Constructing a Comprehensive Picture of Miscanthus Cell Wall to Advance its Deconstruction

A thesis submitted in candidature for the Doctor of Philosophy degree of Aberystwyth University

Ricardo Manuel Fernandes da Costa

INSTITUTE OF BIOLOGICAL, ENVIRONMENTAL & RURAL SCIENCES
ABERYSTWYTH UNIVERSITY
SEPTEMBER 2015

DECLARATION

This work has not previously been accepted in substance for any degree and is not being concurrently submitted in candidature for any degree.

Signed  (Candidate)

Date 8th of September, 2015

STATEMENT 1

This thesis is the result of my own investigations, except where otherwise stated. Other sources are acknowledged by footnotes giving explicit references. A bibliography is appended.

Signed  (Candidate)

Date 8th of September, 2015

STATEMENT 2

I hereby give consent for my thesis, if accepted, to be available for photocopying and for inter-library loan, and for the title and summary to be made available to outside organisations.

Signed  (Candidate)

Date 8th of September, 2015

WORD COUNT OF THESIS: 91,196.

"The time will come when diligent research over long periods will bring to light things which now lie hidden. A single lifetime, even though entirely devoted to the sky, would not be enough for the investigation of so vast a subject… And so this knowledge will be unfolded through long successive ages. There will come a time when our descendants will be amazed that we did not know things that are so plain to them… Many discoveries are reserved for ages still to come, when memory of us will have been effaced. Our universe is a sorry little affair unless it has something for every age to investigate… Nature does not reveal her mysteries once and for all."

– Seneca, Natural Questions,

Book 7, first century

As quoted by Sagan (1980)

SUMMARY

Grasses from the genus *Miscanthus* are among the most promising dedicated lignocellulosic energy crops. Despite their potential, cell wall recalcitrance to deconstruction still hinders widespread use of its biomass as a bioenergy and biomaterial feedstock. Consequently, the advancement of our knowledge concerning the roots of recalcitrance is a pressing matter. To clarify chemical, structural and biological features underpinning recalcitrance in miscanthus cell walls, here are presented the results of an in-depth cell wall analysis following a multidimensional approach, considering: different developmental stages, stem vs. leaf compositional variability and various genotypes. Early results showed inverse correlations between lignin content and ethanol production in stem tissues but not in leaves. FTIR spectroscopy showed that tissue and development-derived compositional differences are mostly associated to structural carbohydrates. Accordingly, subsequent research was shifted to focus on the composition of polysaccharide fractions of the cell wall and on the exploration of structural associations. Glycome profiling allied to glycan immunolocalisation studies further elucidated the nature of compositional variation and provided detailed information about *in situ* distribution of selected carbohydrate epitopes. Key observations demonstrated that stem and leaf biomass is differently modified throughout development, leading to harvest and tissue-specific features at the level of glycan abundance, distribution, composition and ornamentation. These differences have substantial effects on the amenability to deconstruction; however, the results highlighted the limited predictive power of single traits as indicators of cell wall recalcitrance. Instead, a holistic view of the cell wall is promoted, which considers that different components have variable impacts on recalcitrance depending on overall cell wall assembly. These outcomes effectively emphasised the value of the results-driven approach followed in this thesis. Ultimately, the constructed detailed portrait of the cell wall will help steer breeding and engineering strategies for the development of superior energy crops and help advance biorefining strategies.

Key words: Miscanthus, biofuel, plant cell wall, FTIR, lignin, carbohydrate, glycan, glycome profiling, immunolabelling, antibody, recalcitrance, lignocellulose, biomass.

ACKNOWLEDGEMENTS

I would like to begin by expressing my deepest gratitude to my supervisors. To Dr Ana Winters, whose kindness, experience and knowledge, were essential along these last years. Without her contribution most of what has been achieved simply would not exist. To Dr Maurice Bosch, not only for guidance, confidence and esteem that supported me during this work, but also for the valuable support at various levels he gave me over the years. On a more personal level, I wish to heartfully thank my family, friends and everybody who was important to me at one point or another. All your concern, encouragement and particularly your patience will always be very much appreciated. To Dr Gordon Allison, for his valuable suggestions and also for the availability he always showed to comment on and help improve my work. Marian Gray from the Aberystwyth University International Office is another person who, although indirectly, vastly contributed to my project. Thanks to the opportunities given to me by her I was able to establish international collaborations and work with people who have been and will continue to be very important to my career. A big thank you is also due to Dr Michael Hahn, Dr Sivakumar Pattathil, Dr Utku Avci, and others from the Complex Carbohydrate Research Center who helped me and contributed to this project. Since this page cannot accommodate all acknowledgements, to everybody else who has helped me achieve my goals I wish to express my deepest gratitude and ensure that any positive gesture will not be forgotten. Ultimately, as this research was supported by the European Regional Development Funding through the Welsh Government for the BEACON initiative, I thank everyone who was involved and elicited the steady progression of my project.

FREQUENT ABBREVIATIONS

ABSL	Acetyl Bromide Soluble Lignin
AG	Actively Growing
AGN	Arabinogalactan
AGP	Arabinogalactan Protein
ANOVA	Analysis Of Variance
Ara	Arabinose
ATR	Attenuated Total Reflectance
AX	Arabinoxylan
CWM	Cell Wall Material
ELISA	Enzyme-Linked Immunosorbent Assay
FA	Ferulic Acid
FTIR	Fourier transform mid-infrared spectroscopy
Fuc	Fucose
G lignin	Guaiacyl phenylpropanoid lignin unit
Gal	Galactose
GalA	Galacturonic Acid
GAX	Glucuronoarabinoxylan
Glc	Glucose
GlcA	Glucuronic Acid
GP	Glycome Profiling
H lignin	Hydroxyphenyl phenylpropanoid lignin unit
HCA	Hydroxycinnamic Acid
HG	Homogalacturonan
HPAEC-PAD	High-Performance Anion-Exchange Chromatography coupled to Pulsed Amperometric Detection
HPLC	High Performance Liquid Chromatography
IR	Infrared Spectroscopy
mAb	monoclonal Antibody
Man	Mannose
MANOVA	Multivariate Analysis Of Variance
MLG	Mixed-Linkage (1→3, 1→4)-β-Glucan
PB	Peak Biomass (in the context of developmental stage)
PC	Principal Component
*p*CA	*p*-Coumaric Acid
PCA	Principal Component Analysis
PT samples	CWM pretreated with 0.1M KOH to enhance saccharification
RG-I	Rhamnogalacturonan I
RG-II	Rhamnogalacturonan II
Rha	Rhamnose
RI	Refractive Index
S lignin	Syringyl phenylpropanoid lignin unit
SS	Senesced Stage (in the context of developmental stage)
TFA	Trifluoroacetic acid (CF_3CO_2H)
UT samples	Untreated CWM (samples without any applied pretreatment to enhance saccharification)
XG	Xyloglucan
Xyl	Xylose

CONTENTS

1. INTRODUCTION

1. INTRODUCTION

1.1. THE NEED FOR ALTERNATIVE ENERGY SOURCES AND MISCANTHUS AS A RENEWABLE LIGNOCELLULOSIC BIOMASS FEEDSTOCK

The finite nature of our current fossil fuel resources clashes with the ever increasing energy demands derived from rising global populations and improved living standards. Fossil fuel reserves are being consumed at an accelerating speed, leading to higher concentrations of atmospheric carbon dioxide, one of the main greenhouse gases contributing to global climate change (IPCC, 2007). These concerns are main drivers for the development of alternative energy sources.

Plant biomass represents an abundant resource of renewable energy in the form of cell wall polysaccharides. Dedicated energy crops as well as dual-purpose food and energy cultivars from the Panicoideae clade, which includes *Zea mays* (maize), *Miscanthus* spp. (miscanthus), *Sorghum bicolor* (sorghum), *Saccharum* spp. (sugarcane) and *Panicum virgatum* L. (switchgrass), are grasses with C_4 photosynthesis, which generate high yields of biomass (Feltus and Vandenbrink, 2012; van der Weijde *et al.*, 2013). Among these, miscanthus represents one of the most promising dedicated second generation (i.e., lignocellulose-based) bioenergy crops under development (Carroll and Somerville, 2009). Several world-wide breeding programmes focus on harnessing the genotypic and phenotypic variation among and within miscanthus species with the aim of genetically improving miscanthus traits relevant to the enhancement of biomass yield and quality (Heaton *et al.*, 2004; Robson *et al.*, 2013; Yan *et al.*, 2012). Most of the potential energy in lignocellulosic biomass is locked within its cell wall, a heterogeneous mix of predominantly cellulose, xylan and lignin polymers that interact to assemble a complex and dense matrix (McCann and Carpita, 2008; Chundawat *et al.*, 2011).

The relative abundances and interactions among the polymers dictate biomass recalcitrance to saccharification (i.e. amenability to deconstruction to release fermentable sugars). Therefore, one of the key traits for the processing of plant biomass to produce biofuels and biomaterials is cell wall quality (Himmel *et al.*, 2007; DeMartini *et al.*, 2013).

Despite the importance of optimising miscanthus cell wall properties and improving its usefulness as a sustainable and economically viable bioenergy crop, there are substantial gaps in our knowledge concerning the cell wall composition and the biology of this genus. In order to deepen our knowledge of the chemical, structural and biological features of miscanthus cell wall in the context of lignocellulosic feedstocks, as well as to unveil how these characteristics vary among different genotypes, this thesis will present the results and conclusions of an in-depth cell wall analysis of 25 miscanthus genotypes from a larger replicated field trial comprising of 244 genotypes. Several earlier studies on the entire field trial have focussed on a diverse set of physiological and agronomical traits, including senescence (Robson *et al.*, 2012), flowering time (Jensen *et al.*, 2011), and canopy duration and leaf and stem morphology (Robson *et al.*, 2013). In addition, cell wall composition of the full set of genotypes was previously determined using gravimetric analytical methods in combination with near infrared reflectance spectrophotometry (NIRS) -based calibration models (Allison *et al.*, 2011). Extending the level of detail of the latter study, a multidimensional approach has been employed here, considering different developmental stages and stem vs. leaf compositional variability. Each of the chapters in this thesis will present and interpret the results from each related group of experimental approaches. Ultimately, in the final chapter, possible implications of these findings are discussed in terms of future research strategies aimed at developing miscanthus into a sustainable energy crop by means of broadening our understanding of cell wall compositional features, and impacts on biorefining.

1.2. THE GRASS CELL WALL

Plant cell wall biomass is an abundant and renewable organic resource consisting of three main heterogeneous polymeric components (cellulose, hemicelluloses* and lignin), as well as other less abundant components, such as pectins, proteins and hydroxycinnamic acids (Darvill *et al.*, 1980; McNeil *et al.*, 1984; Carpita and Gibeaut, 1993). All these components are interconnected through non-covalent and covalent bonds into an intricate network, that provides structural support to the plant and restricts the accessibility of exogenous enzymes to the cell wall polysaccharides (Fengel and Wegener, 1984; Pauly and Keegstra, 2008). Cell wall recalcitrance to saccharification is the designation used for this conferred resistance to external enzymatic attack, and it can be fundamentally defined as the collective resistance that plant cell walls pose to deconstruction and sugar release by the action of microbes and glycolytic enzymes (Himmel and Picataggio, 2008). More broadly, given that enzymatic hydrolysis of the cell wall to produce fermentable sugars is only one of the energetic applications of lignocellulosic biomass, a new concept has emerged recently, as McCann and Carpita (2015) re-defined recalcitrance as: "those features of biomass which disproportionately increase energy requirements in conversion processes, increase the cost and complexity of operations in the biorefinery, and/or reduce the recovery of biomass carbon into desired products".

Within the scope of producing alternative and renewable fuels derived from lignocellulosic biomass, cell wall recalcitrance represents a serious limiting factor to the full potential of these materials (Pauly and Keegstra, 2008). Currently, harsh and excessive energy consuming pretreatments, followed by high enzyme loadings and prolonged process times are required to reach high hydrolysis rates and fermentable sugar yields (Zheng *et al.*, 2008).

*The term "hemicellulose" is used throughout this thesis as a synonym of "non-cellulosic and non-pectic cell wall polysaccharides", which in grass cell walls essentially consist of xylans, xyloglucans and mixed-linkage (1→3, 1→4)-β-glucan.

Therefore, a deeper understanding of the structure and composition of the plant cell wall is critical for the advancement and optimisation of the processes governing lignocellulosic bioenergy and biorefining applications.

The cell wall is the most external layer of a plant cell, it is what gives shape to and frequently lasts longer than the protoplast which has synthesised it. The wall is also the basis for many vital functions, such as: providing support and resistance to internal turgor; forming defensive barriers (pathogens, dehydration, other environmental factors); mediating intercellular interactions; a source of signalling molecules and developmental cues; controlling rate and direction of growth; regulating diffusion of material through the apoplast; and providing carbohydrate storage (Albersheim, 2011; Burgert, 2006; CCRC, 2007). As a result, plant cell walls may vary in composition depending on specific functions or requirements of different tissues and developmental stages, but also between different plant species or genotypes.

As the plant cell grows, a thin primary wall is deposited mainly consisting of cellulose, hemicellulose and pectins. In dicotyledonous plants, these three classes represent relatively similar percentages of the cell wall: 15% – 30% cellulose; 20% – 25% hemicellulose; and 20% – 35% pectin. However, in commelinoid monocots (e.g., grasses, sedges, rushes, and gingers) the primary wall is reported to contain lower levels of pectins and structural proteins, higher percentages of cellulose, and specifically for the Poales members of the commelinoid monocots, also a special type of glucan hemicellulose, (1→3, 1→4)-β-glucan (MLG) (Carpita, 1996; McCann and Carpita, 2015). The existence of these taxonomically restricted compositional and structural features has led to the classification of the angiosperm primary wall into two distinct classes: Type-I wall, which is characteristic of dicots, non-commelinoid monocots and gymnosperms; and type-II, found only in commelinids (Carpita and Gibeaut, 1993). Cellulose chains are identical between the two types of cell wall. Nevertheless, despite

the presence of small amounts of xyloglucan in type-II walls, cellulose microfibrils are thought to be encased mainly in arabinoxylan hemicelluloses, which functionally replace the predominant pectic substances found in the type-I cell wall (Carpita and Gibeaut, 1993; Carpita, 1996). Additionally, type-II cell walls typically contain larger amounts of hydroxycinnamates (Ishii, 1997b; Vogel, 2008). In this cell wall type, adjacent arabinoxylan chains may have feruloyl groups esterified to arabinose residues, which are then oxidatively coupled to form dimers that cross-link the polymers (Wende and Fry, 1997a; Encina and Fry, 2005).

Lignin is another phenolic component which is found in grass cell walls. This complex aromatic heteropolymer is polymerised from three monolignols derived from the phenylpropanoid pathway: *p*-coumaryl, coniferyl and synapyl alcohols. Monolignol incorporation into lignin occurs in the form of the phenylpropanoid units: *p*-hydroxyphenyl (H), guaiacyl (G), and syringyl (S) (Appendix A). The addition of these polymeric units may vary between different cell types and between species, yielding lignin polymers with varied composition (Fukushima and Dehority, 2000; Boerjan *et al.*, 2003; Bonawitz and Chapple, 2010).

A primary wall is defined as containing cellulose microfibrils which are deposited during cell expansion. At the conclusion of expansion, cellulose deposition into the primary wall ceases, but its composition and mechanical properties may still change; since in certain cell types the wall may be impregnated with other components (Fry, 2010). Impregnation of these walls with lignin is one possibility, yet such layers are still primary walls, even if lignified. Nevertheless, most lignification occurs as secondary cell wall is secreted internally to the primary wall. Cells belonging to vascular tissues, which lack protoplasts at maturity, are frequently lignified and have large amounts of secondary wall; however, not all are lignified (Ishii, 1997b). A secondary cell wall is one whose cellulose microfibrils are laid down after the

cell has ceased to expand (Fry, 2010). At maturity, the secondary cell walls of lignocellulosic feedstocks represent the bulk of the biomass (Pawar *et al.*, 2013), and these walls contain cellulose, hemicellulose and pectin, which is quantitatively and quantitatively different from that of the primary wall (Vogel, 2008). In secondary walls, cellulose is more densely packed and highly ordered than in primary walls (Barnett and Bonham, 2004). However, in both cases it is composed of a polymer of glucose, that is extremely resistant to chemical degradation thanks to the crystalline nature of its microfibrillar (1→4)-β-glucan chains (Fry, 2010; Hall *et al.*, 2010).

Following cellulose, xylans are the dominant group of polysaccharides in grass cell walls (Vogel, 2008). Xylans are more complex than cellulose, as they consist of heteropolymers with (1→4)-β-xylan backbones, frequently acetylated (see chapter 3), and substituted by arabinose (Ara) and glucuronic acid (GlcA) units, attached to some backbone xylose (Xyl) residues (Carpita, 1996)[*]; hence the designations arabinoxylan (AX) and glucuronoarabinoxylan (GAX). However, in secondary walls of tracheary elements, arabinosyl substituents are largely absent, and GlcA or 4-*O*-methyl-GlcA (MeGlcA) is the predominant linkage (McCann and Carpita, 2015). Hydrogen-bonding of cellulose to xylan is generally less efficient than to xyloglucan (XG) and to mixed-linkage (1→3, 1→4)-β-glucan (MLG) (Fry, 2010). XG is much less abundant in grass cell walls than in dicots. Furthermore, despite the presence in both cell wall types of a similar (1→4)-β-Glc backbone frequently substituted by Xyl residues, the ratios between units are different, resulting in xylose-poor xyloglucans in type-II cell walls (Carpita, 1996). On the other hand, significant quantities of MLG occur in grass cell walls, and are functionally analogous to the xyloglucan from type-I wall, as they are especially abundant during periods of rapid cell expansion, firmly hydrogen-bonded to cellulose, and thus may have

[*] It is worth mentioning that in GAX of grass cell walls Ara and GlcA units are linked predominantly to positions 3 and 2 of Xyl residues. However, this linkage structure diverges from what is found in type-I cell walls, where both of these substituents are mainly attached to position 2 of Xyl (Fry, 2010). Appendix B shows the most common monosaccharides contained in the plant cell wall.

a function of tethering its microfibrils (Labavitch and Ray, 1978; Wada and Ray, 1978; Carpita *et al.*, 2001). MLG is an unbranched polymer of glucose but its mixed linkage effectively results in distinct domains within the molecule: ...G3G4G4G3G4G4G4G3G4G4G3G4G4G3G..., where G is β-Glc, and the numbers 3 and 4 represent (1→3) and (1→4) bonds, respectively. Trisaccharide units (cellotriose; DP3) are generally more abundant than tetrasaccharides (cellotetraose; DP4), but the ratios may vary between samples (Meikle *et al.*, 1994). Physical properties of MLG, such as solubility in water, are strongly influenced by these ratios, as glucans where the contribution of DP3 and DP4 is relatively even, are more soluble than glucans where either of these oligomers is more abundant (Collins *et al.*, 2010; Vega-Sánchez *et al.*, 2015). Furthermore, small amounts of longer runs of (1→4)-linked cellodextrins, interrupted by single (1→3) bonds also occur, and it is likely that these cellulose-like domains help MLG to hydrogen-bond cellulose microfibrils (Carpita, 1996; Fry, 2010). Other hemicelluloses, such as mannans may also be found in type-II cell walls, particularly in epidermal tissues, but the amounts are generally very small (Carpita *et al.*, 2001).

There still is no consensus regarding how exactly cellulose interacts with other cell wall polysaccharides. Recurrently, hemicelluloses are described as coating microfibrils (Carpita *et al.*, 2001); however, other lines of research propose that non-cellulosic polysaccharides are adsorbed onto only a small proportion of the microfibril surfaces (Bootten *et al.*, 2004). Regardless, a proposed model stipulates that two co-extensive polymer networks occur in type-II walls, and have distinct roles (Carpita *et al.*, 2001). The first network is the main load-bearing structure of the wall, consisting of AX with low degrees of substitution, and MLG, interacting reversibly through hydrogen-bonds with cellulosic microfibrils. With increased degrees of substitution the affinity for microfibril surfaces decreases, and highly substituted AX and pectin

are considered to comprise the second network; which is thought to determine wall porosity (Harris and Stone, 2008).

Contrary to dicots, the analysis of grass cell wall material (CWM) generally reveals low galacturonic acid (GalA) and rhamnose (Rha) contents, and the reason is that type-II cell walls are generally poor in the pectic polysaccharides which contain these monomers (Carpita, 1996). Qualitatively however, it has been shown that type-II cell wall pectins are similar to those in type-I, except for lower fucose (Fuc) contents (Thomas *et al.*, 1989a). Pectins are polysaccharides which are rich in α-galacturonate, and essentially consist of three interconnected domains linked together by glycosidic bonds: homogalacturonan, rhamnogalacturonan-I and rhamnogalacturonan-II (O'Neill *et al.*, 1990; Fry, 2010). Homogalacturonan (HG) frequently makes up the major portion of cell wall pectins and it comprises of unbranched chains of α-GalA residues, joined by (1→4)-bonds which may or may not be methyl-esterified (Zhang and Staehelin, 1992). GalA residues linked to methyl ester groups (MeGalA) tend to occur contiguously along the HG backbone; an arrangement that probably results from the action of pectin methyl-esterase on a more abundantly methyl-esterified precursor polymer (Fry, 2010). Furthermore, acetylation of HG backbones may occur (Liners *et al.*, 1994), but usually not extensively (Kouwijzer *et al.*, 1996). Rhamnogalacturonan-I (RG-I) may be acetylated; however, it lacks methyl-esters (Schols and Voragen, 1994; Fry, 2010). RG-I is a group of branched polysaccharides composed of a backbone of the repeating disaccharide [→4)-α-GalA-(1→2)-α-Rha-(1→], where most rhamnosyl residues are substituted at C-4 with complex side-chains consisting of galactosyl and arabinosyl residues (O'Neill *et al.*, 1990). Unusually in pectins, some of these side chains may enable RG-I to hydrogen-bond to cellulose (Zykwinska *et al.*, 2005). Rhamnogalacturonan-II (RG-II) was first described by Darvill *et al.* (1978). RG-II is a very complex pectic polysaccharide with a backbone of at least eight (1→4)-linked-α-GalA

residues, substituted by five different types of acidic side-chains, which contain a variety of different sugar residues, including some exclusive to RG-II (Melton *et al.*, 1986; O'Neill *et al.*, 2004). Similarly to RG-I, methyl-esterification has not been reported in RG-II (Fry, 2010), but *O*-acetylation has been detected in certain residues of RG-II side chains (Whitcombe *et al.*, 1995). Generally in this pectic network, calcium contributes to the cross-linking between the de-esterified carboxylic acid groups in HG; whereas RG-II domains are cross-linked by borate di-ester bridges (Ishii *et al.*, 1999; O'Neill *et al.*, 2001). Grass cell walls may also contain galactans, mainly in the form of arabinogalactan (AGN), which typically occur as side-chains of pectic polysaccharides or associated to proteins as arabinogalactan proteins (AGPs) (Carpita, 1996). Moreover, an important discovery has been made recently, as evidence has been found for a proteoglycan containing covalently attached pectin and xylan domains (Tan *et al.*, 2013). However, this discovery has been made using *Arabidopsis* spp. samples, and it is yet unknown if equivalent structures occur in grass cell walls. When compared with dicots and non-commelinoid monocots, grasses contain small amounts of structural proteins and have more abundant phenylpropanoid components, which form an extensive interconnecting network (Iiyama *et al.*, 1990).

All components considered, the grass cell wall can be visualised as an insoluble macromolecular network, where cellulose, matrix polysaccharides (hemicelluloses and pectins), aromatic compounds (e.g., lignin and hydroxycinnamic acids) and aliphatic acids (e.g., acetate) all associate to form a very complex structure, which represents a significant challenge to degradation in either biological and industrial contexts.

1.3. EXPERIMENTAL DESIGN AND PROJECT AIMS

This project followed a cross-cutting approach where knowledge gained from cell biological, biochemical, spectroscopic and imaging methods was integrated in a systematic study of the structure, composition and deconstruction of lignocellulosic biomass. The resulting detailed portrait of the cell wall will in turn contribute to the tailoring of more effective biorefining treatments for specific cell wall types, and also to the breeding of biomass feedstocks with desired characteristics for conversion to biofuels and other biomaterials. This approach was primarily based on the premise that variation in composition, structural architecture and abundance of cell wall polysaccharides and phenolic compounds lead to varying levels of biomass digestibility. In order to conduct an in-depth analysis of lignocellulosic biomass, with a particular focus on the glycome, several miscanthus genotypes were selected from a spaced field trial of 244 accessions (Fig. 1.1), established in 2004 near Aberystwyth, UK (52.437848º, -4.026688º) described by Allison *et al.* (2011). Briefly, the trial field is on a WSW 7% sloping field, relatively exposed to S and W winds. The trial is organised in four randomised blocks perpendicular to the main slope, each surrounded by a dense guard perimeter of a commercially available variety of *M.* × *giganteus*[*]. The soil is characterised by a pH ranging from 5.1 to 6.3, and consists of a stony seasonally waterlogged loam overlying shale, with the stone fraction estimated at 50% of the soil mass in the 0 – 40cm layer.

Genotypes were selected to represent a wide range of compositional variability, estimated by gravimetric measurements of neutral detergent fibre, acid detergent fibre and acid detergent lignin in bulked plant tissue samples (Allison *et al.*, 2011), and on genotype inclusion in association mapping programmes (Slavov *et al.*, 2013). Furthermore, the plant material encompasses genotypes with varying ploidy and belonging to two *Miscanthus* spp., *M. sinensis*

[*] Genotype Mb311, acquired from Biomass Industrial Crops Ltd (BICAL; Devon, UK).

and *M. sacchariflorus*, an inter-specific hybrid *M.* × *giganteus* and other hybrid genotypes with divergent admixtures of *M. sinensis* and *M. sacchariflorus* (Table 1.1). Samples were collected at three time points during the 2012 – 2013 growth season. The time points correspond to three developmental stages: 10 weeks after first shoot emergence, when the plants were actively growing (AG); peak biomass, 18 weeks after emergence, a stage when the plants had mostly ceased their growth (PB); and at 42 weeks after emergence when the plants were completely senesced (SS). At each developmental stage and for each genotype, a single tiller of equal or greater than ¾ of the plant's total height (excluding rhizome and inflorescence when present) was selected randomly and collected from three of the four replicate plots. By the end of the growth season and after tissue separation 18 samples had been collected (3 developmental stages × 3 biological replicates × 2 tissues) for each of the 25 selected lines.

Fig.1.1. Aerial view of the 244-accession trait trial field 2 (2TT).

Table 1.1. Description of the 25 miscanthus genotypes used in this study.

Genotype	Species and "Mb" number	Ploidy	Reason for Choice[†]
gig01	*M.* × *giganteus* (Mb182)	3*n*	High cellulose, low hemicellulose, high lignin, high *p*-coumaric and ferulic acid
gig02	*M.* × *giganteus* (Mb296)	3*n*	Low hemicellulose, high lignin, intermediate *p*-coumaric and ferulic acid
gig03	*M.* × *giganteus* (Mb299)	4*n*	High cellulose, low hemicellulose
hyb01	55% *M. sinensis;* 45% *M. sacchariflorus*[*] (Mb148)	2*n*	♂ parent
hyb02	72% *M. sinensis;* 28% *M. sacchariflorus* (Mb251)	2*n*	High hemicellulose
hyb03	64% *M. sinensis;* 36% *M. sacchariflorus* (Mb307)	3*n*	High ferulic acid, good saccharification results
sac01	*M. sacchariflorus* (Mb297)	2*n*	♀ parent
sin01	*M. sinensis* (Mb014)	2*n*	♂ parent
sin02	*M. sinensis* (Mb016)	2*n*	♂ parent
sin03	*M. sinensis* (Mb019)	2*n*	Low lignin percentage, good saccharification results
sin04	*M. sinensis* (Mb030)	2*n*	♂ parent, intermediate *p*-coumaric and ferulic acids
sin05	*M. sinensis* (Mb031)	2*n*	♂ parent
sin06	*M. sinensis* (Mb037)	2*n*	Low lignin, high yield
sin07	*M. sinensis* (Mb040)	2*n*	Highest *p*-coumaric acid
sin08	*M. sinensis* (Mb102)	2*n*	♂ parent
sin09	*M. sinensis* (Mb108)	3*n*	Frequently included in departmental studies, drought tolerant
sin10	*M. sinensis* (Mb130)	2*n*	♂ parent
sin11	*M. sinensis* (Mb133)	2*n*	♂ parent
sin12	*M. sinensis* (Mb143)	2*n*	Low cellulose
sin13	*M. sinensis* (Mb152)	2*n*	Good saccharification results
sin14	*M. sinensis* (Mb183)	2*n*	Low cellulose, low lignin
sin15	*M. sinensis* (Mb192)	2*n*	♂ parent
sin16	*M. sinensis* (Mb254)	2*n*	High hemicellulose
sin17	*M. sinensis* (Mb312)	2*n*	Low cellulose, low hemicellulose
sin18	*M. sinensis* (Mb314)	2*n*	Low *p*-coumaric and ferulic acid

[*] *M. sinensis* / *M. sacchariflorus* admixture proportions determined from single-nucleotide polymorphism data (Slavov *et al.*, 2013).

[†] Selection based on available compositional data (Allison *et al.*, 2011), and the genotypes selected as parents for association mapping programmes active in late 2011 (Hayes, December 2011. Personal communication).

1.3.1. Secondary trial plot

During the method development stage of the project there was an attempt to establish a secondary trial plot, where the 25 selected lines were included. The main objective of establishing this plot was to simplify sampling and to increase the similarity of environmental conditions for all accessions; given that the slope and the soil composition variation are negligible in the field selected for this trial plot located at Cae Rasus. Rhizomes for all 25 genotypes were collected during the first week of April 2012 from the above mentioned 244-accession plant trial (2TT). Within 24h or 48h from collection, all rhizomes were transported and planted at the Cae Rasus site (52.433420º, -4.026799º). Experimentally, this plot was organised in a single block, with triplicate accessions in a completely randomised design. A *M.* × *giganteus* guard perimeter was also included, plants were spaced 1.25m from each other and the total area of the plot was *circa* 190m^2 (Fig. 1.2).

However, due to extreme weather fluctuations, the survival rate was far from ideal, with almost 50% of plants not surviving the late frosts which occurred during the second quarter of 2012. In an attempt to rescue the dying plants, the field was covered with a perforated plastic film layer with the aim of maintaining relatively constant levels of soil humidity and temperature (Fig. 1.3). Nonetheless, this too had no beneficial impact on the plant survival.

Ultimately it was concluded that extensive rhizome replacement would have to take place and a suitable sampling could only occur after 2 or 3 growth seasons (2014 or 2015). Due to this not being compatible with the duration of the PhD project, the secondary trial plot was abandoned.

giganteus	giganteus	giganteus	giganteus	giganteus	giganteus	giganteus	giganteus	giganteus	giganteus	giganteus
giganteus	Mb 130.C sinensis	Mb 37.B sinensis	Mb 251.A sinensis	Mb 31.C sinensis	Mb 40.B sinensis	Mb 102.C sinensis	Mb 182.A giganteus	Mb 143.B sinensis	Mb 297.C sacc/robustus	giganteus
giganteus	Mb 133.B sinensis	Mb 108.A sinensis	Mb 143.A sinensis	Mb 192.A sinensis	Mb 312.B sinensis	Mb 130.A sinensis	Mb 19.B sinensis	Mb 296.A giganteus	Mb 37.A sinensis	giganteus
giganteus	Mb 16.B sinensis	Mb 314.C sinensis	Mb 297.B sacc/robustus	Mb 152.A sinensis	Mb 314.B sinensis	Mb 297.A sacc/robustus	Mb 182.C giganteus	Mb 251.C sinensis	Mb 30.B sinensis	giganteus
giganteus	Mb 254.C sinensis	Mb 14.C sinensis	Mb 148.A hybrid	Mb 37.C sinensis	Mb 254.A sinensis	Mb 14.B sinensis	Mb 30.C sinensis	Mb 183.C sinensis	Mb 299.C sacchariflorus	giganteus
giganteus	Mb 143.C sinensis	Mb 16.C sinensis	Mb 133.A sinensis	Mb 307.C hybrid	Mb 19.C sinensis	Mb 296.C giganteus	Mb 40.C sinensis	Mb 311.A giganteus (control W)	Mb 108.B sinensis	giganteus
giganteus	Mb 183.B sinensis	Mb 312.A sinensis	Mb 99.A goliath (control T)	Mb 299.B sacchariflorus	Mb 311.C giganteus (control W)	Mb 102.A sinensis	Mb 307.B hybrid	Mb 192.C sinensis	Mb 99.B goliath (control T)	giganteus
giganteus	Mb 31.B sinensis	Mb 299.A sacchariflorus	Mb 192.B sinensis	Mb 182.B giganteus	Mb 254.B sinensis	Mb 31.A sinensis	Mb 251.B sinensis	Mb 183.A sinensis	Mb 14.A sinensis	giganteus
giganteus	Mb 102.B sinensis	Mb 152.C sinensis	Mb 148.C hybrid	Mb 16.A sinensis	Mb 40.A sinensis	Mb 130.B sinensis	Mb 108.C sinensis	Mb 148.B hybrid	Mb 30.A sinensis	giganteus
giganteus	Mb 307.A hybrid	Mb 314.A sinensis	Mb 311.B giganteus (control W)	Mb 296.B giganteus	Mb 312.C sinensis	Mb 19.A sinensis	Mb 99.C goliath (control T)	Mb 152.B sinensis	Mb 133.C sinensis	giganteus
giganteus	giganteus	giganteus	giganteus	giganteus	giganteus	giganteus	giganteus	giganteus	giganteus	giganteus

Fig.1.2. Experimental design used for the trial plot established at the Cae Rasus site in April 2012.

Fig.1.3. Covering of the Cae Rasus trial plot with a perforated plastic film layer (left) and final appearance (right).

2. CHARACTERISATION OF MISCANTHUS AS AN ENERGY CROP

2. CHARACTERISATION OF MISCANTHUS AS AN ENERGY CROP

As part of an approach to characterise the cell wall of miscanthus, practical work was initiated with a study of biomass accumulation and morphology. This was followed by the preparation of the cell wall samples and the measurement of three compositional parameters using moderate to high throughput assays. By following this relatively rapid approach it was intended to gather sufficient information to better understand cell wall modifications throughout the growth season and to help direct subsequent steps of the project. Methods and assessment of the results are described below.

2.1. MISCANTHUS MORPHOLOGICAL CHARACTERISATION

2.1.2. Overview

Native to East Asia, members of the genus *Miscanthus* are perennial, rhizomatous plants, which remobilise nutrients to the rhizome during senescence to ensure regrowth of the crop in the subsequent season (Robson *et al.*, 2012). Consequently, miscanthus is typically harvested during winter or early spring when nutrients have been translocated from above-ground tissues to rhizomes, thus providing a number of environmental advantages over annuals as bioenergy crops, including lower requirements for fertiliser, reduced soil erosion and the potential for soil carbon sequestration (Clifton-Brown *et al.*, 2013). Several varieties of miscanthus give high yields in cool climates, unusual within the C_4 grasses, making miscanthus a potentially viable and sustainable energy crop over a wide range of diverse geographical zones (Purdy *et al.*, 2013). Of the several identified miscanthus species, the most commonly investigated are *Miscanthus sinensis, Miscanthus sacchariflorus* and the vigorous but sterile hybrids between

the two, of which *M.* × *giganteus* is the most widely cultivated variety (Heaton *et al.*, 2008; Dwiyanti *et al.*, 2013; Liu *et al.*, 2013).

In the UK, miscanthus is planted in springtime and once established can be harvested annually for up to 15 years (DEFRA, 2007). In Aberystwyth, where the plants used in these experiments were grown, miscanthus initiates new shoot emergence between March and April. Growth visibly increases in the following months and produces erect and robust stems, which, depending on the genotype, reach heights of several meters by mid-summer. Later in the year, typically after the first autumn frosts, the plants enter senescence, and foliar biomass is greatly reduced.

Furthermore, it is known that leaf and stem differ not only in their relative contributions to total biomass, but also in their cell wall composition and digestibility; as indicated by studies focused on the use of forage grasses and cereal straw for animal nutrition (Love *et al.*, 1998; McCartney *et al.*, 2006). Bearing this in mind and the fact that most studies on cell wall composition in energy crops use total above-ground biomass for their analysis (since this is the most relevant material for downstream applications), it was considered essential not only to characterise miscanthus morphology as a whole but also how biomass accumulation and composition varies between genotypes and throughout development for leaf and for stem independently.

2.1.3. Methods

Immediately after collection, the miscanthus tillers were photographed, measured and left at -20ºC overnight, before being freeze-dried. Once dry, stem and leaf tissue (including sheath) were separated, weighed and leaf contribution was registered as percentage of total biomass dry weight.

Data for tiller length, tiller weight and leaf percentage was statistically assessed to evaluate the effect of genotype (25 levels) and development (3 levels) on the variation of these morphological traits. All statistical calculations were performed using the software Statistica (v. 8.0; StatSoft, Tulsa, Oklahoma) at a 5% significance level (α=0.05). Analyses of variance (ANOVA), Tukey's tests and correlations between variables were determined using natural logarithm transformed data to account for skewed distributions due to the exponential nature of tissue growth. Effect sizes were calculated as eta-squared (η^2) statistics (Cohen, 1973; Levine and Hullett, 2002) according to the equation:

$$\eta^2 = \frac{SS_{effect}}{SS_{total}} \quad (2.1)$$

Where *SS* is the sum of squares.

2.1.4. Results

The mean contribution of leaf material (leaf blade and sheath) to total dry biomass among the genotypes was 63.8% (ranging from 42.2% to 80.4%) at the AG stage, 55.6% (36.3% – 78.8%) for PB stage, and 36.1%, for SS (15.8% – 63.2%). The mean tiller length was 1454mm (1073mm – 2129mm) at AG, 1810mm (1085mm – 2839mm) at PB and 1985mm (1460mm – 2777mm) at SS. For tiller weight, the mean values across the genotypes were 12.0g (4.1g – 35.3g) at AG, 19.4 (6.1g – 56.6g) at PB and 19.8g (6.6g – 72.7g) at SS (Table 2.1). The variance between the three replicates of each genotype was preliminarily tested and shown not to be significantly different for the morphological traits studied here: leaf percentage (P=0.550), tiller length (P=0.092) and tiller weight (P=0.286). Subsequently, ANOVAs used to assess the effect of genotype and developmental stage on morphological variation indicated that both

factors were statistically significant (P<0.001 for the three traits); however, effect sizes varied depending on the morphological trait assessed (Table 2.2).

Box-and-whisker plots of the distribution of leaf percentage, tiller length and tiller weight, show that the contribution of leaf tissue to total biomass decreased as plants matured (Fig. 2.1A). Conversely, tiller length continuously increased until senescence (Fig. 2.1B), and tiller dry weight initially increased but then was not statistically different between PB and SS stages (Fig. 2.1C). Tukey's tests showed that differences in leaf contribution and tiller length from one developmental stage to another were statistically significant, but the same was not observed for tiller weight; as significant change only occurred early in plant growth, and peak biomass and senesced tillers did not differ significantly in their weight.

Further ANOVAs considering each developmental stage on its own showed that there were significant differences between the genotypes at this level (P<0.001 for the three morphological traits). To elucidate where the differences occurred, Tukey's tests were performed to create homogeneous groups for each morphological trait among the genotypes at each developmental stage. Resulting groups are labelled with appropriate superscripts to each value in Table 2.1.

Table 2.1. Morphological traits of the 25 miscanthus genotypes used in this study. Values are expressed as mean ± standard deviation for the three replicated plants at the three developmental stages for each genotype. (AG, Active Growth; PB, Peak Biomass; SS, Senesced Stage). Values within a column sharing a letter in their superscript are not significantly different according to a Tukey's test (α=0.05).

	Leaf Percentage (%)			Tiller Length (mm)			Tiller Weight (g)		
	AG	**PB**	**SS**	**AG**	**PB**	**SS**	**AG**	**PB**	**SS**
gig01	44.5 ± 5.8^{ab}	36.5 ± 0.5^{ab}	16.1 ± 0.8^{a}	2029.3 ± 220.0^{cd}	2690.0 ± 55.0^{cde}	2526.0 ± 143.0^{cde}	26.8 ± 14.9^{bcd}	41.3 ± 0.2^{abcd}	65.1 ± 13.8^{d}
gig02	42.3 ± 3.3^{a}	36.7 ± 3.3^{a}	17.9 ± 3.1^{ab}	1588.7 ± 322.1^{abcd}	2671.5 ± 200.1^{ce}	2592.3 ± 414.8^{de}	35.2 ± 15.1^{cd}	40.3 ± 3.3^{cd}	57.4 ± 31.2^{cd}
gig03	42.2 ± 1.0^{a}	36.3 ± 0.2^{a}	15.8 ± 5.2^{a}	2129.3 ± 328.5^{d}	2839.0 ± 355.0^{e}	2776.7 ± 174.5^{e}	35.3 ± 2.2^{d}	56.6 ± 5.6^{d}	72.7 ± 16.8^{d}
hyb01	55.0 ± 3.4^{abcd}	48.6 ± 1.6^{abc}	26.3 ± 2.9^{abcd}	1665.7 ± 126.7^{abcd}	1779.5 ± 14.8^{abcde}	2211.0 ± 193.8^{bcde}	10.2 ± 5.4^{abcd}	19.0 ± 2.7^{abcd}	13.8 ± 1.0^{a}
hyb02	67.7 ± 3.4^{cde}	45.1 ± 6.9^{abc}	36.6 ± 3.9^{cdefg}	1170.7 ± 161.1^{ab}	1752.5 ± 53.0^{abcde}	1697.3 ± 217.5^{ab}	5.7 ± 3.0^{a}	21.2 ± 6.9^{abcd}	6.8 ± 0.5^{a}
hyb03	53.2 ± 6.9^{abc}	36.6 ± 0.5^{a}	22.1 ± 1.5^{abc}	1890.7 ± 408.1^{bcd}	2269.5 ± 367.0^{bcde}	2565.0 ± 77.0^{de}	16.8 ± 6.8^{abcd}	36.0 ± 0.1^{bcd}	46.5 ± 5.8^{bcd}
sac01	53.2 ± 1.8^{abc}	49.3 ± 1.9^{abc}	32.1 ± 6.2^{bcdef}	1340.7 ± 69.8^{abcd}	1656.0 ± 192.3^{abcd}	1712.3 ± 366.6^{ab}	6.3 ± 2.7^{ab}	10.1 ± 2.8^{abc}	6.6 ± 1.1^{a}
sin01	68.2 ± 1.1^{cde}	59.4 ± 7.1^{bcd}	38.6 ± 2.6^{cdefg}	1202.3 ± 114.0^{ab}	1447.0 ± 46.7^{abd}	1837.7 ± 258.6^{abcd}	11.0 ± 0.9^{abcd}	13.4 ± 0.3^{abcd}	11.3 ± 4.1^{a}
sin02	61.8 ± 4.8^{bcde}	50.9 ± 6.7^{abcd}	31.4 ± 1.9^{bcdef}	1261.7 ± 220.0^{abc}	1730.0 ± 240.4^{abcde}	1798.7 ± 143.0^{abcd}	7.1 ± 2.0^{ab}	11.0 ± 2.7^{abcd}	7.8 ± 1.9^{a}
sin03	68.1 ± 22.1^{cde}	60.6 ± 17.6^{bcd}	46.2 ± 21.3^{cdefg}	1390.7 ± 494.5^{abcd}	1546.5 ± 405.2^{abd}	1766.7 ± 289.7^{abcd}	12.7 ± 11.4^{abcd}	18.5 ± 6.6^{abcd}	15.8 ± 4.3^{a}
sin04	74.3 ± 1.8^{de}	65.6 ± 4.9^{cd}	34.2 ± 0.9^{bcdefg}	1302.0 ± 140.5^{abcd}	1735.0 ± 134.4^{abcde}	2042.0 ± 115.4^{abcde}	9.0 ± 2.7^{abcd}	13.1 ± 1.6^{abcd}	14.7 ± 0.9^{a}
sin05	64.1 ± 4.4^{cde}	56.9 ± 0.6^{abcd}	37.1 ± 3.3^{cdefg}	1553.0 ± 186.2^{abcd}	1879.0 ± 100.4^{bcde}	1980.7 ± 414.4^{abcde}	13.5 ± 3.7^{abcd}	25.9 ± 7.4^{abcd}	15.9 ± 2.0^{a}
sin06	71.6 ± 3.0^{cde}	62.7 ± 0.1^{bcd}	52.7 ± 4.6^{efg}	1384.3 ± 40.7^{abcd}	1825.0 ± 247.5^{abcde}	1723.7 ± 109.4^{abc}	7.8 ± 3.1^{ab}	15.5 ± 9.0^{abcd}	16.1 ± 3.1^{ab}
sin07	66.9 ± 2.0^{cde}	56.6 ± 1.1^{abcd}	28.9 ± 2.5^{abcde}	1441.0 ± 86.4^{abcd}	1795.0 ± 289.9^{abcde}	1756.7 ± 111.8^{abcd}	8.7 ± 2.8^{abc}	19.2 ± 1.1^{abcd}	12.3 ± 1.4^{a}
sin08	69.7 ± 10.2^{cde}	63.4 ± 0.2^{bcd}	37.4 ± 1.3^{cdefg}	1400.3 ± 225.9^{abcd}	1714.5 ± 105.4^{abcde}	2152.3 ± 183.3^{abcde}	8.6 ± 1.6^{abcd}	17.5 ± 3.7^{abcd}	14.1 ± 2.0^{a}
sin09	63.5 ± 1.0^{cde}	59.7 ± 2.6^{bcd}	36.6 ± 1.5^{cdefg}	1570.0 ± 411.5^{abcd}	1830.0 ± 509.1^{abcde}	2074.7 ± 204.8^{abcde}	11.3 ± 5.5^{abcd}	14.5 ± 3.8^{abcd}	10.8 ± 0.4^{a}
sin10	67.0 ± 1.5^{cde}	52.4 ± 2.9^{abcd}	36.4 ± 2.3^{cdefg}	1397.7 ± 162.1^{abcd}	1798.5 ± 313.2^{abcde}	1821.0 ± 184.2^{abcd}	6.1 ± 0.9^{ab}	10.7 ± 5.4^{abc}	6.9 ± 1.0^{a}
sin11	70.2 ± 0.8^{cde}	61.0 ± 1.6^{bcd}	31.0 ± 12.9^{abcde}	1413.0 ± 51.1^{abcd}	1504.0 ± 79.2^{abd}	1837.3 ± 389.5^{abcd}	7.5 ± 1.2^{ab}	11.5 ± 0.4^{abcd}	17.9 ± 16.5^{a}
sin12	76.0 ± 9.5^{de}	66.7 ± 11.8^{cd}	59.9 ± 16.4^{fg}	1116.7 ± 120.1^{a}	1406.5 ± 103.9^{abd}	1597.0 ± 351.3^{ab}	4.1 ± 0.6^{a}	6.3 ± 1.3^{a}	7.5 ± 2.5^{a}
sin13	80.4 ± 2.5^{e}	78.8 ± 0.8^{d}	63.2 ± 11.6^{g}	1072.7 ± 179.6^{a}	1085.0 ± 120.2^{a}	1459.7 ± 44.5^{a}	8.7 ± 5.6^{ab}	10.1 ± 9.3^{ab}	17.5 ± 9.0^{ab}
sin14	69.7 ± 2.7^{cde}	64.5 ± 0.7^{bcd}	50.6 ± 2.8^{defg}	1702.5 ± 611.6^{abcd}	1850.0 ± 50.0^{abcde}	1789.0 ± 15.6^{abcde}	8.5 ± 0.1^{abcd}	20.0 ± 0.2^{abcd}	19.2 ± 8.2^{abc}
sin15	60.5 ± 1.7^{bcde}	54.8 ± 6.1^{abcd}	31.7 ± 1.6^{bcdef}	1620.7 ± 132.2^{abcd}	1978.0 ± 101.8^{bcde}	2537.0 ± 150.4^{cde}	15.3 ± 5.9^{abcd}	17.5 ± 5.4^{abcd}	14.7 ± 1.2^{a}
sin16	66.6 ± 4.1^{cde}	61.8 ± 4.8^{bcd}	39.5 ± 5.2^{cdefg}	1095.0 ± 152.6^{a}	1343.5 ± 23.3^{ab}	1887.7 ± 58.9^{abcde}	4.2 ± 0.5^{a}	6.1 ± 2.3^{a}	6.7 ± 2.3^{a}
sin17	67.4 ± 8.7^{cde}	62.5 ± 16.5^{bcd}	38.3 ± 9.7^{cdefg}	1315.7 ± 136.8^{abcd}	1526.5 ± 301.9^{abd}	1951.7 ± 275.7^{abcde}	8.9 ± 2.7^{abcd}	8.8 ± 4.8^{abc}	7.6 ± 2.8^{a}
sin18	70.9 ± 7.1^{cde}	62.7 ± 1.0^{bcd}	41.9 ± 7.1^{cdefg}	1301.7 ± 210.3^{abcd}	1598.5 ± 143.5^{abcd}	1539.7 ± 185.4^{ab}	10.7 ± 4.0^{abcd}	20.3 ± 5.7^{abcd}	10.5 ± 3.2^{a}
Mean	63.8 ± 10.1	55.6 ± 10.9	36.1 ± 12.1	1454.2 ± 275.2	1810.0 ± 418.2	1985.4 ± 360.8	12.0 ± 8.4	19.4 ± 12.2	19.8 ± 18.9

Table 2.2. ANOVA results for the morphological characterisation traits.

Leaf Percentage

Effect	Degrees of freedom	Sum of squares	Mean square	*F*-ratio	*P*-value	Effect size (η^2)
Genotype	24	10.04	0.42	17.00	<0.0001	0.3302
Developmental stage	2	15.34	7.67	312.40	<0.0001	0.5043
Genotype × Developmental stage	48	2.07	0.04	1.80	0.0074	0.0679
Error	121	2.97	0.03			
Total	195	30.41				

Tiller Length

Genotype	24	5.77	0.24	11.90	<0.0001	0.4504
Developmental stage	2	3.79	1.89	93.70	<0.0001	0.2959
Genotype × Developmental stage	48	0.80	0.02	0.80	0.7758	0.0625
Error	121	2.45	0.02			
Total	195	12.81				

Tiller Weight

Genotype	24	60.20	2.51	15.82	<0.0001	0.6259
Developmental stage	2	9.44	4.72	29.77	<0.0001	0.0981
Genotype × Developmental stage	48	7.36	0.15	0.97	0.5408	0.0765
Error	121	19.19	0.16			
Total	195	96.19				

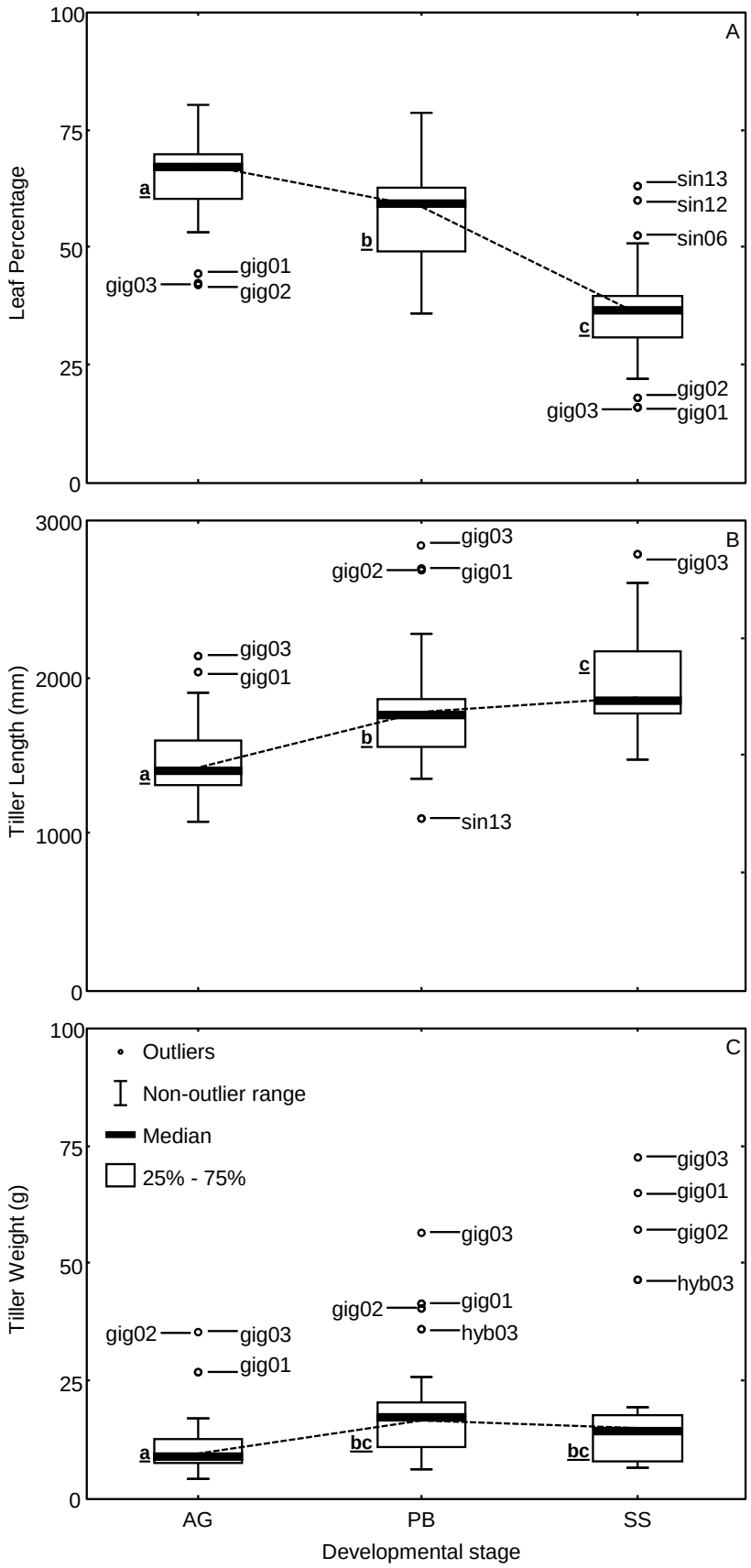

Fig. 2.1. Distribution of morphological measurements for 25 miscanthus genotypes at active growth (AG), peak biomass (PB) and senescence (SS). The non-outlier range is defined as the range of values which fall outside 1.5× the interquartile range of the distribution (height of the 25% – 75% box). Not significantly different developmental stages are indicated by a common underlined letter next to the box (Tukey's test at α=0.05).

2.1.5. Discussion

Clearly demarked homogeneous groups among the genotypes did not emerge from the Tukey's multiple comparisons test (Table 2.1), as there is a continuum between the genotypes. However, for all morphological traits assessed it was observed that the *M.* × *giganteus* and the hyb03 genotypes were frequently clustered in close proximity to each other and at all times on the same end of the range of values for a particular trait. By contrast, the *M. sinensis* genotypes sin12 and sin13 were frequently grouped closely at the other end of the range of values. By looking at the box plots of the distributions (Fig. 2.1) it is apparent that genotypes gig01, gig02 and gig03 are characterised by possessing extremely low values for leaf contribution to total biomass, whereas they do possess unusually high tiller lengths and weights. In contrast, sin12 and sin13 typically have high leaf percentages but shorter and lighter tillers. Furthermore, it is noteworthy that during senescence, a more significant distinction between the homogeneous groups emerged among the values for tiller weight (Table 2.1). These groups may be roughly divided in two sub-groups: the first (a) containing all *M. sinensis*, *M. sacchariflorus*, hyb01 and hyb02 genotypes; and a second group (d) containing the *M.* × *giganteus* and the hyb03 genotypes. Considering that the second group contains the higher values for tiller weight, this provides more evidence for a clear superiority for hybrid genotypes, particularly for *M.* × *giganteus*, concerning total biomass production (Clifton-Brown *et al.*, 2001).

Most studies on cell wall composition in energy crops use total above-ground biomass for their analysis, as this is the most relevant material for downstream applications. However, several studies focussing on the usage of forage grasses and cereal straw for animal nutrition have shown that the leaf fraction is different in terms of cell wall composition and ruminant digestibility when compared to the stem fraction (Love *et al.*, 1998; McCartney *et al.*, 2006). Analysis of biomass accumulation on 25 miscanthus genotypes has shown that leaf material (blade and sheath) contributed on average to more than half of the total dry biomass during the

first two harvest time points. At the senesced stage, the leaf contribution was reduced to an average of 36.1%, mainly due to leaf abscission during senescence. In addition to the significant contribution of leaf biomass to total above-ground biomass, it is important to emphasise the variation of leaf contributions, ranging from 42.2% to 80.4% at actively growing, 36.3% to 78.8% at peak biomass and 15.8% to 63.2% at senescent stages (Table 2.1). These varying tissue contributions can have a substantial performance and economic impact on downstream biorefining processes, as compositional differences between stem and leaf biomass will lead to tissue-specific amenability for enzymatic hydrolysis and to biological conversion into ethanol (discussed in following chapters). Caution is thus required when interpreting cell wall phenotyping data obtained from pooled total above-ground biomass with genetic/genomic data, since part of the observed variation might actually be due to differences in the tissue contributions to total biomass.

To better understand genotype and development-derived variation of allometric traits important for miscanthus cell wall biorefining, mean leaf contribution to total biomass was plotted against tiller length and weight (Fig. 2.2). Throughout development hybrid genotypes ranked high in terms of tiller length and weight, but showed low leaf contributions to total biomass. This trend was predominant in *M.* × *giganteus* genotypes, whereas the other three hybrid genotypes displayed less extreme traits. The *M. sacchariflorus* genotype showed a tendency to fall between the *M. sinensis* genotypes and the other hybrids. The *M. sinensis* genotypes included in this study showed a broader range in the morphological traits studied; of which, sin08, sin14 and sin15 are noteworthy for possessing not only moderate to high values for leaf percentage, but also for biomass production (as expressed by tiller length and weight). By correlating leaf contribution to total biomass with the other two morphological traits, negative associations were observed (tiller length: r=-0.77, P<0.001; (tiller weight: r=-0.59, P<0.001) (Fig. 2.3). These results indicate that low yielding genotypes are more likely

to have higher leaf biomass percentages. Simultaneously: the observed consistency in the genotypes which show extreme morphological traits, the highly significant genotype effect, and the non-significant differences between independent plant replicates of a given genotype, may suggest that the leaf to stem ratio could be at least in part a heritable genotype-specific trait. This may provide valuable opportunities for the breeding of miscanthus cultivars which are simultaneously high yielders and high leaf biomass producers.

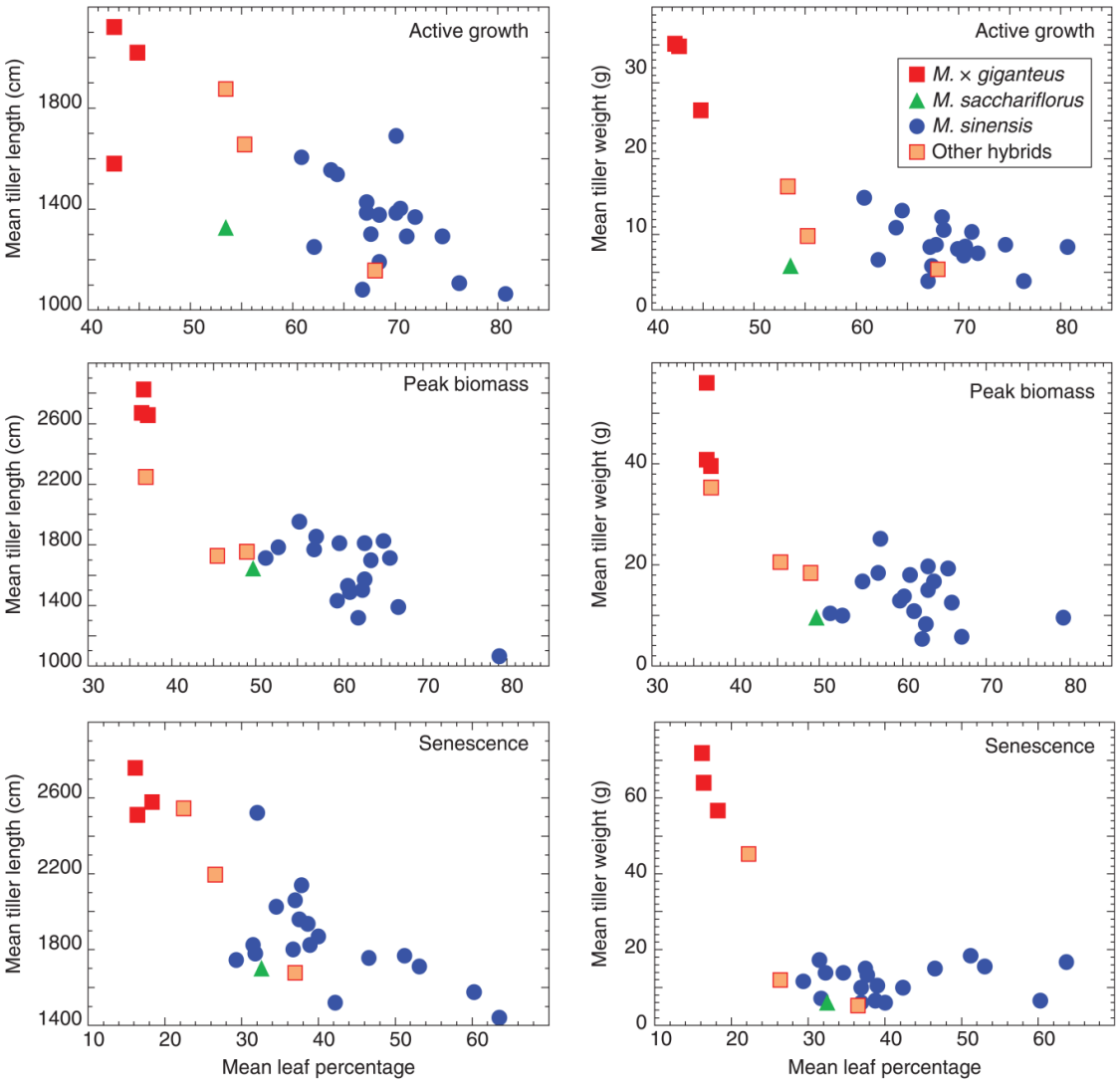

Fig. 2.2. Graphical presentation of the mean leaf percentage of total biomass plotted against mean tiller length and tiller dry weight for the 25 miscanthus genotypes at three developmental stages.

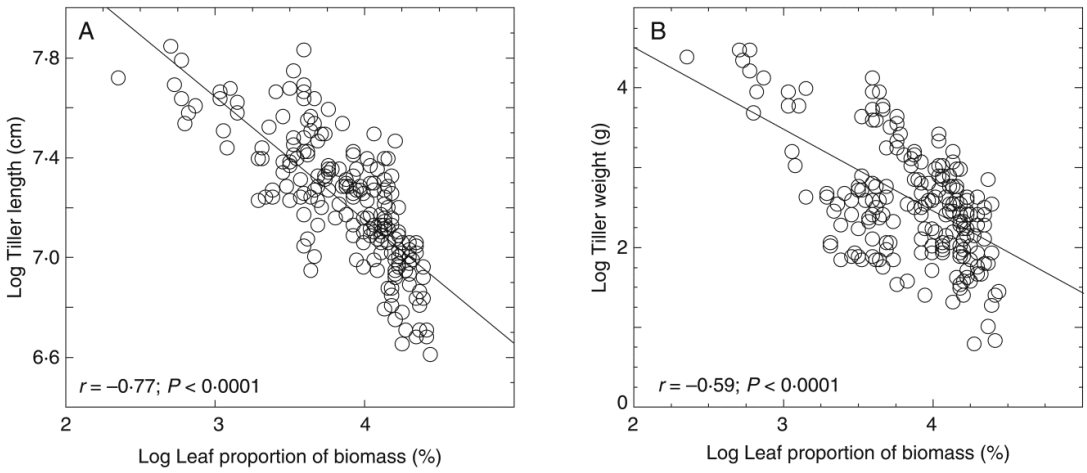

Fig. 2.3. Morphological characterisation of 25 miscanthus genotypes at three developmental stages. Correlation of the natural logarithms of (A) tiller length and (B) total tiller dry weight with percentage leaf contribution to total dry weight biomass for the 25 genotypes at three developmental stages (*r*, Pearson correlation coefficient).

2.2. CELL WALL BIOMASS PREPARATION

2.2.1. Overview

All subsequent compositional analyses and the *Clostridium phytofermentans* bioassay (to be presented in subsequent chapters), were carried out on prepared cell wall material (CWM). The use of these preparations instead of the intact plant biomass greatly minimises or even eradicates interferences from metabolites and other biomass components which are not part of the cell wall.

Several cell wall isolation procedures can be found in the literature. However, modification of methods was required to meet the specific needs of the project; such as to produce higher amounts of CWM for subsequent analyses and to reduce the costs of the enzymes used for starch removal. Furthermore, since all CWM samples were prepared simultaneously, random variations during isolation procedures were minimised.

2.2.2. Materials and methods

Isolated cell wall was prepared following a procedure adapted from a combination of various published methods: organic solvent washing and starch gelatinisation from Foster *et al.* (2010); starch removal from Persson *et al.* (2007) and Kong *et al.* (2011).

After tiller collection, freeze-drying and stem and leaf separation, individual tissues were ground to a particle size in the range of 0.18mm – 0.85mm (mesh sizes 80 and 20). For each sample, approximately 1g of ground plant biomass was extracted sequentially as follows: with 30mL of ethanol 100%, first for 12h and then twice more for 30min in a shaking incubator set at 40ºC/150rpm; three times with 20mL of chloroform/methanol (1:1 v/v), for 30min

incubation times at 25ºC and 150rpm; and finally, three times with 15mL of acetone, for 30min, at 25ºC/150rpm. Between each step of the extraction, the material was collected by centrifugation at 887×*g*[*] for 10min and the supernatants were discarded. Following the third acetone wash, the samples were left to dry overnight in a fume hood. The dried, solvent extracted biomass, was then re-suspended in 15mL of 0.1M sodium acetate buffer (pH=5.0) and heated to 80ºC/20min to induce starch gelatinisation followed by cooling on ice. Subsequently, samples were centrifuged (887×*g*/10min) and supernatants were discarded, after which the resulting pellet was washed twice with 30mL of deionised water, with resuspension, centrifugation (887×*g*/10min) and supernatant removal being performed for each wash. Sodium azide was added at 0.0002% (w/v) to inhibit microbial growth, and starch was removed by incubation with type-I porcine α-amylase (Sigma-Aldrich; 47 units per 100mg cell wall) in 0.1M ammonium formate buffer (pH=6.0) at 25ºC/110rpm. After 48h, digestion was terminated by heating to 95ºC/15min and samples were cooled on ice. The destarched cell wall preparations were then washed three times in 30mL of deionised water and twice with 20mL of acetone, with centrifugation (887×*g*/10min) and supernatant removal, before being freeze-dried.

2.2.2.1. Quick Assessment of Cell Wall Isolation Method

Although the described cell wall isolation procedure is largely based on published and generally used methods[†], it was considered sensible to perform a quick validation of the efficiency of the new adapted methodology. As a result, a brief procedure was performed,

[*] Relative centrifugal force (RCF) acceleration expressed relative to Earth's gravitational acceleration (×*g*).

[†] The adapted cell wall isolation procedure described here has been published as part of a cell wall analysis methodology, and is available in a life science protocol database: DA COSTA, R. M. F., ALLISON, G. & BOSCH, M. 2015. Cell wall biomass preparation and Fourier transform mid-infrared (FTIR) spectroscopy to study cell wall composition. *Bio-protocol,* 5**,** e1494. http://www.bio-protocol.org/e1494.

which consisted of preparing two triplicated batches of CWM starting from the same initial miscanthus biomass: the first, according to the adapted procedure and the second according to the method published by Foster *et al.* (2010). Following isolation, complete CWM hydrolysis was performed with H_2SO_4 to release constituent monosaccharides, and samples were analysed by High-Performance Anion-Exchange Chromatography – Pulsed Amperometric Detection (HPAEC-PAD). For the validation of the CWM isolation method, only the area of the major chromatographic peak (glucose) was utilised, and no extended quantitative analysis was performed at this stage. However, a much wider and exhaustive chromatographic analysis is performed in the context of the data presented in chapter 4. For reasons of practicality and consistency, HPAEC-PAD methodology, and the H_2SO_4 hydrolysis procedure are described in section 4.1.2.

2.2.3. Results

The procedure for cell wall isolation described here is primarily preparative. For this reason, unavoidable and random material loss occurred during the successive washing steps in the preparation of CWM, and accurate determinations of cell wall to total biomass ratios were not possible.

In order to compare the general efficiency of the adapted cell wall isolation method here presented and the one published by Foster *et al.* (2010) in the removal of non-cell wall carbohydrates, isolated cell wall samples were hydrolysed and chromatographically analysed. This simple brief assessment involved only the measurement of the glucose obtained from hydrolysate samples of each isolation method (Table 2.3).

Table 2.3. Glucose content of the CWM samples prepared during the validation of the cell wall isolation procedure. The initial miscanthus biomass used in this assay was the same for all samples, and consisted of the whole above-ground biomass (leaf and stem) of a genotype not used elsewhere in this thesis (Mb188).

Glucose (mg/g CWM)		
Replicate	**Adapted method**	**Foster *et al.* (2010) method**
A	444.50	437.62
B	423.08	415.74
C	418.94	372.41
Mean ± standard deviation	**428.84 ± 13.72**	**408.59 ± 33.19**

2.2.4. Discussion

The aim of this section of the practical work was merely to produce CWM for all subsequent analytical studies. However, despite experimental conditions not having been designed for accurate determination of cell wall percentages of whole biomass, some general trends were observed during the weighing of intact biomass and of the isolated CWM. Namely, it was seen that CWM represented a higher percentage of the intact miscanthus biomass in stem than it does in leaf tissues; and that there is a trend for an increasing CWM to total biomass ratio as development progresses. Further information regarding cell wall proportions in miscanthus biomass have been provided by other authors; such as (Allison *et al.*, 2011) and Lygin *et al.* (2011), who reported that in mature tillers of *M. sinensis* and *M.* × *giganteus* the cell wall percentages vary from 85% to 89% of dry biomass.

There was a concern that by grinding the CWM excessively some information could be lost regarding the impact of different cell wall components on recalcitrance. Size reduction may be considered a procedure that in itself increases cell wall biomass digestibility. It was in order to avoid this that the range of 0.18mm – 0.85mm particle size was chosen. According to Decker *et al.* (2009) biomass can be milled to this particle size range without significantly affecting digestibility. However, reduction below this threshold will increase saccharification, and might therefore mask potential differences in digestibility between genetically different materials.

The development of an adapted version of various published cell wall isolation procedures was performed in order to increase the amounts of CWM produced and to reduce the enzyme costs per batch; the Foster *et al.* (2010) procedure recommends the use of α-amylase from *Bacillus* spp. and pullulanase from *Bacillus acidopullulyticus*, instead of the less expensive type-I porcine α-amylase used here in the adapted protocol. A brief assessment was performed to compare the efficiency of both methods, which involved the comparison of

the variation in glucose amounts obtained from hydrolysate samples of each isolation method (Table 2.3). It was observed that the relative standard deviation (RSD[*]) between the three replicates was 3.20% for the adapted method and 8.12% for the Foster *et al.* (2010) method; whereas, when comparing between methods, the RSD was 6.04%. Considering that the variation in glucose yield between methods was within the same range as the variation between technical replicates of one method, the procedures were considered comparable. Henceforth, in all subsequent analyses, only the more economical, adapted cell wall isolation procedure was employed.

[*] $RSD = {}^{s}/_{\bar{x}} \times 100\%$; where s is equal to the standard deviation, and $\bar{x}$ is equal to the mean.

2.3. Cell Wall Characterisation by FTIR Spectroscopy

2.3.1. Overview

As a strategy to optimise bioenergy and biorefining applications, an increasing amount of effort is being put into the advance of our knowledge concerning the cell wall compositional roots of recalcitrance. For this, Fourier transform mid-infrared spectroscopy (FTIR) may represent a very useful tool, as it allows for a high-throughput, non-destructive and low unit cost procedure to examine cell wall biomass (Allison *et al.*, 2009). Furthermore, the use of Attenuated Total Reflection (ATR) in conjunction with infrared spectroscopy (IR) enables cell wall biomass samples to be examined in solid state without extensive preparation. Nonetheless, the analysis of isolated cell wall preparations instead of the intact plant biomass is highly recommended to minimise interference from components not belonging to the cell wall.

FTIR spectroscopy using ATR, fundamentally consists in using an infrared (IR) beam focused on the ATR crystal at such an angle that it is totally reflected; however, when the ATR crystal is in contact with a sample, its intrinsic absorbance attenuates the intensity of the reflected beam. Hence the use of the terms attenuated total reflectance. The beam then reaches an interferometer, where an interference pattern (i.e., an interferogram) is generated, which is then Fourier transformed into a spectrum; with the net effect of the sample being the alteration of the interference pattern (i.e., the interferogram) of the beam (Smith, 2011). In the resulting spectra the peak positions correlate with molecular structures and this information may be used to decipher the chemical makeup of a sample.

Datasets generated from FTIR spectroscopy can be extensive and complex. In these situations, data-driven modelling techniques are often used as exploratory approaches to identify the most distinctive features of the collected spectra. Here, Principal Component

Analysis (PCA) was used; which consists of a frequently employed method to transform a large set of variables into a smaller set of new variables (principal components), effectively reducing dataset dimensionality.

When the aim is a complete and detailed biomass characterisation, the FTIR-PCA method described here does not exclude the need for parallel wet gravimetric and analytical procedures. However, it does lead to a rapid identification of the major compositional shifts across large sets of samples; thus contributing to steer research pathways, minimise time-draining analytical procedures and reduce overall research costs.

2.3.2. Materials and methods

FTIR was performed on the isolated CWM from all miscanthus samples (25 lines × 3 time points × 2 tissues × 3 plant replicates). Duplicate spectra were collected by ATR in a mid-infrared range of 4000-600cm^{-1} using an Equinox 55 FTIR spectrometer (Bruker Optik, Ettlingen, Germany) equipped with a Golden Gate ATR accessory (Specac, Slough, UK). Spectra were averaged over 32 scans at a resolution of 4cm^{-1} and corrected for background absorbance by subtraction of the spectrum of the empty ATR crystal. Absorbance spectra were converted to text files in Opus (v. 5.0; Bruker Optik), imported into MatLab (v. R2010b; MathWorks, Natick, Massachusetts, USA) and averaged. Full spectra, or fingerprint region spectra (1900cm^{-1} – 800cm^{-1}) were transformed according to the Savitzky-Golay algorithm (order: 3; window: 15 pt.), to improve peak resolution, and mean centre normalised (mean=0; standard deviation=1) prior to PCA using the Eigenvector PLS Toolbox (v. 7; Eigenvector Research, Wenatchee, Washington, USA) to investigate the underlying relationships between the spectra.

2.3.3. Results

FTIR spectroscopy allowed investigation of cell wall composition in miscanthus stem and leaf samples, as well as the identification of major compositional shifts in each of these tissues during development. Comparison of the spectra for stem and leaf samples of the 25 genotypes at each developmental stage showed differences in the relative absorbance of the individual bands. However, they were too numerous and complex for detailed visual interpretation, and PCA was employed as an exploratory approach to identify the most distinctive features of the collected spectra. Following PCA, ten spectral bands were detected as the main discriminant principal component (PC) loadings in the fingerprint region of the spectra (1900cm^{-1} – 800cm^{-1}; Fig. 2.4 A and B). The attribution of spectral areas to their corresponding cell wall components was made according to the literature (Table 2.4). Bands associated with cellulose: 1159cm^{-1} (*d*), 1061cm^{-1} (*f*), 1038cm^{-1} (*g*), and 993cm^{-1} (*i*) (Marry *et al.*, 2000; Wilson *et al.*, 2000; Oh *et al.*, 2005; McCann *et al.*, 2007; Schulz and Baranska, 2007; Adapa *et al.*, 2009; Gwon *et al.*, 2010; Matos *et al.*, 2013; Abidi *et al.*, 2014). Pectin associated loadings: 1746cm^{-1} (*a*), 1105cm^{-1} (*e*), 1017cm^{-1} (*h*), and 951cm^{-1} (*j*) (Séné *et al.*, 1994; Coimbra *et al.*, 1999; Kačuráková *et al.*, 2000; Wilson *et al.*, 2000; McCann *et al.*, 2001; Alonso-Simón *et al.*, 2004). Discriminant bands associated with syringyl monomers of lignin (S-lignin) were found at 1321cm^{-1} (*b*) and 1234cm^{-1} (*c*) (Labbé *et al.*, 2005; Gorzsás *et al.*, 2011; Zhou *et al.*, 2011).

Three PCA models were created, with the first one including all collected spectra (Fig. 2.4C). In this model, the first four PCs accounted for nearly 84% of the variance in the spectral dataset, of which PC1 captured 41.25%. No clustering was detected concerning the various miscanthus species; however, two clear clusters were observed along PC1 comprising spectra from stem and from leaf tissue. The loadings of PC1 for this model (Fig. 2.4F) showed that differences in four regions (designated *a*, *c*, *g* and *j*; as described above) of the FTIR spectra

were the main contributors to the differential clustering of stem and leaf samples. One prevalent positive loading, located at 1234cm^{-1} (*c*) coincides with a band frequently associated with S units in core lignin. However, the other three main loadings of PC1 overlapped spectral regions typically associated with structural carbohydrate in lignocellulosic samples: positive peaks at 1746cm^{-1} (*a*), 1038cm^{-1} (*g*), and a negative peak at 951cm^{-1} (*j*). This indicates that PC1 is mostly correlated with portions of the spectra associated with carbohydrates. Further PCA models were created after the spectral data had been split into separate subsets comprising each tissue type: leaf (Fig. 2.4D) and stem (Fig. 2.4E). For leaf samples, the first five PCs captured slightly more than 83% of the total variance, but no clear clusters could be discerned along any of the PC axes (shown for PC1 and PC2 in Fig. 2.4D). In contrast, analysis of the stem spectral data (the first four principal components accounted for almost 85% of the variance), detected two distinctive clusters correlating to developmental stage along PC1 (Fig. 2.4E); one consisting of stem cell wall samples from actively growing plants, and another of overlapping stem samples collected at peak biomass and after senescence. For this PCA model, six spectral regions featured prominently in the loadings for PC1 (Fig. 2.4G). These loadings, which captured 49.31% of the variance in stem spectral data, showed that this principal component is mostly correlated with spectral regions attributed to cell wall polysaccharide components: positively at 1746cm^{-1} (*a*), 1017cm^{-1} (*h*) and 993cm^{-1} (*i*); and negatively at 1159cm^{-1} (*d*), 1105cm^{-1} (*e*) and 1061cm^{-1} (*f*). In addition, it was also evident that the bands at 1321cm^{-1} (*b*) and 1234cm^{-1} (*c*), associated to S-lignin monomers were perceptible negative loadings, thus suggesting higher amounts of S-lignin in mature stem tissues.

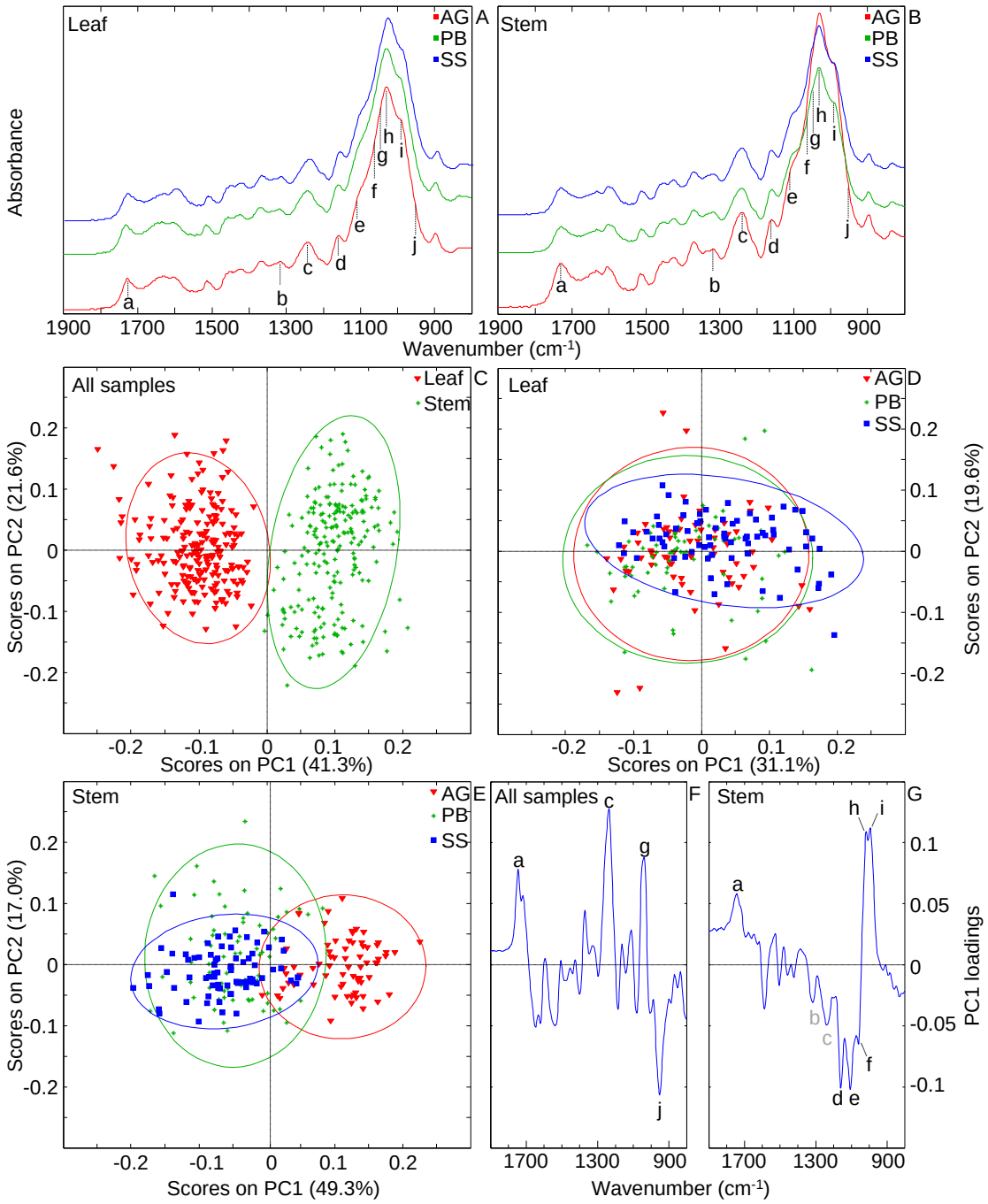

Fig. 2.4. Mean FTIR spectra of (A) leaf and (B) stem samples of 25 miscanthus genotypes at three developmental stages in the 1900-800cm^{-1} range. Plot of principal component one (PC1) and principal component two (PC2) scores for (C) all samples, (D) for stem samples and (E) for leaf samples. PC1 loading plot for (F) all samples and (G) for stem samples. Spectral bands: *a*, 1745cm^{-1}; *b*, 1325cm^{-1}; *c*, 1230cm^{-1}; *d*, 1159cm^{-1}; *e*, 1105cm^{-1}; *f*, 1060cm^{-1}; *g*, 1037cm^{-1}; *h*, 1017cm^{-1}; *i*, 993cm^{-1}; *j*, 950cm^{-1}. Abbreviations: AG, active growth; PB, peak biomass; SS, senesced stage.

Table 2.4. Assignment of relevant FTIR absorption bands characteristic of miscanthus cell wall biomass.

Band	Wavenumber (cm^{-1})	Group	Assignment	Reference
a	1746	Polysaccharides	Ester C=O stretching associated with pectin	1745cm^{-1} (Séné *et al.*, 1994; Wilson *et al.*, 2000; McCann *et al.*, 2001)
b	1321	Lignin	Associated with syringyl units	1320cm^{-1} (Labbé *et al.*, 2005; Gorzsás *et al.*, 2011)
c	1234	Lignin	C=O stretching in syringyl ring	1234cm^{-1} (Zhou *et al.*, 2011)
d	1159	Polysaccharides	C-O-C stretching in cellulose	1161cm^{-1} (Abidi *et al.*, 2014) 1159cm^{-1} (Matos *et al.*, 2013) 1157cm^{-1} (McCann *et al.*, 2007)
e	1105	Polysaccharides	Pectic polysaccharides	1104cm^{-1} (Coimbra *et al.*, 1999) 1100cm^{-1} (Kačuráková *et al.*, 2000) 1105cm^{-1} (McCann *et al.*, 2001)
f	1061	Polysaccharides	C-O stretching and O-C-H in-plane bending vibrations in cellulose	1060cm^{-1} (Wilson *et al.*, 2000; Schulz and Baranska, 2007; Adapa *et al.*, 2009)
g	1038	Polysaccharides	C-O, C=C and C-C-O vibrational stretching in cellulose	1035cm^{-1} (Wilson *et al.*, 2000; Schulz and Baranska, 2007; Adapa *et al.*, 2009)
h	1017	Polysaccharides	Pectic polysaccharides	1014cm^{-1} (Coimbra *et al.*, 1999) 1017cm^{-1} (Kačuráková *et al.*, 2000) 1018cm^{-1} (McCann *et al.*, 2001)
i	993	Polysaccharides	C-O stretching in cellulose	993cm^{-1} (Gwon *et al.*, 2010) 990cm^{-1} (Marry *et al.*, 2000) 993cm^{-1} (Oh *et al.*, 2005)
j	951	Polysaccharides	Pectic polysaccharides	950cm^{-1} (Alonso-Simón *et al.*, 2004) 952cm^{-1} (Coimbra *et al.*, 1999) 951cm^{-1} (Kačuráková *et al.*, 2000)

2.3.4. Discussion

FTIR spectroscopy has become a powerful fingerprinting method to monitor modifications in plant cell wall composition as it provides information about the main polysaccharides and lignin present in the cell wall (Kačuráková *et al.*, 2000; Mouille *et al.*, 2003; Derkacheva and Sukhov, 2008). The multivariate analysis of the FTIR data across the three developmental stages showed a distinct clustering of the spectra obtained from stem and leaf samples (Fig. 2.4C). This spectral segregation suggests significant compositional differences between stems and leaves, which is in accordance with reports in other species, such as maize, sorghum and rice (*Oryza sativa*) (Krakowsky *et al.*, 2006; Murray *et al.*, 2008; Jahn *et al.*, 2011). These studies also showed that there are major differences in the cell wall polymer composition between leaf and stem tissues, suggesting that cell wall composition is under separate genetic control in these tissues. Of the four spectral areas detected as prevalent loadings of PC1 (Fig. 2.4F), one is associated with lignin (*c*), while all others correlate with structural carbohydrates (*a*, *g*, and *j*). As has been reported for sorghum (Petti *et al.*, 2013), the prominence of band *c* in our data is suggestive of higher amounts of S-lignin in stem when compared with leaf tissues. However, given that the remaining three major PC1 loadings coincide with carbohydrate bands, it is likely that overall compositional shifts between leaf and stem cell wall samples are more significant in their polysaccharide fractions. Analysis of the FTIR data from different developmental stages showed that the cell wall composition of stems from actively growing samples differs significantly from those at peak biomass or after senescence, as indicated by the discrete clusters formed during PCA (Fig. 2.4E). This finding most likely relates to the smaller proportion of secondary walls in actively growing stems when compared to samples at peak biomass and senesced stage. Bands associated with S-lignin are noticeable negative loadings (Fig. 2.4G), and suggest a higher occurrence in stem samples

collected during PB and SS. This is in agreement with other reports showing that more S-lignin is deposited in stems when plants mature and cease to elongate, leading to a concomitant increase in the syringyl to guaiacyl ratio of lignin (Chen *et al.*, 2002; Jung and Engels, 2002; Grabber *et al.*, 2004). However, as above, PC1 (which is responsible for the separation between elongating and mature/senesced stem samples), is predominantly correlated with carbohydrate regions of the spectra.

Grass cell walls typically contain less pectin compared to their dicot counterparts (Vogel, 2008; Caffall and Mohnen, 2009). It was therefore unexpected that, in addition to cellulose, variation was detected in spectral regions attributed to pectin while there was no such variation for hemicellulose-associated spectral regions. However, the masking of bands associated with hemicellulose in the spectral region defined between 1200cm^{-1} and 800cm^{-1} (Ridley *et al.*, 2001) remains a possibility until further investigation reveals the precise nature of the structural polysaccharides involved. The presence of negative and positive PC1 loadings associated to pectins (*a*/*j* in Fig. 2.4F; and *a*,*h*/*e* in Fig. 2.4G) might indicate extensive differences in the structure and substitution of pectic polysaccharides between leaf and stem tissue and also as stems mature. This is in agreement with the fact that grasses display a marked developmental preference for accumulating differently modified pectins in specific cell types (Carpita, 1996). Furthermore, in the dicot *Linum usitatissimum* (flax), it has been shown that pectin synthesis and modification is different in stems and in leaves and that stem pectin incurs greater modifications during plant elongation (Bédouet *et al.*, 2006). As for cellulose, the dominant positive band *g* (Fig. 2.4F) could indicate higher cellulose contents in stem samples. On the other hand, the observed opposition of bands *d*, *f* and *i* in the PC1 loading plot (Fig. 2.4G) is suggestive of modifications in cellulose structure as more advanced stages of maturity are reached. In effect, it has been reported that cellulose crystallinity differs between primary and secondary plant cell walls (Kataoka and Kondo, 1998; Park *et al.*, 2013).

With leaf tissue samples (Fig. 2.4D), the compositional differences detected by FTIR were not sufficient to create PCA clusters. This possibly reflects the fact that leaf material is less changeable, and undergoes less secondary cell wall thickening as it matures.

2.4. LIGNIN AND ITS INFLUENCE ON CELL WALL DECONSTRUCTION

2.4.1. Overview

FTIR-derived data suggested that lignin was not the main factor influencing compositional variability of miscanthus cell wall. To assess this directly, lignin content was correlated with cell wall amenability to deconstruction using two moderate to high throughput procedures: Acetyl Bromide Soluble Lignin Measurement (ABSL) and a *Clostridium phytofermentans* bioassay for the determination of biomass digestibility.

The concentration of lignin, its composition and the manner in which it binds holocellulose within the cell wall matrix is often seen as an exacerbating factor of cell wall recalcitrance to enzymatic deconstruction; not only because it makes the biomass resistant to digestion, but also because lignin fractions adsorb enzymes reducing their access to the polysaccharides (Vanholme *et al.*, 2010; Hodgson *et al.*, 2011; Huang *et al.*, 2011; Ding *et al.*, 2012). However, the extent of this effect is not always consistent in literature reports and therefore, recalcitrance should not be attributed solely to the presence of lignin (Grandis *et al.*, 2014). In miscanthus for instance, contrasting influences of lignin content on enzymatic hydrolysis have been reported (Lygin *et al.*, 2011; Zhang *et al.*, 2012).

The ABSL quantification method is a widespread and rapid procedure suitable for lignin determination in small samples. It consists in the solubilisation of lignin into an acetyl bromide solution in glacial acetic acid (Hatfield *et al.*, 1999a; Brunow, 2001). Treatment with acetyl bromide produces very similar extinction coefficients for lignins obtained from different species at a wavelength of 280nm, which is used for the estimation of total lignin content (Chang *et al.*, 2008). It should be mentioned that the employed ABSL method also measures ester-linked hydroxycinnamic acids and it has been reported that these act as synthetic

precursors and form an integral part of the lignin macromolecule (Ralph *et al.*, 1994a; Ralph, 2010; Tobimatsu *et al.*, 2012). To increase the reproducibility and reliability of the ABSL method certain parameters of the procedure were modified from the ones reported in the literature (Fukushima and Hatfield, 2004; Foster *et al.*, 2010). These adaptations, are concerned with the reaction vials, the amounts of sample and the reagent volumes used (a detailed description is provided below).

For the digestibility bioassay, its development and optimisation has been undertaken by Samuel Hazen and his research team (Lee *et al.*, 2012b), based at the University of Massachusetts (Amherst, Massachusetts, USA), with whom collaborative work was established. This is a method consisting of the determination of digestibility as a function of the ethanol yielded after fermentation with *Clostridium phytofermentans*, an anaerobic soil bacterium that can convert a wide range of cell wall carbohydrates to ethanol (Warnick *et al.*, 2002; Lee *et al.*, 2012b). Since no exogenous cellulases and xylanases need to be added to the reaction, the *C. phytofermentans* bioassay here used consists of a consolidated bioprocessing process, in which the fermenting microorganism contributes with cellulolytic enzymes (van Zyl *et al.*, 2007), thus leading to simultaneous saccharification and fermentation.

2.4.2. Materials and methods

For lignin measurement, ABSL was determined in triplicate for all of the miscanthus samples (25 lines × 3 time points × 2 tissues × 3 plant replicates) following the general procedures described by Fukushima and Hatfield (2004) and Foster *et al.* (2010), with some modifications, described as follows. Approximately 7mg of the previously prepared CWM was

weighed into 10mL Pyrex glass tubes fitted with polypropylene caps*. For lignin solubilisation, 500µL of freshly prepared 25% (v/v) acetyl bromide solution in glacial acetic acid was added to the samples, the tubes were capped and placed in a heating block set at 50°C for 2h, after which the tubes were mixed using a vortex mixer every 15min up to a total incubation time of 3h. Following digestion, the tubes were cooled on ice and the contents of each were diluted by the addition of 2000µL of 2M NaOH. A further addition of 350µl of 0.5M hydroxylamine hydrochloride to each tube ensured the decomposition of polybromide ions (Monties, 1989). After vortex mixing, the final volume was adjusted to 10mL with glacial acetic acid. The tubes were recapped, mixed by inversion and centrifuged to produce a particulate-free supernatant, and 200µL of each sample was transferred to UV transparent 96-well plates (UV-Star; Greiner Bio-One, Gloucestershire, UK). The absorbance at 280nm was measured with a plate reader (µQuant; Bio-Tek Instruments, Winooski, Vermont, USA) using KC4 software (v. 3.3; Bio-Tek). An assay control sample of a standard cell wall preparation was included in all batches of the lignin assay as an internal standard. Additionally, negative controls containing no cell wall material were included and their absorbance at 280nm was set as absorbance baseline. A specific absorption coefficient (SAC) of 17.78 g^{-1} L cm^{-1} has been reported for purified HCl-dioxane lignin from miscanthus samples (Lygin *et al.*, 2011) and this was used to calculate the percentages of lignin in the cell wall biomass samples as dry weight using the following equation:

$$ABSL\% = \frac{A_{280}}{SAC \times PL} \times \frac{V_R}{W_S} \times 100\% \qquad (2.2)$$

* By using bigger sample amounts and glassware instead of plasticware, weighing errors caused by electrostatic repulsion were substantially reduced.

Where ABSL% is the acetyl bromide soluble lignin percentage content; A_{280} is the absorption reading at 280nm; PL is the pathlength determined for the 96-well microplates with a volume of 200µL per well used during the analysis (0.556cm)*; V_R is the reaction volume (L); W_S is the sample weight (g).

For the *Clostridium phytofermentans* bioassay of biomass digestibility, the procedures described in Lee *et al.* (2012a) and Lee *et al.* (2012b) were followed. Initially, *C. phytofermentans* strain ISDg (ATCC 700394) was cultured in a defined medium, MQM5.1 prepared as follows: 2g/L NaH_2PO_4, 10g/L K_2HPO_4, 1g/L $(NH_4)_2SO_4$, 1g/L l-cysteine hydrochloride monohydrate; 20mL/L XT solution (5g/L xanthine and 5g/L thymine in 0.06N NaOH); 10ml/L AA1 solution (5g/L of each of the following amino acids: alanine, arginine, histidine, isoleucine, leucine, methinonine, proline and valine), and 10mL/L Balch *et al.* (1979) trace element solution, Resazurin (1mg/L), which was added as an oxidation/reduction indicator. After autoclaving, 10mL/L CPV3 solution (20mg/L *p*-aminobenzoic acid, 1mg/L biotin, 30mg/L folinic acid, 80mg/L nicotinamide, 5mg/L pantethine, 2mg/L pyridoxal hydrochloride, 30mg/L riboflavin, and 10mg/L thiamine) was added. The *C. phytofermentans* inoculum was initially grown in MQM5.1 with 3g/L cellobiose as a carbon source using the anaerobic techniques described by Hungate (1969). Incubations were carried out in 10mL volumes in 18×180mm tubes sealed with neoprene caps.

For the biological conversion quality assay, the isolated leaf and stem CWM from the three replicates of the 25 miscanthus genotypes at 3 developmental stages were analysed. Approximately 20mg of each sample was weighed in triplicate into autoclavable 2.2mL polypropylene 96-well plates (Axygen Scientific, Union City, California, USA), 0.92mL of

* The pathlength was derived experimentally by determining the optical density (OD) difference of water measured at 977nm and 900nm with the instrument used during the analysis, and then comparing it with the standardised measurement of this difference in a 1cm cuvette, at room temperature (0.18OD), using the equation:

$$\frac{OD977_{water} - OD900_{water}}{0.18OD_{1cm\ cuvette\ water}} = Sample\ Pathlength\ (cm)$$

MQM5.1 media was added, and plates were sealed and autoclaved. Subsequently, 0.01mL of the CPV3 solution and 0.01mL of the prepared *C. phytofermentans* inoculum was added to each well, and the samples were incubated without shaking at 37°C/72h. After incubation, the plates were centrifuged and a volume of 1mL of each sample supernatant was collected and filtered through a 0.22µm syringe filter unit (Millipore Corp., Billerica, Massachusetts, USA) and 5µL of each sample was analysed by High Performance Liquid Chromatography (HPLC). The HPLC system (Waters Corporation, Milford, Massachusetts, USA), was equipped with a carbohydrate analysis column (7.8 × 150mm IC-Pak Ion Exclusion, Waters Corporation) and a refractive-index detector. The column was operated at 30°C with 0.005N H_2SO_4 as the running buffer at a flow rate of 0.7mL/min. The retention time for ethanol (17.84±0.02min) was determined using a commercial mix (Fuel Ethanol Residual Saccharides Mix; catalogue number 48468-U; Sigma-Aldrich, St Louis, Missouri, USA) containing glycerol, glucose, maltotriose, maltose monohydrate, lactic acid, acetic acid, dextrin, and ethanol. Standards were analysed at the beginning, middle, and end of every distinct HPLC analysis to ensure accuracy and precision of measurements.

All calculations for descriptive statistics, analyses of variance, Tukey's tests and variable correlations were performed as described in section 2.1.3; with the addition that the effect of tissue type (2 levels) was also tested in addition to genotype and development factors.

2.4.3. Results

Lignin content is expressed as acetyl bromide soluble lignin percentage (ABSL%) of cell wall biomass dry weight (Table 2.5). The mean lignin content of the 25 selected genotypes was observed to increase in both tissues as plants matured, and to range from 18.3% in leaf tissue at AG stage, to 23.7% in stem tissue at SS stage. Additionally, for a given genotype, lignin

content was typically higher in stem samples than in leaf samples at the same developmental stage.

The statistical significance of development, tissue and genotype effects was confirmed by ANOVA (P<0.001 for all three factors), and Tukey's tests showed distinction between AG, PB and SS, and between stem and leaf (Table 2.6 and Fig 2.5). Furthermore, the following effect sizes were determined: $\eta^2_{\text{developmental stage}}$=0.50, η^2_{tissue}=0.10 and η^2_{genotype}=0.06. The variance in lignin content between the three plant replicates of each genotype was preliminarily analysed and shown not to be significant (P=0.605). The interaction between genotype and developmental stage (P=0.845), and the interaction genotype × developmental stage × tissue (P=0.200), were also not significant. On the other hand, the interactions of genotype × tissue and developmental stage × tissue, were both significant (P<0.001). In light of these results, the importance of genotype and tissue on lignin content was assessed at each developmental stage individually (Table 2.6).

The resulting ANOVA showed that tissue was the only factor that had a significant effect at the developmental stages considered (P<0.001 at each of the three developmental stages). Genotype had a significant effect on ABSL% in samples collected during AG (P<0.001) and during PB (P=0.005), but not in senesced samples (P=0.622). The interaction between genotype and tissue was not significant at the actively growing stage (P=0.221), but was significant during peak biomass (P<0.001) and senescence (P=0.030). All these results suggest that although genotype has a significant effect on lignin content, its influence decreases over development, until it has no significant effect on lignin concentration in samples collected during senescence. This decrease in the relevance of genotype is supported by a reduction of its effect size throughout development: η^2_{AG}=0.30, η^2_{PB}=0.13 and η^2_{SS}=0.12. Additionally, the fact that distinct homogeneous groups only emerged for stem samples collected at AG and PB (Fig. 2.4) indicates that the significance of the genotype factor at AG and PB is mostly due to

the variability among stem samples. For all developmental stages no distinct groups were visible among the genotypes in terms of the lignin content of leaves. Later, during senescence when the genotype effect is not significant overall it is visible that no groups emerge among the stem samples as well.

The digestibility of stem and leaf cell wall samples from the 25 genotypes were evaluated based on the ethanol concentration in the supernatant after 72h of incubation with *C. phytofermentans*. Ethanol yields expressed as milligrams of ethanol yielded per gram of the cell wall biomass dry weight ($mg_{ethanol}/g_{biomass}$) ranged from the minimum 36.71mg/g of CWM from leaf of genotype sin16 collected at senescence to a maximum of 63.32mg/g in a stem sample from genotype sin14 during AG (Table 2.7 and Fig. 2.6).

ANOVA detected that the differences in ethanol yielded by the three plant replicates of each genotype were not significant (P=0.090). A significant difference was detected in the ethanol yields of the various genotypes (P=0.006), between the two tissues and between the three developmental stages (P<0.001 for both), with ethanol yields decreasing as plants mature. For each developmental stage there were significant differences in the amount of ethanol yielded from different genotypes: at AG (P=0.040), at PB (P<0.001) and at SS (P<0.001). By Tukey testing the genotype effect on individual tissues at each developmental stage, distinct homogeneous groups emerged in stem samples collected at AG and PB, whereas for leaf they emerged only at PB (Table 2.7). Significant comparisons between lignin content and ethanol yield can be performed for stem collected at AG and at PB, the only situations where both datasets simultaneously displayed distinct groups (Tables 2.5 and 2.7). By looking at the top and bottom ranking genotypes, several simultaneously possess high lignin contents and ethanol yields or low lignin and low ethanol. Namely, the high ranking stem samples from sin04 (54.76mg ethanol/g, 20.00 ABSL%), sin15 (51.39mg ethanol/g, 21.26 ABSL%) at AG, and

from sin10 (48.83mg ethanol/g , 22.85 ABSL%) at PB; and the lower ranking sin08 (46.54mg ethanol/g, 18.09 ABSL%) stem samples at AG.

Table 2.5. Acetyl bromide lignin (ABSL) percentage of cell wall material dry weight (% CWM). Values are mean ± standard deviation for the three replicated plants at the three developmental stages for each genotype. Values within a column sharing a letter in their superscript are not significantly different according to a Tukey's test (α=0.05).

	ABSL (% CWM)					
	Active Growth		Peak Biomass		Senescence	
	Leaf	Stem	Leaf	Stem	Leaf	Stem
gig01	17.27 ± 1.38^{a}	18.72 ± 0.67^{ab}	19.61 ± 0.86^{a}	22.75 ± 0.73^{abc}	20.48 ± 0.84^{a}	24.45 ± 1.22^{a}
gig02	19.48 ± 0.85^{a}	19.87 ± 1.21^{ab}	18.71 ± 0.15^{a}	23.39 ± 0.98^{bc}	20.80 ± 0.70^{a}	24.85 ± 0.78^{a}
gig03	18.19 ± 0.40^{a}	19.74 ± 1.48^{ab}	18.55 ± 0.59^{a}	24.05 ± 1.11^{bc}	21.36 ± 2.88^{a}	24.44 ± 0.93^{a}
hyb01	17.08 ± 0.23^{a}	18.03 ± 1.09^{ab}	19.03 ± 0.71^{a}	21.72 ± 1.80^{abc}	22.18 ± 1.57^{a}	23.55 ± 0.66^{a}
hyb02	17.43 ± 0.33^{a}	19.76 ± 1.22^{ab}	19.17 ± 0.15^{a}	23.15 ± 1.39^{bc}	22.51 ± 0.45^{a}	23.77 ± 0.62^{a}
hyb03	17.91 ± 1.72^{a}	20.07 ± 0.89^{ab}	18.52 ± 0.45^{a}	23.64 ± 0.46^{bc}	20.05 ± 0.51^{a}	24.26 ± 0.62^{a}
sac01	17.38 ± 0.78^{a}	17.18 ± 1.23^{ab}	19.36 ± 1.38^{a}	20.92 ± 0.13^{abc}	22.02 ± 2.31^{a}	23.25 ± 1.16^{a}
sin01	19.70 ± 1.50^{a}	19.76 ± 0.69^{ab}	21.47 ± 1.00^{a}	21.72 ± 0.28^{abc}	23.22 ± 1.92^{a}	22.98 ± 0.04^{a}
sin02	18.63 ± 1.88^{a}	20.41 ± 1.73^{ab}	20.69 ± 0.65^{a}	21.54 ± 1.30^{abc}	23.59 ± 3.03^{a}	23.88 ± 0.81^{a}
sin03	18.07 ± 1.22^{a}	18.18 ± 3.11^{ab}	19.24 ± 1.05^{a}	19.90 ± 2.45^{ab}	23.80 ± 0.87^{a}	22.56 ± 2.19^{a}
sin04	18.68 ± 0.53^{a}	20.00 ± 0.37^{ab}	19.45 ± 1.27^{a}	20.50 ± 1.30^{abc}	24.14 ± 2.33^{a}	22.32 ± 0.39^{a}
sin05	18.88 ± 1.60^{a}	19.45 ± 0.81^{ab}	19.31 ± 1.37^{a}	22.55 ± 0.58^{abc}	23.82 ± 2.48^{a}	23.76 ± 0.87^{a}
sin06	18.95 ± 0.98^{a}	17.68 ± 1.17^{ab}	20.50 ± 1.32^{a}	21.62 ± 1.16^{abc}	22.22 ± 2.70^{a}	22.86 ± 0.43^{a}
sin07	18.63 ± 1.40^{a}	19.35 ± 2.22^{ab}	19.85 ± 1.54^{a}	24.33 ± 1.28^{c}	24.01 ± 2.19^{a}	22.93 ± 0.75^{a}
sin08	17.95 ± 0.66^{a}	18.09 ± 2.15^{ab}	19.43 ± 1.43^{a}	21.34 ± 0.35^{abc}	22.81 ± 2.34^{a}	23.01 ± 1.10^{a}
sin09	18.46 ± 1.38^{a}	21.51 ± 0.65^{b}	19.24 ± 0.99^{a}	22.76 ± 0.32^{abc}	24.41 ± 2.97^{a}	24.05 ± 0.96^{a}
sin10	19.73 ± 0.68^{a}	19.74 ± 1.63^{ab}	20.83 ± 1.46^{a}	22.85 ± 0.70^{abc}	23.11 ± 1.22^{a}	24.10 ± 0.54^{a}
sin11	18.30 ± 0.53^{a}	19.13 ± 2.61^{ab}	19.33 ± 1.12^{a}	22.13 ± 0.87^{abc}	22.22 ± 2.05^{a}	24.06 ± 1.27^{a}
sin12	18.03 ± 1.50^{a}	17.79 ± 2.21^{ab}	18.74 ± 1.12^{a}	21.82 ± 2.67^{abc}	21.68 ± 2.39^{a}	23.70 ± 1.22^{a}
sin13	17.23 ± 0.35^{a}	16.44 ± 0.14^{a}	19.41 ± 0.83^{a}	18.62 ± 3.08^{a}	21.12 ± 1.39^{a}	22.93 ± 0.53^{a}
sin14	17.28 ± 1.43^{a}	19.39 ± 2.10^{ab}	19.10 ± 0.16^{a}	21.99 ± 1.66^{abc}	22.12 ± 0.22^{a}	24.54 ± 0.78^{a}
sin15	19.96 ± 0.14^{a}	21.26 ± 1.56^{ab}	20.77 ± 1.03^{a}	22.49 ± 1.60^{abc}	23.39 ± 0.97^{a}	24.56 ± 0.94^{a}
sin16	17.59 ± 1.13^{a}	19.93 ± 0.76^{ab}	18.47 ± 0.67^{a}	22.88 ± 1.66^{abc}	21.89 ± 1.38^{a}	23.92 ± 0.03^{a}
sin17	17.16 ± 2.02^{a}	21.22 ± 1.13^{ab}	20.85 ± 1.00^{a}	22.52 ± 0.23^{abc}	22.03 ± 0.47^{a}	22.68 ± 1.16^{a}
sin18	19.20 ± 0.60^{a}	20.34 ± 1.24^{ab}	20.24 ± 1.21^{a}	22.67 ± 0.76^{abc}	23.68 ± 2.15^{a}	24.06 ± 0.55^{a}
Mean	18.29 ± 0.88	19.32 ± 1.29	19.59 ± 0.84	22.15 ± 1.28	22.51 ± 1.20	23.66 ± 0.71

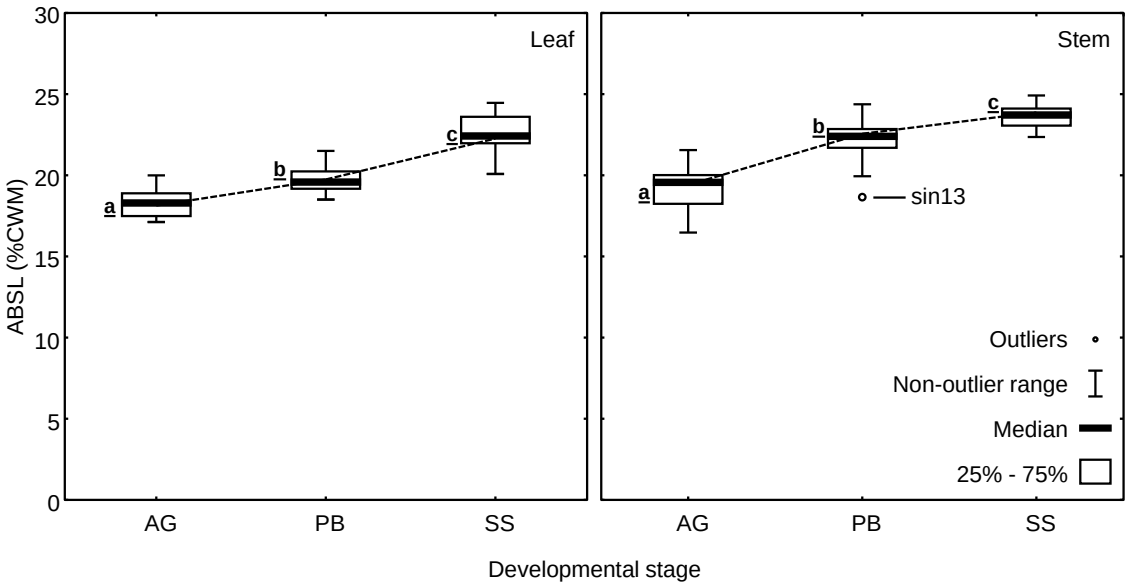

Fig. 2.5. Distribution of acetyl bromide soluble lignin (ABSL) measurements as percentage of CWM from leaf and stem tissue for 25 miscanthus genotypes at active growth (AG), peak biomass (PB) and senescence (SS). The non-outlier range is defined as the range of values which fall outside 1.5× the interquartile range of the distribution (height of the 25% – 75% box). Not significantly different developmental stages are indicated by a common underlined letter next to the box (Tukey's test at α=0.05).

Table 2.6. ANOVA results for lignin content determination.

All Developmental Stages

Effect	Degrees of freedom	Sum of squares	Mean square	*F*-ratio	*P*-value	Effect size (η^2)
Genotype	24	174.00	7.20	3.90	<0.0001	0.0632
Development stage	2	1376.80	688.40	372.10	<0.0001	0.5000
Tissue	1	283.50	283.50	153.30	<0.0001	0.1029
Genotype × Development stage	48	69.70	1.50	0.80	0.8452	0.0253
Genotype × Tissue	24	135.90	5.70	3.10	<0.0001	0.0494
Development stage × Tissue	2	53.60	26.80	14.50	<0.0001	0.0195
Genotype × Development stage × Tissue	48	105.30	2.20	1.20	0.2001	0.0382
Error	300	555.00	1.90			
Total	449	2753.80				

Active Growth

Effect	Degrees of freedom	Sum of squares	Mean square	*F*-ratio	*P*-value	Effect size (η^2)
Genotype	24	120.30	5.01	2.75	0.0002	0.3026
Tissue	1	40.13	40.13	22.00	<0.0001	0.1010
Genotype × Tissue	24	54.65	2.28	1.25	0.2214	0.1375
Error	100	182.43	1.82			
Total	149	397.51				

Peak Biomass

Effect	Degrees of freedom	Sum of squares	Mean square	*F*-ratio	*P*-value	Effect size (η^2)
Genotype	24	75.26	3.14	2.12	0.0052	0.1341
Tissue	1	245.84	245.84	166.26	<0.0001	0.4379
Genotype × Tissue	24	92.42	3.85	2.60	0.0005	0.1646
Error	100	147.86	1.48			
Total	149	561.38				

Senescence

Effect	Degrees of freedom	Sum of squares	Mean square	*F*-ratio	*P*-value	Effect size (η^2)
Genotype	24	48.10	2.00	0.89	0.6119	0.1151
Tissue	1	51.13	51.13	22.75	<0.0001	0.1223
Genotype × Tissue	24	94.09	3.92	1.74	0.0298	0.2251
Error	100	224.73	2.25			
Total	149	418.05				

Table 2.7. Supernatant ethanol concentrations as mg of ethanol yielded per g of dry cell wall biomass after 72h of incubation with *Clostridium phytofermentans*. Values are mean ± standard deviation for the three replicated plants at the three developmental stages for each genotype. Values within a column sharing a letter in their superscript are not significantly different according to a Tukey's test (α=0.05).

	Ethanol Yield (mg Ethanol/g)					
	Active Growth		**Peak Biomass**		**Senescence**	
	Leaf	**Stem**	**Leaf**	**Stem**	**Leaf**	**Stem**
gig01	54.37 ± 7.01^{a}	52.43 ± 6.34^{ab}	50.90 ± 4.39^{ab}	42.21 ± 7.00^{a}	39.49 ± 1.47^{a}	38.68 ± 3.53^{a}
gig02	54.30 ± 9.14^{a}	51.71 ± 5.82^{ab}	51.14 ± 3.55^{ab}	44.32 ± 3.91^{ab}	40.33 ± 3.71^{a}	40.19 ± 2.91^{a}
gig03	54.03 ± 12.43^{a}	46.91 ± 3.14^{a}	51.30 ± 2.74^{ab}	45.05 ± 2.84^{ab}	39.84 ± 2.51^{a}	38.96 ± 2.47^{a}
hyb01	52.72 ± 5.89^{a}	47.47 ± 4.57^{a}	48.65 ± 5.88^{ab}	42.16 ± 3.15^{a}	40.46 ± 3.73^{a}	40.00 ± 1.59^{a}
hyb02	52.61 ± 4.94^{a}	54.00 ± 5.84^{ab}	47.01 ± 6.60^{ab}	45.67 ± 2.75^{ab}	39.58 ± 3.01^{a}	37.91 ± 3.13^{a}
hyb03	51.55 ± 7.51^{a}	49.72 ± 6.88^{a}	49.00 ± 1.15^{ab}	44.36 ± 2.13^{ab}	41.42 ± 2.46^{a}	42.47 ± 3.57^{a}
sac01	52.67 ± 8.68^{a}	47.98 ± 6.76^{a}	47.54 ± 2.71^{ab}	48.03 ± 5.64^{ab}	41.34 ± 3.65^{a}	38.13 ± 1.35^{a}
sin01	51.62 ± 5.86^{a}	46.78 ± 6.72^{a}	50.45 ± 3.08^{ab}	46.04 ± 5.24^{ab}	37.45 ± 4.80^{a}	40.28 ± 0.89^{a}
sin02	49.77 ± 4.86^{a}	46.47 ± 5.94^{a}	47.13 ± 3.05^{ab}	47.55 ± 6.88^{ab}	40.16 ± 0.81^{a}	40.82 ± 2.09^{a}
sin03	48.09 ± 5.22^{a}	50.64 ± 6.48^{a}	50.44 ± 4.30^{ab}	48.62 ± 4.16^{ab}	39.32 ± 1.71^{a}	41.41 ± 0.81^{a}
sin04	53.64 ± 8.56^{a}	54.76 ± 2.87^{ab}	48.19 ± 6.05^{ab}	48.56 ± 6.36^{ab}	37.44 ± 2.81^{a}	40.53 ± 2.11^{a}
sin05	49.15 ± 8.08^{a}	52.15 ± 3.93^{ab}	47.19 ± 5.98^{ab}	43.73 ± 2.05^{ab}	38.19 ± 3.41^{a}	41.09 ± 2.25^{a}
sin06	48.38 ± 8.46^{a}	48.32 ± 4.30^{a}	47.14 ± 3.11^{ab}	48.17 ± 4.55^{ab}	36.78 ± 3.25^{a}	40.34 ± 3.06^{a}
sin07	53.81 ± 6.16^{a}	44.92 ± 5.59^{a}	46.77 ± 2.55^{ab}	46.09 ± 3.30^{ab}	37.92 ± 3.22^{a}	40.40 ± 1.82^{a}
sin08	51.71 ± 9.26^{a}	46.54 ± 3.88^{a}	46.24 ± 2.76^{ab}	47.08 ± 5.90^{ab}	39.68 ± 3.90^{a}	39.42 ± 1.09^{a}
sin09	51.38 ± 6.43^{a}	47.12 ± 7.21^{a}	50.97 ± 4.75^{ab}	46.88 ± 4.02^{ab}	41.34 ± 3.79^{a}	41.04 ± 2.69^{a}
sin10	52.92 ± 7.46^{a}	47.89 ± 7.95^{a}	44.84 ± 4.56^{ab}	48.83 ± 2.91^{ab}	40.36 ± 3.07^{a}	38.63 ± 2.60^{a}
sin11	46.30 ± 7.85^{a}	44.81 ± 4.10^{a}	47.25 ± 2.75^{ab}	45.73 ± 2.48^{ab}	39.39 ± 3.56^{a}	38.05 ± 3.15^{a}
sin12	51.66 ± 7.73^{a}	47.80 ± 4.54^{a}	52.46 ± 3.98^{b}	45.67 ± 3.47^{ab}	40.21 ± 2.42^{a}	41.87 ± 2.42^{a}
sin13	55.22 ± 6.66^{a}	49.38 ± 2.99^{a}	44.76 ± 3.89^{ab}	52.02 ± 3.66^{b}	40.88 ± 1.66^{a}	40.64 ± 2.16^{a}
sin14	51.61 ± 8.02^{a}	63.32 ± 3.79^{b}	51.34 ± 3.36^{ab}	47.07 ± 2.86^{ab}	40.50 ± 3.44^{a}	38.38 ± 1.40^{a}
sin15	48.38 ± 4.94^{a}	51.39 ± 8.01^{a}	43.49 ± 2.67^{a}	47.04 ± 1.51^{ab}	38.92 ± 3.96^{a}	39.53 ± 2.41^{a}
sin16	52.65 ± 8.60^{a}	47.37 ± 4.70^{a}	45.56 ± 3.56^{ab}	43.33 ± 4.87^{ab}	36.71 ± 2.69^{a}	39.27 ± 2.76^{a}
sin17	50.39 ± 6.40^{a}	48.26 ± 7.83^{a}	46.99 ± 3.06^{ab}	45.51 ± 3.39^{ab}	37.49 ± 1.44^{a}	42.68 ± 1.01^{a}
sin18	56.89 ± 7.65^{a}	47.27 ± 4.30^{a}	52.19 ± 6.44^{b}	44.03 ± 1.18^{ab}	39.45 ± 3.24^{a}	41.15 ± 1.45^{a}
Mean	51.83 ± 2.48	49.42 ± 3.92	48.36 ± 2.53	46.15 ± 2.28	39.39 ± 1.43	40.07 ± 1.35

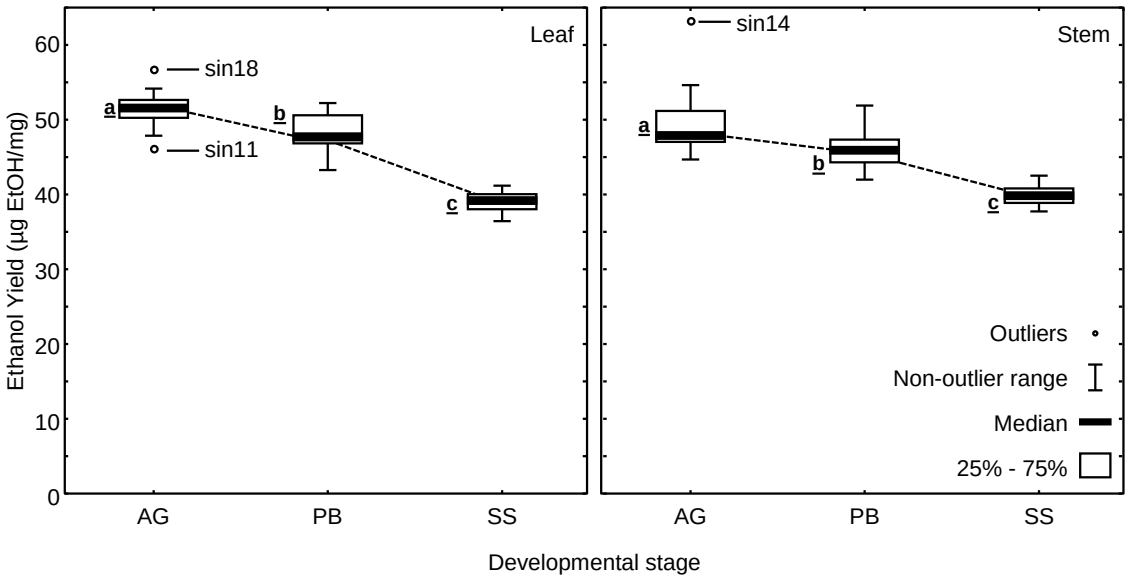

Fig. 2.6. Distribution of measurements of ethanol yielded per g of CWM after 72h of incubation with *Clostridium phytofermentans* for 25 miscanthus genotypes at active growth (AG), peak biomass (PB) and senescence (SS). The non-outlier range is defined as the range of values which fall outside 1.5× the interquartile range of the distribution (height of the 25% – 75% box). Not significantly different developmental stages are indicated by a common underlined letter next to the box (Tukey's test at α=0.05).

2.4.4. Discussion

The ABSL values obtained for lignin content at the senesced stage were in close agreement with other values reported for several miscanthus genotypes (Lygin *et al.*, 2011; Zhang *et al.*, 2012; Domon *et al.*, 2013); although no data for actively growing and peak biomass lignin content in miscanthus is available for comparison. As expected, there was a significant developmental and tissue effect for lignin content with i) an overall increase in lignin as the plants mature, and ii) a higher content of lignin in stem tissues compared with leaf tissues. Higher stem versus leaf lignin content has been reported for a wide range of grasses including switchgrass (Mann *et al.*, 2009; Shen *et al.*, 2009) and *M.* × *giganteus* (Hodgson *et al.*, 2010; Le Ngoc Huyen *et al.*, 2010).

The data also highlighted the limited predictive power of tissue lignin content when measured for a certain developmental stage for a specific genotype. For instance, none of the five lowest ranking genotypes for leaf lignin content at AG stage rank among the five lowest for PB stage and only two of the highest ranking genotypes for stem lignin content at PB rank among the five highest at SS stage. The data also support the concept of distinct genetic control of cell wall composition in leaf and stem tissue. As an example, stem tissue lignin content of the three *M.* × *giganteus* genotypes included in the study ranked among the highest five at SS, while the corresponding leaf content values ranked among the lowest five. While the overall variation in lignin content across the different genotypes remained fairly consistent for leaf tissue with increasing maturity (AG 16.9%, PB 16.2%, SS 21.7%), the variation for stem lignin content is larger for AG and PB (30% and 30.7%, respectively), but decreases at SS (11.3%). The decrease in variation of stem lignin content may reflect a convergence in developmental variability as plants senesce, and most likely accounts for the observed absence of the genotype effect in senesced samples.

The *C. phytofermentans* bioassay showed that CWM amenability to digestion also varies significantly between the tissues, the genotypes and throughout development; with ethanol yields decreasing as plants mature. However, the comparative relation between tissue digestibility was not the same at all developmental stages; since at AG and PB leaf tissue released 4.89% and 4.78% more ethanol respectively, whereas during senescence stem yielded more ethanol, but only with an increase of 1.75% (Table 2.7). Lignin differed between leaf and stem by 5.66% at AG, 13.07% at PB and 5.19% at SS, with stem always containing higher lignin contents (Table 2.5). Furthermore, it has been shown that samples ranking high in lignin content may equally rank high in ethanol yields, with the same being true for samples ranking low in lignin content (Tables 2.5 and 2.7). This suggested that, not only does the degree of tissue lignification not completely account for the convertibility of lignocellulosic biomass, but also that high lignin content in the cell wall is not a predictor of reduced amenability to deconstruction in all experimental conditions.

Additionally, FTIR spectroscopy (Section 2.3) indicated that lignin does not have a predominant influence in most compositional modifications between the cell wall from different tissues and developmental stages; which in fact occur at the level of the structural carbohydrates. Lignin content is frequently seen as an exacerbating factor of cell wall recalcitrance to deconstruction (Vanholme *et al.*, 2010; Hodgson *et al.*, 2011; Ding *et al.*, 2012). As a result, there was a need to assess directly the influence of lignin on cell wall amenability to deconstruction. For this, the ethanol yields obtained from the *C. phytofermentans* assay were correlated with the ABSL concentration of the same samples, thus providing a measure of the interaction of lignin content with biomass amenability to conversion. A very strong negative relationship between lignin content and ethanol yield was observed (r=-0.77; P<0.001; Fig. 2.7), indicating that lignin content does act negatively on CWM digestibility when all developmental stages and tissues are considered. However, high

scattering of data points and an r^2=0.59 for this model suggested other underlying relationships between the variables. By assessing each developmental stage individually (Fig 2.7), for samples collected at AG and SS, no significant relation was detected between ethanol yield and ABSL% (r=–0.13; P≈0.36 for both cases). However, at PB there was a significant correlation between lignin content and ethanol yield, with a Pearson correlation coefficient of r=-0.61 (P<0.001) indicating a negative association between lignin content and amenability to *C. phytofermentans* mediated cell wall deconstruction. Despite this meaningful correlation, the data indicate that other factors besides lignin concentration have an exacerbating effect on recalcitrance, as supported by the individual analysis of stem and leaf data. In stem samples the interaction between ethanol yield and lignin concentration showed a coefficient of r=-0.65 (P<0.001). However, for PB leaf samples the interaction was not significant (r=-0.31, P=0.133). These drastically different coefficients indicate that lignin content has a higher relevance for the recalcitrance of stem tissue than it does for leaf tissue sampled during PB. At this developmental stage, leaf tissue amenability to conversion may be far more influenced by other factors, than it is by lignin concentration. Similar results have been reported by Le Ngoc Huyen *et al.* (2010), who found that foliar tissues show less recalcitrance than stem tissues, despite also containing appreciable amounts of lignin. Moreover, the fact that stem and leaf tissues display distinct behaviours during conversion is indicative of the divergent compositional arrangement of these tissues.

Additionally, PCA of the FTIR spectra obtained for stem and leaf samples collected at PB revealed discriminant loadings and clustering patterns along PC1 similar to the ones seen for the data across the three developmental stages (compare Figs. 2.4F and 2.8). It is very likely that the divergent compositional features at the polysaccharide level and the lignin monomer content may be factors affecting cell wall recalcitrance in addition to mere lignin concentration;

thus making difficult if not impossible the task of solely using the extent of tissue lignification as a predictor of cell wall recalcitrance.

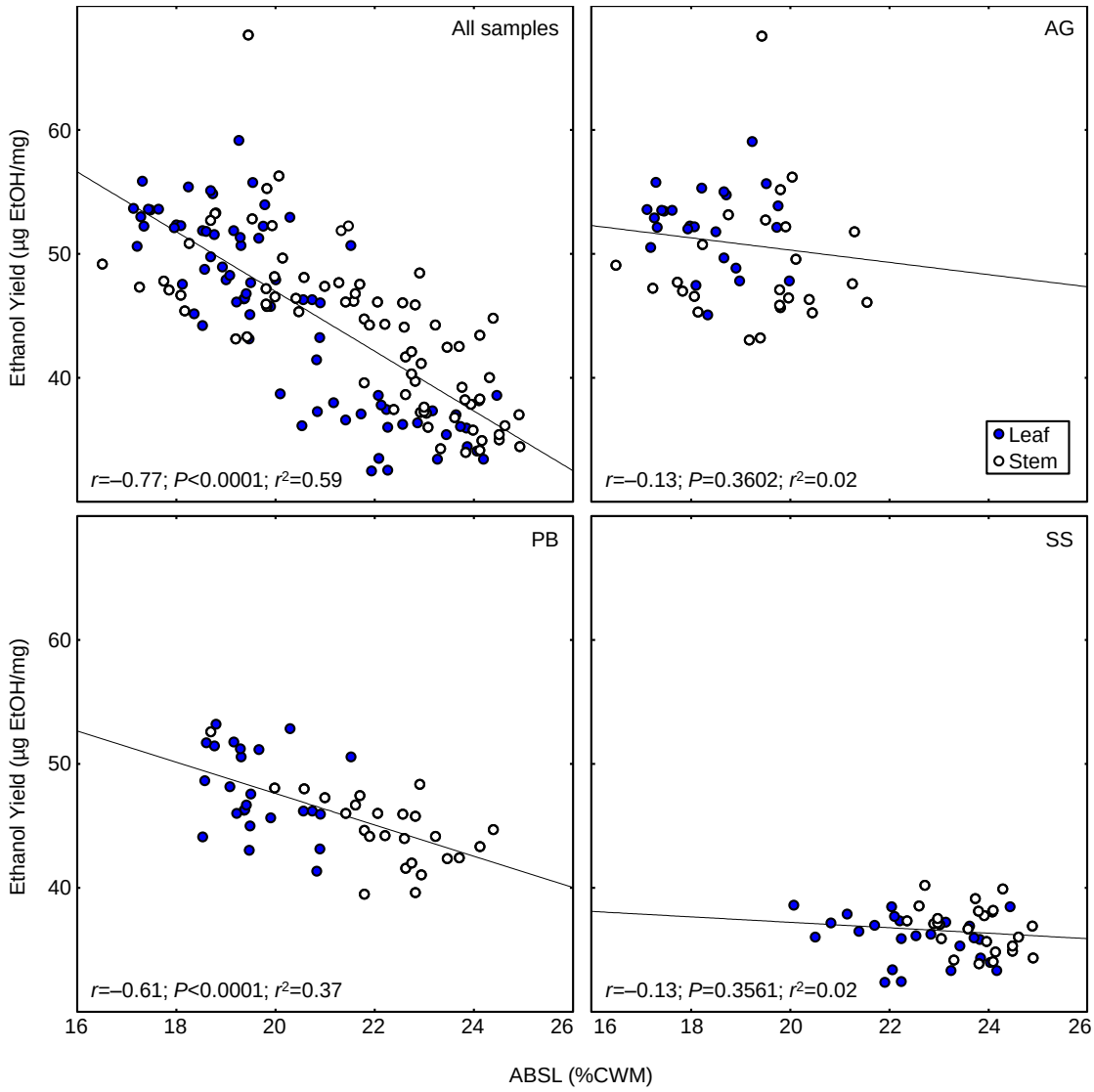

Fig. 2.7. Least square fit of ethanol yield vs. lignin content with the associated Pearson correlation statistic (*r*) and probability (*P*) for 25 miscanthus genotypes during active growth (AG), peak biomass (PB) and senescence (SS) developmental stages (DS).

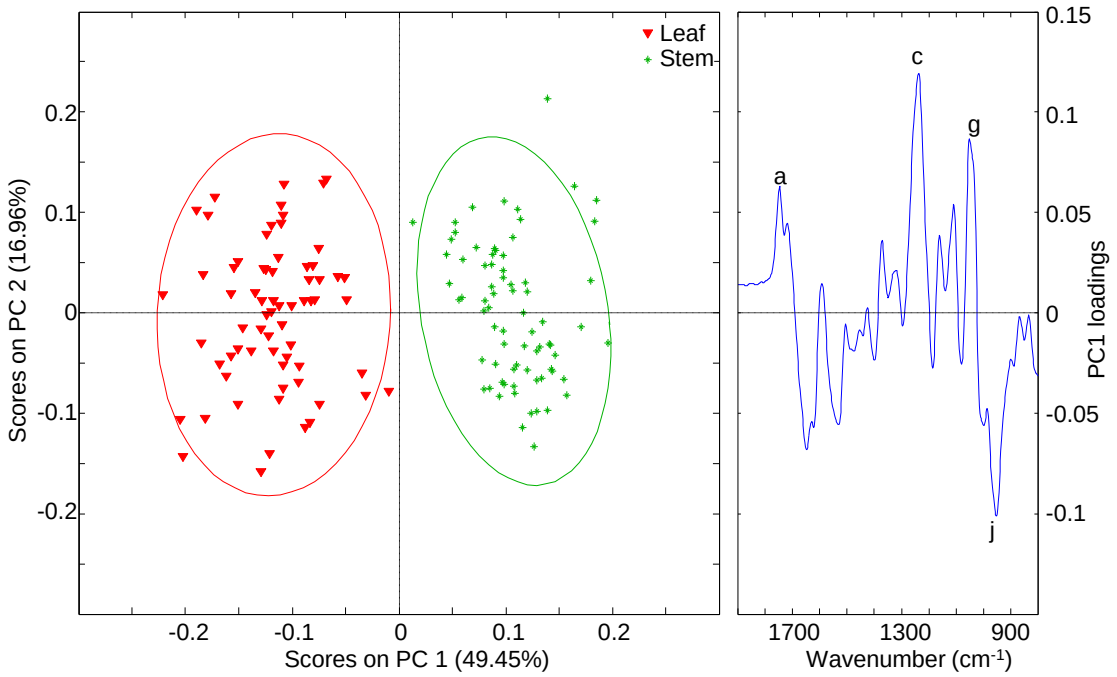

Fig. 2.8. Principal component analysis of FTIR spectra of all samples from 25 miscanthus genotypes at peak biomass stage. Left panel: plot of principal component one (PC1) and principal component two (PC2) scores for all samples at Peak Biomass. Right panel: corresponding PC1 loading plot. Spectral bands: *a*, 1745cm^{-1}; *c*, 1230cm^{-1}; *g*, 1037 cm^{-1}; *j*, 950cm^{-1}

2.5. EXPERIMENTAL DESIGN REFINEMENT

Studies described here clearly demonstrate that recalcitrance of miscanthus tissues cannot be fully explained by lignin content. In order to further elucidate the basis of recalcitrance of miscanthus tissues, detailed studies were undertaken including the use of immunological approaches which are described in following chapters. For the purpose of these studies the analysis of stem and leaf from 25 genotypes collected at three developmental stages would result in an excessively large number of samples, which would effectively make the procedures unfeasible.

In order to retain as much as possible of the original sample diversity while reducing sample redundancy, the 25 genotypes were assessed and preliminarily grouped as presented in Table 2.8, according to the following considerations:

- Data generated in studies described in this chapter to select a wide range of compositional and morphological variability (Sections 2.1, 2.3 and 2.4);
- Inclusion of representatives from the two miscanthus species and hybrids as in the original set of 25 genotypes (Table 1.1);
- Retaining a high number of the parental genotypes originally included in association mapping programmes (Table 1.1);
- Genetic marker information (Slavov *et al.*, 2013):
    - Based on simple sequence repeats (SSR) data, genotypes sin09 and sin16 differed significantly from the remaining *M. sinensis* lines considered in this study;
    - Based on 120 single nucleotide polymorphism (SNP) markers, genotypes sin10 and sin11 strongly differentiated from the remaining *M. sinensis* genotypes, so they were also considered a separate group.

Table 2.8. Preliminary grouping of genotypes for subsequent analyses.

Genotype	Species	Grouping	
sac01	*M. sacchariflorus*	A	*M. sacchariflorus*
gig01	*M.* × *giganteus*	B_1	*M.* × *giganteus* (50/50 *M. sinensis* and *M. sacchariflorus*)*
gig02	*M.* × *giganteus*		
gig03	*M.* × *giganteus*		
hyb01	hybrid	B_2	Other hybrids (non 50/50 admixture)*
hyb02	hybrid		
hyb03	hybrid		
sin09	*M. sinensis*	C_1	Strongly differentiated from remaining *M. sinensis* genotypes based on SSR markers*
sin16	*M. sinensis*		
sin10	*M. sinensis*	C_2	Strongly differentiated from remaining *M. sinensis* genotypes based on SNP markers*
sin11	*M. sinensis*		
sin01	*M. sinensis*	C_3	Subdivided based on lignin content and ethanol yields
sin02	*M. sinensis*		
sin03	*M. sinensis*		
sin04	*M. sinensis*		
sin05	*M. sinensis*		
sin06	*M. sinensis*		
sin07	*M. sinensis*		
sin08	*M. sinensis*		
sin12	*M. sinensis*		
sin13	*M. sinensis*		
sin14	*M. sinensis*		
sin15	*M. sinensis*		
sin17	*M. sinensis*		
sin18	*M. sinensis*		

* (Slavov *et al.*, 2013).

After careful consideration of all conditions one genotype was chosen from groups A, B_1, B_2, C_1 and C_2. From group C_3, three genotypes were chosen based on lignin content: sin08 (intermediate lignin), sin13 (low lignin) and sin15 (high lignin). Selected genotypes are underlined in Table 2.8. Only the biomass from these eight genotypes was used for subsequent analyses.

2.6. CONCLUSIONS

The studies in this chapter provide evidence that structural polysaccharides are main contributors to the compositional variability during stem development and between stem and leaf tissue. Hence, it is hypothesised that the observed differences in recalcitrance between stem and leaf tissues are to a large extent attributed to divergent carbohydrate composition and cross-linking patterns. Variation in the relative contributions of leaf and stem tissues to total above-ground biomass, together with reports indicating that their composition is under separate genetic control, emphasise that improvement of cell wall quality traits for the processing of miscanthus lignocellulosic biomass to biofuels and biomaterials must consider these observations. For gene-trait associations relating to cell wall quality it is best practise to obtain leaf and stem compositional data separately, as tissue-specific traits may be masked by analysis of total above-ground biomass and variability between samples could be largely due to varying tissue contributions to the total biomass.

3. CELL WALL ESTER-LINKED SUBSTITUENTS

3. CELL WALL ESTER-LINKED SUBSTITUENTS

Data from the previous chapter revealed that differences in recalcitrance between developmental stages and tissues are likely to be to a large extent attributed to divergent carbohydrate composition and cross-linking patterns in the cell wall. This chapter will focus particularly on the components involved in this cross-linking between the various cell wall polymers. In grass cell walls, the different polymers are often linked to other components which ornament and contribute to the structure of the wall, namely: ester-linked methyl, acetyl and phenolic acid groups (Saulnier *et al.*, 1999; Grabber *et al.*, 2004; Vogel, 2008; Gille and Pauly, 2012; Fry, 2010).

Glucuronoarabinoxylans may be substituted with glucuronic acid or methyl-glucuronic acid residues (Pauly and Keegstra, 2008), but it is in pectins where methylation has a more predominant effect on polysaccharide structure. Homogalacturonan is synthesised as a highly methyl-esterified polymer (Zhang and Staehelin, 1992). Subsequently, *in muro* pectin methyl-esterase enzymes de-methyl-esterify the polymer to yield carboxyl groups, which may bind calcium, and cross-link pectin chains into rigid "egg-box" structures (Anthon and Barrett, 2006; Lionetti *et al.*, 2010). The formation of these structures leads to greater pectin adhesion and thus contributes to cell wall recalcitrance.

By treating CWM with low molarity alkali metal hydroxide solutions, ester linkages are cleaved by saponification, and several aliphatic and aromatic acids are released, of which acetic acid and the phenolic hydroxycinnamates (HCA) *p*-coumaric (*p*CA) and ferulic (FA) acids are typically the most abundant (Lam *et al.*, 2001; Persson *et al.*, 2002; Buanafina, 2009; Jönsson *et al.*, 2013). While HCAs are thought to be involved in cell wall polymer cross-linking and to negatively affect their deconstruction (Ishii, 1997b; Grabber *et al.*, 2004; Buanafina, 2009; Ralph, 2010), the function of acetylation *in planta* remains enigmatic (Xiong *et al.*, 2013). As

a result, the determination of the abundance of these compounds in the cell wall will contribute to the interpretation of studies on the deconstruction of miscanthus biomass described in subsequent sections.

3.1. Determination of Cell Wall Acetyl Esters

3.1.1. Overview

Substitution by *O*-acetyl groups occurs extensively on the backbone or ramifications of non-cellulosic structural polysaccharides, however, these occur in different abundances depending on the species, tissue, type of cell wall, and ultimately on the nature of the acetylated polymer (Pauly and Scheller, 2000; Gille and Pauly, 2012; Pawar *et al.*, 2013). Arabinoxylans (AX), the most abundant hemicellulose of grass cell walls, are extensively acetylated (Wende and Fry, 1997b; Pawar *et al.*, 2013). *In vivo* functions of acetylation have not yet been completely characterised, but it is known that in xylans, acetyl groups are esterified directly to backbone pyranose rings at carbon positions 2 and 3 (Agger *et al.*, 2010; Chen *et al.*, 2012), where they influence polymer properties and interactions. Opposing results have been reported for the effect of acetylation on cell wall recalcitrance. It has been shown that in *Arabidopsis* spp. mutants with reduced acetylation of xylans, saccharification yields are not higher than in the wild type, presumably because the deposition of xylans with reduced acetyl substituents might lead to tighter xylan–cellulose associations (Xiong *et al.*, 2013). However, it is also known that by chemically removing acetyl esters from lignocellulosic biomass, with little disruption of other fractions (such as lignin), saccharification yields are significantly improved; as studies have demonstrated that de-acetylated xylan becomes 5 to 7 times more digestible, and this renders the cellulose fraction more accessible and 2 to 3 times more digestible in aspen wood and in wheat straw (Grohmann *et al.*, 1989; Kong *et al.*, 1992; Mitchell *et al.*, 1990; Selig *et al.*, 2011). It is likely that acetylation of glycosyl residues of polysaccharides creates steric hindrance for binding of many hydrolytic enzymes, which limits the extent of hydrolysis (Biely, 2012; Pawar *et al.*, 2013). Furthermore, released acetate during cell wall deconstruction

may act as an inhibitor to microbial fermentation (Gille and Pauly, 2012). Lignin acetylation can also occur on aliphatic side chains of S and G monomers, and its levels vary greatly (del Río *et al.*, 2007); however, the function and consequences of such variability in lignin acetylation are still unknown (Pawar *et al.*, 2013).

Acetyl groups can be released by alkali treatment. Bearing this in mind, potassium hydroxide (KOH) aqueous solutions at 0.1M were used for alkaline de-acetylation of miscanthus CWM samples, and ion exclusion HPLC, coupled to Refractive Index (RI) detection allowed quantifying the released acetic acid. Ion exclusion HPLC provides a useful technique for the separation of ionic and non-ionic substances using a stationary phase in which ionic substances are rejected by the resin while non-ionic or partially ionised substances are retained and separated by partition between the liquid inside the resin particles and the liquid outside the particles. The ionic substances therefore pass quickly through the column, but non-ionic or partially ionised substances are held up and are eluted more slowly (Tanaka and Haddad, 2000). An ion exclusion column intended for the separation of organic acids alone or in combination with other compounds, and packed with a cation-exchange resin made of porous polystyrene gel with sulfonic acid groups was used here (Phenomenex, 2015). RI detection uses a differential refractometer that responds to the deflection of a light beam caused by differing refractive indices between the analytes and a reference cell (Morgan and Smith, 2011).

In this section, a method for the de-acetylation of CWM and quantification of released acetate is presented. The variations on yielded acetate amount between developmental stages, tissues and genotypes is discussed, providing the basis for the understanding of the impact of a mild alkaline pretreatment on the enhancement of biomass saccharification (Chapter 4).

3.1.2. Materials and methods

Alkali labile acetyl content was estimated for the stem and leaf samples collected at three developmental stages, from 8 miscanthus genotypes. Acetate release was achieved by an alkaline saponification procedure modified from Manabe *et al.* (2011), according to which 10mg of CWM was incubated in 500µL of 0.1M KOH for 16h (21°C/150rpm). Samples were then centrifuged at 2500×g for 5min, 100µL of the supernatants were mixed with 900µL of 0.005M H_2SO_4 containing 0.01M crotonic acid as an internal standard (IS). Subsequently, the mixtures were filtered through 0.45µm syringe filters (Millipore Corporation, Billerica, Massachusetts, USA) and 25µL of the samples were analysed on an HPLC-RI system (Jasco, Great Dunmow, Essex, UK) equipped with a Rezex ROA-organic acid H^+ column (150×7.8mm) kept at 35°C, with a 0.005M sulphuric acid mobile phase at a flow rate of 0.6mL/min for 16min.

Supernatant concentrations of acetic acid (C_{AA}) were determined using a standard curve prepared with a concentration gradient of an acetic acid standard. All chromatographic peak areas were firstly corrected by multiplication by the ratio between a reference area for the internal standard and the actual area observed in a given sample (IS_{Ref}/IS_{Actual}). Finally, the level of acetylation of cell wall biomass samples was estimated according to the equation:

$$Acetate\% = \frac{C_{AA} \times V_R}{W_S} \times 100\% \quad (3.1)$$

Where Acetate% is the acetate percentage content; C_{AA} is the supernatant concentration (g/L) of acetic acid as determined by HPLC; V_R is the reaction volume (L); W_S is the sample weight (g). All calculations for descriptive statistics, analyses of variance and Tukey's tests

were performed as described in section 2.1.3; with the amendment that the effect of tissue type (2 levels) was also tested in addition to genotype and development factors.

3.1.3. Results

CWM from leaves and stems of 8 miscanthus genotypes (Section 2.5), collected at three developmental stages was analysed for content of alkali labile acetyl esters. Results for genotype sin09 are presented as an example of the typical HPLC-RI chromatogram obtained from the analyses of the supernatants after treating CWM with 0.1M KOH (Fig. 3.1). At the employed experimental conditions, acetic acid has a retention time (RT) of approximately 8.15min. Acetic acid was the predominant compound detected in the extracts of both tissues and at all developmental stages. Various minor peaks were also observed, with smaller retention times than that of acetic acid. However, their identification and quantification would be too imprecise given the low amounts present in the extracts.

Significant differences were observed between the acetate released from leaf and stem tissues at an overall level and also at each developmental stage ($P<0.001$ for all cases; Table 3.1), but cell wall acetylation did not vary equally for both tissues throughout development (Fig. 3.2). Mean overall acetate percentages of leaf tissues increased as plants matured, from 3.15% at AG, to 3.36% at PB and to 4.19% at SS (Table 3.2), and statistically significant differences were observed between all developmental stages ($P<0.001$). By contrast, in the CWM of stems, measured acetate did not change significantly throughout plant development ($P=0.525$), instead, it remained at approximately 4.7% at all developmental stages.

Detected acetate also varied significantly between the genotypes at all developmental stages ($P<0.001$). Tukey testing of the genotype effect lead to the emergence of intricate homogeneous groups at each tissue and developmental stage individually, except for senesced

stems (Table 3.2). This indicates that despite a significant influence of the genotype factor at SS, this effect may be uniquely attributed to the variability among leaf tissues. Whether considering the CWM from stem or from leaf, at all developmental stages the majority of *M. sinensis* genotypes released higher amounts of acetate (Table 3.2), the only exception was the leaf tissue collected from sin13 at PB, which contained lower acetyl abundances than gig01. Specifically considering leaf tissues, genotype sin08 was the highest acetate yielder at all three developmental stages, the *M. sacchariflorus* and hyb03 genotypes were the lowest, whereas the *M.* × *giganteus* genotype had lower than average acetate content. For stem tissues, sin11 and sin13 consistently showed highest acetate levels, sac01 and hyb03 ranked at the lower end of the range, and once again gig01 had lower than average acetate content.

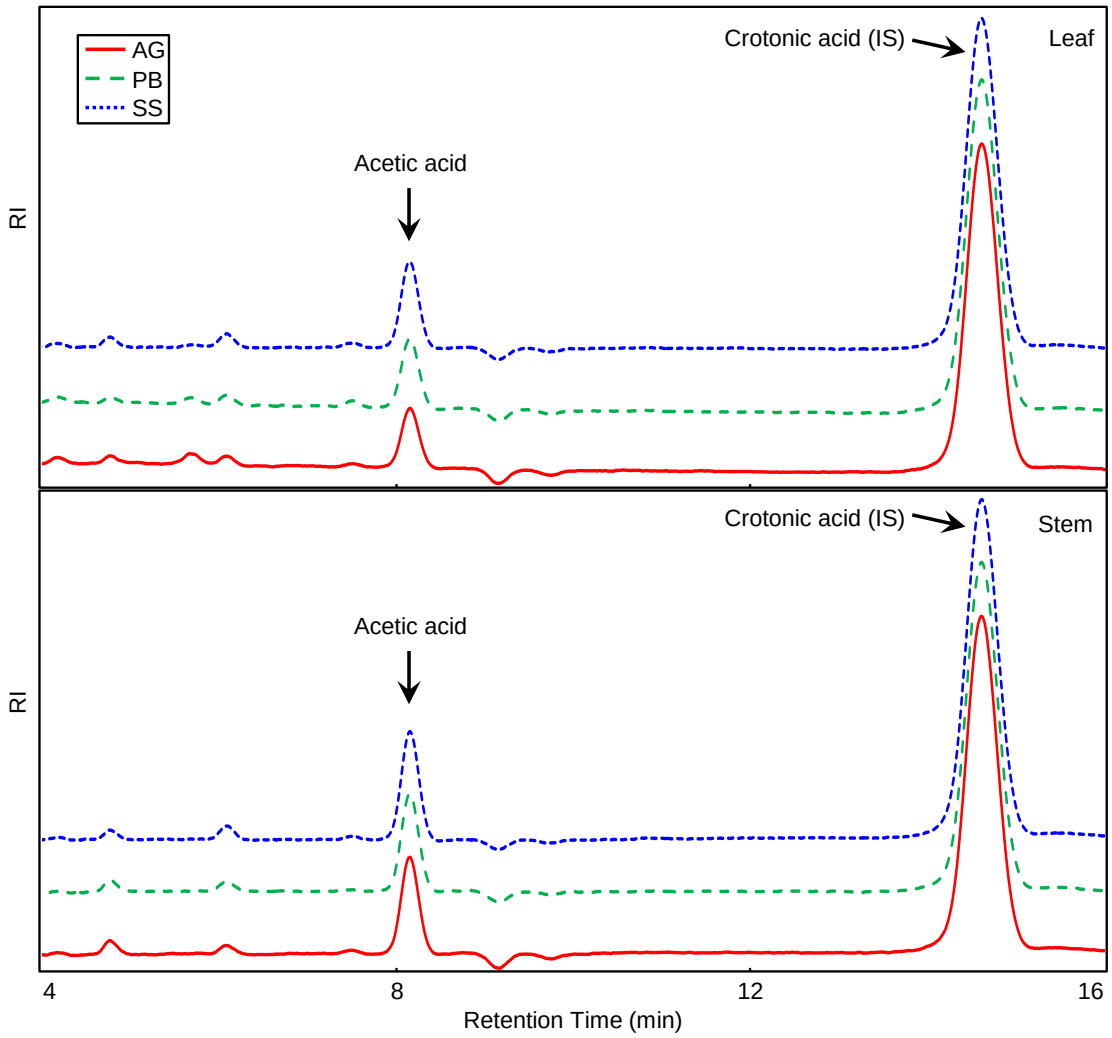

Fig. 3.1. HPLC-RI chromatograms of the supernatant obtained after treating CWM from genotype sin09 with 0.1M KOH. Acetic acid was the predominant detected component from both tissues and at all developmental stages: active growth (AG), peak biomass (PB) and senescence (SS). Void volume regions are omitted; i.e., from t=0min, until the end of the solvent front t=4min. (RI: refractive index; IS: internal standard)

Table 3.1. ANOVA results for released acetate determination.

All Developmental Stages

Effect	Degrees of freedom	Sum of squares	Mean square	*F*-ratio	*P*-value	Effect size (η^2)
Genotype	7	1307.10	186.70	42.57	<0.0001	0.2132
Development Stage	2	400.00	200.00	45.59	<0.0001	0.0652
Tissue	1	3129.90	3129.90	713.49	<0.0001	0.5106
Genotype × Development Stage	14	182.70	13.00	2.97	0.0025	0.0298
Genotype × Tissue	7	275.00	39.30	8.96	<0.0001	0.0449
Development Stage × Tissue	2	580.90	290.50	66.21	<0.0001	0.0948
Genotype × Development Stage × Tissue	14	44.20	3.20	0.72	0.7448	0.0072
Error	48	210.60	4.40			
Total	95	6130.40				

Active Growth

Effect	Degrees of freedom	Sum of squares	Mean square	*F*-ratio	*P*-value	Effect size (η^2)
Genotype	7	269.36	38.48	29.90	<0.0001	0.1101
Tissue	1	2096.77	2096.77	1629.00	<0.0001	0.8572
Genotype × Tissue	7	59.32	8.47	6.58	<0.0001	0.0243
Error	16	20.59	1.29			
Total	31	2446.04				

Peak Biomass

Effect	Degrees of freedom	Sum of squares	Mean square	*F*-ratio	*P*-value	Effect size (η^2)
Genotype	7	293.54	41.93	24.81	<0.0001	0.1578
Tissue	1	1441.44	1441.44	852.88	<0.0001	0.7748
Genotype × Tissue	7	98.38	14.05	8.32	0.0002	0.0529
Error	16	27.04	1.69			
Total	31	1860.40				

Senescence

Effect	Degrees of freedom	Sum of squares	Mean square	*F*-ratio	*P*-value	Effect size (η^2)
Genotype	7	926.90	132.41	13.00	<0.0001	0.6509
Tissue	1	172.84	172.84	16.97	0.0008	0.1214
Genotype × Tissue	7	161.36	23.05	2.26	0.0834	0.1133
Error	16	162.93	10.18			
Total	31	1424.03				

Table 3.2. Acetate release upon 0.1M KOH treatment of miscanthus CWM. Values are expressed as percentage of cell wall material dry weight (% CWM) and are the mean ± standard deviation at three developmental stages for each genotype. Values within a column sharing a letter in their superscript are not significantly different according to a Tukey's test (α=0.05).

	Acetate (% CWM)					
	Active Growth		Peak Biomass		Senescence	
	Leaf	Stem	Leaf	Stem	Leaf	Stem
gig01	3.09 ± 0.07^{ac}	4.49 ± 0.10^{ab}	3.42 ± 0.05^{ad}	4.28 ± 0.11^{a}	4.08 ± 0.16^{cd}	4.10 ± 0.05^{a}
hyb03	2.93 ± 0.17^{c}	4.40 ± 0.06^{a}	2.86 ± 0.04^{c}	4.20 ± 0.11^{a}	3.35 ± 0.02^{b}	3.96 ± 0.05^{a}
sac01	2.51 ± 0.03^{d}	4.29 ± 0.11^{a}	2.77 ± 0.08^{c}	4.47 ± 0.13^{a}	3.12 ± 0.10^{b}	4.09 ± 0.08^{a}
sin08	3.51 ± 0.05^{b}	4.97 ± 0.17^{bcd}	3.74 ± 0.02^{b}	4.77 ± 0.03^{ab}	5.05 ± 0.07^{a}	4.78 ± 0.07^{a}
sin09	3.38 ± 0.12^{ab}	4.97 ± 0.03^{bcd}	3.69 ± 0.05^{ab}	4.71 ± 0.15^{ab}	4.94 ± 0.19^{a}	5.23 ± 0.20^{a}
sin11	3.32 ± 0.12^{ab}	5.02 ± 0.14^{cd}	3.61 ± 0.07^{ab}	5.22 ± 0.19^{b}	4.62 ± 0.06^{ae}	5.09 ± 1.21^{a}
sin13	3.10 ± 0.01^{ac}	5.33 ± 0.01^{d}	3.24 ± 0.11^{d}	5.17 ± 0.24^{b}	3.91 ± 0.15^{c}	5.13 ± 0.05^{a}
sin15	3.39 ± 0.01^{ab}	4.71 ± 0.25^{abc}	3.56 ± 0.14^{ab}	4.81 ± 0.25^{ab}	4.48 ± 0.02^{de}	4.90 ± 0.05^{a}
Mean	3.15 ± 0.32	4.77 ± 0.36	3.36 ± 0.37	4.70 ± 0.38	4.19 ± 0.71	4.66 ± 0.53

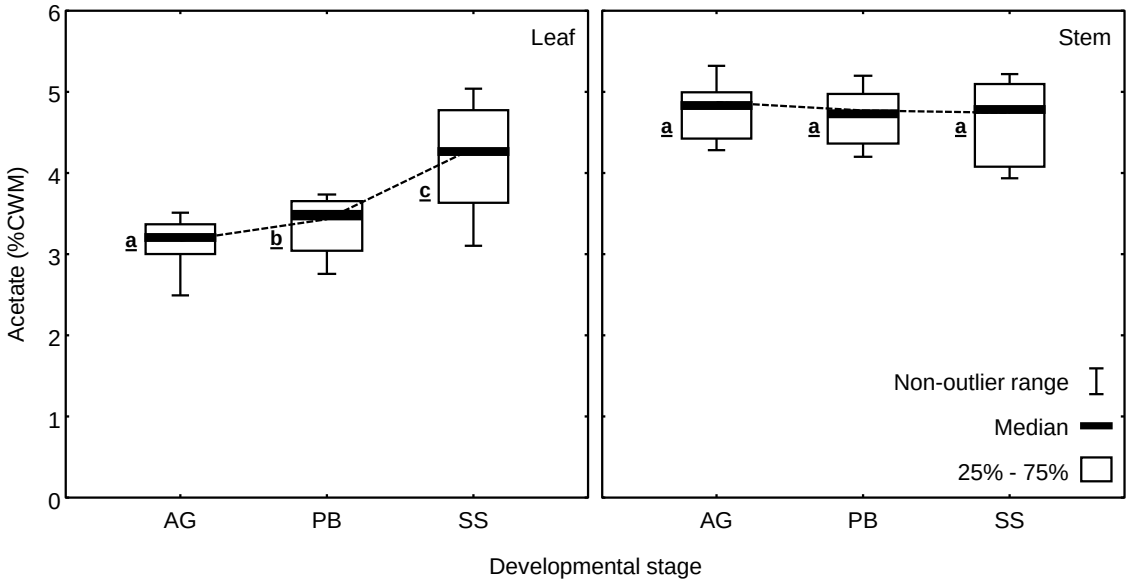

Fig. 3.2. Distribution of measurements of released acetate upon 0.1M KOH treatment of miscanthus CWM. Values are expressed as percentage of cell wall material dry weight (% CWM) from leaf and stem tissue for 8 miscanthus genotypes at active growth (AG), peak biomass (PB) and senescence (SS). The non-outlier range is defined as the range of values which fall outside 1.5× the interquartile range of the distribution (height of the 25% – 75% box). Not significantly different developmental stages are indicated by a common underlined letter next to the box (Tukey's test at α=0.05).

3.1.4. Discussion

The results presented here show that by treating miscanthus cell wall biomass with aqueous solutions of potassium hydroxide, effective removal of acetyl substitutions from the cell polymers is achieved, presumably by saponification; i.e., by release of acetyl ester groups (Marcus *et al.*, 2010; Jönsson *et al.*, 2013). Results from other studies, where similar methods were employed on various lignocellulosic feedstocks, have shown that a near complete cell wall de-acetylation is accomplished at mild alkaline conditions (Kong *et al.*, 1992; Pawar *et al.*, 2013; Chen *et al.*, 2014). Trace amounts of other compounds, detected in the extracts merely as minor peaks and with lower retention times than acetic acid, could not be accurately characterised. However, it can be presumed that they correspond to wall bound compounds; namely carbohydrates or other aliphatic acids, such as formic acid, which may occur as formyl esters (Anderson *et al.*, 1974; Jönsson *et al.*, 2013). The fact that no substantial amounts of sugars were detected in the supernatants of 0.1M KOH-treated samples is in strong agreement with reports that show that by subjecting CWM to mild alkaline treatments, acetyl esters are removed without causing extensive losses of cellulose, hemicellulose or lignin[*] (Kong *et al.*, 1992; Sharma *et al.*, 2013; Jiang *et al.*, 2014).

Furthermore, the employed chromatographic column also is suitable for the detection of simple alcohols such as methanol. Nonetheless, a well demarked peak for this compound was not detected, implying that methyl-esterified polymers are far less abundant in the miscanthus cell wall than acetylated ones. Since methyl esterification tends to be more frequent in pectin, it is possible that methanol release was not detected as a consequence of the relatively lower abundance of pectic polysaccharides in the cell wall (Anthon and Barrett, 2006; Vogel, 2008; Lionetti *et al.*, 2010).

[*] It is possible that polymeric carbohydrates are released but remain undetected at the employed chromatographic conditions. Experimental approaches to assess this possibility will be discussed in chapter 6.

With an average acetyl percentage of 3.57% (2.49% – 5.10%) of the CWM in leaves, and an average of 4.71% (3.92% – 5.95%) in stems (Table 3.2), the range of the values here obtained is in close agreement with data reported for miscanthus by Le Ngoc Huyen *et al.* (2010). However, in comparison to other lignocellulosic feedstocks, miscanthus typically released higher proportions of acetate; e.g., 2.9% in willow (Sassner *et al.*, 2008), 2.2% in corn stover (Kim and Lee, 2005) and 1.7% in wheat straw (Kabel *et al.*, 2007). For miscanthus, values for comparison of the variation observed in acetate release from CWM originating from different tissues and developmental stages are virtually missing. Therefore, results from this assay may contribute to a better understanding of how acetylation is associated to development of miscanthus leaf and stem.

The amount of acetate released from miscanthus leaves increased throughout development, by 6.67% from AG to PB, and by 24.70% from PB to SS (Table 3.2), but without ever achieving the maximum values observed for stems. Stem tissues from actively growing plants contain the highest acetate percentage values, which then slightly decrease (although not significantly) as plants mature and growth rates become lower; by -1.47% from AG to PB, and by -0.85% from PB to SS. These observations could be related to the fact that acetylation is likely to play a fundamental role in providing structural support during plant growth, and therefore there could be a greater need for high cell wall polymer acetylation in stem tissues early in plant development. As is supported by the fact that *Arabidopsis* spp. mutants with reduced wall acetylation exhibit growth deficiencies that become more severe as more copies of the mutation are present (Manabe *et al.*, 2013). Furthermore, in *Arabidopsis* spp., reduced growth phenotypes with collapsed xylem cells are observed in mutants possessing a specific decrease in xylan acetylation (Xiong *et al.*, 2013).

Genotype-derived differences were also detected, as in both tissues it was observed that *M. sinensis* genotypes typically released higher amounts of acetate, followed by the hybrid

genotypes, and ultimately *M. sacchariflorus*, in decreasing order (Table 3.2). It is known that mechanical properties of cell walls can derive from differential polysaccharide acetylation (Manabe *et al.*, 2013), that in the grass primary walls, AX is the main acetylated polymer (Pawar *et al.*, 2013), and that variable proportions of acetylation occur in galacturonate residues in rhamnose-rich portions of pectins (Komalavilas and Mort, 1989; Brown and Fry, 1993). Accordingly, differences in digestibility between the genotypes (as seen in section 2.4 and will be seen in section 4.2), could be partially related to the presence of divergent acetylated polysaccharides in the cell walls of different genotypes. The study of the carbohydrate fraction of the miscanthus cell wall could therefore elucidate if changes in acetylation are dependent on polysaccharide composition and possibly explain the acetate release differences observed between genotypes.

Acetic acid is considered a simultaneous inhibitor of saccharification and of fermentation (Chang and Holtzapple, 2000; Bellissimi *et al.*, 2009), since acetyl substituents cause steric hindrance to cell wall polysaccharide hydrolytic enzymes (Pauly and Scheller, 2000; Biely, 2012; Pawar *et al.*, 2013), and the accumulation of acetic acid inside fermenting microbes causes a toxic acidification of the cytosol (Mira *et al.*, 2010; Gille and Pauly, 2012). Accordingly, by interpreting the variations in acetate release presented here, better knowledge is provided regarding how acetylation impacts miscanthus cell wall recalcitrance. The topic of acetylation linked to cell wall recalcitrance will be addressed again in following chapters.

3.2. Determination of Cell Wall Hydroxycinnamoyl Esters

3.2.1. Overview

Plant cell wall phenylpropanoids are typically divided into two main groups: lignin and HCAs. As for lignin, HCA abundance may vary substantially between species and plant tissues. Type-II cell walls, like those occurring in miscanthus and other grasses, characteristically contain larger amounts of HCAs in comparison with dicotyledonous plants (Ishii, 1997b; Lozovaya *et al.*, 1999). Furthermore, C_4 grasses tend to have higher levels of these phenolic acids than C_3 grasses (Grabber *et al.*, 2004).

Ferulic and *p*-coumaric acids are the main HCAs in the cell wall. Specifically for FA molecules, they are notable for occurring associated to structural polysaccharides as monomers, dimers, or even as larger sized oligomers, cross-linking carbohydrate chains to each other and to lignin (Ralph *et al.*, 1994b; Grabber *et al.*, 2004; Buanafina, 2009; Agger *et al.*, 2010). Furthermore, it has been proposed that the formation of FA cross-links between AX and lignin is a mechanism used by grass cells to end their elongation process and shift from primary to secondary wall development (MacAdam *et al.*, 1992; Jung, 2003). Feruloylation occurs more abundantly in the epidermis, xylem, bundle sheaths and sclerenchyma, while *p*-coumaroylation has been reported to be low in epidermis, moderate in sclerenchyma and high in vascular tissues and pith parenchyma (Faulds and Williamson, 1999; Hatfield *et al.*, 1999c; Grabber *et al.*, 2004; Buanafina, 2009).

In the grass cell wall, FA may occur ester-bound via its carboxylic acid group to O-5 of arabinosyl side chains of arabinoxylan (Wende and Fry, 1997b). FA may also be simultaneously ether-bound to lignin, with its hydroxyl group covalently linked to lignin monomers (Kondo *et al.*, 1990; Buanafina, 2009) thus leading to the anchoring of lignin, and

to its cross-linking to the xylan-cellulose network via the formation of ferulate-polysaccharide-lignin complexes (Iiyama *et al.*, 1994; Ishii, 1997b; Grabber *et al.*, 2004). Additionally, feruloylation of arabinoxylans is important because it provides nucleating sites for the polymerisation and deposition of lignin (Ralph *et al.*, 1995). Peroxidase-mediated oxidative coupling of feruloyl groups leads to the formation of dimers, which cross-link polysaccharides and tighten the cell wall (Ralph *et al.*, 1994a; Wende and Fry, 1997b; Hatfield *et al.*, 1999b). Moreover, it has been suggested that arabinoxylan-pectin networks could also be cross-linked by FA dimers (Ishii, 1997b).

In addition to FA, *p*CA has also been found esterified to O-5 of arabinosyl side chains of arabinoxylan, particularly in immature tissues (Ishii, 1997b; Wen *et al.*, 2011). However, *p*-coumaroylation occurs mainly concomitantly with lignification and it has been reported that S-lignin is pre-acylated with *p*CA before being incorporated into lignin (Lu and Ralph, 1997). Dimerisation of *p*CA also occurs in the cell wall, but since virtually all *p*CA is esterified to lignin, these dimers are probably involved in lignin cross-linking (Grabber *et al.*, 2004).

The formation of these intertwined meshes of polymers has a strong effect on the mechanical properties of the cell wall, such as adherence, extensibility and accessibility. Consequently, *in vivo*, the properties conferred by HCA cross-linking are of great importance to plant growth and development, namely because they contribute to the control of cell wall extensibility (Wende and Fry, 1997b; Lozovaya *et al.*, 1999) and also because they confer protection against predator digestive enzymes and pathogen invasion (Akin *et al.*, 1993; Ikegawa *et al.*, 1996). However, these benefits to the plant are hindrances to the utilisation of lignocellulosic biomass as feedstocks, as they enhance cell wall recalcitrance (Ishii, 1997b; Ralph, 2010). Therefore, there is a need for a better understanding of the roles and distributions of HCAs in the cell walls of different grass tissues and developmental stages.

Experimentally, esterified and etherified HCAs may be distinguished by treating CWM with low molarity aqueous alkaline solutions at room temperature (which cleave ester bonds via saponification), or by hot concentrated alkali at high temperatures (such as 4M KOH at 170°C; which also cleaves ether bonds) (Lozovaya *et al.*, 1999).

To assess the abundance and distribution of ester-linked hydroxycinnamates across the various miscanthus cell wall samples, KOH aqueous solutions at 0.1M and 1M were used for alkaline de-esterification of the wall polymers. The released ester-linked hydroxycinnamates were then analysed by Reversed Phase High Performance Liquid Chromatography coupled to diode array detection (RP-HPLC-DAD). RP-HPLC consists of a method where a hydrophobic stationary phase is used to retain analytes based on their hydrophobicity; i.e., polar compounds are eluted faster than non-polar compounds. To attain this kind of chromatographic separation, octadecyl-bonded silica gel (C_{18}) is the most frequently used column packing (Waksmundzka-Hajnos and Sherma, 2010). Diode array detectors (DAD) are multi-wavelength detectors containing several photodiode arrays, which allow for simultaneous scanning over a range of wavelengths. DAD has two main advantages over other types of detection. Firstly, it allows quantifying each chromatographic peak at its maximum absorption. Secondly, it provides advantages in terms of peak purity since scanning at various wavelengths allows the collection of absorption spectra which help decipher not only the identity of a peak, but also if it represents a single or multiple compounds (Scott, 1998; Lough and Wainer, 1996).

In this section the variation in the contents of the two most abundant HCAs in the miscanthus cell wall is assessed, and similarly to the previous determination of cell wall acetyl esters, the obtained information will be used in subsequent chapters as a contribution to the understanding of how saccharification varies in response to a mild alkaline pretreatment and between developmental stages, tissues and genotypes.

3.2.2. Materials and methods

Alkali labile hydroxycinnamoyl content was estimated for stem and leaf from 8 miscanthus genotypes, collected at three developmental stages. Release of ester-bound HCAs was achieved by using an alkaline saponification method adapted from (Buanafina *et al.*, 2006). For each sample, approximately 10mg of CWM was mixed with 5mL of the degassed extracting solution (0.1M or 1M KOH) under a flow of N_2 to reduce sample oxidation, followed by incubation in the dark for 16h (21°C/150rpm). Samples were then centrifuged at 2500×*g* for 5min, the supernatants were transferred to new tubes and the pellets were washed with 4mL of 100% methanol, and these washes combined with the previous supernatants. Solubilised carbohydrates in the combined extracts were precipitated by incubating the samples at -80°C/20min, after which the supernatants were collected in a new tube, the pellets were washed with 1mL of 100% methanol, and supernatants were once again combined with the wash. Subsequently, the methanol in solution, which composed 50% of the extracts, was centrifugally evaporated, and the resulting aqueous phases were acidified with HCl (pH=2.5). HCAs were then recovered by reverse phase C_{18} solid phase extraction (Sep-Pak C_{18} Vac RC cartridges, 500mg, 3cm^3, 55-105µm particle size, Waters Corporation, Milford, Massachusetts, USA), and the resulting samples were dried under a stream of N_2. Subsequently, samples were reconstituted in 200µL of 70% (v/v) methanol and 20µL were injected for analysis on an RP-HPLC-DAD system (Waters Corp.). A radial compression column was used (8.0×100mm Nova-Pak C_{18} Radial-Pak Cartridge, 4µm particle size, Waters Corp.), with 100% methanol and 5% (v/v) acetic acid as eluents at a linear 20-70% methanol gradient in 25min, at a flow rate of 2mL/min. Chromatograms were monitored using a diode array detector (Waters 996 PAD, Waters Corp.) collecting UV/visible spectra at 240nm – 400nm and linked to Empower Pro software (Waters Corp.). HCA identification was performed in reference to authentic monomer standards and to published diagnostic absorption wavelengths of peaks (Waldron *et*

al., 1996). Supernatant concentrations of each HCA (C_{HCA}) were determined using a standard curve prepared with a concentration gradient of the corresponding HCA (FA or *p*CA). Finally, the content of each HCA expressed as percentage of cell wall biomass dry weight (HCA%) was estimated according to:

$$HCA\% = \frac{C_{HCA} \times V_R}{W_S} \times 100\% \quad (3.2)$$

Where C_{HCA} is the supernatant concentration (g/L) of the corresponding HCA as determined by RP-HPLC; V_R is the reaction volume (L); W_S is the sample weight (g). All calculations for descriptive statistics, analyses of variance and Tukey's tests were performed as described in section 2.1.3; with the exception that the effect of tissue type (2 levels) was also tested in addition to genotype and development factors.

3.2.3. Results

Characterisation of alkali labile hydroxycinnamoyl content was performed after saponification of the CWM with 1M KOH. Two prominent peaks were observed on the RP-HPLC-DAD chromatograms obtained at 340nm for all miscanthus cell wall samples analysed, which were identified as corresponding to *p*-coumaric acid and ferulic acid (RT_{pCA}≈5.86min; RT_{FA}≈6.61min) (Fig. 3.3 for genotype sin09). Several smaller unidentified peaks, mostly with higher RTs than *p*CA and FA were also observed in the chromatograms.

FA content ranged from 0.19% to 0.63% of the cell wall dry weight, on a senesced leaf sample from genotype sin08 and in an actively growing stem sample of genotype sac01, respectively (Table 3.3). When considering all developmental stages together, no significant differences in FA content were detected between tissues (*P*=0.153; Table 3.4). However, at

individual developmental stages a barely significant difference between stem and leaf was detected at PB (P=0.033). As an average, FA content decreased as plants matured and growth ceased (Table 3.3). Similarly for leaf and stem, their FA contents were indistinguishable between PB and SS, but were significantly higher at AG, as indicated by the Tukey homogeneous groupings (Fig. 3.4).

Genotypes showed significant differences among themselves (P<0.001), and interesting relations between them were detected. The *M. sacchariflorus* (sac01) and the hybrid genotypes (hyb03, gig01) were the highest FA releasers in both tissues at most developmental stages (Table 3.3); with stem at AG being the exception, where sin08 released the second highest FA amount. Also exceptional for this genotype, is that despite its high FA content at AG, in subsequent developmental stages it consistently releases among the lowest FA in both tissues, alongside with genotype sin11.

In contrast to FA, *p*CA release was significantly different between tissues (P<0.001; Table 3.5). However, the observation that there are significant differences between the genotypes (P<0.001) is the same as for FA release. The highest *p*CA content was detected in a stem sample collected from hyb03 at PB (2.26%), and the lowest was in sin08 leaf, also from the PB developmental stage (0.42%) (Table 3.6). The highest or second highest *p*CA content is found in genotype gig01 in both tissues at all developmental stages. Remarkably, it was observed that at AG the ranking of genotypes in terms of *p*CA abundance is the same for leaf and stem. At PB and SS this was not true, but it was observed that the rankings did not change much between the two latest developmental stages, as genotypes gig01 and hyb03 consistently released the highest amounts, while sin15, sin09 and sin08 released the lowest (Table 3.6).

Overall standard deviations in *p*CA content were particularly high in stem samples (Table 3.6). It is likely that this high variation was the cause for no Tukey homogeneous groups being detected among the developmental stages in stem samples (Fig. 3.4). However, an overall effect

of development was detected as significant, although less significantly than other effects (P=0.016).

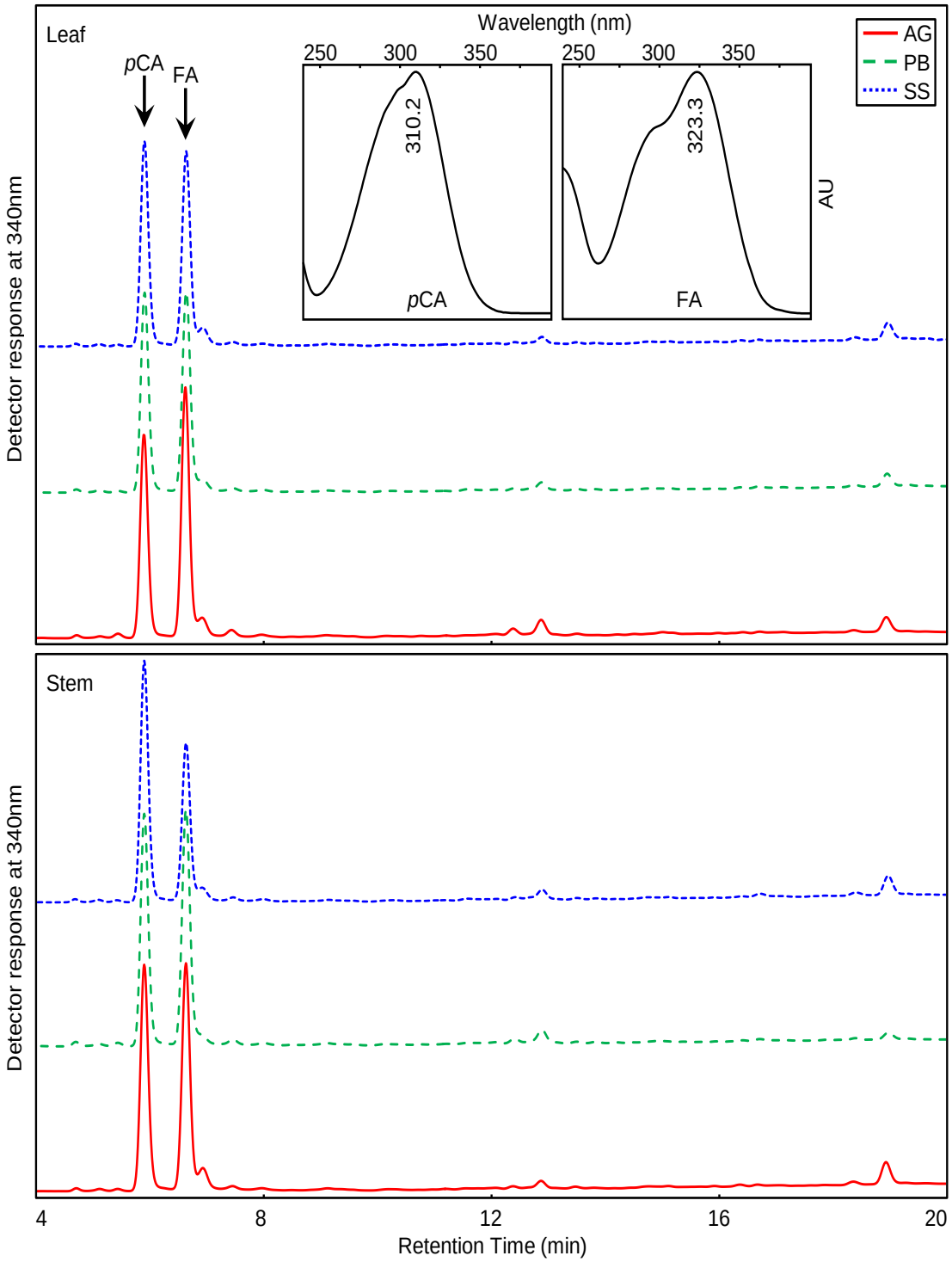

Fig. 3.3. RP-HPLC-DAD chromatograms measured at 340nm obtained after 1M KOH treatment of CWM from leaf and stem tissues of genotype sin09. Absorption spectra at the top correspond to the two predominant peaks in the chromatograms: *p*-coumaric (*p*CA) and ferulic acid (FA). Column void volume region (0-4min) and the portions of the chromatograms after the last peak (20min – 25min) are omitted. (AG: active growth; PB: peak biomass; SS: senescence; AU: arbitrary absorbance units)

Table 3.3. Ferulic acid release upon 1M KOH treatment of miscanthus CWM. Values are expressed as percentage of cell wall material dry weight (% CWM) and are the mean ± standard deviation at three developmental stages for each genotype. Values within a column sharing a letter in their superscript are not significantly different according to a Tukey's test (α=0.05).

	Ferulic acid (% CWM)					
	Active Growth		**Peak Biomass**		**Senescence**	
	Leaf	**Stem**	**Leaf**	**Stem**	**Leaf**	**Stem**
gig01	0.59 ± 0.04^{bc}	0.51 ± 0.05^{bc}	0.44 ± 0.02^{b}	0.43 ± 0.01^{b}	0.49 ± 0.09^{b}	0.38 ± 0.03^{cd}
hyb03	0.62 ± 0.02^{c}	0.45 ± 0.01^{b}	0.49 ± 0.03^{c}	0.59 ± 0.02^{c}	0.49 ± 0.07^{b}	0.52 ± 0.06^{e}
sac01	0.61 ± 0.01^{bc}	0.63 ± 0.07^{c}	0.41 ± 0.07^{b}	0.47 ± 0.05^{b}	0.33 ± 0.04^{ab}	0.44 ± 0.01^{de}
sin08	0.52 ± 0.02^{b}	0.58 ± 0.01^{bc}	0.21 ± 0.02^{a}	0.22 ± 0.02^{a}	0.19 ± 0.02^{a}	0.22 ± 0.01^{a}
sin09	0.28 ± 0.02^{a}	0.27 ± 0.02^{a}	0.24 ± 0.01^{a}	0.29 ± 0.05^{a}	0.24 ± 0.02^{a}	0.22 ± 0.01^{a}
sin11	0.25 ± 0.01^{a}	0.25 ± 0.01^{a}	0.22 ± 0.01^{a}	0.23 ± 0.02^{a}	0.20 ± 0.01^{a}	0.22 ± 0.01^{a}
sin13	0.28 ± 0.03^{a}	0.29 ± 0.05^{a}	0.33 ± 0.05^{ab}	0.28 ± 0.03^{a}	0.25 ± 0.05^{a}	0.23 ± 0.01^{ab}
sin15	0.26 ± 0.01^{a}	0.27 ± 0.02^{a}	0.21 ± 0.01^{a}	0.25 ± 0.01^{a}	0.20 ± 0.02^{a}	0.33 ± 0.01^{bc}
Mean	0.43 ± 0.17	0.41 ± 0.15	0.32 ± 0.11	0.35 ± 0.14	0.30 ± 0.13	0.32 ± 0.12

Table 3.4. ANOVA results for ferulic acid release determination.

All Developmental Stages

Effect	Degrees of freedom	Sum of squares	Mean square	*F*-ratio	*P*-value	Effect size (η^2)
Genotype	7	122.48	17.50	150.77	<0.0001	0.6575
Development stage	2	19.72	9.86	84.95	<0.0001	0.1058
Tissue	1	0.25	0.25	2.11	0.1527	0.0013
Genotype × Development stage	14	28.35	2.03	17.45	<0.0001	0.1522
Genotype × Tissue	7	3.83	0.55	4.71	0.0004	0.0206
Development stage × Tissue	2	1.01	0.50	4.33	0.0186	0.0054
Genotype × Development stage × Tissue	14	5.09	0.36	3.13	0.0016	0.0273
Error	48	5.57	0.12			
Total	95	186.29				

Active Growth

Effect	Degrees of freedom	Sum of squares	Mean square	*F*-ratio	*P*-value	Effect size (η^2)
Genotype	7	71.71	10.24	106.23	<0.0001	0.9287
Tissue	1	0.28	0.28	2.92	0.1070	0.0036
Genotype × Tissue	7	3.68	0.53	5.46	0.0024	0.0477
Error	16	1.54	0.10			
Total	31	77.22				

Peak Biomass

Effect	Degrees of freedom	Sum of squares	Mean square	*F*-ratio	*P*-value	Effect size (η^2)
Genotype	7	42.30	6.04	58.19	<0.0001	0.9229
Tissue	1	0.57	0.57	5.46	0.0328	0.0124
Genotype × Tissue	7	1.30	0.19	1.79	0.1578	0.0284
Error	16	1.66	0.10			
Total	31	45.83				

Senescence

Effect	Degrees of freedom	Sum of squares	Mean square	*F*-ratio	*P*-value	Effect size (η^2)
Genotype	7	36.83	5.26	35.57	<0.0001	0.8460
Tissue	1	0.40	0.40	2.72	0.1184	0.0093
Genotype × Tissue	7	3.93	0.56	3.80	0.0128	0.0903
Error	16	2.37	0.15			
Total	31	43.53				

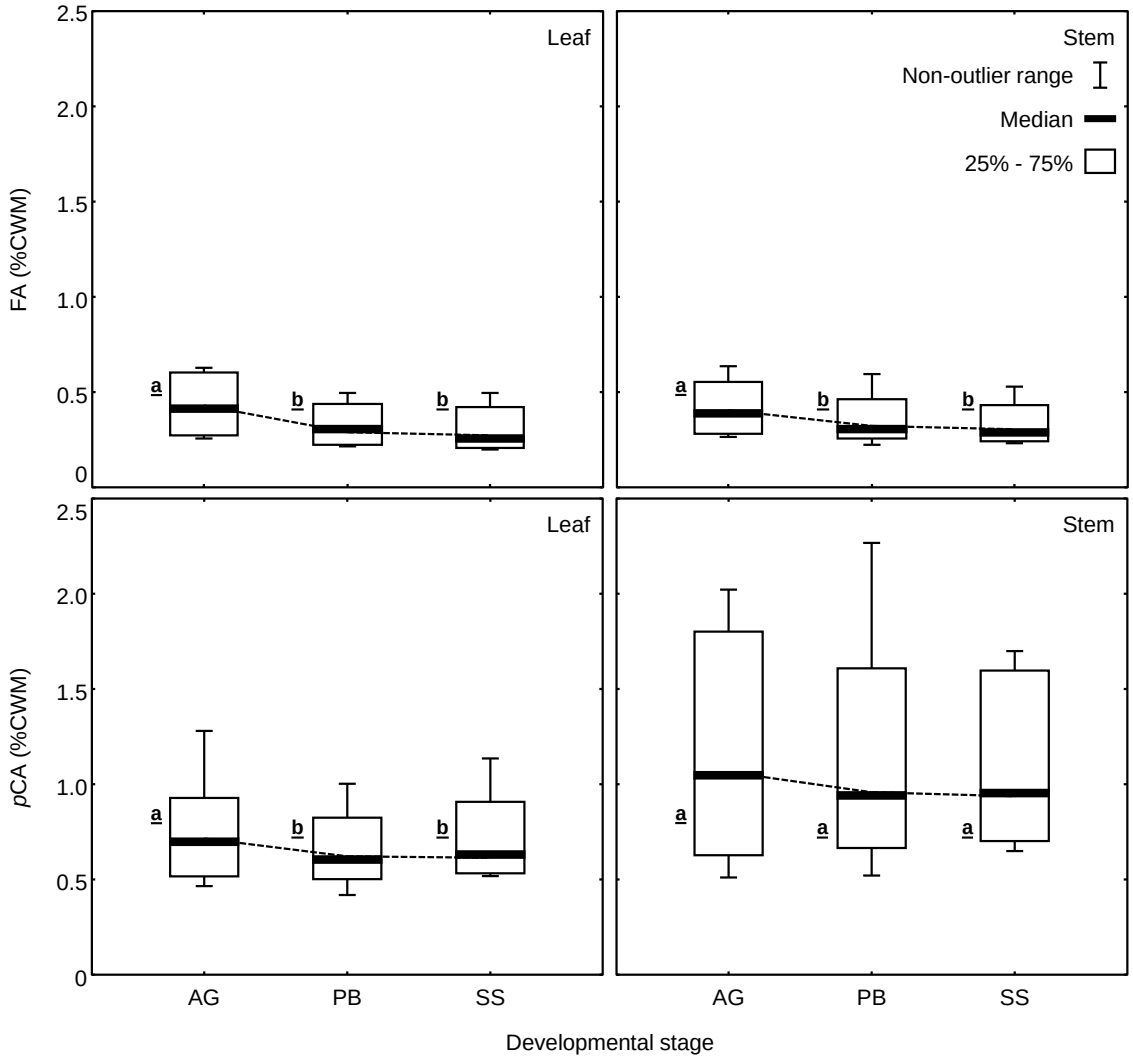

Fig. 3.4. Distribution of measurements of ferulic (FA) and *p*-coumaric (*p*CA) acid released upon 1M KOH treatment of miscanthus CWM. Values are expressed as percentage of cell wall material dry weight (% CWM) from leaf and stem tissue for 8 miscanthus genotypes at active growth (AG), peak biomass (PB) and senescence (SS). The non-outlier range is defined as the range of values which fall outside 1.5× the interquartile range of the distribution (height of the 25% – 75% box). Not significantly different developmental stages are indicated by a common underlined letter next to the box (Tukey's test at α=0.05).

Table 3.5. ANOVA results for *p*-coumaric release determination.

All Developmental Stages

Effect	Degrees of freedom	Sum of squares	Mean square	*F*-ratio	*P*-value	Effect size (η^2)
Genotype	7	1101.48	157.36	174.43	<0.0001	0.5044
Development stage	2	8.20	4.10	4.54	0.0156	0.0038
Tissue	1	445.65	445.65	494.03	<0.0001	0.2041
Genotype × Development stage	14	257.88	18.42	20.42	<0.0001	0.1181
Genotype × Tissue	7	191.40	27.34	30.31	<0.0001	0.0876
Development stage × Tissue	2	3.93	1.96	2.18	0.1246	0.0018
Genotype × Development stage × Tissue	14	131.89	9.42	10.44	<0.0001	0.0604
Error	48	43.30	0.90			
Total	95	2183.73				

Active Growth

Effect	Degrees of freedom	Sum of squares	Mean square	*F*-ratio	*P*-value	Effect size (η^2)
Genotype	7	532.03	76.01	133.85	<0.0001	0.6393
Tissue	1	148.48	148.48	261.49	<0.0001	0.1784
Genotype × Tissue	7	142.63	20.38	35.88	<0.0001	0.1714
Error	16	9.09	0.57			
Total	31	832.23				

Peak Biomass

Effect	Degrees of freedom	Sum of squares	Mean square	*F*-ratio	*P*-value	Effect size (η^2)
Genotype	7	491.25	70.18	82.79	<0.0001	0.5933
Tissue	1	184.70	184.70	217.89	<0.0001	0.2231
Genotype × Tissue	7	138.44	19.78	23.33	<0.0001	0.1672
Error	16	13.56	0.85			
Total	31	827.96				

Senescence

Effect	Degrees of freedom	Sum of squares	Mean square	*F*-ratio	*P*-value	Effect size (η^2)
Genotype	7	336.08	48.01	37.20	<0.0001	0.6521
Tissue	1	116.40	116.40	90.18	<0.0001	0.2259
Genotype × Tissue	7	42.22	6.03	4.67	0.0051	0.0819
Error	16	20.65	1.29			
Total	31	515.35				

Table 3.6. *p*-Coumaric acid release upon 1M KOH treatment of miscanthus CWM. Values are expressed as percentage of cell wall material dry weight (% CWM) and are the mean ± standard deviation at three developmental stages for each genotype. Values within a column sharing a letter in their superscript are not significantly different according to a Tukey's test (α=0.05).

***p*-Coumaric acid (% CWM)**						
	Active Growth		**Peak Biomass**		**Senescence**	
	Leaf	**Stem**	**Leaf**	**Stem**	**Leaf**	**Stem**
gig01	0.93 ± 0.08^{b}	2.02 ± 0.21^{b}	0.87 ± 0.05^{cd}	1.88 ± 0.02^{d}	1.13 ± 0.22^{b}	1.67 ± 0.19^{b}
hyb03	1.27 ± 0.03^{c}	1.34 ± 0.01^{c}	1.00 ± 0.07^{d}	2.26 ± 0.06^{d}	1.11 ± 0.13^{b}	1.69 ± 0.20^{b}
sac01	0.87 ± 0.01^{b}	1.85 ± 0.16^{b}	0.69 ± 0.13^{bc}	1.34 ± 0.25^{c}	0.70 ± 0.10^{ab}	1.52 ± 0.04^{b}
sin08	0.92 ± 0.04^{b}	1.74 ± 0.05^{b}	0.42 ± 0.05^{a}	0.52 ± 0.07^{a}	0.51 ± 0.06^{a}	0.65 ± 0.04^{a}
sin09	0.46 ± 0.01^{a}	0.53 ± 0.01^{a}	0.49 ± 0.01^{ab}	0.55 ± 0.09^{ab}	0.54 ± 0.09^{a}	0.67 ± 0.09^{a}
sin11	0.52 ± 0.01^{a}	0.71 ± 0.04^{a}	0.52 ± 0.00^{ab}	0.81 ± 0.10^{ab}	0.62 ± 0.04^{a}	0.90 ± 0.01^{a}
sin13	0.50 ± 0.06^{a}	0.51 ± 0.08^{a}	0.78 ± 0.07^{cd}	0.99 ± 0.12^{bc}	0.64 ± 0.13^{a}	0.99 ± 0.05^{a}
sin15	0.53 ± 0.01^{a}	0.75 ± 0.01^{a}	0.50 ± 0.03^{ab}	0.77 ± 0.02^{ab}	0.52 ± 0.08^{a}	0.72 ± 0.01^{a}
Mean	0.75 ± 0.29	1.18 ± 0.63	0.66 ± 0.21	1.14 ± 0.64	0.72 ± 0.25	1.10 ± 0.45

3.2.3.1. Effect of 0.1M KOH on the Release of Ester-Linked Hydroxycinnamates

In the following chapter, a pretreatment using 0.1M KOH will be employed before enzymatic hydrolysis of the biomass. Consequently, it was considered pertinent to determine the effect of 0.1M KOH on the release of ester-linked hydroxycinnamates. As for the estimation of acetyl-esterification (Section 3.1), extractions with 0.1M KOH were also performed on a subset of the samples, in order to evaluate its effect in comparison with 1M KOH. Treatment with 0.1M KOH was performed on the CWM from leaf and stem collected at AG, PB and SS from genotypes: gig01, sac01 and sin08. The amounts of both HCAs assessed were lower when extracted with the less concentrated solution, but no consistency was apparent in terms of the percentages extracted with 0.1M in comparison with 1M KOH (Table 3.7). However, the impact of increasing the molarity was more evident for *p*CA, since the differences between the 1M and 0.1M KOH extractions were consistently lower for the FA yields.

Table 3.7. Ferulic and *p*-coumaric acid release upon 0.1M KOH treatment of miscanthus CWM. Values are expressed as percentage of cell wall material dry weight (% CWM). Values inside parenthesis indicate the percent differences between the amount extracted with 1M KOH and 0.1M KOH (also see Tables 3.3 and 3.6).

	gig01	sac01	sin08	Mean
Active Growth				
Leaf				
Ferulic acid	0.39 (-33.90)	0.51 (-16.39)	0.48 (-7.69)	0.46 (-19.33%)
p-Coumaric acid	0.37 (-60.22)	0.47 (-45.98)	0.49 (-46.74)	0.44 (-50.98%)
Stem				
Ferulic acid	0.33 (-34.00)	0.52 (-17.46)	0.40 (-31.03)	0.42 (-27.50%)
p-Coumaric acid	0.49 (-75.74)	0.70 (-62.16)	0.50 (-71.26)	0.56 (-69.72%)
Peak Biomass				
Leaf				
Ferulic acid	0.29 (-34.09)	0.36 (-12.20)	0.20 (-4.76)	0.28 (-17.02%)
p-Coumaric acid	0.31 (-64.37)	0.37 (-46.38)	0.33 (-21.43)	0.34 (-44.06%)
Stem				
Ferulic acid	0.25 (-41.86)	0.37 (-21.28)	0.20 (-9.09)	0.27 (-24.08%)
p-Coumaric acid	0.39 (-79.26)	0.50 (-62.69)	0.29 (-44.23)	0.39 (-62.06%)
Senescence				
Leaf				
Ferulic acid	0.37 (-24.49)	0.30 (-9.09)	0.18 (-5.26)	0.28 (-12.95%)
p-Coumaric acid	0.43 (-61.95)	0.44 (-37.14)	0.44 (-15.38)	0.44 (-38.16%)
Stem				
Ferulic acid	0.22 (-42.11)	0.32 (-27.27)	0.19 (-13.64)	0.24 (-27.67%)
p-Coumaric acid	0.42 (-74.85)	0.47 (-69.08)	0.42 (-35.38)	0.44 (-59.77%)

3.2.4. Discussion

The saponification of miscanthus CWM with solutions of 1M KOH, followed by RP-HPLC-DAD has led to the detection and quantification of HCAs ester-linked to wall polymers (Lam *et al.*, 1990; Ishii, 1997b). Most abundant compounds were identified as *p*CA and FA in all samples analysed. Other peaks, significantly less prominent than *p*CA and FA and with higher RTs were also detected but not identified (Fig. 3.3). It is known that in the plant cell wall a substantial proportion of FA undergoes oxidative coupling, forming a large array of diferulates, which possess different properties not only from monomers but also among themselves, as different dimer linking patterns do occur (Grabber *et al.*, 2004). In RP-HPLC the solid phase is non-polar relative to the polar solvent, this implies that compounds which elute faster than others (i.e., have lower RTs) are more polar. Conversely, slower eluting compounds (i.e., higher RT) are less polar by comparison. Diferulates are typically less polar and, generally have higher RTs than FA monomers (Waldron *et al.*, 1996), so it is likely that unidentified peaks with RTs over 6.61min could correspond to dimers or other oligomers of FA. Furthermore, various forms of ester-bound diferulates have been reported to occur in miscanthus cell walls (Lygin *et al.*, 2011). Additionally, some of the peaks could possibly correspond to caffeic or sinapic acids, since soluble esters of these phenolic acids also occur in the cell wall of grass species (Grabber *et al.*, 2004; Allison *et al.*, 2009).

Wide variability in *p*CA content was observed among the genotypes, particularly in stem samples (Table 3.6 and Fig. 3.4). This is somewhat similar to the data reported by Hatfield *et al.* (2009), who observed higher variation in *p*CA than in FA contents across various grass species. Bonding of *p*CA to lignin occurs mostly by esterification to lignin S units (Grabber *et al.*, 2004), so it is expected that higher levels of *p*CA occur in tissues containing also higher proportions of S-lignin. This is in accordance with the prediction made by FTIR-PCA that stems contain higher S-lignin (Section 2.3.4), and has also been observed in miscanthus by Le

Ngoc Huyen *et al.* (2010). *p*-Coumaric acid was the major saponifiable phenolic compound detected in the samples analysed, which is in accordance with published data for miscanthus (Le Ngoc Huyen *et al.*, 2010; Lygin *et al.*, 2011). Nonetheless, it has been reported that FA content of grass cell walls generally exceeds the *p*CA content (Lozovaya *et al.*, 1999). Therefore, it is important to note that despite *p*CA being the most abundantly detected HCA, FA may indeed be more abundant in the cell wall. There could be various reasons for this. Firstly, since a big portion of FA is ether-linked to cell wall components it is not released during room temperature alkaline treatments (Ishii, 1997b; Lozovaya *et al.*, 1999; Grabber *et al.*, 2004; Li *et al.*, 2014b). Secondly, some phenols may have been lost during the procedure, because while *p*-coumaroyl groups predominantly link to lignin, feruloyl groups can establish ester and ether links with hemicelluloses and other polysaccharides, which are acid precipitated during the sample preparation (Lozovaya *et al.*, 1999; Várnai *et al.*, 2014). Therefore, it is possible that these precipitates may contain ether-linked phenolics, which consequently are not detected under the employed conditions. Thirdly, it has been reported that some linkage patterns involved in FA binding to lignin are not cleanly cleaved by known chemical processes, and therefore total FA content in grass cell walls cannot be measured accurately with current chemical methods (Ralph *et al.*, 1995; Hatfield *et al.*, 2009). Ultimately, most studies reporting higher proportions of FA were not performed in miscanthus cell wall and, as abovementioned, the values here obtained are comparable to values seen in other miscanthus studies; as a result they do allow for a comparative assessment of HCA abundances across developmental stages, tissues and genotypes.

High *p*CA to FA ratios have been associated to low cell wall degradability (Hartley, 1972; Jung *et al.*, 1991; Du *et al.*, 2009). In the samples here analysed, for each genotype, the *p*CA to FA ratio was generally higher in the stem samples of a given developmental stage (Fig. 3.5); and this is consistent with data reported for miscanthus (Lygin *et al.*, 2011) and for

Brachypodium distachyon (Molinari *et al.*, 2013). However, there were some exceptions; namely, among the *M. sinensis* genotypes sin09, sin13 and sin15. Overall, the *p*CA to FA ratio varied from 1.43 to 4.36, with the lowest ratio being found in the leaf of the *M. sacchariflorus* genotype collected at AG, and the highest being in *M.* × *giganteus* senesced stems. These ratios and also the absolute amounts of HCAs are in close agreement with previously reported values for miscanthus (Le Ngoc Huyen *et al.*, 2010; Lygin *et al.*, 2011). Additionally, it is known that grasses with C_4 photosynthesis typically release higher levels of *p*CA than their C_3 counterparts (Hatfield *et al.*, 2009).

Ester-linked HCA contents were not different between the cell wall of mature plants (PB and SS), but actively growing plants did typically have higher amounts of both HCAs studied. This is probably related to the mechanisms involved in the deposition of secondary wall, which is much more abundant in mature than in actively growing plants. It is known that the concentrations of alkali-labile HCAs initially increase during primary wall formation and then peak and decline after secondary wall formation and lignification (Grabber *et al.*, 2004). Higher concentrations of HCAs in the earlier stages of tissue lignification are also in accordance with reports that most *p*CA accretion occurs in tandem with lignin deposition (Grabber *et al.*, 2004), and that ferulates may act as initiation or nucleation sites for lignin polymers (Ralph *et al.*, 1995). Additionally, miscanthus cell walls contain lower amounts of lignin while they are actively growing (Section 2.4), and it is possible that in these condition phenolic acids play important structural roles. In support of this is the fact that FA contents increase substantially in transgenic plants with down-regulated cinnamoyl-CoA reductase, an enzyme involved in the synthesis of lignin precursors (Piquemal *et al.*, 1998). In a similar way, it is possible that when lignin content is lower, such as in actively growing tissues, higher levels of ferulate cross-links serve the function of providing supplemental structural support.

On a different note, the fact that *p*CA is associated to lignin deposition, and the observation that the ranking of genotypes in terms of *p*CA content was relatively constant between PB and SS developmental stages, this could indicate that cell wall composition becomes more unaltered after plant maturation is achieved and the bulk of lignin has been deposited in secondary walls. A similar trend has been observed in section 2.3 (Fig. 2.4 D and E), where the analysis of FTIR data suggested that in stems clear separate clusters are formed according to mature and immature tissues as a result of lower compositional variation as secondary walls are deposited in stem tissues.

Ferulate or diferulate-mediated cross-linking of cell wall polymers is known to negatively correlate with lignocellulose digestion and conversion efficiency (Saulnier *et al.*, 1999; Grabber *et al.*, 2004; Lygin *et al.*, 2011), but the removal of alkali labile phenolics by chemical treatment can be used to increase the biodegradability of CWM (Ishii, 1997b; Buanafina *et al.*, 2006). By treating the miscanthus lignocellulose with 1M KOH, a significant portion of the cell wall HCAs is extracted; however, solutions of this molarity cause a significant removal of matrix polysaccharides, particularly of xylans (Section 5.1). Additionally, by using 1M NaOH solutions, Si *et al.* (2015) have reported that lignin in the cell wall may be at least partially modified when more concentrated alkaline solutions are used. As a consequence, despite the utilisation of higher molarity alkaline solutions for characterisation of HCA content, if the aim is merely their removal to improve cell wall digestibility, then lower molarities would be preferable, as they cause a negligible loss of wall polysaccharides (Section 3.1). To this effect, extractions of HCAs with 0.1M KOH solution were also performed. Their yields were compared to those of 1M KOH (Table 3.7) and it was revealed that 0.1M KOH extractions were less efficient when the removal of total HCAs considered. It was also observed that the difference between the two extraction methods was more evident in the amounts of *p*CA (Table 3.7). By contrast, extracted FA was generally more similar between the two

concentrations, and in leaves the overall difference between methods decreased throughout development. FA is involved in cell wall cross-linking, while most *p*CA in the cell wall is ester-linked to lignin, without being attached to other cell wall polymers (Chabbert *et al.*, 1994; Ralph *et al.*, 1994a; Grabber *et al.*, 2004). As a result, the detected increases in the yields of *p*CA after 1M KOH treatment, in comparison to 0.1M, should not reduce recalcitrance proportionally to the molarity difference. It is expected that an eventual increase in enzymatic sugar yields, solely attributed to the effect of removing HCAs from the cell wall, will not be proportional to the molarity increase from 0.1M to 1M KOH.

Taking this into account, and that 0.1M does not cause substantial losses of cell wall polymers, it was considered that a pretreatment performed with 0.1M KOH would be preferable to be used as part of a screening of CWM recalcitrance to enzymatic saccharification; as the one included in the following chapter; as it is an effective method to break cross-links while minimising polysaccharide degradation.

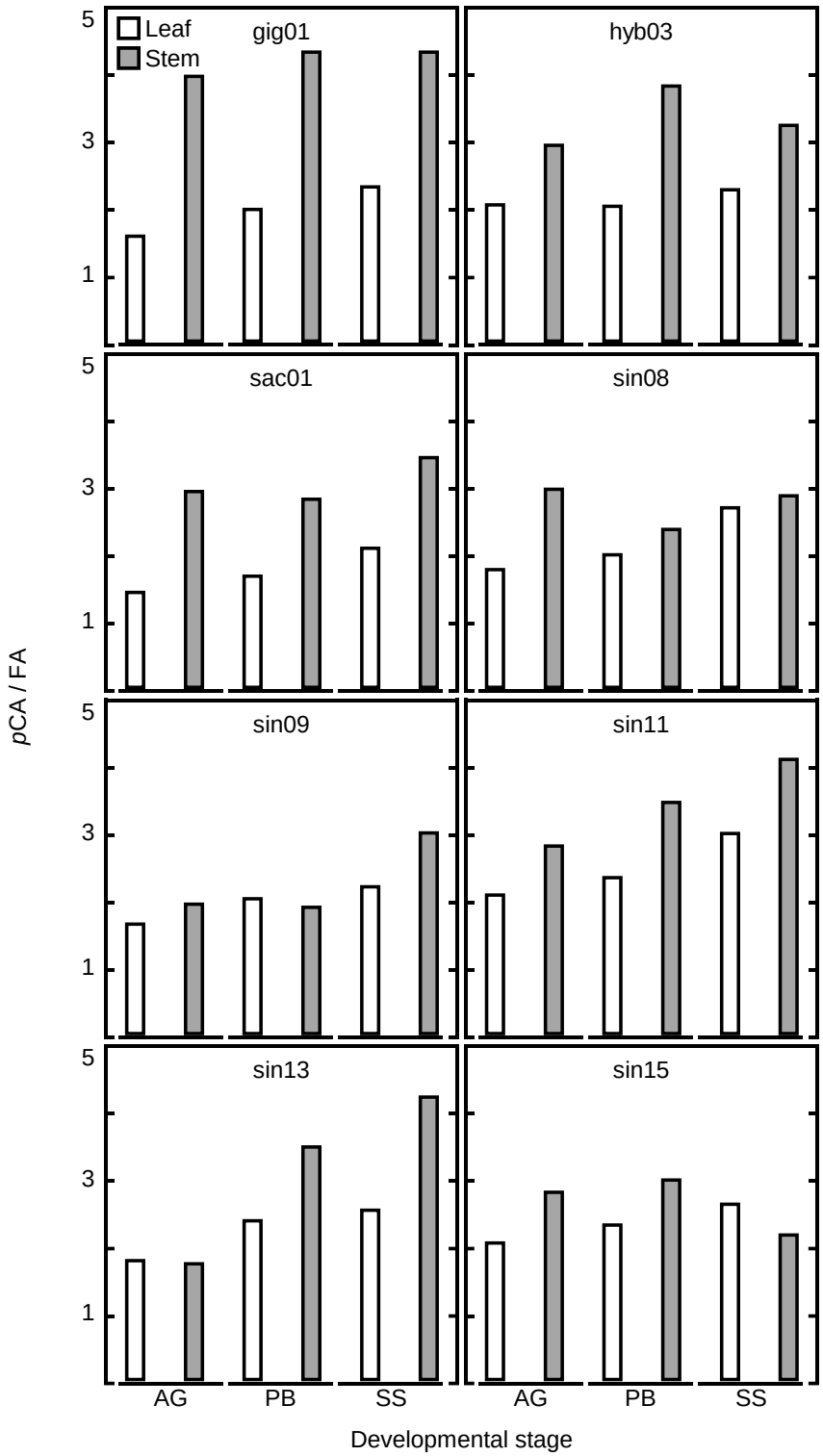

Fig. 3.5. Ratios of cell wall ester-bound *p*-coumaric acid (*p*CA) to ferulic acid (FA). Developmental stages are: active growth (AG), peak biomass (PB) and senescence (SS).

3.3. CONCLUSIONS

In leaf tissues, acetate release increased and HCAs decreased as plants matured, and therefore it was possible that these two cell wall features could inversely vary throughout development. As a result, correlation coefficients were determined between FA and *p*CA content, and acetate release; to detect if there was proportionality between acetylation and hydroxycinnamoylation in miscanthus cell wall biomass (Fig. 3.6). However, the correlation coefficients were low, particularly in the correlation with *p*CA ($r_{acetate \times FA}$=-0.40; $r_{acetate \times pCA}$=0.03), and only the correlation with FA was significant ($P_{acetate \times FA}$=0.0044; $P_{acetate \times pCA}$=0.8044). In this case, there was in fact an inverse proportionality between the two variables.

Significant differences were observed in the relative abundances of ester-linked acetyl groups and HCAs across different tissues, developmental stages and genotypes. Compositional distinctiveness between these levels were in part predicted by the FTIR-PCA approach; that significant structural differences occur between the carbohydrate fractions of CWM collected from different tissues immature or mature tissues (Section 2.6). This conclusion can now be expanded to the fact that differences also occur in the cross-linking of these fractions. Furthermore, it is likely that tissue- and development-derived compositional differences will also have an impact on distinct degrees of cell wall degradation.

By de-acetylating lignocellulosic biomass, it is expected that recalcitrance will be reduced (Grohmann *et al.*, 1989; Kong *et al.*, 1992; Chen *et al.*, 2012). Firstly, it is known that acetate can depress enzymatic hydrolysis of polysaccharides; thus by releasing and removing acetate from the samples, the negative effect of this compound on saccharification is reduced (Selig *et al.*, 2009; Agger *et al.*, 2010; Chen *et al.*, 2012). Secondly, fermentation yields are enhanced, since the acetate toxic effect is greatly reduced if it is removed prior to the inoculation with the fermenting microbes (Chen *et al.*, 2012; Gille and Pauly, 2012). On the

other hand, the removal of ester-linked HCAs is expected to affect cell wall polymer cross-linking, which in turn will interfere with cell wall integrity (Ishii, 1997b; Ralph, 2010), thus facilitating the degradation of CWM. Furthermore, although the mechanism is not well understood, the fermentation of the saccharification products may also be enhanced by HCA removal, as phenolics may have a toxic effect on fermenting microbes, presumably as a result of interference with cell membrane function and modification of protein-to-lipid ratios (Keweloh *et al.*, 1990; Jönsson *et al.*, 2013). As a consequence, it is relevant not only to anticipate the amounts of ester-linked compounds released from the cell wall during downstream processing, but also to develop procedures to de-esterify the biomass while maximising sugar retention. The treatment of CWM with 0.1M KOH could represent a way to achieve both objectives.

Here, it was shown that by treating cell wall biomass with 0.1M KOH, substantial amounts of esterified compounds are released without significantly affecting other fractions of the cell wall. As a result, the data gathered in this chapter suggest that the effect of the 0.1M KOH pretreatment is primarily associated to the removal of hydroxycinnamoyl and acetyl substituents from the cell wall biomass.

The impact of treating CWM with low molarity alkaline solutions will be further discussed in following chapters. Therefore, the information gathered from the analyses of KOH-treated CWM is particularly relevant for the understanding of the effect of an alkaline pretreatment on the improvement of saccharification yields (chapter 4), and the effect of a base treatment used to increase recognition of cell wall polysaccharide epitopes during *in situ* immunolabelling (chapter 5).

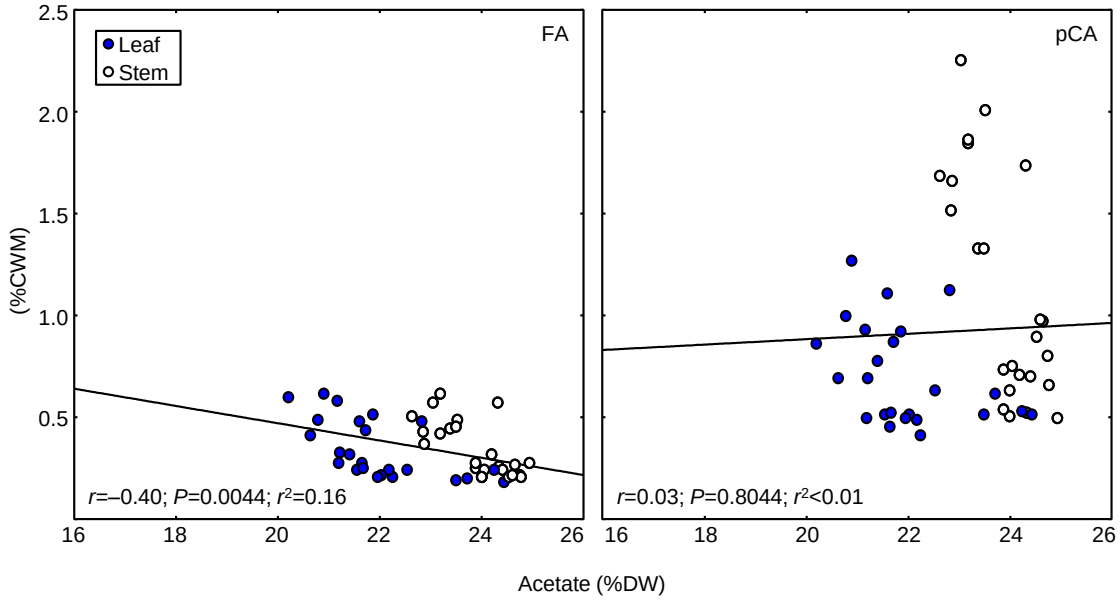

Fig. 3.6. Least square fit of acetate percentage vs. ferulic (FA) and *p*-coumaric (*p*CA) acids, with the associated Pearson correlation statistics (*r*) and probabilities (*P*) for 8 miscanthus genotypes during all developmental stages combined.

4. CELL WALL MONOSACCHARIDES AND SACCHARIFICATION

4. CELL WALL MONOSACCHARIDES AND SACCHARIFICATION

As has been shown in chapter 3, the composition of ester-bound components involved in the linking between cell wall polymers can vary significantly between miscanthus CWM from different developmental stages, tissues and genotypes. However, this type of linkage, designated a cross-link, consists of individual chemical bonds that join together two otherwise separate polymers (e.g., phenolic coupling products) (Fry, 2010). According to this definition, cross-links do not include other types of linkages, such as glycosidic bonds, which have well-defined bonding positions depending on the anomeric centres involved in the linking of the saccharides. Essentially, cross-linking and glycosidic-linking are distinct given the fact that glycosidic bonds never differ in their fundamental nature from any other glycosidic linkage (Fry, 2010); thus producing what is in effect merely a large polysaccharide, albeit with different domains. An example of a network involving glycosidic bonds is the tethering of cellulose microfibrils by hemicelluloses, which in turn can link other polysaccharides, to form the complex matrix of heteropolymers that hinders cell wall saccharification (Himmel and Picataggio, 2008).

As a result, the enhancement of the cost-effectiveness of lignocellulosic biomass utilisation is to a large extent dependent on being able to analyse cell wall fine structures, which in turn relies on the extraction of constituent polysaccharides. Cell wall polysaccharides are best investigated if in aqueous solutions; however, most of them are not water extractable (Fry, 1988). In these cases there are two alternatives. One approach consists of using a series of sequentially more powerful extractants, in order to release cell wall polysaccharides. This will be discussed further in chapter 5. Another approach resorts to deliberate partial degradation of the cell wall, using methodologies to cause partial cleavage of polysaccharide backbones (e.g., acid and enzymatic hydrolysis treatments), which render most of the wall polysaccharides

water soluble. This strategy is the most common procedure for determining the structure of complex polymers, as it yields the constituent monosaccharides and oligosaccharides, which are then separated and investigated by a variety of analytical methodologies (Fry, 1988). By using hydrolysis treatments, individual amounts of the monosaccharides can be determined and then summed to give total sugar contents. Although these procedures do not identify parent polysaccharides, they enable structural predictions, since the typical monosaccharides yielded from cell wall deconstruction have been previously characterised (Melton and Smith, 2001) (Appendix B).

This chapter will mainly characterise and discuss the miscanthus cell wall carbohydrate composition by liquid chromatography, following acid and enzymatic hydrolysis of the CWM. Furthermore, it will also assess the total carbohydrate content and the effect of an alkaline pretreatment on the enhancement of saccharification.

4.1. Total Carbohydrate and Monosaccharide Contents of the Cell Wall

4.1.1. Overview

Depolymerisation of cellulose and other cell wall glycosides can be achieved by similar mechanisms (Rinaldi and Schüth, 2009), which frequently rely on the fact that glycosidic bonds are acid-labile and thus may be hydrolysed in the presence of acid catalysts (Morales-delaRosa *et al.*, 2014). Therefore, methodologies for the analysis of the sugars present in plant cell walls most frequently involve hydrolysis steps, and two commonly used reagents are trifluoroacetic acid (TFA) and sulphuric acid (H_2SO_4). Cell wall hydrolysis with TFA requires shorter reaction times than with H_2SO_4. From this point of view TFA is procedurally more advantageous than H_2SO_4 (Fengel and Wegener, 1979); however, cellulose is relatively resistant to hydrolysis in TFA, although small proportions may be degraded under long hydrolysis times and if its crystallinity is previously compromised (Pettolino *et al.*, 2012). Accordingly, TFA is typically used for the analysis of the more easily extracted matrix polysaccharides, while harsher H_2SO_4 treatments are used for more complete cell wall hydrolysis. A procedure first developed by Saeman *et al.* (1963), modified by Hatfield *et al.* (1999c) and later standardised in an analytical procedure produced by the National Renewable Energy Laboratory (NREL) (Sluiter *et al.*, 2012), is used here to achieve cell wall depolymerisation. This method consists of a two-step acid hydrolysis, where CWM is initially dissolved in H_2SO_4 at high concentration and low temperature, followed by polysaccharide hydrolysis at a higher temperature but lower H_2SO_4 concentration.

Following acid hydrolysis of CWM, the released monosaccharides may be analysed by liquid chromatography. Several forms of HPLC are useful for the separation of monosaccharides and oligosaccharides in cell wall hydrolysates. One of such forms, frequently

abbreviated as HPAEC-PAD, consists of a high-performance anion-exchange chromatography system coupled to a pulsed amperometric detector. HPAEC is a method to separate anionic analytes, yet cell wall monosaccharides are not anions in their common form. However, by using chromatographic eluents at high pH, carbohydrates may be ionised. The reason for this is that most cell wall monosaccharides have dissociation constants (pK_a) in the range 12–14 (e.g., Xyl: 12.15, Glc: 12.28, Gal: 12.39, Ara: 12.43) and are in fact weak acids. As a result, at high pH values the hydroxyl groups of these sugars are partially or totally transformed into oxyanions and may be separated by anion-exchange mechanisms (Zhang and Lee, 2002). HPAEC, thus relies on the usage of alkaline eluents to generate anions, an approach that would not be possible with classical silica-based columns; as these matrices would dissolve at high pH. Historically the development of new column packing materials for HPAEC has been almost exclusively undertaken by Dionex Inc. (Zhang and Lee, 2002). Most notably, the CarboPac series of columns has been specifically designed for carbohydrate anion-exchange chromatography (Dionex, 2000). Within this range, the CarboPac SA10 column has been developed to provide a fast and well resolved separation for most monosaccharides and disaccharides in biofuel research, and is packed with a hydrophobic, polymeric, porous resin, coated with a strong anion-exchange layer of latex nano beads (Dionex, 2013). By using these column packing materials and high pH eluents, cell wall carbohydrates are separated by interaction with quaternary ammonium cation functional groups, and may be eluted in a single run where higher retention times correspond to lower pK_a value (Corradini *et al.*, 2012).

Other types of detector may be used coupled to HPAEC, but PAD is considered superior since it provides advantages in terms of speed and sensitivity, with excellent signal-to-noise ratio even at extremely low analyte concentrations, without requiring derivatisation (Swadesh, 2000). Detection of carbohydrates is achieved by measuring the electrical current generated by their oxidation at the surface of a gold electrode. Only compounds which contain oxidisable

functional groups at the used voltage are detected, and by using optimised waveforms, sensitivity for carbohydrates can be adjusted so it is orders of magnitude greater than for other classes of analytes (Dionex, 2000).

High sensitivity and lack of need for sample derivatisation represent the major advantages of HPAEC-PAD over other methods for carbohydrate detection and quantification. Additionally, no extensive sample preparation is required for analyte detection, since neutral or cationic sample components elute within the void volume of the column, and thus do not usually interfere with analysis of the carbohydrate components of interest (Dionex, 2000; Swadesh, 2000).

The convenience provided by HPAEC-PAD analysis, allied to the efficiency of a modified version of the Saeman *et al.* (1963) method is used in this section to analyse the total abundance of the neutral sugars that compose cell wall polysaccharides. This information alone is relevant, since it enables inferences to be drawn as to how cell wall composition varies throughout development and between tissues and genotypes. Furthermore, information about monosaccharide composition generated in these studies will be relevant to interpreting studies on saccharification described in the subsequent section.

4.1.2. Materials and methods

An acid hydrolysis procedure based on the method described by Sluiter *et al.* (2012) was performed on leaf and stem samples collected from 8 miscanthus genotypes at three developmental stages. Approximately 10mg of the previously prepared CWM (Section 2.2) was weighed into 10mL Pyrex glass tubes fitted with polypropylene caps. 100µL of 72% (w/w) H_2SO_4 was added, the tubes were capped and placed on a heating block set at 30°C for 1h, during which time the samples were mixed every 10min using a vortex mixer. Subsequently, 2500µL of deionised water was added to dilute the acid in solution to 4% (w/w) H_2SO_4[*], samples were mixed to eliminate phase separation, and the sealed tubes were placed in an autoclave at 121°C for 1h. Once at room temperature, the tubes were centrifuged to produce a particulate-free supernatant, and the samples were diluted ten-fold (1:10) by taking 100µL of each sample and mixing with 900µL of deionised water.

Immediately before HPAEC-PAD analysis, samples were diluted once again, this time to a factor of 1:200 and had their pH increased to 7 – 9. This was achieved by mixing 50µL of the 1:10-diluted samples with 950µL of a solution of 0.015M KOH[†]. Aliquots of 400µL of the

[*] By adding 2500µL H_2O the samples are diluted to 4% (w/w) H_2SO_4:
Density 72% H_2SO_4= $d_{72\%\ H2SO4}$= 1.634g/mL
Density H_2O= d_{H2O}=1.00g/mL
Density 4% H_2SO_4= $d_{4\%\ H2SO4}$= 1.025g/mL
Densities taken from Green and Perry (1997)

A. Total weight of 100µL 72% H_2SO_4:
0.10mL 72% H_2SO_4 × $d_{72\%\ H2SO4}$= 0.163g 72% H_2SO_4

B. Composition of 100µL 72% H_2SO_4:
0.163g 72% H_2SO_4 × 72% (acid weight)= 0.118g H_2SO_4
0.163g 72% H_2SO_4 × 28% (water weight)= 0.046g H_2O

C. Concentration of H_2SO_4 after adding 2500µL deionised water:

$$\frac{0.118\text{g } H_2SO_4}{0.163\text{g } 72\%\ H_2SO_4 + 2.5\text{g } H_2O} = 0.044\text{g } H_2SO_4 \text{ per } g \approx 4\%\ (w/w)\ H_2SO_4$$

[†] Given that HPAEC-DAD does not require sample derivatisation, three sample dilution steps were performed during sample preparation, and since only small amounts of the original hydrolysate are injected for chromatographic analysis, no further sample clean-up was deemed to be necessary, except for sample neutralisation. This practice is supported by a Thermo Scientific application note, which states that

diluted samples were then filtered through 0.45μm nylon filter-vials (Thomson SINGLE StEP; Thomson Instrument Company, Oceanside, California, USA). Separation of released carbohydrates was conducted on an ICS-5000 ion chromatography system (Dionex, Sunnyvale, California, USA) operated at 45°C using a CarboPac SA10 (4×250mm) column with a CarboPac SA10G (4×50mm) guard column. An eluent generator coupled to the system continuously prepared a KOH solution at 0.001M for isocratic elution at a flow rate of 1.5mL/min for 14min. In all cases, a volume of 10μL of sample was injected into the column and detection consisted of pulsed amperometric detection (PAD) using a gold working electrode and an Ag/AgCl reference electrode. Chromeleon software (v. 7.1; Dionex) was used for data processing. External calibration standards were used to identify and quantify the five most prominent monosaccharides detected in the chromatograms: Fuc, Ara, Gal, Glc and Xyl. For increased accuracy, minor sugar components (Fuc and Gal) were quantified by using less diluted samples (1:50). To cope with the fact that Gal and Rha coelute at the employed conditions[*], a second run was performed at 30°C with a flow rate of 1.2mL/min, with all remaining HPAEC-DAD parameters unchanged. By following this method, Gal could be separated; however, Rha partially coeluted with the very prominent Glc peaks in the samples and could not be accurately resolved. Concentrations of each monosaccharide (C_{Mns}) were determined using a standard curve prepared with a concentration gradient of the corresponding monosaccharide standard. Finally, the content of each component was estimated as percentage of cell wall biomass dry weight (Mns%) according to:

$$Mns\% = \frac{C_{Mns} \times V_R}{W_S} \times 100\% \quad (4.1)$$

chromatographic performance is not affected by the presence of high concentrations of sulphate in the hydrolysates, and that removal of sulphate is not needed prior to injection (Basumallick and Rohrer, 2014).

[*] Shown in Fig. 4.1. as a peak shoulder at RT≈3.7min, which corresponds to a combination of galactose and rhamnose, which are not separated with the 45°C method.

Where C_{Mns} is the supernatant concentration (g/L) of the corresponding monosaccharide as determined by HPAEC-PAD; V_R is the reaction volume (L); W_S is the sample weight (g). All calculations for descriptive statistics, analyses of variance, Tukey's tests and variable correlations were performed as described in section 2.1.3; with the exception that the effect of tissue type (2 levels) was also tested in addition to genotype and development factors.

4.1.3. Results

Total monosaccharide content of miscanthus CWM was characterised for 8 genotypes, 3 developmental stages and 2 tissues through complete cell wall hydrolysis with H_2SO_4, followed by HPAEC-PAD. The analysis of the hydrolysis products for genotype sin09 is shown in Fig. 4.1 as a typical example of the chromatograms obtained from the hydrolysates. Fucose, arabinose, galactose, glucose and xylose were identified and quantified (Fig. 4.2). A mannose standard was also analysed, revealing an RT of approximately 4.5min; however, the amounts of this monosaccharide in the samples were extremely low and could not be discerned from the chromatogram baseline noise. As a consequence, the trace quantities of mannose in the cell wall could not be quantified. In order to resolve the Gal and Rha peaks, which coelute at 45°C (RT≈3.7min), the HPAEC-PAD method was adapted by reducing the flow rate to 1.2mL/min and the temperature to 30°C (Section 4.1.2). However, only Gal could be separated in these conditions, with Rha still coeluting with another component, this time with Glc. Furthermore, an approach was tested to indirectly obtain the area of Rha peaks, which consisted of subtracting the area obtained for Gal at 30°C from the area obtained for the combined Gal/Rha peak at 45°C; nevertheless, given that detection temperatures were different, the response factor of Gal was not the same for both methods, thus quantitation of Rha was unfeasible.

Total cell wall carbohydrate content was determined as the sum of all quantified monosaccharides (Table 4.1). It should be noted that these amounts do not include rhamnose and other sugar monomers which may also occur in the cell wall, although in minute concentrations, as indicated by observation of the peaks in the HPAEC-PAD chromatograms. In both tissues and at all developmental stages, the highest total sugar content was found in the *M. sacchariflorus* genotype (sac01), with *M.* × *giganteus* (gig01) also consistently ranking in the top four. By contrast, *M. sinensis* sin08 and sin13 always ranked as the bottom two genotypes in terms of total sugar content. When considering the total variation in sugar content from the earliest developmental stage (AG) to the latest (SS), all stem samples had higher proportions of cell wall carbohydrates during active growth. On the other hand, in the leaf tissue of genotypes hyb03, sin08, sin09, sin13 and sin15, carbohydrates made up a bigger proportion of cell wall biomass when the plants were senesced. Looking at the variation from one developmental stage to the next, overall total sugar content of leaf CWM decreased by 7.10% from AG to PB, and increased by 5.79% from PB to SS. As for stem CWM, total sugars were consistently reduced as a percentage of cell wall biomass throughout plant maturation, as they decreased by 5.08% between AG and PB, and 1.49% from PB to SS. However, these trends were not observed in all genotypes. In *M. sinensis* genotypes, total cell wall sugars in leaves increased by over 12% for sin09 and sin11, between PB and SS. In leaf tissues of sac01, total sugar content decreased between all developmental stages, whereas in hyb03 a constant increase was observed up to senescence. For stem tissues, while trends in stem CWM carbohydrate content between developmental stages varied with genotype, there was an overall tendency for sugar content to decrease with maturity. However, there were four exceptions to this: sin15 (+3.53% AG-PB), gig01 (+2.84% PB-SS), sac01 (+0.86% PB-SS) and sin08 (+0.05% PB-SS).

In all samples analysed, Glc, Xyl and Ara were the most abundant monosaccharides, although with a clear predominance of the first two. With an overall average content of 0.21% for Fuc (0.12% – 0.35%) and 0.57% for Gal (0.13% – 1.25%) (Table 4.2), these sugars represented less than 2% of the miscanthus cell wall biomass. Carbohydrates were therefore divided into two groups based on their abundance, consisting of the top three major monosaccharides identified (Ara, Glc, Xyl) and the minor two (Fuc, Gal).

Substantial variation was observed in the amounts of all individual monosaccharides (Table 4.2). Of all detected cell wall sugars, Fuc was the least abundant, varying from 0.12% in stems of genotype sin13, to 0.35% in leaves from genotype sac01, both in senesced samples. The range of Fuc contents did not vary substantially between stem and leaf, and no statistically significant tissue effect was detected (P=0.320; Table 4.3). Differences between developmental stages were significant (P=0.006), but its effect size was relatively low (η^2=0.0118). Tukey testing revealed that a clearly distinct effect of development on Fuc content was only observed in leaf samples collected at PB, while for stem samples two successive developmental stages were not statistically distinguishable from each other (Fig. 4.3). Genotype-derived differences were the only highly significant main source of variation in Fuc cell wall abundance (P<0.001; η^2=0.7842). CWM collected from genotypes sac01 and gig01 ranked within the top three samples in terms of Fuc content at all developmental stages and in both tissues (Table 4.2). In contrast, the lowest Fuc content was consistently detected in sin13. Furthermore, samples from the five *M. sinensis* genotypes analysed here were consistently ranked lowest in terms of Fuc content, except for sin09, which contained the third highest content in stem and leaf tissues collected from senesced plants.

In CWM isolated from miscanthus, tissue-derived differences were the main source of variation in Gal contents (P<0.001; η^2=0.7434; Table 4.4); for all genotypes analysed, leaf cell walls contained higher proportions than stems. Statistical analysis of cell wall Gal abundance

also revealed that despite a significant variation throughout development (P<0.001), plant maturation contributed relatively less to the overall variation in Gal content (η^2=0.0057). Gal increased from AG to PB (+13.79%), particularly in miscanthus stems, but at later stages of development no significant variation was observed (Fig. 4.3). In leaves, Gal content increased while plants were actively growing, reaching a maximum at PB (+4.76%), followed by a marked decrease (-12.50%), with Gal contents reaching their lowest value in senesced biomass. Unlike Fuc, the other minor sugar, Gal abundance was typically higher in genotype sin11, as it contained one of the three highest Gal contents at all developmental stages and in both tissues. However, not all members of this species analysed here ranked similarly in terms of Gal abundance. Namely, sin08, which despite containing the highest Gal content in stem samples harvested at PB, had low to intermediate levels at all other developmental stages in both tissues. Another *M. sinensis* genotype, sin13 had low Gal contents in leaves and high in stems at AG and PB, but at SS this genotype ranked high in both tissues. Compared to other genotypes, the *M. sacchariflorus* genotype generally ranked higher in leaf tissues than in stems at each developmental stage. On the other hand, the *M.* × *giganteus* genotype typically had a below average Gal content in both tissues at all developmental stages.

Glc was by far the most abundant monosaccharide detected in miscanthus CWM (Fig. 4.2). Glc content averaged 44.22% across all leaf and stem samples analysed, ranging from 34.95% to 55.13% in leaf samples and from 39.45% to 61.33% in stems (Table 4.2). Miscanthus tissues diverged significantly in their cell wall Glc content (P<0.001; Table 4.5), which was higher in stems at three developmental stages in all but one genotype; specifically, sin11 at AG and SS, where Glc content was slightly lower in stems than in leaves. Differences between developmental stages were also significant (P<0.001), and Glc abundance was generally higher earlier in development (AG) than at senescence. Nonetheless, this trend was not observed equally for all genotypes, since in the leaf tissue of some genotypes, Glc

abundance was higher at SS than at AG: hyb03 (+6.37%), sin08 (+3.97%), sin13 (+1.57%) and sin15 (+0.02%). Overall, Glc content of stem samples decreased by 4.84% from AG to PB, and subsequently by 2.31% up to senescence, while in leaves it initially decreased as plants reached peak biomass (-7.35%), but then increased as plants senesced (+3.64%) (Table 4.2; Fig. 4.4). As indicated by the overall standard deviation values (Table 4.2) and by a large effect size of the genotype factor at the AG developmental stage (η^2=0.7502; Table 4.5), the variation in Glc abundance among genotypes was the highest when plants were growing. However, variation between genotypes during plant development was not the same for both tissues. In leaf tissues, the standard deviations consistently fell throughout development, with the result that by senescence there was less variation among the genotypes in Glc abundance. By contrast, this trend was not observed in stems, as variation between genotypes was higher at the SS stage than at PB. These inter-genotype differences were highly significant (P<0.001; Table 4.5), and the genotype effect was effectively the largest source of variation in Glc contents, as indicated by an effect size of η^2=0.6117. When genotypes were ranked in terms of Glc abundance, sac01 and gig01 were in the top three for both tissues at all developmental stages, while sin13 consistently contained the lowest or the second lowest Glc content. Interestingly, ranking genotypes at PB and SS in terms of Glc content for both tissues gave a consistent pattern with genotypes sac01, gig01 and hyb03 always in the top three; sin09, sin11 and sin15 showing intermediate values; while sin13 and sin08 showed the lowest.

The second most abundant monosaccharide found in miscanthus cell walls was Xyl (Fig. 4.2), as it made up an average of 14.92% of all CWM samples analysed. Xyl contents ranged from 12.59% to 21.85% in stems, 10.34% to 18.99% in leaves (Table 4.2) and these tissue differences were statistically significant (P<0.001; Table 4.6). Stems generally contained higher proportions of Xyl than leaves, but as plants matured the difference between the tissues decreased, and at SS stems contained an average of only 0.56% more than leaves, and this

difference was not significant (P=0.880; Table 4.6). Xyl amounts differed significantly throughout development (P<0.001), although not in the same way for leaf and stem, despite an initial overall decrease in Xyl content in both tissues between AG and PB. Similarly to observations with Glc, Xyl abundance in leaves generally became higher at SS, but in stems it decreased slightly, although the difference was not substantial (Fig. 4.4). Also in common with Glc trends, the overall abundance of Xyl in stem cell walls was higher at the first harvest time than at senescence. However, in leaves the opposite trend was observed, as Xyl content was higher at the later stages in comparison with early development. Statistical analysis (Table 4.6) also revealed that Xyl content was significantly different between genotypes (P<0.001). Once again monosaccharide contents were high in sac01 hydrolysates, as this genotype contained the highest proportion of Xyl in leaf and stem at all developmental stages (Table 4.2). In fact, sac01 contained unusually high Xyl levels in stems collected at AG and SS (Fig. 4.4). Within the lower ranges, sin08 had the second lowest Xyl content in leaf samples at AG, and the lowest in stems. At PB and SS, sin13 was the genotype with the lowest Xyl content in both tissues. Although not as well differentiated as for Glc, the ranking of genotypes in terms of Xyl abundance showed a consistent pattern after plants achieved maturity; particularly at SS, where the genotypes sac01, sin11 and hyb03 contained the three highest Xyl levels in both tissues, while sin08 and sin13 contained the lowest.

Ara content, the third most abundant monosaccharide (Fig. 4.2), averaged 1.99% of the cell wall for all samples analysed. Significant differences were detected between the tissues (P<0.001; Table 4.7), as the amounts reached 4.13% in leaves and 1.85% in stems (Table 4.2). In fact, contrary to the other two major monosaccharides, for Ara, the abundance primarily varied according to tissue origin of the CWM (η^2=0.6966). For all eight miscanthus genotypes analysed, foliar tissue contained higher proportions of Ara, and the ratios were on average 2.05, 1.92 and 1.87 times greater in leaves than in stems collected at AG, PB and SS, respectively.

In addition, significant differences were detected in the quantitation of Ara (P<0.001) between developmental stages, as the content within the cell wall decreased from one stage to the next in both tissues (Fig. 4.4): in leaves, -11.76% between AG – PB and -4.31% between PB – SS; in stems, -4.90% between AG – PB and -2.94% between PB – SS. The decrease in stems was less accentuated than in leaves, and the difference was not significant between PB and SS (Fig. 4.4). As observed above for other major CW monosaccharides, the variation in Ara content was not the same for all genotypes. These differences were statistically significant (P<0.001), but the genotype effect had a smaller effect size than for other monosaccharides (η^2=0.1910). Inter-genotype variation was observed not only in the Ara content of the CWM (Table 4.2), but also in the fact that in contrast with the general trend for Ara content to decrease with increasing maturity, hyb03 leaf tissues and sac01 and sin09 stem tissues showed an increase with developmental stage. Leaves from sin11 harvested at SS had unusually high Ara levels (Fig. 4.4). Furthermore, this genotype contained the highest Ara content of all leaf samples at all developmental stages. In stems, sin11 also ranked highest for Ara content at AG and SS, and second at PB. At this developmental stage, CWM from the stems of sin15 contained the highest levels of Ara. Regarding the genotypes with the lowest Ara contents, no consistency was observed between tissues, as the lowest ranking leaf samples did not necessarily coincide with the lowest ranking stem samples. However, within the same tissue at each developmental stage, genotype sin09 ranked among the lowest two for leaf Ara content, and gig01 consistently had the lowest Ara content in stems.

Ara and Xyl comprise the most abundant non-cellulosic polysaccharide in the cell wall, arabinoxylan (AX); which consists of a polymer with a (1→4)-β-xylan backbone with Ara attached to some Xyl residues (Carpita, 1996). The degree of xylan backbone substitution with Ara can be indirectly estimated by calculating the ratio of Ara to Xyl in the cell wall (Rancour *et al.*, 2012). Ara/Xyl ratios were observed to vary from 0.06 to 0.12 in stem tissues, and from

0.13 to 0.29 in leaves (Table 4.8), being significantly different between the tissues (P<0.001; Table 4.9). In fact, tissue origin was the main source of variation in the Ara/Xyl ratios (η^2=0.6841), which were typically higher in leaves than in stems by a factor of 2.33 at AG, 2.11 at PB and 1.78 at SS. AX also displayed divergent arabinose ramification throughout development (P<0.001), but the difference was only significant in leaves (Fig. 4.5). For this tissue, an overall decline in the Ara/Xyl ratio was observed from AG to PB (-9.52%) and also between PB and SS (-15.79%) (Table 4.8). In all genotypes, leaf tissues had higher Ara/Xyl ratios when the plants were actively growing, but a constant decrease with increasing maturity was not always observed, as increases were observed in sin09 and sin11 from AG to PB, and in sin13 from PB to SS. *M. sinensis* typically contained more ramified AX, particularly sin11, which had one of the three highest ratios of Ara substitution at all developmental stages and in both tissues; by contrast, the lowest ratios within this species typically occurred in genotype sin09. Leaves and stems of non-*M. sinensis* genotypes (gig01, hyb03 and sac01) contained below average Ara/Xyl ratios for all harvest times. In particular for genotype sac01, the ratio values consistently ranked among the three lowest in both tissues at all developmental stages.

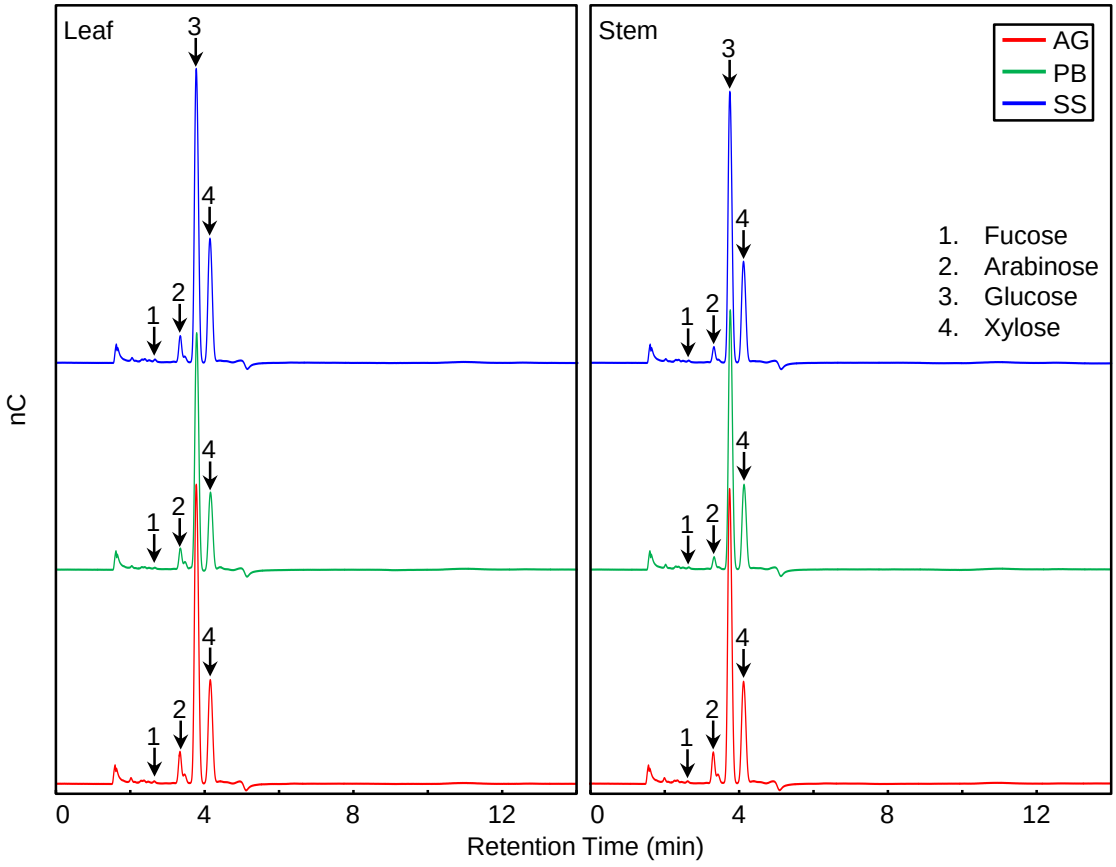

Fig. 4.1. HPAEC-PAD chromatograms obtained after acid hydrolysis of CWM from miscanthus genotype sin09. Glucose, xylose and arabinose were the three most abundant monosaccharides released from both tissues at all developmental stages: active growth (AG), peak biomass (PB) and senescence (SS). Quantification of fucose was performed with less diluted samples. See section 4.1.2 for method details. (nC: nano-Coulomb)

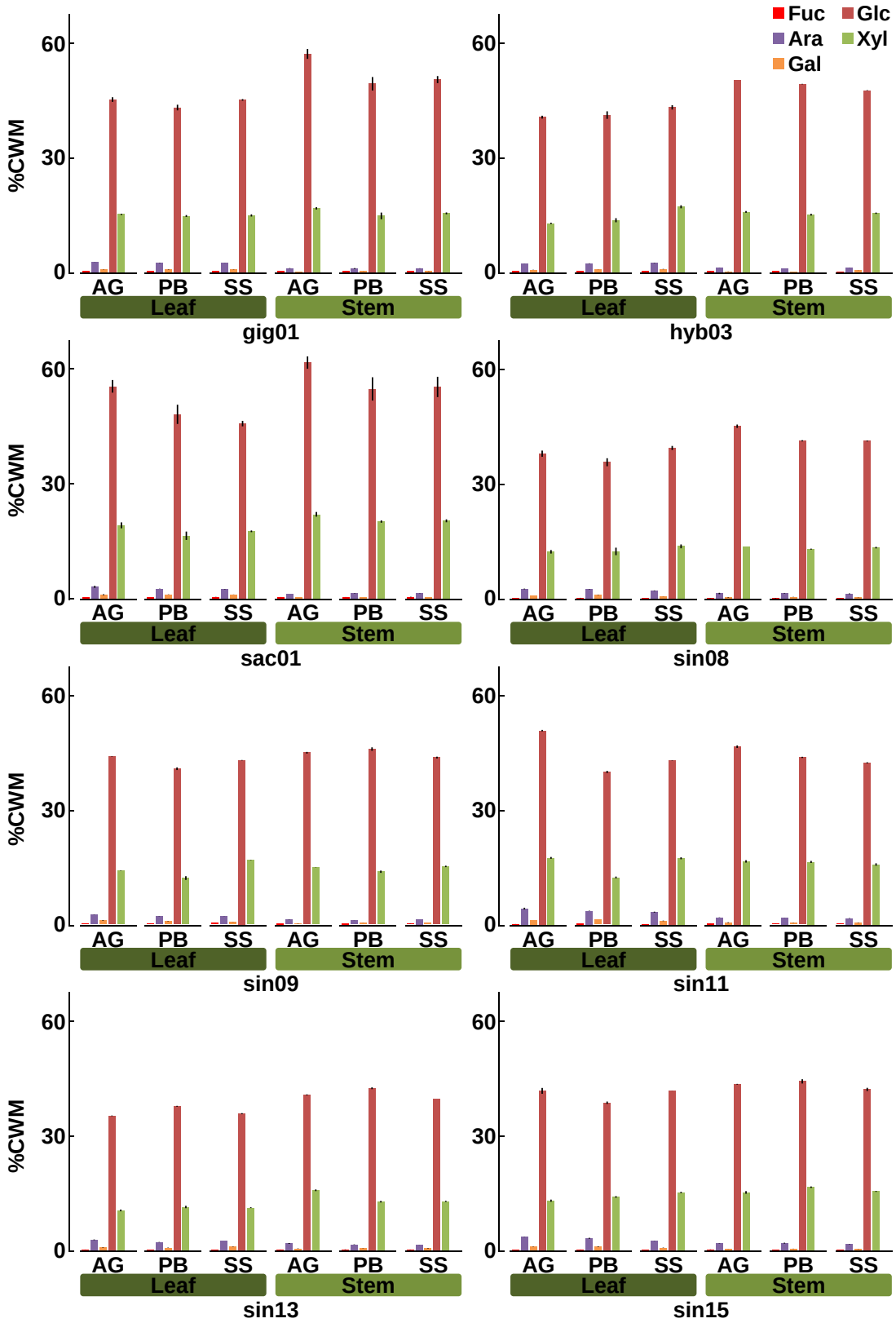

Fig. 4.2. Total monosaccharides released upon acid hydrolysis of CWM from miscanthus genotypes: fucose (Fuc), arabinose (Ara), galactose (Gal), glucose (Glc), and xylose (Xyl). Error bars are the standard deviation of the sample replicates

Table 4.1. Miscanthus cell wall sugar content based on the sum of total sugars quantified after acid hydrolysis of miscanthus CWM. Values are expressed as percentage of cell wall material dry weight (% CWM) and are the sum of the values determined for fucose, arabinose, galactose, glucose and xylose at three developmental stages for each genotype.

Total Sugar (% CWM)						
	Active Growth		**Peak Biomass**		**Senescence**	
	Leaf	**Stem**	**Leaf**	**Stem**	**Leaf**	**Stem**
gig01	63.58 ± 0.76	74.87 ± 1.55	60.91 ± 1.09	65.11 ± 2.76	62.94 ± 0.10	66.96 ± 1.19
hyb03	56.19 ± 0.49	67.37 ± 0.16	57.79 ± 1.54	65.38 ± 0.16	63.44 ± 0.85	64.40 ± 0.25
sac01	78.29 ± 2.54	84.94 ± 2.20	67.94 ± 3.64	76.36 ± 2.71	66.64 ± 0.53	77.02 ± 2.35
sin08	53.41 ± 1.33	60.19 ± 0.32	51.38 ± 2.09	56.13 ± 0.10	55.76 ± 1.12	56.16 ± 0.02
sin09	61.10 ± 0.05	60.99 ± 0.24	55.55 ± 0.83	60.78 ± 0.69	62.29 ± 0.14	60.16 ± 0.45
sin11	73.12 ± 0.65	65.18 ± 0.78	56.87 ± 0.55	62.08 ± 0.38	64.20 ± 0.13	59.88 ± 0.39
sin13	48.75 ± 0.21	58.19 ± 0.08	51.48 ± 0.31	56.71 ± 0.41	49.96 ± 0.09	54.01 ± 0.18
sin15	58.98 ± 1.05	60.60 ± 0.38	56.46 ± 0.08	62.74 ± 0.89	59.71 ± 0.18	59.17 ± 0.59
Mean	61.68 ± 9.88	66.54 ± 9.15	57.30 ± 5.34	63.16 ± 6.34	60.62 ± 5.39	62.22 ± 7.26

Table 4.2. Total monosaccharide content of miscanthus CWM. Values are expressed as percentage of cell wall material dry weight (% CWM) at three developmental stages for each genotype and are the mean ± standard deviation. Values within a column sharing a letter in their superscript are not significantly different according to a Tukey's test (α=0.05).

	Active Growth		Peak Biomass		Senescence	
	Leaf	**Stem**	**Leaf**	**Stem**	**Leaf**	**Stem**
			Fucose (% CWM)			
gig01	0.29 ± 0.02^{d}	0.26 ± 0.02^{bc}	0.25 ± 0.01^{bc}	0.24 ± 0.01^{a}	0.27 ± 0.02^{d}	0.26 ± 0.01^{bc}
hyb03	0.25 ± 0.01^{c}	0.28 ± 0.04^{bc}	0.32 ± 0.01^{d}	0.24 ± 0.01^{ac}	0.23 ± 0.01^{cd}	0.18 ± 0.01^{ab}
sac01	0.25 ± 0.01^{cd}	0.32 ± 0.01^{c}	0.29 ± 0.01^{cd}	0.33 ± 0.01^{c}	0.35 ± 0.03^{e}	0.34 ± 0.05^{c}
sin08	0.16 ± 0.01^{ab}	0.15 ± 0.03^{a}	0.21 ± 0.04^{ab}	0.18 ± 0.05^{ab}	0.19 ± 0.01^{bc}	0.14 ± 0.01^{a}
sin09	0.18 ± 0.01^{ab}	0.22 ± 0.01^{ab}	0.20 ± 0.01^{ab}	0.21 ± 0.01^{ab}	0.24 ± 0.01^{cd}	0.19 ± 0.03^{ab}
sin11	0.17 ± 0.01^{ab}	0.21 ± 0.02^{ab}	0.21 ± 0.01^{ab}	0.18 ± 0.01^{ab}	0.16 ± 0.01^{ab}	0.18 ± 0.01^{ab}
sin13	0.14 ± 0.02^{a}	0.14 ± 0.03^{a}	0.16 ± 0.01^{a}	0.14 ± 0.04^{b}	0.12 ± 0.01^{a}	0.12 ± 0.04^{a}
sin15	0.19 ± 0.01^{b}	0.19 ± 0.03^{ab}	0.18 ± 0.02^{ab}	0.19 ± 0.01^{ab}	0.16 ± 0.01^{ab}	0.16 ± 0.01^{a}
Mean	0.20 ± 0.05	0.22 ± 0.06	0.23 ± 0.05	0.21 ± 0.06	0.22 ± 0.07	0.20 ± 0.07
			Arabinose (% CWM)			
gig01	2.59 ± 0.01^{ab}	1.03 ± 0.05^{a}	2.42 ± 0.05^{a}	0.97 ± 0.12^{a}	2.37 ± 0.01^{a}	1.03 ± 0.02^{b}
hyb03	2.25 ± 0.02^{a}	1.22 ± 0.02^{ab}	2.28 ± 0.06^{ab}	1.05 ± 0.01^{ab}	2.43 ± 0.05^{a}	1.10 ± 0.01^{b}
sac01	2.99 ± 0.25^{bc}	1.21 ± 0.01^{ab}	2.47 ± 0.03^{a}	1.27 ± 0.05^{bc}	2.37 ± 0.04^{a}	1.32 ± 0.03^{a}
sin08	2.56 ± 0.08^{ab}	1.39 ± 0.16^{b}	2.42 ± 0.05^{a}	1.45 ± 0.05^{c}	2.11 ± 0.07^{b}	1.31 ± 0.09^{a}
sin09	2.41 ± 0.03^{a}	1.21 ± 0.02^{ab}	2.11 ± 0.04^{b}	1.04 ± 0.02^{ab}	2.09 ± 0.02^{b}	1.31 ± 0.01^{a}
sin11	4.13 ± 0.22^{d}	1.83 ± 0.04^{c}	3.53 ± 0.05^{d}	1.77 ± 0.02^{d}	3.23 ± 0.11^{c}	1.60 ± 0.04^{c}
sin13	2.68 ± 0.08^{ab}	1.72 ± 0.10^{c}	2.05 ± 0.05^{b}	1.45 ± 0.04^{c}	2.46 ± 0.01^{a}	1.29 ± 0.01^{a}
sin15	3.47 ± 0.03^{c}	1.82 ± 0.04^{c}	3.10 ± 0.13^{c}	1.85 ± 0.12^{d}	2.43 ± 0.04^{a}	1.58 ± 0.05^{c}
Mean	2.89 ± 0.63	1.43 ± 0.32	2.55 ± 0.51	1.36 ± 0.33	2.44 ± 0.35	1.32 ± 0.20
			Galactose (% CWM)			
gig01	0.71 ± 0.04^{a}	0.15 ± 0.01^{a}	0.76 ± 0.05^{ab}	0.20 ± 0.02^{c}	0.70 ± 0.03^{ab}	0.20 ± 0.03^{a}
hyb03	0.63 ± 0.03^{a}	0.19 ± 0.03^{ab}	0.72 ± 0.02^{a}	0.13 ± 0.01^{c}	0.83 ± 0.05^{bc}	0.45 ± 0.01^{b}
sac01	0.93 ± 0.12^{bc}	0.24 ± 0.01^{abc}	1.06 ± 0.02^{d}	0.32 ± 0.01^{a}	1.05 ± 0.02^{d}	0.22 ± 0.01^{a}
sin08	0.72 ± 0.01^{ac}	0.32 ± 0.07^{abcd}	0.92 ± 0.05^{bcd}	0.46 ± 0.03^{b}	0.60 ± 0.01^{a}	0.37 ± 0.02^{bc}
sin09	0.97 ± 0.07^{b}	0.19 ± 0.03^{ab}	0.78 ± 0.05^{abc}	0.32 ± 0.02^{a}	0.58 ± 0.02^{a}	0.28 ± 0.01^{ac}
sin11	1.09 ± 0.01^{b}	0.48 ± 0.08^{d}	1.25 ± 0.01^{e}	0.41 ± 0.04^{ab}	0.92 ± 0.07^{cd}	0.45 ± 0.04^{b}
sin13	0.65 ± 0.05^{a}	0.39 ± 0.04^{cd}	0.63 ± 0.06^{a}	0.43 ± 0.04^{b}	0.85 ± 0.05^{bc}	0.47 ± 0.07^{b}
sin15	0.98 ± 0.04^{b}	0.35 ± 0.02^{bcd}	0.95 ± 0.08^{cd}	0.36 ± 0.03^{ab}	0.64 ± 0.04^{a}	0.30 ± 0.02^{ac}
Mean	0.84 ± 0.18	0.29 ± 0.12	0.88 ± 0.20	0.33 ± 0.11	0.77 ± 0.17	0.34 ± 0.11
			Glucose (% CWM)			
gig01	44.93 ± 0.60^{e}	56.79 ± 1.29^{e}	42.85 ± 0.73^{c}	49.04 ± 1.77^{c}	44.83 ± 0.20^{b}	50.14 ± 0.92^{c}
hyb03	40.35 ± 0.37^{bc}	49.99 ± 0.01^{d}	40.90 ± 0.98^{ac}	48.96 ± 0.07^{bc}	42.92 ± 0.56^{a}	47.31 ± 0.05^{bc}
sac01	55.13 ± 1.65^{g}	61.33 ± 1.62^{f}	47.84 ± 2.50^{d}	54.48 ± 3.03^{d}	45.45 ± 0.72^{b}	54.99 ± 2.64^{d}
sin08	37.74 ± 0.82^{ab}	44.89 ± 0.43^{ab}	35.52 ± 1.05^{b}	41.11 ± 0.15^{a}	39.24 ± 0.53^{d}	41.03 ± 0.11^{a}
sin09	43.66 ± 0.06^{de}	44.61 ± 0.22^{ab}	40.45 ± 0.34^{ac}	45.57 ± 0.44^{abc}	42.66 ± 0.06^{a}	43.35 ± 0.24^{ab}
sin11	50.42 ± 0.19^{f}	46.25 ± 0.34^{b}	39.66 ± 0.27^{abc}	43.47 ± 0.15^{a}	42.68 ± 0.05^{a}	42.05 ± 0.14^{a}
sin13	34.95 ± 0.08^{a}	40.38 ± 0.12^{c}	37.42 ± 0.11^{ab}	42.10 ± 0.24^{a}	35.50 ± 0.14^{c}	39.45 ± 0.01^{a}
sin15	41.46 ± 0.77^{cd}	43.19 ± 0.10^{ac}	38.36 ± 0.32^{ab}	43.93 ± 0.57^{ab}	41.47 ± 0.01^{a}	41.84 ± 0.42^{a}
Mean	43.58 ± 6.61	48.43 ± 7.20	40.38 ± 3.76	46.08 ± 4.47	41.84 ± 3.20	45.02 ± 5.34
			Xylose (% CWM)			
gig01	15.07 ± 0.14^{c}	16.63 ± 0.30^{b}	14.64 ± 0.25^{cd}	14.66 ± 0.86^{b}	14.78 ± 0.29^{b}	15.33 ± 0.23^{a}
hyb03	12.72 ± 0.16^{ab}	15.69 ± 0.24^{ab}	13.56 ± 0.53^{abc}	14.99 ± 0.22^{bc}	17.03 ± 0.40^{a}	15.35 ± 0.17^{a}
sac01	18.99 ± 0.77^{f}	21.85 ± 0.60^{d}	16.28 ± 1.08^{d}	19.96 ± 0.29^{d}	17.43 ± 0.23^{a}	20.16 ± 0.38^{c}
sin08	12.23 ± 0.45^{a}	13.45 ± 0.01^{c}	12.32 ± 0.98^{abc}	12.93 ± 0.11^{a}	13.63 ± 0.50^{d}	13.31 ± 0.19^{b}
sin09	13.87 ± 0.06^{bc}	14.77 ± 0.03^{a}	12.02 ± 0.48^{ab}	13.65 ± 0.28^{ab}	16.73 ± 0.05^{a}	15.02 ± 0.19^{a}
sin11	17.32 ± 0.24^{e}	16.41 ± 0.31^{b}	12.22 ± 0.23^{ab}	16.26 ± 0.26^{c}	17.22 ± 0.25^{a}	15.61 ± 0.31^{a}
sin13	10.34 ± 0.24^{d}	15.56 ± 0.21^{ab}	11.22 ± 0.31^{a}	12.59 ± 0.20^{a}	11.03 ± 0.11^{c}	12.69 ± 0.14^{b}
sin15	12.88 ± 0.28^{ab}	15.05 ± 0.34^{a}	13.87 ± 0.21^{bc}	16.41 ± 0.18^{c}	15.02 ± 0.18^{b}	15.29 ± 0.11^{a}
Mean	14.18 ± 2.83	16.18 ± 2.50	13.27 ± 1.65	15.18 ± 2.39	15.36 ± 2.22	15.35 ± 2.22

Table 4.3. ANOVA results for fucose determination.

Effect	Degrees of freedom	Sum of squares	Mean square	*F*-ratio	*P*-value	Effect size (η^2)
Genotype	7	27.87	3.98	106.91	<0.0001	0.7842
Tissue	1	0.04	0.04	1.01	0.3195	0.0011
Development Stage	2	0.42	0.21	5.65	0.0063	0.0118
Genotype × Tissue	7	0.86	0.12	3.30	0.0061	0.0242
Genotype × Development Stage	14	2.76	0.20	5.29	<0.0001	0.0776
Tissue × Development Stage	2	0.61	0.30	8.16	0.0009	0.0171
Genotype × Tissue × Development Stage	14	1.20	0.09	2.30	0.0166	0.0337
Error	48	1.79	0.04			
Total	95	35.54				

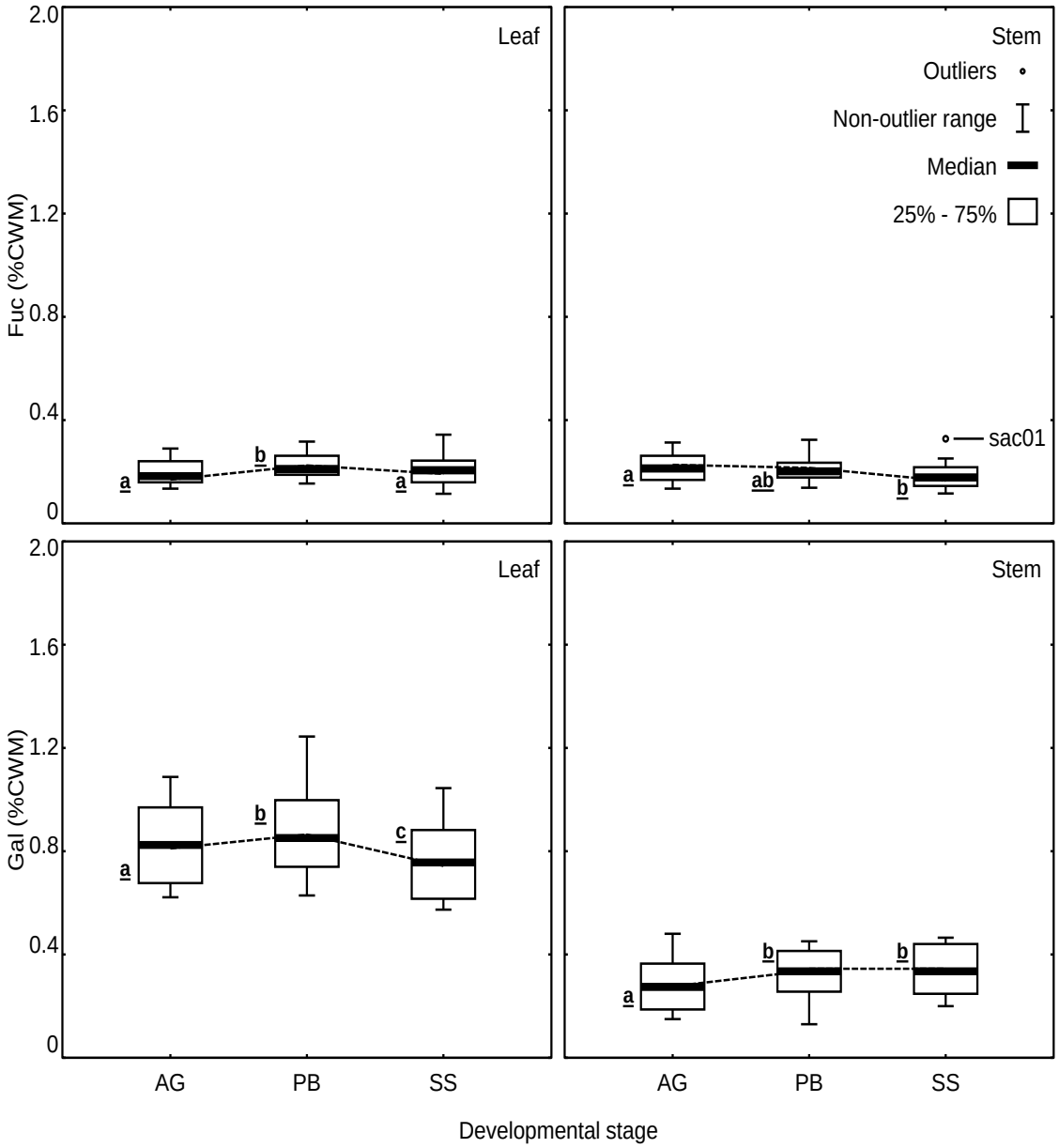

Fig. 4.3. Distribution of measurements of the minor monosaccharides fucose (Fuc) and Galactose (Gal) released upon acid hydrolysis of miscanthus CWM. Values are expressed as percentage of cell wall material dry weight (% CWM) from leaf and stem tissue for 8 miscanthus genotypes at active growth (AG), peak biomass (PB) and senescence (SS). The non-outlier range is defined as the range of values which fall outside 1.5× the interquartile range of the distribution (height of the 25% – 75% box). Not significantly different developmental stages are indicated by a common underlined letter next to the box (Tukey's test at α=0.05).

Table 4.4. ANOVA results for galactose determination.

All Developmental Stages

Effect	Degrees of freedom	Sum of squares	Mean square	*F*-ratio	*P*-value	Effect size (η^2)
Genotype	7	78.97	11.28	63.48	<0.0001	0.0944
Tissue	1	621.93	621.93	3499.55	<0.0001	0.7434
Development Stage	2	4.75	2.38	13.36	<0.0001	0.0057
Genotype × Tissue	7	45.51	6.50	36.58	<0.0001	0.0544
Genotype × Development Stage	14	44.07	3.15	17.71	<0.0001	0.0527
Tissue × Development Stage	2	8.13	4.06	22.87	<0.0001	0.0097
Genotype × Tissue × Development Stage	14	24.76	1.77	9.95	<0.0001	0.0296
Error	48	8.53	0.18			
Total	95	836.64				

Active Growth

Effect	Degrees of freedom	Sum of squares	Mean square	*F*-ratio	*P*-value	Effect size (η^2)
Genotype	7	42.54	6.08	24.89	<0.0001	0.1396
Tissue	1	237.55	237.55	973.03	<0.0001	0.7795
Genotype × Tissue	7	20.75	2.96	12.14	<0.0001	0.0681
Error	16	3.91	0.24			
Total	31	304.74				

Peak Biomass

Effect	Degrees of freedom	Sum of squares	Mean square	*F*-ratio	*P*-value	Effect size (η^2)
Genotype	7	48.47	6.92	46.70	<0.0001	0.1500
Tissue	1	246.66	246.66	1663.60	<0.0001	0.7635
Genotype × Tissue	7	25.57	3.65	24.64	<0.0001	0.0792
Error	16	2.37	0.15			
Total	31	323.08				

Senescence

Effect	Degrees of freedom	Sum of squares	Mean square	*F*-ratio	*P*-value	Effect size (η^2)
Genotype	7	32.03	4.58	32.51	<0.0001	0.1570
Tissue	1	145.85	145.85	1036.23	<0.0001	0.7147
Genotype × Tissue	7	23.94	3.42	24.30	<0.0001	0.1173
Error	16	2.25	0.14			
Total	31	204.06				

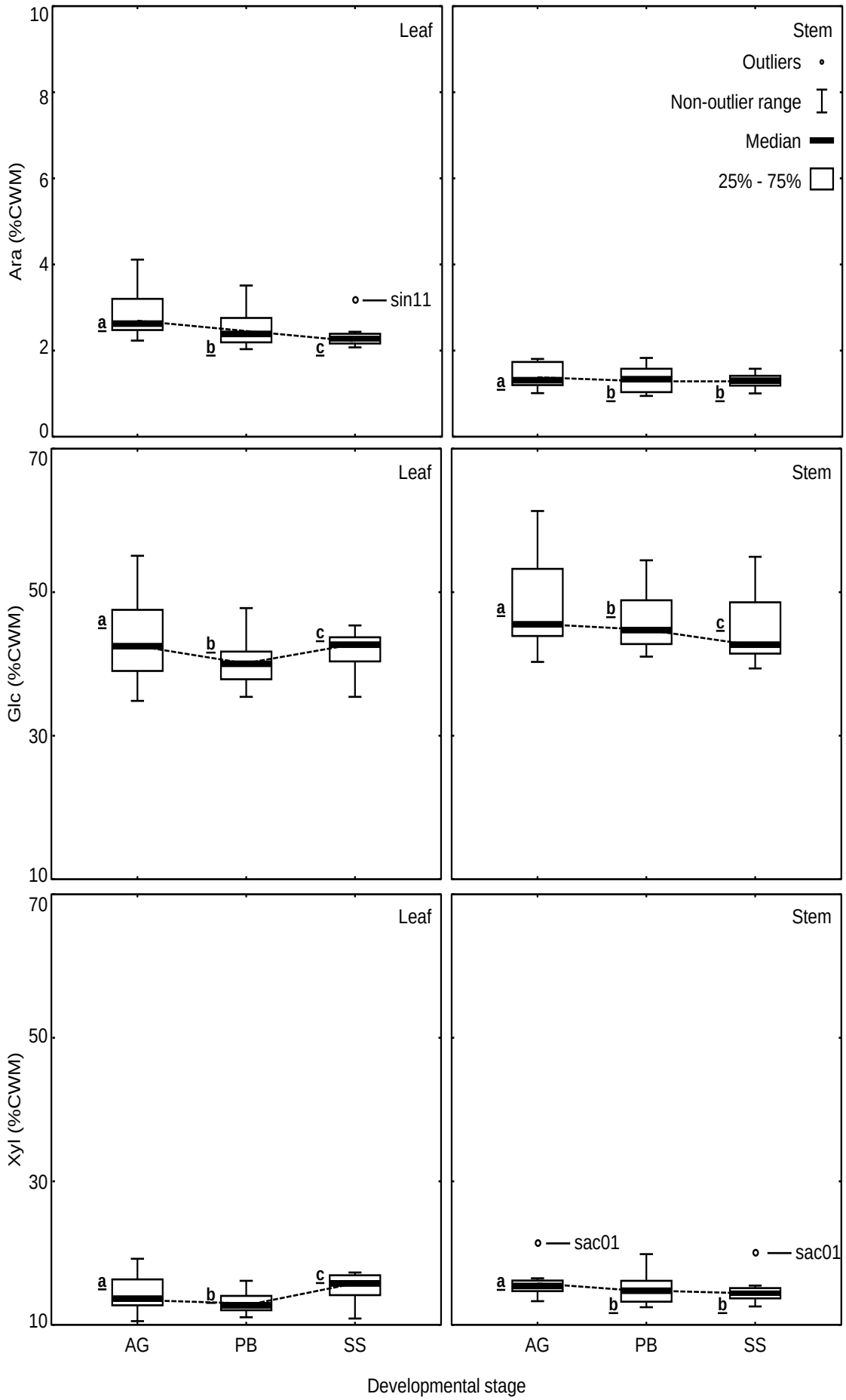
Leaf
Stem
Outliers
Non-outlier range
Median
25% - 75%
Ara (%CWM)
Glc (%CWM)
Xyl (%CWM)
sin11
sac01
a
b
c
AG
PB
SS
Developmental stage

Fig. 4.4. (Previous page). Distribution of measurements of the major monosaccharides Arabinose (Ara), Glucose (Glc) and Xylose (Xyl) released upon acid hydrolysis of miscanthus CWM. Values are expressed as percentage of cell wall material dry weight (% CWM) from leaf and stem tissue for 8 miscanthus genotypes at active growth (AG), peak biomass (PB) and senescence (SS). The non-outlier range is defined as the range of values which fall outside 1.5× the interquartile range of the distribution (height of the 25% – 75% box). Not significantly different developmental stages are indicated by a common underlined letter next to the box (Tukey's test at α=0.05).

Table 4.5. ANOVA results for glucose determination.

All Developmental Stages

Effect	Degrees of freedom	Sum of squares	Mean square	*F*-ratio	*P*-value	Effect size (η^2)
Genotype	7	188433.00	26919.00	318.70	<0.0001	0.6117
Tissue	1	50298.00	50298.00	595.40	<0.0001	0.1633
Development Stage	2	15329.00	7664.00	90.70	<0.0001	0.0498
Genotype × Tissue	7	18007.00	2572.00	30.50	<0.0001	0.0585
Genotype × Development Stage	14	19765.00	1412.00	16.70	<0.0001	0.0642
Tissue × Development Stage	2	2644.00	1322.00	15.70	<0.0001	0.0086
Genotype × Tissue × Development Stage	14	9518.00	680.00	8.00	<0.0001	0.0309
Error	48	4055.00	84.00			
Total	95	308049.00				

Active Growth

Effect	Degrees of freedom	Sum of squares	Mean square	*F*-ratio	*P*-value	Effect size (η^2)
Genotype	7	115111.00	16444.00	286.90	<0.0001	0.7502
Tissue	1	18803.00	18803.00	328.10	<0.0001	0.1226
Genotype × Tissue	7	18601.00	2657.00	46.40	<0.0001	0.1212
Error	16	917.00	57.00			
Total	31	153432.00				

Peak Biomass

Effect	Degrees of freedom	Sum of squares	Mean square	*F*-ratio	*P*-value	Effect size (η^2)
Genotype	7	46623.00	6660.00	48.21	<0.0001	0.6130
Tissue	1	26055.00	26055.00	188.60	<0.0001	0.3426
Genotype × Tissue	7	1166.00	167.00	1.21	0.3547	0.0153
Error	16	2210.00	138.00			
Total	31	76054.00				

Senescence

Effect	Degrees of freedom	Sum of squares	Mean square	*F*-ratio	*P*-value	Effect size (η^2)
Genotype	7	46464.00	6638.00	114.50	<0.0001	0.7348
Tissue	1	8084.00	8084.00	139.50	<0.0001	0.1278
Genotype × Tissue	7	7759.00	1108.00	19.10	<0.0001	0.1227
Error	16	927.00	58.00			
Total	31	63234.00				

Table 4.6. ANOVA results for xylose determination.

All Developmental Stages

Effect	Degrees of freedom	Sum of squares	Mean square	*F*-ratio	*P*-value	Effect size (η^2)
Genotype	7	35770.00	5110.00	355.90	<0.0001	0.6522
Tissue	1	4059.00	4059.00	282.80	<0.0001	0.0740
Development Stage	2	2373.00	1187.00	82.70	<0.0001	0.0433
Genotype × Tissue	7	2476.00	354.00	24.60	<0.0001	0.0452
Genotype × Development Stage	14	4328.00	309.00	21.50	<0.0001	0.0789
Tissue × Development Stage	2	2077.00	1038.00	72.30	<0.0001	0.0379
Genotype × Tissue × Development Stage	14	3073.00	220.00	15.30	<0.0001	0.0560
Error	48	689.00	14.00			
Total	95	54845.00				

Active Growth

Effect	Degrees of freedom	Sum of squares	Mean square	*F*-ratio	*P*-value	Effect size (η^2)
Genotype	7	17745.10	2535.00	224.69	<0.0001	0.7590
Tissue	1	3198.10	3198.10	283.46	<0.0001	0.1368
Genotype × Tissue	7	2257.40	322.50	28.58	<0.0001	0.0966
Error	16	180.50	11.30			
Total	31	23381.10				

Peak Biomass

Effect	Degrees of freedom	Sum of squares	Mean square	*F*-ratio	*P*-value	Effect size (η^2)
Genotype	7	10431.10	1490.20	59.52	<0.0001	0.6880
Tissue	1	2937.90	2937.90	117.35	<0.0001	0.1938
Genotype × Tissue	7	1392.90	199.00	7.95	0.0003	0.0919
Error	16	400.60	25.00			
Total	31	15162.50				

Senescence

Effect	Degrees of freedom	Sum of squares	Mean square	*F*-ratio	*P*-value	Effect size (η^2)
Genotype	7	11922.00	1703.10	252.20	<0.0001	0.8559
Tissue	1	0.20	0.20	0.00	0.8795	<0.0001
Genotype × Tissue	7	1899.30	271.30	40.20	<0.0001	0.1364
Error	16	108.00	6.80			
Total	31	13929.50				

Table 4.7. ANOVA results for arabinose determination.

All Developmental Stages

Effect	Degrees of freedom	Sum of squares	Mean square	*F*-ratio	*P*-value	Effect size (η^2)
Genotype	7	1038.69	148.38	263.06	<0.0001	0.1910
Tissue	1	3787.83	3787.83	6715.04	<0.0001	0.6966
Development Stage	2	134.29	67.15	119.04	<0.0001	0.0247
Genotype × Tissue	7	213.32	30.47	54.03	<0.0001	0.0392
Genotype × Development Stage	14	110.25	7.88	13.96	<0.0001	0.0203
Tissue × Development Stage	2	50.78	25.39	45.01	<0.0001	0.0093
Genotype × Tissue × Development Stage	14	75.64	5.40	9.58	<0.0001	0.0139
Error	48	27.08	0.56			
Total	95	5437.88				

Active Growth

Effect	Degrees of freedom	Sum of squares	Mean square	*F*-ratio	*P*-value	Effect size (η^2)
Genotype	7	548.33	78.33	74.16	<0.0001	0.2277
Tissue	1	1699.56	1699.56	1608.96	<0.0001	0.7058
Genotype × Tissue	7	143.26	20.47	19.37	<0.0001	0.0595
Error	16	16.90	1.06			
Total	31	2408.05				

Peak Biomass

Effect	Degrees of freedom	Sum of squares	Mean square	*F*-ratio	*P*-value	Effect size (η^2)
Genotype	7	438.30	62.61	151.99	<0.0001	0.2636
Tissue	1	1137.62	1137.62	2761.48	<0.0001	0.6841
Genotype × Tissue	7	80.38	11.48	27.87	<0.0001	0.0483
Error	16	6.59	0.41			
Total	31	1662.89				

Senescence

Effect	Degrees of freedom	Sum of squares	Mean square	*F*-ratio	*P*-value	Effect size (η^2)
Genotype	7	162.32	23.19	103.53	<0.0001	0.1317
Tissue	1	1001.43	1001.43	4471.16	<0.0001	0.8124
Genotype × Tissue	7	65.32	9.33	41.66	<0.0001	0.0530
Error	16	3.58	0.22			
Total	31	1232.65				

Table 4.8. Arabinose to xylose ratio (Ara/Xyl) in miscanthus CWM. Values were calculated by dividing the percentage of Ara by the percentage of Xyl in each sample, and are expressed as the mean of the replicates at three developmental stages, two tissues and eight genotypes (standard deviations were below 0.01 in all cases). Values within a column sharing a letter in their superscript are not significantly different according to a Tukey's test (α=0.05).

Ara/Xyl ratio						
	Active Growth		**Peak Biomass**		**Senescence**	
	Leaf	**Stem**	**Leaf**	**Stem**	**Leaf**	**Stem**
gig01	0.17^{a}	0.06^{bc}	0.17^{ab}	0.07^{a}	0.16^{a}	0.07^{b}
hyb03	0.18^{a}	0.08^{bc}	0.17^{abc}	0.07^{a}	0.14^{cd}	0.07^{b}
sac01	0.16^{a}	0.06^{b}	0.15^{a}	0.06^{a}	0.14^{bc}	0.07^{b}
sin08	0.21^{d}	0.10^{ad}	0.20^{cd}	0.11^{b}	0.15^{ad}	0.10^{ac}
sin09	0.17^{a}	0.08^{cd}	0.18^{abc}	0.08^{a}	0.13^{b}	0.09^{c}
sin11	0.24^{b}	0.11^{a}	0.29^{e}	0.11^{b}	0.19^{e}	0.10^{a}
sin13	0.26^{bc}	0.11^{a}	0.18^{bc}	0.12^{b}	0.22^{f}	0.10^{ac}
sin15	0.27^{c}	0.12^{a}	0.22^{d}	0.11^{b}	0.16^{a}	0.10^{a}
Mean	0.21 ± 0.04	0.09 ± 0.02	0.19 ± 0.04	0.09 ± 0.02	0.16 ± 0.03	0.09 ± 0.02

Table 4.9. ANOVA results for Ara/Xyl ratio determination.

All Developmental Stages

Effect	Degrees of freedom	Sum of squares	Mean square	*F*-ratio	*P*-value	Effect size (η^2)
Genotype	7	0.06	0.01	288.54	<0.0001	0.1807
Tissue	1	0.23	0.23	7645.52	<0.0001	0.6841
Development Stage	2	0.01	0.01	171.13	<0.0001	0.0306
Genotype × Tissue	7	0.01	0.00	32.01	<0.0001	0.0201
Genotype × Development Stage	14	0.01	0.00	24.55	<0.0001	0.0308
Tissue × Development Stage	2	0.01	0.00	125.35	<0.0001	0.0224
Genotype × Tissue × Development Stage	14	0.01	0.00	21.55	<0.0001	0.0270
Error	48	0.00	0.00			
Total	95	0.34				

Active Growth

Effect	Degrees of freedom	Sum of squares	Mean square	*F*-ratio	*P*-value	Effect size (η^2)
Genotype	7	0.03	0.00	107.33	<0.0001	0.2190
Tissue	1	0.11	0.11	2582.00	<0.0001	0.7525
Genotype × Tissue	7	0.00	0.00	11.72	<0.0001	0.0239
Error	16	0.00	0.00			
Total	31	0.14				

Peak Biomass

Effect	Degrees of freedom	Sum of squares	Mean square	*F*-ratio	*P*-value	Effect size (η^2)
Genotype	7	0.03	0.00	119.41	<0.0001	0.2226
Tissue	1	0.09	0.09	2660.43	<0.0001	0.7086
Genotype × Tissue	7	0.01	0.00	34.61	<0.0001	0.0645
Error	16	0.00	0.00			
Total	31	0.12				

Senescence

Effect	Degrees of freedom	Sum of squares	Mean square	*F*-ratio	*P*-value	Effect size (η^2)
Genotype	7	0.01	0.00	112.47	<0.0001	0.2076
Tissue	1	0.04	0.04	2705.58	<0.0001	0.7133
Genotype × Tissue	7	0.00	0.00	40.57	<0.0001	0.0749
Error	16	0.00	0.00			
Total	31	0.06				

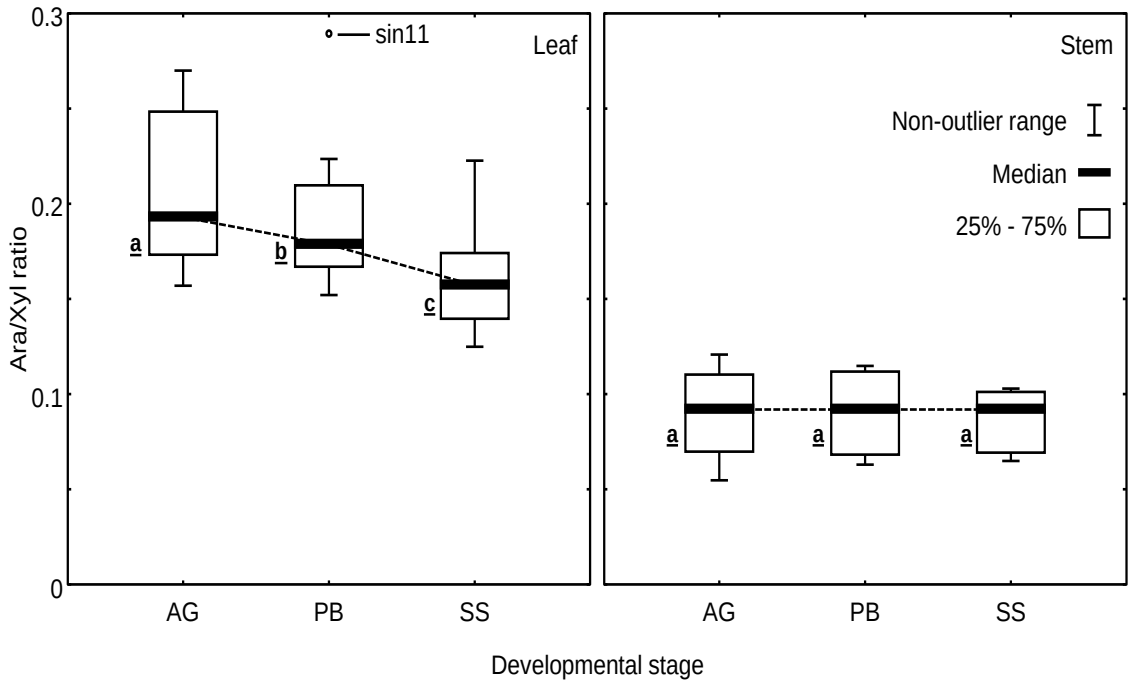

Fig. 4.5. Distribution of measurements of the arabinose to xylose ratio (Ara/Xyl) of miscanthus CWM. Values were calculated by dividing the percentage of Ara by the percentage of Xyl in each cell wall sample from leaf and stem tissue of 8 miscanthus genotypes at active growth (AG), peak biomass (PB) and senescence (SS). The non-outlier range is defined as the range of values which fall outside 1.5× the interquartile range of the distribution (height of the 25% – 75% box). Not significantly different developmental stages are indicated by a common underlined letter next to the box (Tukey's test at α=0.05).

4.1.4. Discussion

Neutral sugars in the cell wall of miscanthus were characterised by employing a procedure consisting of the total acid hydrolysis of CWM samples followed by HPAEC-PAD separation and detection. Leaf and stem biomass collected from eight genotypes at three distinct developmental stages of maturity were used in this analysis. Two HPAEC-PAD separation methods differing in temperature and flow rate (Section 4.1.2) allowed for five monosaccharides to be identified and quantified (Fig. 4.2). The results were then used to estimate total sugar content of the cell wall and to draw conclusions with respect to the abundance of the different cell wall structural polysaccharides, across tissues, developmental stages and different genotypes.

Analysed stem samples showed an overall decrease in total sugar contents throughout development (Table 4.1), most notably in the CWM from the *M.* × *giganteus* genotype. In contrast, despite the overall trend in leaves for a decrease from AG to SS, total sugars only fell an average of 1.72%, and for most genotypes (5 out of 8) sugar contents were actually higher in the senesced tissues. Reduced total sugar content at later time points could be at least partially explained by the accumulation of non-carbohydrate components in the cell wall, most prominently lignin, which has been determined to become more abundant in the tissues as development progresses (Section 2.4). By contrast, in order to gain more detailed information regarding the differences between genotypes and tissues during development, each cell wall monosaccharide was assessed individually.

Cell wall neutral sugars were divided into two groups based on their relative abundance: major cell wall monosaccharides (Glc, Xyl, Ara) and minor monosaccharides (Fuc, Gal) (Fig. 4.2). The abundance of both minor sugars, Fuc and Gal were consistent with the values from other miscanthus studies (Le Ngoc Huyen *et al.*, 2010; Lygin *et al.*, 2011). Fuc is typically associated with xyloglucans and with pectic polysaccharides, both frequently considered to be

less abundant in type-II cell walls of grasses than in type-I walls, found in other plant groups such as dicots or non-commelinoid monocots (Thomas *et al.*, 1989a; Carpita, 1996). Furthermore, it is known that contrary to dicot species, pectic RG-I in grass cell walls does not possess fucosyl residues (Thomas *et al.*, 1989b). These observations could explain the extremely low amounts at which Fuc was found in miscanthus cell wall. However, despite these reduced values, variation in Fuc content was found to be significant between genotypes; significant (with relatively low effect size) between developmental stages; and not significant at all between tissues. These results are in accordance with results from other grass species, such as in *Brachypodium distachyon*, where it was shown that Fuc abundance did not significantly differ between samples collected from different organs at various stages of maturity (Rancour *et al.*, 2012).

Gal, in grass cell walls, is predominantly derived from galactans, mainly in the form of arabinogalactans, which typically occur as side-chains of pectic polysaccharides or as part of AGPs (Carpita, 1996). For all miscanthus genotypes analysed, CWM isolated from leaves had higher Gal content than stems. This is in strong agreement with Le Ngoc Huyen *et al.* (2010), who also observed that Gal occurred in minor amounts but at significantly higher proportions in leaves and leaf-sheaths than in stem internodes. In terms of developmental variation, Gal initially increased in both tissues during growth, from AG up to PB. After this point, Gal content in stems remained relatively constant and did not change significantly as plants senesced. However, in senesced leaves, Gal content became markedly lower (Fig. 4.3). High Gal contents in cell walls during early stages of plant maturity have also been observed in *Brachypodium distachyon* (Rancour *et al.*, 2012). Since galactans are the main Gal-containing cell wall polysaccharides and occur mostly associated with pectins and AGPs, which are less abundant in secondary cell walls (Ishii, 1997b; O'Neil and York, 2003), low Gal contents were predicted later on during development, when primary cell walls made up a smaller proportion

of the plant biomass. Furthermore, it was observed that Fuc and Gal contents do not vary equally throughout development for all genotypes. Given the fact that these variations were significant, and that grasses contain extremely low amounts of structural AGPs (Carpita, 1996), it may be inferred that the composition of the pectin fraction of the cell wall is quantitatively different between genotypes, and that the deposition of secondary wall with its concomitant reduction of pectin abundance does not occur at the same rate in all genotypes.

Glc was the most abundant cell wall monosaccharide in all miscanthus samples analysed. Cellulose and MLG are the main sources of Glc in Poales cell walls (Carpita, 1996). Nonetheless, the quantified Glc is essentially derived from cellulose, since MLG, and other glucose-containing hemicelluloses, such as xyloglucan, represent smaller proportions of the cell wall than cellulose in type-II cell walls (Vogel, 2008). A comparable value for the average Glc content across all analysed samples (44.22%), and higher abundances in stems than in leaves have been reported for miscanthus (Le Ngoc Huyen *et al.*, 2010; Zhang *et al.*, 2012) and for *Brachypodium distachyon* (Rancour *et al.*, 2012). Similarly, variation in Glc content of cell wall biomass according to genotype has been reported in a study where cell wall composition was assessed in *M. sinensis* and in *M.* × *giganteus* samples (Lygin *et al.*, 2011). Higher contents of Glc and of total sugars in CWM from stems, when compared with leaves, is associated with higher amounts of structural polysaccharides, which represent the main load-bearing network in the thickened walls of specialised cell types, that are more abundant in stems (Harris and Stone, 2008; Xu, 2010; Leroux, 2012).

Divergence in Glc abundance between genotypes was particularly high at the AG developmental stage (Table 4.2). The miscanthus genotypes studied here differed substantially in terms of tiller length and weight (Section 2.1), which implies different rates of plant growth. This genotype-derived morphological divergence could explain a higher variation in glucan cell wall contents at AG, since it is known that grass cell walls incorporate MLG specifically

during cell expansion (Carpita, 1996), and given different growth rates, MLG incorporation may not be similar for all genotypes. It has been shown that MLG may occur in mature grass tissues (Vega-Sánchez *et al.*, 2013); nonetheless, the influence of MLG is expected to be reduced after the AG stage, as these glucans are at least partially enzymatically hydrolysed following cell expansion (Buckeridge *et al.*, 2004).

After AG, it was found that Glc contents of leaves became continuously less differentiated between genotypes as plants matured, however, in stems, inter-genotype variability decreased from AG to PB, but then increased at SS. It is known that during senescence the translocation of nutrients from above-ground tissues to the rhizome occurs at a faster rate in leaves than it does in stems (Smith and Slater, 2011). As a result, by the time SS samples were harvested, most leaf biomass was at an equally advanced stage of senescence. By contrast, since translocation in stems happens more gradually over the winter period (Smith and Slater, 2011), it is possible that when the whole tillers were harvested at the end of the growth season (SS), not all stems were equally senesced. Additionally, it has been reported that during senescence there is a decrease in cell wall content in carnation (*Dianthus caryophyllus*) biomass, which is largely due to a loss of Gal and Ara (de Vetten and Huber, 1990). Bearing this in mind, it is likely that in the cell walls of miscanthus samples studied here, the leaves were similarly senesced when harvested, and consequently the translocation of nutrients had progressed to an equivalent stage, thus leading to less variable cellulose proportions between genotypes. This is further supported by the fact that in the miscanthus samples here analysed, the abundance of Gal and Ara also decreased in leaves as they senesced, but not in stems (Fig. 4.3 and Fig. 4.4). In stems, progression of senescence may occur at different rates in different genotypes, leading to different degrees of senescence in harvested stems, and varying proportions of non-cellulosic cell wall components, ultimately influencing the percentage of cellulose in the CWM of senesced plants. It is likely that absolute cellulose contents remain

relatively unchanged for a given tissue after maturity is reached, as synthesis of new cell walls is expected to decrease as plants reach peak biomass and enter senescence. In this scenario, Glc levels change primarily as a consequence of fluctuations in non-cellulosic components of the cell wall, as cellulose contents should remain relatively unchanged for a given tissue after maturity. This view may be supported by the ranking of genotypes in terms of Glc content, which mostly derives from cellulose abundance and becomes constant in both tissues at PB and SS; with *M. sacchariflorus* as the genotype with highest Glc content, followed by *M.* × *giganteus* and hyb03, with the *M. sinensis* genotypes showing the lowest levels.

Senesced leaf and stems generally had lower Glc contents than actively growing samples. These observations are in agreement with the lower Glc content reported in miscanthus stems and leaves at later harvest times (Le Ngoc Huyen *et al.*, 2010). However, despite this being true for all stem samples analysed, in the leaf of four miscanthus genotypes, Glc was up to 6.37% more abundant at senescence (Table 4.2). Furthermore, while in stems Glc abundance continuously decreased from one developmental stage to the next, in leaves Glc contents initially fell between AG and PB, but then increased as plants senesced. A decrease in Glc would be expected after AG, as primary walls are more abundant at this developmental stage and contain higher amounts of MLG, which is enzymatically reduced at later stages (Buckeridge *et al.*, 2004). However, an increase in abundance at SS in leaf tissues is observed, not only for Glc, but also for Xyl (Fig. 4.4). This may provide support to the hypothesis that structural polysaccharides (mostly cellulose and xylan) achieve higher proportions within the biomass of senesced leaves as a consequence of a faster progressing senescence-induced remobilisation of Gal and Ara associated polysaccharides (such as arabinogalactan) and non-structural components in leaves than in stems.

Contrary to the overall trend of decreasing Glc and Xyl content from AG to PB, the abundance of both these monosaccharides in genotypes hyb03 and sin13 was higher in leaf

tissues at PB. This demonstrates that variations throughout development in the abundance of the two major cell wall monosaccharides does not happen in a similar way for all genotypes.

The genotypes used in this study represent flowering and non-flowering genotypes, for example, the two highest yielding genotypes do not usually flower under UK conditions and are sterile triploids[*]. Therefore, cell wall modifications that occur, namely to support the flowering panicle will only be represented in flowering genotypes and not be present in non-flowering types. Senescence and flowering are linked and so earlier flowering genotypes may be more developmentally mature at an earlier time-point than non-flowering genotypes.

Specifically, compositional divergence between the genotypes may arise from at least two situations. Firstly, it is possible that given different genotype morphologies (Section 2.1), there are different requirements from the cell walls, in terms of plant support and transport, which are reflected in wall composition and structure, possibly giving rise to genotype-specific cell wall compositions. Secondly, as discussed above, it is possible that some genotypes achieve different stages of development at different rates and consequently, at a given harvest time, the relative abundances of cell wall components differ between the genotypes; namely the abundance of primary or secondary walls at PB. This second hypothesis may be supported by the fact that examples which diverge from the general trend of Glc and Xyl abundance are observed primarily in foliar biomass. In leaf samples, some of the compositional variability among genotypes is expected to derive from the fact that the abundance of leaf tissue also varies between the genotypes (Section 2.1), which will affect the extent of leaf formation and tissue expansion between genotypes. This will be responsible for differing proportions of primary and secondary walls in the leaf biomass. The FTIR-PCA results reported in chapter 2 corroborates this theory (Fig. 2.4 D and E), since these showed that, with the exception of

[*] Purdy, December 2015. Personal communication.

senesced leaf samples, which clustered more closely together, there was much more compositional variability in the samples from other developmental stages.

Ara content in the cell wall varied primarily according to tissue origin. Leaf generally contained almost twice as much Ara than stems, but this difference decreased slightly throughout development. Ara decreases as plants mature for both tissues, but in stems the contents were statistically indistinguishable between PB and SS (Fig. 4.4). Given that in grass cell walls, a big proportion of Ara occurs as substituents of xylan backbones (Carpita, 1996), the variation of Ara abundance can be interpreted to a great extent as a result of changes in arabinoxylan (AX) ornamentation. However, it is worth noting that in miscanthus there are other less abundant Ara-containing cell wall polysaccharides; namely arabinogalactans, which may occur as side chains of the complex multi-domain pectic glycan RG-I, and associated to proteins (Xue *et al.*, 2013) (see also chapter 5). Ara and Xyl combined ranged from 13.02% of the cell wall to 21.97% in leaves, and from 13.98% to 23.06% in stems, which is comparable to published values for miscanthus (Le Ngoc Huyen *et al.*, 2010; Zhang *et al.*, 2012; Si *et al.*, 2015), and confirms that AX is the main hemicellulose in miscanthus, similar to other grass lignocellulosic feedstocks such as corn stover, wheat straw, rice straw and sorghum biomass (Pauly and Keegstra, 2008). The combined Ara and Xyl contents indicate that on average the total AX contents were not considerably different between leaf and stem tissues; however, the estimation of AX ramification according to the Ara/Xyl ratio showed significant differences between tissues, developmental stages and genotypes.

The Ara/Xyl ratio positively accounts for the degree of Ara substitutions in xylan. For a given genotype, the CWM from leaves had higher Ara/Xyl ratios than stems at all developmental stages (Table 4.8), indicating that in the foliar tissues of miscanthus AX is more substituted than in stems. Overall, xylan substitution with Ara, as indicated by the Ara/Xyl ratio, was approximately two times higher in leaves than in stems, although the difference

between tissues reduced slightly as plants matured. Nonetheless, Ara/Xyl ratios always varied primarily according to tissue origin. Differences between genotypes were the second biggest source of variation in Ara/Xyl ratios, followed by developmental variation in leaves, but not in stems, since no significant differences were detected between developmental stages (Fig. 4.5; Table 4.9). Ara/Xyl ratios typically decreased in leaves as plants matured and entered senescence, and for all genotypes they were higher at AG than at SS. These differences between tissues and developmental stages are in agreement with previously reported values for miscanthus (Le Ngoc Huyen *et al.*, 2010) and for *Brachypodium distachyon* (Rancour *et al.*, 2012). Additionally, in sugarcane it has been reported that the degree of AX branching is higher in leaf than in culm (de Souza *et al.*, 2013).

At all developmental stages, *M. sinensis* genotypes contained the highest Ara/Xyl ratios, particularly sin11, which in fact has an unusually high degree of Ara substitution in leaves at PB (Fig. 4.5). By contrast, below average degrees of substitution were typically found in non-*M. sinensis* genotypes (gig01, hyb03 and sac01 in Table 4.8). At PB and SS, the ranking order of genotypes in terms of their Ara/Xyl ratio was more consistent in stems than in leaves (Table 4.8). This observation was also made for the contents of Glc and *p*CA (Section 3.2), and this trend is also very similar to that observed with the FTIR-PCA analysis (Fig. 2.4 D and E). These results showed that after maturation of the plant, stem cell wall composition does not change much, while in leaves higher compositional variability impedes the formation of clear separate clusters, probably because different leaves were at various stages of development at a given harvest time.

It has been shown that low-branched xylans are often associated to lignification, and that highly substituted AXs are more frequently found in primary cell walls, while less substituted xylans are more abundant in secondary cell walls (Suzuki *et al.*, 2000). Bearing this in mind, and that samples with lower Ara/Xyl ratios have lower arabinose ramification, the collected

data strongly suggest that higher proportions of secondary walls are found in stems, in leaves at later development stages and in genotypes with below average Ara/Xyl ratios at a given developmental stage; such as gig01, hyb03, sac01 and sin09. This is also in accordance with reported observations that older miscanthus internodes are richer in thick secondary walls than leaves and sheaths (Le Ngoc Huyen *et al.*, 2010).

Extensive AX branching may partially restrict the ability of enzymes to degrade wall polysaccharides, since it is known that xylanases are unable to efficiently deconstruct AX forms that are highly substituted with Ara (Correia *et al.*, 2011). By contrast, it has also been reported that the degree of arabinose substitution in xylans enhances lignocellulose enzymatic digestibility, as it negatively affects cellulose crystallinity (Li *et al.*, 2013a). In addition, the fact that dilute alkali may extract xylans with many side chains, but higher concentrations are required for more un-substituted structures (Fry, 2010) attests that xylan recalcitrance varies inversely in relation to how substituted the polymers are. This clearly demonstrates cell wall complexity and how the same aspects may oppositely influence the availability of wall monosaccharide for biorefining applications. As a result, the identification and quantification analyses performed in this section are key steps in the process of optimising the utilisation of miscanthus cell wall biomass. Accordingly, the information collected regarding the cell wall monosaccharides and the estimated degrees of AX branching will play a fundamental role not only in the subsequent section, where the enzymatic hydrolysis of the cell wall will be assessed with and without a pretreatment to improve saccharification results, but also in chapter 6, where relations between cell wall features and recalcitrance will be further discussed.

4.2. Enzymatic Cell Wall Hydrolysis and the Effect of an Alkaline Pretreatment

4.2.1. Overview

As living organisms adapted to their ecological surroundings, plants have evolved complex mechanisms to maintain the structural integrity of their cell walls, thus resisting attacks on their structural glycans. This cell wall recalcitrance, or resistance to depolymerisation by enzymes, is largely dependent on the ability of these hydrolytic agents to access their substrates in the walls (Harris and Stone, 2008). From a biorefining point of view, restricted enzyme access is mostly related to two features of the cell wall biomass. Firstly, the exposed surface area of the biomass plays a major role, as smaller particle sizes of the material lead to greater surfaces susceptible to enzyme action (Chundawat *et al.*, 2007). Secondly, at a molecular level, several structural elements of the cell wall polymers represent severe hindrance to enzyme action. Namely: the arrangement of cellodextrins in the crystalline core of cellulose microfibrils renders this polymer highly resistant to chemical and biological hydrolysis (Nishiyama *et al.*, 2002); covalent linking of lignin with other wall polymers significantly restricts the action of degradative enzymes (Harris and Stone, 2008); and the presence of FA and *p*CA in the cell walls, which not only enables polymer cross-linking, but also inactivates certain fungal glucosidases (Scheller and Ulvskov, 2010; Ximenes *et al.*, 2011). Additionally, it has been observed that by de-acetylating cell wall biomass, its digestibility is increased (Grohmann *et al.*, 1989; Kong *et al.*, 1992). AX branching also has an influence on the enzymatic hydrolysis of wall polysaccharides, but its effect may be complex; on the one hand, it has been reported that highly decorated forms of AX are poorly degraded, as steric constraints restrict xylanase access (Pell *et al.*, 2004; Correia *et al.*, 2011), whereas on the other

hand, the degree of arabinose substitution in xylans may enhance saccharification, as substituents negatively affect cellulose crystallinity (Xu *et al.*, 2012; Li *et al.*, 2013a).

At a biorefinery level, pretreatments are essential and are conducted early on in the biomass processing pipeline to enhance the efficiency of subsequent enzymatic hydrolysis and fermentation processes (Mosier *et al.*, 2005). Physical size reduction of the feedstock is considered a pretreatment on its own, as well as hot water and steam explosion pretreatments (Sørensen *et al.*, 2008; Li *et al.*, 2013b), but chemical treatments of the biomass are often used to further and extensively increase cell wall saccharification. Diverse acid and alkaline pretreatments have been extensively characterised (Li *et al.*, 2013a). Dilute acid pretreatments mainly act by breaking glycosidic linkages, releasing individual monosaccharides (Saha *et al.*, 2005; Xu *et al.*, 2012; Wyman *et al.*, 2013), primarily from hemicelluloses, which is thought to expose crystalline cellulose (Himmel *et al.*, 2007) and alter anatomical and topochemical features of the tissues (Ji *et al.*, 2015), improving enzymatic digestibility.

Alkaline pretreatments have been considered particularly promising procedures to increase the biodegradability of lignocellulosic feedstocks (Jackson, 1977; Sharma *et al.*, 2013). In contrast to acid pretreatments, mild alkaline does not cause a significant release of individual monosaccharide components, as these pretreatments primarily lead to solvation and saponification of the CWM thus swelling the biomass, and breaking ester bonds that cross-link polysaccharides with each other and with lignin, thereby making cellulose more accessible to hydrolytic enzymes (Hendriks and Zeeman, 2009; Xu *et al.*, 2012; Li *et al.*, 2013a; Wyman *et al.*, 2013). By studying how plant cell wall saccharification is affected by alkaline pretreatments, not only may more efficient methods for biomass conversion be developed, but also valuable information can be generated regarding cell wall assembly.

At a laboratory level, in order to reliably assess differences in digestibility between lignocellulosic samples, efforts must be made not only to downscale biomass processing steps,

but also to avoid the attenuation of differences in recalcitrance between CWM samples, which may happen when very harsh pretreatments are used. Instead, mild pretreatments are considered to be better suited to be used as part of sensitive screening methods to identify biomass characteristics affecting saccharification potential (Gomez *et al.*, 2008; Gomez *et al.*, 2010). In the present study, the aim was not to determine the most efficient pretreatment method to facilitate saccharification of miscanthus CWM, but instead to assess the biomass saccharification potential when a pretreatment that maintains near total cell wall carbohydrate content is used; hence permitting comparisons between genotypes, developmental stages and tissues. For this aim, the 0.1M KOH treatment discussed in chapter 3 was considered to be appropriate for the following reasons: 1) The solubilised fractions resulting from this treatment were analysed by HPLC and its impact on the cell wall is at least partially known; 2) As this is a very mild pretreatment, no extensive modification of the cell wall composition is expected, thus allowing the detection of differences in recalcitrance between the samples, while still being potentially able to enhance the amenability to saccharification.

In comparison with acid pretreatments, but also with other alkaline pretreatments, there has been relatively less use of KOH as a pretreatment chemical (Sharma *et al.*, 2013). However, KOH pre-treatments have been characterised in several lignocellulosic feedstocks, such as switchgrass (Sharma *et al.*, 2013), rice straw (Ong *et al.*, 2010) and poplar (Chang and Holtzapple, 2000). Additionally, KOH pretreatment seems to have several advantages, specifically: its ability to de-acetylate and reduce biomass hydroxycinnamoyl substituents, which acid pretreatments do not (Chang and Holtzapple, 2000; Kumar and Wyman, 2009) (Chapter 3), and at equal enzyme loadings and similar experimental conditions it has been reported that KOH pretreatments lead to higher carbohydrate yields than NaOH treatments (Ong *et al.*, 2010). Furthermore, it has been reported that KOH has higher reactivity with carbon structures than NaOH does, as has been shown by Raymundo-Piñero *et al.* (2005), who

compared the effect of KOH and NaOH as carbon activating agents on the structural pattern of carbon nanotubes, and observed that KOH could degrade highly ordered tubular structures, whereas NaOH was only effective with disordered materials.

Notwithstanding its obvious usefulness for the study of cell wall saccharification, assays using hydrolytic enzymes are also valuable as a means to better understand cell wall structures; given that by assessing how prone CWM is to enzymatic hydrolysis before and after pretreatments, conclusions may be drawn regarding the structural diversity of the cell wall polymers. In this section, the yield of individual monosaccharides was determined by enzymatic hydrolysis of the CWM, followed by HPAEC-PAD analysis with the aim of estimating enzymatic release of cell wall carbohydrate and to assess the impact of a pretreatment on biomass saccharification. Based on data presented in other chapters of this thesis, a mild alkaline pretreatment with 0.1M KOH was considered to be the most suitable for the aim of performing a multilevel assessment of cell wall recalcitrance, while exploring the effects of pretreatment and enzymatic hydrolysis on cell wall disassembly.

4.2.2. Materials and methods

The digestibility of CWM from 8 miscanthus genotypes was determined following an approach consisting of the enzymatic hydrolysis of un-pretreated (UT) and pretreated (PT) biomass, followed by HPAEC-PAD analysis of released sugars. Previously isolated CWM was used for this assay (Section 2.2).

Pretreated samples were prepared following a procedure identical to that described in section 3.1.2, according to which, approximately 10mg of CWM was incubated in 500µL of 0.1M KOH for 16h (21°C/150rpm). Once pretreated, the samples were centrifuged at 2500×g for 5min, the supernatants were discarded, and the pellets were washed 5 times in 850µL of

0.025M potassium acetate buffer (KOAc; pH=5.6[*]) to remove interfering chemicals and to optimise the pH for enzymatic hydrolysis (Lan *et al.*, 2013).

Enzymatic hydrolysis of UT and PT samples was achieved using an enzyme cocktail consisting of a mixture of Celluclast (NS 50013; cellulase) and Novozyme 188 (NS 50010; β-glucosidase) at a 4:1 ratio (both obtained from Novozymes, Bagsvaerd, Denmark). Supplementation with the β-glucosidase was to reduce the inhibitory effect of cellobiose accumulation on cellulase activity[†]. Specifically, an incubation mixture was prepared and dispensed in such a way that per each CWM sample there were 997μL of KOAc buffer at 0.025M (pH=5.6), 2.4μL of Celluclast, and 0.6μL of Novozyme 188, with added sodium azide at 0.04% (w/v) to inhibit microbial growth. Subsequently, both UT and PT biomass samples were incubated at 50°C/150rpm. Cocktails were prepared so that cellulase loadings were in excess of 14 filter paper units per gram (FPU/g) of CWM, based on a cellulase activity value of 60FPU/mL for Celluclast (Lan *et al.*, 2013). Some well-established published saccharification assays use lower cellulase loadings than the ones used here (Gomez *et al.*, 2010; Gomez *et al.*, 2011). Higher concentrations were used to ensure enzyme amounts would not be limiting to the reactions; thus maximising hydrolysis and ensuring that digestion results would reflect biomass recalcitrance as much as practically possible.

After 36h of incubation each sample was diluted ten-fold (1:10) by adding 9mL deionised H_2O, followed by centrifugation to produce a particulate-free supernatant. Monosaccharide chromatographic separation and quantitation were performed similarly to the method described

[*] 0.025M potassium acetate (KOAc) buffer (pH = 5.6)
1. Prepare:
   A: 0.2M acetic acid by mixing 138.6μL glacial acetic acid in 12mL H_2O
   B: 0.2M potassium acetate by dissolving 2217.06mg potassium acetate in 113mL H_2O
2. Prepare 250mL of 0.1M KOAc by mixing 12mL of A, 113mL of B, and 125mL H_2O
3. Prepare 1000mL of 0.025M KOAc by adding 250mL of 0.1M KOAc to 750mL H_2O
4. Confirm pH=5.6 (5.5 – 5.6).

[†] Novozymes NS 50013: contains a cellulase from *Trichoderma reesei* that hydrolyses (1→4)-β-glucosidic linkages in cellulose and other β-glucans into glucose, cellobiose and other oligomers. Novozymes NS 50010: contains a β-glucosidase from *Aspergillus niger* that hydrolyses cellobiose to glucose.

in section 4.1.2. Briefly: immediately before HPAEC-PAD, samples were diluted by mixing 50µL of the 1:10-diluted samples with 950µL deionised H_2O, resulting in a dilution factor of 1:200. Subsequently, 400µL of these diluted samples were transferred to filter-vials and analysed by HPAEC-PAD on an ICS-5000 ion chromatography system with a CarboPac SA10 column, operated at 45°C with isocratic elution at a flow rate of 1.5mL/min. All samples were analysed in duplicate. Identification and supernatant concentrations of enzymatically released Ara, Glc and Xyl were determined using a standard curve prepared with a concentration gradient of the appropriate monosaccharide standards, and contents were expressed as percentage of CWM dry weight according to equation 4.1. These enzymatically released monosaccharide amounts were then used to determine what percentage they would represent of the total corresponding monosaccharide contained within the cell wall:

$$Percentage_{Total\ Mns} = \frac{Enz.\ Mns}{Total\ Mns} \times 100\% \quad (4.2)$$

Where Enz. Mns is the amount of enzymatically released monosaccharide from the sample; Total Mns is the total amount of monosaccharide in the sample, previously determined by total acid hydrolysis of the cell wall (Section 4.1). All statistical tests were performed as described in section 4.1.2.

4.2.3. Results

Enzymatic saccharification of miscanthus CWM was assessed with and without a mild alkaline pretreatment consisting of incubating CWM samples with 0.1M KOH for 16h at 21°C. Subsequently, the products were analysed by HPAEC-PAD, revealing that only the major cell wall monosaccharides (Glc, Xyl and Ara) could be detected at appreciable amounts after

enzymatic deconstruction of the CWM. Figure 4.6 shows the separation of enzymatic hydrolysis products of un-pretreated (UT) and pretreated (PT) CWM from genotype sin09 in an example of a typically obtained chromatogram. In UT and in PT samples, Glc was the most prominent peak in all chromatograms, followed by Xyl and then Ara (Fig. 4.6). By comparing peak prominence between developmental tissues, for Glc and Ara the peaks were proportionally more pronounced in leaf than in stems. By contrast, for Xyl at AG and SS, stem samples revealed more pronounced peaks, whereas at PB the opposite was observed. Concerning the application of the 0.1M KOH treatment, for all samples analysed there was a decidedly obvious increase in detected sugar in pretreated samples. These observations were suggestive of substantial differences in abundance of released monosaccharide between tissues, developmental stages and following pretreatment action.

The yields of the three major cell wall monosaccharides were assessed, rather than merely the yield of the main cell wall hexose, with the aim of evaluating saccharification potential, as well as providing insight into cell wall assembly and into the mechanisms affecting polymer destruction by enzyme action. When expressed, as a sum of the three monosaccharides, total enzymatically released sugars reached maxima of 22.60% and 49.01% of the CWM, respectively in UT and PT samples of actively growing stems from genotype sac01 (Table 4.10). The lowest total sugar release was observed from senesced stem samples, but in different genotypes in PT (gig01, 27.06% of the CWM), and in UT samples (sin09, 5.40% of the CWM).

In UT samples (Table 4.11), the highest value for enzymatically released Ara was observed in leaf samples harvested from actively growing plants of genotype sac01 (0.43% CWM), while the minimum was observed in senesced stems from sin08 (0.05% CWM). Ara release increased substantially with pretreatment (Table 4.12), and the observed maximum was in AG leaf from sin11 (1.39% CWM), whereas the minimum was in SS stems from gig01 (0.57% CWM). Similarly to the total sugar yields, the absolute extent of Glc release was the

highest from actively growing stems of sac01, as maxima of 7.07% and 34.14% CWM were observed for UT and PT samples respectively (Tables 4.11 and 4.12). Samples with the lowest absolute Glc yields did not coincide before and after pretreatment, as genotype sin09 released 4.23% CWM as Glc in UT samples, whereas after pretreatment genotype sin15 released the minimum amount of 17.79% CWM (Tables 4.11 and 4.12); however, in both cases these values were observed in senesced stems. Absolute enzymatic yield of Xyl as a proportion of the CWM dry weight was also noticeably increased after pretreatment. As seen for Glc, the highest Xyl yields were observed in actively growing stems before and after pretreatment, but in this case, the maximum values were detected in genotype sin13: 5.40% CWM in UT and 14.69% CWM in PT samples (Tables 4.11 and 4.12). Contrary to the other two analysed sugars, the minimum Xyl yields were observed in leaves, at the senesced stage: 0.45% CWM for UT samples (sin09) and 6.63% CWM for PT samples (sin08).

Quantifying the absolute enzymatic release of cell wall monosaccharides as percentage of the cell wall dry weight is useful to assess how amenability to saccharification varies across miscanthus CWM samples collected from different genotypes, developmental stages and tissues. Nevertheless, to better understand and compare the impact of pretreatment and enzymatic hydrolysis on the release of cell wall sugars between samples, it is necessary to express the yields of individual sugars as a percentage of the total respective monosaccharide occurring in the cell wall (previously determined in section 4.1); these percentages are presented in tables 4.13 and 4.14 The statistical significance of the pretreatment, genotype, tissue and development stage factors on the extractability of Ara, Glc and Xyl were assessed by ANOVA (Table 4.15), revealing that these factors had a significant influence on the saccharification of the cell wall (P<0.001 for all monosaccharides). The application of pretreatment was the main source of variation in the yields of the three monosaccharides, as a statistical effect size greater than 0.8 for the pretreatment effect was the biggest for all three

sugars (Table 4.15). By interpreting the remaining effect sizes it was seen that the genotype factor was the second strongest influence on the variation in the yields of the three monosaccharides (η^2_{Ara}=0.0467; η^2_{Glc}=0.0328; η^2_{Xyl}=0.0191); however, relevant trends were also observed according to the tissue and development stage from where the CWM samples were taken.

In UT samples, enzymatic release of Ara as percentage of total Ara in the cell wall ranged from 2.41% to 21.48% (Table 4.13), and between 31.20% and 94.77% in PT samples (Table 4.14). The maximum value for the proportion of released Ara was observed in actively growing samples, while the lowest was seen at senescence in UT biomass. However, after pretreatment the lowest percentage of released Ara was found in an AG sample, and the highest at PB. Higher percentages of total Ara were typically extracted from stems in UT and in PT samples (Tables 4.13 and 4.14). By looking at the overall variation of Ara release along development it is observed that different trends occur before and after pretreatment (Fig. 4.7). In UT CWM from leaves, the overall Ara release decreased by 48.93% between AG and PB and then by 17.24%, between this developmental stage and SS. After pretreatment, despite a slight increase of 1.86% from AG to PB, and then 1.18% from PB to SS (Table 4.14 and Fig. 4.7), the percentages of released Ara were not statistically different from one developmental stage to the next. As observed with leaves, Ara release decreased throughout development in UT stem samples (-33.77 AG – PB and -27.25 PB – SS; Table 4.13), but after pretreatment Ara extractability decreased between the two first developmental stages and then increased as plants senesced (Table 4.14), although the difference between PB and SS was not significant (Fig. 4.7).

The overall proportions of enzymatically extracted Glc were higher in leaves than in stems, and noticeably increased after pretreatment, as they ranged from 9.76% to 38.17% in UT biomass, and from 37.45% to 72.39% after pretreatment (Tables 4.13 and 4.14). UT leaf

cell wall samples showed an overall decrease in enzymatically released Glc from AG to PB (-34.64%) and from PB to SS (-17.42%; Table 4.13 and Fig. 4.7). By contrast, in pretreated leaf CWM, despite most genotypes showing a decrease in enzymatically released Glc from AG to PB, the overall trend was for a slight, but non-significant, increase in Glc extractability between these two developmental stages, followed by a statistically significant 2.85% decrease as plants senesced (Table 4.14 and Fig. 4.7). For the CWM from stems there was a decrease in Glc extractability throughout development in both UT and PT samples (Tables 4.13 and 4.14), but this trend was more pronounced in the non-treated samples (Fig. 4.7).

The positive effect of the 0.1M KOH pretreatment was particularly noticeable in Xyl yields, as released proportions were never below 48.66% and reached up to 94.40% of total Xyl in the cell wall (Table 4.14), contrasting with a range of 2.68% – 34.73% in UT samples (Table 4.13). In all CWM samples not subjected to pretreatment the highest percentages of extracted Xyl were found to be in stems, averaging 2.57 times higher when compared to leaves. In pretreated samples, the Xyl yields were more similar between tissues, as the overall ratio of stem to leaf Xyl release was 1.09. As observed for the other monosaccharides, in UT samples the percentage of extracted Xyl decreased throughout development (Table 4.13 and Fig. 4.7). In pretreated stems, this same trend of overall decreasing Xyl yields along development was also observed (-9.43% AG – PB and -5.45% PB – SS; Table 4.14). However, in pretreated leaf the overall proportion of extracted Xyl became 8.93% higher at the PB stage, and then decreased 9.94% at SS (Table 4.14 and Fig. 4.7). Notwithstanding these overall trends in the extractability of Ara, Glc and Xyl, not all genotypes had an identical variation throughout development or in different tissues, suggesting genotype-specific responses to the pretreatment and to enzymatic hydrolysis.

Compared to other genotypes, the extractability of Ara from *M. sacchariflorus* (sac01) UT samples was generally above average, in both tissues and at all developmental stages (Table

4.13). However, in UT senesced stems and leaves, despite the samples from sac01 still displaying the fourth highest extracted Ara value, the three top ranking genotypes were hyb03, gig01 and sin13. In pretreated samples, the extractability of Ara from sac01 genotypes was not particularly high; the highest value was observed with genotype hyb03, at all developmental stages and in both tissues, with the exception of stem at PB, where hyb03 had the second highest value (Table 4.14).

UT and PT samples from genotype sin13 displayed generally high proportions of released Xyl. In fact, this was the only genotype that always released above average Xyl quantities, independent of tissue and developmental stage. By contrast, the genotypes sin11 and sin15 frequently displayed intermediate to low yields (Tables 4.13 and 4.14). However, there was extensive variation in the relationships between genotypes concerning their proportions of released Xyl, since for a particular tissue at a given developmental stage, the pretreatment not only enhanced the proportions of released monosaccharide, but in some cases it also altered how the different genotypes compared to each other (compare Tables 4.13 and 4.14). Specifically, in UT samples from actively growing stems and leaves of sac01 and hyb03 intermediate levels of released Xyl were observed, with slightly higher values for sac01. However, after pretreatment, the hyb03 genotype showed the third highest value, while sac01 showed the lowest. A similar observation was made for genotypes gig01 and sin09 in stems collected at PB, which showed intermediate values in UT samples, however once pretreated their samples respectively released the lowest and the highest ratio proportion of Xyl. In addition or SS stage stems, Xyl release from genotype sin09 increased from the lowest value pretreatment, to the highest in PT samples.

Of the eight studied genotypes, in both tissues and at all developmental stages, sin15 consistently showed below average proportions of released Glc. No genotype showed a predominantly high proportion of Glc release in all situations. Nonetheless, for each individual

tissue it was observed that sin09 leaves and sin13 stems generally showed above average values in UT and in PT samples (Tables 4.13 and 4.14). As seen for Ara and Xyl, when comparing proportions of Glc release between UT and PT samples, the ranking of Glc extractability for some genotypes was very distinct; namely, stems and leaves at PB and SS from genotypes sac01 and gig01 showed relatively high levels of released Glc in UT samples, but were among the lowest in PT samples (Tables 4.13 and 4.14).

These observations on the enzymatic release of the three major cell wall monosaccharides clearly demonstrate that the positive influence of the pretreatment on released sugars is not equivalent among the genotypes. This is true for the three sugars analysed, but in the case of Glc extractability it is also important to note that the samples that showed the highest or lowest proportion of released Glc did not necessarily coincide with the samples which showed high or low saccharification yields; measured as Glc release as percentage of the dry weight of the CWM (compare Tables 4.11 and 4.12 with Tables 4.13 and 4.14). To give some examples: UT samples from AG leaves from genotype sin11 showed a well below average proportion of released Glc (Table 4.13), but the third highest yield of Glc as percentage of CWM dry weight (Table 4.11); pretreated senesced leaves from sin13 showed the third highest proportion of extracted Glc (Table 4.14), but in terms of absolute release as percentage of the cell wall it showed the second lowest yield (Table 4.12); and for genotype sac01, its pretreated senesced stems showed the third highest saccharification yield (Table 4.12), but its percentage of extracted Glc was the second lowest (Table 4.14).

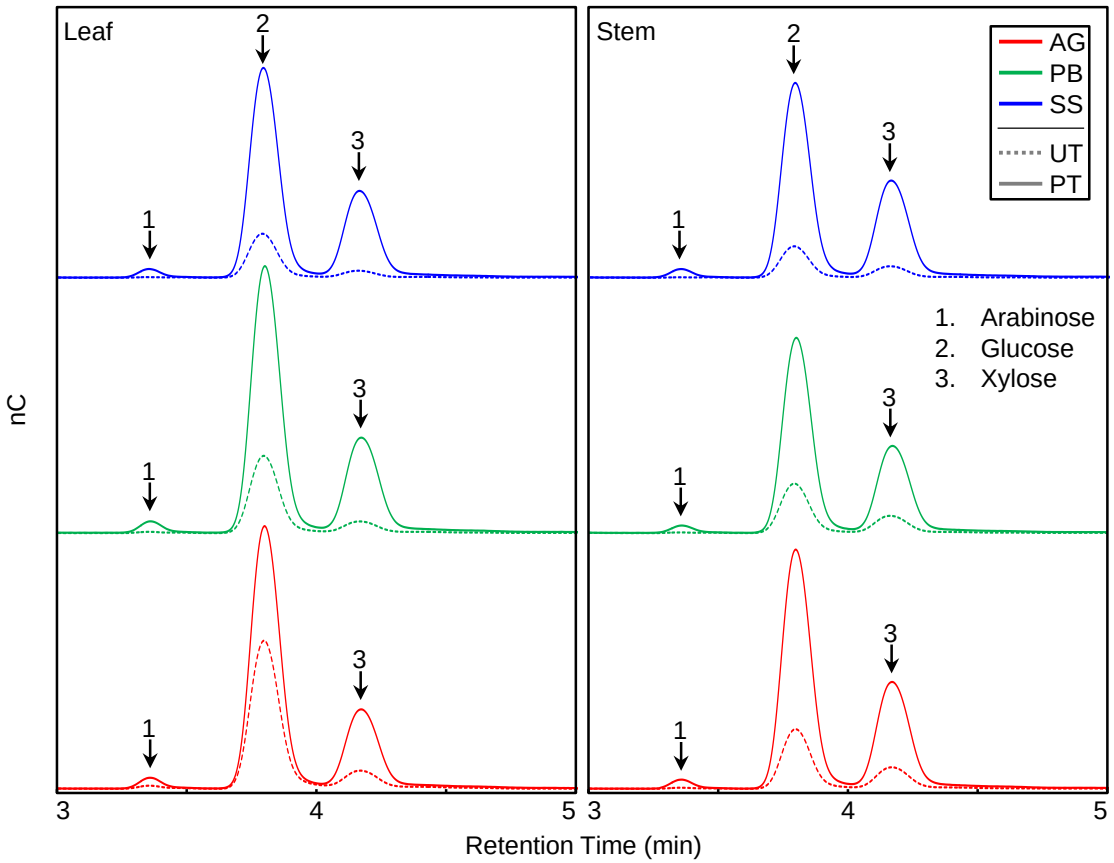

Fig. 4.6. HPAEC-PAD chromatograms obtained from enzymatic hydrolysis (cellulase supplemented with β-glucosidase) of CWM from miscanthus genotype sin09. Chromatograms are shown between minutes 3 and 5, the retention time interval where arabinose, glucose and xylose are eluted. Dotted lines indicate hydrolysis products obtained from un-pretreated samples (UT), and full lines correspond to enzymatically hydrolysed CWM pretreated with 0.1M KOH (PT). See section 4.2.2 for method details. Developmental stages: active growth (AG), peak biomass (PB) and senescence (SS). (nC: nano-Coulomb)

Table 4.10. Total monosaccharides released upon enzymatic hydrolysis (cellulase supplemented with β-glucosidase) of pretreated (PT) and un-pretreated (UT) miscanthus CWM. Values are given for three developmental stages, two tissues and consist of the sum of arabinose, glucose and xylose yields expressed as a percentage of cell wall material dry weight (% CWM) for each genotype.

	Active Growth		**Peak Biomass**		**Senescence**	
	Leaf	**Stem**	**Leaf**	**Stem**	**Leaf**	**Stem**
			Total (% UT CWM)			
gig01	14.40	16.42	9.70	10.45	9.86	8.41
hyb03	12.50	14.56	8.56	9.14	10.39	9.77
sac01	17.59	22.60	10.00	11.79	7.00	13.32
sin08	14.85	17.31	7.00	10.14	5.71	5.90
sin09	18.64	10.09	10.55	8.61	5.97	5.40
sin11	14.98	10.74	9.65	9.20	6.74	5.53
sin13	15.09	20.39	6.96	14.30	7.47	8.12
sin15	7.32	8.49	6.42	10.33	5.79	5.67
Mean	14.42	15.07	8.60	10.50	7.37	7.76
			Total (% PT CWM)			
gig01	38.65	42.22	34.35	29.47	34.23	27.06
hyb03	35.90	45.59	39.36	36.09	42.17	38.01
sac01	41.99	49.01	36.44	36.12	34.82	37.05
sin08	34.28	45.02	32.66	31.55	33.32	31.35
sin09	42.18	36.18	38.06	39.40	37.43	36.63
sin11	40.49	34.87	37.40	35.34	39.13	34.08
sin13	31.59	44.99	29.54	36.22	31.59	29.29
sin15	27.20	32.28	31.13	31.69	31.16	27.18
Mean	36.53	41.27	34.87	34.48	35.48	32.58

Table 4.11. Monosaccharides released upon enzymatic hydrolysis (cellulase supplemented with β-glucosidase) of un-pretreated (UT) miscanthus CWM. Values are given for three developmental stages, two tissues and are expressed as mean percentage (± standard deviation) of cell wall material dry weight (% CWM) for each genotype.

	Active Growth		**Peak Biomass**		**Senescence**	
	Leaf	**Stem**	**Leaf**	**Stem**	**Leaf**	**Stem**
			Arabinose (% CWM UT)			
gig01	0.32 ± 0.01	0.13 ± 0.00	0.17 ± 0.00	0.09 ± 0.02	0.16 ± 0.03	0.09 ± 0.01
hyb03	0.30 ± 0.01	0.17 ± 0.01	0.13 ± 0.00	0.09 ± 0.02	0.21 ± 0.01	0.11 ± 0.01
sac01	0.43 ± 0.01	0.19 ± 0.01	0.19 ± 0.02	0.11 ± 0.01	0.10 ± 0.00	0.09 ± 0.03
sin08	0.28 ± 0.01	0.19 ± 0.01	0.11 ± 0.02	0.10 ± 0.01	0.06 ± 0.01	0.05 ± 0.00
sin09	0.34 ± 0.01	0.14 ± 0.01	0.16 ± 0.02	0.09 ± 0.01	0.07 ± 0.00	0.07 ± 0.00
sin11	0.25 ± 0.00	0.17 ± 0.00	0.13 ± 0.00	0.10 ± 0.01	0.08 ± 0.01	0.06 ± 0.01
sin13	0.31 ± 0.02	0.37 ± 0.01	0.11 ± 0.00	0.20 ± 0.02	0.14 ± 0.01	0.11 ± 0.01
sin15	0.17 ± 0.01	0.14 ± 0.01	0.11 ± 0.01	0.14 ± 0.01	0.08 ± 0.00	0.06 ± 0.01
Mean	0.30 ± 0.07	0.19 ± 0.08	0.14 ± 0.03	0.12 ± 0.04	0.11 ± 0.05	0.08 ± 0.03
			Glucose (% CWM UT)			
gig01	12.71 ± 0.04	12.79 ± 0.10	8.78 ± 0.02	8.24 ± 0.11	8.88 ± 0.31	6.65 ± 0.04
hyb03	10.98 ± 0.03	11.16 ± 0.07	7.81 ± 0.01	7.12 ± 0.08	9.21 ± 0.07	7.60 ± 0.58
sac01	15.22 ± 0.20	17.07 ± 0.19	9.01 ± 0.14	9.43 ± 0.09	6.44 ± 0.03	9.97 ± 0.28
sin08	12.85 ± 0.02	12.99 ± 0.04	6.25 ± 0.07	7.79 ± 0.03	5.08 ± 0.01	4.69 ± 0.01
sin09	16.52 ± 0.03	7.63 ± 0.18	9.36 ± 0.01	6.64 ± 0.04	5.46 ± 0.01	4.23 ± 0.06
sin11	13.65 ± 0.01	7.96 ± 0.03	8.97 ± 0.02	7.26 ± 0.01	6.05 ± 0.01	4.32 ± 0.01
sin13	13.34 ± 0.04	14.62 ± 0.01	6.18 ± 0.05	11.80 ± 0.02	6.77 ± 0.09	6.40 ± 0.01
sin15	6.10 ± 0.03	6.40 ± 0.01	5.86 ± 0.03	7.68 ± 0.05	5.13 ± 0.01	4.44 ± 0.03
Mean	12.67 ± 3.14	11.33 ± 3.74	7.78 ± 1.46	8.24 ± 1.66	6.63 ± 1.61	6.04 ± 2.04
			Xylose (% CWM UT)			
gig01	1.37 ± 0.01	3.50 ± 0.04	0.76 ± 0.01	2.12 ± 0.05	0.82 ± 0.16	1.66 ± 0.01
hyb03	1.23 ± 0.01	3.24 ± 0.04	0.62 ± 0.02	1.93 ± 0.01	0.97 ± 0.08	2.06 ± 0.19
sac01	1.93 ± 0.03	5.35 ± 0.08	0.80 ± 0.02	2.25 ± 0.02	0.47 ± 0.02	3.26 ± 0.11
sin08	1.72 ± 0.01	4.12 ± 0.07	0.64 ± 0.01	2.26 ± 0.01	0.56 ± 0.01	1.16 ± 0.01
sin09	1.78 ± 0.01	2.33 ± 0.07	1.03 ± 0.01	1.87 ± 0.01	0.45 ± 0.01	1.10 ± 0.07
sin11	1.08 ± 0.01	2.61 ± 0.01	0.55 ± 0.01	1.84 ± 0.01	0.61 ± 0.01	1.15 ± 0.03
sin13	1.44 ± 0.08	5.40 ± 0.06	0.68 ± 0.08	2.30 ± 0.01	0.56 ± 0.01	1.61 ± 0.01
sin15	1.05 ± 0.02	1.95 ± 0.01	0.45 ± 0.04	2.51 ± 0.01	0.58 ± 0.01	1.17 ± 0.01
Mean	1.45 ± 0.33	3.56 ± 1.31	0.69 ± 0.18	2.14 ± 0.24	0.63 ± 0.18	1.64 ± 0.74

Table 4.12. Monosaccharides released upon enzymatic hydrolysis (cellulase supplemented with β-glucosidase) of miscanthus CWM pretreated with 0.1M KOH (PT). Values are given for three developmental stages, two tissues and are expressed as mean percentage (± standard deviation) of cell wall material dry weight (% CWM) for each genotype.

	Active Growth		**Peak Biomass**		**Senescence**	
	Leaf	**Stem**	**Leaf**	**Stem**	**Leaf**	**Stem**
			Arabinose (% CWM PT)			
gig01	1.25 ± 0.01	0.77 ± 0.02	1.02 ± 0.01	0.61 ± 0.00	1.00 ± 0.01	0.57 ± 0.01
hyb03	1.15 ± 0.01	0.96 ± 0.02	1.31 ± 0.05	0.81 ± 0.01	1.36 ± 0.00	0.84 ± 0.04
sac01	1.25 ± 0.01	0.91 ± 0.01	1.05 ± 0.00	0.72 ± 0.01	1.11 ± 0.02	0.96 ± 0.02
sin08	1.04 ± 0.01	0.89 ± 0.05	0.79 ± 0.05	0.61 ± 0.03	0.83 ± 0.01	0.59 ± 0.02
sin09	1.23 ± 0.00	0.87 ± 0.02	1.10 ± 0.02	0.98 ± 0.05	1.00 ± 0.02	0.99 ± 0.01
sin11	1.39 ± 0.01	0.89 ± 0.01	1.28 ± 0.01	0.91 ± 0.03	1.23 ± 0.01	0.88 ± 0.02
sin13	1.19 ± 0.03	1.06 ± 0.02	1.02 ± 0.00	0.80 ± 0.02	0.95 ± 0.10	0.87 ± 0.04
sin15	1.08 ± 0.00	0.90 ± 0.01	1.10 ± 0.03	0.77 ± 0.02	1.06 ± 0.02	0.62 ± 0.02
Mean	1.20 ± 0.11	0.91 ± 0.08	1.08 ± 0.16	0.77 ± 0.13	1.07 ± 0.17	0.79 ± 0.17
			Glucose (% CWM PT)			
gig01	27.96 ± 0.07	29.92 ± 0.24	23.76 ± 0.05	20.84 ± 0.01	23.70 ± 0.04	18.78 ± 0.03
hyb03	25.71 ± 0.01	31.45 ± 0.33	27.38 ± 0.02	24.63 ± 0.09	28.93 ± 0.11	25.95 ± 0.23
sac01	30.95 ± 0.11	34.14 ± 0.01	25.97 ± 0.05	24.35 ± 0.06	23.99 ± 0.07	22.63 ± 0.03
sin08	24.37 ± 0.01	31.73 ± 0.69	22.81 ± 0.28	21.17 ± 0.14	25.87 ± 0.06	22.31 ± 0.02
sin09	31.42 ± 0.03	24.40 ± 0.06	27.25 ± 0.04	26.64 ± 0.07	25.77 ± 0.04	23.84 ± 0.04
sin11	29.68 ± 0.02	22.53 ± 0.08	26.50 ± 0.07	22.56 ± 0.24	26.58 ± 0.07	21.57 ± 0.10
sin13	22.42 ± 0.01	29.23 ± 0.16	20.52 ± 0.11	24.62 ± 0.28	22.32 ± 1.54	19.85 ± 0.02
sin15	18.82 ± 0.01	20.33 ± 0.02	22.54 ± 0.36	21.03 ± 0.03	20.87 ± 0.01	17.79 ± 0.02
Mean	26.42 ± 4.42	27.97 ± 4.94	24.59 ± 2.54	23.23 ± 2.14	24.75 ± 2.55	21.59 ± 2.70
			Xylose (% CWM PT)			
gig01	9.44 ± 0.04	11.53 ± 0.14	9.57 ± 0.03	8.03 ± 0.06	9.53 ± 0.02	7.72 ± 0.01
hyb03	9.04 ± 0.02	13.18 ± 0.21	10.67 ± 0.01	10.65 ± 0.02	11.88 ± 0.04	11.22 ± 0.14
sac01	9.80 ± 0.14	13.96 ± 0.02	9.42 ± 0.01	11.06 ± 0.03	9.72 ± 0.08	13.46 ± 0.05
sin08	8.87 ± 0.01	12.39 ± 0.04	9.06 ± 0.33	9.77 ± 0.01	6.63 ± 0.05	8.45 ± 0.04
sin09	9.53 ± 0.02	10.92 ± 0.05	9.71 ± 0.01	11.78 ± 0.06	10.66 ± 0.05	11.80 ± 0.15
sin11	9.42 ± 0.01	11.45 ± 0.10	9.62 ± 0.07	11.87 ± 0.24	11.33 ± 0.03	11.62 ± 0.08
sin13	7.98 ± 0.02	14.69 ± 0.03	8.00 ± 0.05	10.80 ± 0.03	8.33 ± 0.54	8.57 ± 0.04
sin15	7.29 ± 0.03	11.04 ± 0.02	7.49 ± 0.01	9.90 ± 0.04	9.23 ± 0.03	8.77 ± 0.05
Mean	8.92 ± 0.86	12.40 ± 1.41	9.19 ± 1.01	10.48 ± 1.25	9.66 ± 1.69	10.20 ± 2.07

Table 4.13. Monosaccharides released upon enzymatic hydrolysis (cellulase supplemented with β-glucosidase) of un-pretreated (UT) miscanthus CWM. Values are given for three developmental stages, two tissues and are expressed as mean percentage (± standard deviation) of the total amount of the corresponding monosaccharide for each genotype (previously determined as described in section 4.1). Values within a column sharing a letter in their superscript are not significantly different according to a Tukey's test (α=0.05).

	Active Growth		Peak Biomass		Senescence	
	Leaf	**Stem**	**Leaf**	**Stem**	**Leaf**	**Stem**
			Arabinose (UT % total arabinose)			
gig01	12.31 ± 0.44^{cd}	12.90 ± 0.01^{ad}	6.81 ± 0.01^{cde}	9.50 ± 2.24^{ab}	6.70 ± 1.12^{c}	9.14 ± 0.56^{b}
hyb03	13.17 ± 0.26^{de}	13.79 ± 0.56^{a}	5.56 ± 0.01^{bcd}	8.52 ± 1.45^{a}	8.68 ± 0.26^{d}	10.06 ± 0.57^{b}
sac01	14.54 ± 0.39^{f}	15.34 ± 1.14^{a}	7.85 ± 0.81^{e}	8.97 ± 1.06^{a}	4.00 ± 0.01^{ab}	6.84 ± 2.15^{ab}
sin08	10.79 ± 0.26^{b}	13.95 ± 0.50^{a}	4.67 ± 0.74^{ab}	6.58 ± 0.44^{a}	3.05 ± 0.33^{a}	3.53 ± 0.01^{a}
sin09	14.10 ± 0.22^{ef}	11.17 ± 1.06^{cd}	7.32 ± 0.84^{de}	9.01 ± 1.27^{a}	3.27 ± 0.01^{a}	4.92 ± 0.01^{a}
sin11	6.10 ± 0.01^{a}	9.21 ± 0.01^{bc}	3.68 ± 0.01^{ab}	5.71 ± 0.30^{a}	2.41 ± 0.15^{a}	3.86 ± 0.42^{a}
sin13	11.41 ± 0.56^{bc}	21.48 ± 0.36^{e}	5.13 ± 0.01^{abc}	13.97 ± 1.32^{b}	5.52 ± 0.27^{bc}	8.84 ± 1.05^{b}
sin15	4.93 ± 0.35^{a}	7.56 ± 0.35^{b}	3.60 ± 0.19^{a}	7.56 ± 0.35^{a}	3.29 ± 0.01^{a}	3.60 ± 0.85^{a}
Mean	10.92 ± 3.58	13.18 ± 4.24	5.58 ± 1.62	8.73 ± 2.49	4.61 ± 2.17	6.35 ± 2.72
			Glucose (UT % total glucose)			
gig01	28.29 ± 0.08^{e}	22.52 ± 0.18^{b}	20.49 ± 0.05^{f}	16.82 ± 0.22^{b}	19.82 ± 0.69^{c}	13.27 ± 0.09^{b}
hyb03	27.20 ± 0.07^{ab}	22.31 ± 0.13^{b}	19.10 ± 0.02^{a}	14.55 ± 0.15^{a}	21.46 ± 0.16^{d}	16.07 ± 1.22^{c}
sac01	27.63 ± 0.35^{b}	27.84 ± 0.31^{d}	18.85 ± 0.30^{a}	17.33 ± 0.16^{c}	14.16 ± 0.07^{b}	18.16 ± 0.51^{d}
sin08	34.06 ± 0.06^{f}	28.95 ± 0.09^{e}	17.60 ± 0.19^{e}	18.94 ± 0.06^{d}	12.95 ± 0.03^{a}	11.44 ± 0.01^{ab}
sin09	37.84 ± 0.06^{c}	17.10 ± 0.41^{a}	23.16 ± 0.01^{b}	14.58 ± 0.10^{a}	12.79 ± 0.01^{a}	9.76 ± 0.14^{a}
sin11	27.07 ± 0.02^{a}	17.21 ± 0.06^{a}	22.61 ± 0.04^{b}	16.69 ± 0.01^{b}	14.19 ± 0.02^{b}	10.27 ± 0.01^{a}
sin13	38.17 ± 0.11^{c}	36.20 ± 0.01^{f}	16.50 ± 0.14^{d}	28.02 ± 0.04^{e}	19.08 ± 0.25^{c}	16.22 ± 0.01^{c}
sin15	14.72 ± 0.06^{d}	14.81 ± 0.02^{c}	15.28 ± 0.09^{c}	17.49 ± 0.12^{c}	12.37 ± 0.03^{a}	10.61 ± 0.07^{a}
Mean	29.37 ± 7.56	23.37 ± 7.25	19.20 ± 2.78	18.05 ± 4.29	15.85 ± 3.65	13.22 ± 3.21
			Xylose (UT % total xylose)			
gig01	9.07 ± 0.03^{ab}	21.02 ± 0.23^{b}	5.18 ± 0.03a^{b}	14.52 ± 0.36^{d}	5.53 ± 1.10^{cd}	10.81 ± 0.01^{b}
hyb03	9.68 ± 0.04^{a}	20.67 ± 0.23^{b}	4.57 ± 0.17^{a}	12.89 ± 0.08^{b}	5.70 ± 0.45^{d}	13.40 ± 1.25^{c}
sac01	10.15 ± 0.14^{a}	24.51 ± 0.35^{d}	4.90 ± 0.12^{a}	11.26 ± 0.10^{a}	2.68 ± 0.09^{a}	16.16 ± 0.53^{d}
sin08	14.09 ± 0.08^{d}	30.59 ± 0.50^{e}	5.24 ± 0.04^{ab}	17.51 ± 0.07^{f}	4.14 ± 0.01^{abcd}	8.73 ± 0.01^{a}
sin09	12.86 ± 0.06^{c}	15.79 ± 0.48^{a}	8.59 ± 0.11^{d}	13.72 ± 0.04^{c}	2.70 ± 0.05^{a}	7.30 ± 0.49^{a}
sin11	6.26 ± 0.02^{e}	15.93 ± 0.01^{a}	4.53 ± 0.01^{a}	11.32 ± 0.03^{a}	3.52 ± 0.06^{ab}	7.35 ± 0.16^{a}
sin13	13.93 ± 0.75^{cd}	34.73 ± 0.41^{f}	6.08 ± 0.70^{b}	18.27 ± 0.11^{g}	5.10 ± 0.09^{bcd}	12.67 ± 0.04^{bc}
sin15	8.15 ± 0.18^{b}	12.97 ± 0.09^{c}	3.21 ± 0.28^{c}	15.28 ± 0.09e	3.89 ± 0.03^{abc}	7.62 ± 0.01^{a}
Mean	10.52 ± 2.84	22.03 ± 7.57	5.29 ± 1.56	14.34 ± 2.61	4.16 ± 1.19	10.50 ± 3.31

Table 4.14. Monosaccharides released upon enzymatic hydrolysis (cellulase supplemented with β-glucosidase) of miscanthus CWM pretreated with 0.1M KOH (PT). Values are given for three developmental stages, two tissues and are expressed as mean percentage (± standard deviation) of the total amount of the corresponding monosaccharide for each genotype (previously determined as described in section 4.1). Values within a column sharing a letter in their superscript are not significantly different according to a Tukey's test (α=0.05).

	Active Growth		**Peak Biomass**		**Senescence**	
	Leaf	**Stem**	**Leaf**	**Stem**	**Leaf**	**Stem**
			Arabinose (PT % total arabinose)			
gig01	48.17 ± 0.24^{f}	74.49 ± 1.85^{a}	42.30 ± 0.51^{b}	62.81 ± 0.01^{b}	42.20 ± 0.28^{ab}	55.34 ± 0.98^{c}
hyb03	51.00 ± 0.26^{b}	78.65 ± 1.63^{a}	57.39 ± 2.08^{d}	76.86 ± 0.53^{d}	55.98 ± 0.01^{c}	76.22 ± 3.14^{a}
sac01	41.85 ± 0.20^{a}	75.27 ± 0.56^{a}	42.33 ± 0.01^{b}	56.77 ± 0.98^{ab}	47.00 ± 0.78^{b}	73.09 ± 1.59^{ad}
sin08	40.53 ± 0.47^{a}	64.81 ± 3.66^{c}	32.53 ± 1.91^{a}	41.77 ± 2.19^{c}	39.30 ± 0.56^{a}	45.29 ± 1.54^{b}
sin09	50.97 ± 0.01^{b}	71.93 ± 1.68^{a}	52.15 ± 0.72^{c}	94.77 ± 4.57^{e}	47.80 ± 0.88^{b}	75.69 ± 0.47^{a}
sin11	33.71 ± 0.26^{d}	48.79 ± 0.33^{b}	36.23 ± 0.18^{a}	51.51 ± 1.71^{a}	38.04 ± 0.41^{a}	55.30 ± 1.31^{c}
sin13	44.43 ± 1.06^{e}	62.03 ± 0.88^{c}	49.79 ± 0.10^{c}	55.11 ± 1.62^{ab}	38.48 ± 3.91^{a}	67.49 ± 3.26^{d}
sin15	31.20 ± 0.00^{c}	49.49 ± 0.57^{b}	35.50 ± 0.88^{a}	41.60 ± 1.00^{c}	43.55 ± 0.94^{ab}	39.07 ± 1.19^{b}
Mean	42.73 ± 7.45	65.68 ± 11.58	43.53 ± 8.84	60.15 ± 18.04	44.04 ± 6.07	60.93 ± 14.28
			Glucose (PT % total glucose)			
gig01	62.24 ± 0.15^{d}	52.70 ± 0.41^{b}	55.44 ± 0.12^{a}	42.52 ± 0.01^{d}	52.87 ± 0.08^{c}	37.45 ± 0.06^{b}
hyb03	63.70 ± 0.01^{e}	62.91 ± 0.65^{e}	66.95 ± 0.04^{b}	50.31 ± 0.18^{a}	67.40 ± 0.26^{b}	54.85 ± 0.49^{a}
sac01	56.15 ± 0.21^{b}	55.69 ± 0.02^{c}	54.36 ± 0.10^{a}	44.76 ± 0.10^{e}	52.79 ± 0.14^{c}	41.20 ± 0.05^{c}
sin08	64.59 ± 0.01^{g}	70.70 ± 1.53^{d}	64.24 ± 0.78^{d}	51.50 ± 0.33^{ab}	65.92 ± 0.15^{ab}	54.36 ± 0.05^{a}
sin09	71.96 ± 0.07^{h}	54.69 ± 0.13^{bc}	67.37 ± 0.09^{b}	58.47 ± 0.15^{c}	60.41 ± 0.08^{a}	54.99 ± 0.09^{a}
sin11	58.87 ± 0.04^{c}	48.71 ± 0.18^{a}	66.82 ± 0.17^{b}	51.89 ± 0.56^{b}	62.27 ± 0.16^{ab}	51.30 ± 0.25^{f}
sin13	64.15 ± 0.04^{f}	72.39 ± 0.40^{d}	54.84 ± 0.29^{a}	58.48 ± 0.68^{c}	62.87 ± 4.35^{ab}	50.33 ± 0.06^{e}
sin15	45.40 ± 0.01^{a}	47.08 ± 0.04^{a}	58.77 ± 0.94^{c}	47.87 ± 0.06^{f}	50.34 ± 0.02^{c}	42.53 ± 0.05^{d}
Mean	60.88 ± 7.78	58.11 ± 9.58	61.10 ± 5.83	50.72 ± 5.77	59.36 ± 6.51	48.38 ± 6.96
			Xylose (PT % total xylose)			
gig01	62.67 ± 0.28^{d}	69.34 ± 0.83^{a}	65.40 ± 0.22^{e}	54.88 ± 0.38^{a}	64.46 ± 0.13^{ab}	50.36 ± 0.02^{c}
hyb03	71.11 ± 0.14^{f}	84.03 ± 1.35^{e}	78.80 ± 0.08^{a}	71.07 ± 0.14^{b}	69.75 ± 0.26^{bd}	73.07 ± 0.93^{b}
sac01	51.68 ± 0.72^{a}	63.90 ± 0.09^{d}	58.01 ± 0.09^{d}	55.39 ± 0.14^{a}	55.77 ± 0.45^{c}	66.79 ± 0.23^{a}
sin08	72.55 ± 0.11^{g}	92.09 ± 0.31^{c}	73.79 ± 2.65^{b}	75.57 ± 0.07^{e}	48.66 ± 0.36^{e}	63.51 ± 0.26^{e}
sin09	68.70 ± 0.13^{e}	73.95 ± 0.33^{b}	80.87 ± 0.10^{a}	86.26 ± 0.41^{c}	63.74 ± 0.27^{ab}	78.54 ± 1.01^{f}
sin11	54.38 ± 0.05^{b}	69.78 ± 0.63^{a}	78.72 ± 0.55^{a}	73.04 ± 1.50^{b}	65.79 ± 0.20^{ab}	74.50 ± 0.50^{b}
sin13	77.19 ± 0.17^{h}	94.40 ± 0.16^{c}	71.34 ± 0.48^{b}	85.81 ± 0.23^{c}	75.51 ± 4.89^{d}	67.57 ± 0.33^{a}
sin15	56.64 ± 0.22^{c}	73.43 ± 0.15^{b}	54.00 ± 0.03^{c}	60.32 ± 0.25^{d}	61.47 ± 0.17^{ac}	57.36 ± 0.31^{d}
Mean	64.36 ± 9.40	77.62 ± 11.22	70.11 ± 10.06	70.29 ± 12.48	63.14 ± 8.22	66.46 ± 9.31

Table 4.15. ANOVA tables of results for the determination of the major monosaccharides released upon enzymatic hydrolysis of miscanthus CWM.

Effect	Degrees of freedom	Sum of squares	Mean square	*F*-ratio	*P*-value	Effect size (η^2)
Arabinose						
Pretreatment (1)	1	95553.60	95553.60	64103.10	<0.0001	0.8112
Genotype (2)	7	5505.50	786.50	527.60	<0.0001	0.0467
Tissue (3)	1	5394.00	5394.00	3618.60	<0.0001	0.0458
Development Stage (4)	2	653.10	326.50	219.10	<0.0001	0.0055
Pretreatment × Genotype	7	2925.20	417.90	280.30	<0.0001	0.0248
Pretreatment × Tissue	1	3243.30	3243.30	2175.80	<0.0001	0.0275
Genotype × Tissue	7	500.80	71.50	48.00	<0.0001	0.0043
Pretreatment × Development Stage	2	188.20	94.10	63.10	<0.0001	0.0016
Genotype × Development Stage	14	879.80	62.80	42.20	<0.0001	0.0075
Tissue × Development Stage	2	98.90	49.50	33.20	<0.0001	0.0008
Pretreatment × Genotype × Tissue	7	723.30	103.30	69.30	<0.0001	0.0061
Pretreatment × Genotype × Development Stage	14	730.70	52.20	35.00	<0.0001	0.0062
Pretreatment × Tissue × Development Stage	2	114.20	57.10	38.30	<0.0001	0.0010
Genotype × Tissue × Development Stage	14	582.40	41.60	27.90	<0.0001	0.0049
1 × 2 × 3 × 4	14	553.70	39.60	26.50	<0.0001	0.0047
Error	96	143.10	1.50			
Total	191	117789.80				
Glucose						
Pretreatment (1)	1	64232.90	64232.90	217625.60	<0.0001	0.8462
Genotype (2)	7	2491.80	356.00	1206.10	<0.0001	0.0328
Tissue (3)	1	1533.30	1533.30	5194.80	<0.0001	0.0202
Development Stage (4)	2	2510.70	1255.30	4253.20	<0.0001	0.0331
Pretreatment × Genotype	7	977.30	139.60	473.00	<0.0001	0.0129
Pretreatment × Tissue	1	274.90	274.90	931.40	<0.0001	0.0036
Genotype × Tissue	7	687.90	98.30	332.90	<0.0001	0.0091
Pretreatment × Development Stage	2	319.90	159.90	541.90	<0.0001	0.0042
Genotype × Development Stage	14	1304.60	93.20	315.70	<0.0001	0.0172
Tissue × Development Stage	2	47.00	23.50	79.60	<0.0001	0.0006
Pretreatment × Genotype × Tissue	7	75.20	10.70	36.40	<0.0001	0.0010
Pretreatment × Genotype × Development Stage	14	254.60	18.20	61.60	<0.0001	0.0034
Pretreatment × Tissue × Development Stage	2	386.90	193.40	655.40	<0.0001	0.0051
Genotype × Tissue × Development Stage	14	649.50	46.40	157.20	<0.0001	0.0086
1 × 2 × 3 × 4	14	136.40	9.70	33.00	<0.0001	0.0018
Error	96	28.30	0.30			
Total	191	75911.20				
Xylose						
Pretreatment (1)	1	158835.00	158835.30	324505.40	<0.0001	0.9103
Genotype (2)	7	3331.00	475.90	972.30	<0.0001	0.0191
Tissue (3)	1	2540.80	2540.80	5191.00	<0.0001	0.0146
Development Stage (4)	2	1833.10	916.60	1872.60	<0.0001	0.0105
Pretreatment × Genotype	7	2036.60	290.90	594.40	<0.0001	0.0117
Pretreatment × Tissue	1	137.60	137.60	281.20	<0.0001	0.0008
Genotype × Tissue	7	430.80	61.50	125.70	<0.0001	0.0025
Pretreatment × Development Stage	2	257.60	128.80	263.10	<0.0001	0.0015
Genotype × Development Stage	14	1974.10	141.00	288.10	<0.0001	0.0113
Tissue × Development Stage	2	625.00	312.50	638.40	<0.0001	0.0036
Pretreatment × Genotype × Tissue	7	356.90	51.00	104.20	<0.0001	0.0020
Pretreatment × Genotype × Development Stage	14	751.20	53.70	109.60	<0.0001	0.0043
Pretreatment × Tissue × Development Stage	2	226.60	113.30	231.50	<0.0001	0.0013
Genotype × Tissue × Development Stage	14	711.90	50.80	103.90	<0.0001	0.0041
1 × 2 × 3 × 4	14	384.40	27.50	56.10	<0.0001	0.0022
Error	96	47.00	0.50			
Total	191	174480.30				

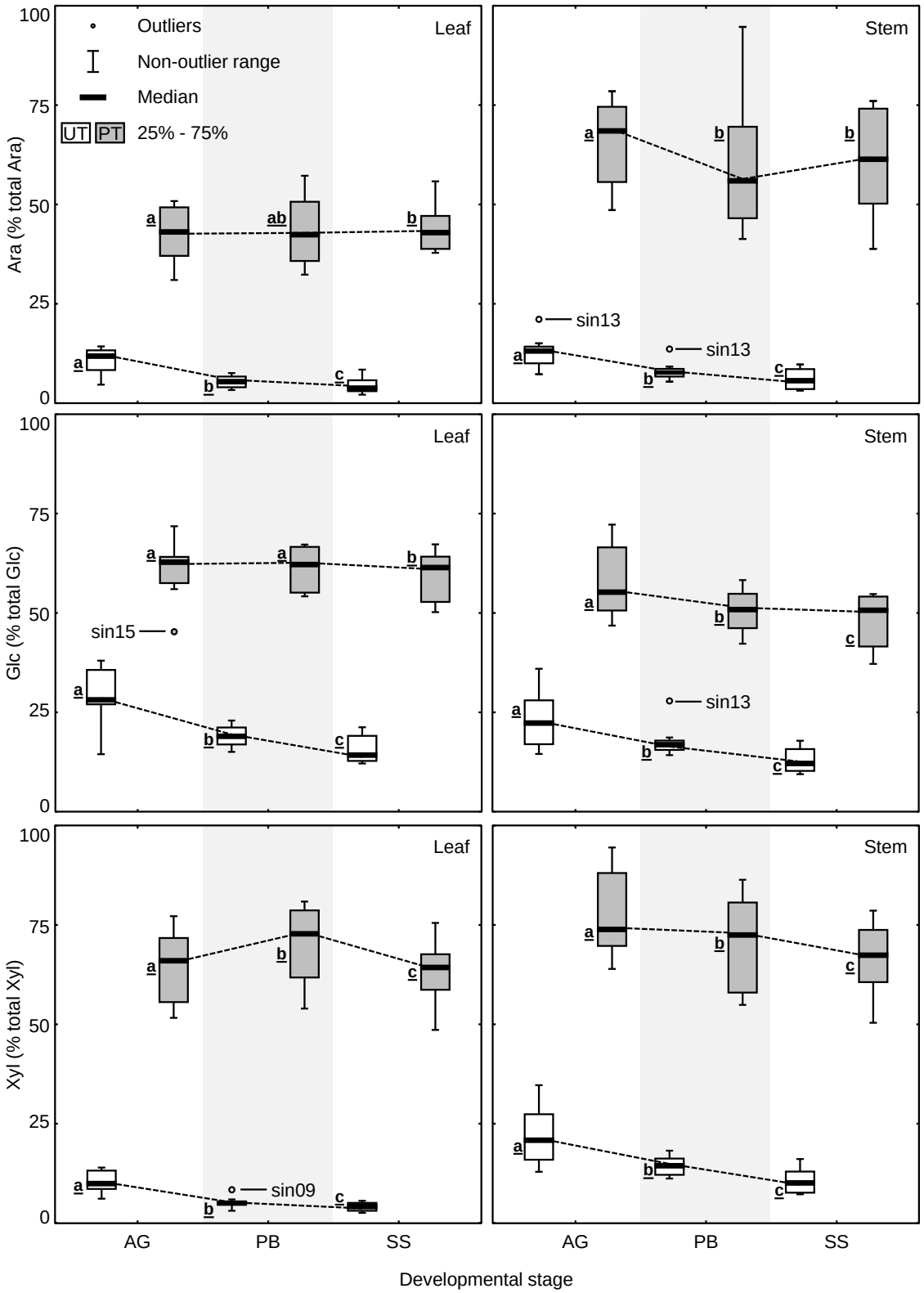

Fig. 4.7. Box plots showing the distribution of measurements of the major monosaccharides Arabinose (Ara), Glucose (Glc) and Xylose (Xyl) released upon enzymatic hydrolysis of miscanthus CWM. Shaded boxes represent the distribution of values obtained from samples pretreated (PT) with 0.1M KOH and the blank boxes correspond to un-pretreated samples (UT). Values are expressed as percentage of the total amount of the corresponding monosaccharide present in the CWM of leaf and stem tissues collected from 8 miscanthus genotypes at active growth (AG), peak biomass (PB) and senescence (SS). The non-outlier range is defined as the range of values which fall outside 1.5× the interquartile range of the distribution (height of the 25% – 75% box). Underlined letters beside boxes indicate Not significantly different developmental stages are indicated by a common underlined letter next to the box (Tukey's test at α=0.05).

4.2.4. Discussion

The enzymatic hydrolysis of miscanthus CWM only allowed for the detection of substantial amounts of Glc, Xyl and Ara. As seen in section 4.1, these are the major cell wall polysaccharide units in miscanthus, which in part explains the high detectability of these sugars. However, it is also possible that the release of certain matrix sugars, such as Gal from pectin, was restricted by the inability of the enzymes used here to adequately degrade the polysaccharides containing this monosaccharide (Hatfield *et al.*, 2009). By observing the HPAEC-PAD chromatograms (Fig. 4.6) it is immediately visible that a pretreatment consisting of incubating cell wall biomass with 0.1M KOH for 16h at 21°C has a marked effect in increasing detected monosaccharide. The usage of KOH solutions as a pretreatment has been previously reported, namely in one case where a range of conditions were tested in switchgrass; revealing that KOH pretreatments are generally very effective at generating high saccharification yields during hydrolysis, even at mild conditions, such as 0.5% KOH, for 12h at 21°C. (Sharma *et al.*, 2013).

Nevertheless, the aim of the enzymatic hydrolysis assay performed in the present study was primarily to monitor differences in saccharification between genotypes, developmental stages and tissues, rather than to improve pretreatment conditions. In addition, it was intended to assess the impact of a pretreatment on saccharification, without extensively modifying cell wall composition. For this end, the previously characterised mild alkaline pretreatment was determined as being an appropriate choice (Chapter 3). The implementation of the mild 0.1M KOH pretreatment has also permitted not only to minimise losses in hemicellulose and lignin content, but also to avoid the camouflaging of differences in recalcitrance between samples; which are known to happen when harsher pretreatments are used (Gomez *et al.*, 2010).

For all analysed samples, by pretreating the CWM with 0.1M KOH, the cell wall polysaccharides were made more accessible for enzymatic hydrolysis, and significant increases

were observed in the saccharification yields (Tables 4.10, 4.11, 4.12), and on the proportions of extracted Glc, Xyl and Ara (Tables 4.13, 4.14).

The *M. sacchariflorus* genotype studied here (sac01) consistently showed high total sugar yields with all PT and UT samples. Total sugar release typically decreased as plants matured for UT samples, and at all developmental stages the total saccharification yields were higher from stem tissues (Table 4.10). However, PT stems typically released higher amounts of total sugar than leaves at the AG stage, but not at PB and SS. These results are comparable to those of Le Ngoc Huyen *et al.* (2010), who used a similar enzyme cocktail and an alkaline pretreatment with aqueous ammonia to assess enzymatic hydrolysis in miscanthus, revealing that the saccharification yields were lower at later harvest times, and that the degradation of cellulose in mature tissues was higher in leaf and sheath tissues than in stem internodes.

For the individual monosaccharides, all three analysed sugars had the highest yields in AG samples, while the lowest were observed in SS samples (Tables 4.11 and 4.12). Actively growing stem samples from genotype sac01 released the highest amounts of Glc as a proportion of the cell wall from UT and PT samples, while for Xyl the maxima were seen in AG stems from sin13 (Tables 4.11 and 4.12). Nevertheless, this agreement in the genotypes between PT and UT samples was not always observed, for example maximum and minimum yields of Ara and the minimum yields of Glc and Xyl did not coincide in the PT and the UT samples. These observations indicate that the effect of the pretreatment in increasing the yield of a given monosaccharide is not equal for all genotypes, even in tissues collected at the same developmental stage. It was also observed that 0.1M KOH does not enhance the extractability of each of the major cell wall monosaccharides equally for all samples, demonstrating that even in the same genotype different sugars respond in different ways to the pretreatment (Tables 4.13 and 4.14). This non-proportional effect of the pretreatment on monosaccharide extractability across the different genotypes supports observations made in previous chapters

that there are fundamental differences in cell wall structural and compositional features, which may be genotype-specific.

As seen in section 4.1, Glc content in the cell wall is typically higher in stem samples (Table 4.2), but this higher abundance did not always equate to higher enzymatic yields of Glc from stems. Table 4.11 shows that upon enzymatic hydrolysis of UT samples the overall Glc yield from stems is only higher than from leaves at the PB developmental stage. In PT samples, actively growing stems released higher absolute amounts of Glc than leaves, but the opposite was observed at PB and SS (Table 4.12). This indicates that cell wall Glc content in the biomass is not a proportional indicator of saccharification yields, thus providing evidence for the concept that interactions between polymers and other structural features of the cell wall represent a strong influence on sugar extractability in addition to mere carbohydrate abundances in the biomass. Also, support for this is the fact that Glc extractability was typically higher from leaves than from stems, before and after pretreatment (Tables 4.13 and 4.14).

In terms of the extractability of the three major cell wall monosaccharides (Tables 4.13, 4.14 and Figure 4.7) not only were significant development and tissue derived differences observed (Table 4.15), but also different responses to pretreatment for each sugar. For UT samples, the yields of the three analysed monosaccharides were significantly higher in AG samples than in more mature samples, from both tissues (Table 4.13 and Fig. 4.7), indicating that the amenability to deconstruction of miscanthus biomass progressively declines throughout development. After applying the pretreatment, despite some differences between developmental stages still remaining significant, they were generally less marked than in UT samples, particularly in leaves (Table 4.14 and Fig. 4.7). However, a notable variation was observed in the trend of Xyl extractability throughout development in PT samples, since it continuously decreased in stems, but in leaves it increased at PB and then declined at SS (Fig. 4.7). Another distinctive feature of the effect of the pretreatment on Xyl yields was that it

caused a marked reduction of the average difference in Xyl extractability between leaf and stem tissues for a given developmental stage, in comparison to non-treated samples (compare Tables 4.13 and 4.14). Both these observations may be attributed to a greater effectiveness of the pretreatment on the enhancement of Xyl extractability from leaves than from stems (see also Table 4.16). Glc extractability from PT leaf samples did not vary very much between developmental stages. By contrast, in pretreated stems a continuously significant decrease in Glc yields was observed throughout development (Fig. 4.7). This suggests that, at least in leaf samples, the amenability to saccharification of the biomass is primarily dependent on the presence of compounds involved in polymer linking, which are partially removed during the pretreatment (Chapter 3). These observations indicate that the disruptive effect of the pretreatment on lignocellulosic biomass was not the same for the three major cell wall monosaccharides, as the ratios between the percentage of total monosaccharide enzymatically released from PT and UT samples (PT/UT) varied substantially (Table 4.16). These ratios provide a measure for the pretreatment effectiveness on increasing the extractability of monosaccharides. For Ara and Glc the pretreatment was more effective at increasing monosaccharide yields in later developmental stages than in earlier stages. However, for Xyl yields there was a more marked effect of the pretreatment in leaves than in stems (Table 4.16). As a proportion of each total monosaccharide in the cell wall, upon enzymatic hydrolysis, the pretreated samples typically released approximately seven times more of Ara and three times more Glc than before the treatment. For Xyl extractability, the pretreatment had a clearly different effect on the different tissues, since overall extractability increased more than eleven times in leaves, but less than five times in stems. Although no continuous increase along development was observed for any of the monosaccharides in terms of their saccharification yields or extractability, the PT/UT ratios clearly indicate that the effectiveness of the pretreatment increased as plants matured.

One of the effects of the 0.1M KOH pretreatment was the partial removal of HCAs and acetate (Chapter 3), so it is conceivable that these compounds do in fact have a role as enhancers of cell wall recalcitrance. However, on a first analysis, higher or lower abundances of these ester bound compounds do not seem to vary in strict accordance with the lesser or greater effect of the pretreatment in promoting saccharification. One possible explanation could be related to the fact that in later harvest times 0.1M KOH generally becomes less efficient at removing HCAs from the cell wall, particularly in stems (as shown in the comparative table 3.7); which may indicate that later in plant maturity a higher proportion of the cross-links is maintained, even after pretreatment. This in turn would cause a lesser disruption of the cross-links which sustain cell wall structural integrity (Ishii, 1997b; Ralph, 2010), and thus contribute to higher recalcitrance in more mature tissues. Additionally, it has been reported that Ara substitution degree in xylan may affect the digestibility of CWM from miscanthus, namely after a pretreatment has been employed (Li *et al.*, 2013a). In section 4.1, it was seen that Ara and Xyl contents of the cell wall do not change significantly between developmental stages in mature stem tissues (PB and SS in Fig. 4.4), and particularly for the Ara/Xyl ratio (Fig. 4.5), it remained unchanged throughout the development of stem tissues. By comparing these results with the fact that there is a decline in the amount of enzymatically released Glc from stem tissues as they mature and enter senescence (Fig. 4.7), no general trend is apparent for Ara ornamentation in xylans and Glc extractability such as proportional variation to each other, in a positive or negative way. This may indirectly provide further evidence for the hypothesis that cell wall cross-linking has a more determining influence on cell wall disassembly than polymer abundances do[*].

[*] Further insight on how recalcitrance is associated with Ara ornamentation and with other cell wall features is provided in chapter 6, which contains correlations between cell wall saccharification and various other aspects of cell wall architecture and composition.

The highest or lowest yields of enzymatically released Glc, Xyl and Ara (Tables 4.11 and 4.12) did not always coincide with the highest or lowest extractability values of the corresponding monosaccharide (Tables 4.13 and 4.14). By correlating the sugar yields with monosaccharide extractability (Table 4.17) it was shown that typically high and significant correlations were observed in UT samples. In contrast, for all cell wall monosaccharides investigated, the proportions of total extracted monosaccharide from PT samples were less or even non-significantly correlated with the saccharification yields, despite the absolute sugar yields being significantly higher than from UT samples. The true meaning of these observations remains to be clarified, but they do indicate a complex relation between saccharification yield and sugar extractability, and is highly suggestive that biomass usability is likely to be more influenced by structural features of the cell wall than by mere structural carbohydrate abundance.

The action of the mild alkaline pretreatment used here has been characterised to some extent (Chapter 3), revealing that 0.1M KOH causes little loss of the cell wall major polymers (lignin, cellulose and xylans)[*], suggesting that it is the partial removal of esterified substituents that is mainly responsible for the positive effect of this pretreatment on saccharification (Grohmann *et al.*, 1989; Kong *et al.*, 1992; Ishii, 1997b; Buanafina *et al.*, 2006; Pawar *et al.*, 2013). Consequently, a partial explanation for the mechanism behind the positive effect of 0.1M KOH on saccharification yields could be associated with the saponification of ester-linked diferulates which cross-link matrix polysaccharides (Williamson *et al.*, 1998; Buanafina, 2009). Furthermore, the removal of ester-linked *p*CA may also decrease recalcitrance. Despite the absence of evidence for *p*CA-mediated cross-links between lignin and hemicellulose, it is known that this HCA occurs associated to lignin (Grabber *et al.*, 2004)

[*] However, it should be noted that despite 0.1M KOH causing little disruption of the cell wall major polymers, mild alkaline extractants may remove some of the cell wall pectin, as will be seen in the following chapter. As a result, it should not be excluded at this point that potential pectin removal also has an effect on saccharification enhancement (this topic will be revisited in chapter 6).

and negative correlations have been reported between *p*CA abundance and digestibility of lignocellulosic biomass (Méchin *et al.*, 2000). The disruption of intermolecular ester bonds in the wall would loosen the cell wall network, resulting in increased porosity of CWM. In chapter 3 it was seen that of the cell wall phenolic acids, *p*CA was typically released in greatest abundance. It may thus be conjectured that concerning the impact of the HCAs on saccharification, a great part of the effect of the 0.1M KOH pretreatment is associated to the removal of ester-linked *p*CA; which is known to be mostly bound to lignin (Sun *et al.*, 1998; Grabber *et al.*, 2004). Concerning negative effects on saccharification, they could derive from lignin-related limitations that may lead to non-productive associations with hydrolases (Berlin *et al.*, 2006), i.e., steric hindrance of productive hydrolase binding. As a result, it may be presumed that by employing the 0.1M KOH pretreatment some of the functions performed by *p*CA and lignin on the maintenance of cell wall integrity are deteriorated. Alternatively, some separation of lignin from the structural polysaccharides may be promoted, thus facilitating the access of hydrolytic enzymes and increasing cell wall digestibility. A similar hypothesis has been presented by Paripati and Dadi (2014) as an explanation for the mechanism of action of a mild alkaline treatment. Another possibility for the mechanism of action of the 0.1M KOH pretreatment could be associated to the acetylation of xylan. Enhanced Glc release from miscanthus CWM has been observed after addition of a xylanase supplement to cellulase, indicating that glucose release is enhanced by xylose removal (Le Ngoc Huyen *et al.*, 2010). However, various studies have shown that during saccharification, acetyl groups in xylans create steric hindrance for binding of hydrolytic enzymes, limiting the extent of hydrolysis (Biely, 2012; Pawar *et al.*, 2013). It is known that the enzyme preparation Celluclast used in this assay contains a broad spectrum of cellulolytic enzyme activities, including various cellobiohydrolases and endo-(1→4)-β-glucanases. Most notably, one endo-(1→4)-β-glucanase, EGII, has been reported to have some xylanase activity (Rosgaard *et al.*, 2007).

Given that the 0.1M KOH treatment also causes de-acetylation of the CWM, it may be postulated that the removal of acetyl groups facilitates the hydrolysis of xylans, which in turn leads to an increase in Glc release; since it is known that low amounts of certain xylans lead to reduced wall recalcitrance (Biswal *et al.*, 2015), and that the removal of hemicelluloses can facilitate cellulose enzymatic conversion by promoting cellulase accessibility (Kumar and Wyman, 2009; Qing *et al.*, 2010). Further possibilities to elucidate the effect of pretreatment, and to establish associations between how and why pretreatment effectiveness varies depending on the abundance of cell wall elements with adverse effects on saccharification will be explored in subsequent sections.

Table 4.16. Effectiveness of pretreatment measured as the mean ratio between the percentage of total corresponding monosaccharide enzymatically released from pretreated (PT) and from un-pretreated (UT) CWM.

PT/UT ratio of the percentage of total monosaccharide extracted								
	Active Growth		**Peak Biomass**		**Senescence**		**Mean**	
	Leaf	**Stem**	**Leaf**	**Stem**	**Leaf**	**Stem**	**Leaf**	**Stem**
Arabinose	3.91	4.98	7.81	6.89	9.54	9.60	7.09	7.16
Glucose	2.07	2.49	3.18	2.81	3.74	3.66	3.00	2.98
Xylose	6.12	3.52	13.26	4.90	15.19	6.33	11.52	4.92

Table 4.17. Pearson coefficients of the correlations between the total enzymatic yield of each major cell wall monosaccharide (%CWM) and the percentage of total monosaccharide (% monosaccharide) released from pretreated (PT) and un-pretreated (UT) cell wall samples. Marked correlations (*) are significant at $P<0.05$. For each correlation coefficient N=16, consisting of two replicates from each tissue, of each genotype, at a given developmental stage.

	Active Growth		**Peak Biomass**		**Senescence**	
	Leaf	**Stem**	**Leaf**	**Stem**	**Leaf**	**Stem**
			Arabinose			
UT	0.88*	0.86*	0.86*	0.74*	0.99*	0.96*
PT	0.01	-0.14	0.48	0.58*	0.62*	0.82*
			Glucose			
UT	0.80*	0.85*	0.89*	0.91*	0.94*	0.94*
PT	0.52*	0.62*	0.62*	0.62*	0.74*	0.68*
			Xylose			
UT	0.67*	0.88*	0.90*	0.56*	0.85*	0.93*
PT	-0.24	0.43	0.61*	0.56*	0.49	0.70*

4.3. CONCLUSIONS

Given that variation in cell wall constituents between different developmental stages, tissues and genotypes are reported to have an influence on the wall mechanical properties, extensibility and biodegradability (Jung and Deetz, 1993; Jung, 2012), two assays were employed to assess total monosaccharide composition and amenability to saccharification of miscanthus cell wall biomass (all previously presented data is now summarised in Fig. 4.8).

Significant differences were observed in the carbohydrate fraction of miscanthus cell wall (Tables 4.9 and 4.15). For all studied monosaccharides substantial variation was observed in their cell wall abundance between genotypes, tissues and developmental stages. This observation provides support to the conclusion based on FTIR-PCA that structural polysaccharides are main contributors to the compositional variability during stem development and between stem and leaf tissue (Section 2.3).

Despite higher percentages of cellulose being expected in grass lignocellulosic biomass as tissues mature and secondary wall is deposited (Vogel, 2008), in both leaves and stems it was observed that Glc content in the wall decreased from AG to PB. This reduction in total Glc

in the wall is presumed to result from loss of MLG, since it is known that the quantities of this polymer decrease when cell expansion is complete, indicating breakdown, rather than simply dilution by continued deposition of different polysaccharides (Buckeridge *et al.*, 2004; Fry, 2010). From PB to SS, Glc and Xyl abundance increases in leaves, but decreases in stems, and it is likely that this difference between tissues is a consequence of different rates of senescence-induced remobilisation of cell wall components, such as of Gal and Ara (Shane *et al.*, 2014). The total AX content did not vary substantially between tissues, but their Ara/Xyl ratios were significantly different. The Ara/Xyl ratio can positively account for the degree of Ara substitution of xylan, and generally it was higher in leaves than in stems, decreased along development in leaf tissues, but remained constant in the stems of plants as they matured and entered senescence (Fig. 4.5).

A mild alkaline pretreatment consisting of incubating samples in 0.1M KOH for 16h at 21°C was applied and the amenability of miscanthus cell wall biomass to enzymatic hydrolysis was assessed. With and without the pretreatment, significant differences between genotypes were observed in both tissues at the various developmental stages, in the enzymatic yields of the three main cell wall monosaccharides. No genotype showed a general tendency for a typically high or low sugar yield in all conditions studied. However, for individual tissues it was seen that some genotypes displayed generally above or below average values; which provides further evidence for the hypotheses that there may be a genotype-specific component in cell wall assembly (perhaps associated to the structural requirements demanded by their phenotypes), and that there is an independent control of cell wall composition in different tissues (Murray *et al.*, 2008).

Enzymatic saccharification generally declined throughout development, but in pretreated samples, the differences between developmental stages were much less prominent than in UT samples. Total sugar, and particularly Glc contents were typically higher in stem tissues than

in leaf tissues (Table 4.2), but the enzymatic release of Glc was higher in pretreated mature leaf samples (Table 4.12), confirming that the usability of the monosaccharides contained in miscanthus lignocellulosic biomass is distinct between different tissues. These observations are also clear evidence that harvesting time and tissue origin are very relevant factors which affect saccharification, and should be considered in strategies to optimally maximise lignocellulose biorefining. In addition, the fact that Glc content in the biomass is not proportional to saccharification yields suggests that the interaction between cell wall structural and compositional features is highly influential on sugar extractability.

In line with this is the fact that 0.1M KOH did not enhance the extractability of the major cell wall monosaccharides equally, as the effectiveness of the pretreatment was extremely variable between monosaccharides; and specifically for Xyl release the overall effectiveness was also different between tissues (Table 4.16). Moreover, for a given monosaccharide the influence of the pretreatment on the enhancement of yield varied between developmental stages, being higher later in maturity. Between genotypes, it was also seen that at the same developmental stage and tissue, the effectiveness of the pretreatment on a specific monosaccharide was not the same for all genotypes; thus suggesting that this non-proportional effect of the pretreatment on monosaccharide extractability across the genotypes is a consequence of fundamental differences in cell wall structural and compositional features, which may be genotype-specific. More generally, these observations demonstrate that different structural features, amenable to modification by the pretreatment, have a distinct influence on the recalcitrance of different sugars.

The application of a mild alkaline pretreatment using 0.1M KOH mostly results in a controlled de-esterification of the biomass samples, thus minimising lignin and carbohydrate losses, which may exceed 30% of the hemicellulose contents when harsher pretreatments are used (Kong *et al.*, 1992; Chen *et al.*, 2013; Pawar *et al.*, 2013; Chen *et al.*, 2014; Liu *et al.*,

2014). The use of KOH as a reagent was chosen to comply with the previous assays of biomass acetylation estimation (Section 3.1), characterisation of HCAs (Section 3.2), sequential extraction for glycome profiling (Section 5.1), and also with the application of a base treatment to allow the immunolocalisation of key epitopes in tissue sections (Section 5.2). Furthermore, given that by treating the biomass with 0.1M KOH its effect may be largely characterised, and that the composition of the main wall polymers is not extensively affected (Chapter 3), positive impacts on enzymatic hydrolysis are likely to be predominantly associated to specific cell wall structural disturbance, rather than profound compositional modification.

Results presented in this chapter strongly suggest that in different genotypes, different cell wall features contribute differently to recalcitrance. Also, as different proportions of cell wall components lead to different structural interactions, the overall effect on recalcitrance of a specific cell wall component is also expected to be enhanced or reduced.

Hydrolysis-based assays are limited in the amount of information they can provide, as the quantification of released monosaccharides only allows for indirect conclusions about the *in muro* polymers where they were contained. Consequently, in order to better understand cell wall assembly in miscanthus and how this affects recalcitrance, there is a need to obtain further information regarding the polysaccharides as they occur and how tightly they are bound in the wall ultra-structure. This demonstrates a necessity for additional analyses of the structural polysaccharide contents, which may be satisfied by the immunological approaches presented in the subsequent chapter.

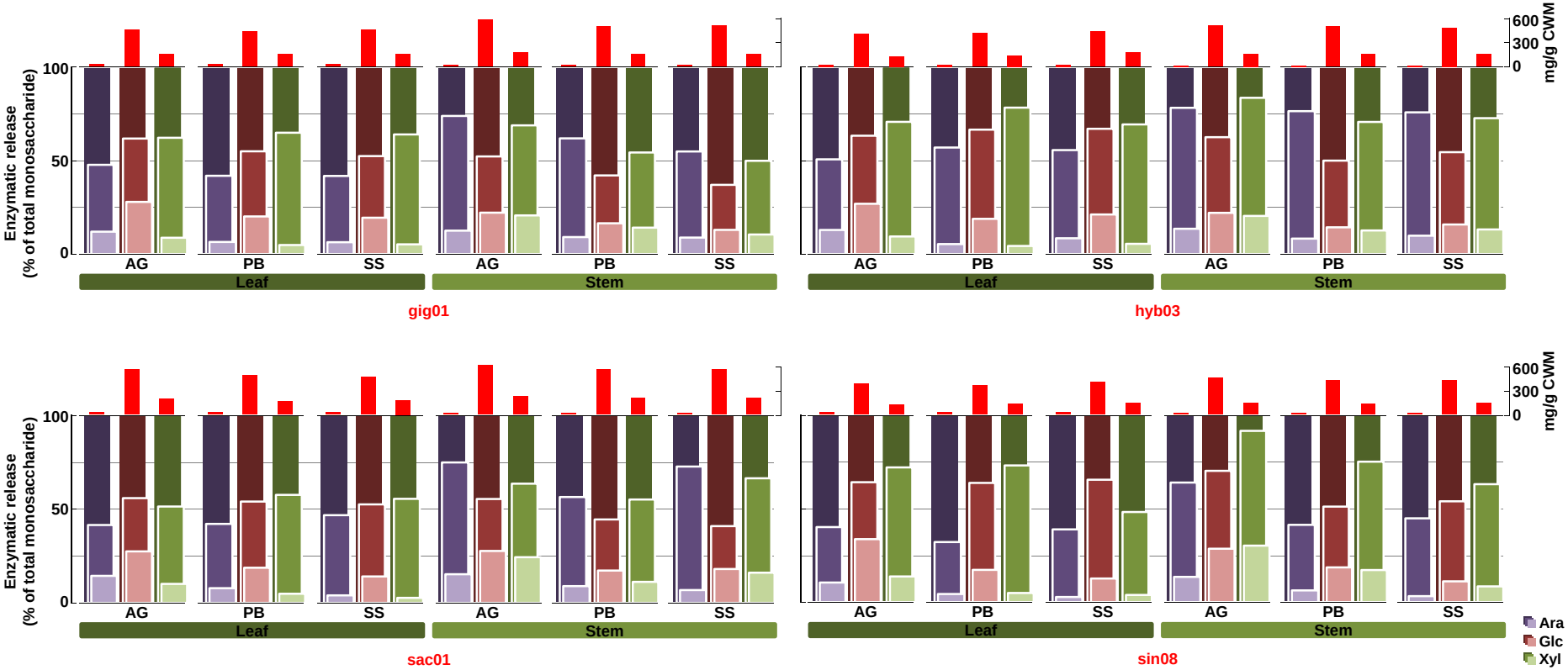

Fig. 4.8. Percentages of total monosaccharide released upon enzymatic hydrolysis of miscanthus CWM with and without a 0.1M KOH pretreatment. Each colour indicates a specific monosaccharide: arabinose (purple), glucose (bordeaux) and xylose (green). The darker tone represents the total of monosaccharide present in the cell wall (100%), and percentages of this total which are released during enzymatic hydrolysis are shown by the intermediate tone (pretreated biomass) and the lightest tone (un-pretreated biomass). The red bars above indicate the total amount in mg of monosaccharide per g of cell wall material (CWM). Developmental stages: active growth (AG), peak biomass (PB) and senescence (SS).

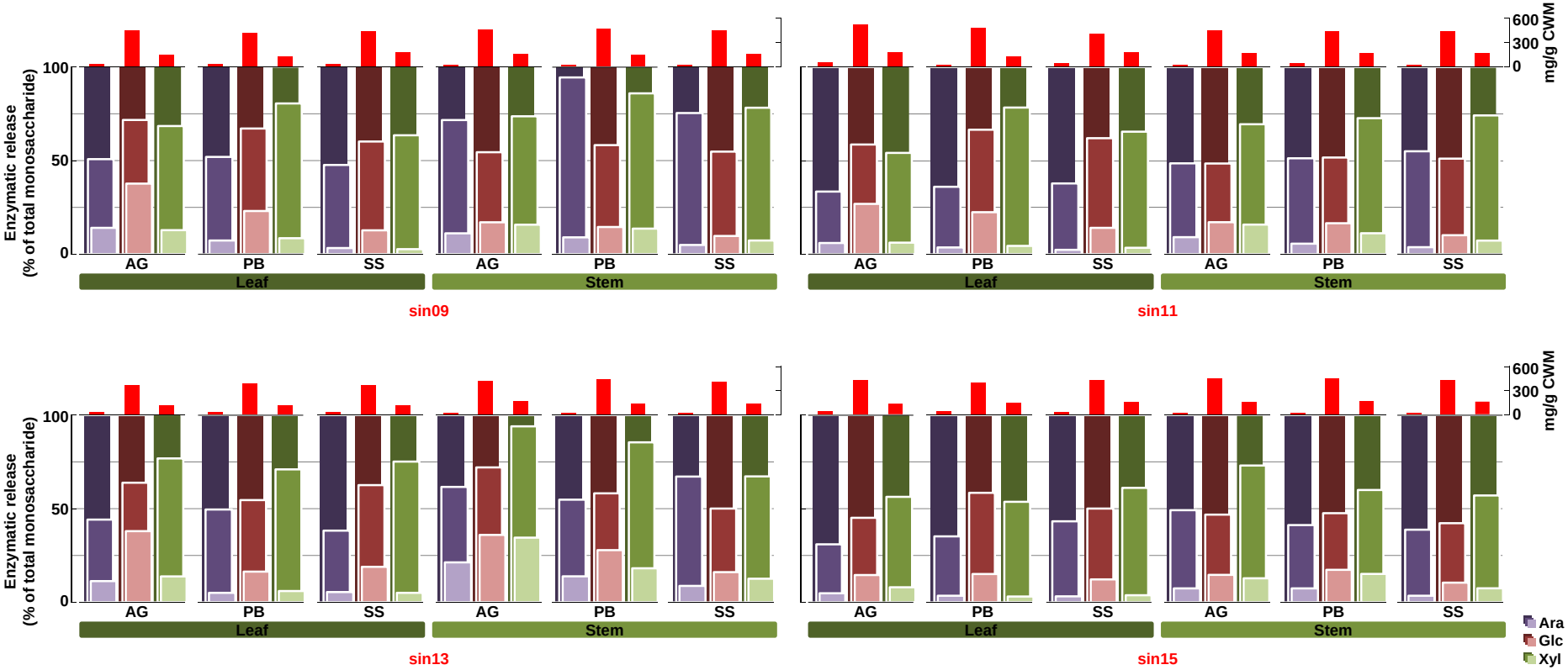
Enzymatic release
(% of total monosaccharide)
100
50
0
600
300
0
mg/g CWM
AG
PB
SS
Leaf
Stem
sin09
sin11
sin13
sin15
Ara
Glc
Xyl

Fig. 4.8. (cont.).

5. IMMUNOLOGICAL STUDY OF NON-CELLULOSIC CELL WALL GLYCANS

5. IMMUNOLOGICAL STUDY OF NON-CELLULOSIC CELL WALL GLYCANS

As seen previously, miscanthus cell walls are very complex composites, which may differ significantly in their composition, depending on the tissue, genotype and the developmental stage being examined. In addition, structural features of the cell wall polymers not only vary between tissues and developmental stages, but also at subcellular levels (Keegstra, 2010; McCann and Knox, 2010; Pauly and Keegstra, 2010). The determination of released carbohydrates in cell wall hydrolysates, as performed in the previous chapter, is of crucial importance for lignocellulosic biomass characterisation. However, these assays are limited in the amount of information they can provide, in what concerns the structure of cell wall polysaccharides. As a result, for an improved understanding of the structural complexity of the cell wall, complementary analytical tools are required.

Monoclonal antibodies (mAbs) may be used as highly specific molecular probes for the characterisation of structural carbohydrates, and their potential has long been recognised (Roberts *et al.*, 1985). Nonetheless, high heterogeneity has been demonstrated in structural carbohydrates, as several structural forms have been identified for most non-cellulosic cell wall polysaccharides, such as hemicelluloses (York and O'Neill, 2008) and pectins (Mohnen, 2008). Expansion of our knowledge regarding which epitopes are recognised by the mAbs is thus essential to maximise the usefulness of immunological methods to characterise cell wall glycans (Puhlmann *et al.*, 1994; Knox, 1997; Pattathil *et al.*, 2010; Sørensen and Willats, 2011).

Benefiting from this continuous accumulation of mAb specificity information, several research groups have generated numerous glycan-directed mAbs, which today total to over 200 probes capable of binding to epitopes occurring in most cell wall matrix polysaccharides (Willats *et al.*, 2000b; Pattathil *et al.*, 2010). This worldwide collection of mAbs is considered to be sufficiently diverse and extensive in its binding specificities to allow the development of

several immunology-based methods for the study of most non-cellulosic classes of plant cell wall glycans.

Two of such immunological approaches have been employed in this project, both in collaboration with Michael Hahn's research team based at the Complex Carbohydrate Research Center (CCRC) of the University of Georgia (Athens, Georgia, USA): glycome profiling (Pattathil *et al.*, 2012) and *in situ* immunolabelling of glycan epitopes (Avci *et al.*, 2012) (Fig. 5.1). Glycome profiling (GP) essentially consists of an enzyme-linked immunosorbent assay (ELISA)-based screen which uses a recently assembled toolkit of plant cell wall glycan-directed mAbs (Pattathil *et al.*, 2010) to identify the polysaccharides removed at different steps of an increasingly harsh sequential extraction to fractionate the cell wall. On the other hand, immunolabelling may be performed after GP, using a subset of the mAb toolkit, in order to visualise the occurrence of particular polysaccharide epitopes *in muro*.

A few studies have recently utilised mAb probes to characterise miscanthus cell walls, in comparison with various model grasses (Kulkarni *et al.*, 2012), in 3 different *M. sinensis* genotypes (de Souza *et al.*, 2015), and across various internodes in *M. lutarioriparius* (Cao *et al.*, 2014). However, according to our knowledge no study has yet employed immunological probe technology to provide a comprehensive picture of the miscanthus cell wall encompassing different species and genotypes (*M. sinensis*, *M. sacchariflorus*, and two hybrid genotypes including *M.* × *giganteus*), across successive harvest time points and different plant tissues.

In this chapter, mAb probes are used to further elucidate the abundance and structure of the cell wall matrix polysaccharides and how they are distributed *in muro*. The acquired information will complement our understanding of how miscanthus cell wall compositional and structural features change with time, how they differ between tissues, and how divergent the genotypes are. In the subsequent and final chapter of this thesis, possible associations

between immunological information and the remaining datasets will be explored with the aim of drawing inferences regarding how saccharification efficiency is affected.

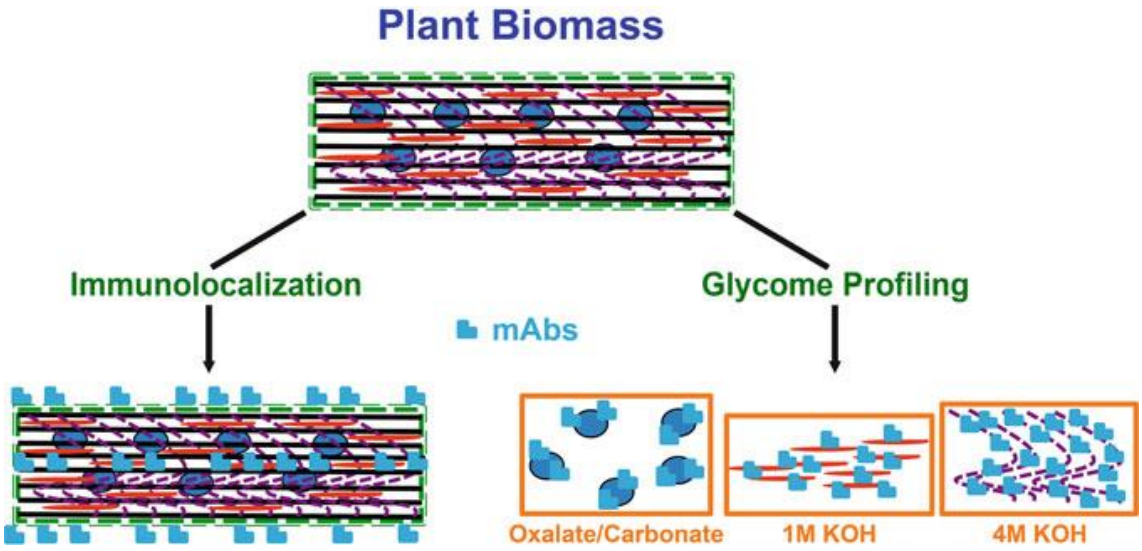

Fig. 5.1. Schematic representation of the two approaches for immunological characterisation of miscanthus CWM employed in this chapter. (Adapted from Avci *et al.* (2012))

5.1. GLYCOME PROFILING

5.1.1. Overview

The CCRC-developed glycome profiling platform has been widely used to characterise cell wall material from a wide variety of plant materials, such as commelinid monocots species: maize (*Zea mays*), switchgrass (*Panicum virgatum*), miscanthus (*Miscanthus* spp.), rice (*Oryza sativa*), brachypodium (*Brachypodium distachyon*), foxtail millet (*Setaria italica*) and sugarcane (*Saccharum* sp.) (Kulkarni *et al.*, 2012; de Souza *et al.*, 2013; de Souza *et al.*, 2015; Pattathil *et al.*, 2015); dicot species: poplar (*Populus* spp.), black locust (*Robinia pseudoacacia*), goldenrod (*Solidago* sp.), alfalfa (*Medicago sativa*), and arabidopsis (*Arabidopsis* sp.) (DeMartini *et al.*, 2011; DeMartini *et al.*, 2013; Tan *et al.*, 2014; Biswal *et al.*, 2015; Pattathil *et al.*, 2015); and even gymnosperm species, such as loblolly pine (*Pinus taeda*) and Douglas fir (*Pseudotsuga menziesii*) (Pattathil *et al.*, 2015). Cell wall GP represents a moderate to high throughput method to obtain a comprehensive picture of the glycan epitope composition of cell wall biomass samples, which simultaneously provides insight into the amenability of glycan epitopes to be removed from CWM (Pattathil *et al.*, 2012) (an overview of the glycome profiling procedure is provided in Fig. 5.2). Firstly, the wall is subjected to a sequential extraction, where at each step a specific fraction is removed. In the study presented here, these extractions were performed using a sequence of increasingly harsher chemical extractants: 0.05M ammonium oxalate, 0.05M sodium carbonate, 1M KOH, 4M KOH, acidic sodium chlorite and 4M KOH PC (post-chlorite treatment). It is this succession of extractants that allows inferences about how tightly bound to the wall the epitopes are, and hence the polysaccharides in which they are contained. In addition, the fact that the cell wall polysaccharides are solubilised in aqueous solutions has the advantage of making the

compounds freely accessible for detection (Pattathil *et al.*, 2012), thus preventing possible epitope masking by the presence of other wall components, as has been reported in the literature (Puhlmann *et al.*, 1994; Marcus *et al.*, 2008; Marcus *et al.*, 2010).

Each extraction step is intended to remove specific types of cell wall polysaccharides, namely: loosely bound pectins (oxalate and carbonate extracts); xyloglucans, xylans and varying amounts of strongly bound pectin (1M and 4M KOH); lignin-associated glycans (chlorite); and remaining tightly bound wall glycans (4M KOH PC) (Li *et al.*, 2014a). Subsequently, the sugar concentration of each cell wall fraction is determined using the phenol-sulphuric acid method for the estimation of total sugar contents in a sample. In this method, the hot concentrated sulphuric acid breaks down any polysaccharides, oligosaccharides, and disaccharides to monosaccharides. Pentoses are then dehydrated to furfural, hexoses to hydroxymethyl furfural, and by adding phenol a reaction is initiated where carbohydrates are derivatised and a yellow-brown coloured product is produced, which has maximum absorption at 490nm (Dubois *et al.*, 1956; Nielsen, 2010). This property allows for total carbohydrate content in the solution to be determined according to the intensity of the developed colour. The phenol-sulphuric acid method is an easy and rapid way of estimating virtually all classes of carbohydrates, especially if performed in a 96-well plate format (Masuko *et al.*, 2005). Nonetheless, the percentage of saccharide conversion into furfural is not complete, and the absorptivity of the different carbohydrates may vary (Dubois *et al.*, 1956; Nielsen, 2010). As a consequence, the quantitation results must be expressed arbitrarily as equivalents of one carbohydrate (e.g., glucose). The information obtained from the phenol-sulphuric acid assay is useful to estimate and compare the total carbohydrate removed from the cell wall at each extraction step. In addition, it allows for the dilution of the cell wall fractions to a comparable concentration before ELISA; since the various cell wall fractions are loaded onto the ELISA plates in equal sugar amounts. This makes GP essentially a qualitative assay. However, semi-

quantitative conclusions are also possible, since information about the amount of carbohydrate released at each extraction step is provided together with the ELISA data, and thus allows meaningful comparisons of relative epitope abundances.

After dilution to an equal predetermined concentration, all cell wall fractions are subjected to ELISA against a toolkit of antibodies (Pattathil *et al.*, 2010) directed to most cell wall glycans (with the exception of cellulose and RG-II; Appendix C). Hence, this allows the nature of the polysaccharides present in the CWM samples to be identified.

ELISA is a highly versatile and sensitive analytical test for the detection of virtually any kind of antigenically active molecule (Engvall and Perlmann, 1971). Various formats of ELISA have been developed, but all involve an interaction between antibody and antigen with one of the reactants immobilised on a solid support (Paulie *et al.*, 2005). The ELISA procedure employed in the present study (Pattathil *et al.*, 2010) utilises an indirect method of detection, which involves two binding processes, one with a primary mAb and another with a labelled secondary mAb (Appendix D). The first step of the ELISA is the coating of the ELISA plates, and consists of the immobilisation of epitopes contained in the extracts to the wells of the plates (Butler *et al.*, 1992). The coating step takes advantage of the ability of various plastics to adsorb carbohydrates, and several commercially available microtitre plates have been tested by Pattathil *et al.* (2010) during GP method development. These tests showed that the ability of the polysaccharides to bind to the plates does not depend on their glycosyl composition or charge; however, it was seen that unmodified oligosaccharides and low molecular mass polysaccharides (such as RG-II) do not effectively adsorb to the plates, and therefore GP does not yield information on small glycan molecules. Once plate coating is complete, residual non-specific binding sites are blocked with an excess of an unrelated protein (such as non-fat milk), followed by incubation with primary glycan-directed mAbs. After removal of unbound mAbs, detection is achieved by an enzyme-conjugated secondary mAb, which binds to the primary

mAbs and reacts with a chromogenic substrate; thus allowing detection by spectrophotometric measurement of the coloured product in a plate reader.

Following the observations made in previous chapters that miscanthus cell wall samples originating from different genetic, developmental and tissue sources have varying degrees of recalcitrance, it is pertinent to clarify the role of cell wall structure in biomass degradability. Chromatographic analyses of cell wall hydrolysates on their own cannot reveal all underlying structural features of the cell wall. By providing information about cell wall glycan abundance and about how tightly different epitopes are bound to the wall, the GP results presented in this section will expand on the information already gathered concerning the monosaccharide composition of miscanthus cell wall. The comprehensive picture of the glycan epitope composition reported here will firstly encompass different tissues and harvest time points, in order to characterise the most significant alterations polysaccharide cell wall composition. Secondly, attempts will be made to emphasise differences in epitope occurrence between the genotypes. Ultimately, based on the results, a subset of the mAbs used for GP will be selected for immunolabelling studies, with the aim of determining epitope distributions *in muro*.

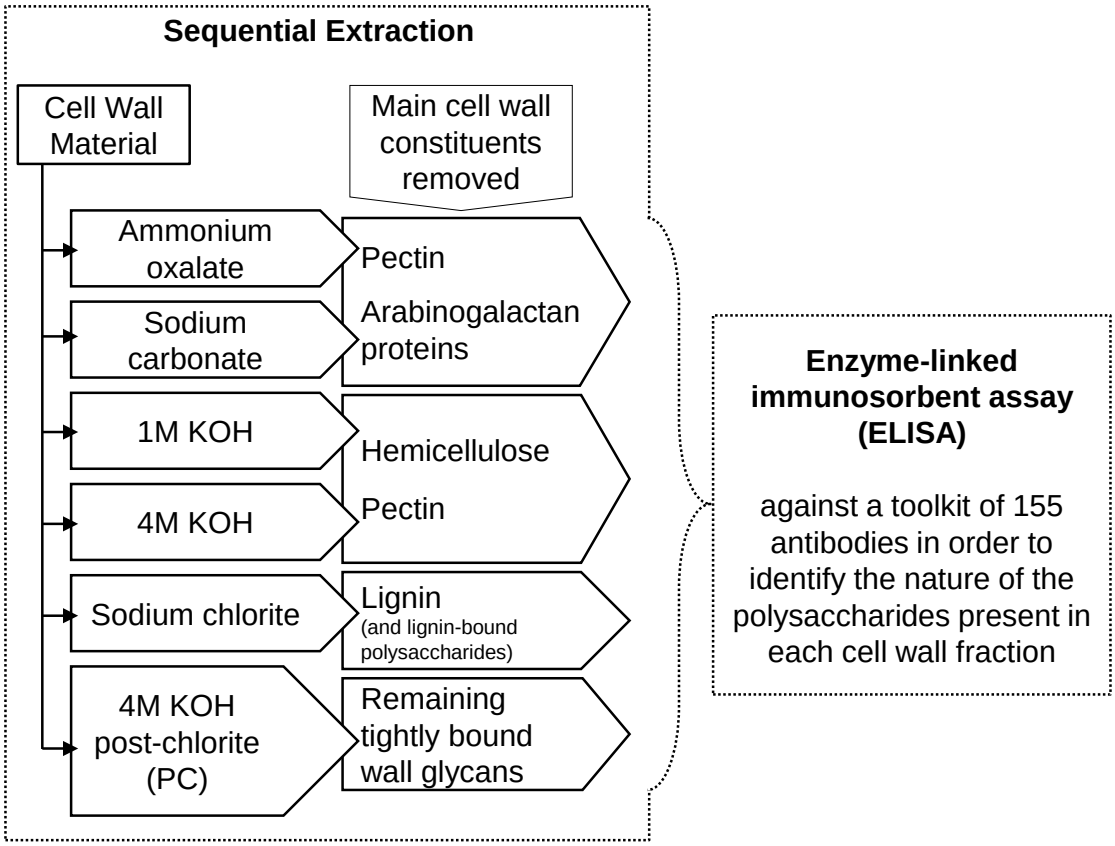

Fig. 5.2. Glycome profiling procedure.

5.1.2. Materials and methods

The experimental procedures presented in this section can be divided into four steps: cell wall isolation, sequential extraction, total carbohydrate estimation and glycome profiling. The first step was achieved following the isolation methods described in section 2.2, the remaining steps are described below.

5.1.2.1. Sequential extraction

Sequential extractions were performed in 10mg/mL suspensions based on the initial weight of the CWM (Pattathil *et al.*, 2010; Pattathil *et al.*, 2012). Firstly, samples were suspended in 0.05M ammonium oxalate (pH 5.0) and incubated for 24h at 25ºC with constant shaking. After incubation, mixtures were centrifuged (2500×*g*/10 min) and supernatants were decanted and kept at 4ºC. The resulting pellets were subsequently washed three times in the same volume of deionised water, centrifuged (2500×*g*/10 min) and the supernatants were discarded. This procedure was subsequently repeated with three other extractants: 0.05M (Na_2CO_3; pH=10.0) containing 0.5% (w/v) $NaBH_4$[*]; 1M KOH containing 1% (w/v) $NaBH_4$; and 4M KOH containing 1% (w/v) $NaBH_4$. The samples were then delignified by an acidic sodium chlorite treatment (Ahlgren and Goring, 1971), which consists of suspending the material in 20mL of deionised water kept at 70°C, followed by three additions of 0.125g of $NaClO_2$ and 50µL of glacial acetic acid (each separated by 1h incubations). Dissolved chlorine gas was then removed by slowly bubbling air through the sample. Finally, the solid material

[*] Hydroxyl radicals of the carbohydrates are ionised at the high pH of the extracting solutions:

$$R–OH + OH^- \rightarrow R–O^- + H_2O$$

As a result, sugar molecules become negatively charged and repel each other, helping to maintain their solubility (Fry, 2010). However, under these alkaline conditions a stepwise depolymerisation of cell wall polysaccharides may occur from the reducing end groups, in a process designated peeling (Spiridon and Popa, 1998). Peeling may therefore lead to the formation of new end groups and consequently alter the glycan epitopes. As a precautionary measure against peeling the alkaline solutions were supplemented with sodium borohydride ($NaBH_4$), which is a powerful reducing agent (Istek and Gonteki, 2009), to reduce polysaccharide oxidation.

remaining after this treatment (post-chlorite, PC) was subjected to a final extraction with 4M KOH containing 1% (w/v) $NaBH_4$. The six cell wall extracts produced were respectively designated: Oxalate, Carbonate, 1M KOH, 4M KOH, Chlorite, and 4M KOH PC. The KOH extracts were neutralised, on ice, using glacial acetic acid. 2-octanol (5 drops per sample) was added to prevent foaming. All extracts were dialysed against four changes of deionised water (sample:water ≈1:60) at room temperature for a total of 48h (3.5kDa molecular weight cut-off tubing, no.S632724; Spectrum laboratories Inc., California, USA) and subsequently freeze-dried. By the end of the sequential extraction, 288 samples enriched in various cell wall components had been produced (8 genotypes × 2 tissues × 3 developmental stages × 6 extractions)[*].

5.1.2.2. Phenol-sulphuric acid method for total carbohydrate estimation

Total carbohydrate content was estimated using the phenol-sulphuric acid method in a 96-well microplate format (Dubois *et al.*, 1956; Masuko *et al.*, 2005). Assays were performed in duplicate, in disposable 13×100mm glass test tubes. All cell wall fractions prepared during the sequential extraction were dissolved in deionised H_2O at a concentration of 0.2mg of the dry extract per mL. Subsequently, and for each sample, 100µL of the resulting solubilised extract, 100µL of 5.0% (w/v) phenol and 500µL of 18M H_2SO_4 were added in succession to the bottom of the test tube. Each sample was gently mixed and left incubating for 20min at room temperature in a fume hood. After incubation, 250µL of each reaction mixture was transferred to transparent 96-well plates (Costar 3598; Corning Inc., Corning, New York, USA), and the absorbance at 490nm was measured with a plate reader (µQuant; Bio-Tek Instruments, Winooski, Vermont, USA) using KC4 software (v. 3.3; Bio-Tek). A standard

[*] The final insoluble residue remaining after the sequential extraction was subjected to compositional analyses, discussed in appendix F.

curve prepared using solutions with varying Glc concentrations was used to determine Glc-equivalents of the sugars in each extract. Negative controls without cell wall extract samples were included in all plates and their absorbance at 490nm was set as absorbance baseline[*].

5.1.2.3. Enzyme-Linked Immunosorbent Assay

ELISA plates (384-well, clear, flat bottom, polystyrene, no.3700; Corning Inc. Life Sciences, Tewksbury, Massachusetts, USA) were coated with the previously sequentially extracted samples diluted to a final concentration of 13.4µg of carbohydrates per mL, and allowed to dry overnight at 37°C (Appendix D). The ELISAs were then conducted using a suite of 155 cell wall glycan-directed mAbs as described by Pattathil *et al.* (2012). All employed mAbs were obtained as hybridoma cell culture supernatants from the CCRC laboratory stocks (Appendices C and E), but are commercially available from CarboSource (CCRC series, PN series, JIM series, MAC series; http://www.carbosource/net) or from BioSupplies (BG1, LAMP; http://www.biosupplies.com.au/). A 0.1M Tris-buffered saline (pH=7.6) was prepared by adding 5.85g NaCl, 12.10g Tris-HCl and 2.78g Tris-base to 1L deionised H_2O. Non-specific binding sites in the previously coated ELISA plates were blocked with a 1% (w/v) non-fat powdered milk solution in 0.1M Tris-buffered saline (blocking buffer) for 1h. All subsequent aspiration and wash steps were performed using an ELx405 microplate washer (Bio-Tek Instruments; Winooski, Vermont, USA). Blocking agent was removed by aspiration and undiluted primary mAbs were added to each well and plates were incubated for 1h at room temperature. Supernatants were then removed and wells were washed three times with 0.1% (w/v) non-fat powdered milk in Tris-buffered saline (wash buffer). Peroxidase-conjugated goat

[*] In addition to being used to estimate carbohydrate content of each extract, the phenol sulphuric method was also used to estimate the total sugar contents of the CWM before the sequential extraction. For this, CWM was acid hydrolysed as described in section 4.1.2 (see appendix F).

anti-mouse immunoglobulin G (IgG) or goat anti-rat IgG secondary antibodies (Sigma-Aldrich), depending on the primary antibody used, were dispensed and incubated for 1h (diluted at 1:5000 in the wash buffer) followed by washing. A freshly prepared substrate consisting of 3,3',5,5'-tetramethylbenzidine solution (TMB Peroxidase Substrate Kit SK-4400; Vector Laboratories, Inc., Burlingame, California, USA) was added to each well, left incubating for blue colour development (Josephy *et al.*, 1982), and after 20min the reaction was terminated by the addition of 0.5N H_2SO_4. Immediately after, net OD values of the colour formation in the wells were measured at 450nm, subtracting a background reading at 655nm. Additionally, negative controls consisting of water and the same primary and secondary antibodies but no immobilised glycans were included in all assays and their absorbance was subtracted from the readings.

5.1.2.4. Data analysis

For the total carbohydrate quantitation dataset, ANOVA was used to test the factor effect of extractant (6 levels), genotype (8 levels), development (3 levels) and tissue (2 levels), on the amounts of total carbohydrate recovered from the CWM samples. Tukey's tests were used for multiple comparisons between factor levels. All ANOVA and Tukey's tests were performed using the Statistica software (v. 8.0; StatSoft, Tulsa, Oklahoma) at a 5% significance level (α=0.05). ANOVA effect sizes were calculated as eta-squared statistics as described in equation 2.1 (Section 2.1.3).

For the ELISA dataset, a multivariate analysis of variance (MANOVA) was performed to test for the significance of the different factors (Statistica software; 5% significance level). Optical densities obtained for individual mAbs were averaged across the 8 genotypes for leaf and stem at each developmental stage, thus providing a general picture of the glycome profile of miscanthus cell wall, and how it varies between tissues and throughout development (Fig.

5.4). The mAbs are grouped into several clades based on commonalities in their recognition of most non-cellulosic cell wall glycans (Pattathil *et al.*, 2010).

Matrices were then created with the ELISA responses and imported into MatLab (v. R2010b; MathWorks, Natick, Massachusetts, USA), prior to principal components analysis (PCA) using the Eigenvector PLS Toolbox (v. 7.0.3; Eigenvector Research, Wenatchee, Washington, USA) to investigate the underlying relationships between the samples. To balance the weight of the different variables (mAbs) and avoid biased results, ELISA data were normalised (Jensen and Janes, 2012). For this, the PLS Toolbox autoscale function was used, which centres each variable by subtracting its mean followed by the scaling of the centred variable by division by its standard deviation.

Differences between genotypes in terms of binding intensities to the mAb clusters were evidenced by calculation of standard deviations from the mean, which were plotted as heat maps (Figs. 5.16), where ELISA responses are used to produce a colour gradient indicating variations in antibody binding intensities against the cell wall glycans. For this, a modified version of R-console software was used (R Development Core Team, 2006) (Pattathil *et al.*, 2010; Pattathil *et al.*, 2012).

5.1.3. Results

5.1.3.1. Total Carbohydrate Estimations of Cell Wall Fractions

Carbohydrate content was measured by the phenol-sulphuric acid assay following sequential extractions. In comparison with other extractants, 1M KOH removed the highest proportion of cell wall carbohydrates per gram of CWM. The remaining fractions showed the following decreasing order of quantities of total recovered sugars: 4M KOH, 4M KOH PC, carbonate, chlorite and oxalate (Fig. 5.3 and Table 5.1).

The statistical significance of the effect of extraction and tissue on sugar release was confirmed by ANOVA (P<0.001 for both factors; Table 5.2). Tukey's tests showed a distinction between the amount of sugar recovered from stem and leaf, and between all extracts except carbonate and chlorite, which did not release significantly different absolute amounts of carbohydrate. As indicated by its effect size (η^2=0.77), the extract factor was the main source of variation observed in the data. The secondly highest source of variation, albeit contributing far less to the variability among samples, was the tissue factor with a η^2=0.03. The genotype factor also showed a marginally significant effect (P=0.042), but Tukey's tests did not show a distinction between the genotypes. The interactions of extract with tissue, genotype and development factors were also significant ($P_{extract\times tissue}$<0.001; $P_{extract\times genotype}$<0.001; $P_{extract\times development}$=0.014).

Interestingly, despite no significance being observed for the development factor overall (P=0.449), when the oxalate extracts were analysed separately, a significant effect was detected (P=0.007). Moreover, with the most effective extractant (1M KOH) the development factor showed a significant effect on resulting extracts (P=0.047); although differences were only

observed between AG and SS, with PB not being discernible from either, according to the Tukey's test.

The amounts of extracted carbohydrate were typically higher in leaf samples than in stem samples for all extracts, at all developmental stages, except for the carbonate fractions at AG and SS. In this extract the stem samples typically released slightly more total carbohydrates than leaves (Table 5.1). However, these differences between tissues were not significant in the carbonate extracts (Table 5.2). Similarly, no significant differences were detected between tissues in the 4M KOH PC fractions. As for the 4M KOH and the chlorite fractions, there was a significant difference between tissues (P=0.007 for 4M KOH and P=0.017 for chlorite), which, nonetheless was not significantly altered along plant development (P=0.870 for 4M KOH and P=0.683 for chlorite). There was also a significant variation between the tissues in the oxalate extracts (P<0.001). However, the most striking difference between leaf and stem samples in terms of total extracted carbohydrate was observed with 1M KOH (the extractant which removed the highest amount of cell wall carbohydrates), where leaves released on average approximately 1.7 times more carbohydrate than stems. The differences between tissues were the main cause of variation in the amounts of extracted sugars in the 1M KOH extracts (P<0.001; η^2=0.53). It was also observed in these extracts that the overall amounts of extracted sugars increased in both tissues as plants matured.

By the end of the sequential extraction, the mean summed total carbohydrate released from leaf tissues was 191mg/g CWM (ranging from 116 to 236mg/g; Table 5.1), whereas from stem it was 130mg/g CWM (89 – 161mg/g; Table 5.1). The greatest proportion of extracted carbohydrates was released before tissue delignification (chlorite treatment); specifically, 80% from leaf tissues and 77% from stems. A trend was also observed along development, by which pre-delignification sugar release was higher in the earlier developmental stages for both tissues: leaf, 83% (AG), 80% (PB), 77% (SS); and stem, 78% (AG), 78% (PB) and 75% (SS).

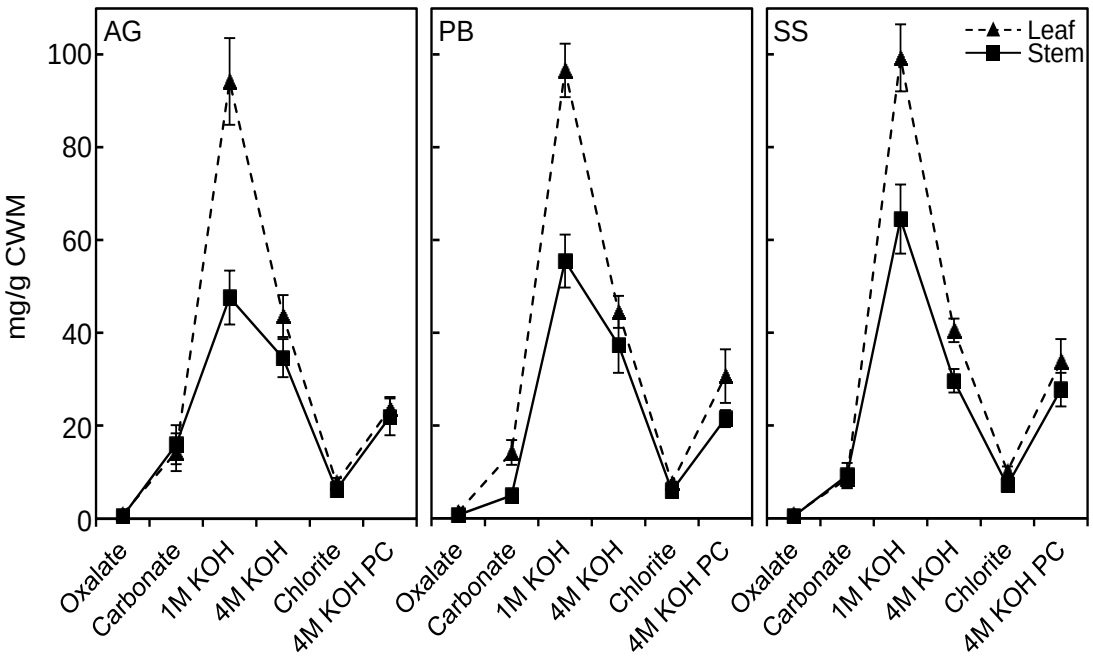

Fig. 5.3. Total carbohydrate recovered from each sequential extraction step per gram of isolated cell wall material (mg/g CWM) estimated by the phenol-sulphuric acid assay. Values are the mean and standard deviation (error bars) of eight genotypes. (AG: actively growing; PB: peak biomass; SS: senescence)

Table 5.1. Amount of carbohydrate recovered at each extraction step per gram of isolated cell wall material (mg/g CWM) based on phenol-sulphuric acid assay for total sugar estimation. (AG: actively growing; PB: peak biomass; SS: senescence; $\bar{x}$: mean; E: extract; T: tissue; DS: developmental stage)

	Ammonium Oxalate						**Carbonate**						**1M KOH**					
	Leaf			**Stem**			**Leaf**			**Stem**			**Leaf**			**Stem**		
	AG	**PB**	**SS**	**AG**	**PB**	**SS**	**AG**	**PB**	**SS**	**AG**	**PB**	**SS**	**AG**	**PB**	**SS**	**AG**	**PB**	**SS**
gig01	1.03	1.34	0.48	0.39	0.43	0.43	26.42	3.96	12.65	4.66	2.89	1.92	94.24	89.02	67.86	40.35	38.11	42.61
hyb03	1.10	1.29	1.11	0.35	0.64	0.39	11.09	17.23	10.78	32.34	5.57	1.28	85.05	72.54	112.77	42.98	65.71	103.09
sac01	1.19	1.99	1.76	1.11	1.87	0.54	2.39	13.78	5.17	11.65	11.87	8.18	59.80	104.93	115.48	23.06	38.79	61.36
sin08	0.87	1.69	0.39	0.35	0.58	0.33	22.13	14.18	3.09	36.92	1.73	25.64	101.07	112.11	93.56	61.96	77.16	49.49
sin09	1.53	1.14	0.50	0.39	0.50	0.45	2.86	27.67	7.35	12.66	2.32	6.98	71.12	75.30	120.67	28.99	35.43	72.21
sin11	1.19	1.60	0.44	0.39	0.64	0.30	8.96	9.74	2.11	6.91	1.77	10.01	121.94	99.30	80.19	54.49	64.08	47.79
sin13	0.34	0.99	0.74	1.03	0.75	0.60	33.22	19.98	19.42	11.78	8.25	13.02	81.05	102.82	84.37	67.30	55.35	54.19
sin15	0.69	0.81	0.78	0.38	0.44	0.49	7.65	7.12	7.56	10.82	4.89	6.75	139.95	117.21	119.96	62.38	69.54	85.85
$\bar{x}_{(E)}$	0.81						11.19						76.35					
$\bar{x}_{(E+T)}$	1.04			0.57			12.35			10.03			96.76			55.93		
$\bar{x}_{(E+T+DS)}$	0.99	1.36	0.78	0.55	0.73	0.44	14.34	14.21	8.52	15.97	4.91	9.22	94.28	96.65	99.36	47.69	55.52	64.57

Table 5.1. (cont.).

	4M KOH						Chlorite						4M KOH PC					
	Leaf			Stem			Leaf			Stem			Leaf			Stem		
	AG	PB	SS	AG	PB	SS	AG	PB	SS	AG	PB	SS	AG	PB	SS	AG	PB	SS
gig01	55.47	38.84	47.67	31.49	42.33	27.43	7.09	9.02	10.24	3.06	6.23	8.46	15.57	17.02	34.01	12.00	24.34	26.01
hyb03	66.05	44.30	46.14	38.39	25.71	21.31	6.80	7.77	5.75	3.44	4.37	6.02	22.39	20.78	17.94	13.06	18.15	28.65
sac01	31.58	41.51	41.87	27.11	45.64	30.64	6.67	8.18	9.50	16.65	5.96	8.93	14.79	19.98	15.77	25.21	12.75	21.43
sin08	30.86	47.05	42.10	12.49	15.32	32.95	6.27	6.52	11.35	7.45	7.41	5.24	22.10	41.91	46.84	37.27	26.74	17.78
sin09	45.17	63.76	32.65	31.50	58.34	43.11	7.09	7.70	9.06	5.30	5.35	7.16	32.55	21.11	28.32	10.16	28.50	30.88
sin11	43.58	51.53	32.78	46.87	43.80	31.28	13.58	7.85	16.24	6.05	7.63	5.54	19.32	66.01	56.41	35.17	19.91	20.87
sin13	46.50	36.24	49.29	47.56	54.17	20.12	4.45	7.47	9.30	3.45	5.32	7.10	32.72	29.79	40.21	12.93	18.66	50.85
sin15	30.37	33.15	32.00	41.71	13.89	30.63	10.32	6.46	9.69	4.74	5.30	8.54	30.01	28.94	30.79	29.92	23.11	25.63
$\overline{x}_{(E)}$	38.42						7.48						26.57					
$\overline{x}_{(E+T)}$	42.94			33.91			8.51			6.45			29.39			23.75		
$\overline{x}_{(E+T+DS)}$	43.70	44.55	40.56	34.64	37.40	29.68	7.78	7.62	10.14	6.27	5.94	7.12	23.68	30.69	33.79	21.96	21.52	27.76

Table 5.2. ANOVA results for the amount of total carbohydrate recovered from miscanthus CWM based on the phenol-sulphuric acid assay.

Effect	Deg. of freedom	Sum of squares	Mean	*F*-ratio	*P*-value	Effect size
All extracts						
Extract	5	186348.7	37269.7	447.5	<0.0001	0.7718
Genotype	7	1296.8	185.3	2.2	0.0423	0.0054
Development	2	135.0	67.5	0.8	0.4489	0.0006
Tissue	1	7285.9	7285.9	87.5	<0.0001	0.0302
Extract × Genotype	35	8323.0	237.8	2.9	<0.0001	0.0345
Extract × Development	10	2043.6	204.4	2.5	0.0142	0.0085
Genotype × Development	14	1521.3	108.7	1.3	0.2271	0.0063
Extract × Tissue	5	14201.6	2840.3	34.1	<0.0001	0.0588
Genotype × Tissue	7	200.8	28.7	0.3	0.9306	0.0008
Development × Tissue	2	79.4	39.7	0.5	0.6230	0.0003
Extract × Genotype × Development	70	9746.3	139.2	1.7	0.0166	0.0404
Extract × Genotype × Tissue	35	3131.9	89.5	1.1	0.3907	0.0130
Extract × Development × Tissue	10	639.1	63.9	0.8	0.6592	0.0026
Genotype × Development × Tissue	14	666.0	47.6	0.6	0.8784	0.0028
Error	70	5830.2	83.3			
Total	287	241449.6	48691.4			
Oxalate extract						
Tissue	1	2.6	2.6	24.9	0.0002	0.2568
Genotype	7	2.7	0.4	3.6	0.0196	0.2605
Development	2	1.5	0.8	7.4	0.0065	0.1521
Tissue × Genotype	7	0.7	0.1	1.0	0.4979	0.0689
Tissue × Development	2	0.2	0.1	0.8	0.4608	0.0169
Genotype × Development	14	1.0	0.1	0.7	0.7474	0.1004
Error	14	1.5	0.1			
Total	47	10.2	4.1			
Carbonate extract						
Tissue	1	64.6	64.6	0.9	0.3527	0.0171
Genotype	7	779.0	111.3	1.6	0.2174	0.2061
Development	2	380.2	190.1	2.7	0.1006	0.1006
Tissue × Genotype	7	548.2	78.3	1.1	0.4039	0.1451
Tissue × Development	2	293.9	146.9	2.1	0.1592	0.0778
Genotype × Development	14	734.3	52.4	0.7	0.7012	0.1943
Error	14	979.1	69.9			
Total	47	3779.2	713.6			
1M KOH extract						
Tissue	1	20009.3	20009.3	158.3	<0.0001	0.5299
Genotype	7	5711.5	815.9	6.5	0.0016	0.1513
Development	2	966.4	483.2	3.8	0.0473	0.0256
Tissue × Genotype	7	1316.6	188.1	1.5	0.2490	0.0349
Tissue × Development	2	279.2	139.6	1.1	0.3586	0.0074
Genotype × Development	14	7707.5	550.5	4.4	0.0047	0.2041
Error	14	1769.3	126.4			
Total	47	37759.8	22313.0			
4M KOH extract						
Tissue	1	978.2	978.2	9.8	0.0073	0.1440
Genotype	7	1357.7	194.0	2.0	0.1357	0.1999
Development	2	287.1	143.6	1.4	0.2688	0.0423
Tissue × Genotype	7	797.9	114.0	1.1	0.3896	0.1175
Tissue × Development	2	27.8	13.9	0.1	0.8704	0.0041
Genotype × Development	14	1953.7	139.6	1.4	0.2665	0.2876
Error	14	1390.5	99.3			
Total	47	6792.8	1682.5			
Chlorite extract						
Tissue	1	51.4	51.4	7.4	0.0166	0.1377
Genotype	7	75.4	10.8	1.6	0.2285	0.2022
Development	2	32.4	16.2	2.3	0.1337	0.0867
Tissue × Genotype	7	57.3	8.2	1.2	0.3733	0.1537
Tissue × Development	2	5.4	2.7	0.4	0.6831	0.0146
Genotype × Development	14	54.0	3.9	0.6	0.8581	0.1447
Error	14	97.1	6.9			
Total	47	373.0	100.0			
4M KOH PC extract						
Tissue	1	381.4	381.4	2.4	0.1464	0.0597
Genotype	7	1693.5	241.9	1.5	0.2454	0.2652
Development	2	511.1	255.5	1.6	0.2399	0.0800
Tissue × Genotype	7	611.9	87.4	0.5	0.7894	0.0958
Tissue × Development	2	112.1	56.0	0.3	0.7126	0.0175
Genotype × Development	14	817.2	58.4	0.4	0.9665	0.1280
Error	14	2258.8	161.3			
Total	47	6385.9	1242.0			

5.1.3.2. Cell Wall Glycome Profile Variation across Tissues and Developmental Stages

The sequential extraction was very effective at removing matrix polysaccharides and lignin from the cell wall, as by the end of the sequential extraction near total non-cellulosic components had been removed (in Appendix F it is shown that apart from glucans, only xylose and lignin were detected, although at an average of less than 2.6% of the residues; Tables F2 and F3). Each solvent of the sequential extraction process was mainly aimed at extracting specific fractions of the cell wall polymers (Li *et al.*, 2014a): ammonium oxalate for weakly bound pectins, sodium carbonate for more tightly bound pectins, 1M KOH to remove more labile hemicelluloses along with tightly bound pectins, 4M KOH to remove tightly bound hemicelluloses along with tightly bound pectins, acid sodium chlorite to oxidise and solubilise lignin while releasing lignin-embedded polysaccharides, and another 4M KOH post-chlorite treatment to remove additional lignin-bound polysaccharides. Sequential extraction of CWM samples followed by ELISA screening of the resulting cell wall fractions provided detailed information regarding compositional changes in miscanthus cell wall between tissues and throughout development (a list of all used mAbs can be found in Appendix C). Observed signals allow semi-quantitative inferences, as intensities indicate relative abundances of particular epitopes. Additionally, the presence of particular classes of glycan epitopes at a given cell wall fraction provides information related to differences in extractability.

MANOVA revealed significant differences in the glycome profiles between the various miscanthus cell wall extracts ($P<0.001$), and also within each extract, between tissue type, genotype and developmental stage ($P<0.001$ for all two-way interactions with the extract factor; Appendix G). The mean OD values obtained for each mAb during the glycome profiling of leaf and stem tissues of the 8 miscanthus genotypes at various developmental stages are shown in Fig. 5.4 (part A and B contain the same data organised differently to facilitate

comparisons between tissues or developmental stages). The vast majority of the mAb classes used in the glycome screening of miscanthus samples did effectively bind to cell wall components. Exceptions were the xylan-2 subclass and the mannan-directed mAbs (galactomannan-1 and 2, and glucomannan); although for one galactomannan-2 mAb (CCRC-M166) minimal signals were detected in samples extracted with 4M KOH after delignification (4M KOH PC). Also absent were the binding signals to rhamnogalacturonan-I epitopes from the RG-Ia subclass (CCRC-M2 and CCRC-M5), and to mAbs CCRC-M94 and CCRC-M98, which recognise pectins found in cell wall preparations from the bryophyte *Physcomitrella patens* (more detail on the OD observed for each mAb during the ELISA is provided in appendix I). All glycome profiling results are summarised in Fig. 5.4 (A and B), a detailed interpretation of these data is presented below.

Antibodies directed at non-fucosylated XG showed highest binding signals in the 4M KOH extractions (pre and post sodium chlorite treatment) with generally more of these epitopes being removed from stem tissue in comparison to leaves; particularly before lignin removal. Little non-fucosylated XG-5 epitope was removed in the 4M KOH PC fraction in comparison to the other non-fucosylated XG classes. In actively growing leaf samples, non-fucosylated XG was more readily extractable with 1M KOH than in more mature tissues or stems; particularly for subclasses non-fucosylated XG1 and 2. Signals from the non-fucosylated XG-6 epitope CCRC-M57 were absent or minimal throughout all samples. Fucosylated xyloglucan showed a very similar epitope abundance pattern to non-fucosylated XG in that a marked increase in binding was observable in the 4M KOH extracts. Furthermore, binding was generally higher in senesced samples after the sodium chlorite treatments.

Xylan epitopes were released in all extraction steps, but their abundance varied throughout development and tissue type depending on mAb subclass. Binding to xylans and non-fucosylated xyloglucans from the xylan-1/XG subclass was highest in the 4M KOH

extracts, with greater abundance in stem tissues. By contrast, xylan-3 epitopes generally occurred at higher amounts in leaf samples, particularly those recognised by CCRC-M117 and CCRC-M113, which were noticeably more detectable in the cell wall fractions obtained with KOH. For xylan subclasses 4 to 7, some more loosely bound epitopes found in oxalate and carbonate extracts were typically more abundant in stem tissues and in actively growing plants. For the more tightly bound epitopes released with the harsher alkaline extractants, a different pattern was observed. For xylan-5, 6 and 7, no substantial variation between tissues or developmental stages was observed in their detected signals in any of the KOH fractions; although the levels were slightly higher for leaves when extracted with 1M KOH, and slightly higher for stems in both 4M KOH fractions. Finally, for the xylan epitopes released during delignification, xylan-4, 5 and 7 were more abundant in leaves than in stems and in actively growing plants, as shown by the higher signals displayed for the corresponding mAbs in the chlorite fractions.

The β-glucan class of mAbs is particularly relevant for miscanthus cell wall analysis, since it includes the BG1 mAb, which binds to mixed linkage (1→3),(1→4)-β-glucans (MLG). Release of epitopes associated with β-glucans increased with the use of the harsher KOH extractants. In both 4M KOH fractions the epitope abundances were either similar between tissues, or slightly higher in stems. However, in the remaining cell wall extracts, leaf tissues released β-glucan epitopes more abundantly. Remarkably, in the chlorite cell wall fractions from leaf tissues higher signals were detected for BG1 binding than in stems.

Homogalacturonan epitopes were probed with two subclasses of mAbs, each with a different detection pattern. HG backbone-1 epitopes occurred in all cell wall fractions, but binding intensities were higher in the carbonate extracts. In what concerns differences between tissues, the OD values were typically higher in leaf CWM, but the differences between tissues were less marked in both 4M KOH fractions. Of these HG backbone-1 epitopes, those removed

in the oxalate extracts were more abundant in senesced CWM, whereas for the fractions obtained with KOH, the differences between developmental stages were less noticeable, although with a slight tendency to be higher in actively growing plants. In chlorite extracts, all probed HG backbone-1 epitopes were detected and binding intensities to JIM5 were particularly high. By contrast, binding signals for HG backbone-2 epitopes were minimal in all fractions, except for the ammonium oxalate.

Binding signals to the backbone of rhamnogalacturonan-I (RG-I) epitopes were generally low, and almost exclusively perceptible in the extracts performed with KOH and notably in the chlorite fractions. Nevertheless, RG-I backbone epitopes identified by CCRC-M14 were found to be more abundant in leaf tissues relative to stem, and were particularly low in senesced samples. Other RG-I epitopes were probed with a series of mAbs which gave varied responses. Generally, the highest binding intensities to RG-Ib and RG-Ic epitopes were observed in carbonate fractions, but some level of variation was observed in the signals of these epitopes. For example, RG-Ib was detected in the carbonate extracts of both tissues at PB and SS, but this epitope was detected at extremely low amounts in AG samples. Furthermore, considering the total carbohydrate removed at each step of the sequential extraction, a big portion of RG-Ib epitopes was removed in the 4M KOH PC fractions, particularly in PB and SS leaf tissues. Epitopes akin to RG-I found in linseed (*Linum usitatissimum*) mucilage were detected in all extractions, but more abundantly in the 4M KOH extractions.

The RG-I/AGN class of mAbs, which detects arabinogalactan side-chain epitopes of RG-I, showed the highest binding values in the oxalate fractions from actively growing tissues; although proportionally to the amount of carbohydrate removed by the extractants, the bulk of these epitopes was removed from the cell wall by the harsher KOH solvents. In the first three steps of the sequential extraction there was a general tendency for higher signals of RG-I/AGN mAbs to be found in leaves and in actively growing samples, when compared to stems, or PB

and SS, respectively. By contrast, in the chlorite and both 4M KOH extractions, more variation was observed, and a specific tissue did not consistently release more of these epitopes at all developmental stages. In the 4M KOH fractions, binding values for RG-I/AGN were typically higher in AG samples, but depending on the mAb, leaf or stem had higher signals. For the chlorite extractions within the same tissue there were no substantial differences between developmental stages; although leaves typically released more RG-I/AGN epitopes than stems at AG and PB. Finally, for the 4M KOH PC fractions, higher binding intensities were seen in leaves at AG and PB, but in senesced tissues the differences between tissues was less visible and more mAb-dependent.

Pectic structures bound by mAbs from the AGN-1 to AGN-4 subclasses may occur in arabinogalactan-containing polysaccharides as well as in glycoproteins. Highest total signal for these epitopes was detected in the oxalate extractions from actively growing plants, particularly from stems. However, OD values diverged substantially across the various cell wall extractions. Certain mAbs from the AGN-1 subclass (MAC204 and JIM20) and from AGN-3 (JIM15, JIM8, CCRC-M85 and CCRC-M81) had higher total binding values in the oxalate and carbonate extracts from actively growing stems. Detectability of AGN-1 was then severely reduced in all later harsher steps of the sequential extractions, suggesting that these more labile epitopes had all been extracted with the mildest extractants. By contrast, the signal for AGN-3 slightly increased in the chlorite extractions, particularly in stems; suggesting that a population of these epitopes had not been previously released due to being directly linked to lignin. A similar trend was also observed in the AGN-4 subclass, as the binding values for JIM13 gradually decreased until the chlorite fraction, where they typically increased, especially in stem samples. Within the AGN-2 subclass, JIM14, JIM19 and JIM12 showed high signals in the weaker extractions; whereas CCRC-M133 and CCRC-M107 binding intensities increased

with harshness, typically peaking in the 4M KOH PC extractions, after a smaller fraction being removed together with lignin during the sodium chlorite treatment.

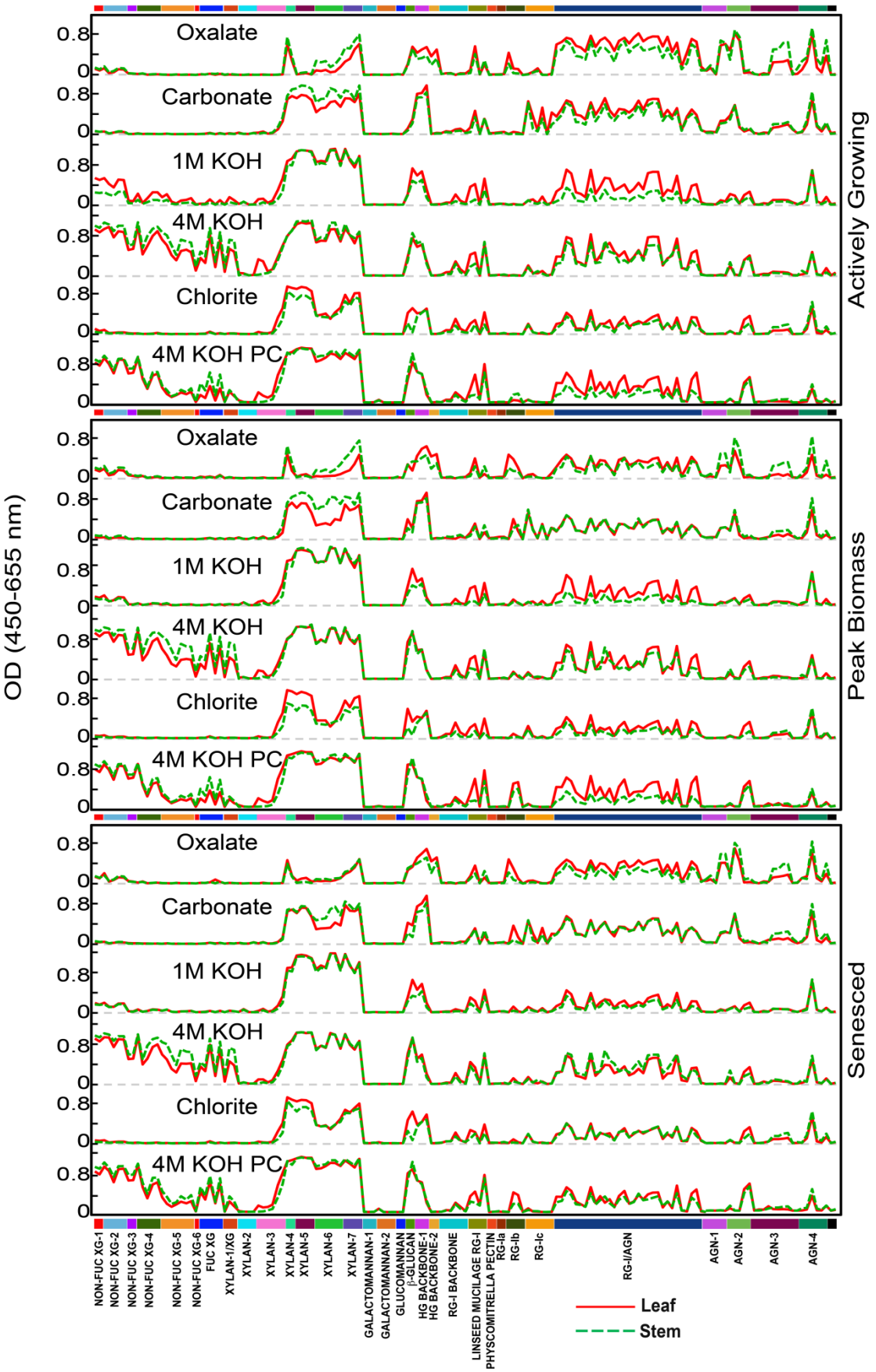

Fig. 5.4A. Mean binding values to different classes of cell wall glycan epitopes released at sequential extraction steps from leaf and stem samples from 8 miscanthus genotypes at 3 developmental stages. (See appendix C for a list of all mAbs, and appendix I for more detail on this figure)

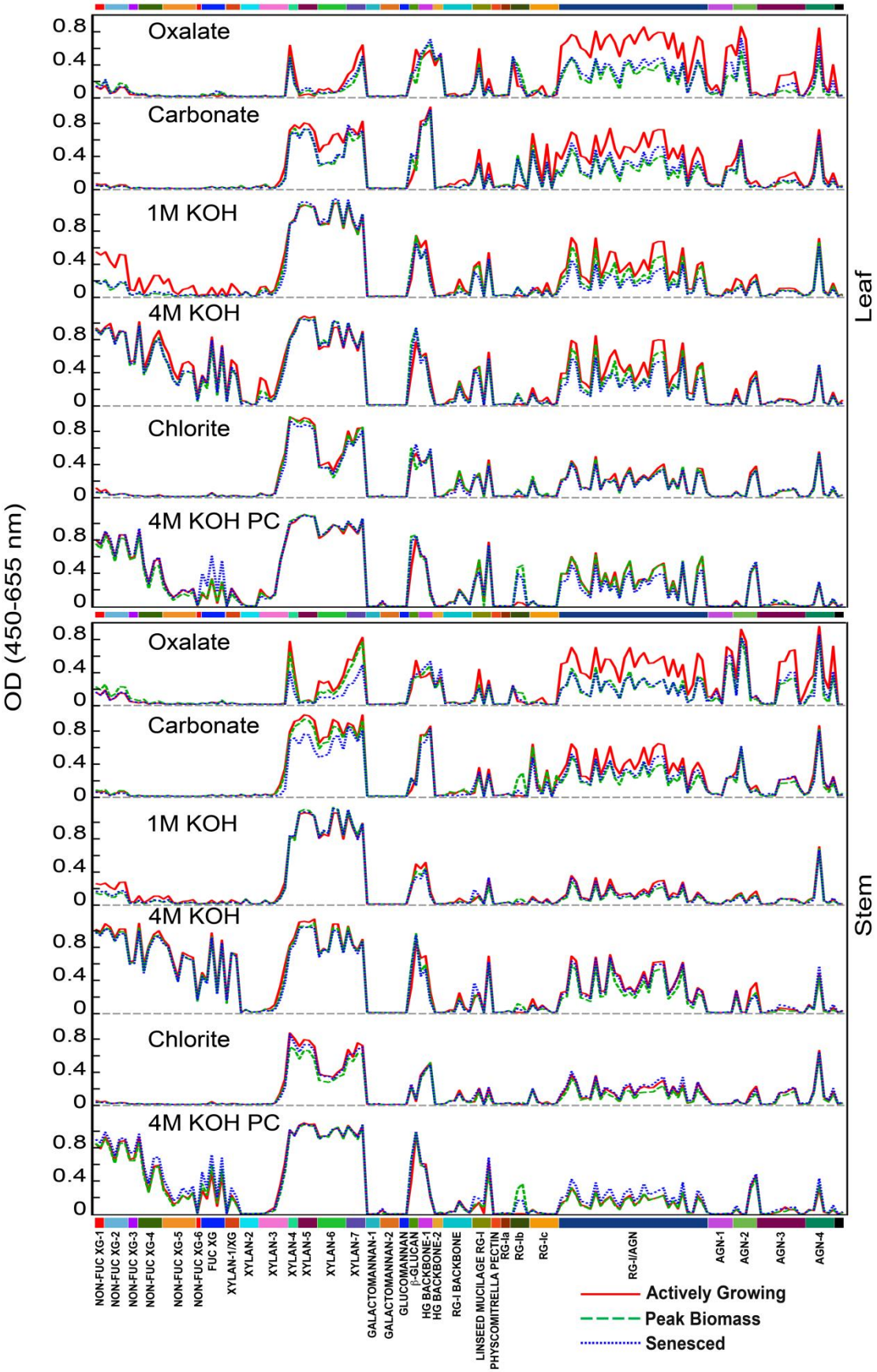

Fig. 5.4B. Mean binding values to different classes of cell wall glycan epitopes released at sequential extraction steps from leaf and stem samples from 8 miscanthus genotypes at 3 developmental stages. (See appendix C for a list of all mAbs, and appendix I for more detail on this figure)

5.1.4. Discussion

5.1.4.1. Diverging Cell Wall Glycomic Profiles across Developmental Stages and Tissues

A sequence of solutions was utilised to fractionate the cell wall from miscanthus biomass samples collected from different tissues and developmental stages. Each extractant represented successive steps of increasing solvent alkalinity, with the exception that an acid sodium chlorite treatment was employed to delignify the CWM before the final alkaline extraction. The highest proportion of released sugars was achieved without tissue delignification being required. However, to attain a more complete release of matrix polysaccharides, removal of lignin was essential; particularly in stems and in more mature plants.

At the end of the sequential extraction, the composition of the resulting residues was analysed, indicating that glucans, essentially cellulose, represented almost the totality of the composition of all samples (Appendix F). Only trace amounts of other compounds were detected, namely lignin and Xyl; with higher amounts of this sugar occurring in stem samples and in senesced plants. This may suggest that in stems and in the latest developmental stage there are strongly bound Xyl-containing hemicelluloses, which cannot be removed by the sequential extraction. In what concerns the nature of these polymers, it is very likely that they consist of xylans, since these are the most abundant hemicelluloses in grass cell walls (Carpita, 1996), and the occurrence of xylans strongly bound to cellulose has been reported for miscanthus (de Souza *et al.*, 2015). However, it is known that XG can bind more effectively to cellulose, and thus establish more stable associations (Carpita and Gibeaut, 1993; Fry, 2010). It is also known that complete XG removal requires higher alkaline concentrations than those used during the sequential extraction (Edelmann and Fry, 1992). Consequently, it could be

hypothesised that strong XG-cellulose links may resist the sequential extraction, with the result that at least some of the Xyl found in the residues occurs in XG.

The various extractants removed different portions of the cell wall structural carbohydrates; which in decreasing order were: 1M KOH, 4M KOH, 4M KOH PC, carbonate, chlorite and oxalate. The amount of carbohydrate per fraction varied primarily as a result of the extractant used, then according to tissue and thirdly according to genotype (Table 5.2). Differences between developmental stages were only significant for the oxalate and 1M KOH fractions, and differences between tissues were not significant for the carbonate and 4M KOH PC extracts. Several factors may affect the recalcitrance of the cell wall polymers removed during the sequential extraction (Li *et al.*, 2014a), namely: the level of intertwining of the polysaccharides and of their embedding within lignin (non-covalent associations); the location of the polysaccharides within the cell wall (superficiality); and the age, function or type of tissue being analysed, which may, for example, present differing degrees of cell wall thickening (histology). As a means to monitor extractability changes, and thus derive conclusions about what affects recalcitrance in miscanthus biomass, all samples were screened with a toolkit of 155 mAbs (Appendix C) to determine the typical glycome profile for each of the cell wall fractions (Pattathil *et al.*, 2010).

Obtained glycome profiles differed significantly between stem and leaf (MANOVA; appendix G), and between the various developmental stages. To better understand which glycan epitopes contributed mostly to the differentiation between these factors, PCA was utilised as an approach to elucidate underlying relations in the GP data (GP-PCA). By including all glycome profiling data, a preliminary model was generated, where according to binding intensities of the various groups of the glycan-directed mAbs, the distinct cell wall extracts were discretely distributed mainly along PC1 (Fig. 5.5A). Specifically, the oxalate, carbonate, chlorite and 1M KOH extracts diverged significantly from both 4M KOH fractions. This

revealed that despite some overlap, the six cell wall fractions obtained during the sequential extraction effectively removed distinct fractions of the cell wall polysaccharides. By analysing the loadings of PC1 (Fig. 8.8.A. in appendix H) it could be determined to which mAbs PC1 is mostly correlated, and infer which cell wall epitopes contribute the most to the divergence between fractions. These loadings suggested that the clusters located on the positive side of PC1 (Fig. 5.5A) typically contained higher abundances of XG and xylan epitopes. This was expected, as wall fractionation methods conventionally extract hemicelluloses by employing KOH and other strong aqueous alkaline solutions, which act as chaotropic agents; i.e., to disrupt the hydrogen bonding network between hemicelluloses and cellulose (Fry, 2010). By contrast, the extracts which formed clusters on the negative side of PC1 were characterised by having higher binding signals to most pectic epitopes, with the exception of certain AGN-2 and 3 epitopes; which were positively correlated with PC1. These considerations derived from PCA about the most significant contributors to the variation between the cell wall fractions were indeed confirmed by comparing binding intensities between different extracts (Fig. 5.4A).

Higher signals for most pectic epitopes were observed in the cell wall fractions obtained with milder extractants. Nonetheless, there were exceptions. For the AGN-2 epitopes recognised by CCRC-M133 and CCRC-M107, binding intensities increased as solvents became harsher, suggesting an association to very tightly bound pectins in miscanthus cell walls. Epitopes bound by JIM13 were detected in all cell wall fractions, but its binding intensities declined in each successive extraction step, except with sodium chlorite, as the signals increased slightly with this treatment. This is suggestive of an association of these epitopes with lignin. HG backbone-1 epitopes had higher binding intensities in carbonate fractions. Nonetheless, given that these extractants removed lower percentages of the cell wall carbohydrate, these more loosely bound HG epitopes removed with sodium carbonate are presumably less abundant in the intact CWM than the more tightly bound epitopes removed

with harsher alkaline extractants. For the chlorite cell wall fraction, particularly high binding signals were detected for the mAbs CCRC-M38 and JIM5; also suggesting an association of HG to lignin in both studied miscanthus tissues. Previous studies have proposed associations between lignin and pectic epitopes, namely in the cell wall of miscanthus (de Souza *et al.*, 2015), poplar (DeMartini *et al.*, 2011) and switchgrass (Shen *et al.*, 2013). In addition, overlapping deposition patterns have been reported for pectin and lignin in the middle lamella of alfalfa tissues (Wi *et al.*, 2005). By employing sodium chlorite as the fifth step of the sequential extraction, it is unlikely that this delignification treatment extensively affects other wall components, and thus pectin epitopes detected in this cell wall fraction are presumably released only as a consequence of the destruction of bound lignin structures. However, it should be recognised that direct lignin-pectin associations are not a common trend of thought found in the literature (Shen *et al.*, 2013), and hence further investigation is required. Support for this view may also arise from the observation that binding intensities of several RG-I related epitopes become more intense in harsher extracts (RG-I backbone, RG-Ib and linseed mucilage RG-I; Fig. 5.4). In addition, for all these subclasses of mAbs in the chlorite fraction, higher signals are seen in leaf samples than in stems.

HG is synthesised in a highly methyl-esterified form, is subsequently de-esterified *in muro*, producing sequences of un-esterified galacturonic acid residues, which may establish Ca^{2+} linkages and form egg-box structures (Liners *et al.*, 1989; Wolf *et al.*, 2009; Lionetti *et al.*, 2010), thus contributing to maintain correct cell adhesion. In the GP study presented here, four mAbs were included which bind to HG epitopes with different levels of esterification: CCRC-M38, CCRC-M131 and JIM5, which partially bind to fully, or relatively un-esterified HG epitopes; and JIM7, which binds to a heavily esterified HG epitope (Knox *et al.*, 1990; Pattathil *et al.*, 2010). In oxalate fractions, binding to these four mAbs was detected, and specifically for CCRC-M38 and JIM5, their binding intensities were lower in AG samples and

then became higher in later developmental stages in both tissues, but particularly in leaves (refer to appendix I for more detail). This suggests that the abundance of un-esterified HG epitopes increases as plants mature, which is consistent with progressive de-esterification of these pectins. In subsequent alkaline cell wall fractions binding to CCRC-M38 and JIM5 remained detectable, but undetected for JIM7. It cannot be excluded that this is an outcome of the saponifying action of alkaline solvents, which de-esterify cell wall polymers. As a consequence, inferences regarding the variation of esterification of HG across tissues and developmental stages could only be drawn at the level of the more labile ammonium oxalate-extracted HG epitopes. In all subsequent extractions no information could be attained concerning how extensively the polymers are esterified *in muro*. However, the immunolabelling studies which will be presented in the subsequent section will provide further information in this regard.

Also in accordance with the GP-PCA data, the XG epitopes showed more intense signals in both 4M KOH extracts and in the 1M KOH fractions from leaves, particularly at the AG developmental stage (Fig. 5.4). Conspicuously, the origin of the PC1 axis intersects the 1M KOH cluster (Fig. 5.5A), almost dividing between tissues, with stem extracts being plotted closely to the mildest extractants, and leaf nearer to the 4M KOH clusters. This suggests that leaf is less recalcitrant, and thus requires less harsh solvents (1M KOH) in order to yield extracts which have more features in common with the 4M KOH clusters; than do the 1M KOH extracts from stem, which are more resistant to extraction. These differences in recalcitrance between tissues are also supported by saccharification data (Section 4.2).

During the sequential extraction, the 1M KOH fractions initiate a trend of increased release of XG epitopes which continues in the 4M KOH extracts. This is in agreement with reports for switchgrass (Shen *et al.*, 2013) and sugarcane (de Souza *et al.*, 2013). In another study performed on miscanthus cell wall, it has been reported that high amounts of XG are

released with sodium chlorite, suggesting that portions of these polymers may be branched with lignin (de Souza *et al.*, 2015). In the data presented here, XG epitopes were not substantially detected in the chlorite fractions, suggesting that these glycans are not extensively associated directly to lignin. However, this does not contradict entirely with what has been proposed by de Souza *et al.* (2015). It has been shown that by treating CWM with concentrated alkaline solutions, some degradation of phenylpropanoid cell wall components may be effected, namely to HCA (Section 3.2) and also to lignin (Si *et al.*, 2015). As a result, it is possible that some of the XG epitopes detected in the 1M KOH and the first 4M KOH fraction could be associated to more labile portions of lignin. For the subsequent 4M KOH PC extraction, the release of XG epitopes is presumed to have been previously blocked by lignin, or lignin-associated polysaccharides, which were present in the wall before delignification with sodium chlorite.

High variation was also detected in the binding to xylan epitopes, and although the KOH-produced cell wall fractions presented a somewhat similar profile, for each extract it was observed that different xylan subclasses presented different intensities of binding. Xylan 4 and 7 typically displayed relatively high signals in all extracts, xylan 5 epitopes were more noticeable in all but the oxalate fraction, whereas xylan 6 detection was more abundant in the KOH-mediated extraction steps; which suggests that the detected structures occur in distinct xylan populations. Of these xylans, it is evident that some are easily removed with mild treatments, whereas others require much harsher extractants, including solvents for lignin removal. These observations point to the likelihood of the more labile xylans differing in structure from the more recalcitrant ones, as has also been hypothesised in another study of miscanthus cell wall (de Souza *et al.*, 2015). Furthermore, it is possible that a portion of the xylans in miscanthus cell walls, which are more abundant in leaves than in stems (Fig. 5.4), do

occur associated to lignin. This is corroborated by the fact that a similar conclusion has been reported by DeMartini *et al.* (2013) for poplar cell wall fractions.

Detection of mannan epitopes was extremely low or even absent in analysed samples. Only in the 4M KOH PC fractions, particularly of senesced samples, were these epitopes detected, nonetheless, with extremely low binding intensities. This is in accordance with that expected for type-II cell walls (Carpita *et al.*, 2001), and consistent with cell wall compositional data of all but one miscanthus genotypes studied by de Souza *et al.* (2015). It is worth noting that the fact that these authors could identify mannan structures in one genotype provides evidence for the competence of GP in the identification of these epitopes. As a consequence, their non-detection in the miscanthus profiles reported here is not due to procedural artefacts, such as epitope modification, but instead, corresponds to a real absence in the analysed samples. This is supported by the fact that total cell wall hydrolysis did not release quantifiable amounts of mannose (Section 4.1).

Subsequently, the glycome profiling data from each extract was modelled independently, and for all cell wall fractions two separate clusters emerged, one comprising the glycome profiles from stems and another from leaves (Fig. 5.5 B – E and Fig. 8.8.B. in appendix H). Depending on the PC responsible for the separation, its corresponding loadings were interpreted in order to infer the main glycan contributors to the differentiation between tissues. PC loadings revealed that in the oxalate and carbonate extracts, significant differences occur between tissues in terms of the binding intensities to specific glycan epitopes. Concerning the loosely bound RG-I/AGN epitopes removed in these extracts, PCA suggested that a higher abundance for these epitopes in leaves is a main diverging factor in relation to stems. By contrast, higher signals in stems than in leaves for most AGN-3 and AGN-4 epitopes were determined to be a distinctive characteristic of the oxalate and carbonate fractions of miscanthus stem cell wall.

Differences in labile xylan epitopes were demonstrated to be a discriminating characteristic between tissues, as certain subclasses showed lower binding intensities in leaf samples. Specifically for the carbonate fraction, binding signals for xylan-5, 6 and 7 epitopes were generally more intense in stem samples. This was more noticeable at the PB developmental stage, but in senesced samples, particularly for xylan-5 and 7, the intensities showed less variation between stems and leaves. Given that these mAbs are directed at linear xylan epitopes, i.e., unsubstituted polymers (unpublished data from the Hahn laboratory), it is likely that a smaller proportion of the xylan structures extracted with sodium carbonate are substituted in stem tissues. Furthermore, the fact that the signal difference between leaves and stems is not so marked at SS could indicate that at this developmental stage there is a smaller difference in the amounts of xylan substitution between tissues; which in turn may be interpreted as being suggestive of a decline in substituted xylan proportions in leaves as plants senesced. Both these observations are in agreement with the Ara/Xyl ratios reported in section 4.1; which were significantly lower in stem samples, and in senesced leaf samples when compared to younger tissues.

In the PC1 loadings of the 1M KOH fraction no prominent difference between tissues was restricted to a particular group of epitopes (Fig. 8.8.B. in appendix H), instead, the analysis just emphasised the generally higher degree of binding found in leaf CWM for most of the tested mAbs. For the 4M KOH fractions, PCA revealed that many of the major variations between tissues are identical in the extracts obtained before and after the chlorite treatment. Specifically, it emphasised that in both 4M KOH fractions stems typically released higher abundances of fucosylated and non-fucosylated XG, and more xylan from subclasses 5, 6 and 7. On the other hand, it highlighted that distinctive characteristics of leaf cell wall fractions extracted with 4M KOH are higher binding values for most RG-I related epitopes (RG-I Backbone, and RG-I/AGN) and xylan epitopes from subclasses 3 and 4. The loadings plot

emphasised that for the chlorite fractions, the binding intensities are generally higher in leaf cell wall samples and that this is mainly for xylans, β-glucans, HG backbone, RG-1 backbone and RG-I/AGN. Conversely, the PCA identified that higher abundances of certain AGN epitopes from subclasses AGN-3 and AGN-4 are characteristic of stem samples.

Stronger binding intensities for LAMP2H12H7 (LAMP) and BG1 mAbs in the first three cell wall fractions in the extraction series of leaf samples suggests that miscanthus leaves contain higher proportions than stems of both β-glucan epitopes probed. Specifically for MLG epitopes probed by BG1, these structures are detected in all cell wall fractions, agreeing with data reported for corn stover (Li *et al.*, 2014a). Considering the proportions of cell wall polysaccharides removed by each extractant, the bulk of MLG is presumed to have been released with 1M KOH. In this cell wall fraction, samples from the AG developmental stage exhibit the most intense signals for MLG binding, indicating that the CWM from younger plants contains higher amounts of MLG. This is in agreement with reported findings that despite MLG accumulating preferentially in younger tissues, it is also found in mature tissues (Vega-Sánchez *et al.*, 2013), although with a reduction in abundance due to the action of endogenous enzymes (Buckeridge *et al.*, 2004). By contrast, in the more harshly extracted 4M KOH fractions, higher abundances of MLG epitopes were detected in CWM from PB and SS stages, and in stems when compared to the AG stage and leaves, respectively. In the chlorite fraction, senesced and leaf samples contained higher abundances of MLG epitopes. The fact that MLG is removed from the wall by extractants of very different harshness is in agreement with reports that these glycans can present different levels of solubility; which in turn are strongly influenced by the ratio between trisaccharide and tetrasaccharide structural domains of this polymer (Collins *et al.*, 2010; Vega-Sánchez *et al.*, 2015). Furthermore, several authors have proposed that certain domains of the MLG polymers interact directly with cellulose microfibrils (Carpita, 1996; Fry, 2010; Kiemle *et al.*, 2014). These proposals are in agreement

with the observations here reported for miscanthus, that the glycome profile of the three cell wall fractions produced by the harshest extractants exhibit the highest binding signals to β-glucan epitopes, which suggests that the recognised epitopes are strongly bound to the wall.

To find epitopes showing the most variation between developmental stages, PCA models were created for the glycome profiling data of the different cell wall fractions for each tissue (Fig. 5.5 F – H and Fig. 8.8.C. in appendix H). In the stem models, an almost complete overlap of the samples collected at different developmental stages was observed, and thus no clear clusters could be discerned along the PC axes, for any of the cell wall fractions analysed (Fig. 8.8.C. in appendix H). An implication of this observation is that compositional differences in the abundance of most cell wall matrix epitopes in stems are not sufficiently significant to originate clear clusters of samples according to developmental stage. Given that the most abundant non-cellulosic polysaccharides in miscanthus cell wall are hemicelluloses (Le Ngoc Huyen *et al.*, 2010; Allison *et al.*, 2011; Lygin *et al.*, 2011), it is likely that the overall abundance of these glycans does not vary substantially between developmental stages. In fact, this is supported by the GP binding intensities, as signals to most tightly bound xylan epitopes were generally similar between developmental stages in all stem cell wall KOH-mediated extracts (Fig. 5.4), which represent the fractions with the biggest proportion of extracted matrix polysaccharides.

By direct comparison of the glycome profiles obtained for stem samples (Fig. 5.4), it is seen that actively growing stems exhibit markedly higher signals for less abundant loosely bound pectic epitopes, extracted with ammonium oxalate and sodium carbonate (RG-I/AGN and AGN subclasses of mAbs). Additionally, in these cell wall fractions, lower signals were observed for xylan epitopes at PB and SS indicating that despite tightly bound xylans not varying significantly between developmental stages, there is a population of more labile, yet less abundant xylans, which occur at higher proportions in the stems of immature plants.

Similarly, for leaf cell wall fractions removed during the last three steps of the sequential extraction (4M KOH, chlorite and 4M KOH PC), compositional differences in cell wall glycans were insufficient to create PCA clusters according to developmental stages (Fig. 8.8.C. in appendix H). As for stems, this presumably indicates that the occurrence of the more abundant, tightly bound xylans does not vary significantly between harvest time points. However, in contrast to the glycome profiles from stems, distinct clusters related to developmental stage were detected in the scores plots of leaf samples, for the oxalate, carbonate and 1M KOH fractions. Two clusters emerged in all cases, one consisting of overlapping leaf samples collected at peak biomass and after senescence and another from actively growing plants (Fig. 5.5 F – H). Overall, these observations suggest that changes attributed to plant growth in the cell wall glycome of leaf tissues are mainly prominent in the more labile epitopes released with the mildest extractants. Specifically, by analysing the loading plots of PC1 (Fig. 8.8.C. in appendix H), it was concluded that there are three main points of variation between developmental stages concerning more labile leaf cell wall glycan epitopes: (1) higher amounts of loosely bound pectins in AG samples extracted during the first three extraction steps; (2) lower abundances of loosely bound xylans, particularly in the carbonate cell wall fractions of mature plants; and (3) more abundant XG in actively growing plants than at later stages.

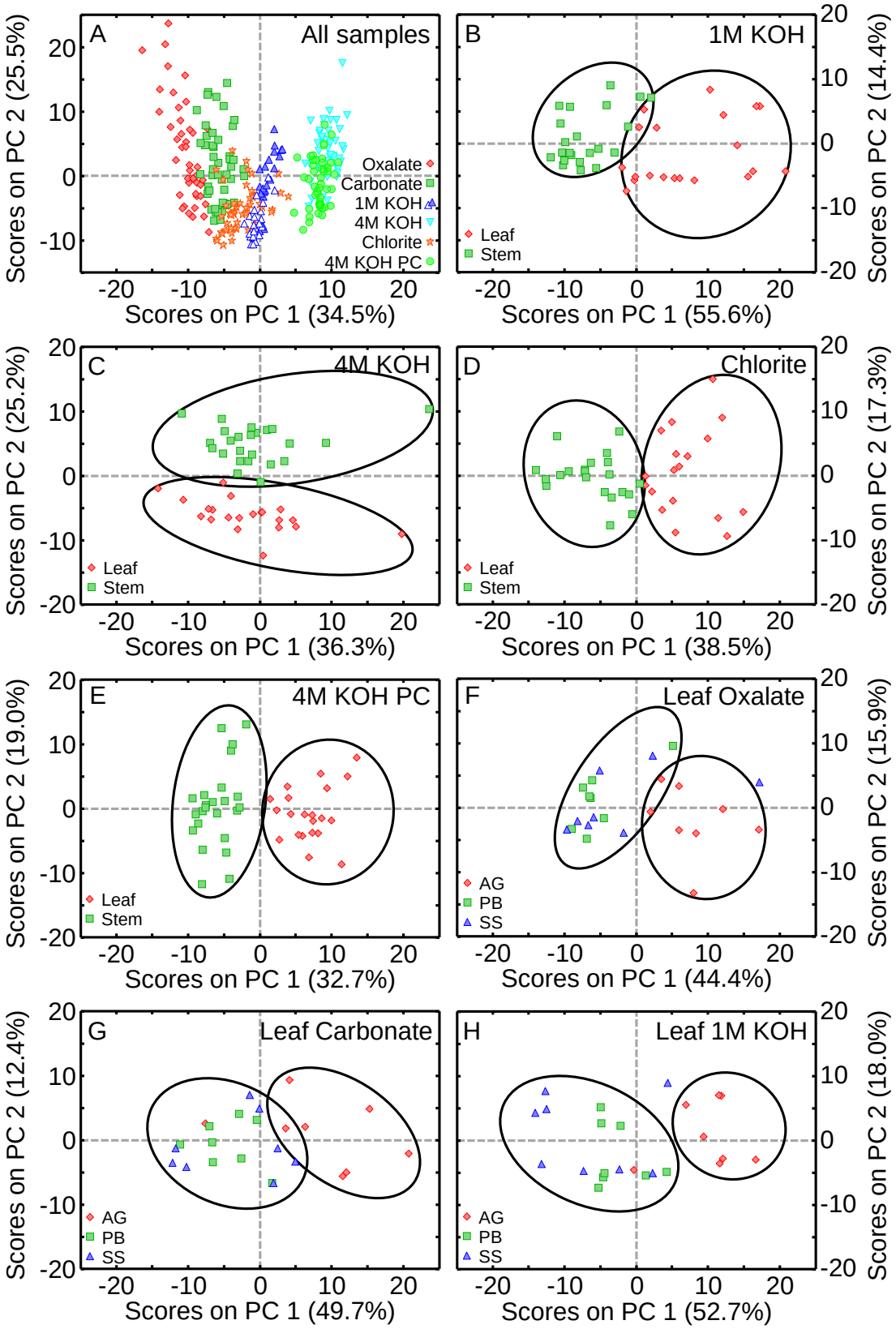

Fig. 5.5. Principal components analysis of glycome profiling data. Plot of principal component one (PC1) and principal component two (PC2) scores for all samples (A; open triangles in the 1M KOH extract are stem samples and blue-filled triangles are leaf samples), for samples extracted with 1M KOH (B), 4M KOH (C), sodium chlorite (D) and 4M KOH again post-chlorite (PC) treatment; F, G and H show leaf tissue samples extracted with ammonium oxalate, sodium carbonate and 1M KOH. Abbreviations: AG, active growth; PB, peak biomass; SS, senesced stage.

5.2. *IN SITU* IMMUNOLABELLING

5.2.1. Overview

Cell wall polysaccharides represent a highly heterogeneous and dynamic component of the plant cell, and this structural complexity has to date a not completely understood impact on its recalcitrance to saccharification. GP, the technique discussed in the previous section, has the ability to extensively elucidate the polymeric nature of the cell wall carbohydrates. However, one inconvenience of the technique is the fact that no amount of information is attainable concerning the subcellular distribution of the epitopes. Immunohistochemistry, in the form of *in situ* immunolabelling of glycan epitopes, is a technique which has the ability to complement GP in this matter, as it provides information on the distribution of specific glycan epitopes. In the context of cell walls, immunolabelling involves the use of cell wall glycan-directed mAbs in conjunction with fluorescence microscopic imaging to perform ultra-structural studies and thus determine the distribution of structural polysaccharides across different regions of the tissues under analysis. Immunolabelling differs from GP in that it does not involve the extraction of the glycans from the cell wall, and thus it results in minimal, if any, modification of the epitopes. Nevertheless, when using this technique not all epitopes are freely accessible for detection, whether as a consequence of them not being in the plane of the sections taken for immunohistochemistry, or because other wall components (such as ester-linked groups) may interfere with *in situ* access of the mAbs to the epitopes (Avci *et al.*, 2012).

Very limited information is currently available concerning the location of cell wall glycan epitopes in miscanthus tissues (Xue *et al.*, 2013; Cao *et al.*, 2014). Therefore, this is a subject which remains under-explored, namely concerning the characterisation of the variation across different tissues and genotypes. However, immunolabelling does have the unique potential to

further our understanding of the structure and role of polysaccharides within the cell wall, as it currently is the only effective methodology which allows the determination of the distribution of specific polysaccharide structures in the cell wall (Marcus *et al.*, 2010). A possible contributor to this lack of studies in miscanthus is the fact that immunolabelling is a laborious procedure, which makes it unfeasible to perform single studies encompassing a very large collection of mAbs. To cope with this, in the present study the previously determined glycome profile of the miscanthus cell wall was used to narrow down the selection of mAbs to be included in immunolabelling studies. In this section the results of these analyses are presented, where a subset of the mAb toolkit used for GP (Appendix C) was employed in a study aimed at determining the location of specific glycan epitopes across leaf and stem tissues from 8 miscanthus genotypes. It is expected that the gathering of data at the level of subcellular distributions of glycan epitopes will allow inferences on the architecture of the miscanthus cell wall, and thus possibly aid in the design of more advanced approaches to enhance saccharification yields.

5.2.2. Materials and methods

A single tiller cut immediately above the rhizome was collected at the peak biomass (PB) developmental stage. Sampling uniformity across 8 miscanthus genotypes with varying phenotypes (Section 2.1) was achieved by collecting leaf and stem samples from an internode in all cases located halfway through the length defined between the uppermost fully formed ligule and the base of the tiller[*]. Subsequently, smaller sections measuring approximately 1mm to 5mm were cut from the middle portion of the leaf blade and from the middle of the internode (Fig. 5.6). Samples were immediately immersed in a fixative solution consisting of 1.6% (v/v) paraformaldehyde with 0.2% (v/v) glutaraldehyde in 0.025M sodium phosphate buffer (pH=7.1). After being left fixing for 16h, tissues were washed with the same buffer (3 times, 15min each), and with deionised H_2O (2 times, 15min each). For dehydration, samples were left 30min at each step of a 35%, 50%, 70% and 95% (v/v) aqueous ethanol series, then at 100% (v/v) ethanol (16h) and finally again at 100% (v/v) ethanol for 1h. Subsequently, the dehydrated samples were moved to 4ºC and then gradually infiltrated with cold LR White embedding resin[†] (medium grade, 18181; Ted Pella Inc., Redding, California, USA) as follows: 1:3 resin:absolute ethanol; 1:1 resin:absolute ethanol; 3:1 resin:absolute ethanol; and 3 times 100% resin; each step for 24h. Infiltrated samples were then transferred to gelatine capsules

[*] Given the impossibility to conveniently sample a homologous representative internode from all genotypes, a medial internode was chosen as an attempt to uniformly sample all genotypes, while simultaneously producing sections which were more representative of the whole biomass of the tissue in question (compared with sections taken solely from older or younger internodes, if they were chosen for sampling).

[†] LR White is a hydrophilic acrylic resin, which as other plastic/resin-based embedding media yield sections that are impenetrable to the mAbs. Labelling of tissue is therefore limited to those cellular structures that are exposed on the cut surface of the section. In the case of wax-embedded tissues, the wax embedding medium is removed prior to immunolabelling, leading to exposure of additional tissue surfaces that can subsequently be accessed by mAbs during labelling of the sections. Such differences in the nature of the sections must be taken into account when interpreting the results of immunohistochemical studies. For example, changes in labelling patterns using probes against xylan or mannan epitopes have been observed after treatment of wax-embedded sections with pectic-degrading enzymes (Marcus *et al.*, 2008, Marcus *et al.*, 2010), but were not observed when LR White is used as the embedding medium (Brennan and Harris, 2011; Avci *et al.*, 2012; Donaldson and Knox, 2012).

(Snap-Fit capsules, 130-14; Ted Pella), containing 100% LR White resin for embedding, which was polymerised at 4ºC under UV light (365nm) for 48h.

The polymerised blocks were then trimmed with a sharp razor blade under a dissecting microscope to create a sectioning surface. For stem and leaf tissues from 8 miscanthus genotypes, cell wall glycan epitopes were analysed by fluorescence immunolabelling according to procedures described in Pattathil *et al.* (2010) and Avci *et al.* (2012). Transverse semi-thin sections (250nm) were cut with a Leica EM UC6 ultramicrotome (Leica Microsystems Inc., Buffalo Grove, Illinois, USA) and mounted on glass slides (colorfrost/plus; Fisher Scientific Ltd., Pittsburgh, Pennsylvania, USA). Immunolabelling was performed at room temperature by applying and removing a series of 10µL droplets of the appropriate reagents to the sections using the following protocol. Non-specific binding in the sections was blocked with 3% (w/v) non-fat dry milk in 0.01M potassium phosphate buffered saline containing 0.5M NaCl (KPBS; pH=7.1). After 30min, the sections were washed once for 5min with the same KPBS buffer. Undiluted hybridoma supernatant of the mAbs under study was applied and incubated for 90min. Sections were then washed with KPBS three times for 5min. Goat anti-mouse IgG or goat anti-rat IgG conjugated to Alexa-fluor 488 (Invitrogen, Waltham, Massachusetts, USA) diluted 1:100 in KPBS was applied and incubated for 90min. Sections were then washed three times with KPBS for 5min, and then twice with deionised H_2O for 5min. Furthermore, for each genotype, leaf and stem sections were treated following this same procedure, but using primary mAbs known not to bind to epitopes in the plant tissues. These sections represent negative immunological controls (Avci *et al.*, 2012). Prior to placing a coverslip, Citifluor antifadent mounting medium AF1 (Electron Microscopy Sciences, Hatfield, Pennsylvania, USA) was applied.

In situ immunolabelling represents a complementary dataset to GP. However, between the two procedures, one significant difference is that the alkaline extractants used during the

sequential extraction lead to de-esterification of the wall polysaccharides, which in turn may alter the epitopes recognised by the mAbs. Certain xylan-directed and HG-directed mAbs used in this study are known to only strongly bind to de-esterified forms of the polymers. To account for this, miscanthus sections were subjected to a base treatment with 0.1M KOH (1h followed by three 5min washes with deionised H_2O) as a first step, before blocking and incubation with primary and secondary mAbs. Microscopic inspection of the sections was performed using an Eclipse 80i microscope (Nikon Inc., Melville, New York, USA) equipped with epifluorescence optics. Different exposure times were tested during microscopic examination of the sections. For the final figures, all micrographs for a given mAb were captured at the same exposure time with a Nikon DS-Ri1 camera head using NIS-Elements Basic Research software (Nikon).

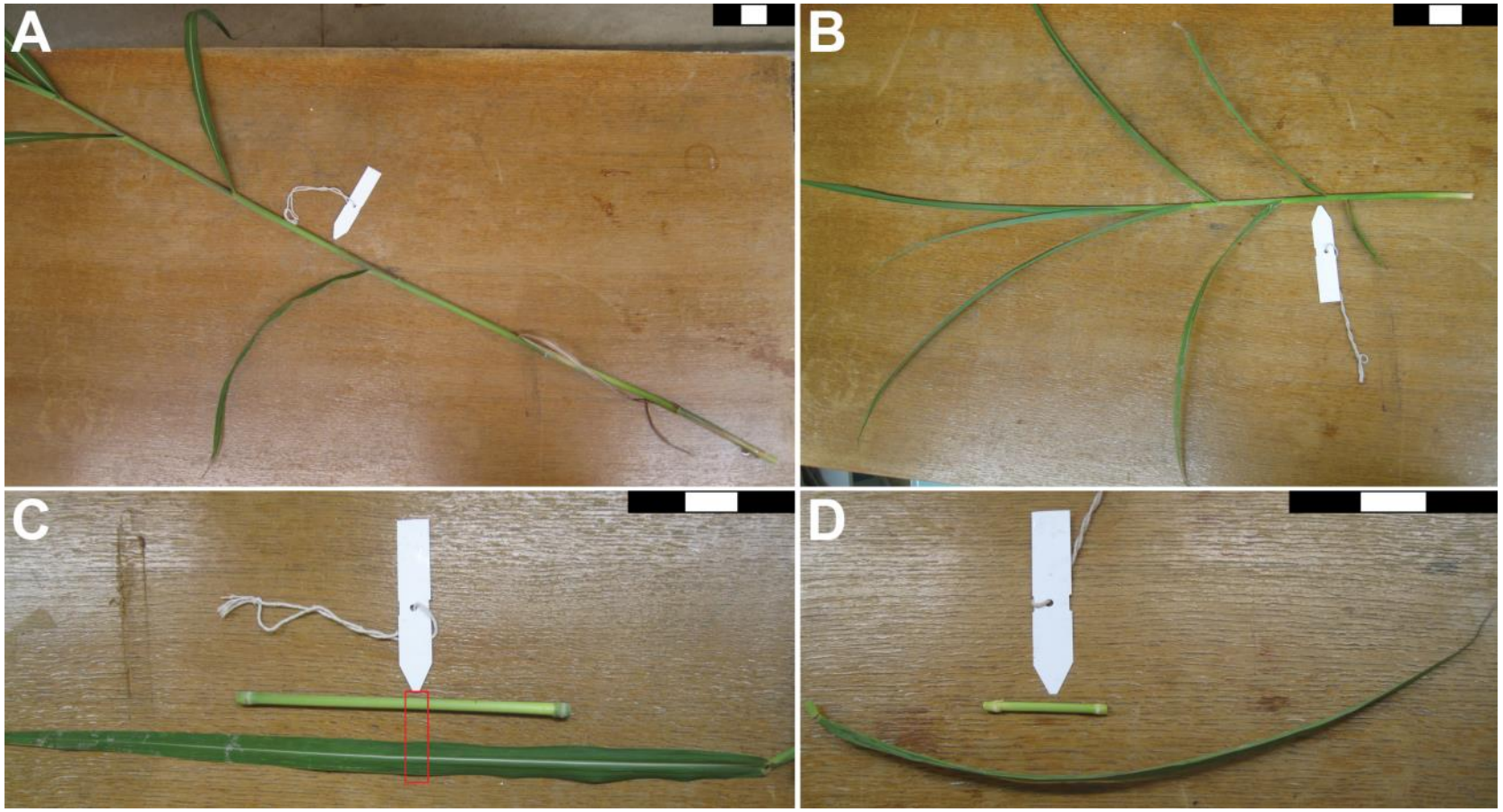

Fig. 5.6. Appearance of the tillers taken from genotypes gig01 (A, C) and sin13 (B, D). Red box indicates the portions of stem and leaf used for *in situ* immunolabelling studies, and scale bars represent 15cm.

5.2.3. Results

In order to validate and verify *in situ* the results obtained from the glycome profiling of miscanthus tissues, an immunohistochemical study was performed on stem and leaf midrib semi-thin sections. Given that it would not be feasible to probe samples from all eight genotypes with the large set of mAbs used for GP, only the gig01 genotype was utilised at this stage. The choice of this genotype has to do with the well disseminated use of *M.* × *giganteus* at both research and commercial levels (Allison *et al.*, 2011). This approach maximised the number of mAbs that could be used, while ensuring the feasibility, comparability and relevance of the immunolabelling study, in terms of characterising and highlighting differences in cell wall glycan distribution patterns in miscanthus tissues. Furthermore, given the complexity of the observed *in situ* immunofluorescence patterns, not all details mentioned in the context of the immunolabelling study could be illustrated. As a result, micrographs were included with the aim of providing an overview of the appearance of immunolabelled *M.* × *giganteus* tissues, and higher resolution versions of all figures are available upon request[*].

The immunolabelling study of miscanthus tissues was preceded by microscopic inspection of leaf and stem sections stained with toluidine blue, as a means to characterise their histological complexity (Fig. 5.7). Toluidine blue is a basic thiazine metachromatic dye, which can be used for polychromatic staining of plant tissues (O'Brien *et al.*, 1964; Sridharan and Shankar, 2012). Transverse sections of miscanthus leaves revealed that vascular bundles are surrounded by two layers of cells, one forming the bundle sheath, and another forming the mesophyll (Fig. 5.7). This type of structural organisation is also seen in other C_4 plants, such as sugarcane (Colbert and Evert, 1982) and maize (Russell and Evert, 1985), and it is

[*] Also available in the supplemental materials of this thesis and online: https://mega.co.nz/#!rBNgQLzD!9ypu0nCjIv6GlcWSl3V4o6QfDuDBFagRk-2CGgw-f6c.

designated *kranz* anatomy[*] (Esau, 1977). Furthermore, within mesophyll and bundle sheath cells, chloroplasts are visible, stained with a dark purple hue, and above the mesophyll, stomatal complexes occur, consisting of guard cells, subsidiary cells and substomatal chambers. In miscanthus midribs, the vascular bundles are concentrated on the abaxial face of the leaf, and a sequence of large bundles is interrupted by typically 2 or 3 smaller bundles. Both in leaves and stems, cell walls associated with the xylem typically yielded a bluish tone with toluidine blue staining, which indicates lignification of the wall (O'Brien *et al.*, 1964). By contrast, in the phloem, neither the sieve tube elements nor the companion cells showed this bluish hue. A similar pattern of lignin occurrence has been reported in sugarcane sections stained with phloroglucinol (de Souza *et al.*, 2013). Large parenchymatous cells of ground tissue make up the core of the leaf midrib. By contrast, in stems, despite ground tissue also becoming more abundant towards the centre of the transverse sections, the cells are substantially smaller. The overall organisation of the stem tissues is distinct from leaves, primarily as a result of the absence of *kranz* anatomy. Here, bundle sheaths are not visible, but several layers of sclerenchyma cells surround the bundles. These sclerified cells are more abundant around the smaller vascular bundles which occur closer to the epidermis. Additionally, certain un-stained structures detected in the cytosolic compartment of stem parenchyma cells were identified as amyloplasts, based on the fact that starch remains colourless after toluidine blue staining (O'Brien *et al.*, 1964).

Cell wall glycans of leaves and stems from *M.* × *giganteus* were probed with a total of 34 mAbs (Table 5.3) aimed at various classes of hemicelluloses and pectins (Appendix C), including 6 which are directed at XG epitopes. For two of these mAbs, CCRC-M50 and CCRC-M58, which bind to non-fucosylated XG from subclasses 4 and 5 respectively, labelling was extremely low, albeit slightly more noticeable in stem tissues, particularly in phloem cell walls

[*] Derived from the German word for wreath.

(Fig. 8.10A in appendix J). Similarly, labelling with CCRC-M106, a fucosylated XG-binding mAb, was also very faint but more noticeably in the phloem. Although in this instance no apparent difference in labelling intensity was observed between stems and leaves (Fig. 8.10A in appendix J).

Immunolabelling of non-fucosylated XG epitopes with CCRC-M101 was generally less intense than with CCRC-M88 (Fig. 5.8), but in both cases a pattern of fluorescence was visible in leaves and stems which consisted of strong labelling of the phloem and fainter labelling of the xylem and the epidermis[*]. Occasional labelling of the middle lamella in the parenchymatous ground tissue of leaves was observed with both mAbs, although more intensely with CCRC-M88. In stems, labelling of non-fucosylated XG in the middle lamella of all parenchymatous and sclerenchymatous tissues was more intense than in leaves, when probed with CCRC-M88, but not with CCRC-M101.

For fucosylated XG, epitopes identified by CCRC-M1 showed a much less distributed pattern. In addition, labelling of cell walls from leaves was clearly less abundant than in stems; despite the fact that even in this tissue labelling was not abundant, as it was mostly restricted to phloem cells (Fig. 5.8).

Xylan epitopes were probed with 9 mAbs (Table 5.3). Five of these mAbs, CCRC-M154 (xylan-4), CCRC-M150 (xylan-4), CCRC-M140 (xylan-6), CCRC-M139 (xylan-6) and CCRC-M149 (xylan-7), displayed distinct labelling pattern, within and between miscanthus tissues (Fig. 5.9). In leaf cell walls probed with CCRC-M154, labelling was observed in all cell types, although with differences in intensity. Phloem cells were the structures where fluorescence was more intense, but xylem parenchyma and lacunae, bundle sheaths, and epidermis (including the stomatal complexes), were also labelled. In sclerenchymatous cells, the secondary wall seems to be more intensely labelled than the primary wall; conversely, in

[*] Consult supplemental high resolution version of Fig. 5.8 for further detail.

parenchymatous ground tissue cells, primary walls and middle lamellae are more intensely labelled. In stems, fluorescence intensity was generally lower, but labelling patterns in vascular bundle, sclerenchyma and parenchymatous cell walls were similar to those observed in leaves. However, in the epidermis labelling was much fainter in stems, although the outer part of epidermal cells, i.e., the cuticle, was found to be labelled by CCRC-M154 in leaves and in stems. Despite CCRC-M150 also binding xylan-4 epitopes, the labelling patterns of this mAb were substantially different from CCRC-M154; most strikingly because immunolabelling with CCRC-M150 was less distributed. With CCRC-M150, immunofluorescence was mainly concentrated in the phloem, particularly in companion cells, both in stems and in leaves. However, while in stems labelling was restricted to these walls, in leaves, a slightly less marked, but still intense labelling was observed in sieve tube elements. CCRC-M140 and CCRC-M139 belong to the xylan-6 subclass of mAbs, and in both cases it was observed that their patterns were similar, except for the fact that CCRC-M139 yielded more intense fluorescence. This observation is more clearly visible in stem sections, where the walls of all cell types are labelled, with the exception of phloem and protoxylem. In leaves, the labelling pattern of CCRC-M140 and CCRC-M139 in vascular bundles was identical to stem, as xylem and associated sclerenchymatous cells (particularly their thickenings) were substantially more labelled than phloem and protoxylem. Strong labelling of epidermis cell walls was also visible with both mAbs, but in ground tissue cells of leaves, labelling occurred more visibly in the primary wall, and was stronger with CCRC-M139. The xylan-7 mAb, CCRC-M149, showed a very abundant labelling pattern, which included the walls of all cell types in stems, and all cell types except mesophyll in leaves; which were faintly labelled. Furthermore, contrary to that observed with the other xylan-directed mAbs, labelling of parenchyma and sclerenchyma cell walls with CCRC-M149 did not vary between primary and secondary walls.

Very low reactivity was detected while probing the tissues of *M.* × *giganteus* with the remaining xylan-directed mAbs (Table 5.3) from subclasses xylan-3 (Fig. 8.10A in appendix J) and xylan-5 (Fig. 5.10). Xylans may be extensively esterified, as they form ester links with acetyl groups (Wende and Fry, 1997b; Pawar *et al.*, 2013). Additionally, in the case of AX, FA may occur ester-bound to arabinosyl side chains (Wende and Fry, 1997a). Alkaline extractants used during GP are known to cause carbohydrate de-esterification, which allied to the fact that xylan-specific mAbs were developed for de-acetylated, alkali-extracted xylans (Li *et al.*, 2014a), does lead to alterations in mAb recognition of cell wall glycan epitopes. The use of a base treatment in immunolabelling studies has been previously reported (Marcus *et al.*, 2010), where KOH was employed as a saponifying agent to remove ester-linked groups. As shown in chapter 3, compounds released by treating miscanthus CWM with 0.1M KOH include HCAs and acetate. Nonetheless, as a proportion of the CWM, the 0.1M KOH treatment primarily causes the release of acetyl groups (compare tables 3.2 and 3.7, which respectively show acetate and HCA release upon 0.1M KOH treatment). Bearing this in mind, a base treatment was performed, consisting of subjecting the sections to 0.1M KOH for 1h, before incubation with primary mAbs[*]. With this treatment it was intended to: (1) account for the fact that ester-linked substituents interfere with the binding of xylan-directed mAbs, particularly of those in the xylan-5 and -6 subclasses; (2) partially replicate the de-esterification effect of the sequential extraction performed as part of GP; and (3) provide information regarding the level of xylan esterification.

For xylan-3 mAbs, CCRC-M117 and CCRC-M113, the base treatment did not enhance epitope recognition, and their immunolabelling with and without the base treatment only showed very weak reactivity in both tissues (Fig. 8.10A in appendix J). Nevertheless, minimal

[*] It is important to note that non-recognition of esterified glycan epitopes derives from the fact that the mAbs were generated using de-esterified cell wall glycans. As a result, the base treatment is only a technical approach to allow epitope detection. The esterified forms of the epitopes are the native form, as they occur in the tissues.

labelling could be seen in leaves (xylem, sclerenchyma, and in some cells of phloem), and in stems (parts of xylem).

By contrast, with the xylan-5 subclass of mAbs, epitope recognition was significantly enhanced after the base treatment (Fig. 5.10). In sections treated with 0.1M KOH, CCRC-M144 and CCRC-M155 presented very similar labelling patterns; which effectively revealed where esterified xylan epitopes occur in intact cell walls. The walls of bundle sheaths and of stomata subsidiary cells (in leaves) were strongly labelled with CCRC-M144 and CCRC-M155. Within the vascular bundles of leaves and stems, labelling was more intense in the phloem and in xylem parenchyma. However, epitope detection was clearly enhanced in the walls of cells associated with the xylem of leaves, while in stems, the labelling of phloem was essentially restricted to companion cells. Secondary walls of sclerenchymatous cells were more strongly labelled with both mAbs, and despite this being true for leaves and stems, given that sclerified walls are more abundant in stem sections, labelling distributions appear wider. Immunofluorescence of CCRC-M144 and CCRC-M155 epitopes is mostly observed adjacent to the innermost face of stem parenchyma cell walls. Interestingly, in leaves, a different pattern is observed, as the walls of parenchyma cells which are closer to the vascular bundles have stronger labelling for CCRC-M144. However, in some cases the various layers of the wall are labelled equally, and in ground tissue closer to the core of leaf, labelling is more intense in corner junctions and even in the middle lamella of some cells. Finally, in epidermal cells, labelling with CCRC-M144 and CCRC-M155 was seen to be stronger on the cuticle.

In line with GP results, which suggested that mannan occurs at extremely low amounts in miscanthus genotypes analysed here, immunolabelling with CCRC-M174 (Table 5.3), a galactomannan-directed mAb, showed extremely low signals in leaf and in stem sections from *M.* × *giganteus* (Fig. 8.10A in appendix J). However, some residual immunofluorescence could be observed, particularly in sclerenchyma cells.

In *M.* × *giganteus*, (1→3)-β-glucan epitopes recognised by LAMP (Table 5.3) were detected in several cell types and in both tissues. Labelling was more intense in the phloem, in protoxylem vessels and lining the lacunae (Fig. 5.11). Distinct tissue-specific labelling patterns were also observed. In leaf sections, strong labelling occurred on the walls of epidermis, but only on inner-facing sides of the cells. Strong immunofluorescence was detected in cells of parenchymatous ground tissue in cells that are near the vascular bundles, specifically in some portions of the outer layers of the walls, presumably including the middle lamella. Generally, labelling with LAMP was less widespread in stem tissues, although in vascular bundles, the probed epitopes showed a more abundant distribution, particularly on xylem parenchyma. Another detail which was more observable in stem tissues was the fact that the walls of parenchyma and sclerenchyma were punctuated by small areas of more intense immunofluorescence[*].

BG1, the second β-glucan-directed mAb used in immunolabelling studies, generated more intense labelling patterns than LAMP (Fig. 5.11). This difference was more visible in leaf sections, where labelling with BG1 was visible in most cell types. Notable exceptions to this were the walls of metaxylem, mesophyll and stomatal subsidiary cells, where minimal or no labelling was observed. Furthermore, different cell wall structures presented varying labelling intensities. In leaves, bundle sheath cells appear to be more strongly labelled in their secondary walls, and within the phloem, peripheral sieve tube elements were more intensely labelled. Epidermal cells were also labelled, but while in leaves, labelling with BG1 was observed in most cells; in stems, MLG accumulation was restricted to just a few epidermal cells (per section). In sclerenchyma of leaves, layering of the wall is visible, as the secondary and primary walls show different labelling intensities. By contrast, in the sclerenchyma surrounding the

[*] These *puncta* of higher LAMP epitope detection presumably correspond to plasmodesmata. This labelling pattern for LAMP contrasts with the patterns observed for BG1 (discussed ahead), where the plasmodesmata remained unlabelled. This was particularly visible on the sections of another miscanthus genotype, sin11 (Fig. 8.10B in appendix J).

vascular bundles of stems, MLG detection was observed associated to the primary walls. Parenchymatous ground tissues generally showed labelling in the middle lamella and corner junctions of the cells. However, some variation was observed, as ground tissue parenchyma in leaf sections showed strong labelling of the middle lamella, and noticeable but less intense fluorescence of the primary wall, whereas in stems, the labelling was less intense. Furthermore, it is noteworthy that labelling differences were seen within the same tissue, as some parenchymatous cells seemed to accumulate BG1 epitopes in a layer lining the cytosolic content of the cell; perhaps the plasma membrane or adjacent to it (visible in the supplemental high resolution figures).

The distribution of epitopes associated with three pectic domains was studied in *M.* × *giganteus* tissues using 16 mAbs (Table 5.3). For HG, the most abundant pectic domain (Atmodjo *et al.*, 2011), seven mAbs were utilised. Additionally, given that the structure and function of HG may be altered by the addition of ester-linked groups to the polymers (Willats *et al.*, 2001a), the degree of HG esterification was probed by mAbs directed at esterified epitopes, and by employing a base treatment identical to that described above for the detection of esterified xylan.

Three of the tested HG-directed mAbs did not show substantial immunolabelling of epitopes in *M.* × *giganteus* sections. Although the epitope recognised by the first mAb, CCRC-M34, has not yet been completely characterised (Zabotina *et al.*, 2008), it is known to bind a partially methyl-esterified, base-sensitive HG epitope (unpublished data from the Hahn laboratory). On this basis, CCRC-M34 was tested on *M.* × *giganteus* stem sections with and without a base treatment (Fig. 8.10A in appendix J), but in both cases, labelling was minimal and often undistinguishable from wall auto-fluorescence. LM19, which preferentially binds unesterified HG epitopes (Verhertbruggen *et al.*, 2009), showed almost negligible labelling; although after close inspection, very faintly labelled structures were seen to be slightly more

abundant in the vascular bundles of leaves (Fig. 8.10A in appendix J). Another LM-series mAb, LM20, which requires methyl-esters for HG epitope recognition (Verhertbruggen *et al.*, 2009) did not show substantial visible labelling in any of the *M.* × *giganteus* sections analysed, as only auto-fluorescence could be detected (Fig. 8.10A in appendix J).

The GP analysis (Section 5.1) showed that four mAbs were relevant in assessing the level of HG esterification in miscanthus biomass: JIM7, JIM5, CCRC-M38 and CCRC-M131 (Table 5.3). JIM7 and JIM5, are widely used and are thought to bind to low-ester and high-ester HG epitopes, respectively (Willats *et al.*, 2000a). Methyl-esterified HG recognised by JIM7 could not be detected in either leaf or stem sections from mature *M.* × *giganteus* plants, since only wall auto-fluorescence was observed (Fig. 5.12). With JIM5, which recognises partially methyl-esterified, but can also bind un-esterified HG epitopes (Clausen *et al.*, 2003), faint labelling was observed, yet more notably than with JIM7. Labelling was more evident in leaves, particularly in portions of the wall of phloem and mesophyll cells. In parenchyma of the midrib ground tissue, labelling of the lining of intercellular spaces of cell junctions was observed, with an accumulation at the corners of said spaces. Stem sections showed very faint labelling with JIM5, but some labelling was seen on the walls of the phloem and epidermis, and lining of protoxylem lacunae (visible in the supplemental high resolution figures).

Un-esterified HG epitopes were probed in *M.* × *giganteus* tissues with CCRC-M38 and CCRC-M131, and produced similar labelling patterns to each other (Fig. 5.12). Also comparable, was the epitope detection in vascular bundles of leaves and stems, as only phloem and protoxylem structures were labelled in both tissues. However, while in stem sections neither CCRC-M38 nor CCRC-M131 labelled wall structures in the parenchymatous ground tissue; in leaves, different parenchyma labelling patterns were observed. On interfascicular parenchyma and on flanking mesophyll, epitopes labelled by CCRC-M38 and CCRC-M131 were abundantly detected on the middle lamella, with a higher accumulation on intercellular

spaces. Also in leaf sections, unesterified HG epitopes identified by CCRC-M38 and CCRC-M131 were seen to accumulate on the corners and on the lining of intercellular spaces of cell junctions in the parenchyma of ground tissue.

Additionally, a treatment with 0.1M KOH for 1h prior to immunolabelling procedures was used in conjunction with CCRC-M38 and CCRC-M131 in the probing of *M.* × *giganteus* leaf sections (Fig. 5.12). The aim of this base treatment was to determine (indirectly) the abundance of esterified versions of the epitopes recognised by these mAbs, given that by saponifying ester-linked groups before applying the HG-directed mAbs, any differences in the labelling patterns may be attributed to previously esterified epitopes. It should be noted that by employing this treatment, the extent to which the HG backbones were de-methyl-esterified cannot be estimated. However, differences in labelling patterns between treated and un-treated sections indicate the occurrence of HG epitopes which were at least partially esterified before the base treatment. After 0.1M KOH-mediated removal of ester-linked groups, there was an increase in the detection of HG epitopes recognised by CCRC-M38 and CCRC-M131 (Fig. 5.12); although more perceptibly with CCRC-M38, which binds to fully un-esterified HG. However, for both mAbs the more readily detected difference between un-treated and base-treated sections was an increase of the labelling of middle lamellae. Particularly in pretreated sections probed with CCRC-M38, the borders of the various cells which make up leaf tissues were very well defined, as the middle lamella of all cell types became more labelled.

RG-I related epitopes were probed with four mAbs (Table 5.3). For CCRC-M129 and JIM101, no epitope recognition was detected (Fig. 8.10A in appendix J). With CCRC-M72 and CCRC-M164, labelling was generally faint, but patterns could be observed (Fig. 5.13). In leaves, the most intense labelling with CCRC-M72 was seen on portions of the lining of the protoxylem lacuna, and on the portion of the wall at the base of stomatal subsidiary cells.

With CCRC-M164, the labelling was also faint, but more intense than with CCRC-M72, and was seen more abundantly on the walls of protoxylem parenchyma, of stomatal guard cells, and also of some bundle sheath and parenchyma cells near the vascular bundles. In stems, labelling with both mAbs was even fainter than in leaves, as CCRC-M72 only labelled the lining of protoxylem lacuna to a minimal extent, and CCRC-M164 epitopes were restricted to phloem cell walls. It is also noteworthy that when phloem was labelled with CCRC-M164, epitope detection appeared restricted to sieve tube element cells.

CCRC-M128 is included in the RG-I/AGN class of mAbs, which contains probes directed at AGN side chains of RG-I (Appendix C). In the analysed *M.* × *giganteus* sections, labelling of cell wall structures was faint with this mAb, but in plasmatic and cytosolic membranous structures, more intense labelling was observed (Fig. 5.14). In leaves, these included, chloroplasts and plasma membranes, but epitope recognition declined, and eventually ceased towards the core of the leaf midrib. In stems too, membranes and cytosolic elements, such as amyloplasts, were more strongly labelled than whole wall layers. For both tissues, the only occasion where CCRC-M128 highlighted the cell wall proper was in the thickening of some sclerenchyma cells surrounding the vascular bundles. CCRC-M133 recognised galactan and arabinogalactan epitopes on walls of certain ground tissue cells near the vascular bundles, and of interfascicular parenchyma, in leaves. In a few instances, labelling was also observed on portions of the wall of cells closer to the core of the midrib. Furthermore, closer to the leaf surface, some mesophyll and epidermis cells (stomata included), had their walls more strongly labelled on the sides facing the areas of contact between these cells. For stem sections, CCRC-M133 only labelled parenchyma walls to a minimal extent, the only exception being small clusters of sub-epidermal parenchymatous cells. In the phloem, of stems and leaves, labelling with CCRC-M133 was restricted to areas adhered to plasma membranes of companion cells. In common with CCRC-M128, the strongest labelling intensities observed for JIM13 were

associated with membranous structures in stems and in leaves. For the remaining two mAbs included in the AGN clade of probes, JIM20 and JIM19, *M.* × *giganteus* sections showed faint labelling, and stronger immunofluorescence was only detected on accumulations adhered to the plasma membrane and on the membrane of amyloplasts in stem sections (Fig. 8.10A in appendix J).

Table 5.3. Cell wall glycan-directed mAbs used in the study of *in situ* immunolabelling of *M.* × *giganteus* leaf and stem tissues (further information on all mAbs used here can be found in Appendix C).

	mAb	mAb subclass – based on Pattathil *et al.* (2010)	Reference
Hemicelluloses	CCRC-M101	Non-fucosylated xyloglucan-1	Pattathil *et al.* (2010)
	CCRC-M88	Non-fucosylated xyloglucan-2	Pattathil *et al.* (2010)
	CCRC-M58	Non-fucosylated xyloglucan-4	Pattathil *et al.* (2010)
	CCRC-M50	Non-fucosylated xyloglucan-5	Pattathil *et al.* (2010)
	CCRC-M1	Fucosylated xyloglucan	Pattathil *et al.* (2010)
	CCRC-M106	Fucosylated xyloglucan	Pattathil *et al.* (2010)
	CCRC-M113[BT]	Xylan-3	Pattathil *et al.* (2010)
	CCRC-M117[BT]	Xylan-3	Pattathil *et al.* (2010)
	CCRC-M150	Xylan-4	Pattathil *et al.* (2010)
	CCRC-M154	Xylan-4	Pattathil *et al.* (2010)
	CCRC-M144[BT]	Xylan-5	Pattathil *et al.* (2010)
	CCRC-M155[BT]	Xylan-5	Pattathil *et al.* (2010)
	CCRC-M139	Xylan-6	Pattathil *et al.* (2010)
	CCRC-M140	Xylan-6	Pattathil *et al.* (2010)
	CCRC-M149	Xylan-7	Pattathil *et al.* (2010)
	LAMP	(1→3)-β-glucan	Meikle *et al.* (1991)
	BG1	Mixed-linkage (1→3, 1→4)-β-glucan	Meikle *et al.* (1994)
	CCRC-M174	Galactomannan-2	Pattathil *et al.* (2010)
Pectins	JIM7	Homogalacturonan backbone-2 (heavily esterified)	Knox *et al.* (1990)
	JIM5	Homogalacturonan backbone-1 (partially esterified and un-esterified)	Knox *et al.* (1990)
	CCRC-M38[BT]	Homogalacturonan backbone-1 (fully un-esterified)	Pattathil *et al.* (2010)
	CCRC-M131[BT]	Homogalacturonan backbone-1 (un-esterified)	Pattathil *et al.* (2010)
	CCRC-M34[BT]	Homogalacturonan (partially esterified; base-sensitive epitope)	Pattathil *et al.* (2010)
	LM19	Homogalacturonan (partially un-esterified)	Verhertbruggen *et al.* (2009)
	LM20	Homogalacturonan (methyl-esterified; different epitope from that recognised by JIM7)	Verhertbruggen *et al.* (2009)
	CCRC-M72	Rhamnogalacturonan-I backbone	Pattathil *et al.* (2010)
	CCRC-M164	Epitopes akin to linseed mucilage rhamnogalacturonan-I	Pattathil *et al.* (2010)
	JIM101	Rhamnogalacturonan-Ib	Pattathil *et al.* (2010)
	CCRC-M129	Rhamnogalacturonan-I backbone	Pattathil *et al.* (2010)
	CCRC-M128	RG-I/AGN (arabinogalactan side chains of rhamnogalacturonan-I)	Pattathil *et al.* (2010)
	CCRC-M133	Arabinogalactan-2	Pattathil *et al.* (2010)
	JIM13	Arabinogalactan-4 (arabinogalactan and arabinogalactan proteins)	Knox *et al.* (1991)
	JIM20	Arabinogalactan-1 (glycoprotein-associated)	(Knox *et al.*, 1995)
	JIM19	Arabinogalactan-2 (glycoprotein-associated)	(Knox *et al.*, 1995)

[BT] mAbs used in combination with a 0.1M KOH base treatment.

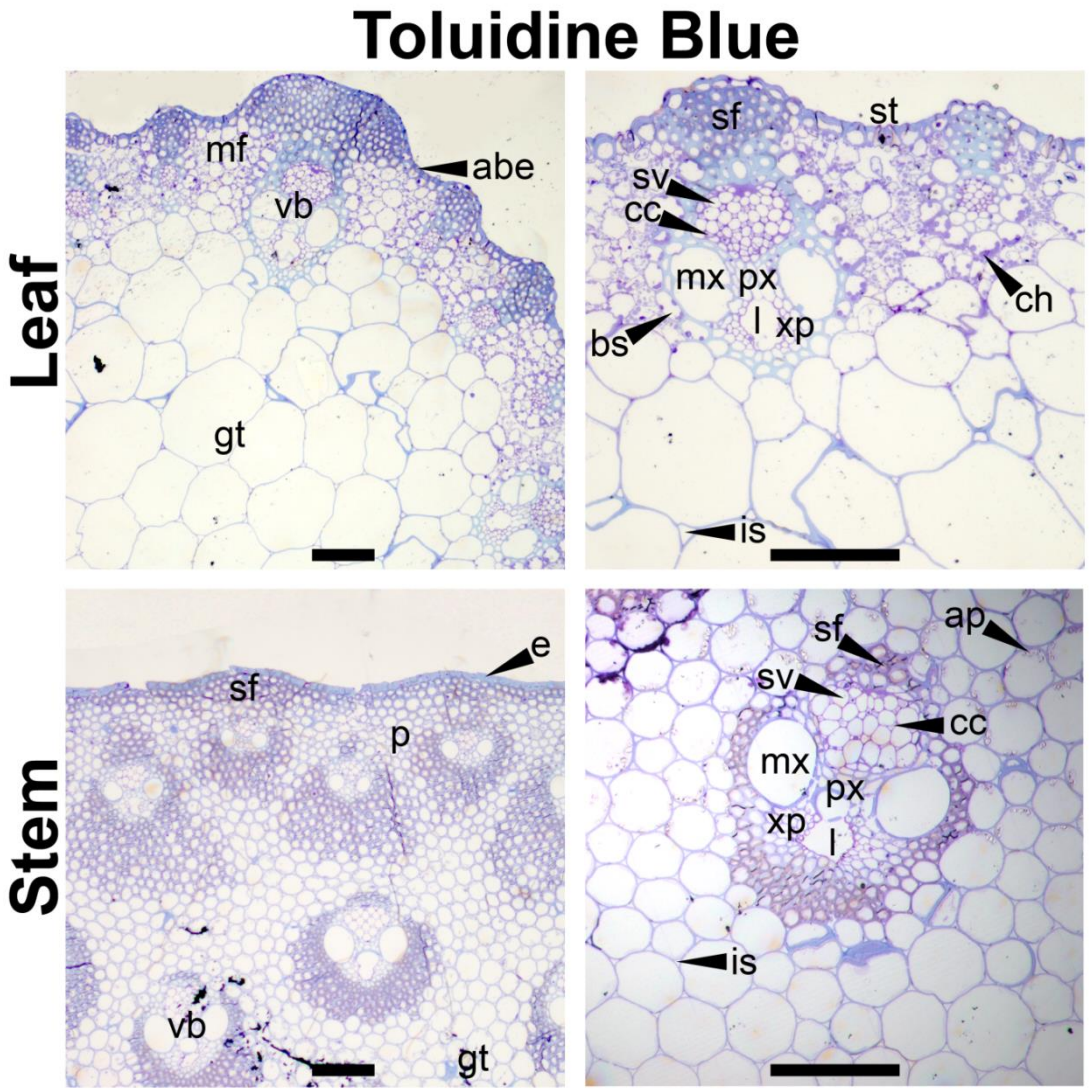

Fig. 5.7. Transverse sections of leaf and stem samples of *M.* × *giganteus* (gig01), stained with toluidine blue. Legend: abaxial surface epidermis (abe), amyloplast (ap), bundle sheath (bs), companion cell (cc), chloroplasts (ch), epidermis (e), ground tissue (gt), intercellular space of ground tissue (is), protoxylem lacuna (l), mesophyll cells (mf), metaxylem (mx), interfascicular parenchyma (p), protoxylem (px), sclerenchyma fibres (sf), stomatal complex (st), sieve tube element (sv), vascular bundle (vb), xylem parenchyma (xp). Scale bars=100µm.

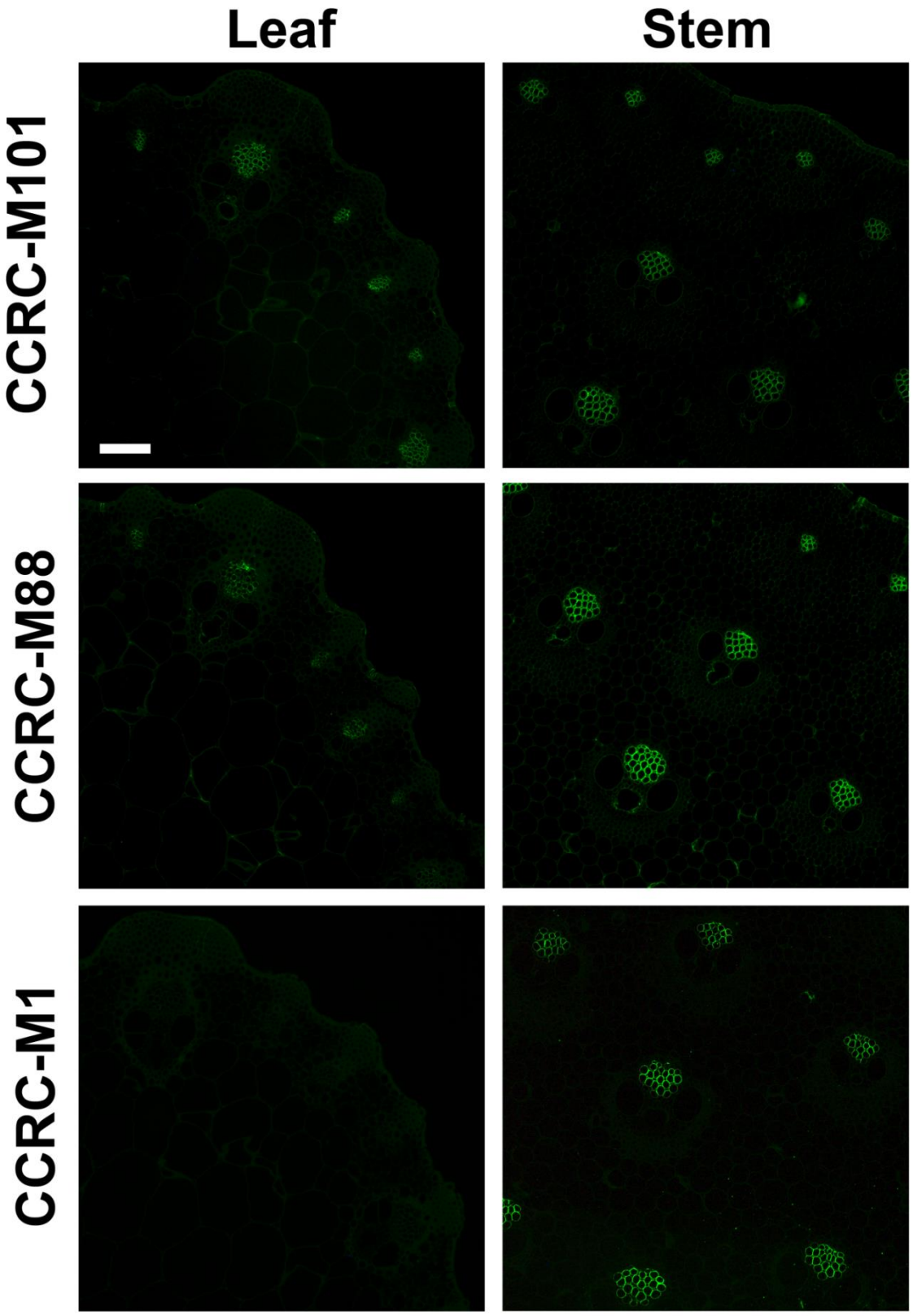

Fig. 5.8. Immunofluorescent labelling of transverse sections from leaves and stems from *M.* × *giganteus* (gig01) with xyloglucan binding mAbs. Scale bar: 100µm.

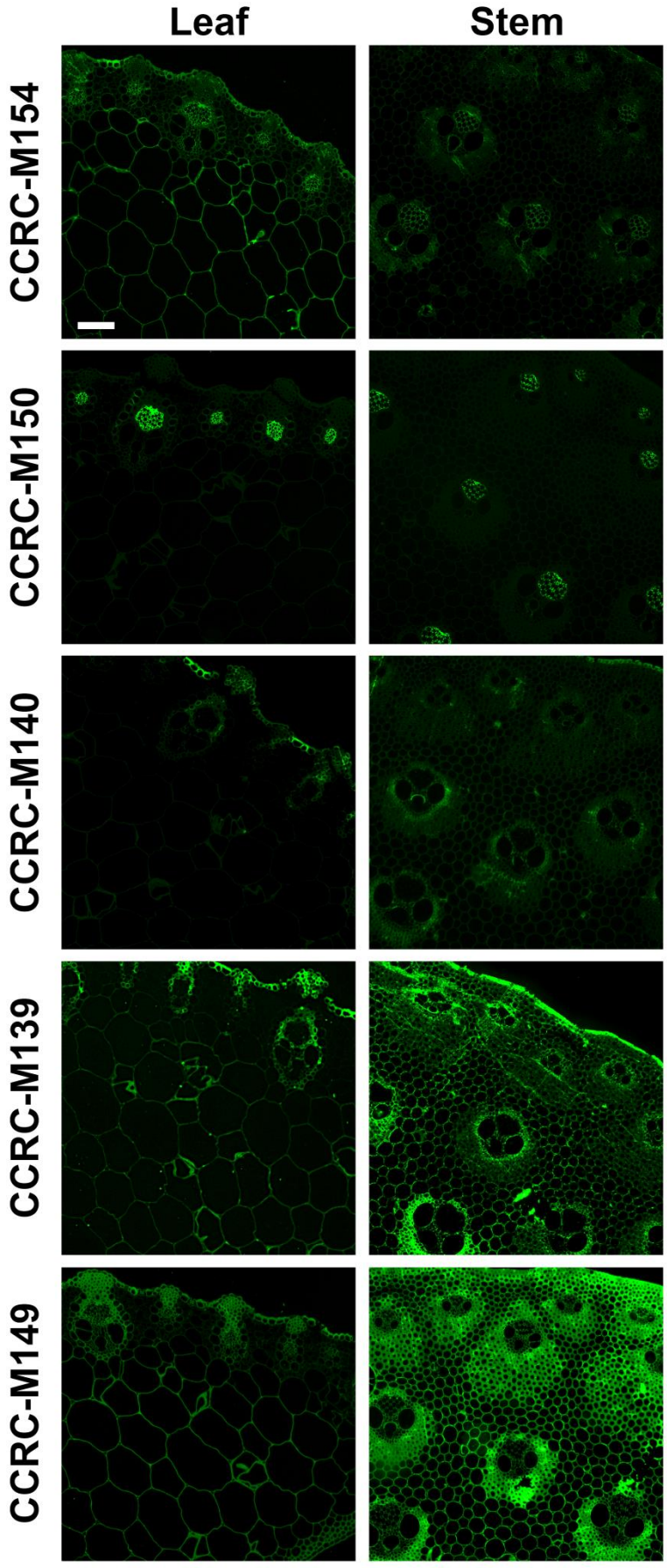

Fig. 5.9. Immunofluorescent labelling of transverse sections from leaves and stems from *M.* × *giganteus* (gig01) with xylan binding mAbs. Scale bar: 100µm.

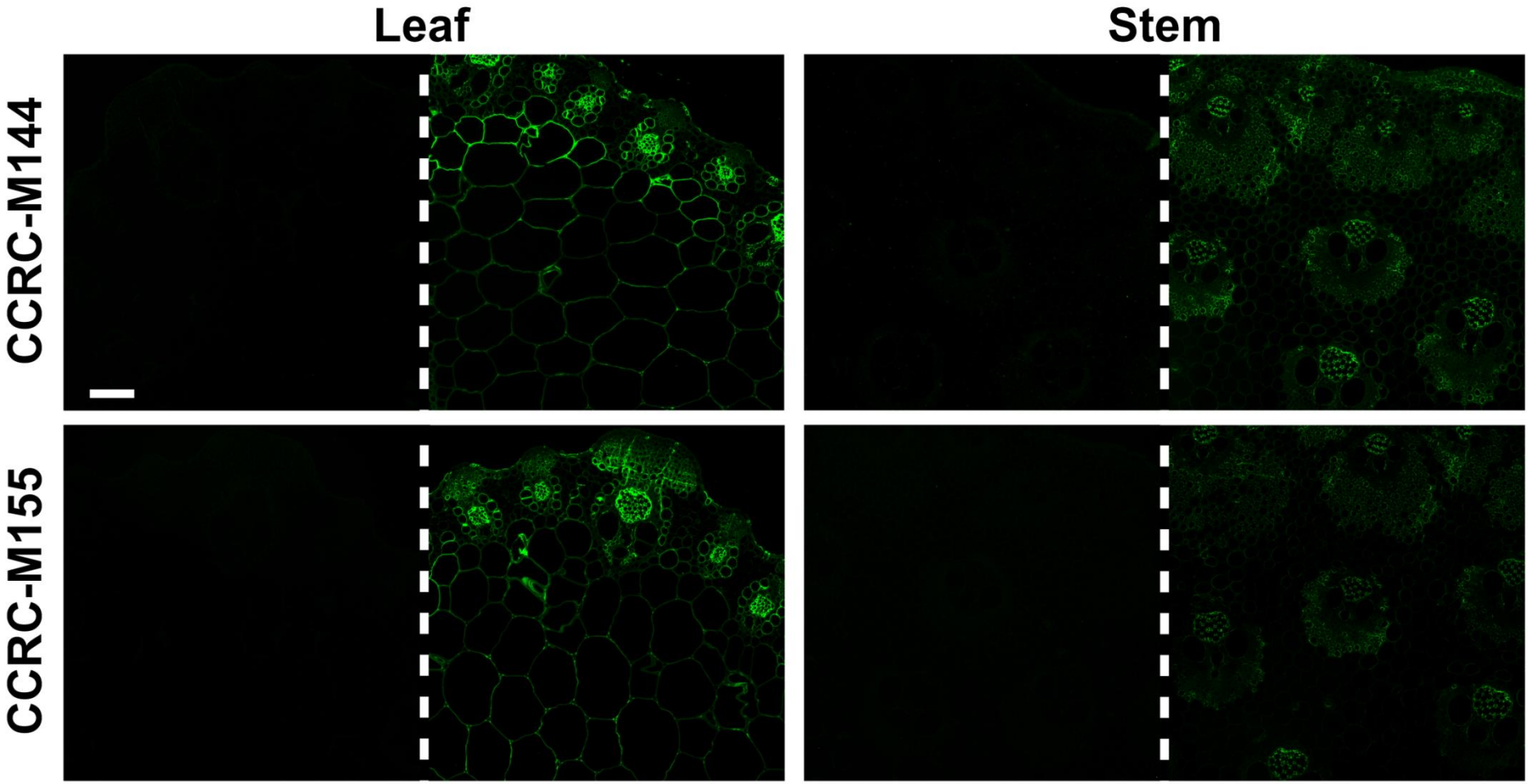

Fig. 5.10. Immunofluorescent labelling of transverse sections from leaves and stems from *M.* × *giganteus* (gig01) with xylan binding mAbs before and after (left and right side of dashed line respectively) a base treatment with 0.1M KOH. Scale bar: 100µm.

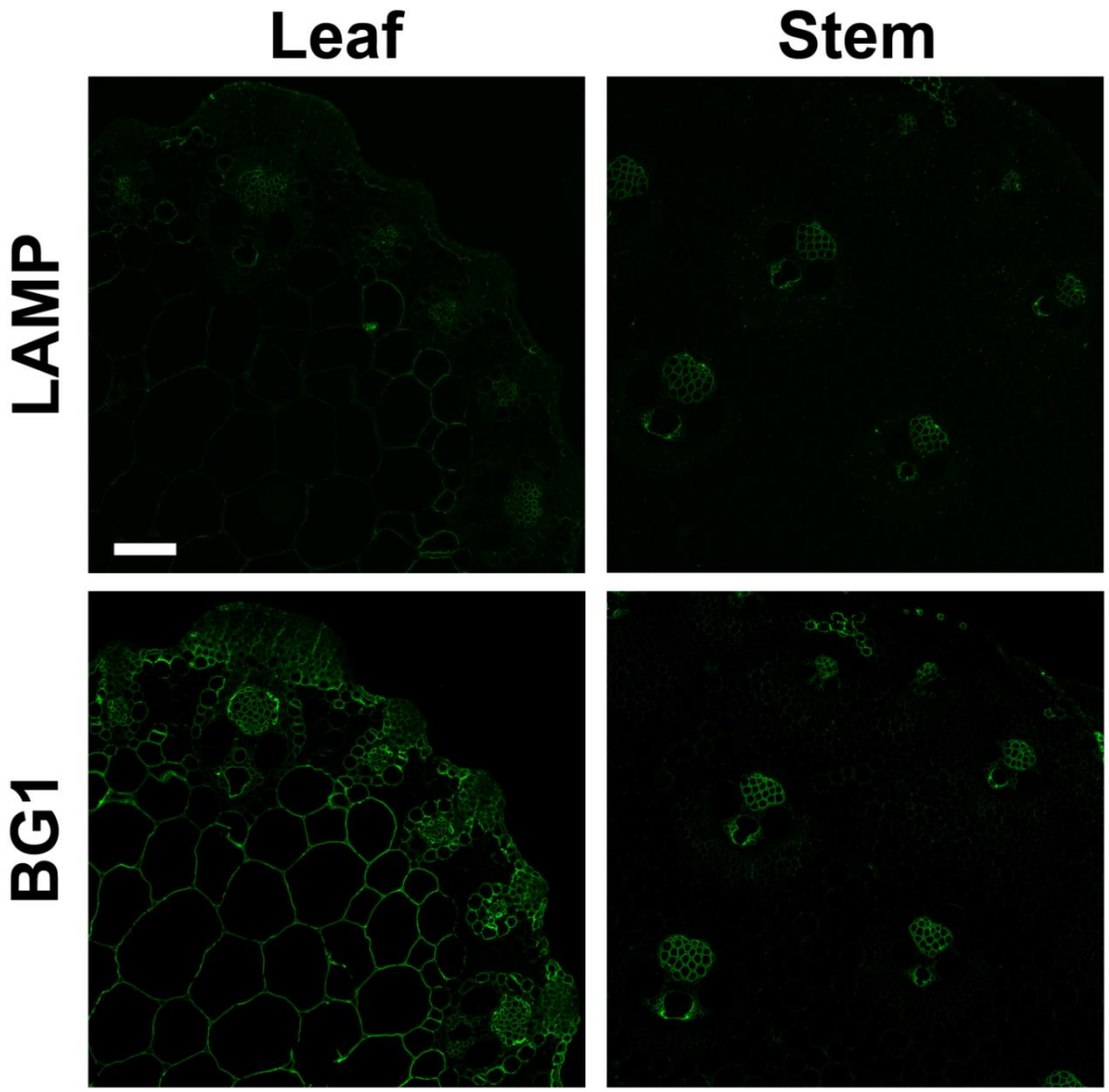

Fig. 5.11. Immunofluorescent labelling of transverse sections from leaves and stems from *M.* × *giganteus* (gig01) with β-glucan binding mAbs. Scale bar: 100μm.

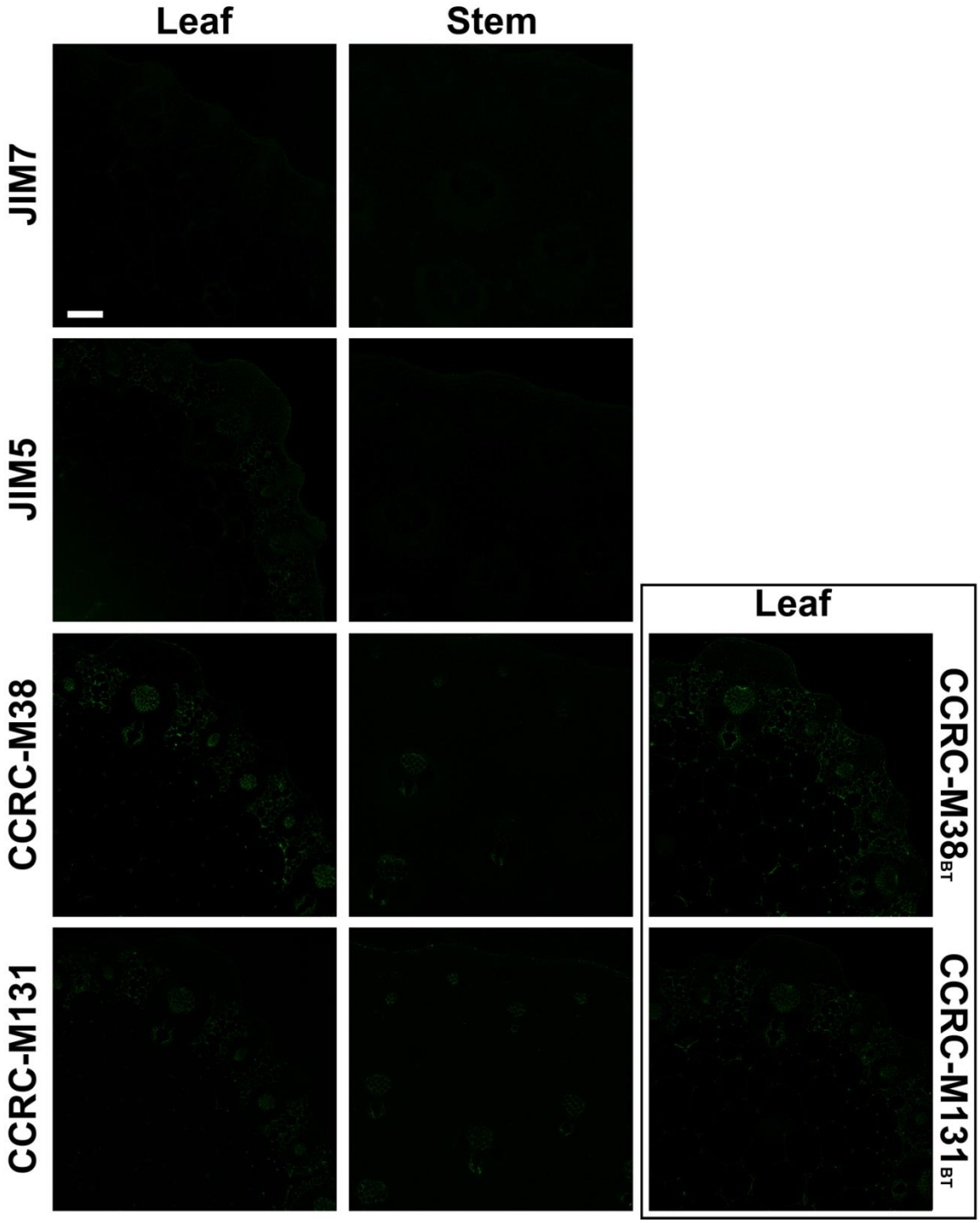

Fig. 5.12. Immunofluorescent labelling of transverse sections from leaves and stems from *M.* × *giganteus* (gig01) with homogalacturonan binding mAbs. For CCRC-M38 and CCRC-M131, immunolabelling of leaf sections was performed before and after a base treatment (BT) with 0.1M KOH (inside box). Scale bar: 100µm.

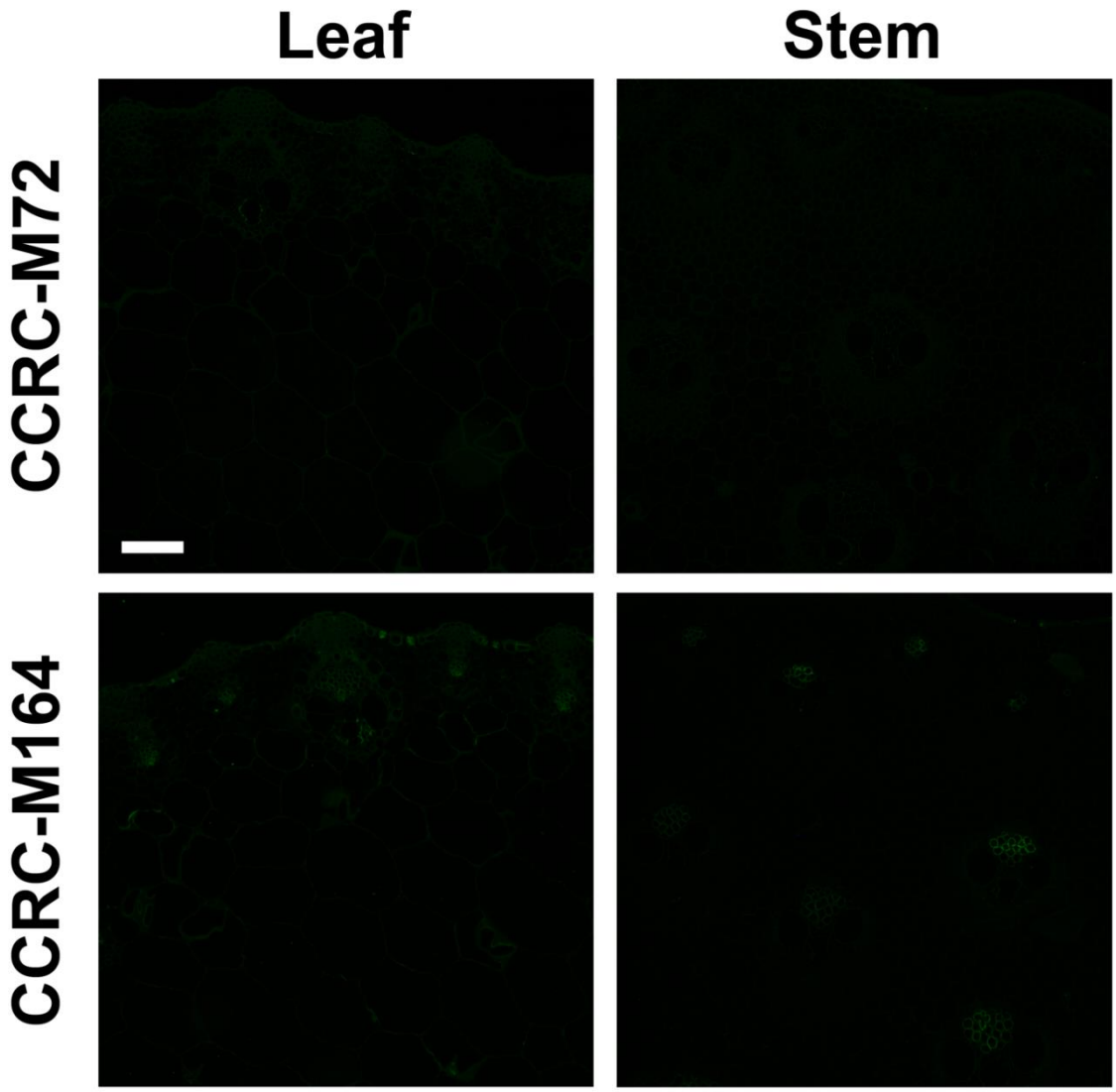

Fig. 5.13. Immunofluorescent labelling of transverse sections from leaves and stems from *M.* × *giganteus* (gig01) with rhamnogalacturonan-I binding mAbs. Scale bar: 100µm.

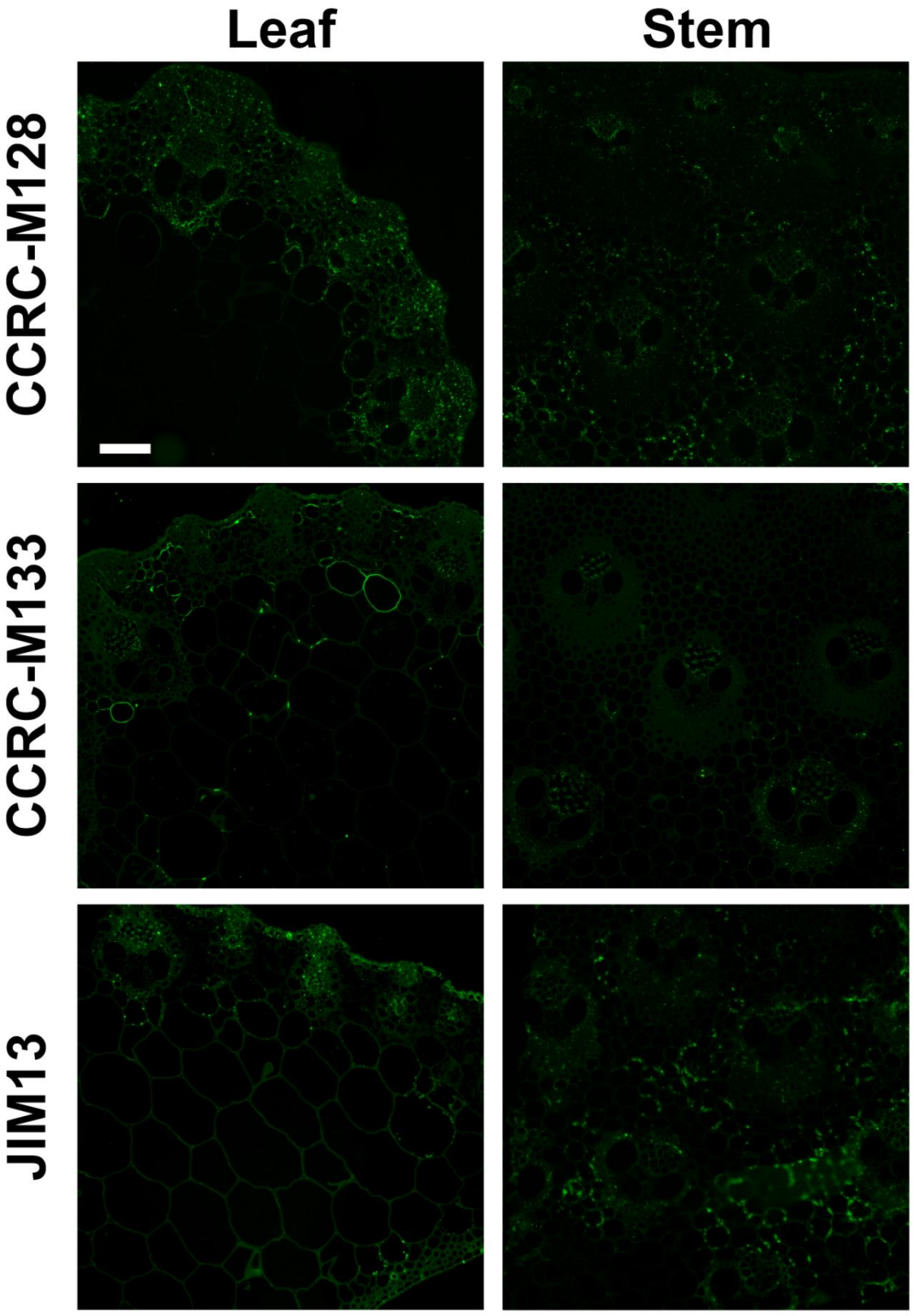

Fig. 5.14. Immunofluorescent labelling of transverse sections from leaves and stems from *M.* × *giganteus* (gig01) with arabinogalactan binding mAbs. Scale bar: 100µm.

5.2.4. Discussion

As would be expected for the type-II cell wall of grasses, immunolabelling of *M.* × *giganteus* tissues with mAbs directed at non-xylan hemicellulosic epitopes typically yielded less distributed and less intense immunofluorescence results (Carpita, 1996).

For the mannan epitopes recognised by CCRC-M174, minimal labelling in all examined *M.* × *giganteus* sections (Fig. 8.10A in appendix J) is consistent with detected low signals of mannan epitopes during GP (discussed in section 5.1.4). However, more abundant labelling patterns have been reported for miscanthus when using another heteromannan-directed mAb (Xue *et al.*, 2013; Cao *et al.*, 2014), and thus a possibility remains that mannan possessing different epitopes than the one recognised by CCRC-M174 may occur in miscanthus cell walls. Furthermore, it has been suggested that mannan esterification may impede epitope recognition by specific mannan-directed mAbs (Marcus *et al.*, 2010), as a KOH-mediated base treatment of the sections improved mannan epitope recognition. In the present study, no base treatment has been used in combination with mannan-directed mAbs for the probing of *M.* × *giganteus* tissues. However, the sequential extraction performed as part of GP procedures also de-esterifies cell wall glycan epitopes. It may therefore be deduced that if ester-linked groups were indeed affecting mannan epitope recognition, saponifying agents of the sequential extraction would have removed such groups, and consequently the epitopes would have been detected in cell wall fractions during the ELISA. As a result, in miscanthus tissues analysed here, the recognition of epitopes by all mannan-directed mAbs included in this study (Appendix C) is not likely to be affected by ester-linked groups. However, the data does not exclude the possibility that mannan structures recognised by mannan-directed mAbs, other than those included here, may occur in miscanthus cell walls (with or without ester-linked groups).

In what concerns the labelling with XG-directed mAbs (Fig. 5.8), its distribution is in agreement with the known low abundance of XG in the cell wall of grasses (Carpita, 1996);

whereas the more abundant distribution of XG labelling in stem sections is in agreement with GP data, which showed that epitopes associated with these glycans are generally more abundant in stem biomass (Section 5.1). Despite their limited distribution patterns, binding intensities of XG-directed mAbs were higher in phloem cell walls, suggesting that most XG in miscanthus cell walls occurs in phloem tissues. Higher abundance in the phloem, or sometimes exclusive occurrence of XG in phloem walls has been observed in several commelinoid monocots (Brennan and Harris, 2011), including in *M. lutarioriparius* (Cao *et al.*, 2014). However, despite labelling of XG epitopes being more abundant in the phloem, these are not the only hemicelluloses detected in these vascular tissues (shown below); nor are phloem walls the only structures where XG epitopes are detected. In parenchyma cells, labelling of the middle lamella is also observed, particularly with CCRC-M88. However, while this labelling is only occasional in leaf sections, in stems it is more abundant. Labelling of XG epitopes in middle lamellae has been reported previously, namely in suspension-cultured sycamore cells (Moore *et al.*, 1986). The middle lamella binds cells together in tissue systems, functioning as an "intracellular cement" (Bateman, 1976); a functionality that may be enhanced by the presence of XG, which is strongly bound and presumed to interact directly with the cellulosic microfibril network (Hayashi, 1989). The probing of *M.* × *giganteus* sections with CCRC-M1 showed very faint labelling patterns, especially in leaves, but even in stems it was mostly restricted to phloem sieve tube elements. These labelling patterns suggest that fucosylated XG is less distributed than non-fucosylated XG, and that leaves contain lower amounts of these epitopes than stems; which is in agreement with the very low abundance of Fuc found in miscanthus tissues (Section 4.1), and with the fact that higher binding intensities to fucosylated XG were observed in stem tissues during the GP analysis (Fig. 5.4).

Predictably for a grass species, of all the matrix glycan-directed mAbs used in this study, those which bind xylan epitopes showed the most widespread distribution (Figs. 5.9 and 5.10).

All cell types in *M.* × *giganteus* sections had at least one xylan epitope detected in their walls. Information regarding which mAb recognised the different epitopes, and immunofluorescence intensity, are two factors which clearly indicate that the xylan polymers occurring in *M.* × *giganteus* cell walls have distinct structures and abundances. It is very likely that these features are associated with glycan function, and may affect cell wall biomass recalcitrance to saccharification. Many of the xylan-directed mAbs belong to the same subclasses of glycan probes (Pattathil *et al.*, 2010) (Table 5.3). However, all displayed distinct epitope labelling patterns, and thus it is likely that they recognise distinct xylan structures; although the exact recognised epitopes remain unknown for various mAbs. Glucuronoarabinoxylan is known to occur in the interstitial space between cellulose microfibrils in primary cell walls (McCann and Carpita, 2008; Li *et al.*, 2014a), and the labelling patterns of CCRC-M154, CCRC-M139 and CCRC-M149 in areas of the primary wall of *M.* × *giganteus* is in agreement with this. Some xylan-directed mAbs labelled phloem cell walls, with particularly strong immunofluorescence for epitopes recognised by CCRC-M150, and by CCRC-M144 and CCRC-M155, when used in conjunction with the base treatment. By contrast, epitopes recognised by xylan-6 (CCRC-M140, CCRC-M139), and xylan-7 (CCRC-M149) classes of mAbs, which bind linear, unsubstituted xylan epitopes (unpublished data from the Hahn laboratory) were less detected in phloem, but more abundantly in sclerified cell walls. This may indicate that phloem cells have walls rich in certain xylan polymers, among which some bear ester-linked substituents; whereas in sclerenchyma cell walls, the detected xylan is presumably less substituted. Data from other type-II cell wall-containing species, *M. lutarioriparius* (Cao *et al.*, 2014), sugarcane (de Souza *et al.*, 2013) and maize (Suzuki *et al.*, 2000) have shown that lignification is low in phloem, but higher in other cell types, such as sclerenchyma. As a result, to a certain extent it seems apparent that xylan epitopes which are less substituted are detected primarily in lignified cell walls, while more substituted polymers, namely by ester-linked groups, are more abundant

in cell types with lower lignin content. Indeed, by using polyclonal antibodies which recognise highly substituted glucuronoarabinoxylans, and low-branched xylans, Suzuki *et al.* (2000) demonstrated that in maize, low-branched xylans are distributed in all lignified walls, while most highly substituted polymers are distributed in un-lignified tissues. For CCRC-M144 and CCRC-M155 used in conjunction with the base treatment, it should also be noted that despite epitope detection being more abundant in phloem, labelling is also seen in the wall of other cell types, namely in sclerenchyma. However, this does not contradict the presented hypothesis, as 0.1M KOH does also remove FA (Section 3.2), which is known to cross-link structural carbohydrates to lignin (Ralph *et al.*, 1994b; Grabber *et al.*, 2004; Buanafina, 2009; Agger *et al.*, 2010). As a result, the increased labelling of sclerenchyma in base-treated sections could be attributed to the inability of CCRC-M144 and CCRC-M155 to bind feruloylated xylan epitopes; which may be associated with lignin. Bearing in mind that the sequential extraction also does de-esterify the cell wall, support for this claim could be derived from the GP analysis, where it was shown that xylan-5 mAbs have particularly high signals in the chlorite and 4M KOH PC cell wall fractions; which contain epitopes presumed to be directly or indirectly associated with lignin. Further studies would be essential to confirm or revoke these hypotheses, but given that the associations of lignin with cell wall carbohydrates are known to enhance lignocellulosic biomass recalcitrance, the relative abundance of more or less branched xylans is likely to be a very important factor in the improvement of dedicated energy crops such as miscanthus.

As the outermost layer of organs, the epidermis has the function of, amongst other things, protecting the plant against enzyme-mediated microbial attack (Glover, 2010). Strong labelling of epidermal cell walls was detected for all except one of the tested xylan-directed mAbs (CCRC-M150). During the GP analysis, it was observed that only the harsher KOH-mediated extraction steps were able to remove substantial amounts of xylan epitopes from the walls, this

being more patent for xylan-5 and xylan-6 subclasses of mAbs (Fig. 5.4). It is thus likely that the presence of recalcitrant xylan may confer epidermal walls with greater resistance to external attacks. As in other species, the epidermis in miscanthus is coated by a cuticle; which consists of a protective membrane made up of two layers, one more external, essentially composed of waxes, which covers an internal matrix that contains glycan polymers thought to extend from the underlying cell wall (Kerstiens, 2010).

Hemicellulosic polymers detected in the cuticles of several plant species such as eucalyptus, poplar, pear and tomato have been suggested to yield epidermal structures highly resistant to enzymatic digestion (López-Casado *et al.*, 2007; Guzmán *et al.*, 2014). Interestingly, following base treatment of *M.* × *giganteus* tissues which removed ester groups from the wall glycans, labelling with CCRC-M144 and CCRC-M155 was particularly intense in the cuticle of some epidermal cells; indicating that esterified xylan epitopes are abundant in cuticular layers. It is known that xylans bearing acetyl-ester groups are more resistant to enzymatic attack (Selig *et al.*, 2009), and HCAs, which are involved in ester-mediated cross-linking, have a negative effect on cell wall deconstruction and are able to confer protection against predator digestive enzymes and pathogen invasion (Akin *et al.*, 1993; Ikegawa *et al.*, 1996). Additionally, the presence of HCAs on the epidermis would also make sense as providers of protection against ultraviolet (UV) radiation, as phenolic compounds have been implicated as protective elements against the mutagenic effect of UV-B insolation (Flenley, 2011). From a bioconversion perspective, these observations may be particularly relevant in the study of which glycans may have a more adverse effect on cell wall saccharification, given the possibility that the deposition of certain xylan epitopes in cell structures which are more prone to external attack, may be indicative of higher recalcitrance of the glycans where the epitopes are present. As a result, biomass from different sources may

contain different abundances of these more recalcitrant epitopes and thus generate different fermentable sugar yields.

LAMP is a (1→3)-β-glucan-directed mAb, which does not show cross-reactivity against MLG or cellulose, thus allowing the probing of callose in the cell wall (Meikle *et al.*, 1991). Callose consists of linear (1→3)-β-glucan, which may play different roles in the wall, depending on the cell and tissue type where it occurs (Stone, 2006; Chen and Kim, 2009; Nedukha, 2015). In *M.* × *giganteus*, labelling with LAMP is generally more widely distributed in leaf tissues, and particularly intense in phloem cells, an observation which would be expected; since it has long been known that this vascular structure is rich in callose and that callose has a role in the formation of sieve pores of the phloem (van Bel, 2003; Xie *et al.*, 2011). Portions of the protoxylem are also labelled by LAMP, particularly in stem tissues, where immunofluorescence extends onto the xylem parenchyma cells. From a developmental perspective, protoxylem matures before plant organs undergo intensive elongation; whereas metaxylem typically only matures after elongation is completed (Evert, 2006). As a result, the fact that protoxylem-associated structures are labelled, but not metaxylem, may have implications on cell wall development. Yet another pattern of labelling with LAMP which may be related to tissue maturation is observed in the ground tissue of leaf samples, where the cells that are near the vascular bundles exhibit more intense immunofluorescence in centre-facing portions of the cell wall layers and middle lamellae. By contrast, labelling of the walls in parenchyma at the core of the midrib is much less intense. This could be a consequence of different cells being at various maturation stages. Indeed, callose is known to be involved in the formation of the cell plate during cytokinesis, remaining the dominant polysaccharide in the recently formed wall, until it is enzymatically removed, and replaced by cellulose and other glycans during cell wall maturation (Samuels *et al.*, 1995; Staehelin and Hepler, 1996; Stone, 2006; Chen and Kim, 2009). Additionally, ground tissue cells in stems are typically smaller

and more abundant than in leaves. Based on this morphology, it may be speculated that in leaves cell expansion plays a more important role than in stems, where cell division may contribute more to tissue growth. As a result, it could be possible that a more abundant presence of the β-glucan epitopes recognised by LAMP in the parenchyma of leaves has influence on organ elongation[*]. Also in leaves, labelling with LAMP was particularly intense on the inner-facing side of epidermal cells, which could be associated with plant defence. It has been reported that callose may confer mechanic rigidity and resistance against external attack, namely by fungi (Aist, 1976; Jacobs *et al.*, 2003; van Bel, 2003; Chowdhury *et al.*, 2014). It is conceivable that this callose barrier, which *in vivo* has a protective function, will have a negative effect on cell wall deconstruction for industrial applications.

Also of interest is a punctuated pattern of labelling with LAMP which occurs on the walls of parenchyma and sclerenchyma cells (particularly visible in genotype sin11; Fig. 8.10B in appendix J), which after closer examination was observed to be located on the plasmodesmata. It is known that plasmodesmatal canals are permanently lined by a callose layer between the wall and the plasma membrane, thus regulating transportation of water and aqueous solutions between contiguous cells (Stone, 2006; Xie and Hong, 2011). However, callose may also be deposited very rapidly, sealing the plasmodesmata in response to mechanical wounding (Stone, 2006); which does occur during preparation for tissue fixation. As a result, the possibility should not be eliminated that labelling of plasmodesmatal regions with LAMP may be affected by this plant response mechanism. Furthermore, callose is known to typically occur in stomatal guard cells (Albersheim, 2011); in the *M.* × *giganteus* sections here analysed, stomatal cells were not particularly labelled.

[*]Stem tissues may undergo anisotropic elongation (i.e. generate narrow long cells), which would not be visible in the transverse sections taken for immunolabelling studies. As a result, hypotheses presented in this paragraph are mostly speculative and further studies will be needed to assess their veritableness.

Labelling with BG1 in *M.* × *giganteus* tissues was expected, as this mAb binds to mixed-linkage (1→3, 1→4)-β-glucan, which is abundant in type-II cell walls (Carpita, 1996). More abundant labelling of leaves in comparison to stems is in agreement with GP results, that overall MLG levels are higher in foliar biomass. Additionally, the observed pattern of MLG distribution was similar to that reported by Xue *et al.* (2013) for *M.* × *giganteus* stems, as the strongest labelling was also seen in vascular bundles and portions of interfascicular parenchyma. However, those authors used less mature plants in their studies, and this is possibly the reason behind the fact that they observed more abundant labelling in xylem and interfascicular parenchyma. MLG has been traditionally considered as a transiently accumulated glycan, which is mostly associated with the cell wall of immature, expanding tissues (Carpita *et al.*, 2001; Gibeaut *et al.*, 2005; Christensen *et al.*, 2010). During GP studies it was observed that MLG epitopes are more abundant earlier in development. Consistent with this, MLG detection was observed to be more intense in the middle lamellae and primary walls of parenchyma cells; metaphloem appears less labelled than protophloem, which is formed earlier in development and then crushed on the edges of the phloem. However, a big proportion of MLG remains detectable in mature plants, which suggests it plays a more permanent function (Vega-Sánchez *et al.*, 2013). This possibility may also be supported by the data collected in the present study for miscanthus biomass, where MLG epitopes are detected in the glycome profile of senesced samples; in many cases so tightly bound to the wall that they were only removed from the wall in the 4M KOH and 4M KOH PC fractions (Fig. 5.4). These observations are consistent with reports that MLG may occur in the cell walls of tissues involved in transport and support functions; namely in miscanthus stems (Xue *et al.*, 2013) and rice leaves and stems (Vega-Sanchez *et al.*, 2012). Similar observations have been made here during the immunolabelling of sections taken from mature *M.* × *giganteus* plants, as MLG accumulation was detected in structures associated with transport and support: in leaves,

labelling was observed in secondary walls of sclerenchyma cells; in stem sclerenchyma, but more associated with primary walls and middle lamellae; and for both tissues, in the walls of cells associated with protoxylem. MLG accumulation was detected in the ground tissue of leaf and stem sections, although in leaves, labelling was seen to be more intense. In all labelled ground tissue cells, fluorescence intensity was higher in the middle lamella, but occasionally, some cells also showed labelling of a thin layer, presumably corresponding to the plasma membrane or adjacent wall portions. References in the literature concerning the occurrence of MLG in the plasma membrane are not common, but Philippe *et al.* (2006) reported the accumulation of MLG at the plasma membrane of wheat endosperm cells. Despite the fact that samples used in the immunolabelling studies were collected from mature plants, it may be possible that some MLG synthesis still occurs (Vega-Sánchez *et al.*, 2015). Bearing this in mind, it is possible that the detection of MLG epitopes in plasma membrane-related areas is linked to its secretion and deposition on the wall. This hypothesis is supported by two models proposed for MLG synthesis: one, which holds that MLG is synthesised in Golgi membranes, packaged into vesicles, and exported to the plasma membrane to be integrated into the wall; and another, which shows in various grass species that in common with other glucans (cellulose and callose), MLG is in fact assembled at the plasma membrane (Wilson *et al.*, 2015).

Additionally, the identification of BG1 and LAMP epitopes was marked in some interfascicular parenchyma cells near the epidermis in stems. These differences in immunolabelling are indicative of a distinct composition and structure in the wall of these parenchyma cells. A similar observation has been made by Xue *et al.* (2013) while studying miscanthus stems collected at an earlier developmental stage. In their samples, these authors observed a higher distribution of this compositionally distinct interfascicular parenchyma than observed in the present study; which may indicate that its abundance in miscanthus stem tissue is development-dependent.

The degree of HG esterification has implications on the structure and function of these pectic polysaccharides; namely by affecting their elasticity (Willats *et al.*, 2001a). Acetyl-esterification of HG may occur, although to a typically lower extent (Liners *et al.*, 1994; Kouwijzer *et al.*, 1996). More importantly, HG polymers are synthesised in a highly methyl-esterified state (Zhang and Staehelin, 1992; Mohnen, 1999), and once *in muro*, enzymatic removal of methyl-esters promotes the formation of cross-links between pectin chains into more rigid structures, promoting cell adhesion, and thus cell wall recalcitrance to deconstruction (Anthon and Barrett, 2006; Lionetti *et al.*, 2010). Abundance and patterns of methyl-esterification are known to vary along the HG chains and also in different cell wall structures and plant tissues (Liberman *et al.*, 1999; Willats *et al.*, 2001a; Bosch *et al.*, 2005), and this has also been shown here for *M.* × *giganteus* sections. In section 5.1, it was hypothesised that the observed low or even absence of JIM7 epitopes detected during the GP studies could be a consequence of the saponifying action of alkaline solvents used during the sequential extraction. However, no base treatment was used during *in situ* immunolabelling with JIM7, and yet, negligible binding signals were observed in *M.* × *giganteus* sections. These observations suggest that, at least in mature tissues, harvested from *M.* × *giganteus* plants at the PB stage, the levels of esterified HG recognised by JIM7 are extremely low. Furthermore, this is also substantiated by the reduced labelling obtained with LM20; another mAb directed at methyl-esterified HG. More abundant labelling with LM20 in miscanthus stems has been reported (Xue *et al.*, 2013). However, this apparent disparity is explained by the fact that stem tissues analysed in the present study were collected at a more advanced stage of maturity, and consequently possessed larger proportions of de-methyl-esterified HG in the wall; which is not recognised by LM20. These observations are not indicative of a complete absence of methyl-esterified HG in mature *M.* × *giganteus* tissues; given that by employing a base treatment in

conjunction with mAbs aimed at un-esterified HG (Table 5.3), it was possible to detect HG epitopes which were originally at least partially esterified.

For *M.* × *giganteus* stem tissues, un-esterified HG was detected particularly in protoxylem and vascular bundles. In *M. lutarioriparius,* more abundant labelling than observed here for JIM5 has been reported (Cao *et al.*, 2014). This difference may be species-related, but most likely, should have a development-related component, as the *M.* × *giganteus* stem tissues analysed in the present study represent a later harvest time, and it is likely that *in muro* HG was at a more advanced stage of de-esterification.

In un-treated leaf sections of *M.* × *giganteus* (Fig. 5.12), labelling patterns for partially and un-esterified HG epitopes recognised by JIM5 were detected in greater abundance than in stems. Similar patterns were also observed with CCRC-M38 and CCRC-M131 in un-treated tissues. However, this apparent redundancy served to substantiate observations made for JIM5 and the results obtained during GP studies; which suggested that pectic HG, particularly with a low degree of esterification, is more abundant in leaf tissues. Despite no references having been found for comparison of the distribution pattern of HG epitopes in miscanthus leaves, an interpretation of the results may be derived from the fact that leaf tissues typically contain lower amounts of Glc than stems (Section 4.1). Less Glc implies lower abundance of glucans, which in miscanthus cell walls essentially corresponds to cellulose. It has been reported that HG with a low degree of esterification may increase in response to cellulose depletion (Wolf *et al.*, 2009), whether after treatment with cellulose synthesis inhibitors (Manfield *et al.*, 2004) or in response to reduced cellulose synthase expression (Burton *et al.*, 2000). Thus, it is possible that the apparent more distributed labelling pattern of un-esterified HG in leaves (Fig. 5.12, without the base treatment), when compared to stems, could be at least partially explained as an adaptation aimed at increasing cell wall adherence in tissues with lower cellulose content. A future study aimed at detecting cellulose distribution and abundance in leaf sections would

be pertinent as an approach to establish if areas of low cellulose abundance coincide with areas of lower HG esterification.

CCRC-M38 and CCRC-M131 analysis of saponified sections allowed indirect determination of differences in the abundance of esterified HG epitopes; given that labelling pattern differences between saponified and un-saponified tissues correspond to esterified HG epitopes. In these base-treated tissues, labelling was increased for both mAbs, most strikingly on the middle lamellae between the primary wall of two adhered cells, suggesting that these areas are abundant in methyl-esterified HG. This is in agreement with reported high levels of methyl-esterification in middle lamellae between adhered cells (Liners *et al.*, 1994). Despite the impossibility of determining the exact degree to which HG backbones were methyl-esterified prior to saponification, the base treatment revealed that HG epitopes exclusively detected after the base treatment are more extensively esterified than those also detected in un-treated sections. Bearing this in mind there may be a functional requirement for lower levels of methyl-esterification of the HG in the corners of intercellular spaces. In plant tissues, turgor pressure tends to force the cells towards a spherical form, thus subjecting three-way cell junctions to tension tending towards cell separation and formation of intercellular spaces. As a consequence, tensile stress is mostly induced at regions of adhered walls bordering the separated cell walls and the intercellular space (Jarvis, 1998; Willats *et al.*, 2001a); i.e., on the corners of the intercellular spaces. One of the most interesting aspects observed during the immunohistochemical study of *M.* × *giganteus* sections was the labelling patterns of these intercellular spaces with HG and xylan epitopes. Un-esterified HG epitopes were readily detected in the corners of intercellular spaces by CCRC-M38 and CCRC-M131 (Fig. 5.15). By contrast, labelling of middle lamellae in areas of two adjacent primary walls was only detected after the base treatment. This is suggestive that HG epitopes bound by CCRC-M38 and CCRC-M131 on the middle lamella between two adjacent cells are esterified to a greater extent than

epitopes found on the corners of the intercellular spaces. Given that reduced methyl-esterification of HG promotes the formation of Ca^{2+} linkages, which reinforce cell adhesion, the observed differences in HG esterification are very likely to have a role in providing support to cell wall structures (Liners *et al.*, 1989; Wolf *et al.*, 2009; Lionetti *et al.*, 2010).

Interestingly, when probing base-treated sections with xylan-directed CCRC-M144 and CCRC-M155 (Fig. 5.13), labelling of the middle lamella and intercellular spaces was increased. As has been shown in previous chapters, a 0.1M KOH pretreatment, which led to a very positive effect on enhancing saccharification yields, has the effect of predominantly removing ester-linked acetate and HCA substituents from the cell wall (Chapter 3). As mentioned above, given that these acetate and HCA groups may be specifically ester-linked to xylan polymers (Ishii, 1997b; Wende and Fry, 1997b; Pawar *et al.*, 2013), it is likely that the epitopes recognised by CCRC-M144 and CCRC-M155 in base-treated sections were acetylated and/or hydroxycinnamoylated in the intact cell wall. Of the HCAs, FA is notable for cross-linking carbohydrate chains (Grabber *et al.*, 2004; Buanafina, 2009). As for acetate, despite its biological role not being well understood (Manabe *et al.*, 2011; Manabe *et al.*, 2013), it is known that acetylated xylan may interact with cellulose (Busse-Wicher *et al.*, 2014), and that deconstruction of cell wall glycans is negatively affected by the presence of acetyl esters (Grohmann *et al.*, 1989; Mitchell *et al.*, 1990; Kong *et al.*, 1992; Selig *et al.*, 2009). An interpretation of these observations could be that esterified xylan and unesterified HG epitopes occur on the corners of intercellular spaces as a means to provide structural support against uncontrolled separation of adhered cells along the middle lamella. A similar concept for the role of HG in intercellular space corners has been previously proposed by Willats *et al.* (2001a). However, that study was performed on a dicot species, and the authors did not assess the distribution of xylan epitopes. If confirmed, this possibility that *M.* × *giganteus* plants accumulate esterified xylan and unesterified HG in areas where structural reinforcement is

required, may imply that localised heterogeneity in particular portions of the cell wall matrix has the ability of altering the physical properties of the cell wall, and thus affecting biomass saccharification.

CCRC-M72, a mAb directed at the RG-I backbone, and CCRC-M164, which binds epitopes akin to RG-I found in linseed, were the probes which showed better labelling results to RG-I related cell wall structures in the *M.* × *giganteus* sections analysed (Fig. 5.16). The glycome profiles of miscanthus (Section 5.1) revealed that epitopes akin to RG-I found in linseed mucilage occur abundantly in the cell wall fractions produced during sequential extraction. Furthermore, of the glycan probes included in the toolkit used for GP (Appendix C), Pattathil *et al.* (2010) have shown that the linseed mucilage RG-I clade, to which CCRC-M164 belongs, is one of the few classes of mAbs which show polymer-specific binding patterns. Consequently, it was pertinent to assess the distribution of the RG-I epitopes recognised by CCRC-M164. As was later revealed, this mAb labelled several structures in *M.* × *giganteus* tissues.

Previously, the distribution of RG-I related epitopes in miscanthus tissues was probed in *M. lutarioriparius* (Cao *et al.*, 2014) and in *M.* × *giganteus* (Xue *et al.*, 2013). However, in both cases *in situ* immunofluorescence assays were performed on still elongating stems, and using a different set of mAbs than those utilised in the present study. Of the labelling patterns observed in *M. lutarioriparius*, all were distinct from those obtained with CCRC-M72 and CCRC-M164. By contrast, some similarities were observed between labelling of CCRC-M164 (Fig. 5.16), and the pattern obtained with a β-galactan-directed mAb (LM5) on immature *M.* × *giganteus* stems (Xue *et al.*, 2013). In both cases, the epitopes were only weakly detected in stem sections and mostly restricted to phloem cell walls. Reduced labelling with RG-I directed mAbs is consistent with the expected low abundance of pectin in type-II cell walls (Carpita, 1996). However, it should not be excluded that *M.* × *giganteus* contains other RG-I epitopes.

One possibility is that other RG-I epitopes, perhaps with different ornamentations, and thus not recognised by CCRC-M72 or CCRC-M164, may occur in the tissues; as is suggested when enzymatic pretreatments which modify the epitopes are applied in miscanthus tissues (Xue *et al.*, 2013).

The results obtained from GP suggested that RG-I is more abundant in leaf biomass, and higher *in situ* detectability of RG-I epitopes in leaf sections may support this observation. In leaves, each of these RG-I directed mAbs showed a different labelling pattern, as CCRC-M72 labelled the lining of protoxylem lacuna and the wall of stomatal subsidiary cells, whereas CCRC-M164 labelled the walls of protoxylem parenchyma, of stomatal guard cells, and of certain bundle sheath and parenchyma cells near the vascular bundles. It has been proposed that RG-I is functionally involved with cell and tissue development, but little is still known about how the structure of these polymers correlates with their function (Lee *et al.*, 2013). It may be associated to providing structural support to the tissues, as it has been suggested that side chains may enable RG-I to associate with cellulose microfibrils, at least in some specialised cell types (Zykwinska *et al.*, 2005). It is also known that RG-I is highly variable not only in structural terms, but also in its occurrence within cell walls (Willats *et al.*, 2001b). Therefore, modification of RG-I structure and abundance is presumed to be associated with its function, which may explain why the patterns obtained with CCRC-M72 and CCRC-164 are distinct, even in equivalent sections from *M.* × *giganteus* tissues; as the roles played by RG-I may vary in relation to specific requirements from the wall in different locations.

An example of this distinct distribution of structurally different RG-I epitopes in the walls of cells known to perform different functions in plant tissues may be observed in stomatal complexes. During stomatal opening, guard cells must undergo large and reversible deformation, as they accumulate potassium salts, causing an osmotically driven uptake of water, while subsidiary cells may assist in the execution of stomatal movements (Roelfsema

and Hedrich, 2009). Labelling with CCRC-M72 was observed on subsidiary cell walls, and with CCRC-M164, on guard cells, but not *vice versa*[*]. Additionally, JIM13 AGN epitopes were also detected in guard cells. It has been suggested that arabinan side chains of RG-I provide steric hindrance to the association of neighbouring domains of HG, thus preventing these polymers from forming tight associations (Jones *et al.*, 2003). It is thought that reversible modification of arabinan helps maintaining flexibility in the guard cell walls, thus allowing them to cope with the deformation required for stomatal opening and closing. Accordingly, it may be speculated that in *M.* × *giganteus* the occurrence of AGN structures in guard cells, and of distinct RG-I epitopes in the walls of subsidiary and guard cells is associated to structurally divergent polymers, which are likely to be implicated in the specific role of each cell type in the regulation of stomatal opening. Also relevant for stomatal functions may be the labelling of wall structures with CCRC-M88 in stomatal subsidiary and guard cells. In this case, a non-fucosylated XG epitope, its occurrence may be associated to unequal thickening of the wall, which allied to variable turgor pressure allows distortion of cell shape and thus the opening and closing of the stoma (Albersheim, 2011).

Arabinans, galactans, and highly branched AGN of various configurations and sizes occur at low amounts in grass cell wall biomass, where they can be associated to RG-I, and as part of AGPs, which are a family of extensively glycosylated hydroxyproline-rich glycoproteins (HRGP) (Carpita, 1996; Showalter, 2001). AGPs predominate and cover the plasma membrane (Lamport *et al.*, 2014), to which most are anchored by a glycosylphosphatidyl-inositol (GPI) anchor (Youl *et al.*, 1998; Svetek *et al.*, 1999). Several processes of plant growth and development have been proposed to be mediated by AGPs. Among these various roles is a possible involvement on secondary wall deposition; as data from several plant species, reviewed by Seifert and Roberts (2007), have suggested that

[*] These different labelling patterns can also be seen in other genotypes Figs. 5.25, 5.26, 5.34 and 5.35.

GPI-anchored AGPs are secreted to the cell surface with cellulose synthase, and that as they bind to cellulose, they are released from GPI anchors and incorporated into wall thickenings, such as those of sclerenchyma cells (Ito *et al.*, 2005). In agreement with this possible function of AGPs, most of the AGN-directed mAbs used in the present study (Table 5.3) did in fact bind to membranous elements of the cells, or areas of the wall adhered to membranes (Fig. 5.17). Furthermore, for one of the mAbs, CCRC-M128, the thickening of some sclerenchyma cells surrounding the vascular bundles was often labelled.

CCRC-M128, has been characterised as binding to AGN side chains of RG-I, and JIM13 is a mAb directed at AGN epitopes of AGPs. However, in the analysed *M.* × *giganteus* sections, these mAbs presented some similarities in their labelling patterns, in the sense that in both cases whole wall layers were less frequently and less intensely labelled than membranous structures; namely, chloroplasts in leaves and amyloplasts in stems.

Epitopes bound by AGN-directed mAbs were also seen in phloem cells, with distinct labelling patterns for different mAbs. With CCRC-M133, immunofluorescence was restricted to areas adhered to plasma membranes of companion cells. It is possible that this distinct labelling is indicative of different AGN structures; however, the functional implication of this observation are unknown.

Published examples of the usage of AGN-directed mAbs for *in situ* immunolabelling studies of miscanthus tissues are not common. Xue *et al.* (2013) and Cao *et al.* (2014) have reported epitopes distributions of some arabinan- and galactan-directed mAbs, but no pattern similarity with the results presented here could be found. CCRC-M128 and CCRC-M133 immunofluorescence observed here in *M.* × *giganteus* sections diverged considerably from patterns reported using AGN-binding mAbs in arabidopsis tissues (Pattathil *et al.*, 2010); as would be expected for a dicot species with a type-I cell wall. Therefore, minimal labelling to cell wall structures for mAbs which are known to bind carbohydrate components of

glycoproteins is in agreement with reported low levels of protein in type-II cell walls (Carpita, 1996), and reveals that *M.* × *giganteus* cell walls conform to the norm for grasses.

JIM19 and JIM20 have been characterised as recognising epitopes from carbohydrate moieties of HRGPs (Knox *et al.*, 1995). In an ELISA-based screen against diverse plant polysaccharide preparations, Pattathil *et al.* (2010) characterised the carbohydrate binding patterns of these mAbs. As a result: JIM20 was included in a mAb clade characterised for binding to gum tragacanth (an exudate where the predominant glycan component is AGN), and to certain RG-I preparations; JIM19 was included in a mAb clade characterised by binding to linear and branched arabinans and RG-I preparations from diverse plants (Appendix C). Bearing this in mind it is likely that the epitopes recognised by JIM19 and JIM20 in *M.* × *giganteus* tissues consist of glycoproteic complexes mostly associated to cell membranous structures.

For all AGN-directed mAbs used for immunolabelling, GP results showed that (Fig, 5.4): (1) JIM19 and JIM20 had higher binding values in the cell wall fractions produced with the weakest extractants, particularly in stem tissues; (2) the epitopes recognised by CCRC-M128 were more abundant in the oxalate and carbonate extracts; (3) epitopes bound by JIM13 had declining binding intensities in each successive extraction step prior to the sodium chlorite treatment; and (4) for CCRC-M133, epitope removal from miscanthus biomass increased with extractant harshness, and the highest signals were seen with the 4M-KOH PC fractions. This indicates that different AGN-related epitopes have very different amenabilities to be extracted from the wall. For the more labile epitopes, immunolabelling patterns primarily associated with membranous structures may justify their easier release; as in the milled CWM used for GP, the extracting solutions presumably fill the luminal spaces of the cells. Consequently, epitopes observed to occur associated with membranous structures, should be more accessible, and thus would be more readily removed from the wall. As for CCRC-M133, this was the AGN-directed

mAb which showed a labelling pattern less associated with membranous structures and more frequently associated with wall layers. Such locations in the tissues may partially explain why this epitope is less labile. Furthermore, the fact that the signals for CCRC-M133 were higher in the glycome profiles of cell wall fractions produced with harsher solvents, may suggest that it recognises an epitope which may be directly or indirectly associated to more recalcitrant molecular structures of the wall. These associations could give rise to epitopes which are not recognised by the CCRC-M133 mAb *in situ*; thus explaining why the labelling patterns are restricted to just a few cellular structures, in contrast with the moderately high signals observed in GP.

As mentioned above, several mAbs used in this study to probe hemicellulose and pectin epitopes, showed that the walls of certain large parenchymatous cells, which are near the vascular bundles of leaves, showed more intense labelling than parenchyma cells of ground tissue. The contribution of these walls to the overall biomass of *M.* × *giganteus* should be limited. However, future studies exploring the reasons behind this distinct labelling pattern are relevant to understand the role of the identified cell wall structures. Gathered information may eventually contribute to optimise miscanthus lignocellulosic biomass applications.

5.3. Genotypic Variation in Cell Wall Glycan Contents – Quick Assessment

Previously, in sections 5.1 and 5.2, the data derived from two immunological approaches were used to characterise the non-cellulosic glycans of miscanthus cell wall, with a focus on the differences between tissues and developmental stages. As part of these studies a total of eight miscanthus genotypes were analysed. These were the same genotypes included in studies described in the previous chapters of this thesis (Table 1.1): sac01, gig01, hyb03, sin09, sin11, sin08, sin13 and sin15. The detailed analysis of each genotype represents a very valuable dataset, which will allow identifying key factors of genotype- and species-specific cell wall heterogeneity. This information can potentially contribute to at least three areas of miscanthus-related research, it can: (1) improve our basic understanding of how cell wall composition and structure is modified in different genotypes, some of which have very distinct anatomies; (2) identify genotype-specific features with a positive or negative effect on cell wall saccharification, and thus help direct efforts to breed improved miscanthus varieties to be used as dedicated lignocellulosic crops; and (3) determine if the various genotypes possess distinct types of cell wall composition or structure, which would justify the development and application of different approaches to achieve optimal biomass conversion into industrially relevant products. Nevertheless, due to time and space constraints, these genotypic differences could not be discussed as part of the thesis. It is anticipated that this information will be explored in the context of at least one peer-reviewed journal article to be submitted for publications in the near future.

In the following sections, illustrations for glycome profiling and glycan immunolabelling results are presented for individual genotypes. For each dataset, a brief assessment is also included, in order to provide the reader with an overview of the gathered data.

5.3.1. Cell Wall Glycome Reference and Genotype-specific Heterogeneities

The glycome profiling data, presented in section 5.1, were summarised in heat maps, together with corresponding bar graphs indicating the total carbohydrate recovered from each sequential extraction step. The resulting graphical interpretations are shown in Fig. 5.15 (A and B), where the mean of 8 miscanthus genotypes in terms of their binding intensities to glycan-directed mAbs is shown for leaf and stem CWM extracts at three developmental stages. Additionally, the standard deviation from the mean binding intensity was calculated for each mAb, and also represented as heat maps (Fig. 5.16 A and B), this time with a different colour pallet to avoid confusion with the heat maps of the means.

This re-interpretation of the data is intended to graphically represent the concept of a cell wall glycome reference. In this novel approach to data analysis, the heat map of the means initially shows the typical OD values obtained with the different mAbs for the miscanthus genotypes used in the study, against which the glycome profile of individual genotypes may be compared; secondly, the heat map of standard deviations indicates portions of the glycome profiles where greater variability occurs, thus identifying the cell wall glycan epitopes which vary the most between genotypes. Furthermore, the heat map of standard deviations also provides information regarding epitope extractability between different cell wall fractions, developmental stages and tissues. For example, standard deviations are typically higher for pectic mAbs in the ammonium oxalate fractions, suggesting that labile pectin may be quantitatively more variable than the more tightly bound epitopes which are only removed with harsher extractants. An extension of this observation is that inter-genotypic variation is not homogeneous for all classes of cell wall glycans, as standard deviations are typically lower in cell wall fractions produced with harsher extractants, suggesting that between the 8 miscanthus genotypes used in this study, the labile epitopes tend to be more variable than the abundance of the more recalcitrant ones. One instance of such heterogeneities is found in the detected

abundances of xylan epitopes amenable to extraction with 1M KOH, which varied much less between the genotypes than for example, labile pectic epitopes extracted with ammonium oxalate.

Once key epitopes have been identified based on the reference glycome profile, individual genotypes may be assessed. The glycome profiles for the leaf and stem CWM extracts of each genotype at a given developmental stage are presented in Fig. 5.17 A – F. By observing these heat maps it is immediately observable that certain genotypes display very distinct binding values for certain epitope classes; e.g.: for genotype sac01, XG and xylan epitopes have particularly high signals in the 4M KOH cell wall fraction of actively growing stems (AGS; Fig. 5.17D). Another type of relevant differences is epitope shifting between extracts in different genotypes. One example for this is found in leaves collected at the actively growing harvest time (AGL; Fig. 5.17A), where for genotypes gig01, hyb03 and sac01, the signals for the RG-I/AGN class of epitopes are visibly higher in the ammonium oxalate fraction than in the subsequent carbonate fraction. However, in the *M. sinensis* genotypes, the predominance of RG-I/AGN epitopes in the ammonium oxalate extracts is not so clear, and indeed for sin09, the signals are typically higher in the carbonate fraction.

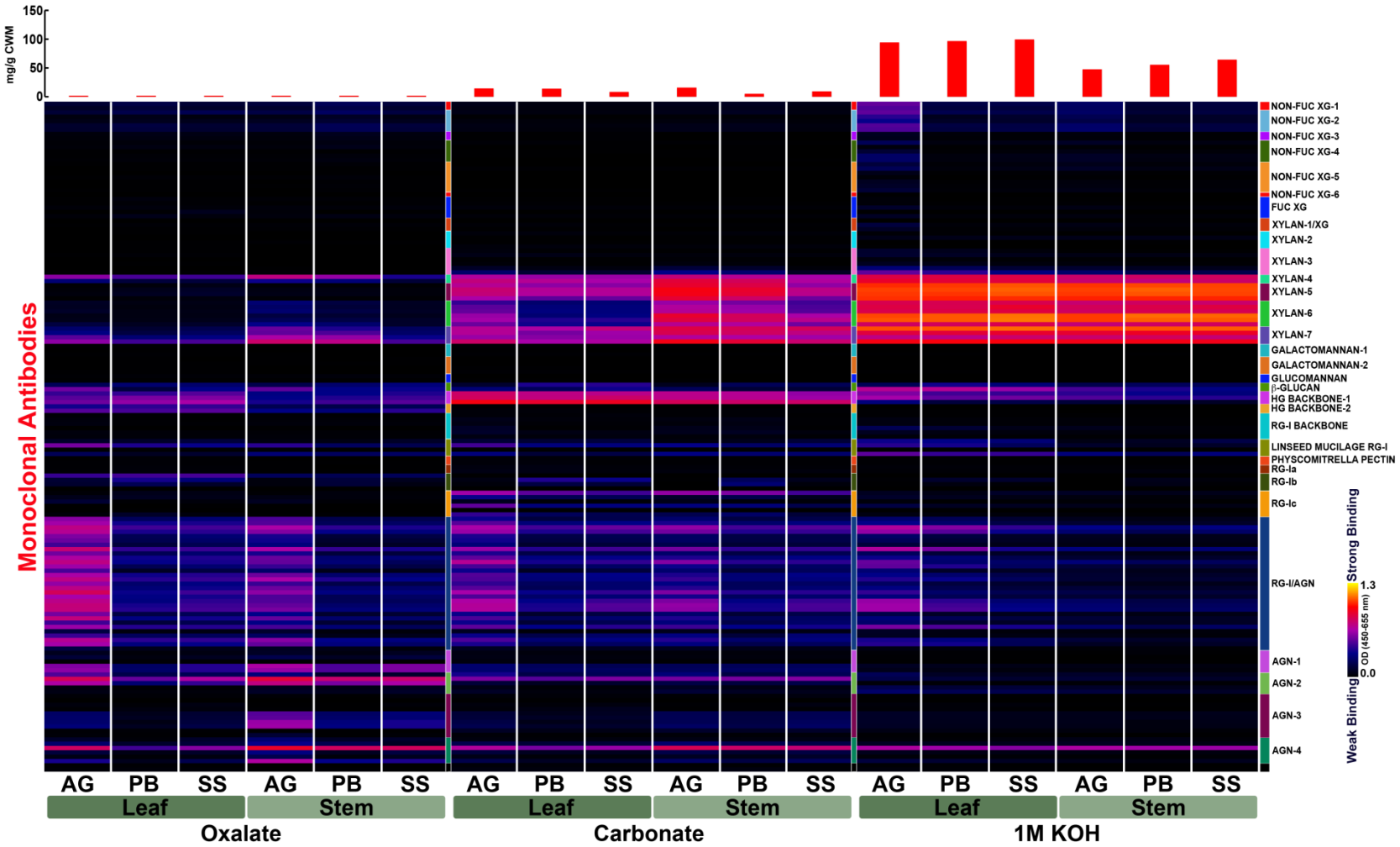

Fig. 5.15A. Glycome profile of miscanthus cell wall material (CWM) extracted sequentially with ammonium oxalate, sodium carbonate and 1M KOH. Corresponding tissues and developmental stages are labelled below each profile: AG, actively growing; PB, peak biomass; SS, senesced. Each extract was probed against an array of plant glycan-directed monoclonal antibodies (panel on the right of the figure; Appendix C). Antibody binding strength depicted in function of optical density (OD) is presented as a colour gradient ranging from black (no binding) to yellow (OD=1.3). Binding intensities are the average of the 8 genotypes here studied. The bar graphs at the top indicate the amount of sugars recovered in the solubilised extracts per gram of CWM.

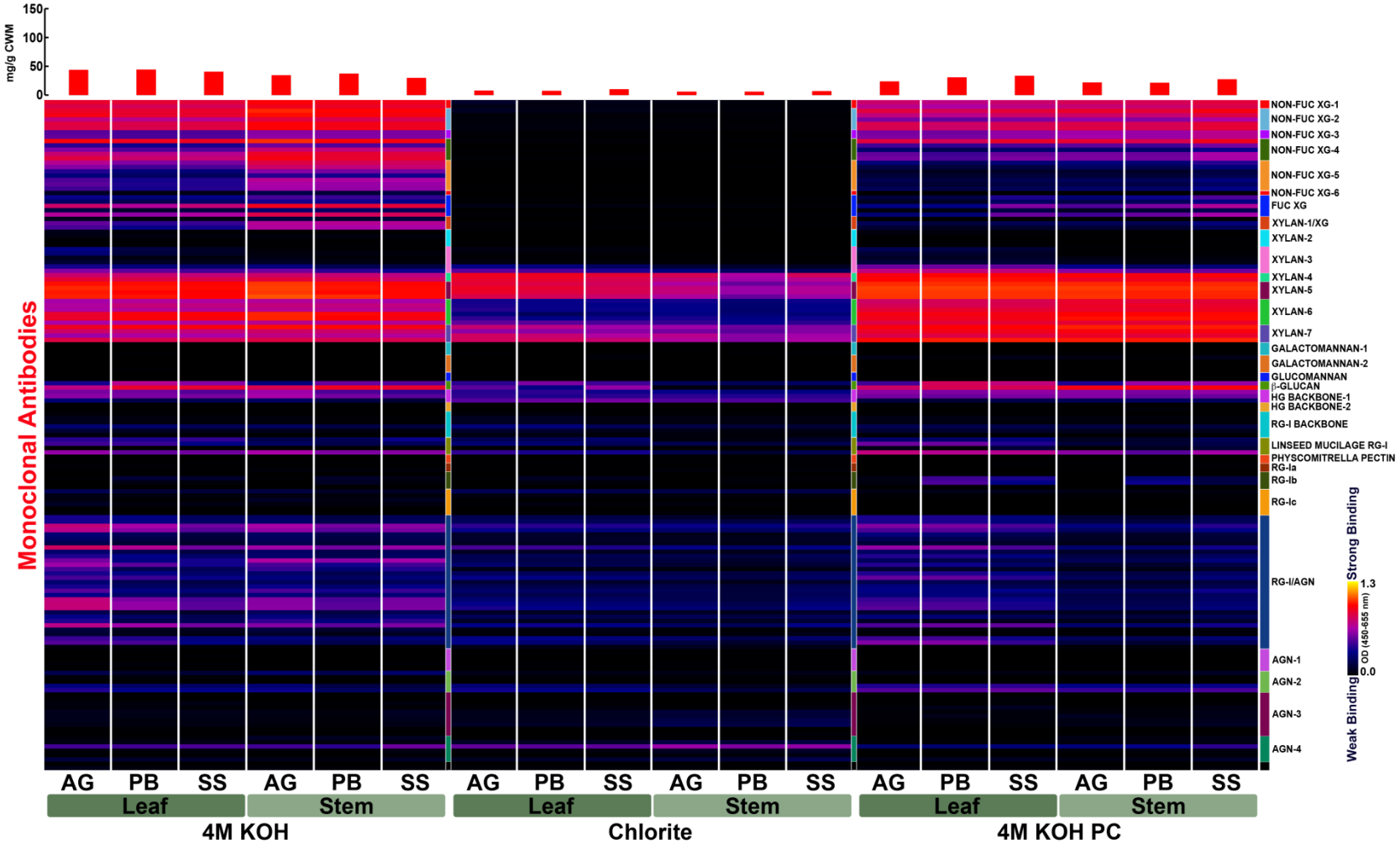

Fig. 5.15B. Glycome profile of miscanthus cell wall material (CWM) extracted sequentially with 4M KOH, sodium chlorite and 4M KOH post-chlorite treatment (PC). Corresponding tissues and developmental stages are labelled below each profile: AG, actively growing; PB, peak biomass; SS, senesced. Each extract was probed against an array of plant glycan-directed monoclonal antibodies (panel on the right of the figure; Appendix C). Antibody binding strength depicted in function of optical density (OD) is presented as a colour gradient ranging from black (no binding) to yellow (OD=1.3). Binding intensities are the average of the 8 genotypes here studied. The bar graphs at the top indicate the amount of sugars recovered in the solubilised extracts per gram of CWM.

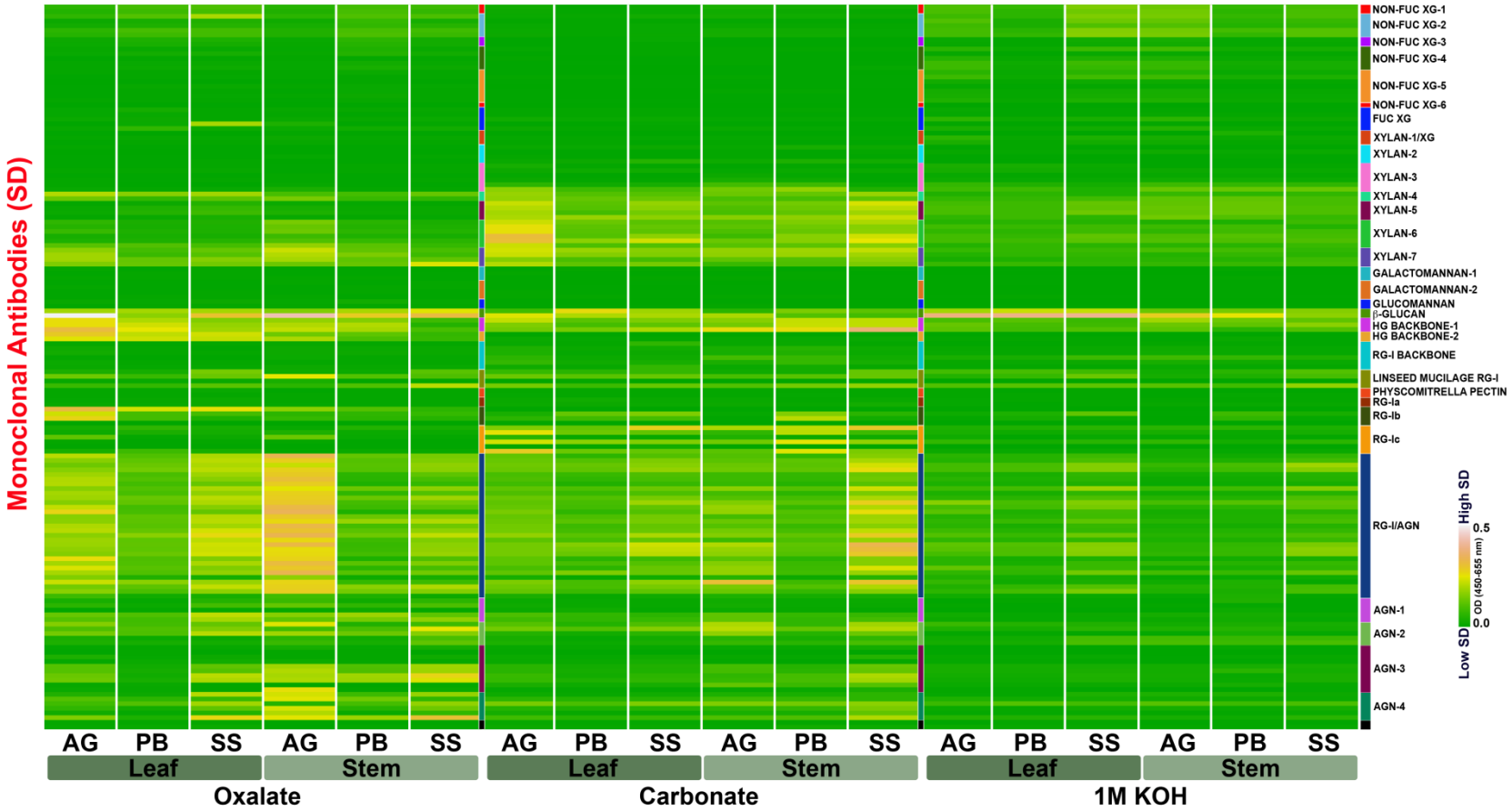

Fig. 5.16A. Standard deviations (SD) from the mean binding intensities shown in Fig. 5.15A. Cell wall glycan classes are indicated to the right, and corresponding extract, tissue and developmental stage are labelled below each column. SD values are given in optical density (OD) units and the maximum value is 0.4755 (≈0.5).

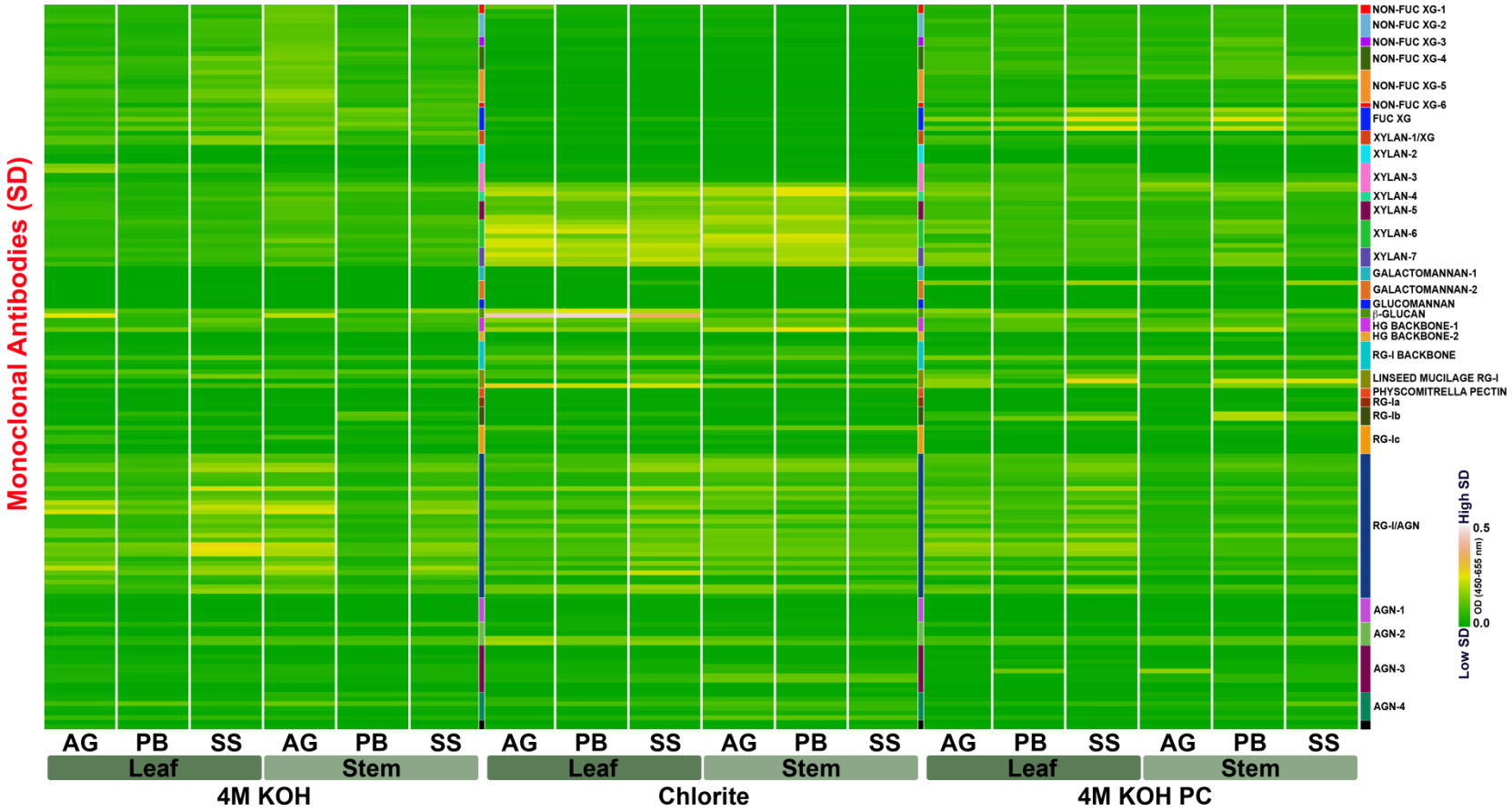

Fig. 5.16B. Standard deviations (SD) from the mean binding intensities shown in Fig. 5.15B. Cell wall glycan classes are indicated to the right, and corresponding extract, tissue and developmental stage are labelled below each column. SD values are given in optical density (OD) units and the maximum value is 0.4755 (≈0.5).

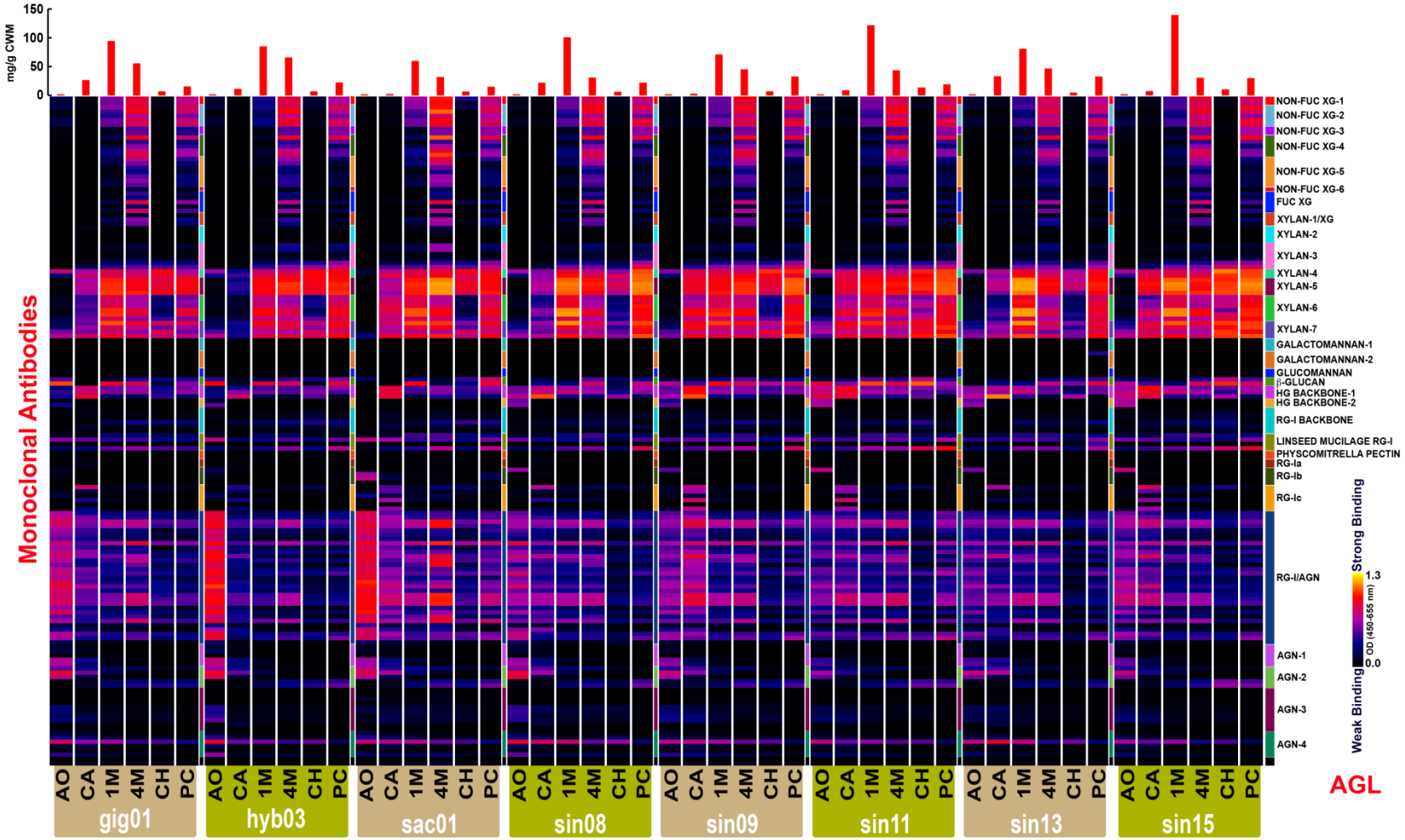

Fig. 5.17A. Glycome profile of cell wall material (CWM) from the leaves of actively growing miscanthus (AGL). The CWM of eight miscanthus genotypes was sequentially extracted with ammonium oxalate (AO), sodium carbonate (CA), 1M KOH (1M), 4M KOH (4M) and delignified with sodium chlorite (CH) followed by another extraction with 4M KOH post-chlorite (PC). Corresponding genotypes and extracts are labelled below each profile. Each extract was probed against an array of plant glycan-directed monoclonal antibodies (panel on the right of the figure; Appendix C). Antibody binding strength depicted in function of optical density (OD) is presented as a colour gradient ranging from black (no binding) to yellow (OD=1.3). The bar graphs at the top indicate the amount of sugars recovered in the solubilised extracts per gram of CWM.

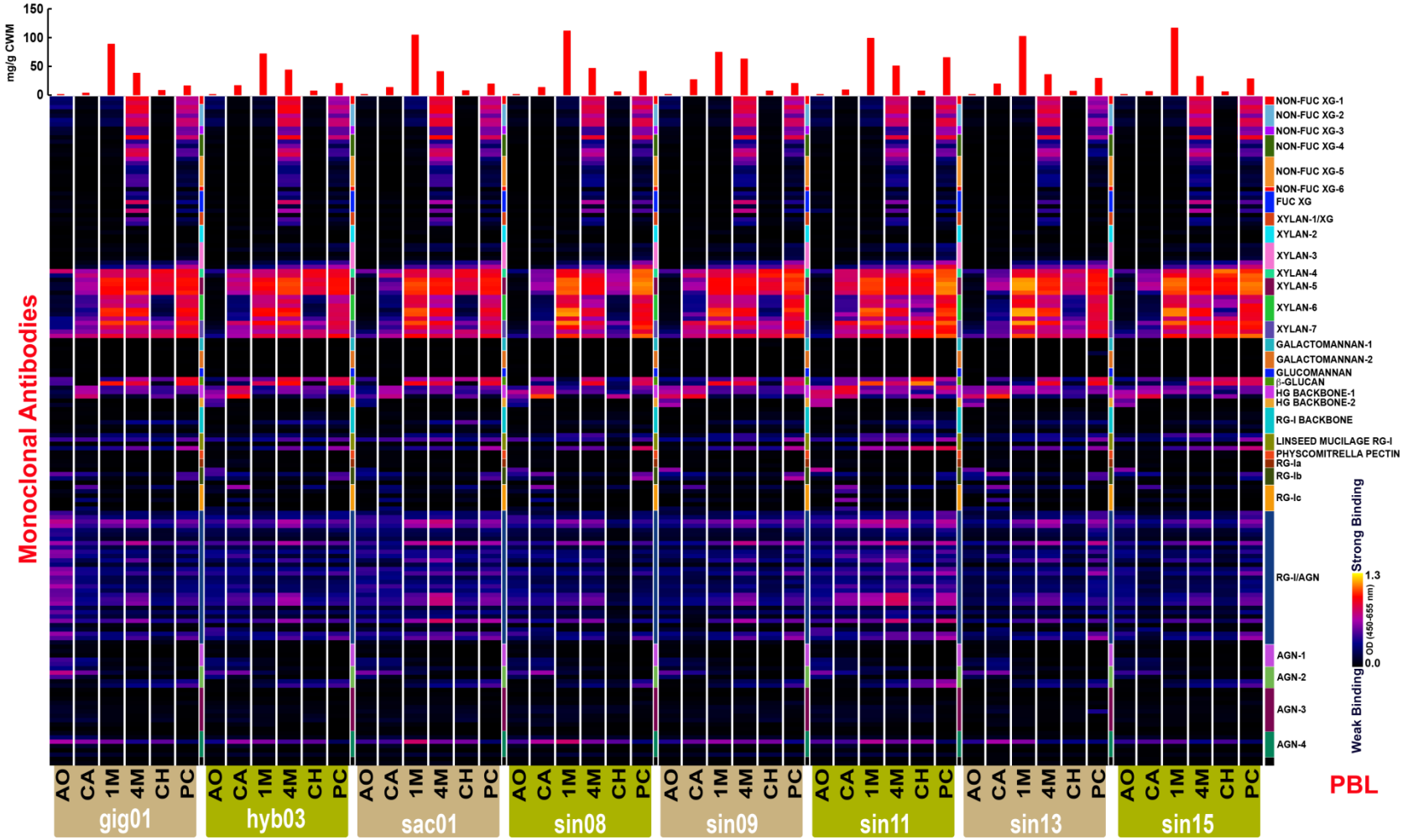

Fig. 5.17B. Glycome profile of cell wall material (CWM) from the leaves of miscanthus at the peak biomass stage (PBL). The CWM of eight miscanthus genotypes was sequentially extracted with ammonium oxalate (AO), sodium carbonate (CA), 1M KOH (1M), 4M KOH (4M) and delignified with sodium chlorite (CH) followed by another extraction with 4M KOH post-chlorite (PC). Corresponding genotypes and extracts are labelled below each profile. Each extract was probed against an array of plant glycan-directed monoclonal antibodies (panel on the right of the figure; Appendix C). Antibody binding strength depicted in function of optical density (OD) is presented as a colour gradient ranging from black (no binding) to yellow (OD=1.3). The bar graphs at the top indicate the amount of sugars recovered in the solubilised extracts per gram of CWM.

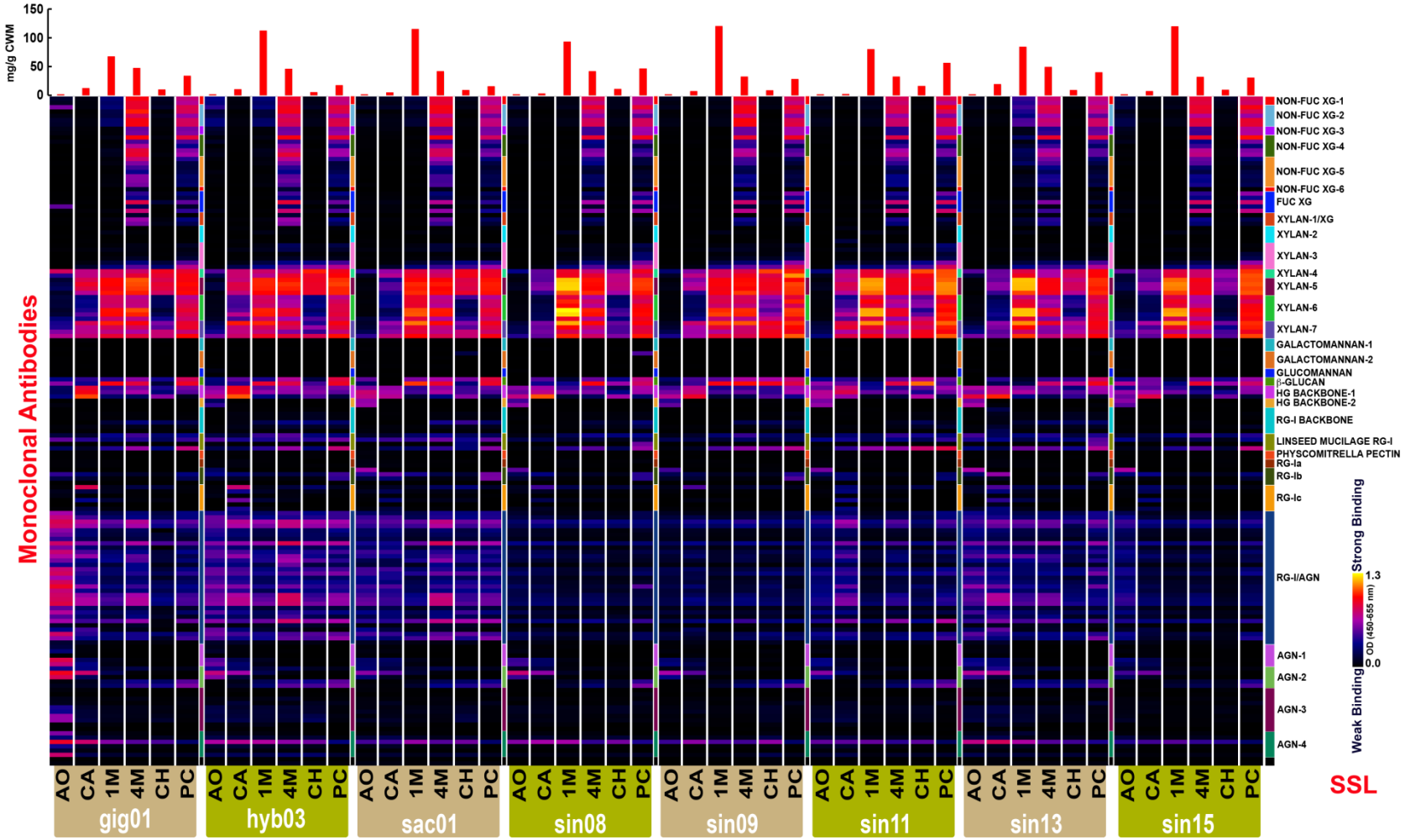

Fig. 5.17C. Glycome profile of cell wall material (CWM) from the leaves of senesced miscanthus (SSL). The CWM of eight miscanthus genotypes was sequentially extracted with ammonium oxalate (AO), sodium carbonate (CA), 1M KOH (1M), 4M KOH (4M) and delignified with sodium chlorite (CH) followed by another extraction with 4M KOH post-chlorite (PC). Corresponding genotypes and extracts are labelled below each profile. Each extract was probed against an array of plant glycan-directed monoclonal antibodies (panel on the right of the figure; Appendix C). Antibody binding strength depicted in function of optical density (OD) is presented as a colour gradient ranging from black (no binding) to yellow (OD=1.3). The bar graphs at the top indicate the amount of sugars recovered in the solubilised extracts per gram of CWM.

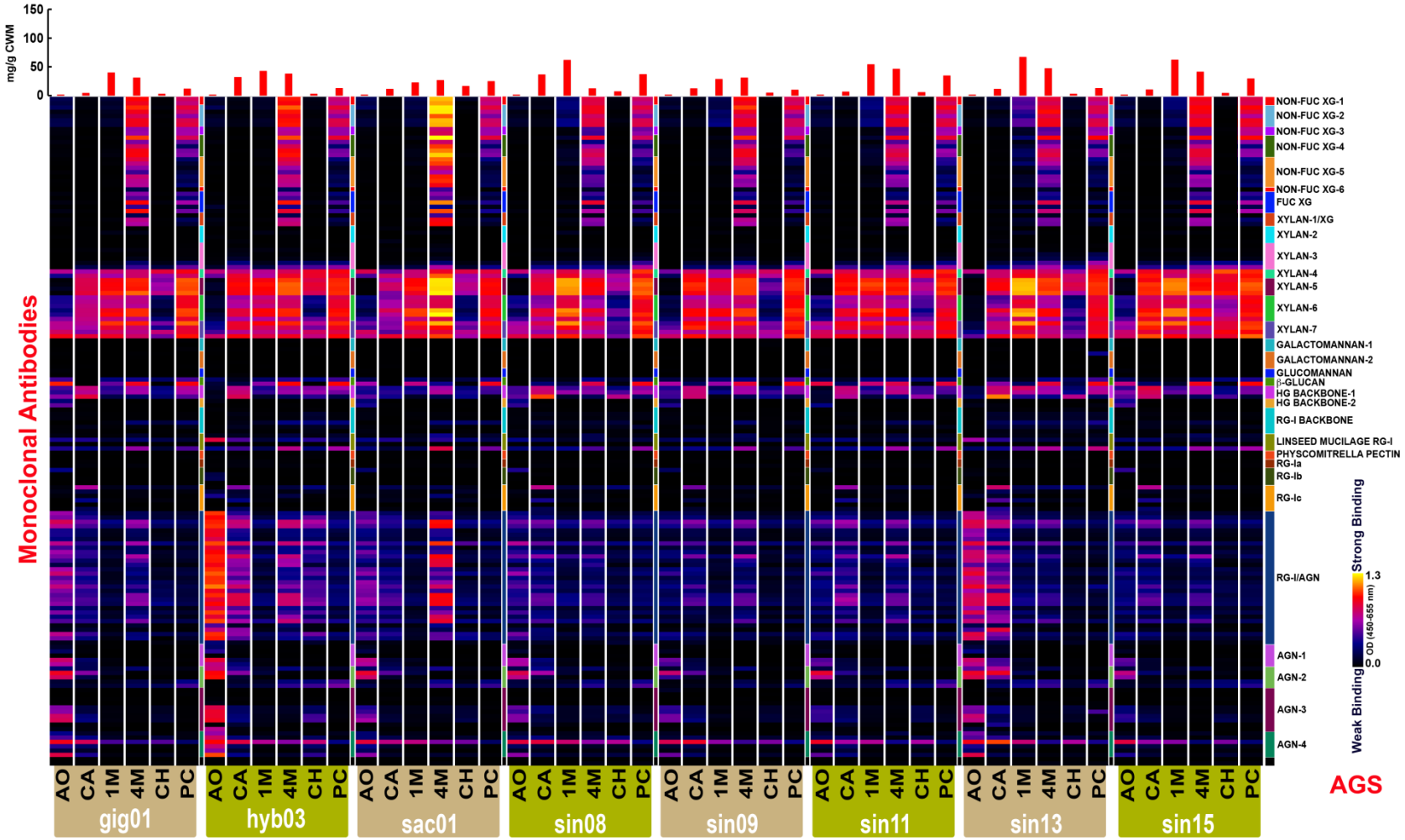

Fig. 5.17D. Glycome profile of cell wall material (CWM) from the stem of actively growing miscanthus (AGS). The CWM of eight miscanthus genotypes was sequentially extracted with ammonium oxalate (AO), sodium carbonate (CA), 1M KOH (1M), 4M KOH (4M) and delignified with sodium chlorite (CH) followed by another extraction with 4M KOH post-chlorite (PC). Corresponding genotypes and extracts are labelled below each profile. Each extract was probed against an array of plant glycan-directed monoclonal antibodies (panel on the right of the figure; Appendix C). Antibody binding strength depicted in function of optical density (OD) is presented as a colour gradient ranging from black (no binding) to yellow (OD=1.3). The bar graphs at the top indicate the amount of sugars recovered in the solubilised extracts per gram of CWM.

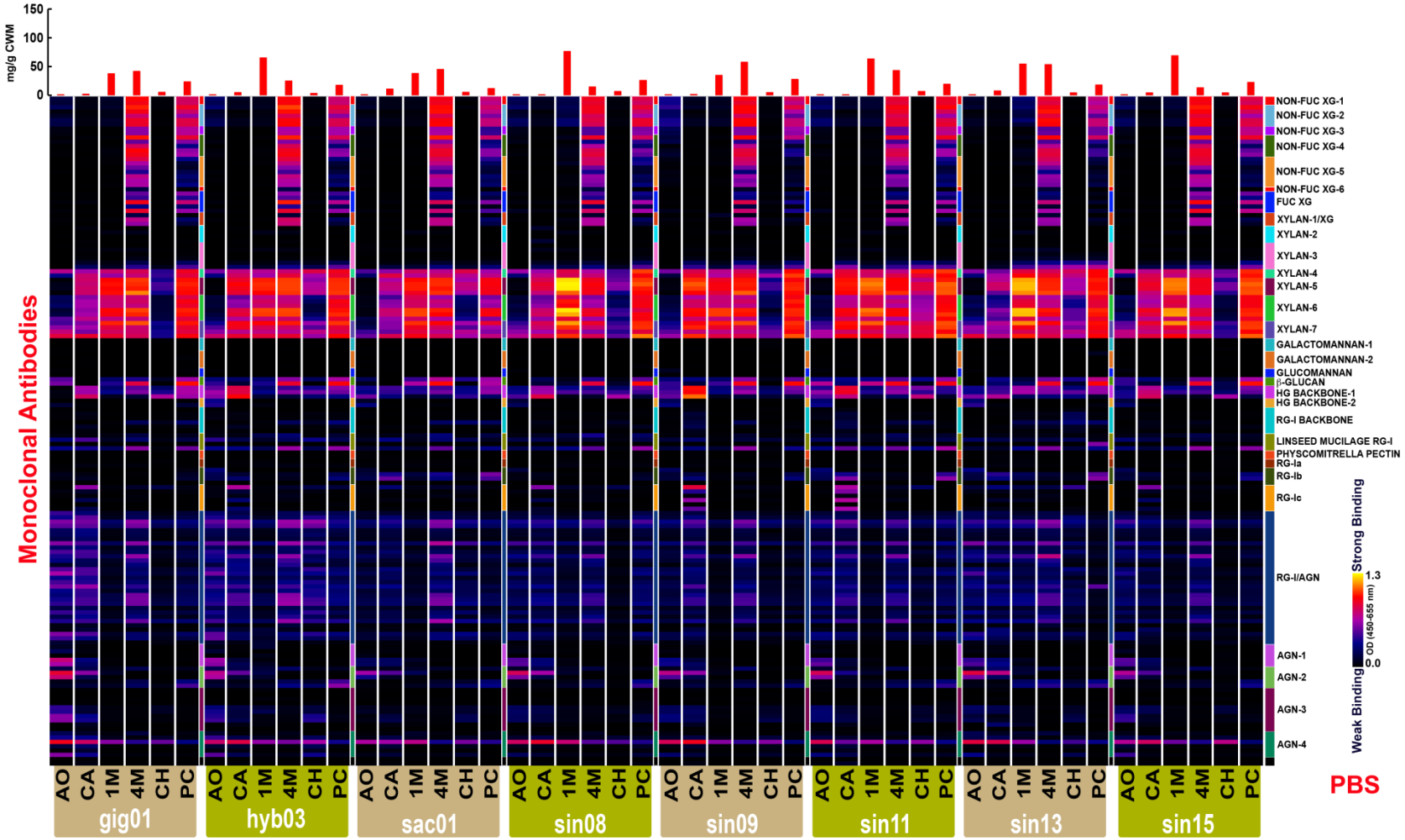

Fig. 5.17E. Glycome profile of cell wall material (CWM) from the stem of miscanthus at the peak biomass stage (PBS). The CWM of eight miscanthus genotypes was sequentially extracted with ammonium oxalate (AO), sodium carbonate (CA), 1M KOH (1M), 4M KOH (4M) and delignified with sodium chlorite (CH) followed by another extraction with 4M KOH post-chlorite (PC). Corresponding genotypes and extracts are labelled below each profile. Each extract was probed against an array of plant glycan-directed monoclonal antibodies (panel on the right of the figure; Appendix C). Antibody binding strength depicted in function of optical density (OD) is presented as a colour gradient ranging from black (no binding) to yellow (OD=1.3). The bar graphs at the top indicate the amount of sugars recovered in the solubilised extracts per gram of CWM.

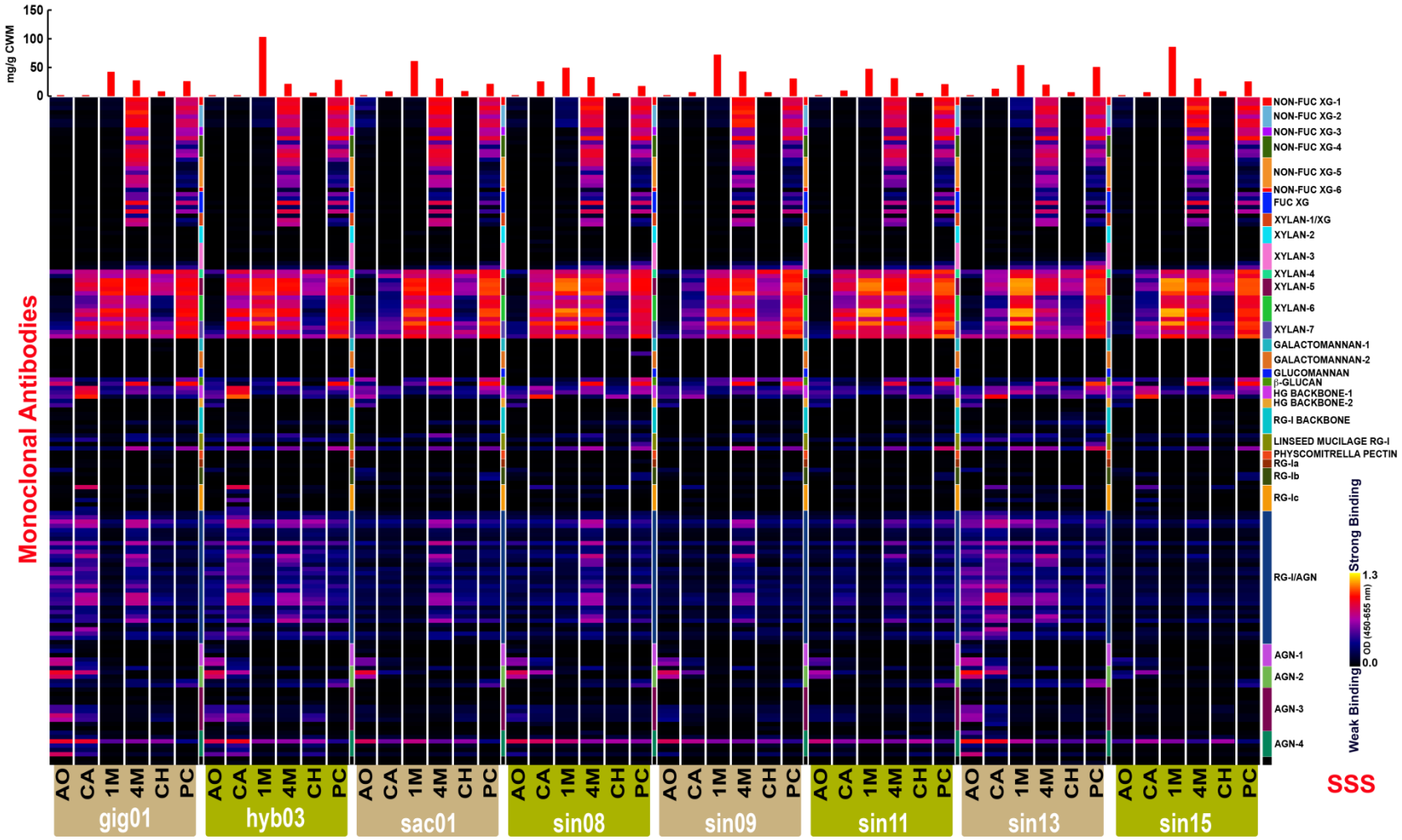

Fig. 5.17F. Glycome profile of cell wall material (CWM) from the stem of senesced miscanthus (SSS). The CWM of eight miscanthus genotypes was sequentially extracted with ammonium oxalate (AO), sodium carbonate (CA), 1M KOH (1M), 4M KOH (4M) and delignified with sodium chlorite (CH) followed by another extraction with 4M KOH post-chlorite (PC). Corresponding genotypes and extracts are labelled below each profile. Each extract was probed against an array of plant glycan-directed monoclonal antibodies (panel on the right of the figure; Appendix C). Antibody binding strength depicted in function of optical density (OD) is presented as a colour gradient ranging from black (no binding) to yellow (OD=1.3). The bar graphs at the top indicate the amount of sugars recovered in the solubilised extracts per gram of CWM.

5.3.2. Genotype-specific Cell Wall Glycan Immunolabelling Patterns

As in section 5.2, the binding to different glycan-directed mAbs observed in the GP of each individual genotype was subsequently verified by *in situ* immunolabelling. For this, a subset of 22 mAbs out of the 155 used for GP studies (Appendix C) was chosen to perform a screening of the 8 miscanthus genotypes studied. This set of mAbs (Table 5.4) contains many probes not included in section 5.2 for the characterisation of *M.* × *giganteus*; thus non-redundant data is also presented for this genotype. A characterisation of toluidine blue-stained sections from each genotype is included to facilitate the identification of the observed histological structures (Fig. 5.18). Furthermore, in this wider comparative study, the aim was not to focus on an overview of the appearance of leaf and stem sections, but instead to focus on specific portions of the tissues, thus more magnified micrographs are presented.

As described in the methods section (5.2.2), sampling uniformity was achieved by collecting leaf and stem samples from an internode in all cases located halfway along the length defined as being between the uppermost fully formed ligule and the base of the tiller. However, despite all immunolabelled sections having been obtained from plants harvested at the peak biomass stage (PB), given the different phenotypes of the miscanthus genotypes, the internode taken from sin13 was at an apparently less mature stage; as indicated by the fact that it was shorter and softer than those from other genotypes (Fig. 5.6 B and D). Furthermore, flowering of this genotype is typically delayed in comparison to others or even non-occurring[*]. As a result, clear differences may be observed in the immunolabelling patterns of certain glycan epitopes between sin13 and other genotypes (Figs. 5.19 – 5.26)[†]. One such example is the labelling observed for the β-glucan epitope recognised by the LAMP mAb (Fig. 5.23). This

* Jensen, September 2015. Personal communication.
† As previously mentioned, higher resolution versions of the figures are available on the supplemental materials of this thesis and online: https://mega.co.nz/#!rBNgQLzD!9ypu0nCjIv6GlcWSl3V4o6QfDuDBFagRk-2CGgw-f6c.

type of observations may allow conclusions related to changes in wall composition and structure as a function of tissue differentiation along intrinsic developmental gradients that exist in the plant (Avci *et al.*, 2012). Apart from this, other clear differences between the genotypes are also revealed; for example in the labelling patterns of CCRC-M160 (Fig. 5.20). Additionally, a base treatment intended to determine the degree of xylan and HG esterification has also been employed in conjunction with selected mAbs (Table 5.4), and the results are shown in Figs. 5.21 and 5.22., for xylan epitopes, and in Fig. 5.24 for HG epitopes.

Table 5.4. Cell wall glycan-directed mAbs used in the study of *in situ* immunolabelling of leaf and stem tissues from 8 miscanthus genotypes (further information on all used mAbs can be found in Appendix C).

	mAb	**mAb subclass – based on Pattathil *et al.* (2010)**	**Reference**
Hemicelluloses	CCRC-M95	Non-fucosylated xyloglucan-1	Pattathil *et al.* (2010)
	CCRC-M87	Non-fucosylated xyloglucan-2	Pattathil *et al.* (2010)
	CCRC-M1	Fucosylated xyloglucan	Pattathil *et al.* (2010)
	CCRC-M114[BT]	Xylan-3	Pattathil *et al.* (2010)
	CCRC-M150	Xylan-4	Pattathil *et al.* (2010)
	CCRC-M154	Xylan-4	Pattathil *et al.* (2010)
	CCRC-M144[BT]	Xylan-5	Pattathil *et al.* (2010)
	CCRC-M155[BT]	Xylan-5	Pattathil *et al.* (2010)
	CCRC-M160	Xylan-7	Pattathil *et al.* (2010)
	CCRC-M137	Xylan-7	Pattathil *et al.* (2010)
	LAMP	(1→3)-β-glucan	Meikle *et al.* (1991)
	BG1	Mixed-linkage (1→3, 1→4)-β-glucan	Meikle *et al.* (1994)
Pectins	JIM7	Homogalacturonan backbone-2 (heavily esterified)	Knox *et al.* (1990)
	JIM5	Homogalacturonan backbone-1 (partially esterified and un-esterified)	Knox *et al.* (1990)
	CCRC-M38[BT]	Homogalacturonan backbone-1 (fully un-esterified)	Pattathil *et al.* (2010)
	CCRC-M14	Rhamnogalacturonan-I backbone	Pattathil *et al.* (2010)
	CCRC-M164	Epitopes akin to linseed mucilage rhamnogalacturonan-I	Pattathil *et al.* (2010)
	JIM137	Rhamnogalacturonan-Ib	Pattathil *et al.* (2010)
	CCRC-M7	RG-I/AGN (arabinogalactan side chains of rhamnogalacturonan-I)	Pattathil *et al.* (2010)
	CCRC-M12	RG-I/AGN (arabinogalactan side chains of rhamnogalacturonan-I)	Knox *et al.* (1991)
	CCRC-M133	Arabinogalactan-2	Pattathil *et al.* (2010)
	JIM13	Arabinogalactan-4 (arabinogalactan and arabinogalactan proteins)	Knox *et al.* (1991)

[BT] mAbs used in combination with a 0.1M KOH base treatment.

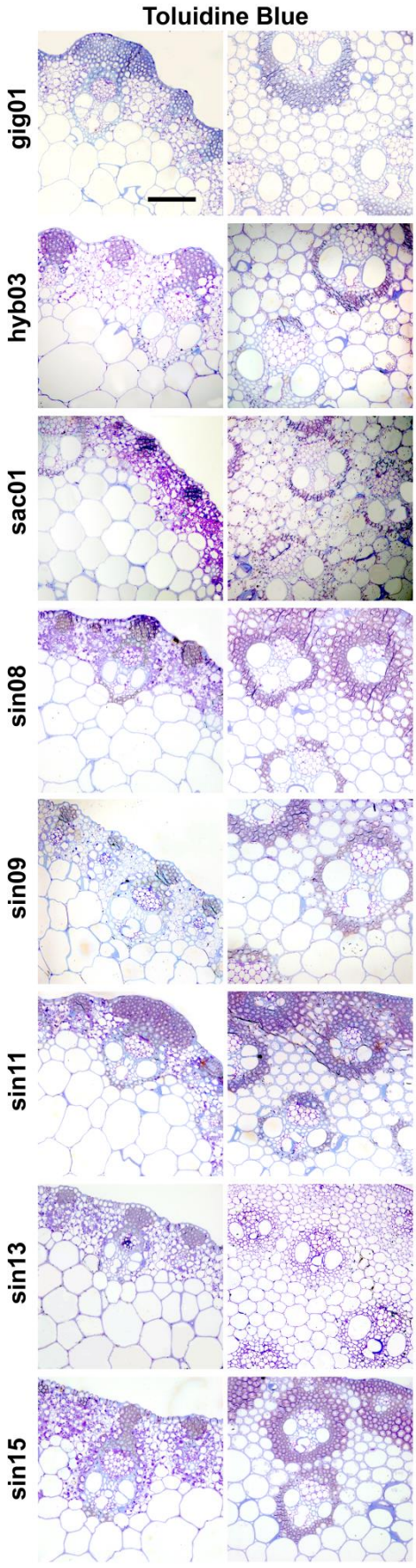

Fig. 5.18. Transverse sections stained with toluidine blue of the eight miscanthus genotypes used for *in situ* immunolabelling. Leaf tissue of each genotype is in the left column and stem is in the right. Scale bar: 100µm.

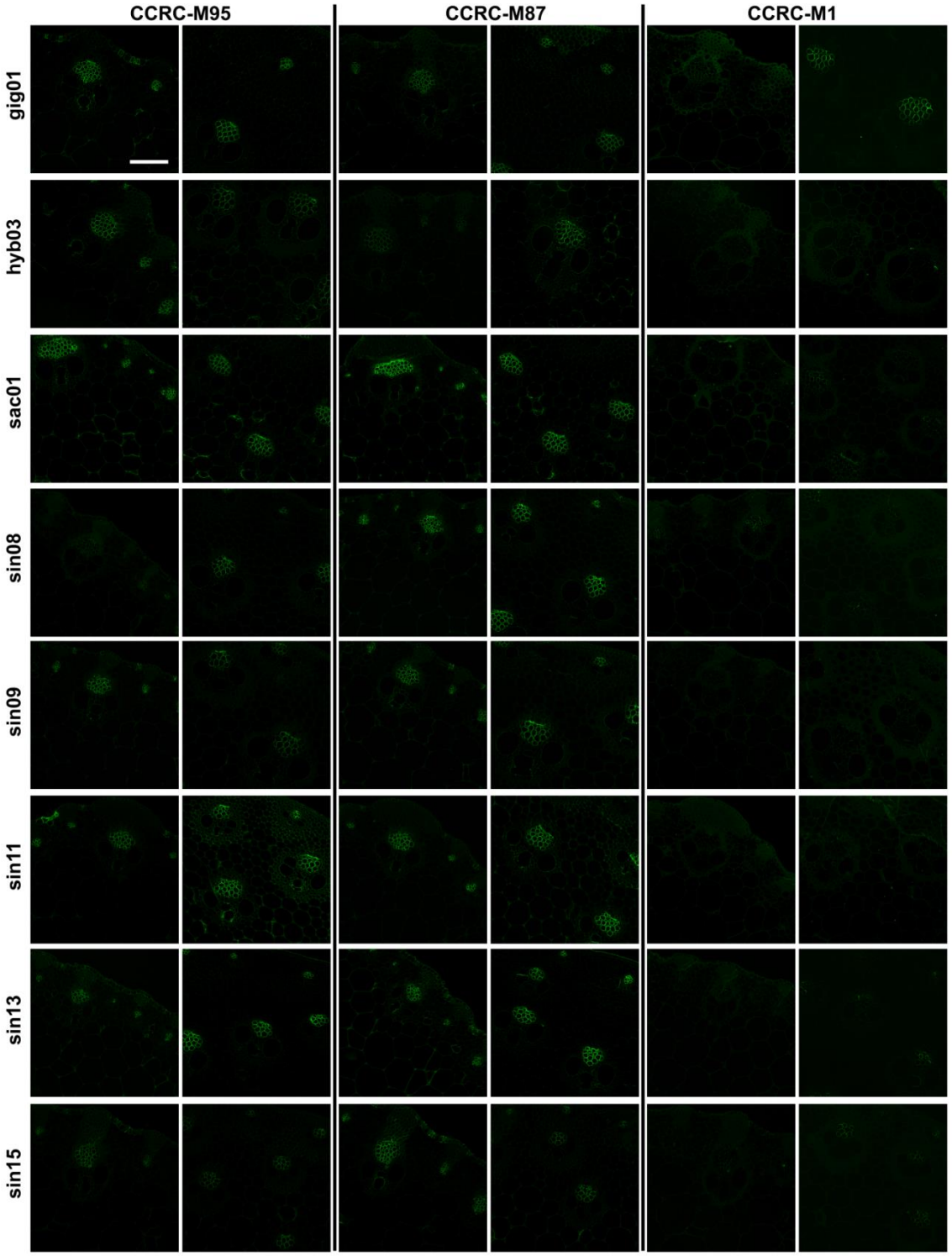

Fig. 5.19. Immunofluorescent labelling of transverse sections from leaves and stems of eight miscanthus genotypes with xyloglucan binding mAbs. For each mAb, leaf is in the left column and stem is in the right. Scale bar: 100µm.

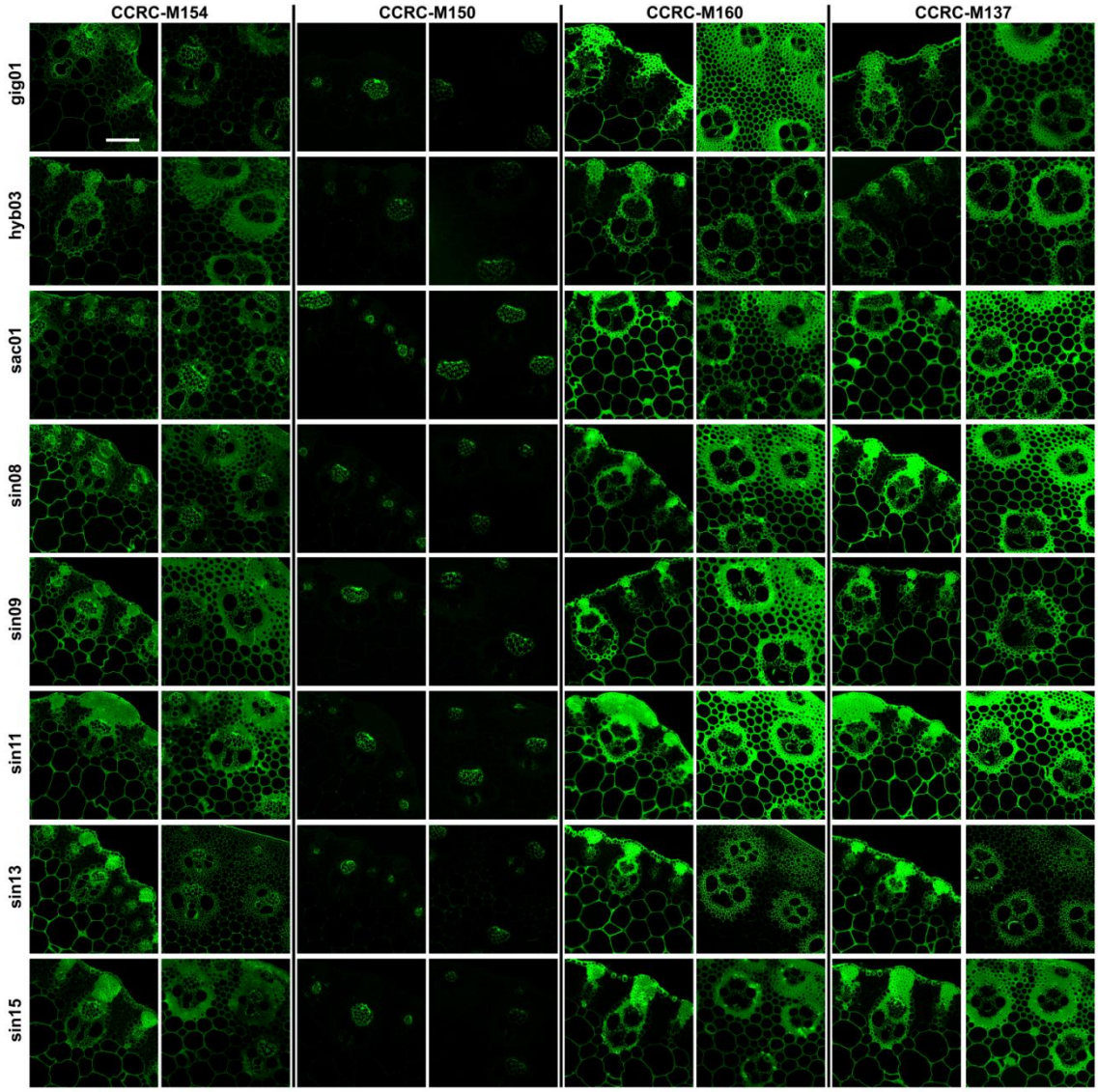

Fig. 5.20. Immunofluorescent labelling of transverse sections from leaves and stems of eight miscanthus genotypes with xylan binding mAbs. For each mAb, leaf is in the left column and stem is in the right. Scale bar: 100µm.

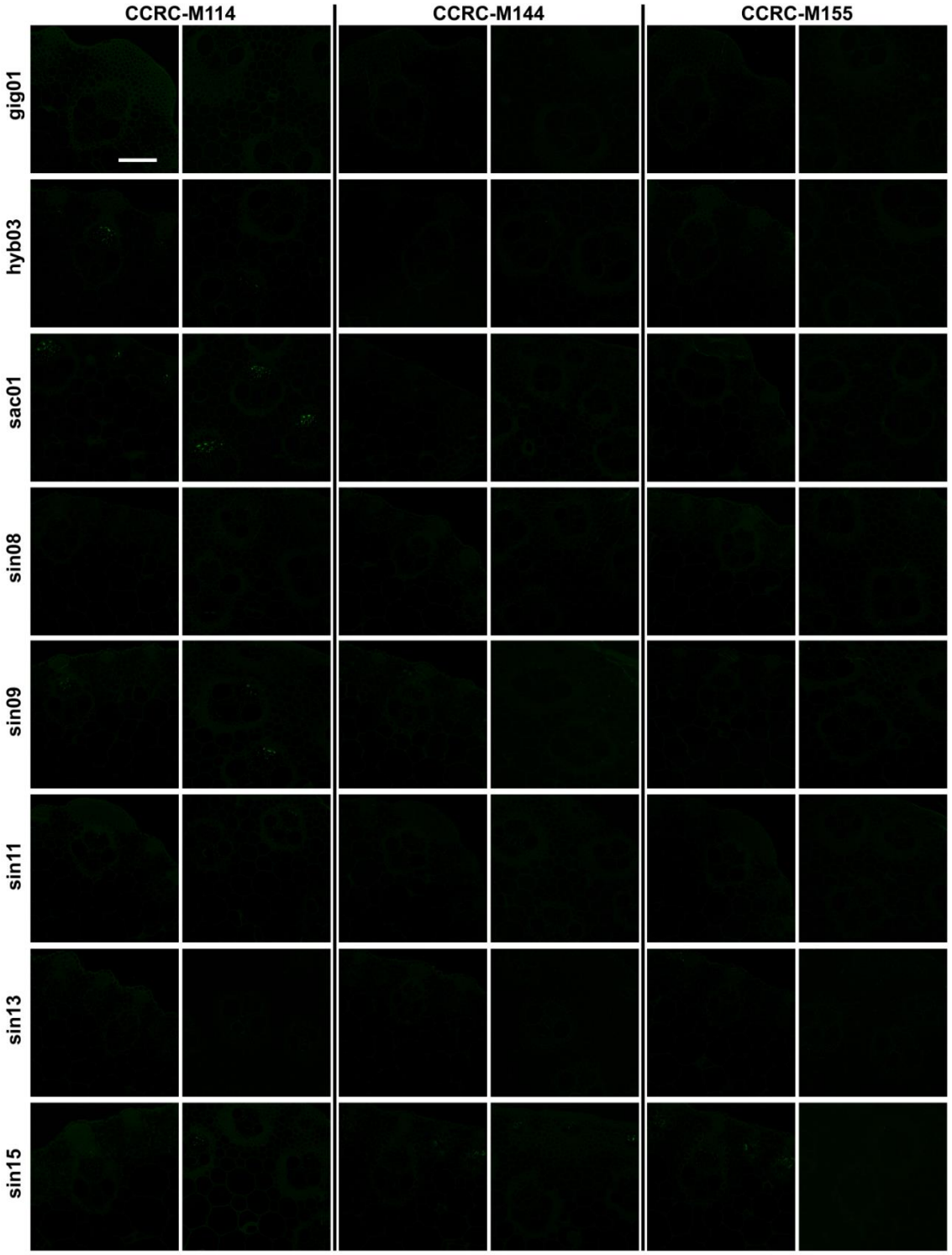

Fig. 5.21. Immunofluorescent labelling of transverse sections from leaves and stems of eight miscanthus genotypes with xylan binding mAbs, before a base treatment with 0.1M KOH. For each mAb, leaf is in the left column and stem is in the right. Scale bar: 100µm.

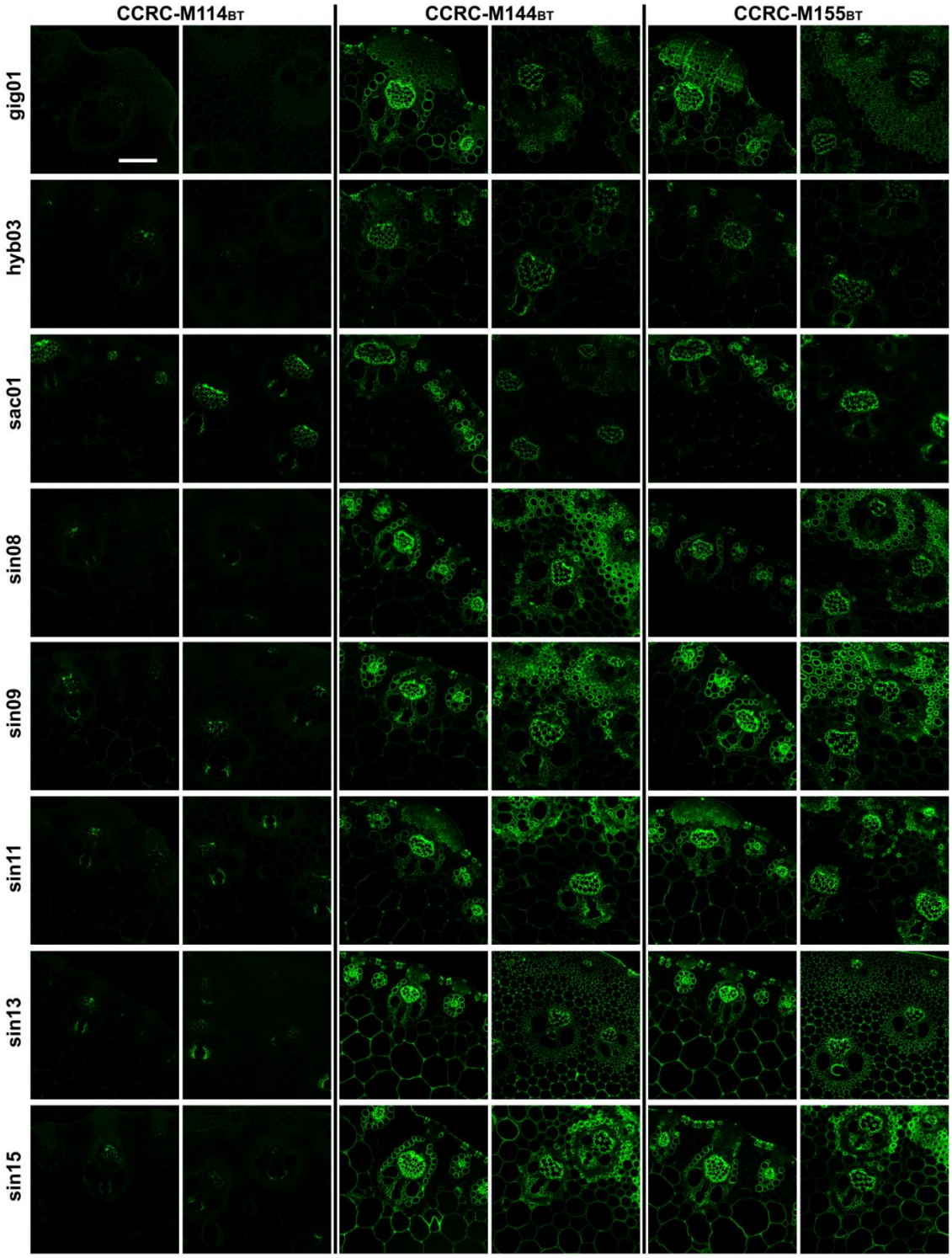

Fig. 5.22. Immunofluorescent labelling of transverse sections from leaves and stems of eight miscanthus genotypes with xylan binding mAbs, after a base treatment (BT) with 0.1M KOH. For each mAb, leaf is in the left column and stem is in the right. Scale bar: 100µm.

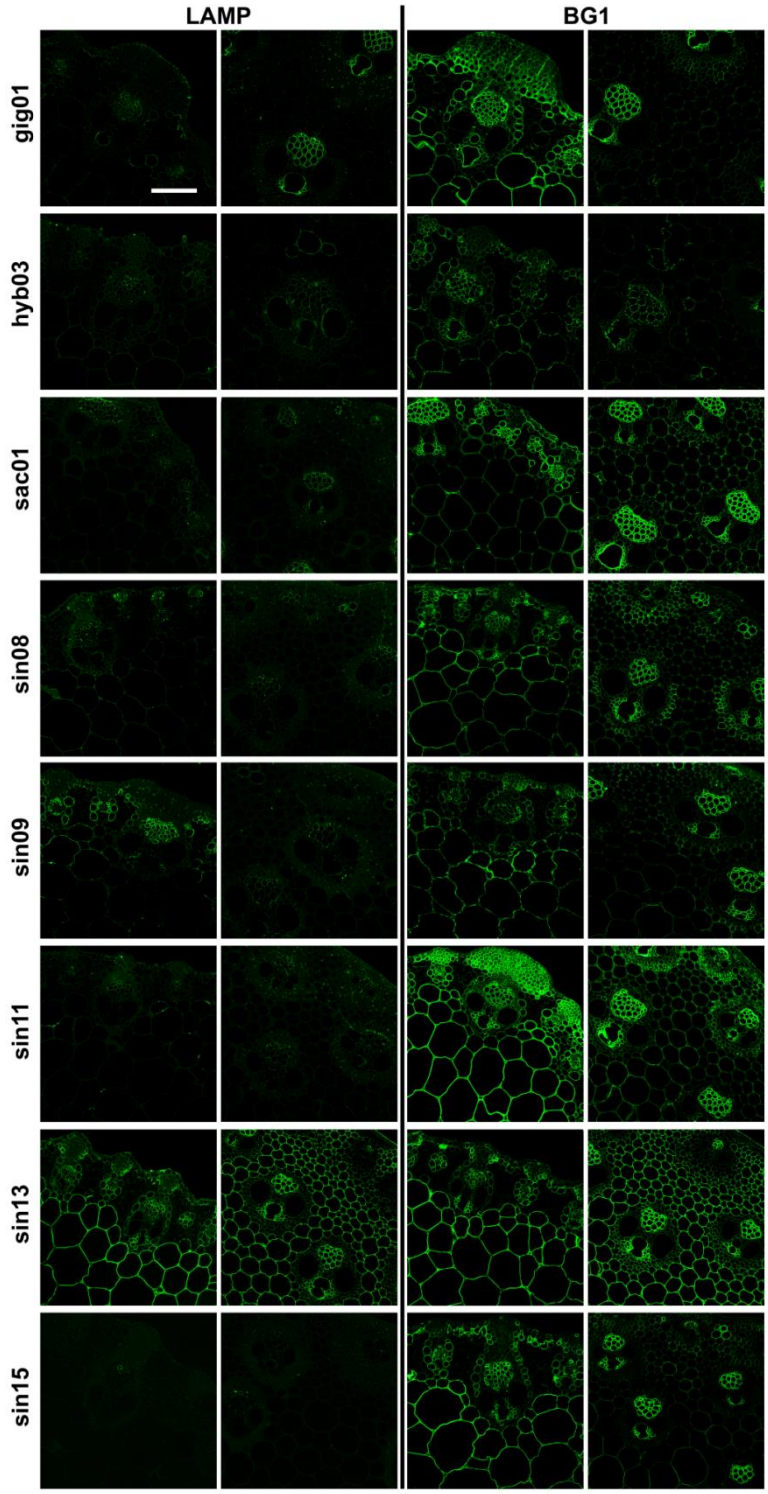

Fig. 5.23. Immunofluorescent labelling of transverse sections from leaves and stems of eight miscanthus genotypes with β-glucan binding mAbs. For each mAb, leaf is in the left column and stem is in the right. Scale bar: 100µm.

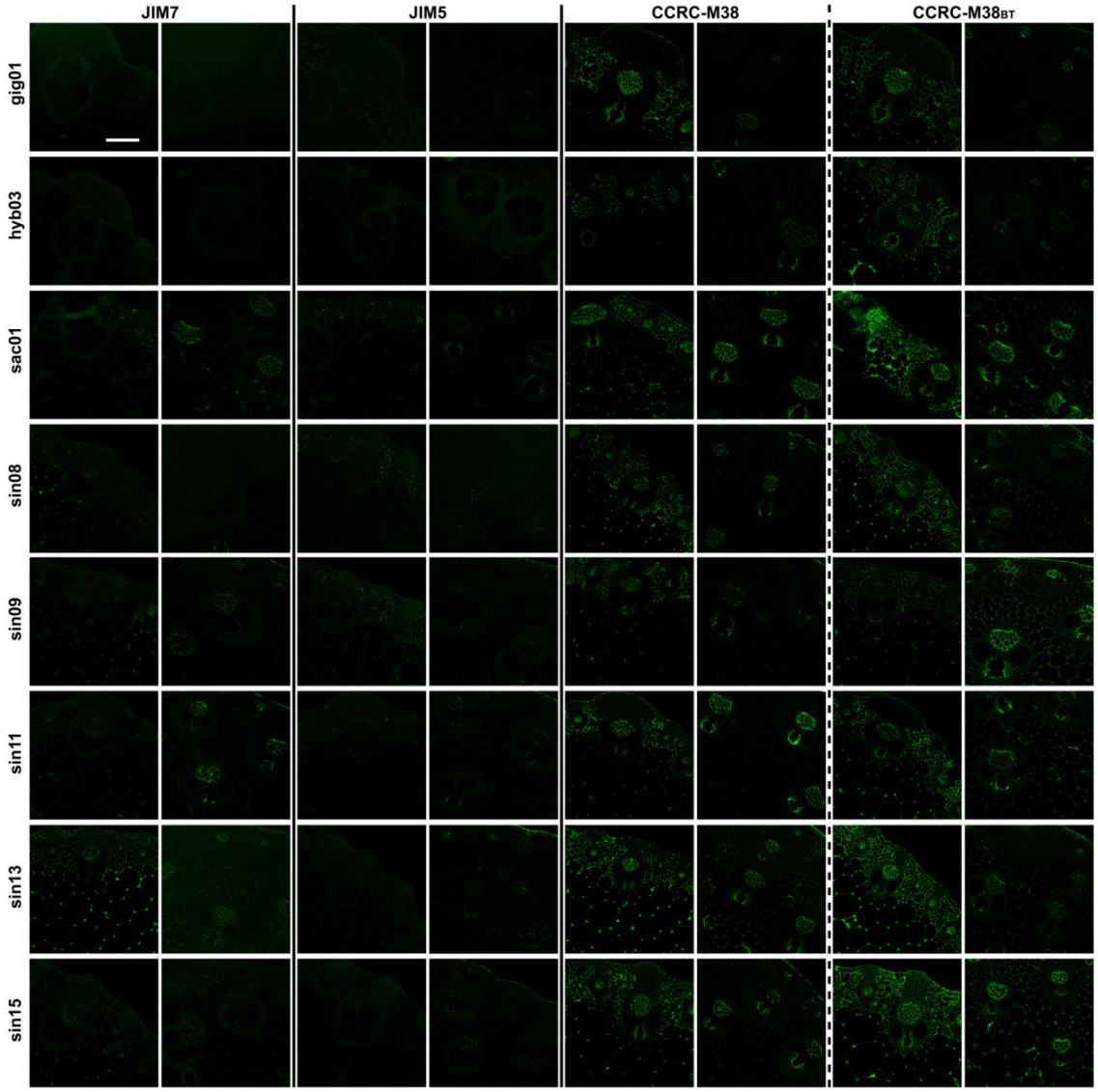

Fig. 5.24. Immunofluorescent labelling of transverse sections from leaves and stems of eight miscanthus genotypes with homogalacturonan binding mAbs. For each mAb, leaf is in the left column and stem is in the right. For CCRC-M38 immunolabelling was performed before and after a base treatment (BT) with 0.1M KOH. Scale bar: 100µm.

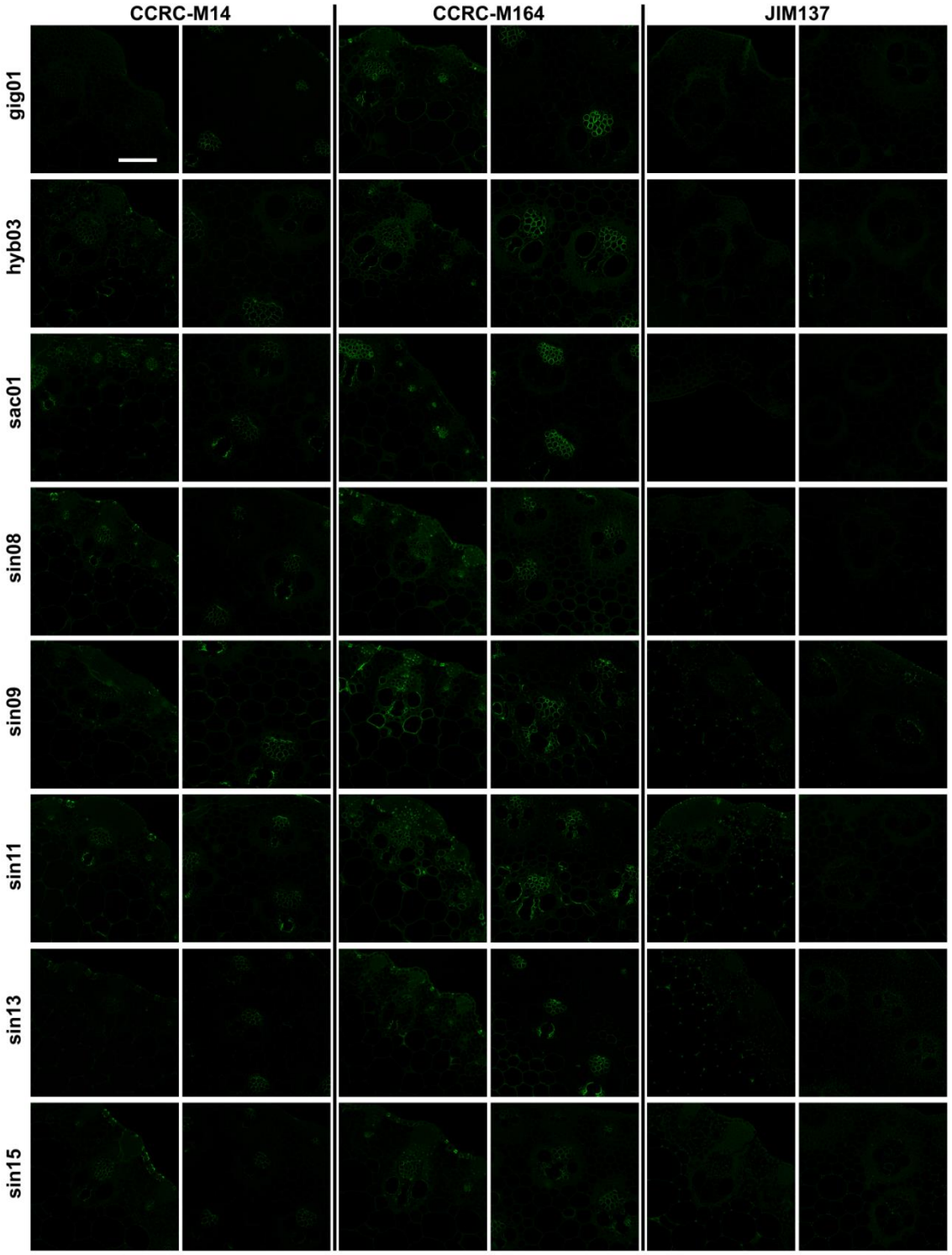

Fig. 5.25. Immunofluorescent labelling of transverse sections from leaves and stems from *M.* × *giganteus* (gig01) with rhamnogalacturonan-I binding mAbs. Scale bar: 100µm.

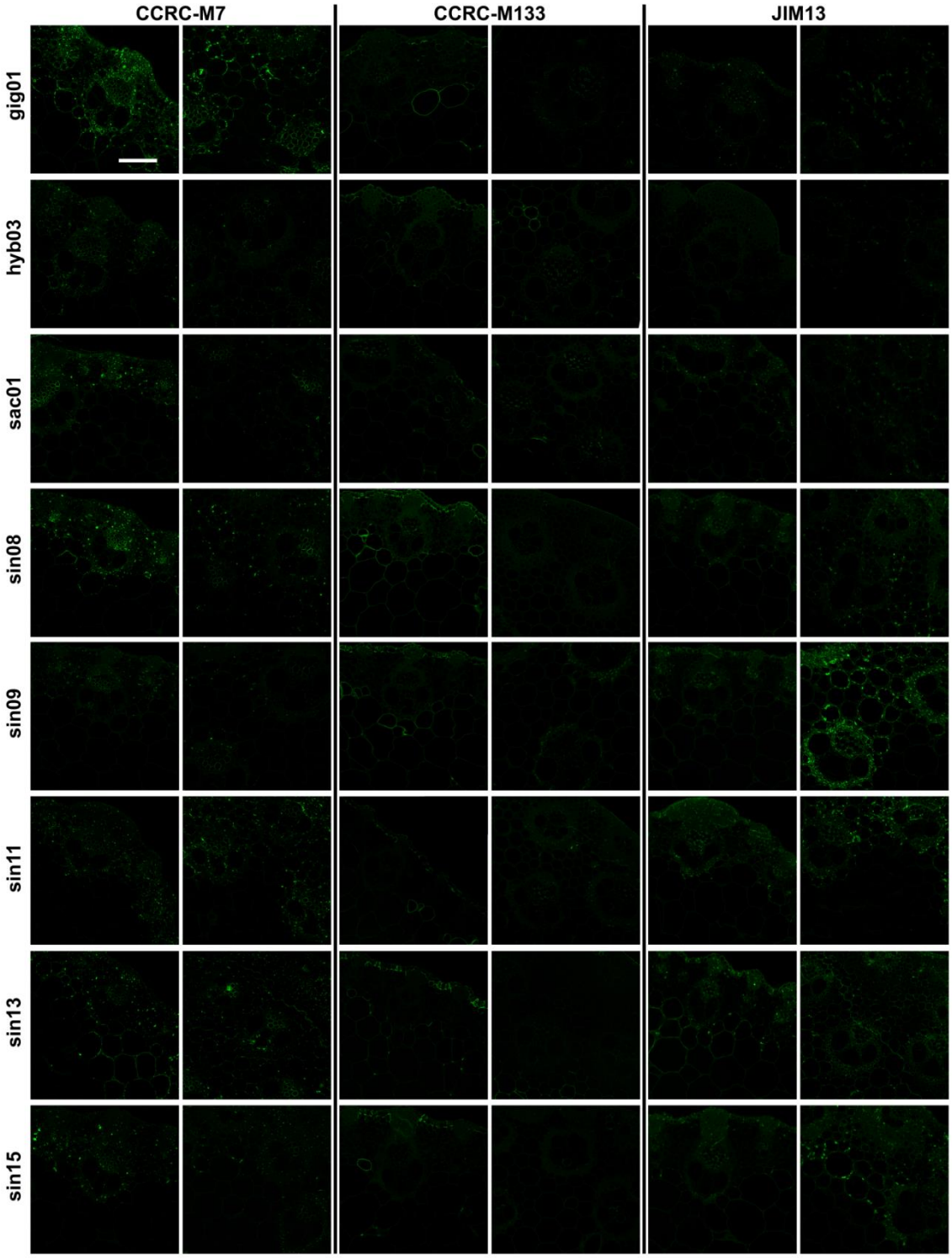

Fig. 5.26. Immunofluorescent labelling of transverse sections from leaves and stems of eight miscanthus genotypes with arabinogalactan binding mAbs. For each mAb, leaf is in the left column and stem is in the right. Scale bar: 100µm.

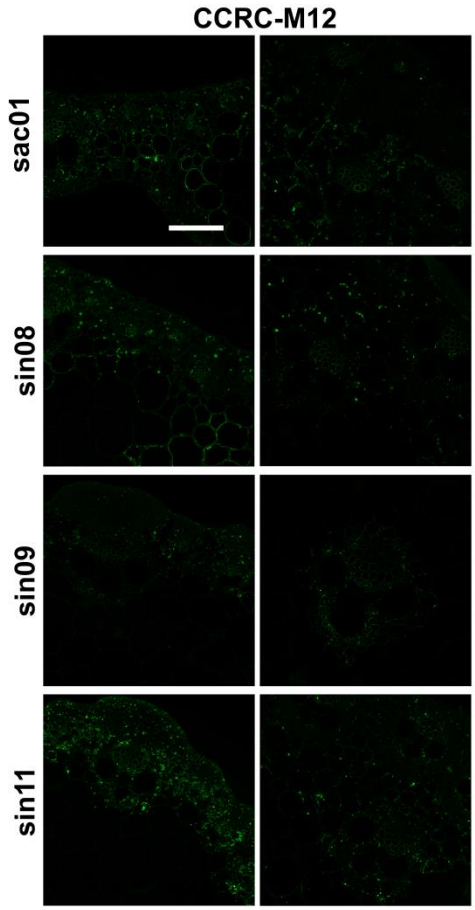

Fig. 5.27. Immunofluorescent labelling of transverse sections from leaves and stems of genotypes sac01, sin08, sin09 and sin11 with CCRC-M12, an arabinogalactan binding mAb. Leaf sections are on the left column and stem sections are on the right. Scale bar: 100µm.

5.3.3. Immunolabelling of Glycans in Leaf Margin Anatomical Structures

In order to validate GP results and to compare the glycan distribution patterns between miscanthus tissues, an immunolabelling study was performed, where sections of stems and of leaf midribs were compared (Chapter 5). However, during these histochemical studies it was observed that leaf marginal portions displayed labelling patterns which are unique to certain leaf-exclusive anatomical features; namely, bulliform cells, larger-sized stomatal complexes, and mesophylls. It was considered that this information was not essential to the aim of this thesis. Studies focused on the characterisation of cell wall glycans in miscanthus leaves are scarce in the literature. In view of that, a histochemical study was performed on six miscanthus genotypes, as a means to characterise glycan distribution patterns in leaf-specific anatomical structures. Results of this study are presented in the following figures. It is projected that the collected information will constitute the basis of a future publication, where possible functional implications of the presence of certain glycans on the cell wall of foliar tissues will be explored.

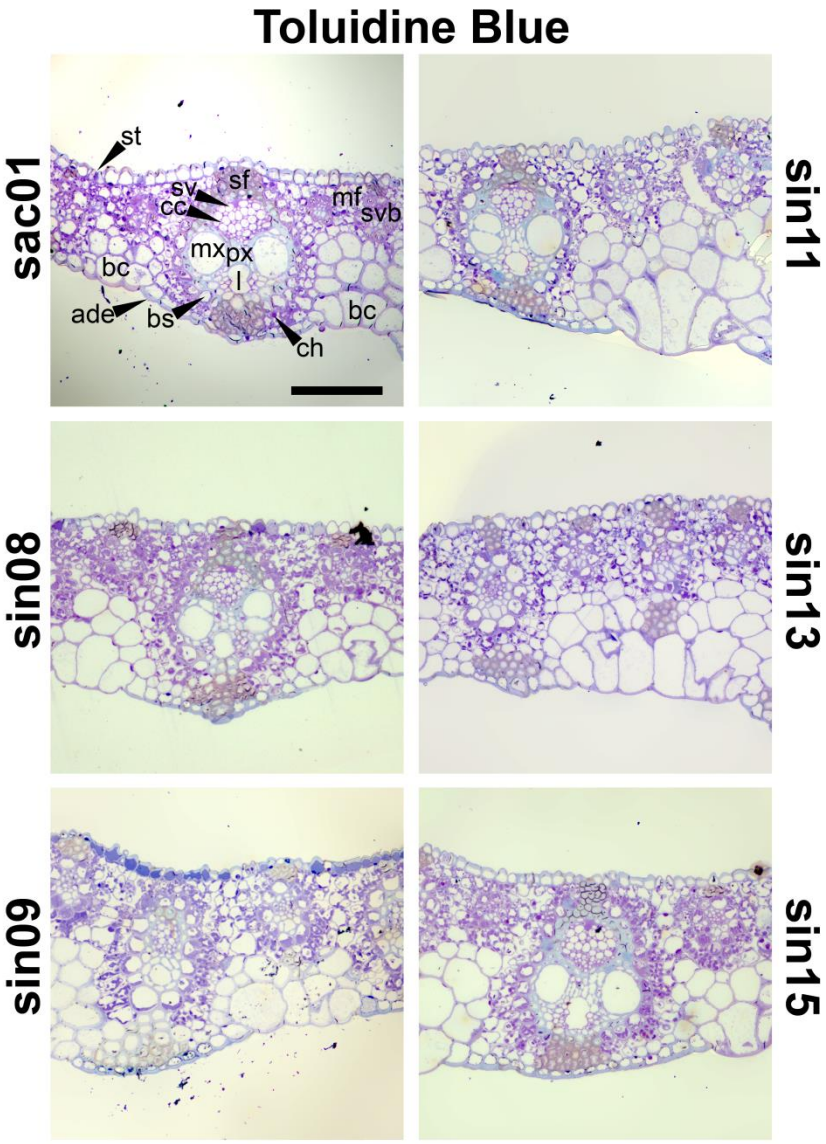

Fig. 5.28. Transverse sections of leaf margins from six miscanthus genotypes used for *in situ* immunolabelling, studies stained with toluidine blue. Legend: adaxial face epidermis (ade), bulliform cells (bc), bundle sheath (bs), chloroplasts (ch), companion cell (cc), mesophyll cells (mf), metaxylem (mx), protoxylem (px), protoxylem lacuna (l), sclerenchyma fibres (sf), sieve tube element (sv), small vascular bundle (svb), stomatal complex (st). Scale bar: 100µm.

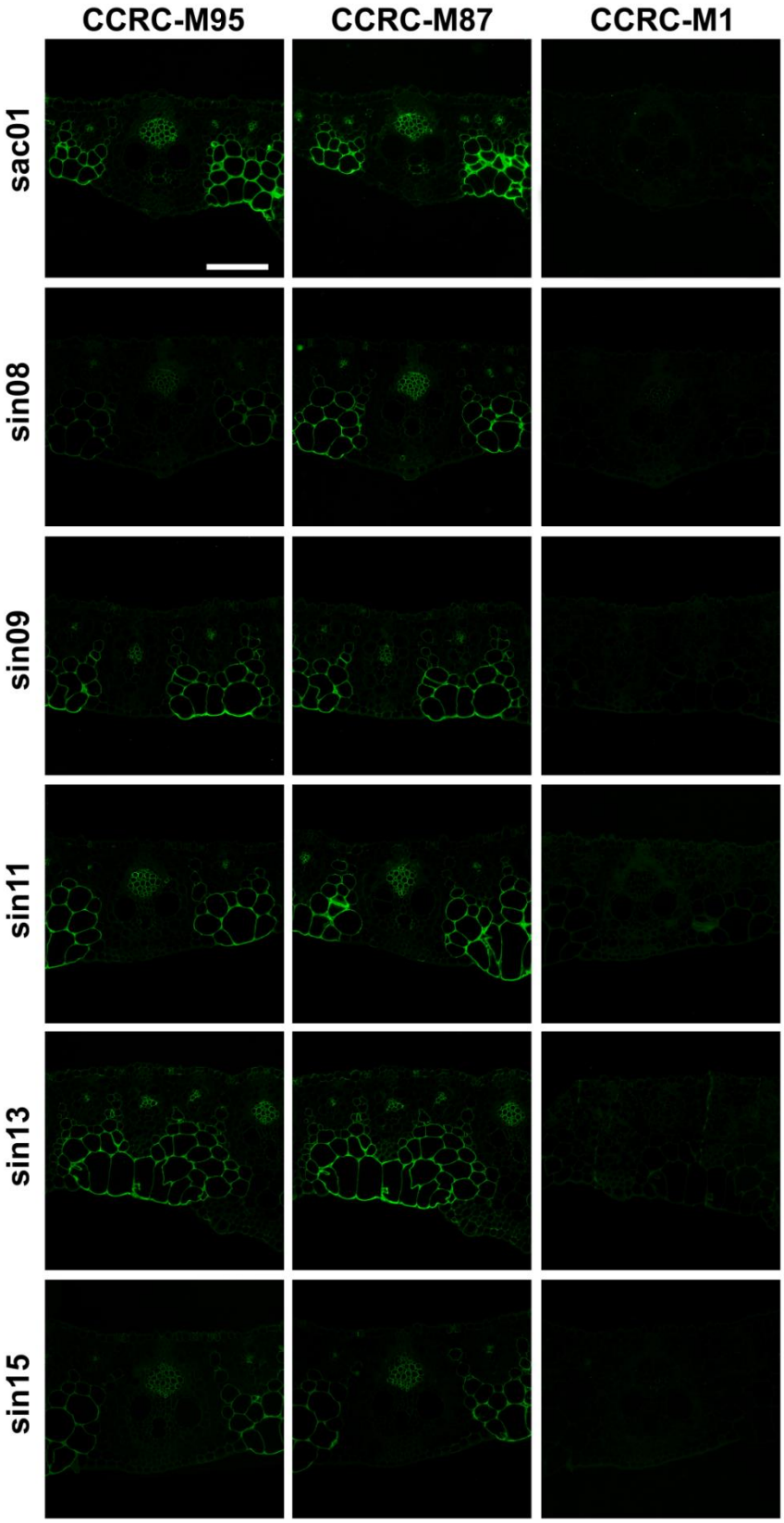

Fig. 5.29. Immunofluorescent labelling of transverse sections from leaf margins of six miscanthus genotypes with xyloglucan binding mAbs. Scale bar: 100µm.

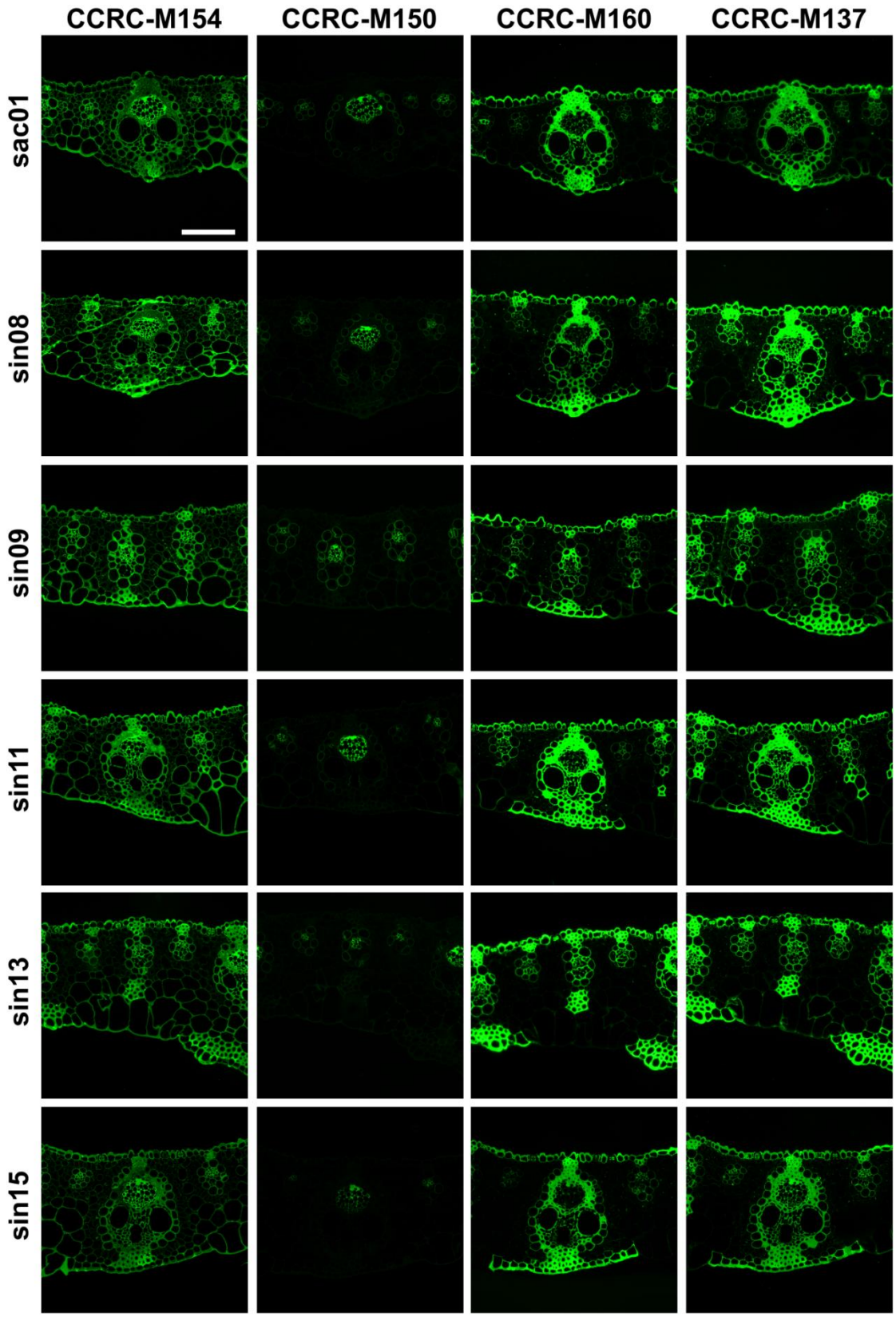

Fig. 5.30. Immunofluorescent labelling of transverse sections from leaf margins of six miscanthus genotypes with xylan binding mAbs. Scale bar: 100µm.

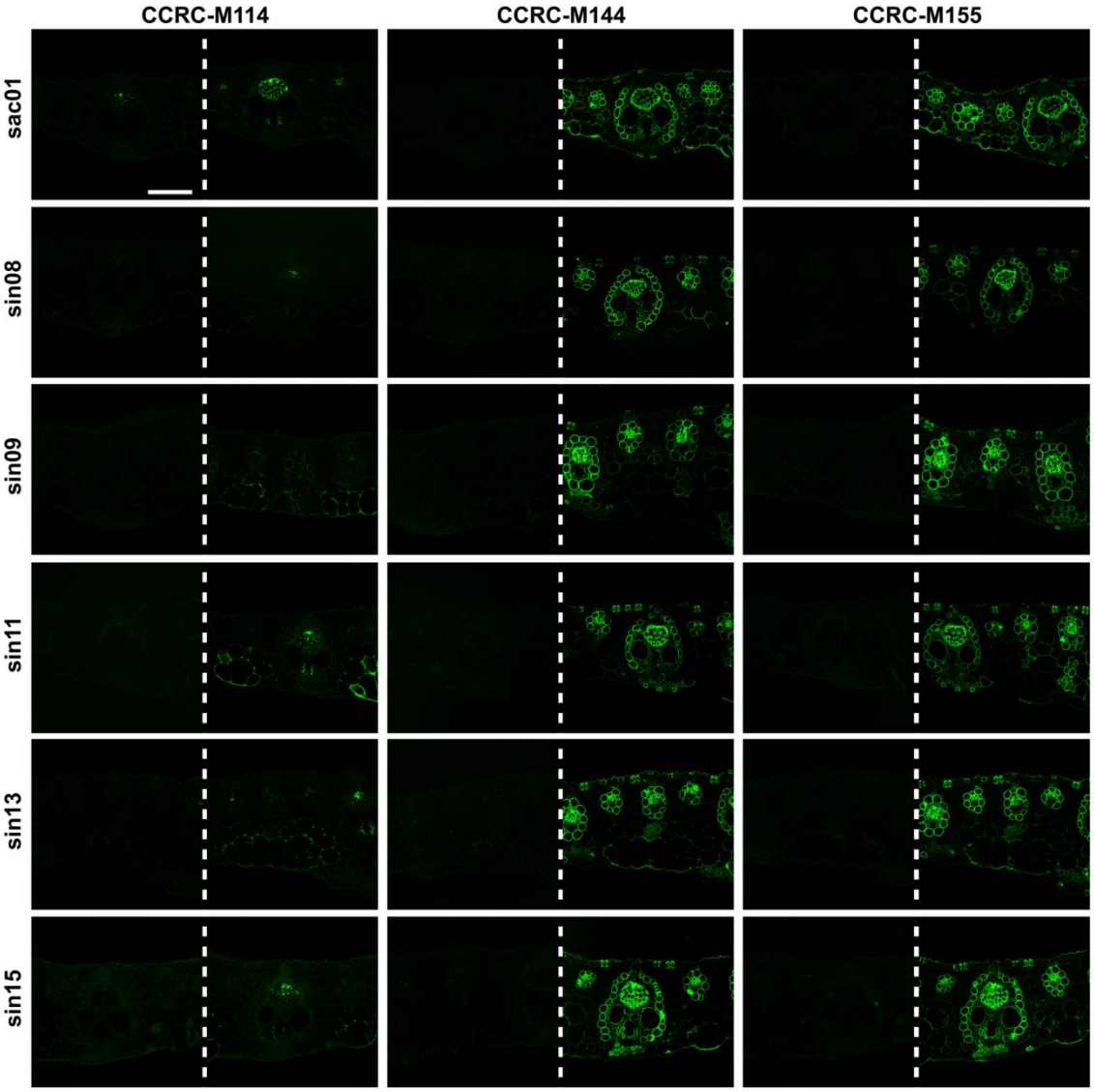

Fig. 5.31. Immunofluorescent labelling of transverse sections from leaf margins of six miscanthus genotypes with xylan binding mAbs, before and after (left and right side of dashed line respectively) a base treatment with 0.1M KOH. Scale bar: 100µm.

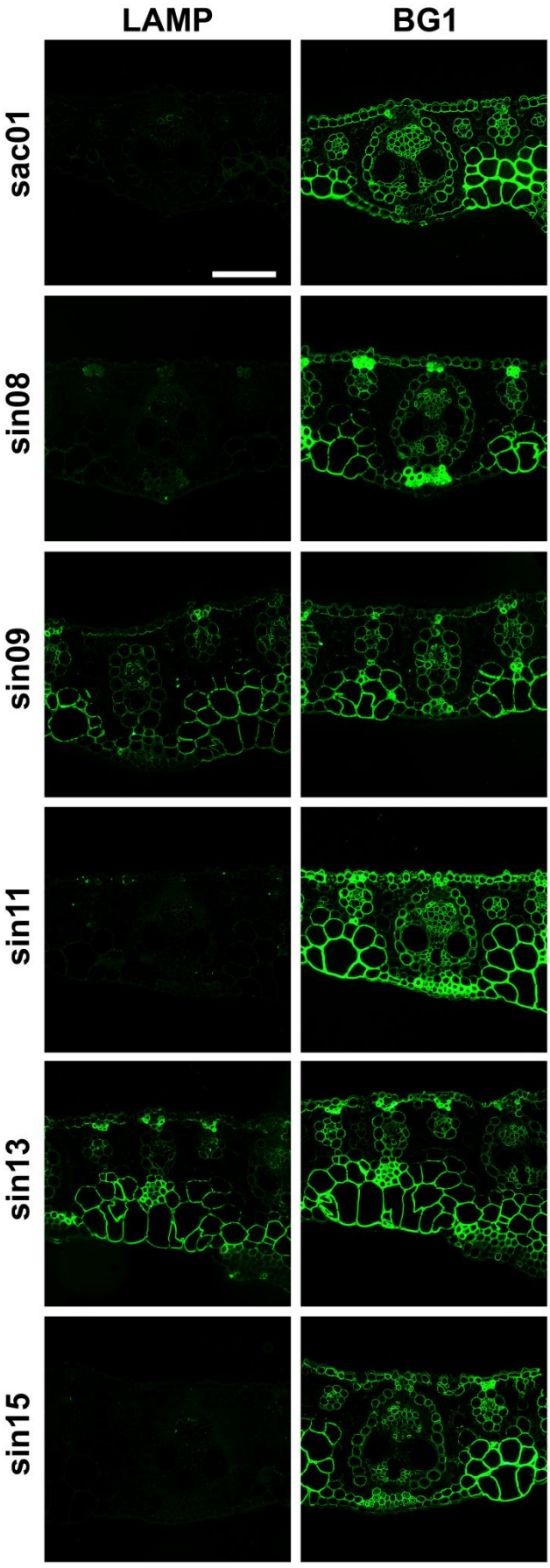

Fig. 5.32. Immunofluorescent labelling of transverse sections from leaf margins of six miscanthus genotypes with β-glucan binding mAbs. Scale bar: 100µm.

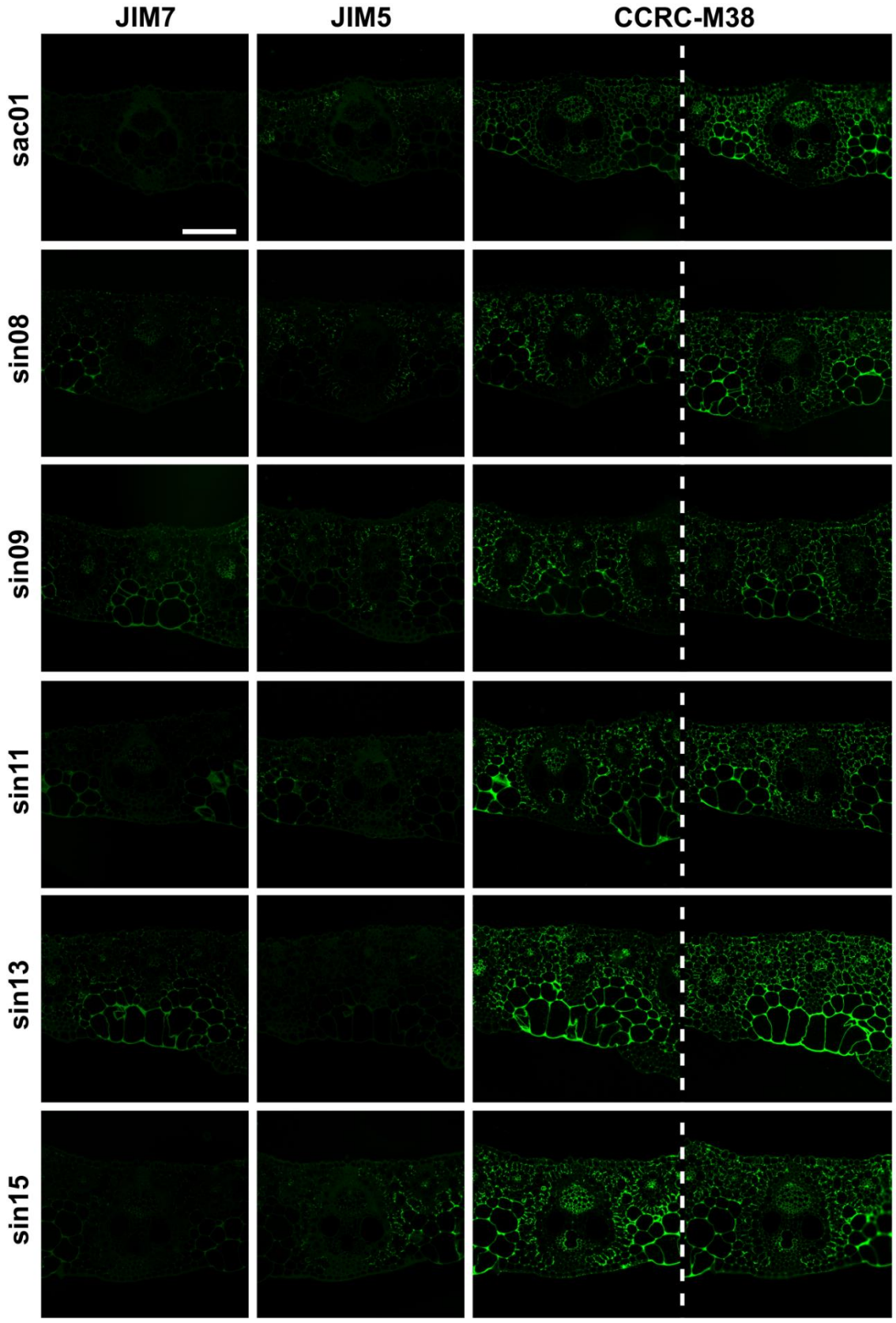

Fig. 5.33. Immunofluorescent labelling of transverse sections from leaf margins of six miscanthus genotypes with homogalacturonan binding mAbs. For CCRC-M38, immunolabelling was performed before and after (left and right side of dashed line respectively) a base treatment with 0.1M KOH. Scale bar: 100µm.

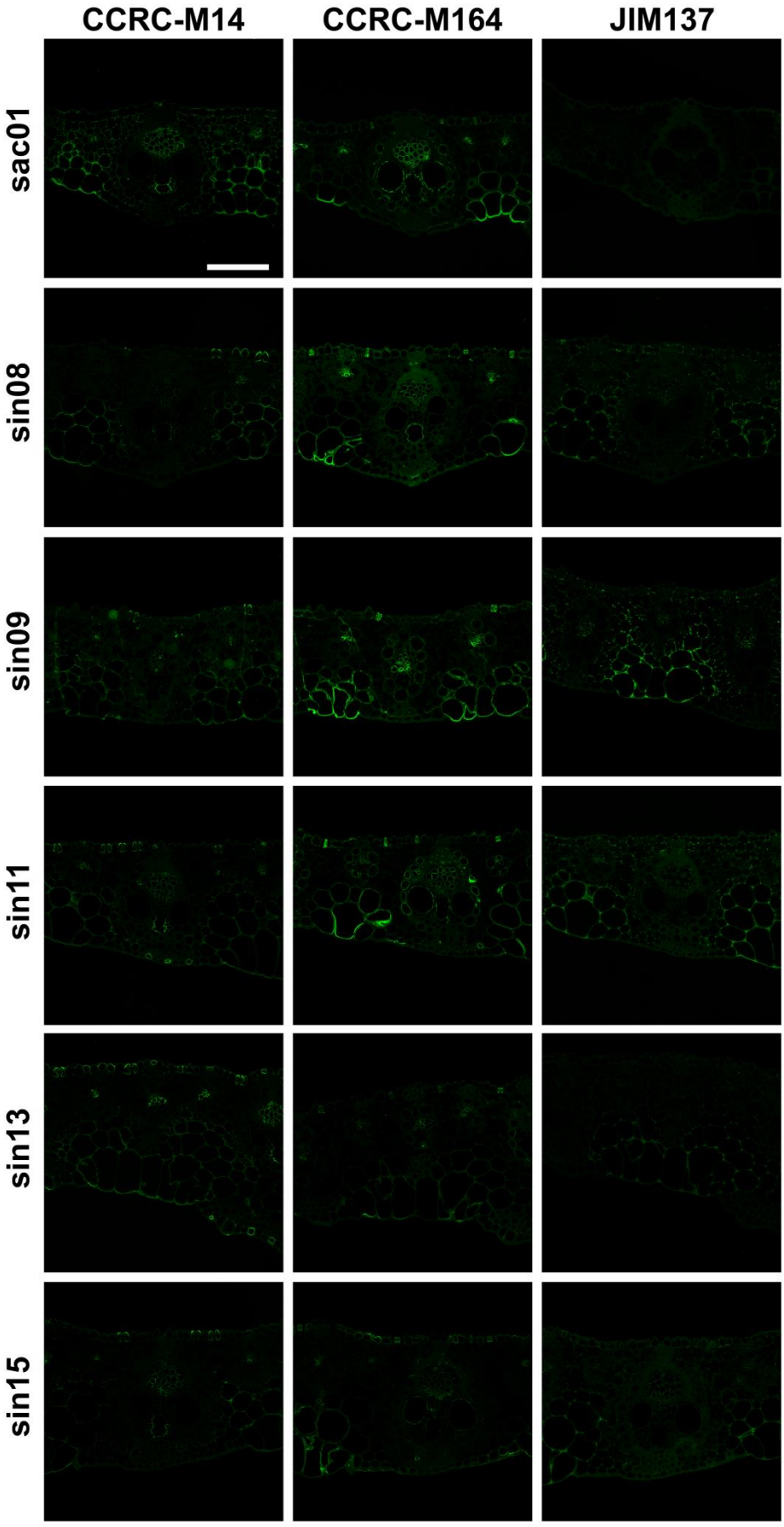

Fig. 5.34. Immunofluorescent labelling of transverse sections from leaf margins of six miscanthus genotypes with rhamnogalacturonan-I binding mAbs. Scale bar: 100µm.

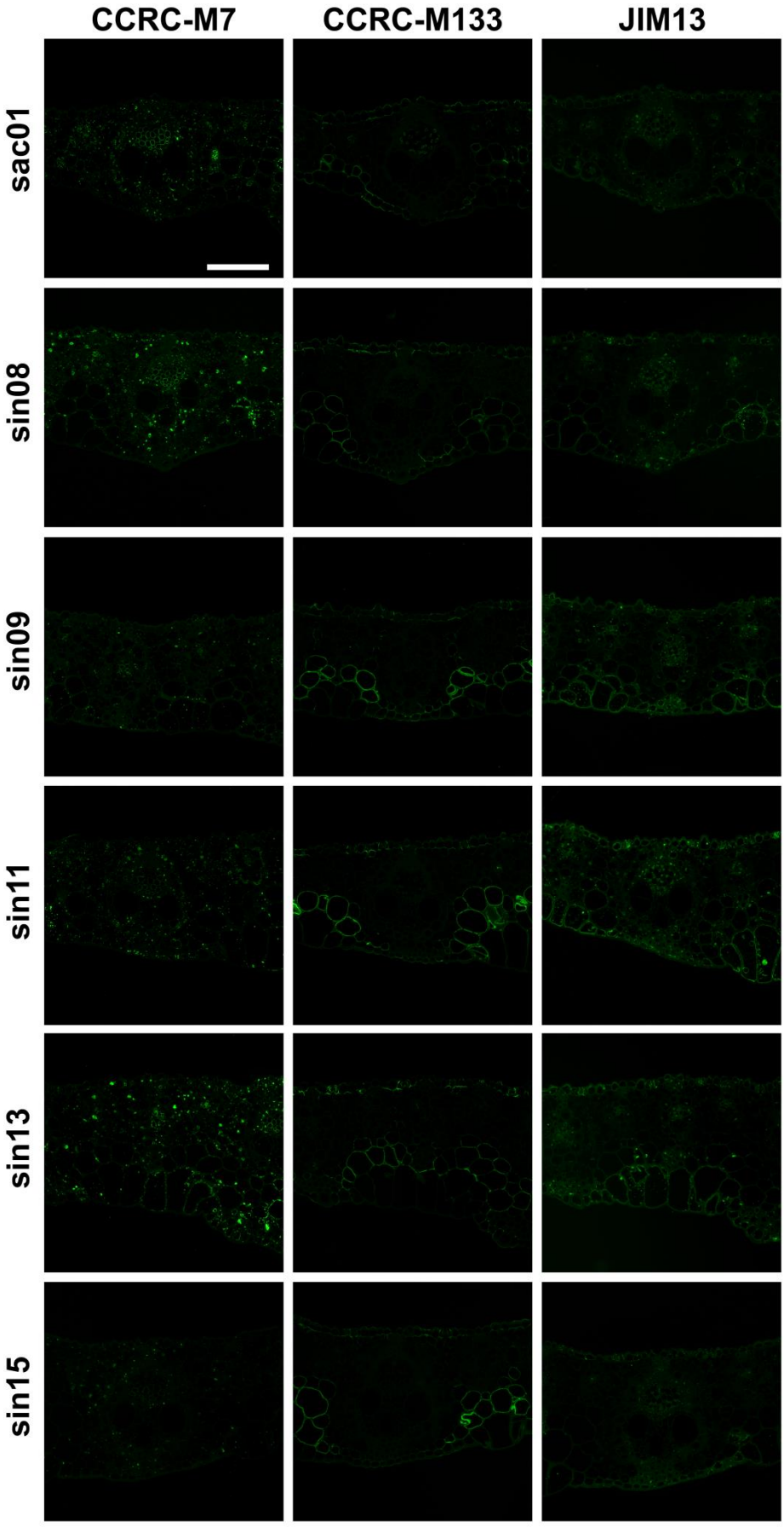

Fig. 5.35. Immunofluorescent labelling of transverse sections from leaf margins of six miscanthus genotypes with arabinogalactan binding mAbs. Scale bar: 100µm.

5.4. Conclusions and Summary of Findings

A study of structural glycan composition and distribution in miscanthus tissues originating from different sources is of interest not only to further our fundamental understanding of the cell wall, but also for the optimisation of lignocellulosic biomass utilisation as a feedstock for renewable bioproduct and bioenergy solutions. For these aims, two distinct but complementary immunological approaches were put in practice to characterise the carbohydrate fraction of miscanthus cell wall and the results are presented in this chapter. Several relevant observations related to composition, structure and possible interactions between cell wall polysaccharides are reported. Furthermore the results of a comparative study have identified key cell wall glycan differences between developmental stages and tissues.

The molecular probes used in these studies possess enough variability to allow the probing of most classes of plant cell wall polysaccharides (Appendix C), and for the first time this array of glycan-directed mAbs was used to comprehensively characterise the cell wall glycome of miscanthus across different harvest times, tissues and genotypes. Despite most of the mAbs used here having been characterised in terms of their binding affinities (Pattathil *et al.*, 2010), the recognised epitope structures are not always completely known. Nevertheless, the lack of precise knowledge of epitope structures does not eliminate the usefulness of implementing cell wall glycan-focused immunological approaches, as it still permits identifying and drawing conclusions regarding essential differences between samples, which help steer research directions.

During the first immunological approach presented here, it was seen that miscanthus cell wall samples present complex and at times significantly variable glycome profiles between developmental stages and tissues. Most of the tightly bound xylan epitopes found in the KOH-produced cell wall fractions do not vary considerably between developmental stages. However, in other extracts there are variations in some subclasses of epitopes, which may indicate deep

structural differences and varied associations between the polymers; in particular with lignin. Indeed, the glycome profile of chlorite fractions, which contain glycans associated to lignin, has shown that different abundances of xylan, β-glucan and several pectin epitopes may vary quite notably between tissues and developmental stages (Fig. 5.4). For the more labile epitopes removed from the wall in the first steps of the sequential extraction, differences were observed in the abundances of hemicelluloses and pectins along development; which are overall more significant in leaves than in stems. In both tissues the proportions of more labile oxalate- and carbonate-extracted xylan, RG-I and AGN were small, but more abundant in actively growing plants. For other probed pectin epitopes, higher abundances were detected in later developmental stages; namely, binding to RG-Ib epitopes was extremely low in the carbonate extracts from actively growing plants, but increased in later developmental stages, and also with the utilisation of harsher solvents.

Some of the differences between tissues in the 4M KOH fractions are common to the pre- and post-chlorite versions of these extracts. This observation allowed inferences about the occurrence of the more recalcitrant 4M KOH-extracted glycan epitopes; namely that tightly bound xylans (5 – 7) and XG are more abundant in stems, whereas tightly bound epitopes associated with RG-I and xylan (3 and 4) are more common in leaves. However, fraction-specific differences between tissues were also detected, depending on whether the CWM had been de-lignified or not. In 4M KOH PC fractions, in addition to all probed XG epitopes being more abundant in stems, they were also more abundant in senesced samples; suggesting that after senescence, miscanthus cell walls contain bigger proportions of these tightly bound hemicellulosic epitopes associated with lignin, than in earlier developmental stages. Furthermore, 1M KOH-extractable XG is strikingly more abundant in samples from younger plants in general, but particularly from leaves. Given that these epitopes were extractable with the weakest of the employed KOH solutions, they are presumably more loosely bound to the

other wall polymers. It has been reported for type-I cell walls that XG associates with cellulose to form a network, which provides structural support for the growing cell wall (Hayashi, 1989; Pauly *et al.*, 1999). In type-II cell walls, XG is typically present in reduced amounts, with AX (specifically GAX) thought to perform roles structurally analogous to XG from type-I cell walls (Carpita and Gibeaut, 1993; Carpita, 1996). Furthermore, it is known that as miscanthus tissues mature, the AX from the GAX-cellulose framework becomes far more abundant in the cell wall, and that there is a higher abundance of secondary walls in older internodes than leaves and sheaths (Le Ngoc Huyen *et al.*, 2010). Altogether, this could suggest that XG epitopes are more abundant in the earliest developmental stage and in leaves as a result of lower proportions of cells which have completed secondary wall deposition.

Loosely bound MLG epitopes were released more abundantly from younger tissues in the first three cell wall fractions of the extraction series, whereas more tightly bound epitopes were more abundant in leaf tissues than in stems. Generally high binding signals were detected for β-glucans in the harsher alkaline cell wall fractions, and also in the chlorite fractions of leaves. These findings are in accordance with data reported for switchgrass (Shen *et al.*, 2013), sugarcane (de Souza *et al.*, 2013), corn stover (Li *et al.*, 2014a), and with various studies proposing associations of MLG with cellulose (Carpita, 1996; Fry, 2010; Kiemle *et al.*, 2014). It should also be noted that the results presented here are not entirely concordant with another glycome profiling study on miscanthus cell wall (de Souza *et al.*, 2015); however, the data reported by these authors may not be completely comparable with the results presented here, as the order of the sequential extraction was not the same, and NaOH was used instead of KOH. It is possible that these alterations produce distinct patterns of cell wall fractionation.

For the more easily extracted RG-I and AGN side-chains, leaves typically contained higher abundances, whereas loosely bound AGN epitopes (3 and 4) and xylans (3 and 4) tended to be more abundant in stems. In the 1M KOH fraction, which represents the biggest proportion

of extracted polysaccharides, the main varying characteristic between tissues was the fact that the CWM from leaves typically contained higher abundances of almost all probed glycans. However, for some epitopes the discrepancy between leaf and stem was more significant; namely concerning β-glucans, HG and non-fucosylated XG. Leaf cell wall samples had higher binding signals for HG backbone in the first three extraction steps, but differences between tissues were reduced in both 4M KOH fractions. This suggests that despite more loosely bound HG epitopes found in oxalate, carbonate and 1M KOH fractions being more abundant in leaves, there is a population of tighter bound HG epitopes which does not differ substantially between tissues.

Remarkably, binding to tightly bound RG-Ib epitopes was extremely low in actively growing samples, but at the later PB and SS stages, intensities were increased, particularly in the CWM from leaves. However, the highest release of these epitopes was observed in the 4M KOH fractions after lignin removal. These observations indicate that the release of a population of these epitopes was initially blocked by lignin, and could only be extracted after the chlorite treatment with 4M KOH. Binding to RG-I backbone structures was typically low in all miscanthus cell wall fractions. Nevertheless, for the epitopes recognised by CCRC-M14 the signals became slightly higher in the later steps of the sequential extraction. Differences between tissues and developmental stages were not substantial, but were higher for leaf samples. The fact that distinct binding to CCRC-M14 could only be detected in the cell wall fractions extracted with KOH and sodium chlorite suggests that the recognised epitopes occur in tightly bound pectic structures, which could be involved in linkage to lignin, as has also been proposed by other authors (Wi *et al.*, 2005; DeMartini *et al.*, 2013; Shen *et al.*, 2013). Finally, binding intensities to tightly bound RG-I/AGN epitopes in the chlorite and 4M KOH PC fractions were found to be higher in leaves at the AG and PB stages, but in senesced plants the differences between tissues were not substantial.

Many of the most interesting comparative observations made between the CWM from stem and leaf, as indicated by GP, were verified by using key mAbs for *in situ* epitope immunolocalisation. Within the hemicellulose-directed mAbs, more intense labelling of XG epitopes in stem sections is consistent with the glycome profiles observed for leaves and stems. Mixed results for xylan immunolabelling, are in agreement with information derived from GP, showing that some of the more labile epitopes are more abundantly detected in stem extracts, but for more recalcitrant xylans, abundance differences between tissues are less marked. Both β-glucan-directed mAbs, but particularly for the MLG-binding BG1, epitopes were more abundantly detected in leaf cell wall fractions, and in the *in situ* immunolabelling patterns of foliar sections.

Within pectin-binding mAbs, for the first three steps of the sequential extraction, the glycome profiles of leaves were particularly high in HG backbone epitopes compared to stems. Similarly, for RG-I epitopes, GP suggested that they are more abundant in leaves; based on the fact that, when compared to stems, binding intensities were higher for leaf samples in most cell wall fractions produced during the sequential extraction. Immunolabelling results appear to substantiate both these observations, as HG backbone-2 mAbs (JIM5, CCRC-M38, CCRC-M131) and RG-I related mAbs (CCRC-M72 and CCRC-M164) showed more abundant labelling patterns in leaf sections (Figs. 5.12 and 5.13).

For AGN, based on GP results, epitope abundances vary depending on the mAb subclass used. CCRC-M133 (AGN-3) showed particularly higher binding intensities in leaves; whereas signals for JIM13 (AGN4) were typically more intense in stem cell wall extracts. To a certain extent these disparities between AGN classes were also detected in the *in situ* immunolabelling study (Fig. 5.14), as the cellular structures labelled by CCRC-M133 and JIM13 seem respectively more abundant in leaf sections, and in stem sections. The relevance of comparing relative immunolabelling abundances between leaves and stems is reasonably valid when data

derived from parallel analytical procedures (such as GP) is also taken into consideration. However, it is important to note that inferences regarding epitope abundances in the overall leaf or stem biomass should not be solely based on immunolabelling data. Indeed, some epitopes may remain undetected as a consequence of other wall components interfering with *in situ* mAb access to epitopes, and some glycan epitopes may be located in specific cells or subcellular structures, which are not in the plane of the section taken for immunohistochemistry study (Avci *et al.*, 2012).

Altogether, these compositional disparities in the carbohydrate composition of miscanthus cell walls are in strong agreement with the FTIR-PCA results (Section 2.3). The GP-PCA approach employed in this chapter allowed the detection of significant variation between developmental stages and tissues. These differences are largely coincident with the main FTIR-PCA conclusion that structural polysaccharides are main contributors to the compositional variability during plant development and between stem and leaf tissues (See discriminant wavenumbers in Fig. 2.4 F, G and in Table 2.4). The PCA analysis of the FTIR and GP datasets may also indicate the occurrence of differences between tissues, and developmental stages in the structure of specific polymers. Namely for pectin polysaccharides, both approaches suggested that structurally different pectins may occur in leaf and stem tissues and also in plants of varying maturation. Ultimately, the FTIR-PCA approach indicated that the composition of the cell wall does not vary substantially throughout development for leaves, whereas it does for stems. Conversely, in GP-PCA clear clusters along developmental stages emerged in the scores plots of some cell wall fractions from leaves, but never from stems (Compare Figs. 5.5 F – H and Fig. 8.8.C. in appendix H). Since FTIR provides an overall picture of both carbohydrate and non-carbohydrate components of the cell wall (Carpita and McCann, 2015), the fact that significant differences were observed for stem samples by FTIR-PCA, but not by GP-PCA, could indicate that the variation along development in stems is not

primarily associated to the most abundant matrix polysaccharides; which are xylan hemicelluloses in type-II cell walls (Carpita, 1996). Indeed, of the cell wall components detected by FTIR-PCA as significantly varying between mature and immature stem tissues, all were associated with cellulose, pectin and lignin (Fig. 2.4G and Table 2.4). Further support comes from comparison of the glycome profiles of stem cell wall fractions from different developmental stages (Fig. 5.4), this shows that AG samples have higher abundances of pectic epitopes, but xylans vary comparably less between developmental stages. On the other hand, for leaves, FTIR-PCA did not detect significant differences between developmental stages, however, GP-PCA detected clusters comprising of mature and immature samples, but only in the first three steps of the sequential extraction. This could indicate that between leaf cell wall samples from different developmental stages, the more labile matrix polysaccharides do vary significantly, but the same is not observed for most of the more tightly bound polysaccharides. Considering that more labile epitopes are also less abundantly released, this may explain why these differences between developmental stages were not detected during FTIR-PCA. In short, it appears that variation in structural cell wall components, between mature and immature stems, are primarily associated to non-matrix cell wall components, and to a lesser extent to pectin. By contrast, the overall composition in leaf biomass originating from different harvests is less varied than in stems, but differences could be statistically identified in more labile and less abundant glycan epitopes amenable extraction with ammonium oxalate and sodium carbonate.

Immunolabelling data further suggested that biomass compositional differences between leaves and stems are likely to be associated with distinct abundances of certain cell types and cellular structures, which have different roles in the tissues and therefore require function-specific compositional features. Furthermore, observations that certain immunolabelling patterns are tissue-exclusive suggested that the occurrence and location of certain glycan

epitopes is associated with functional requirements of the tissues. Although overall HG epitope levels are typically detected in greater abundance in leaf samples, higher and lower degrees esterification have opposed effects on cell wall properties. Therefore, the observed higher abundance of un-esterified HG in foliar tissues could be associated to a coping mechanism intended to increase cell adhesion and thus rigidify the tissues as a response to lower cellulose and lignin content when compared to stems (Willats *et al.*, 2001a; Wolf *et al.*, 2009). In other cases, certain glycan epitopes, which based on their location, may be involved in providing structural reinforcement (e.g., corners of intercellular spaces), or protection against external attack (e.g., epidermal cells and cuticles), are presumably integrated in polysaccharide structures which enhance tissue resistance to deconstruction. Consequently, higher abundances of these epitopes may suggest higher recalcitrance of the polymers where they are included; and thus the study of their distribution may provide further insights into which glycan epitopes have more relevant effects on lignocellulosic biomass saccharification. Some of these cases may explain why the yields of enzymatically released Glc are lower in stem biomass including at later developmental stages (Fig. 4.7). Namely, XG epitopes were only abundantly released with harsh 4M KOH solutions, which indicates that associated glycans are tightly bound to the wall, presumably interacting with cellulose microfibrils. The immunolabelling data presented in this chapter is in agreement with this possibility, as XG epitopes were found to occur in middle lamellae and primary walls of *M.* × *giganteus* tissues. Additionally, when compared with leaves, XG is detected in greater abundance in stem biomass, thus possibly contributing to the greater recalcitrance to saccharification observed in this tissue. Additionally, GP showed an increase in the abundance of un-esterified HG epitopes as plants mature. Considering that HG de-esterification has the effect of promoting cell adhesion, and recalcitrance to saccharification (Lionetti *et al.*, 2010), it is possible that the higher levels at which less methyl-esterified HG occurs in mature plants represents a reason for biomass from later harvests

typically having lower saccharification yields. In previous sections of this thesis, the carbohydrate component of the cell wall has been determined to be a main contributor to compositional variability between miscanthus samples from different origins. This variability was hypothesised to have an effect on cell wall digestibility (Chapter 2) and amenability to enzymatic hydrolysis (Chapter 4). With the data reported in the present chapter, some possible explanations for possible impact of glycan structures on recalcitrance have been presented. However, it is important to mention that other factors are known to affect cell wall deconstruction, such as interactions with cellulose, and esterification of xylan polymers, which allows acetylation, hydroxycinnamoylation and the formation of linkages with lignin[*]. Ultimately, another structural feature that might enhance saccharification yields in leaves is the structure of these tissues, which are to a great extent composed of mesophyll and large parenchymatous cells in the ground tissue, with typically thinner walls than in stems. It is likely that these finer structural features are more amenable to hydrolytic enzyme access, and thus contribute to sugar release.

[*] These topics will be mentioned again in the final chapter of the thesis.

6. GENERAL DISCUSSION, CONCLUSIONS AND FUTURE WORK

6. General Discussion, Conclusions and Future Work

The lignocellulosic materials encased in the plant cell walls represent a largely untapped renewable resource for the production of biofuels, and other biomaterials with relevant economic and industrial applications. However, with an estimated 10% of plant genomes encoding proteins involved in the synthesis, modification and deconstruction of the cell wall (Carpita and McCann, 2015), these structures emerge as very complex and intricate networks of biopolymers. Accordingly, for the aim of optimally utilising cell wall biomass as a renewable source of useful molecules, it is vital to further our knowledge regarding how walls are compositionally and structurally assembled.

Lignocellulosic feedstocks may consist of agricultural residues, forestry wastes, municipal solid waste, industrial and food processing wastes, and dedicated energy-crops, such as *Miscanthus* spp.. Miscanthus was the subject of the studies in this thesis, as its cell wall was dissected by a diverse set of tools, which were employed in order to cope with the complexity of plant cell walls. Studies were performed in terms of wall composition, structure and digestibility, initially on 25 miscanthus genotypes (Table 1.1), using FTIR, acetyl bromide lignin quantitation, and a bioassay for the measurement of *Clostridium phytofermentans*-mediated digestibility. Subsequently, the focus was shifted to 8 of these genotypes (Section 2.5), and more detailed studies were performed on their cell wall, namely: determination of cell wall acetylation, ester-linked HCAs, total carbohydrate and individual monosaccharides; assessment of the enzymatic saccharification with and without an alkaline pretreatment; and two immunological approaches for the study of non-cellulosic cell wall glycans, glycome profiling and *in situ* immunolabelling.

Previous chapters of this thesis have described each of these approaches and reported results from the relevant experiments. In this final chapter the aim is to establish associations

between cell wall constituents in miscanthus and, make inferences about their effect on cell wall saccharification, so that new and relevant information may be provided. Final data and conclusions are presented with the aim of contributing to our understanding of the complexity and diversity of plant cell wall constituents and help underpin their respective roles. Ultimately, it is expected that this information may lead to new research directions and contribute to the optimal industrial utilisation of lignocellulosic feedstocks.

6.1. Cell Wall Constituents, Associations, and Impacts on Saccharification

6.1.1. Composition of Miscanthus Cell Walls

As seen in previous chapters, cell wall composition of the miscanthus genotypes used in this study show significant differences between tissues and developmental stages. However, in all analysed samples, glucose is the single most abundant monosaccharide in the cell walls (Fig. 6.1), indicating that glucans, essentially cellulose, and to a lesser extent MLG (Domon *et al.*, 2013), are the predominant carbohydrates in leaf and stem biomass at all harvest times considered. Lignin makes up the second biggest proportion of the cell wall, followed by xylose, acetate and arabinose. For the minor constituents of miscanthus cell walls, the relative proportions differ between tissues. In leaf cell wall biomass, the abundance of galactose is typically higher than that of individual HCAs. By contrast, in stems, when compared to leaves, *p*CA typically represents a bigger proportion, and galactose levels are lower. Based on glycome profiling results (Fig. 5.4), galactose in miscanthus cell walls is essentially associated with AGN polymers, which were predominantly detected as side chains of RG-I (Chapter 5). In terms of the relative abundances of these carbohydrates, bigger proportions of galactose in leaf tissues are in accordance with the typically higher signals observed for the RG-I/AGN class of

mAbs in the glycome profile of leaves. Arabinose is also an integral part of AGN polymers; however, in the cell wall of miscanthus and of other grasses, most of the arabinose occurs as arabinosyl substituents of xylan, giving rise to AX, which is the main hemicellulose in miscanthus (Pauly and Keegstra, 2008; Le Ngoc Huyen *et al.*, 2010; Lygin *et al.*, 2011). This reported information, together with the glycome profiles, which showed high binding intensities to xylan epitopes (Fig. 5.4), confirm that the high abundance of xylose in the cell wall, may indeed be attributed to xylan. Additionally, as shown in Fig. 4.5, higher Ara/Xyl ratios in leaf CWM provides evidence for more ramified AX in this miscanthus tissue. Notably, acetate released upon de-esterification of the cell wall with 0.1M KOH, on average represented 4% of the miscanthus cell wall biomass dry weight. Considering that xylans are the main acetylated cell wall component (Pawar *et al.*, 2013), acetate abundance provides an indication of the acetylation levels of these polymers.

Given that *p*CA essentially occurs associated with lignin (Grabber *et al.*, 2004), the higher abundance of this HCA in stems is in agreement with the higher degree to which these tissues are lignified. It is thought that virtually all *p*CA is esterified to lignin (Grabber *et al.*, 2004). As a consequence, given that HCA quantitation was performed via de-esterification of the CWM, it is likely that the bulk of *p*CA has been released and estimated. However, a greater proportion of FA establishes ether-links to lignin, and may also form dimers and larger sized oligomers (Ralph *et al.*, 1994b; Buanafina, 2009; Agger *et al.*, 2010), which were not determined in the present study. Other undetermined cell wall components presumably include uronic acids, methyl groups, proteins, mineral components, or even small amounts of oligosaccharides resulting from incomplete hydrolysis of cell wall glycans. Percentages of these undetermined components are typically higher in leaves, become more abundant at the PB stage, and then reach a minimum in the CWM of senesced samples. Concerning the uronic acids, GlcA and GalA may occur as part of GAX and of pectic polymers. Glycome profiling

has shown that the binding of RG-I and HG epitopes are higher in leaves than in stems (Fig. 5.4), which would indicate higher proportions of these pectins in leaves. Poalean cell walls typically contain low protein levels (Carpita, 1996). However, in the intact biomass of leaves, crude protein levels are considerably higher than in stems (Mowat *et al.*, 1965), so it is plausible that in the prepared CWM of these tissues, protein also makes up a bigger proportion of leaf biomass. Other unaccounted components which make up cell wall biomass are ash, which is mainly composed of silica, and also other minerals. For miscanthus and other grass species, at an overall level, mineral components have been reported to be typically higher in the cell wall of leaves than of stems (Monti *et al.*, 2008; Xu, 2010).

Based on the principal components analyses of the FTIR and the GP data (Figs. 2.4 and 5.5), temporal variations in the structural composition of the cell wall, between mature and immature stems, appears to be primarily associated with non-cell wall matrix components (cellulose and lignin) and to a lesser extent with matrix polysaccharides (pectins). By contrast, the overall composition of leaf biomass originating from different harvests is less varied than that of stems, as the only differences which could be statistically identified were for more labile and less abundant glycan epitopes[*]. On the one hand, for lignin in stems, the FTIR-based prediction was that S-lignin is more abundant in mature stems (PB and SS), which is consistent with the larger overall variation in total lignin content observed between AG – PB (+2.7%) than between PB – SS (+2.0%; Fig. 6.1). For cellulose, in stems, the difference between mature and immature biomass was predicted to be mostly associated with structural features. The reason for this is the observed opposition of bands *d*, *f* and *i* in the PC1 loading plot for stem CWM (Fig. 2.4G). In lignocellulosic biomass, all three of these FTIR spectral bands have been attributed to cellulose (Table 2.4). Furthermore, based on previously reported differences in cellulose crystallinity between primary and secondary cell walls (Kataoka and Kondo, 1998;

[*] Detailed discussion in section 5.4.

Park *et al.*, 2013), it was proposed that differences in cellulose structure between immature and mature stems are a consequence of different degrees of secondary wall deposition.

As a percentage of the cell wall biomass, glucose levels typically decrease in stems and in leaves between AG and PB, which might be a reflection of the reduction in MLG abundance in biomass from later harvests (Section 5.1.4), as it is known to preferentially accumulate in younger tissues (Vega-Sánchez *et al.*, 2013). However, while the decrease in glucose continues into senescence for stem biomass, for leaves, glucose abundance increases between PB and SS. As previously discussed (Section 4.1.4), this is likely to be a consequence of a faster progressing senescence-induced nutrient remobilisation which primarily affects non-structural cell wall components. This conclusion may be supported by the observed more accentuated decline on the percentage of undetermined cell wall components between PB and SS in leaves (-6.8%), than in stems (-0.9%). Further support comes from the fact that xylose abundance follows the same trend as glucose; as it also increases in senesced biomass, which translates into higher cell wall proportions attributed to hemicellulosic structural polysaccharides.

The overall analysis of miscanthus cell walls suggests that despite the relative abundance of the main components being similar between tissues and developmental stages, there are key alterations which affect the fine structure and composition of the wall. This added complexity is likely to have different repercussions on the cell wall structure, which are deemed to affect the assembly of the wall. In order to elucidate how these features vary in relation to each other, ratios and correlations are presented in the final sections of this thesis. It is expected that the knowledge provided here will contribute to our understanding of how a varying structure and composition of the cell wall affects its deconstruction.

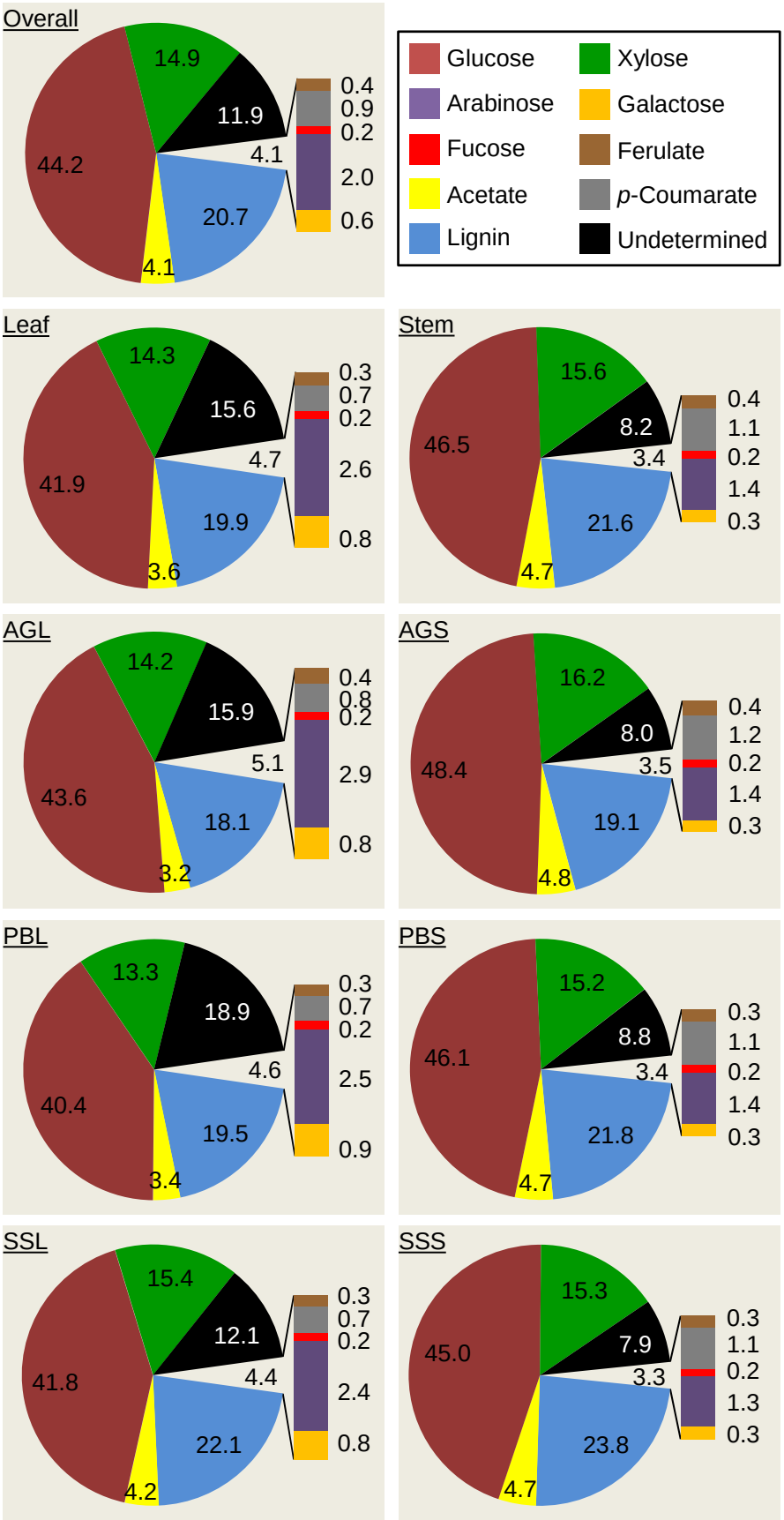

Fig. 6.1. Percentage (%) composition of miscanthus cell wall based on the mean of each component for the 8 miscanthus genotypes used in this study (see previous chapters for more detail). Overall this indicates the composition for leaf and stem tissues at all developmental stages combined. (AG, active growth; PB, peak biomass; SS, senescence; L, leaf; S, stem).

6.1.2. Associations between Cell Wall Components

Beyond mere composition, the interaction between different cell wall components incorporates most of the complexity of lignocellulosic biomass. As has been discussed previously, miscanthus biomass contains substantial proportions of xylans, which play essential roles in maintaining cell wall integrity. In comparison to cellulose, xylans are distinctively more heterogeneous, as their backbones are often linked to other components, thus profoundly affecting xylan structure and composition. However, xylan ornamentation is a controversial topic in the study of cell wall recalcitrance, as frequently conflicting effects on amenability to saccharification have been reported in the literature. The abundance of three cell wall components known to occur as substituents in xylan chains has been presented in previous chapters. Here, it is intended to explore possible associations between the abundance of these components and that of xylan. In the subsequent section these associations will be further explored in the context of their impact on cell wall deconstruction.

Further insight into xylan ornamentation with acetyl, arabinosyl and feruloylated arabinosyl substituents may be estimated by calculating ratios between these components (Table 6.1). For acetyl ornamentation, nearly all cell wall polymers, with the exception of cellulose and MLG may be acetylated (Gille and Pauly, 2012), but the main source of acetate from the cell wall are xylans (Pawar *et al.*, 2013). Each monomer of xylan backbones may be mono- or di-acetylated (Teleman *et al.*, 2000; Gille and Pauly, 2012; Lee *et al.*, 2014), with the acetyl groups linked at the O-2 or O-3 positions of the xylosyl residues (Carpita, 1996). As an average of the miscanthus genotypes studied here, acetyl groups are never present in the cell wall at acetate to xylose residue ratios (Acet/Xyl) lower than 58:100. This suggests that xylans in miscanthus cell walls are heavily acetylated, as potentially more than half of the xylose residues could be substituted with an acetyl group. This observation is corroborated by *in situ* immunolabelling studies, where xylan epitope detection was enhanced considerably after a

base treatment which de-esterified the cell wall (Fig. 5.10). Between tissues, developmental stages and genotypes, the Acet/Xyl ratios generally followed the same trends as the absolute acetate proportions presented in section 3.1; as higher values are typically seen in stem biomass and there is a trend for increasing acetylation along development, which is more noticeable in leaf samples. Notably, at a genotype level it was observed that in most cases the highest Acet/Xyl ratios did not occur in the same genotypes which released the highest proportions of acetate. Also important is the fact that the values for the acetate to xylose ratios are larger than one (Acet/Xyl > 1) for PB and SS stems of genotype sin13. Both these observations indicate that the structural contribution of acetyl substituents is different between the genotypes. While in some cases the number of xylose residues surpasses the number of acetyl residues, suggesting that most acetyl groups could be in fact associated to xylans. In other cases, such as for sin13 stems, the ratios indicate that, on a molar basis, acetate in the cell wall is more abundant than xylose. This could be interpreted as an indication that non-xylan cell wall components are also acetylated. Alternatively, it could imply that di-acetylation of xylosyl residues is more prevalent in these samples. As previously mentioned, sin13 plants had particular morphological traits (Fig. 5.6), as the tillers were typically shorter, tissues were softer, and at each developmental stage the harvested plants appeared to be developmentally behind the remaining genotypes. This observation is further substantiated by the fact that flowering times for sin13 are typically delayed in comparison to other genotypes[*]. It is possible that these differences in morphology and development have repercussions at the level of cell wall composition and structure, which in turn may explain the high Acet/Xyl ratios obtained for sin13 stems. In the current study it was not possible to provide further explanations for these values. Nonetheless, despite AX typically being the most abundantly acetylated polysaccharide in grass cell walls, acetylation of HG, RG-I and lignin has also been reported (Ishii, 1997a;

[*] Jensen, September 2015. Personal communication.

Mohnen, 2008; Gille and Pauly, 2012). It is possible that the higher Acet/Xyl ratio in sin13 stems is derived from higher acetylation of non-xylan components. However, it is also valid to speculate that non-xylan structures are substituted with acetyl to similar extents in different genotypes, and that the difference in sin13 is in fact derived from more extensive mono- and di-acetylation of xylans. This second possibility could be supported by observations made during immunolabelling studies; where detection of xylan epitopes recognised by CCRC-M144 and CCRC-M155 was more enhanced in sin13 stems than in other genotypes (Fig. 5.22).

Despite its occurrence in AGN polymers, most of the arabinose in grass cell walls is found as a substituent of xylan backbones (Carpita, 1996). As a result, arabinose to xylose ratios (Ara/Xyl[*]) are frequently used as indicators of the degree of arabinosyl substitution of AX. The Ara/Xyl ratio positively accounts for the degree of arabinosylation of xylan backbone, its values are typically lower in stems, and a decline is observed throughout development in leaf samples (Fig. 6.2). Xylan polymers substituted to different degrees have different distributions in the cell wall, as highly substituted AXs are more abundant in primary cell walls, and more linear xylans are often associated with lignification and secondary cell walls (Suzuki *et al.*, 2000). This is an indicator that the degree of arabinosylation may vary in accordance to structural roles. However, conflicting explanations exist for the contribution of arabinosyl substituents to the formation of tight cell wall structures. From one point of view, it has been reported that higher concentrations of alkali are required to extract less substituted xylans (Fry, 2010), and that the number of arabinose substituents is positively correlated with cell wall deconstruction; presumably as a result of a negative effect on cellulose crystallinity (Li *et al.*, 2013a). Conversely, extensive AX branching may partially restrict the ability of enzymes to degrade wall polysaccharides (Correia *et al.*, 2011). Furthermore, higher arabinosylation may also provide more opportunities for FA-mediated cross-linking, leading to more rigid

[*] Ara/Xyl ratios have already been discussed in section 4.1.

structures. The reason for this is that in grass cell walls, FA is typically found linked to arabinosyl substituents of AX (Ralph *et al.*, 1994b; Wende and Fry, 1997b), where it may simultaneously ether-link to lignin monomers (Kondo *et al.*, 1990; Buanafina, 2009), or even form dimers and other oligomers, which cross-link carbohydrate chains to each other (Grabber *et al.*, 2004; Agger *et al.*, 2010).

Similar trends were observed between developmental stages for the variation of ester-linked FA abundance in the cell wall (Table 3.3 and Fig. 3.4) and the FA/Ara molar ratio (Table 6.1 and Fig. 6.2). In both cases, typical values are higher in AG samples and then decrease in samples from more mature plants. However, the average ratio of FA substituents per each arabinose residue is twice as high in stems than in leaves. Similar differences between the FA/Ara ratios of leaves and stems have also been reported in *Brachypodium distachyon* cell wall biomass (Rancour *et al.*, 2012). Given that the abundance of FA is not substantially different between tissues (Table 3.4), high values for the FA/Ara ratio in stems may be explained by lower abundance of arabinose in these tissues (Fig. 6.1). Conversely, in the CWM from leaves, GP data suggests that AGN side chains of RG-I are more abundant than in stems (Fig. 5.4). This suggests that a bigger proportion of the arabinose residues in the cell wall of leaves is not substituted by FA, as it is associated with pectins and thus does not participate in AX crosslinking.

To better understand how FA abundance varies in relation to the Ara/Xyl ratio, correlation coefficients were calculated between these variables (Table 6.2). It was shown that arabinose substitution of xylans is not generally proportional to feruloylation. However, it should be kept in mind that only ester-linked FA monomers have been quantified, which excludes all FA dimers and ether-linked residues. In stem biomass at PB and SS, significant negative correlations between FA abundance and Ara/Xyl ratio could imply that the ester-linked FA content is lower when AX ramification is higher. This may be explained by

the fact that as plants mature and more ferulate cross-links are formed between AX polymers, the number of ester-linked FA monomers decreases as a result of being oxidatively coupled to form cross-linking oligoferulates (Wende and Fry, 1997a; Encina and Fry, 2005; Buanafina, 2009). This is corroborated by the fact that throughout stem maturation the Ara/Xyl ratio remains unaltered, but the FA/Ara ratio decreases (Fig. 6.2). In leaves, despite a significant negative correlation having been detected at the AG stage, FA abundance and Ara/Xyl ratio are not generally correlated to each other (Table 6.2). The structural features of the cell wall which influence these observations could not be further discerned in the present work. However, as indicated by the GP analysis, AGN side chains of RG-I are more abundant in the CWM of actively growing leaves (Fig. 5.4), and it is possible that in these tissues pectin-associated arabinose has a bigger influence on the Ara/Xyl ratios than it does in stems and in more mature tissues. Ultimately, these opposing observations of leaf and stem biomass provides further evidence for the marked compositional and structural disparity of miscanthus stem and leaf cell walls, and confirms that it is best practise to obtain independent tissue-specific compositional data, as has been previously mentioned (Section 2.6).

It has been reported that *p*CA accretion occurs in tandem with lignin deposition (Grabber *et al.*, 2004), and it is presumed that higher levels of *p*CA occur in tissues which also contain also higher proportions of S-lignin, as these units are known to be pre-acylated with *p*CA before being incorporated into lignin (Lu and Ralph, 1997). The data reported here on miscanthus is consistent with this, as the analysis of FTIR data suggested that stem biomass contains higher S-lignin levels (Section 2.3), and the determination of cell wall content of *p*CA showed that it is indeed typically more abundant in stems (Section 3.2), when compared to leaves. To determine how *p*CA in miscanthus cell walls is associated to overall lignin content, correlations were determined. No significant proportionality was detected between *p*CA and lignin content, at an overall level (r=0.07; P=0.625; Fig. 6.3), nor for individual tissues: leaf (r=-0.32;

P=0.127) and stem (*r*=-0.05; *P*=0.829). As a result, despite the fundamental role of *p*CA in lignin cross-linking, their absolute abundances are not correlated. Nevertheless, positive correlations have been reported between lignin units and several other phenolics in miscanthus cell walls (Li *et al.*, 2014b), therefore future studies could help determine whether *p*CA is correlated specifically to S-lignin abundance.

Table 6.1. Ratios of different xylan substitution groups in miscanthus CWM. Values for the arabinose/xylose ratio are reproduced from Table 4.8. Each value is the mean of the replicates at each developmental stage, and tissue for eight genotypes. Note that ratios of acetate to xylose and ferulic acid to arabinose were calculated considering the molar mass of the components.

	Acetate/Xylose molar ratio					
	Active Growth		**Peak Biomass**		**Senescence**	
	Leaf	**Stem**	**Leaf**	**Stem**	**Leaf**	**Stem**
gig01	0.51	0.68	0.58	0.73	0.69	0.67
hyb03	0.58	0.70	0.53	0.70	0.49	0.64
sac01	0.33	0.49	0.43	0.56	0.45	0.51
sin08	0.72	0.92	0.76	0.92	0.93	0.90
sin09	0.61	0.84	0.77	0.86	0.74	0.87
sin11	0.48	0.76	0.74	0.80	0.67	0.82
sin13	0.75	0.86	0.72	1.03	0.89	1.01
sin15	0.66	0.78	0.64	0.73	0.75	0.80
Mean	0.58	0.75	0.65	0.79	0.70	0.78
	Arabinose/Xylose ratio					
gig01	0.17	0.06	0.17	0.07	0.16	0.07
hyb03	0.18	0.08	0.17	0.07	0.14	0.07
sac01	0.16	0.06	0.15	0.06	0.14	0.07
sin08	0.21	0.10	0.20	0.11	0.15	0.10
sin09	0.17	0.08	0.18	0.08	0.12	0.09
sin11	0.24	0.11	0.29	0.11	0.19	0.10
sin13	0.26	0.11	0.18	0.12	0.22	0.10
sin15	0.27	0.12	0.22	0.11	0.16	0.10
Mean	0.21	0.09	0.19	0.09	0.16	0.09
	FA/Arabinose molar ratio					
gig01	0.18	0.38	0.14	0.34	0.16	0.29
hyb03	0.21	0.29	0.17	0.43	0.16	0.37
sac01	0.16	0.40	0.13	0.29	0.11	0.26
sin08	0.16	0.32	0.07	0.12	0.07	0.13
sin09	0.09	0.17	0.09	0.22	0.09	0.13
sin11	0.05	0.11	0.05	0.10	0.05	0.11
sin13	0.08	0.13	0.12	0.15	0.08	0.14
sin15	0.06	0.11	0.05	0.10	0.06	0.16
Mean	0.12	0.24	0.10	0.22	0.10	0.20

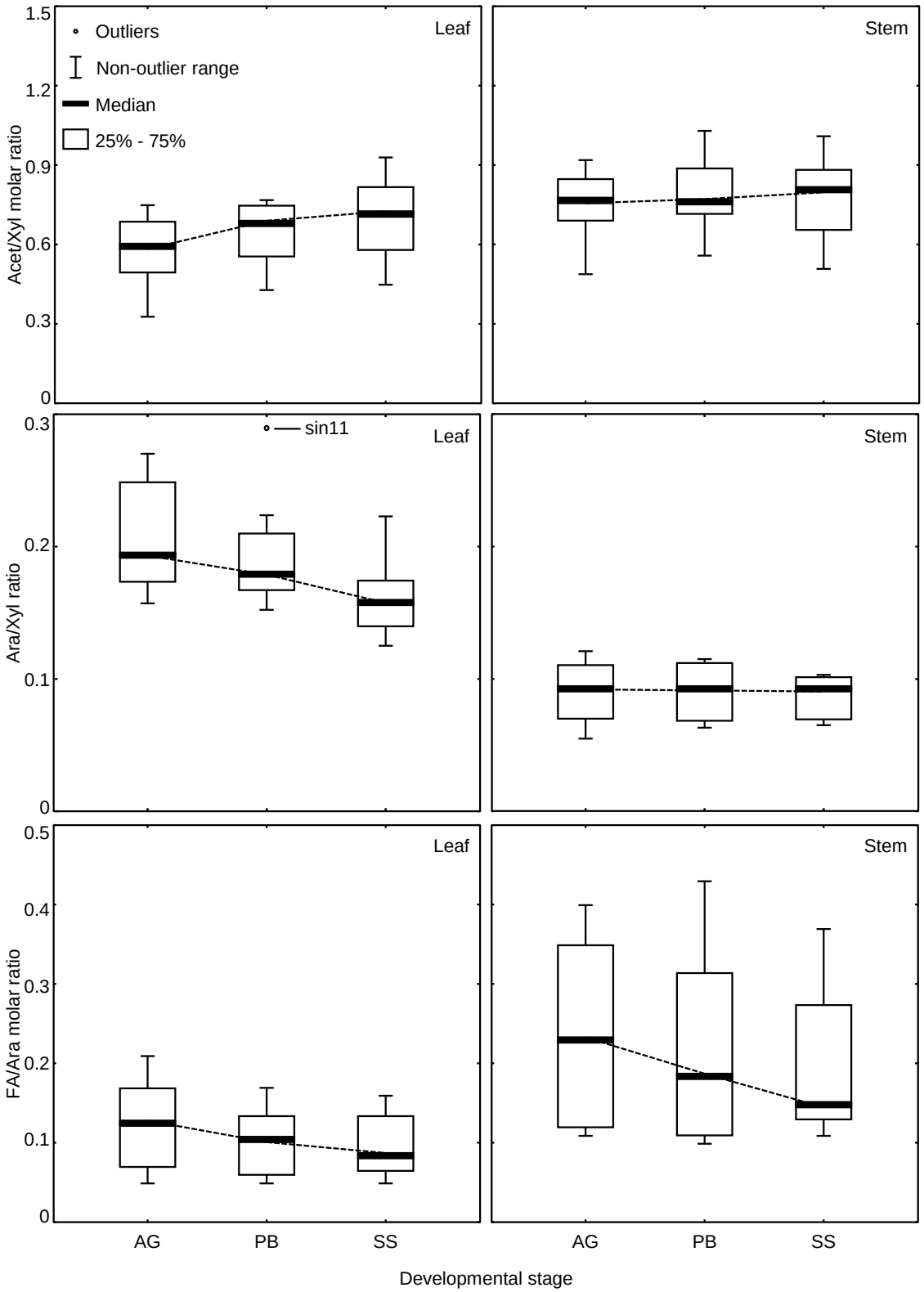

Fig. 6.2. Distribution of measurements of the acetate to xylose molar ratio (Acet/Xyl), arabinose to xylose ratio (Ara/Xyl; reproduced from Fig. 4.5), and ferulate to arabinose molar ratio (FA/Ara) of miscanthus CWM. Note that the Acet/Xyl and the FA/Ara ratios were calculated considering the molar mass of the components. Developmental stages are: active growth (AG), peak biomass (PB) and senescence (SS). The non-outlier range is defined as the range of values which fall outside 1.5× the interquartile range of the distribution (height of the 25% – 75% box).

Table 6.2. Pearson coefficients of the correlations (*r*) between the arabinose to xylose ratio (Ara/Xyl, which gives an indication of xylan arabinosylation) and ferulic acid (FA) content of cell wall material (CWM). Marked correlations (*) are significant at $P<0.05$. For each coefficient at a given combination of developmental stage and tissue N=16, consisting of two replicates from each tissue, for 8 genotypes. For correlations at tissue level N=48, and overall N=96. Developmental stages: AG, active growth; PB, peak biomass; SS, senescence.

	FA (% CWM)					
	Overall					
Ara/Xyl ratio	-0.27					
	Leaf			**Stem**		
	-0.34			-0.70*		
	AG	**PB**	**SS**	**AG**	**PB**	**SS**
	-0.74*	-0.66	-0.27	-0.67	-0.82*	-0.78*

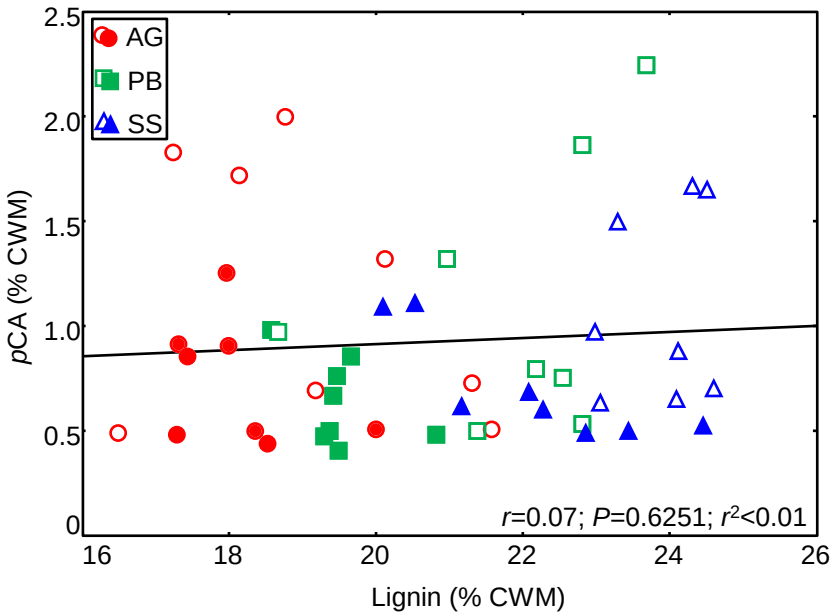

Fig. 6.3. Least square fit of lignin vs. *p*-coumaric acid (*p*CA) content in miscanthus cell wall material (CWM), with the associated Pearson correlation statistics (*r*) and probabilities (*P*) for 8 miscanthus genotypes. Developmental stages: AG, active growth; PB, peak biomass; SS, senescence. Open shapes (circles, squares and triangles) represent stem samples and filled shapes are leaf samples.

6.1.3. Correlation between Cell Wall Digestibility Assessment Methods

Miscanthus and other lignocellulosic crops have been traditionally used for bioenergy applications, and different mechanisms have been employed for the conversion from biomass, to some kind of energy form. Two of the most relevant applications consist of the generation of heat and power via combustion processes, and deconstruction of cell wall energy-rich carbohydrate polymers for biological production of liquid fuels (Hodgson *et al.*, 2010; Allison *et al.*, 2011). In the present study, the focus has been on the latter approach, as different cell wall components have been examined, while assessing their possible impacts on cell wall recalcitrance to saccharification. However, the deconstruction of the cell wall has more varied potential industrial applications than simply their conversion into fermentable sugars for ethanol production. Namely, various classes of biomaterials may be produced to add value to lignocellulosic biofuel production pipelines, butanol may be produced instead of ethanol, and as new biochemical, chemical and thermochemical conversion pathways emerge, even lignin may become a useful source of industrially relevant molecules (Ragauskas *et al.*, 2014; McCann and Carpita, 2015). Cell wall recalcitrance to deconstruction will still remain one of the most significant hindering factors to widespread utilisation of lignocellulosic feedstocks. Although, given the continuously emerging novel forms of utilising these materials, it has been suggested that definitions of recalcitrance should be updated, as this concept should reflect more than how strongly cell wall biomass may be resistant to the release of fermentable sugars (McCann and Carpita, 2015). Paradoxically, while novel biomass conversion methods are on course to being developed and optimised, at a research level, the determination of enzyme-mediated digestibility and the quantitation of released Glc, still remain viable and common ways of assessing cell wall recalcitrance. Firstly, as cellulose is the most abundant component of lignocellulosic biomass and the centrepiece of the cell wall structural core, it directly or indirectly interacts with most cell wall components. Therefore, by employing enzyme-

mediated cell wall deconstruction methods, an overview is provided of how the wall is recalcitrant as a whole, and together with compositional data, allows inferences about how structures are assembled. Secondly, from a biomass fermentation point of view, although progress is being made on the development of microorganisms which will metabolise pentose sugars (such as xylose), most microorganisms in current use are more efficient at utilising hexose sugars (such as glucose) as substrates for fermentation (Hatfield *et al.*, 2009; Vega-Sánchez *et al.*, 2015). Thus, high Glc yields is a desirable biomass trait, and one which may be assessed by enzymatic saccharification trials. Thirdly, by using microorganisms which express enzymes capable of deconstructing the cell wall, and also have the capacity of fermenting the products, simultaneous saccharification and fermentation is achieved. These methods have the advantage that since hexoses may be rapidly converted to an industrially useful product (such as ethanol) by the fermentation process, digestibility indicators derived from this kind of bio-assays are theoretically good predictors of the industrial usefulness of the biomass samples being analysed. However, there are disadvantages, mainly concerned with the fact that microbe mechanisms of action and the catalogue of expressed enzymes have not been completely characterised, which limits the range of inferences that may be made concerning cell wall assembly, and disassembly.

The amenability of miscanthus biomass to deconstruction has been assessed by three different methodologies, and the results are summarised in Table 6.3. The procedure of two of these methods only differed in the application of an alkaline pretreatment (0.1M KOH, 16h, 21°C; characterised in chapter 3), and involved the direct use of an enzyme cocktail, essentially containing cellulase and β-glucanase activity (Section 4.2). The third method consists of a *C. phytofermentans*-mediated simultaneous saccharification and fermentation procedure, which utilises ethanol yield as an indicator of biomass digestibility (Section 2.4). By assessing digestibility by more than one method, the aim was to better understand how different cell wall

biomass samples may potentially respond to distinct lignocellulose conversion processes. Moreover, by determining how the methods are correlated to each other, inferences may be made about how cell wall composition and structure are affected.

Despite having a different mechanism of action and thus different impacts on the cell wall, at an overall level all three methods correlated positively and significantly with each other (Fig. 6.4). Enzymatically released Glc from UT samples showed the strongest correlation with the ethanol yields from the *C. phytofermentans* assay (r=0.70; P<0.001). A common feature of the enzymatic saccharification assay and the *C. phytofermentans*-mediated fermentation of CWM is that no pretreatment was employed aimed at enhancing biomass digestibility. Bearing this in mind, compositional and structural features of the cell wall should have comparable influences on the action of both digestibility assessment methods; which in turn leads to very correlatable results at an overall level. At a tissue level, differences were observed in the correlation patterns between methods. A strong, significant and positive correlation was detected (r=0.78; P<0.001) for leaves; but despite a positive and significant correlation in stem biomass, it was not as strong (r=0.55; P=0.006). Data from previous chapters have suggested that CWM from leaves is less recalcitrant than from stems; as indicated by generally higher ethanol yields (Fig. 2.6), higher enzymatically released Glc from UT and from PT samples (Fig. 4.7), and higher total carbohydrate released during cell wall fractionation (Fig. 5.3), in leaf biomass. As a result, a higher correlation coefficient in leaves than in stems, between ethanol yields and Glc yields in UT samples, could be explained on the basis that stems are less digestible. Given that structural and compositional factors are associated with recalcitrance, it is likely that there are cell wall features in stems, more than in leaves, which potentially have a different influence on the action of *C. phytofermentans*-mediated fermentation and the action of the enzyme cocktail used; ultimately leading to more varied results between these two digestibility assessment methods.

The effect of the 0.1M KOH pretreatment on the enhancement of enzymatic saccharification yields has been discussed in chapter 4. Here (Fig. 6.4), it is shown that the Glc yields from UT and PT samples are correlated at the mean (r=0.59; P<0.001), leaf (r=0.48; P=0.019), and stem (r=0.67; P<0.001) levels. The fact that a significant correlation is observed when all samples are included in the calculation indicates that enzymatic saccharification of CWM with or without a pretreatment are both valid and correlatable procedures to determine biomass amenability to digestion. Nonetheless, how the values are correlated differs substantially between leaf and stem samples, reflecting the effect of the pretreatment; given that the enzymatic hydrolysis procedure *per se* was identical for UT and PT samples. By calculating ratios between the Glc yield from PT and UT samples (PT/UT; Table 4.16), it was seen that PT leaf samples typically release 2.07 times more Glc than UT samples at the AG developmental stage, whereas for stems the ratio was 2.49. By contrast in mature tissues (PB and SS), the pretreatment was more effective in leaf samples; as the ratios for leaf were 3.18 (PB) and 3.74 (SS), and for stem, 2.81 (PB) and 3.66 (SS). These ratios firstly indicate that the pretreatment is largely more effective in leaf biomass, and secondly, it shows that the application of 0.1M KOH is more effective at enhancing biomass digestibility in mature tissues. This clearly demonstrates that samples originating from different tissues and harvest times do not respond in similar ways to the pretreatment. This is particularly noticeable when plotting PB and SS data points, which are generally associated with proportionally higher Glc yield values in the PT axis of the leaf plot, when compared to the stem plot (Fig. 6.4). As a consequence, tissue and development-related differences in responses to pretreatment have divergent effects on the correlation of Glc yields from UT samples with those from PT samples; which in turn account for the disparities observed in the correlation coefficients for Glc yields from leaf and stem samples.

In the previous two discussed correlations, the methods had in common the fact that no pretreatment had been applied, or that the enzymatic digestion was identical. However, between the *C. phytofermentans* assay and the enzymatic hydrolysis of PT samples, no procedural steps are directly comparable. Nevertheless, a positive and significant correlation coefficient was detected (r=0.39; P=0.007; Fig. 6.4); which despite indicating only a moderately strong association, does show that digestibility indicators from these methods are correlatable to a certain extent. A slightly stronger correlation (r=0.45; P=0.027) was observed with stem biomass, but no significance was detected (r=0.32; P=0.128) with leaves. As discussed above, correlations with differing degrees of significance between leaf and stem samples may be explained by the effect of the pretreatment and its divergent impact on biomass from different origins. By observing the distribution of values along the axis of PT samples it is visible that there is a bigger spread of data points from the same developmental stage. Particularly, it is seen that, contrary to enzymatically released Glc from UT samples and the ethanol yields, where a clustering is observed between samples of different maturation, for PT samples such clustering is not always clearly detected. This is more evident with leaf samples, where the action of the pretreatment is more efficient, with the result that PT leaf biomass may differ more extensively from the UT leaf samples, than do PT stems from UT stems. Therefore, structural and compositional features of the stem biomass used for *C. phytofermentans*-mediated fermentation, and the PT biomass used for enzymatic saccharification, may be more similar between each other, than are PT and UT leaf samples. As a result, the digestibility indicators of these methods are more correlatable in stems than in leaves, which have been more extensively modified by the pretreatment.

For each individual tissue at a given developmental stage, the correlations between methods were recurrently non-significant (Table 6.4). At this level of the data, the correlation coefficients reflect how the biomass from each miscanthus genotype, collected at a given

developmental stage and tissue, responds to the different digestibility assessment methods (illustrated in Fig. 6.4 by the differently shaped markers on the leaf and stem plots). Here, the only situations where significance emerged was for the correlation between the enzymatic release of Glc from UT and PT CWM collected from actively growing leaf and stem samples: r_{leaf}=0.91 (P=0.002); r_{stem}=0.86 (P=0.007). As mentioned above, differences in correlations between UT and PT samples reflect the effect of the pretreatment. Consequently, the fact that AG samples were the only ones that showed significant correlations could be explained by the higher digestibility of these less mature tissues (Fig. 4.7), which in turn minimises the importance of the pretreatment. In fact, the effectiveness of the pretreatment is the lowest in AG samples (Table 4.16), making the Glc yields from UT and PT biomass more correlatable between both enzymatic saccharification methods. In all remaining situations no significant associations were detected, implying that the ranking of the 8 miscanthus genotypes in terms of their digestibility is not always well correlated between different assessment methods.

Overall good concordance among the three digestibility assays was observed for genotypes sin08 and sin13 (Fig. 6.5). However, agreement between the results can also be variable, depending on the developmental and tissue origin of the cell wall biomass. Namely, sin15 showed the lowest digestibility indicators, as measured by ethanol and Glc yields from UT and PT samples, in actively growing leaves and in senesced leaves; but in stem and in other harvest times, more variation is seen in how the digestibility results ranked in different methods. In other cases, even bigger discrepancies have been observed, namely: in senesced leaf samples from hyb03, in senesced stem from sac01, and in sin09 for peak biomass leaf and senesced stem samples. As previously discussed, these differences in how the same sample responds to different digestibility assessment methods suggests that features associated with cell wall structure and composition lead to differences in how biomass reacts to the alkaline pretreatment, and how hydrolytic enzymes may interact with cell wall polymers. Essentially,

three inferences may be made when big discrepancies occur in the ranking of a specific genotype in terms of its glucose yield from un-pretreated CWM (UT Glc), glucose yield from pretreated CWM (PT Glc) and ethanol yields from the *C. phytofermentans*-mediated fermentation (EtOH):

- UT Glc ≈ PT Glc ≠ EtOH: There are cell wall features which either have a particularly positive or negative effect on *C. phytofermentans*-mediated digestion, but have proportionally comparable effects on enzymatic saccharification regardless of the implementation of the 0.1M KOH pretreatment.
- UT Glc ≠ PT Glc ≈ EtOH: This type of discrepancy may be explained based on the fact that the 0.1M KOH pretreatment is known to remove ester-linked components from the cell wall, an effect which might be replicated to some extent during *C. phytofermentans*-mediated digestion; as it has been reported that a variety of esterases are highly expressed by this bacterium (Tolonen *et al.*, 2011). As a consequence, when the UT Glc rank is much lower than for the other two methods, it is likely that cell wall traits in the sample are more susceptible to the effect of the 0.1M KOH pretreatment, and to the action of *C. phytofermentans* auxiliary enzymes, leading to a substantial rise in amenability to digestion. By contrast when the UT Glc rank is much higher than for the other two methods, it suggests that the sample has a low cell wall recalcitrance, which gives rise to high Glc yields in UT samples, but that application of an alkaline pretreatment and the possible effect of secondary clostridial enzymes does not lead to equally high ranking digestibility results.
- UT Glc ≈ EtOH ≠ PT Glc: In these situations, when PT Glc ranks are higher, it could be attributed to a specific effect of the 0.1M KOH in the reduction of recalcitrance. Conversely, when the UT Glc and the EtOH ranks are higher, it

could imply that the biomass is very digestible and does not depend on the action of 0.1M KOH, nor of *C. phytofermentans* auxiliary enzymes to produce high ranking digestibility indicators.

Further implications of particular cell wall traits on digestibility, and how different genotypes rank in terms of these traits, will be discussed in the following section. When comparing digestibility assessment methods, it was observed that biomass from different tissues, harvest times and genotypes do not respond similarly to various conversion approaches despite some significant correlations having been observed at overall levels. This observation gives relevance to the importance of cell wall traits for the improvement of miscanthus varieties to be used in biofuel and other biomaterial applications. As a result, while it is true that various procedures may yield comparable results and correlate with each other, to a certain extent, in larger screenings of biomass samples, this may not be the case with smaller screens; as evidenced when individual tissues are analysed at a given developmental stage (Fig. 6.5). Indeed, if only one method is chosen to assess digestibility, valuable information may be overlooked or lost concerning the impact of the finer structural and compositional biomass features. Furthermore, as biomass downstream processing methods are simultaneously being improved, the development of new energy crop varieties should not focus on a single processing method for biomass quality assessment, but instead should consider various potential, industrially adaptable, biomass conversion procedures.

Table 6.3. Summary of results of three digestibility assessment methods: enzymatic release of glucose from un-pretreated (UT) and pretreated (PT) cell wall material, and ethanol yield from the *C. phytofermentans* digestibility bioassay. Data for glucose yields is reproduced from Tables 4.13 and 4.14. Data for the ethanol yields are a subset of Table 2.7, consisting of the values obtained for the leaf and stem samples harvested from the same miscanthus tillers as used for the enzymatic saccharification assays. Values are the mean ± standard deviation of duplicated samples at three developmental stages for each genotype.

	Active Growth		**Peak Biomass**		**Senescence**	
	Leaf	**Stem**	**Leaf**	**Stem**	**Leaf**	**Stem**
			Glucose (UT % total glucose)			
gig01	28.29 ± 0.08	22.52 ± 0.18	20.49 ± 0.05	16.82 ± 0.22	19.81 ± 0.69	13.27 ± 0.09
hyb03	27.20 ± 0.07	22.31 ± 0.13	19.10 ± 0.02	14.55 ± 0.15	21.46 ± 0.16	16.07 ± 1.22
sac01	27.63 ± 0.35	27.84 ± 0.31	18.85 ± 0.30	17.33 ± 0.16	14.16 ± 0.07	18.16 ± 0.51
sin08	34.06 ± 0.06	28.95 ± 0.09	17.60 ± 0.19	18.94 ± 0.06	12.95 ± 0.03	11.44 ± 0.01
sin09	37.84 ± 0.06	17.10 ± 0.41	23.15 ± 0.01	14.58 ± 0.10	12.79 ± 0.00	9.76 ± 0.14
sin11	27.07 ± 0.02	17.21 ± 0.06	22.61 ± 0.04	16.69 ± 0.00	14.19 ± 0.02	10.27 ± 0.00
sin13	38.17 ± 0.11	36.20 ± 0.00	16.50 ± 0.14	28.02 ± 0.04	19.08 ± 0.24	16.22 ± 0.00
sin15	14.71 ± 0.06	14.81 ± 0.02	15.28 ± 0.09	17.49 ± 0.12	12.37 ± 0.02	10.61 ± 0.07
Mean	29.37 ± 7.56	23.37 ± 7.25	19.20 ± 2.78	18.05 ± 4.29	15.85 ± 3.65	13.23 ± 3.21
			Glucose (PT % total glucose)			
gig01	62.24 ± 0.15	52.70 ± 0.41	55.44 ± 0.12	42.52 ± 0.01	52.87 ± 0.08	37.45 ± 0.06
hyb03	63.70 ± 0.00	62.91 ± 0.65	66.95 ± 0.04	50.31 ± 0.18	67.40 ± 0.26	54.85 ± 0.49
sac01	56.15 ± 0.21	55.69 ± 0.02	54.36 ± 0.10	44.76 ± 0.10	52.79 ± 0.14	41.20 ± 0.05
sin08	64.59 ± 0.01	70.70 ± 1.53	64.24 ± 0.78	51.50 ± 0.33	65.92 ± 0.15	54.36 ± 0.04
sin09	71.96 ± 0.07	54.69 ± 0.13	67.37 ± 0.09	58.47 ± 0.15	60.41 ± 0.08	54.99 ± 0.09
sin11	58.87 ± 0.04	48.71 ± 0.18	66.82 ± 0.17	51.89 ± 0.56	62.27 ± 0.16	51.30 ± 0.25
sin13	64.15 ± 0.04	72.39 ± 0.40	54.84 ± 0.29	58.48 ± 0.68	62.87 ± 4.35	50.33 ± 0.06
sin15	45.40 ± 0.01	47.08 ± 0.03	58.77 ± 0.94	47.87 ± 0.06	50.34 ± 0.02	42.53 ± 0.05
Mean	60.88 ± 7.78	58.11 ± 9.58	61.10 ± 5.83	50.72 ± 5.77	59.36 ± 6.51	48.38 ± 6.96
			Ethanol Yield (mg ethanol/g)			
gig01	57.45 ± 6.77	51.58 ± 2.93	46.71 ± 1.29	44.12 ± 3.92	38.02 ± 0.49	41.12 ± 0.33
hyb03	49.78 ± 2.13	50.24 ± 2.76	49.71 ± 1.62	43.03 ± 0.25	38.38 ± 0.31	39.45 ± 0.06
sac01	51.99 ± 13.94	44.01 ± 11.62	50.71 ± 0.66	44.36 ± 9.08	38.94 ± 0.59	39.30 ± 0.25
sin08	59.61 ± 7.91	45.75 ± 1.58	49.35 ± 2.73	53.66 ± 2.91	39.88 ± 0.38	40.60 ± 0.26
sin09	51.32 ± 12.95	41.72 ± 1.36	46.63 ± 0.69	49.90 ± 0.95	38.57 ± 0.89	44.45 ± 0.49
sin11	51.17 ± 14.41	41.69 ± 1.17	48.48 ± 0.19	43.42 ± 1.28	40.59 ± 1.07	39.29 ± 1.51
sin13	55.22 ± 6.03	49.38 ± 1.89	43.41 ± 4.11	54.51 ± 4.79	41.81 ± 0.15	41.23 ± 0.28
sin15	44.65 ± 4.21	45.25 ± 2.18	45.32 ± 1.41	47.88 ± 2.82	37.30 ± 1.70	40.72 ± 0.14
Mean	52.65 ± 4.70	46.20 ± 3.81	47.54 ± 2.46	47.61 ± 4.64	39.19 ± 1.48	40.77 ± 1.69

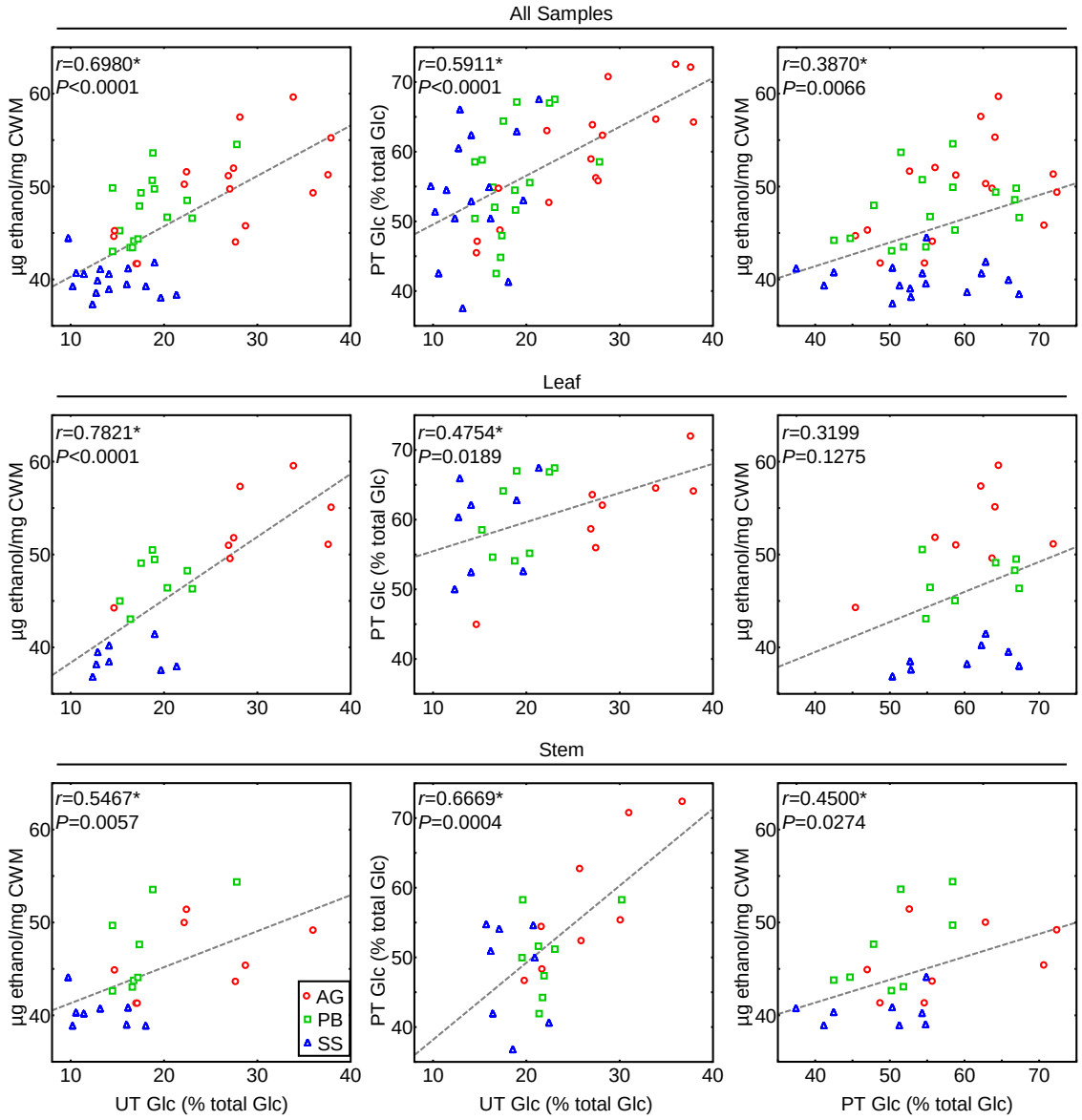

Fig. 6.4. Least square fit of the cell wall material (CWM) digestibility assessment results, with the associated Pearson correlation statistics (*r*) and probabilities (*P*). The first column shows the correlations between the enzymatically released Glc from un-pretreated (UT) CWM, vs. ethanol yield from the *C. phytofermentans* digestibility bioassay. The second column shows the correlations between the enzymatic release of Glc from UT and pretreated (PT) CWM (0.1M KOH, 16h, 21°C). The third column shows the correlations between the Glc yield from PT samples and the ethanol yield from the *C. phytofermentans* digestibility bioassay. The values for UT and PT are expressed as percentage of total Glc in the cell wall. Each value consists of the mean of duplicated samples from leaf and stem biomass harvested from the same tiller for the 8 miscanthus genotypes studied. Developmental stages: AG, active growth; PB, peak biomass; SS, senescence. Marked correlations (*) are significant at $P<0.05$.

Table 6.4. Pearson coefficients of the correlations (*r*) between three digestibility assessment methods: enzymatically released glucose from un-pretreated cell wall material (UT Glc); ethanol yield from the *C. phytofermentans* digestibility bioassay (Cphy EtOH); and enzymatically released Glc from pretreated cell wall material (PT Glc). Marked correlations (*) are significant at $P<0.05$. For each coefficient at a given combination of developmental stage and tissue, N=16, consisting of two replicates from each tissue, for 8 genotypes. Developmental stages: AG, active growth; PB, peak biomass; SS, senescence.

	Leaf			**Stem**		
	AG	**PB**	**SS**	**AG**	**PB**	**SS**
UT Glc *vs.* Cphy EtOH	0.67	0.30	0.10	0.43	0.68	-0.46
UT Glc *vs.* PT Glc	0.91*	0.53	0.28	0.86*	0.39	-0.25
PT Glc *vs.* Cphy EtOH	0.58	0.32	0.55	0.41	0.64	0.22

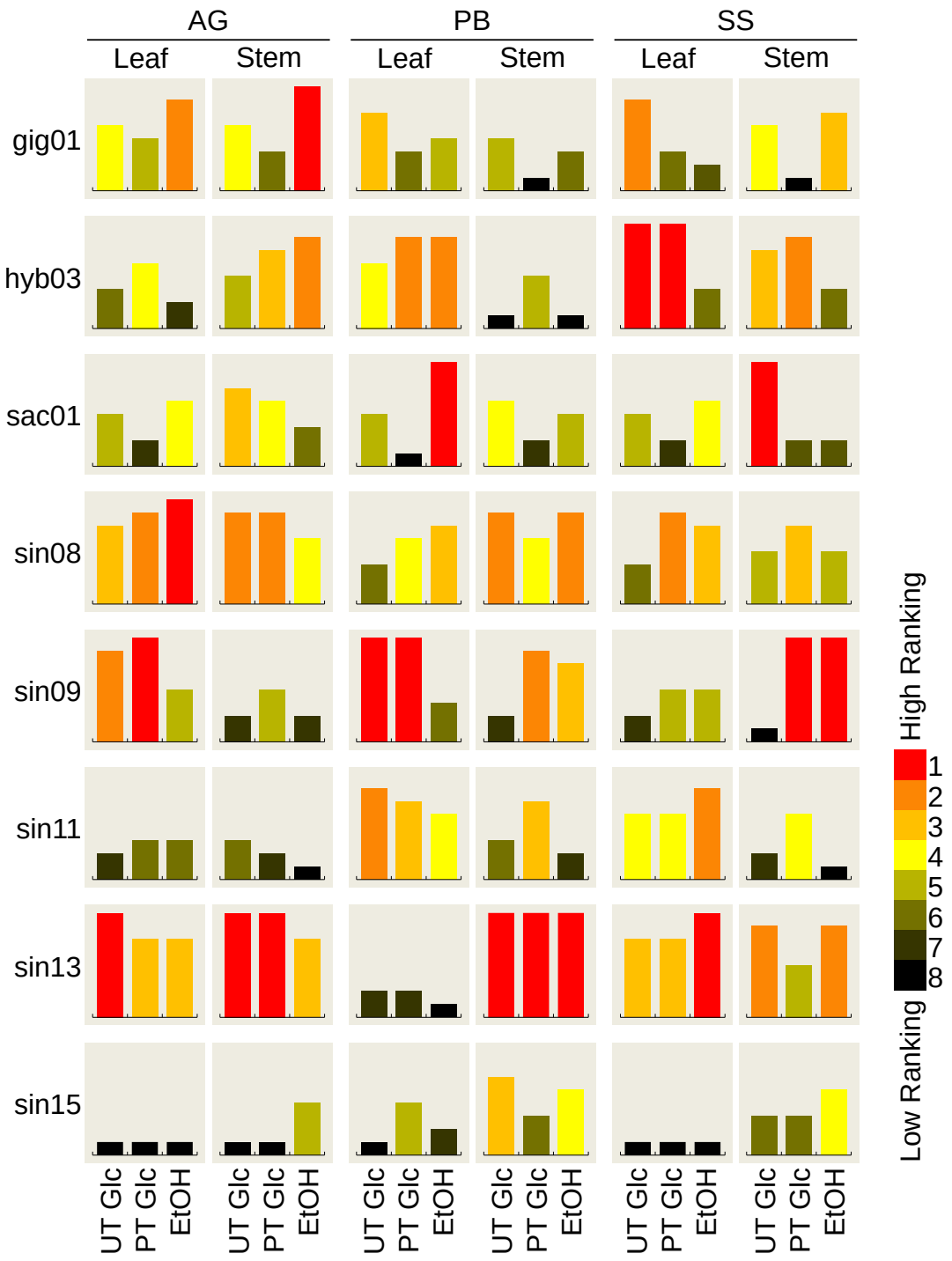

Fig. 6.5. Rankings of leaf and stem biomass from eight miscanthus genotypes in terms of their amenability to digestion across developmental stages (AG, active growth; PB, peak biomass; SS, senescence). Digestibility was assessed through the measuring of enzymatically released glucose from un-pretreated cell wall material (UT Glc) and pretreated cell wall material (PT Glc), and the ethanol yield from the *C. phytofermentans*-mediated fermentation (EtOH).

6.1.4. Genotype Considerations

The present study has demonstrated that miscanthus cell wall composition may vary significantly, not only between tissues and developmental stages, but also between genotypes. In previous chapters, the different genotypes were ranked in terms of each quantifiable measured cell wall characteristic. The impact on recalcitrance of these cell wall configuration differences will be assessed in the following section. Here, it is intended to provide a summary of how the genotypes compare to each other in terms of cell wall characteristics which may affect biomass deconstruction.

By comparing Glc saccharification indicators (Glc release by enzymatic hydrolysis from UT and PT samples) with the abundance of lignin (Fig. 6.6.), in many cases it is visible that samples with below average lignin contents have above average Glc release. *Vice versa*, in other cases of the leaf or stem tissue of a given genotype, at a specific developmental stage, above average lignin content co-occurred with low Glc release. However, this inverse proportionality was not always observed. In fact, for some samples, such as senesced stem and PB leaf from genotype gig01, lignin content is high, and yet, Glc release from UT samples was above the average. In other cases, such as stem biomass collected from genotypes hyb03 and sin09 at the PB developmental stage, high lignin content and low Glc release from UT samples were observed; however, after the application of the 0.1M KOH pretreatment, Glc release soared up and was among to the highest 25% of the range of values obtained for stem biomass at the peak yield harvest. These observations are suggestive that the role of lignin in recalcitrance is complex, and not a straight-forward direct association between its content and recalcitrance. Moreover, the application of a weak alkaline pretreatment may also deeply affect biomass responses to enzymatic saccharification. Many other compositional and structural cell wall features may affect recalcitrance, namely the abundance cell wall ferulic acid, which may be found ester- or ether-bonded to cell wall polymers, and is involved in their cross-linking

(Buanafina, 2009). Only ester-bonded FA monomers were quantified in the present study, and as observed for lignin abundances, clear, positive or negative proportionality between FA abundance and Glc saccharification was not detected. Further detail into how FA levels, and other cell wall features, such as hemicellulose content and ornamentation vary in relation to Glc saccharification will be provided in section 6.1.5.

In addition to cell wall features *per se*, from the perspective of the whole harvested miscanthus biomass, the fact that different genotypes and developmental stages contain varying proportions of leaf and stem also has an impact on biomass amenability to deconstruction. The reason for this is related to different properties of the harvested biomass arising from the fact that leaf, stem and presumably also other plant tissues, contain cell walls which differ in their composition and structure. A morphological characterisation of the different miscanthus genotypes was described in section 2.1. Chapter 4 describes experiments where total Glc content of the cell wall biomass, and its enzymatic release were determined. A summary of these data is provided in Fig. 6.7. Subsequently, the values were used to estimate Glc content and saccharification yields of whole above-ground CWM, with and without a pretreatment (Fig. 6.8). Bearing in mind that only single tillers from each genotype at a given developmental stage were harvested (Section 1.3), it is noteworthy that the values provided for tiller weight may not be accurately representative. However, given that in all cases they represented at least ¾ of the total height of the plant, comparisons may be made concerning differences in scale between genotypes. The aim of Fig. 6.8 is to provide a summarised graphical representation of the yield, composition and amenability to deconstruction for the biomass from different genotypes, at different harvest times. Several inferences may be made from the interpretation of the data. Nevertheless, an important observation is that at the end of the miscanthus growth cycle (February-March; senescence), *M.* × *giganteus* is the highest biomass producer, followed by hyb03. With all genotypes having been harvested at identical time points, it is interesting to

observe that for these two hybrid genotypes, peak biomass yield appears to only be reached after the PB harvest time, explaining why tiller weights are higher in senesced biomass. Furthermore, when comparing the Glc content, it can be observed that some genotypes which have higher Glc proportions do not seem to produce proportionally higher yields of enzymatically released Glc. As an example, in senesced biomass, gig01 tillers contain approximately 490mg of Glc per gram of CWM, whereas for hyb03, the equivalent value is 460mg/g CWM. When the CWM is subjected to enzymatic hydrolysis, for gig01 approximately 70mg and 196mg of Glc are released from 1g of un-pretreated and pretreated CWM, respectively. However, for hyb03, samples release 80mg (UT) and 266mg (PT) from each gram of CWM. This demonstrates that higher Glc content of the CWM is not always synonymous with high saccharification efficiency, as different cell wall properties, such as cellulose crystallinity may affect deconstruction. Furthermore, as complex effects of different cell wall properties interfere with cell wall disassembly, different genotypes may have specifically variable levels of recalcitrance, and thus different biomass utilisation potentials. As a consequence, genotypes which are high biomass producers may not always be the most cost-effective varieties.

The percentages that the cell wall represents in the above-ground biomass of miscanthus were considered to further explore these observations. Using miscanthus plants from the same experimental field trials as those used in the present study, Allison *et al.* (2011) reported neutral detergent fibre (NDF; a measure of total cell wall) proportions of total biomass, which averaged at approximately 86% over three consecutive years. In all cases, the studies were performed on senesced whole tiller biomass (pooled leaf and stem), collected in February, at the end of miscanthus growth cycle as a crop. These values are in accordance with data from Lygin *et al.* (2011), which reported that cell wall percentages of total miscanthus biomass ranges from 85% to 89%. NDF proportions of pooled leaf and stem senesced biomass for each individual

genotype are shown in Table 6.5. Based on these values, Fig. 6.9 shows the approximate amounts of pretreated senesced biomass (0.1M KOH for 16h at 21°C) needed from each of the 8 miscanthus genotypes used in the present study to achieve the same amount of enzymatically released Glc. The choice of pretreated biomass for these associations has to do with the fact that it was with these samples that the best saccharification yields were achieved in the present study (Chapter 4). It is also important to note that only cell wall-derived Glc is included in the present study. In the total harvested biomass, Glc content will presumably be higher, as Glc-containing soluble sugars may occur in the biomass, even if at very low proportions. Nevertheless, despite the values presented being specific for the experimental conditions employed in the present study, it is clear that different genotypes do present varying amenabilities to conversion. An example is gig01, which although it typically produced the highest amounts of biomass at the SS harvest, almost 600g of biomass is needed to obtain 100g of Glc by enzymatic saccharification. By contrast, with hyb03 only slightly more than 400g are needed to yield the same amount of Glc. Once again, these results indicate that higher biomass does not guarantee that proportionally high saccharification will be achieved. Additionally, various genotypes will present differing levels of utilisation cost-effectiveness depending on harvest time. Concerning the impact of varying tissue proportions on the overall recalcitrance, the correlation coefficient was calculated between the amounts of biomass needed to obtain 100g of Glc and the mean leaf contribution of each genotype. No significance was detected (r=0.30; P=0.256), indicating that at an overall level, the contribution of leaf to total biomass does not have a strong effect on amenability to deconstruction. However, by plotting these two variables against each other (Fig. 6.9B), it was observed that the most outlying genotypes were those with the more extreme values for the amount of biomass needed for 100g of Glc; namely, hyb03 as the lower extreme, and sin13 and sin15 as the highest extremes. By excluding these values and recalculating the correlation, a very high and significant coefficient of r=-0.97

(P<0.001) was determined. It is essential to keep in mind that these values are approximations, and that further and larger studies are required to confirm or deny the significance of relative tissue proportions on biomass digestibility. However, such a markedly high coefficient observed at the senesced stage, which is when leaf proportions are the lowest (due to leaf abscission), is highly suggestive of a real influence of tissue proportions on miscanthus biomass amenability to deconstruction.

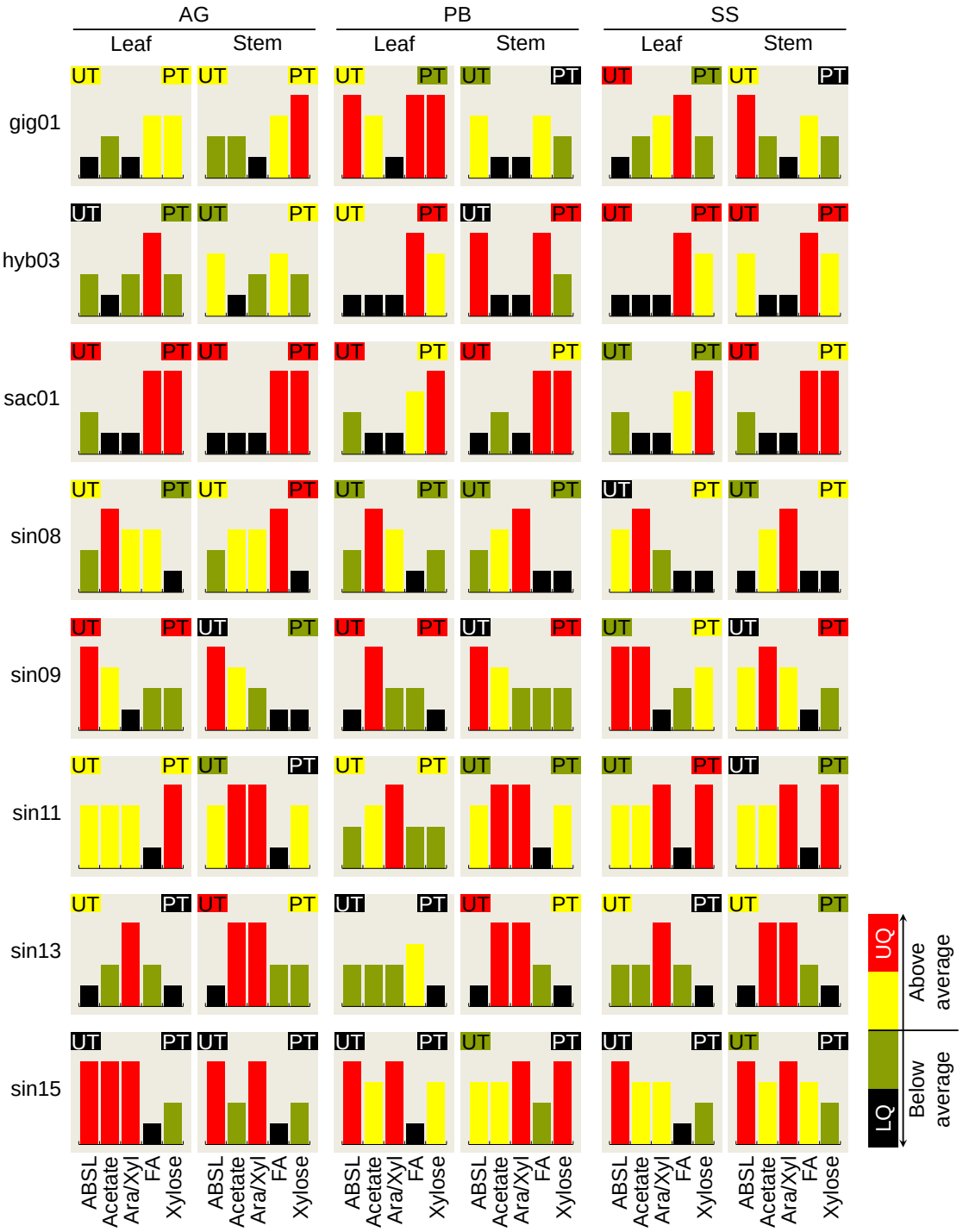

Fig. 6.6. Relative abundance profiles of five cell wall features thought to affect cell wall recalcitrance. Relative abundance is shown in relation to the average value for each compositional and structural feature in the cell wall of leaf and stem from 8 miscanthus genotypes at a given developmental stage. Red colour represents the upper quartile of the values (UQ; within the highest 25% of the range of values), black colour represents the lower quartile of the values (LQ; within the lowest 25% of the range of values). Abbreviations: AG, actively growing; PB, peak biomass; SS, senescence; ABSL, acetyl bromide soluble lignin; Ara, arabinose; Xyl, xylose; FA, ester-linked ferulic acid; UT and PT, enzymatically released glucose yields from un-pretreated and pretreated CWM, respectively.

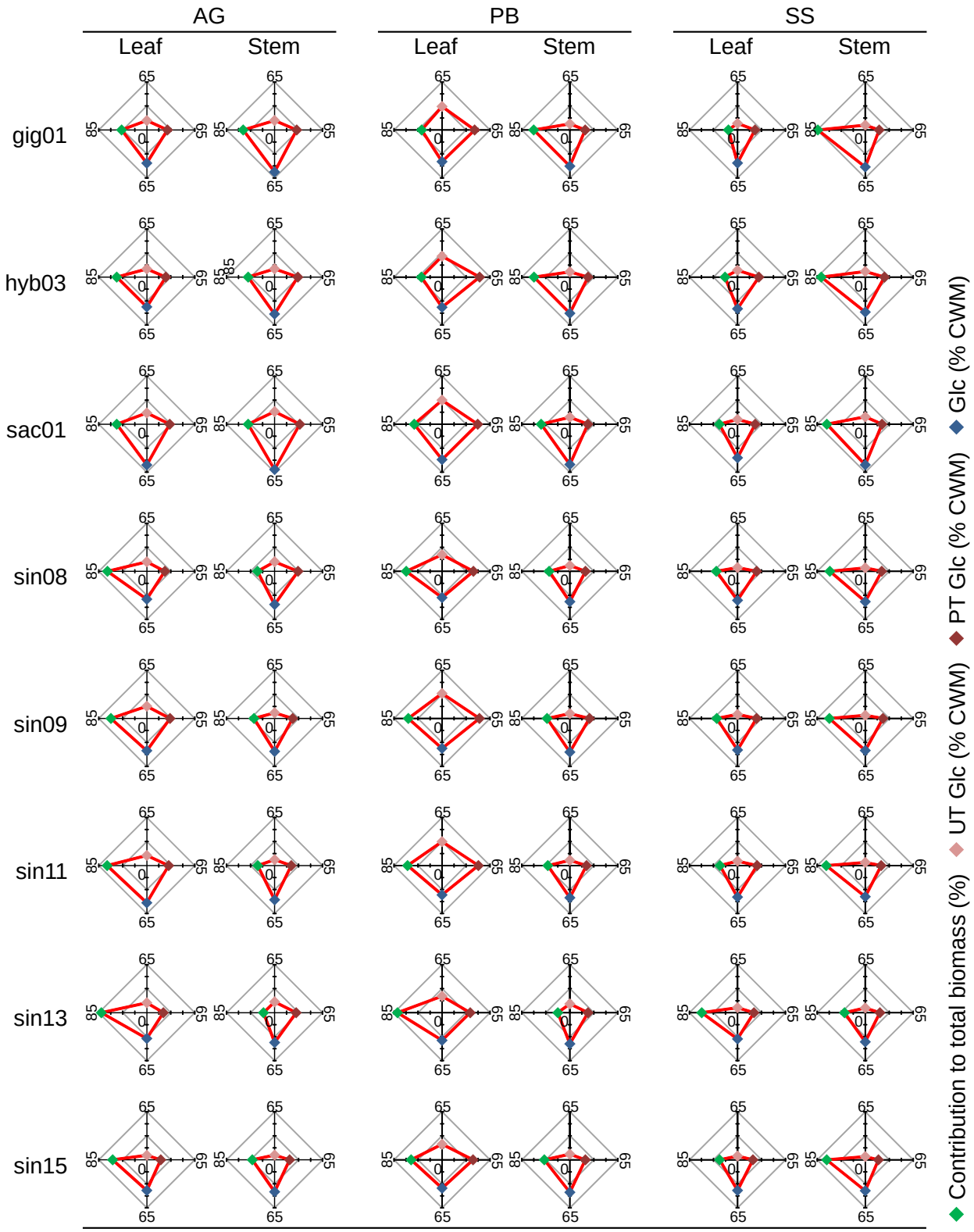

Fig. 6.7. Comparison of relative contributions of stem and leaf to total biomass, total cell wall glucose contents, and glucose saccharification yields from un-pretreated (UT) and pretreated (PT) cell wall material (CWM). Data is shown for leaf and stem biomass harvested from 8 miscanthus genotypes at actively growing (AG), peak biomass (PB) and senesced (SS) developmental stages.

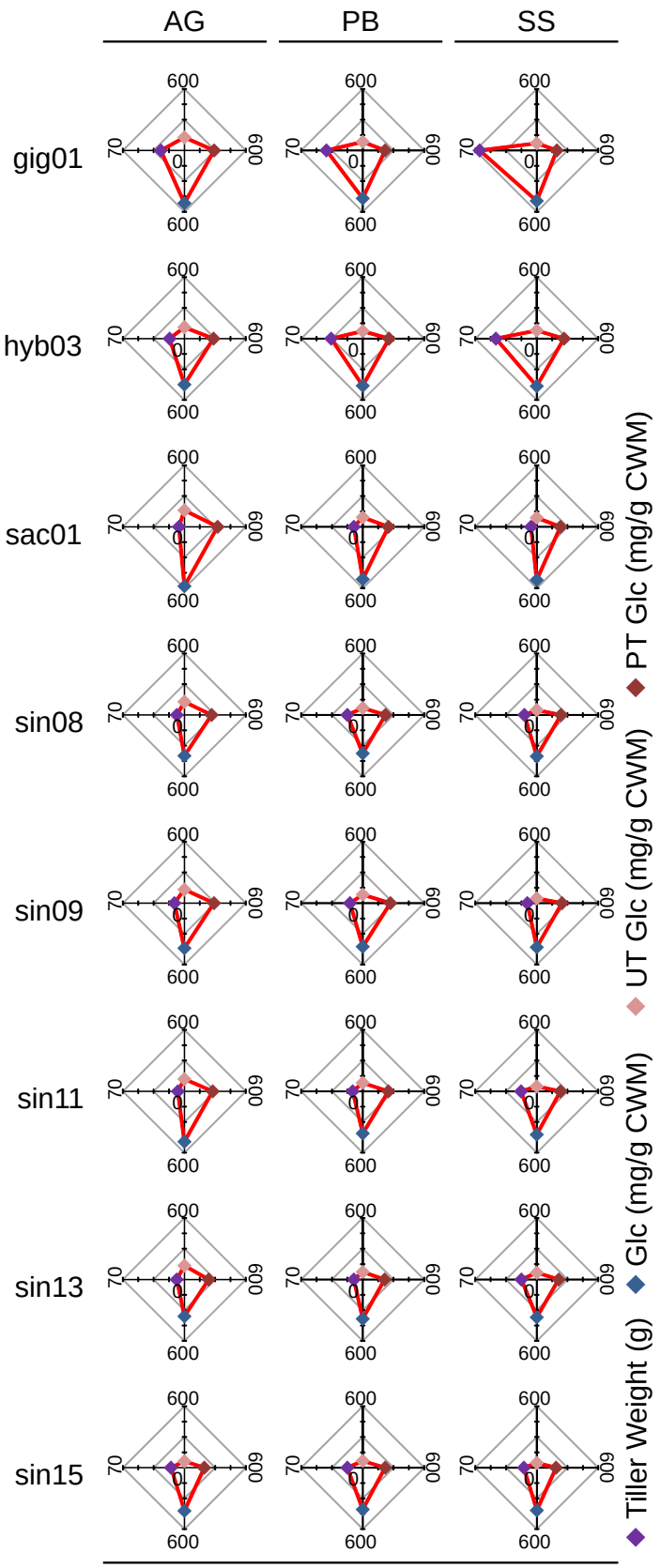

Fig. 6.8. Tiller mean weight and estimation of total cell wall glucose contents, and glucose saccharification yields from un-pretreated (UT) and pretreated (PT) cell wall material (CWM). Values take into account the relative contributions of stem and leaf tissue to total tiller biomass. Developmental stages: actively growing (AG), peak biomass (PB) and senescence (SS).

Table 6.5. Neutral detergent fibre (NDF) proportions of pooled leaf and stem total senesced biomass (dry weight, DW). Values were determined by Allison *et al.* (2011) and are available at http://mscan.ibers.aber.ac.uk (IBERS intranet only).

	NDF (% Biomass DW)
gig01	89.12
hyb03	87.05
sac01	85.51
sin08	88.62
sin09	88.76
sin11	87.33
sin13	78.06
sin15	87.14

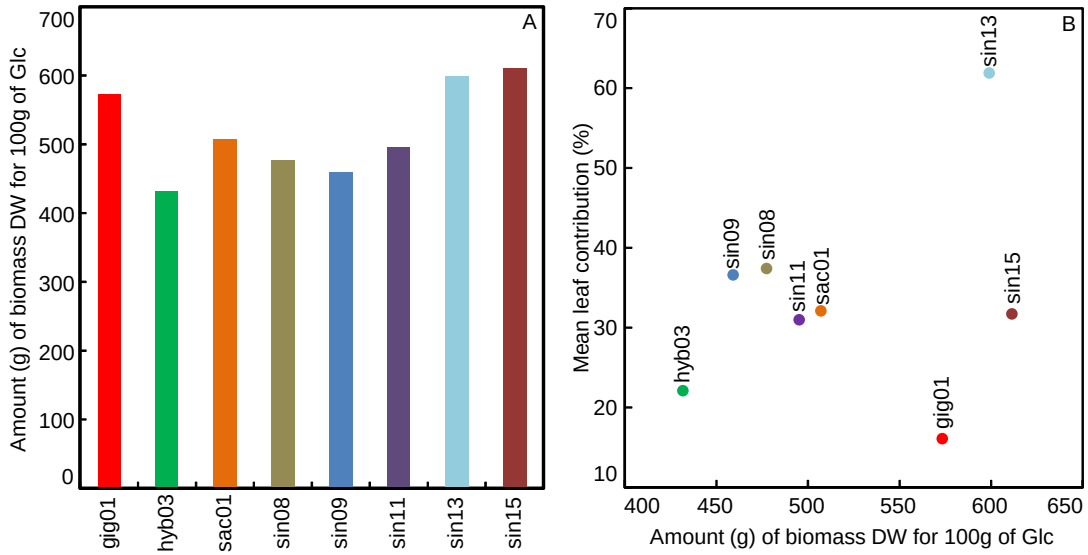

Fig. 6.9. Estimation of pooled leaf and stem total senesced biomass (dry weight, DW) needed to release 100g of glucose form pretreated samples (0.1M KOH; 16h; 21°C; Chapter 4) through enzymatic hydrolysis (4:1 Celluclast and Novozyme 188) (A). Plotting of the amounts of biomass needed to achieve 100g of glucose vs. the mean leaf contribution to total biomass (Chapter 2).

6.1.5. Cell Wall Features and their Impact on Recalcitrance

A network of cellulose and AX, which is mainly constituted by glucose and xylose, represents the main load-bearing glycan structure of the cell wall of miscanthus (Fig. 6.1), and of other Poales (Carpita, 1996). Cellulose microfibrils may enhance recalcitrance, because of their crystalline nature (Himmel *et al.*, 2007; McCann and Carpita, 2015), and it has been reported that reduction of cellulose crystallinity results in efficient cellulase enzyme penetration and higher affinity to the cellulose substrate (Yoshida *et al.*, 2008). Moreover, hemicellulose has been demonstrated to be a positive factor on saccharification enhancement in pretreated biomass, as it forms hydrogen bonds with cellulose and negatively affects its crystallinity (Xu *et al.*, 2012). Conversely, when considering hydrolysis efficiency, it has been suggested that xylobiose and other xylooligomers may inhibit enzymatic hydrolysis of pure glucan and pure xylan, in pretreated corn stover (Kumar and Wyman, 2009; Qing *et al.*, 2010), and in *M. lutarioriparious* biomass, pretreated with liquid hot water, lower hemicellulose content has been associated with higher effectiveness of cellulose deconstruction for ethanol production (Li *et al.*, 2013b). These reports are broadly in agreement with the observed findings in the present study.

In order to assess how Glc saccharification yields vary in response to the abundance of Glc and Xyl, the values for the cell wall content in these monosaccharides were correlated (Fig. 6.10) with: (1) enzymatically released Glc from UT and PT samples, expressed as percentage of cell wall biomass (%CWM); and (2) proportion of total Glc released upon enzymatic hydrolysis of UT and PT samples (%Glc). The aim of the second set of correlations is to assess how Glc and Xyl abundance is associated with saccharification efficiency. As would be expected, total Glc content in the cell wall was significantly and positively correlated with the yields of enzymatically released Glc from cell wall samples, before and after the pretreatment; despite correlation strength only being moderately high. For UT biomass: r_{All}=0.40 (P<0.001),

r_{Leaf}=0.41 (P=0.004) and r_{Stem}=0.53 (P<0.001). For PT samples: r_{All}=0.42 (P<0.001), r_{Leaf}=0.60 (P<0.001), and r_{Stem}=0.48 (P<0.001). By contrast, when correlating total Glc content in the cell wall with the proportions of removed Glc by enzymatic action, significant correlations were only detected in PT biomass, and even here, they were of moderate strength, negative, and non-significant in stem samples: r_{All}=-0.40 (P<0.001), r_{Leaf}=-0.30 (P=0.036) and r_{Stem}=-0.23 (P=0.119). These observations reveal that Glc abundance in the cell wall is not well correlated with the efficiency at which Glc may be released from the glucans in UT CWM from both tissues, and in PT biomass from stem. Specifically for pretreated leaf cell wall biomass, the significant negative correlation reveals that the higher the levels of Glc in the cell wall, the lower the proportions of extracted Glc. This observation is presumably a consequence of crystalline cellulose structures, which should become more abundant as cell wall glucan contents become higher, which in turn generates higher proportions of Glc in cellulose structures that are less accessible to hydrolytic enzymes. Furthermore, this suggests that the negative influence of cellulose crystallinity in saccharification yields is more significant in pretreated leaf biomass, as opposed to UT samples and stem tissues, where other cell wall features are likely to play more predominant roles as saccharification inhibitors. Namely, more abundant diferulate cross-links in UT samples, and higher lignin content in stems.

Similarly to what has been seen for the correlation between total Glc content in the cell wall, also for the Xyl abundance, significant correlations were detected with the enzymatic Glc yield from PT samples (r_{All}=0.33, P=0.001; r_{Leaf}=0.50, P<0.001; r_{Stem}=0.30, P=0.042). In contrast, however, was the observation that Xyl abundance is not correlated with Glc enzymatic release yields in UT leaf samples (r_{Leaf}=0.09, P=0.5416), but is significant at an overall level and for stem tissues (r_{All}=0.20, P=0.030; r_{Stem}=0.42, P=0.003). In all cases where the correlations were significant, the association between Xyl abundance and enzymatic release of Glc was positive. This positive association between Xyl content and saccharification yields

could be explained by the above mentioned negative effect xylans have on cellulose crystallinity. Furthermore, the positive correlation between Glc enzymatic yields and Xyl abundance may be associated with the fact that Xyl and Glc are the main carbohydrates of the cell wall, and both follow similar trends in terms of their abundance between different tissues and developmental stages (Fig. 4.4). Very different associations were observed when correlating total cell wall Xyl content and the proportion of enzymatically removed Glc, as only one of the calculated correlations was significant: PT CWM at an overall level (r_{All}=-0.35, P<0.001). These results suggest that in most cases Xyl abundance is not correlated with the efficiency at which Glc may be extracted from the cell wall, and when it is significantly correlated, the effect is negative; which is in agreement with the above mentioned reports that xylan interferes with enzymatic hydrolysis efficiency.

To provide further understanding of how hemicellulosic components are associated with biomass deconstruction, correlations were calculated between the abundance of cell wall components, which are known to occur associated with xylan, and the yield (Fig. 6.11) and efficiency (Fig. 6.12) of enzymatic Glc release. Xylan ornamentation with arabinosyl, feruloyl and acetyl groups has been discussed in previous chapters of this thesis. Furthermore, the hemicellulose-related ratios calculated in section 6.1.3 (Ara/Xyl, FA/Ara and Acet/Xyl) have also been correlated with the Glc saccharification indicators.

Ara/Xyl ratios are not significantly correlated with enzymatic Glc saccharification yields from UT cell wall biomass (Fig. 6.11), but in PT samples from leaf (r=-0.30, P=0.041), stem (r=-0.35, P=0.016) and actively growing plants (r=-0.48, P=0.005), the correlations are significant, albeit negatively associated with enzymatic Glc saccharification yields. The fact that Glc saccharification yields are only correlated with xylan arabinosylation in plants from earlier harvest times could suggest that arabinosyl substituents of AX do have a negative effect on enzymatic saccharification yields, but only in alkaline pretreated cell wall biomass from

young plants. Given that, at the AG developmental stage, lower proportions of the tissues have their secondary wall deposited, this immaturity factor may suggest that a negative effect of AX ramification is more pronounced before extensive tissue lignification takes place. In parallel, in PT samples, the effect of AX ramification on enzymatic deconstruction may be more relevant than in UT samples as a result of other recalcitrance-enhancing cell wall features being removed during the pretreatment. This could imply that in UT samples, cell wall features, such as ester bond-mediated cross-linking, play more substantial roles in recalcitrance than AX ramification does. Interestingly, when the Ara/Xyl ratio is correlated with the proportions of released Glc (Fig. 6.12), which provides an indication of saccharification efficiency, positive and significant associations are seen between the two variables in PT samples at PB (r=0.74, P<0.001) and SS (r=0.65, P<0.001) developmental stages. Coincidentally, it is also in PT samples at these developmental stages where the ratio of FA/Ara is more negatively correlated with Glc release proportions (Fig. 6.12; r_{PB}=-0.58, P<0.001; r_{SS}=-0.51, P=0.003). Given that ester-linked FA occurs associated to arabinosyl residues of AX, and that the ester-linked fraction of these phenolic acids is removed during the alkaline pretreatment, it is plausible that the existence of de-feruloylated arabinosyl residues in AX polymers of PT CWM has a positive effect on the efficiency at which Glc is enzymatically released. Two hypotheses may justify this observation. Firstly, it has been suggested that the degree of arabinose substitution in xylan is a key factor that positively affects biomass digestibility of miscanthus after various pretreatments, as Ara in AX is partially associated with cellulose, negatively affecting cellulose crystallinity, and in turn saccharification efficiency (Li *et al.*, 2013a). Secondly, it is possible that gaps in the cell wall structure between AX chains, left after the removal of ester-linked diferulates during the pretreatment, allows for improved enzyme accessibility to the glucans. Moreover, given that less substituted xylans are less recalcitrant, the fact that they are more easily removed may improve access of hydrolytic enzymes to cellulose fibres.

In UT CWM, when significance is detected in the correlations of ester-linked FA monomer abundance with Glc enzymatic yields (Fig. 6.11) and with the proportions of released Glc (Fig. 6.12), these associations are always positive. For Glc (UT % CWM): r_{All}=0.53 (P<0.001), r_{AG}=0.44 (P=0.013), r_{SS}=0.78 (P<0.001), r_{Leaf}=0.49 (P<0.001), r_{Stem}=0.57 (P<0.001); for Glc (UT % total Glc): r_{All}=0.35 (P<0.001), r_{SS}=0.62 (P<0.001), r_{Leaf}=0.39 (P=0.006), r_{Stem}=0.34 (P=0.017). Ester-linked FA monomers may be oxidatively coupled to form dimers and oligomers which cross-link AX polymers (Wende and Fry, 1997a; Encina and Fry, 2005; Buanafina, 2009). Since cell wall structures become tighter, and thus more recalcitrant as more ferulate monomers are coupled to form cross-links between AX chains, it may be conjectured that in CWM samples where higher abundances of ester-linked FA monomers occur, lower proportions of these HCAs have been coupled, which leads to cell wall structures which are less recalcitrant to enzymatic deconstruction. Hence providing an explanation for the positive correlations observed between ester-linked FA monomers and Glc saccharification indicators.

As previously discussed, acetyl is another substituent which occurs in cell wall polysaccharides, most abundantly in xylan. The correlation between cell wall acetylation and the indicators of enzymatic Glc saccharification has been determined in two different ways. Initially, with acetate abundance values on their own, and secondly, as a molar ratio between acetate and Xyl (Acet/Xyl). In all cases, the trends of correlation significance were generally similar for acetate abundance and for the Acet/Xyl ratio (Figs. 6.10 and 6.11). Thus only the correlations with acetate abundance will be discussed. The role of acetate in plant cell walls is not completely understood, but it is known that CWM which has been de-acetylated by the action of an alkaline pretreatment does exhibit better saccharification results (Chapters 3 and 4), and it has been reported that the pattern of xylan acetylation may influence how xylan interacts with cellulose in secondary cell walls (Busse-Wicher *et al.*, 2014). How

lignocellulosic biomass deconstruction is affected by acetyl substituents also remains unclear, but available information suggests that even if acetate does not affect saccharification directly, its abundance in the cell wall may be associated with the prevalence of structural features, which in turn do enhance recalcitrance. In the miscanthus CWM analysed in the present study, significant and negative correlations between acetate content and enzymatically released Glc yields were observed for UT samples at an overall level (r=-0.32, P=0.002), in senesced plants (r=-0.65, P<0.001) and in leaf biomass (r=-0.57, P<0.001). These negative correlations indicate that in fact Glc saccharification yields are inversely associated with the degree of cell wall acetylation. Acetate abundance in leaf cell wall biomass increases throughout development (Fig. 3.2), which may explain the particularly higher correlation coefficients detected in the biomass from leaves and senesced plants. By correlating acetate abundance with the proportions of released Glc from UT samples, significant correlation coefficients were always negative (r_{All}=-0.35, P=0.001; r_{SS}=-0.62, P<0.001; r_{Leaf}=-0.50, P<0.001); indicating that cell wall acetylation not only hinders Glc saccharification yields, but also the efficiency at which Glc may be released. Similarly, for PT samples at an overall level (r=-0.22, P=0.029) and at the PB developmental stage (r=-0.45, P=0.010) Glc release efficiency is also negatively correlated with acetate content. However, in stem samples, the proportions of released Glc are positively correlated with acetate abundance (r=0.38, P=0.007), which may be explained on the basis that the typically higher acetate content in stem biomass (Fig. 3.2) makes a bigger contribution to the maintenance of correct cell wall integrity than it does in leaves. As a result, once the 0.1M KOH pretreatment is applied, and acetyl-ester bonds are cleaved, the cell wall becomes substantially more susceptible to the action of hydrolytic enzymes.

Ratios between the abundance of *p*CA and FA have been reported in Fig. 3.5, and it has been suggested that high values for this ratio are associated with low cell wall degradability (Hartley, 1972; Jung *et al.*, 1991; Du *et al.*, 2009). Similar observations have been made in the

miscanthus cell wall samples here analysed, as the *p*CA/FA ratio is negatively correlated with the Glc yields (Fig. 6.11): for UT samples at a global level, and in leaf samples (r_{All}=-0.28, P=0.007; r_{Leaf}=-0.72, P<0.001); for PT samples, at an overall level, PB, SS and in leaf biomass (r_{All}=-0.28, P=0.006; r_{PB}=-0.43, P=0.015; r_{SS}=-0.40, P=0.024; r_{Leaf}=-0.35, P=0.014). Also concerning correlations with the proportions of released Glc (Fig. 6.12), significant and negative correlations were detected at the overall level of the samples (r=-0.41, P<0.001), at the AG developmental stage (r=-0.45, P=0.011) and in leaf samples (r=-0.65, P<0.001) for UT samples; whereas for PT samples, significant correlations were more frequent, as they were detected at an overall level (r=-0.52, P<0.001), PB (r=-0.62, P<0.001), SS (r=-0.46, P=0.008) and in stem samples (r=-0.43, P=0.002). These observations suggest that *p*CA/FA ratios are frequently negatively associated with Glc saccharification yields, and with the efficiency at which Glc may be released from the CWM, particularly in PT samples. However, despite being known that *p*CA in the cell wall is predominantly associated with lignin, the structural role of this HCA has not yet been fully characterised, and thus there is a lack of understanding of the molecular specificities by which the *p*CA/FA ratios are correlated with cell wall recalcitrance.

The elucidation of how different cell wall features affect the *C. phytofermentans*-mediated fermentation is in many cases not possible, given that the mechanism of action of this bacterium has not been completely characterised. Nonetheless, in most cases the trends in correlation significance with the ethanol yields were not too dissimilar to those observed for Glc release yields (Fig. 6.11). Therefore, analogous inferences may be drawn to some extent, in what concerns the impact of the different cell wall features on amenability to deconstruction. However, in senesced samples (Fig. 6.11) opposing effects were observed concerning the impact of cell wall acetylation, as a positive correlation was detected between ethanol yields and acetate abundance (r=0.40, P=0.024). This observation is also in

opposition to the observed in earlier developmental stages, and thus could not be reasonably explained in the current study.

As discussed in chapter 2, lignin has traditionally been described as the cell wall component which mostly contributes to lignocellulosic biomass recalcitrance to deconstruction. Results from the present study have shown that lignin is in fact always negatively correlated with Glc saccharification yields from UT samples (Fig. 6.11; r_{All}=-0.82, P<0.001; r_{AG}=-0.80, P<0.001; r_{PB}=-0.63, P<0.001; r_{SS}=-0.60, P<0.001; r_{Leaf}=-0.80, P<0.001; r_{Stem}=-0.90, P<0.001). However, in PT samples, lignin content is not significantly correlated with Glc yields in peak biomass samples (r=-0.24, P=0.183), suggesting that at this developmental stage Glc saccharification yields are more influenced by other factors beyond lignin content. Additionally, according to the correlations with the efficiency of Glc saccharification from PT samples (Fig. 6.12), the negative effect of lignin appears to be even lower; as the only single developmental stage where a significantly negative correlation was detected is in actively growing plants (r=-0.62, P<0.001), and only with stem biomass (r=-0.57, P<0.001). AG samples are typically the least recalcitrant of all developmental stages, possibly indicating that in biomass from this time point cell wall features which tighten cell wall structures have lower impacts on saccharification efficiency, than in samples collected at later harvests. This is corroborated by the fact that in pretreated samples from actively growing plants only lignin content has a significantly negative effect on saccharification efficiency. Therefore, although lignin is less abundant in biomass harvested at earlier developmental stages, given that other cell wall components do not significantly affect saccharification efficiency, this low lignin abundance may still become the most significant recalcitrance enhancing factor. Furthermore, in later developmental stages, this predominance of the negative effect of lignin content is not observed, as other cell wall features become significantly and negatively correlated with saccharification indicators. The 0.1M KOH pretreatment is

known to remove ester-linked components from the cell wall (Chapter 3). Minimal interference on lignin content has been observed with other chemical pretreatments, which notwithstanding still do have very positive effects on saccharification (Kristensen *et al.*, 2008; DeMartini *et al.*, 2011). However, as the correlations of lignin abundance and Glc saccharification are altered in UT and PT samples (Figs. 6.10 and 6.11), it is evident that the pretreatment altered the role of lignin in the cell wall. Thus, these data support the concept that it is not lignin content per se that affects recalcitrance. Rather, the integration of lignin and polysaccharides within the cell wall, and their mutual associations, appear to play a larger role. Moreover, ester-linked components, such as FA, acetate, and *p*CA, removed during the pretreatment are directly or indirectly involved in polymer cross-linking, and this may have affected the role of lignin in the cell wall in terms of its association with glycans. This is not only supported by the distinct correlation coefficients with lignin in PT and UT samples, but also by the fact that several glycans are detected in chlorite fractions of the cell wall during glycome profiling (Fig. 5.4). Ultimately, these results give relevance to the importance of cell wall structural features in Glc saccharification efficiency, in detriment of mere lignin content, in the situations where no significant correlations are detected.

Between tissues, different compositional traits are likely to respond differently to pretreatment. As discussed in chapter 5, it is likely that HG makes a bigger contribution to maintaining correct cell wall structure in leaves than in stems, possibly as a consequence of lower cellulose and lignin contents than in stems (Burton *et al.*, 2000; Manfield *et al.*, 2004; Wolf *et al.*, 2009). Perhaps this may help explain the higher efficiency of the pretreatment in enhancing Glc and Xyl release from leaf biomass (Table 4.16), as the 0.1M KOH treatment is known to remove HG from the wall in switchgrass (DeMartini *et al.*, 2013) and presumably also from miscanthus biomass. Especially in grasses, this could lead to weaker cell to cell adhesion in pretreated tissues, and thus enhance enzyme accessibility.

Also related to compositional differences between tissues, is the fact that despite the abundance of ester-linked FA not varying substantially between leaf and stem (Fig. 3.4. and Table 3.7.), the Ara/Xyl ratio is higher in leaves (Fig. 4.5). An interpretation of this could be that, whereas in stems higher abundances of lignin imply that bigger proportion of FA are involved in cross-linking lignin to xylan; in leaves, because of lower proportions of lignin, the bigger proportion of arabinosyl to xylosyl residues would provide more opportunities for ester-bonded FA cross-linking between AX chains. As a result, when 0.1M KOH is applied, the xylan chains in leaves likely represent a lower hindrance to enzymatic accessibility. Whereas in stems, higher lignin content, would imply more abundant links between xylan and lignin, which occur by covalent bonds via ether linkages (Williamson *et al.*, 1998; Buanafina, 2009) and thus are not broken by 0.1M KOH. As a conclusion, higher effectiveness of 0.1M KOH on leaves is relevant to optimise biomass conversion approaches, but also to understand differences in how the cell wall structure is maintained in leaf and stem tissues of miscanthus. Moreover in this case it suggests that lignin plays a bigger role in stems, while in leaves carbohydrate-carbohydrate structure reinforcement seems to play more relevant roles than in stems.

Although the determinants behind the impact of pectin content on cell wall recalcitrance are poorly understood, it has been shown that arabidopsis *quasimodo* mutants, which carry mutations on certain galacturonosyltransferases (putative pectin methyl-transferases), display deficient cellular adhesion (Bouton *et al.*, 2002; Mouille *et al.*, 2007). Furthermore, it has also been reported that a decrease in HG content of the cell wall enhances polymer flexibility (Ralet *et al.*, 2008). In grass cell walls, despite a lower abundance, pectin may also be a key contributor to cell wall integrity (McCann and Carpita, 2015), and thus may influence biomass recalcitrance. As discussed in chapter 5, this effect of pectin may be at the level of HG polymers, which, when de-methyl-esterified, promote cell adhesion, and thus cell wall

recalcitrance to deconstruction (Zhang and Staehelin, 1992; Mohnen, 1999; Anthon and Barrett, 2006; Lionetti *et al.*, 2010). The 0.1M KOH pretreatment de-esterifies cell wall polymers, which from the point of view of cell wall structure conceivably could initially contribute to cell wall adhesion. However, it is known that polysaccharide ornamentations do have negative effects on hydrolytic enzyme activity, namely by steric hindrance (Pauly and Scheller, 2000; Pell *et al.*, 2004; Correia *et al.*, 2011; Biely, 2012; Pawar *et al.*, 2013; Buckeridge and de Souza, 2014). Therefore, although KOH-mediated de-esterification of the cell wall would reduce the degree of HG methyl-esterification, it could simultaneously make cell wall polysaccharides more prone to enzymatic attack. Additionally, as briefly mentioned above, in switchgrass, a closely related species to miscanthus, it has been reported that 0.1M KOH causes the release of HG epitopes (DeMartini *et al.*, 2013). It is likely that in the miscanthus biomass analysed in the present study, the 0.1M KOH pretreatment also causes the removal of some HG. Given that HG occurs abundantly in middle lamellae (Chapter 5), and contributes to cell adhesion, the removal of HG, effected by 0.1M KOH, may be an additional factor, alongside the severing of ester-bonded cross-links; altogether contributing to the disruption of cell wall integrity, and thus enhancing amenability to deconstruction. Additionally, during glycome profiling of miscanthus CWM it was observed that several pectic epitopes which are removed with the weakest steps of the sequential extraction (perhaps somewhat analogously to the effect of the 0.1M KOH pretreatment) are also found in chlorite extracts, which de-lignify the cell wall. Therefore the possibility that glycans, namely pectins, are removed during the alkaline pretreatment, and that these polymers could be involved in lignin associations is plausible, and has been suggested by other authors in studies focused on grass cell wall (DeMartini *et al.*, 2013; de Souza *et al.*, 2015). In older literature, as mentioned in Shen *et al.* (2013), references are found suggesting that pectins may be removed with lignin during the delignification by chemical treatments. Furthermore, it has been shown that in beech

(*Fagus crenata*) lignocellulosic biomass, lignin-carbohydrate complexes (LCC) contain ester linkages between lignin and glucuronoxylan, and that about a third of the glucuronic acid present in the LCC is involved in this ester linkage (Takahashi and Koshijima, 1988). These data may provide support for the hypothesis that pectin removal during alkaline pretreatment does have a positive effect on recalcitrance attenuation. Studies focusing on interactions between lignin and pectin are not abundant in the literature, thus the confirmation of these theories requires further studies. However, relatively recent identification of pectin-containing proteoglycan cell wall structures (Tan *et al.*, 2013), and the identification of potential inter-linkages between xylan and pectin, and between xylan and AGPs (Cornuault *et al.*, 2015) suggest that current models of the plant cell wall are incomplete, and that they are even more complex than traditionally thought. Accordingly, there is the possibility for the occurrence of polymer interactions which have not been previously considered.

The data presented here reveals that several structural features associated with carbohydrate and non-carbohydrate cell wall components play substantial roles in maintaining cell wall integrity, and thus affect amenability to deconstruction. These factors may not only be associated with how hemicellulose polysaccharides interact with each other and with cellulose and lignin, at a whole biomass level (as shown by the correlations discussed in this section), but also with differences in the distribution and esterification of other specific cell wall polysaccharides. Namely, pectic HG, which revealed distinct esterification patterns in different tissues and in certain cell types (discussed in chapter 5). Altogether, the results that have been presented throughout this thesis point to the general conclusion that single cell wall components, such as lignin, should not be considered as sole indicators of biomass recalcitrance. Cell wall assembly, and consequently its disassembly, are complex multifactor phenomena, which are heavily dependent on: (1) the procedures used to hydrolyse the cell wall; (2) the application and the nature of pretreatments; (3) structural and compositional differences

between tissues and developmental stages in the carbohydrate component of the cell wall; (4) the occurrence and abundance of cell wall micro domains where glycans possess different properties; (5) physiological mechanisms, such as the translocation of carbohydrates during senescence, which affect relative proportions of lignocellulosic biomass components. Moreover, as was shown in the previous section, different miscanthus genotypes have distinct cell wall compositional and structural profiles. This creates an additional layer of complexity on cell wall deconstruction, where it is possible that different synergies could occur, which in turn, would cause varying effects of individual cell wall feature in biomasses from different origins. Ultimately, this would depend on how the different components interact in the cell wall as a whole, creating an overall positive or negative net effect on recalcitrance.

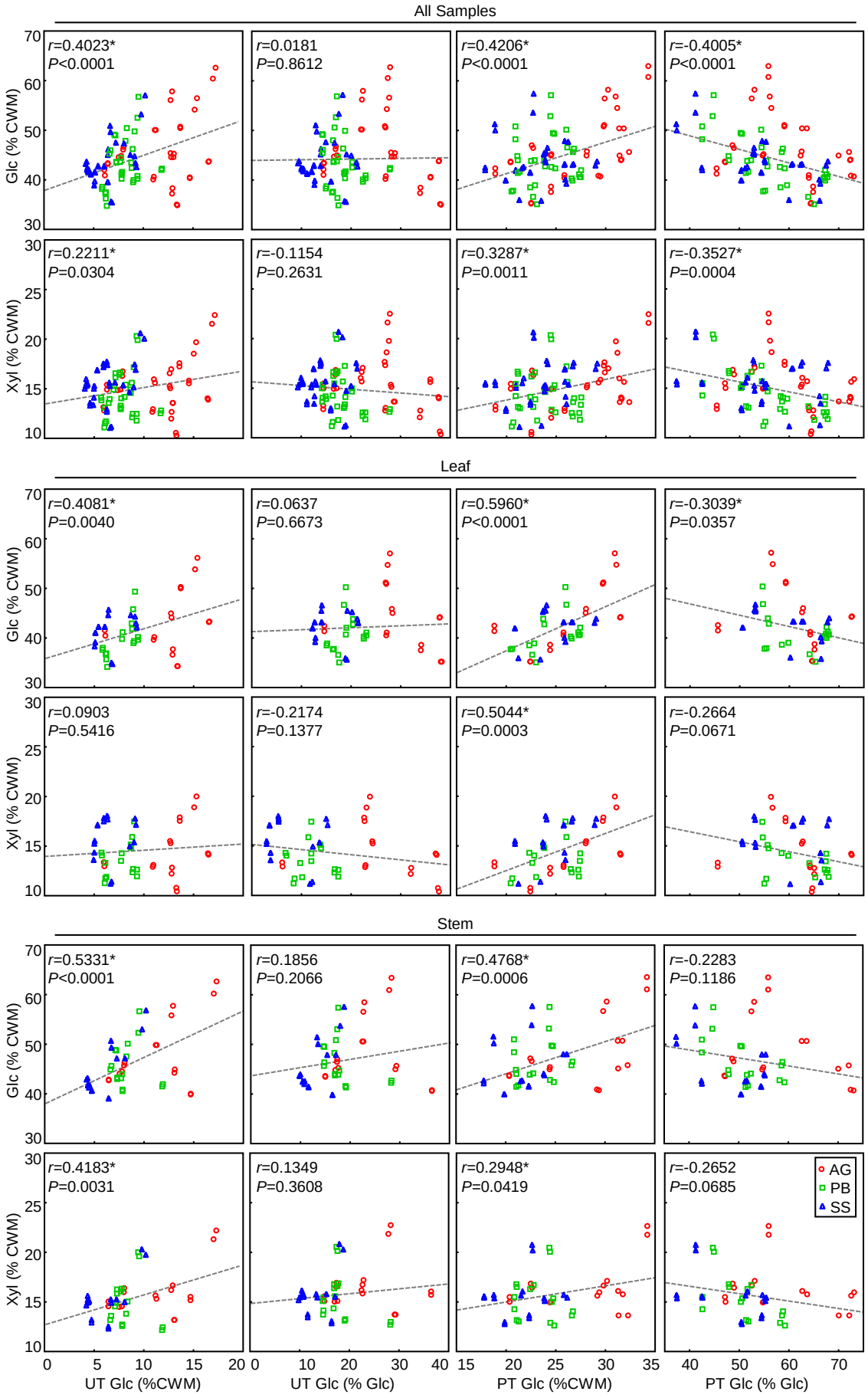
All Samples
r=0.4023*
P<0.0001
r=0.0181
P=0.8612
r=0.4206*
P<0.0001
r=-0.4005*
P<0.0001
r=0.2211*
P=0.0304
r=-0.1154
P=0.2631
r=0.3287*
P=0.0011
r=-0.3527*
P=0.0004
Leaf
r=0.4081*
P=0.0040
r=0.0637
P=0.6673
r=0.5960*
P<0.0001
r=-0.3039*
P=0.0357
r=0.0903
P=0.5416
r=-0.2174
P=0.1377
r=0.5044*
P=0.0003
r=-0.2664
P=0.0671
Stem
r=0.5331*
P<0.0001
r=0.1856
P=0.2066
r=0.4768*
P=0.0006
r=-0.2283
P=0.1186
r=0.4183*
P=0.0031
r=0.1349
P=0.3608
r=0.2948*
P=0.0419
r=-0.2652
P=0.0685
AG
PB
SS
Glc (% CWM)
Xyl (% CWM)
UT Glc (%CWM)
UT Glc (% Glc)
PT Glc (%CWM)
PT Glc (% Glc)

Fig. 6.10. (Previous page). Least square fit and associated Pearson correlation statistics (*r*) and probabilities (*P*) for the correlations between the total content of miscanthus cell wall most abundant monosaccharides (glucose and xylose), against the yields of enzymatically released glucose from pretreated (PT) and un-pretreated (UT) cell wall material (CWM). Enzymatically released glucose yields expressed as percentages of total glucose in the cell wall provides an indication of the saccharification efficiency. Developmental stages: AG, active growth; PB, peak biomass; SS, senescence. Marked correlations (*) are significant at $P<0.05$.

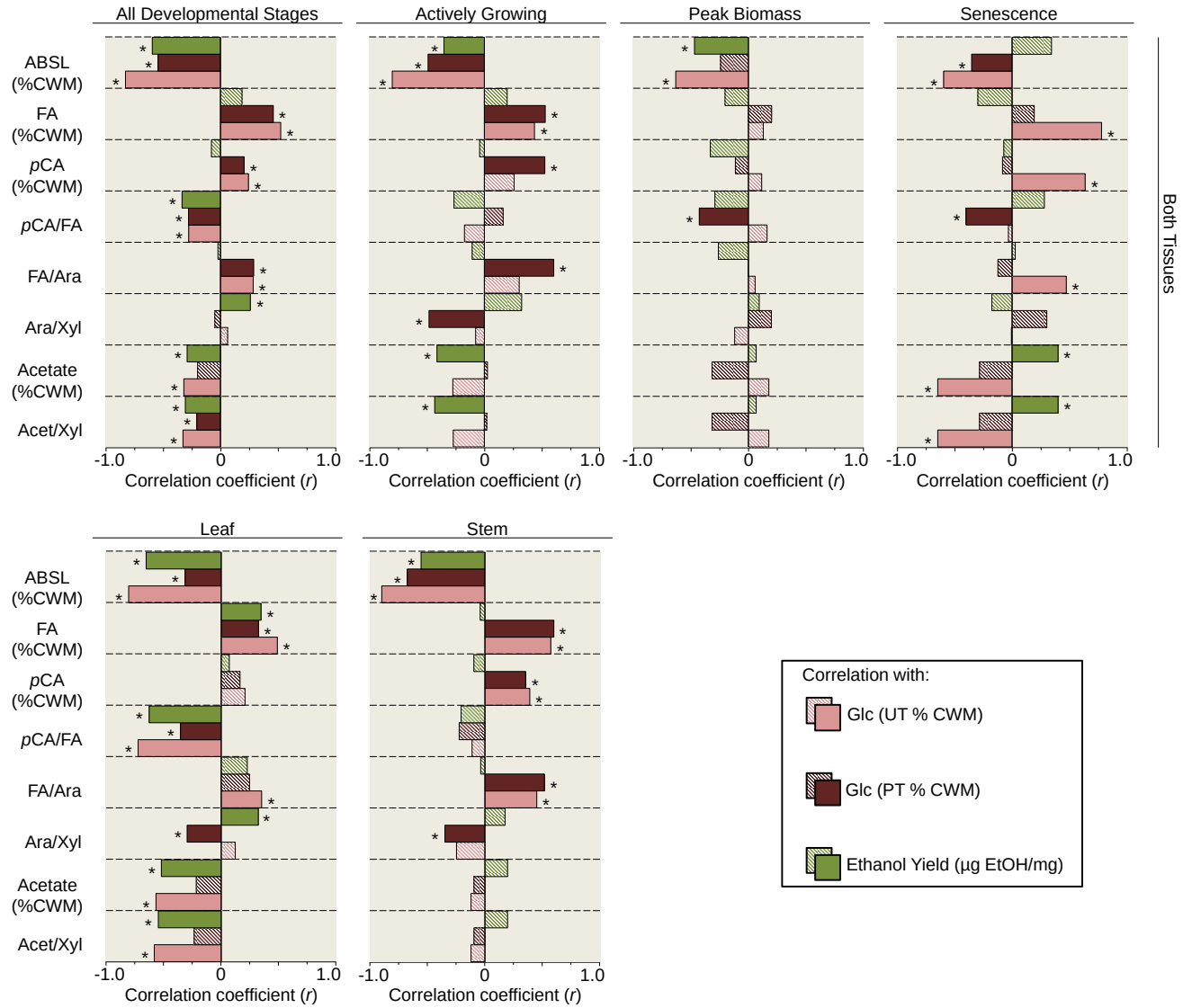

Fig. 6.11. Pearson coefficients of the correlations between the results obtained for the three digestibility assessment assays, and several cell wall features. For each correlation coefficient N=96 for all developmental stages, N=48 for individual tissues, and N=32 at each developmental stage. Marked correlations (*) are significant, and columns filled with a diagonal lines pattern are non-significant at $P<0.05$. Abbreviations: UT, un-pretreated; PT, pretreated; ABSL, acetyl bromide soluble lignin; FA, ester-linked ferulic acid, *p*CA, *p*-coumaric acid; Ara, arabinose; Acet/Xyl, molar ratio between acetate and xylose in the cell wall material (CWM); EtOH, ethanol yielded from the *C. phytofermentans*-mediated fermentation.

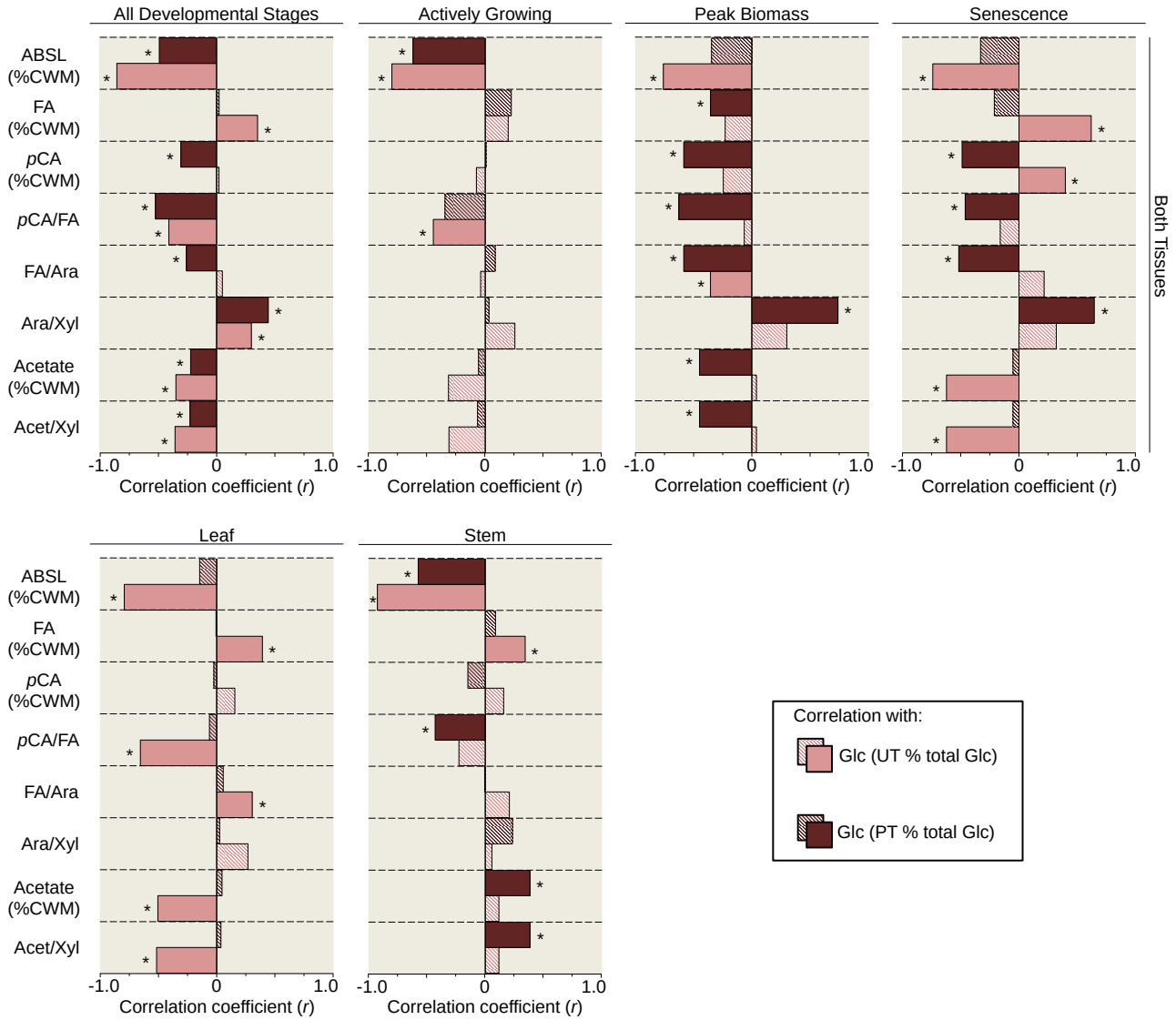

Fig. 6.12. Pearson coefficients of the correlations between glucose saccharification efficiency, and several cell wall features. For each correlation coefficient N=96 for all developmental stages, N=48 for individual tissues, and N=32 at each developmental stage. Marked correlations (*) are significant, and columns filled with a diagonal lines pattern are non-significant at $P<0.05$. Abbreviations: UT, un-pretreated; PT, pretreated; ABSL, acetyl bromide soluble lignin; FA, ester-linked ferulic acid, *p*CA, *p*-coumaric acid; Ara, arabinose; Acet/Xyl, molar ratio between acetate and xylose in the cell wall material (CWM).

6.2. Final Considerations, Publication Output and Future Research Directions

The studies presented in this thesis provided evidence that different miscanthus genotypes have significantly different properties with regard to biomass production and the proportions of leaf and stem biomass in the whole above-ground harvested biomass. Hybrid genotypes, particularly *M.* × *giganteus*, are typically the highest biomass producers at all developmental stages considered. By contrast, the lowest measured tiller weights were observed in *M. sinensis*, but these genotypes display a wider range of morphological properties. Most studies on cell wall composition in energy crops use total above-ground biomass for their analysis, as this is the most relevant material for downstream applications. However, different tissues possess cell walls with very distinct properties, likely to be controlled by separate mechanisms, which ultimately have distinct effects on biomass recalcitrance to deconstruction. Varying tissue contributions can have a substantial performance and economic impact on downstream biorefining processes, as compositional differences between stem and leaf biomass will lead to tissue-specific amenability to enzymatic hydrolysis, to biological conversion into ethanol and to the generation of other economically relevant products.

FTIR spectroscopy allied to PCA allowed investigation of the underlying relationships between the spectra, thus leading to the determination of the overall compositional shifts of miscanthus cell wall samples collected from different tissues at different developmental stages. The interpretation of spectral segregation patterns and of the corresponding principal component loadings suggested that overall compositional shifts between leaf and stem predominantly occur at the level of the cell wall structural carbohydrates. Between immature and mature stems, in addition to the variation in the cell wall polysaccharide fractions, lignin emerged as a main source of compositional variation between actively growing plants and plants which had reached their peak biomass yield. The predictions derived from the FTIR-PCA approach were subsequently confirmed by gravimetric and other methodologies,

which directly assessed the cell wall composition in terms of specific components, or groups of chemically related components.

For lignin composition, the acetyl bromide method was employed. Previously to the present study, no data for lignin content was available for the cell wall of actively growing and peak biomass miscanthus plants. Significant developmental and tissue effects were detected in the lignin abundances, as it typically increased as plants matured, and stem biomass was more lignified when compared to leaves. However, the variation in lignin abundance between tissues and developmental stages was much lower than initially expected. Moreover, at the senesced harvest time point, no significant differences were detected between the lignin abundances of different genotypes; neither in their leaf nor in their stem biomass. Although indirectly, these observations represented an initial confirmation of the FTIR-based hypotheses that carbohydrates are major contributors to cell wall compositional variation between tissues and developmental stages, and that stem cell walls are subjected to more extensive modification throughout development than leaves.

By employing a bioassay which used ethanol yields from *C. phytofermentans*-mediated fermentation, as a means to assess biomass quality, it was revealed that CWM amenability to digestion varies significantly between the tissues, genotypes and development. Two other approaches were employed to assess digestibility; both based on the measurement of released Glc (in addition to Xyl and Ara) following the enzymatic hydrolysis of cell wall biomass samples with and without a mild alkaline pretreatment. Given that these three approaches rely in distinct mechanisms to deconstruct the cell wall, the agreement between them was heavily influenced by cell wall properties of the specific samples under scrutiny. However, at an overall level, in all cases the amenability to deconstruction was typically higher in younger plants, and in leaves when compared to stems.

Correlation coefficients were determined between the results derived from these digestibility assessment methods, and the abundance of lignin and other cell wall compositional and structural features; to determine their impact on cell wall recalcitrance to deconstruction. These studies highlighted the limited predictive power of single traits as indicators of cell wall recalcitrance. Results strongly suggested that at different developmental stages, the biomass from different plant tissues, and even from different genotypes, present properties which are sufficiently divergent to cause distinct effects on recalcitrance. It is likely that in cell wall biomass from different origins these cell wall features contribute differently to recalcitrance, as different proportions of cell wall components lead to different interactions, which enhance or reduce the influence of a given feature. These conclusions do not contribute to the formulation of reductionist explanations for cell wall recalcitrance. However, the observation that no universally significant correlation has been detected between a specific cell wall component and a negative effect on cell wall deconstruction may lead to the development of new approaches to improve the efficiency of Poalean lignocellulosic biomass deconstruction.

Specifically for lignin, which is frequently considered the main recalcitrance-enhancing cell wall component; its effect is complex, and not a straight-forward negatively proportional association between its content and recalcitrance. A key observation derived from the present study was that in pretreated biomass from mature miscanthus plants, lignin abundance is not correlated with the efficiency at which Glc is enzymatically released from the cell wall. The employed pretreatment involved treating CWM with 0.1M KOH (21°C, 16h), and a significantly positive effect was observed on saccharification efficiency and yields. To a certain extent, the effect of 0.1M KOH may be explained by the fact that it leads to a partial release of esterified acetyl and hydroxycinnamoyl substituents of cell wall polymers. Furthermore, it is noteworthy that it causes little disruption of cell wall polymers; as no substantial amounts of

aromatic compounds (besides *p*CA and FA), and mono- or oligosaccharides were detected as being released during pretreatment.

Overall lignin contents of the cell wall remain largely unaltered in the pretreated biomass, and they are at times poorly correlated with saccharification efficiency. This supports the view that research approaches aimed at better understanding cell wall cross-linking are at least as relevant as studies focused on simply reducing lignin content. The reason for this is that an improved elucidation of cell wall structure may allow the development of pretreatments or genetic engineering approaches aimed at minimising interaction with lignin, without a reduction of cell wall lignin abundance. Perhaps genetically modified plants with lignin contents comparable to un-modified varieties, but with less interconnected cell wall structures, may lead to higher saccharification yields, without compromising plant structural integrity. Indeed, this approach of redesigning lignin structure has already shown promising results, as reported by Wilkerson *et al.* (2014); who have improved cell wall digestibility via the introduction of chemically labile linkages into the lignin backbone. There are numerous economic benefits of maintaining normal *in planta* lignin levels. Namely, as new conversion pathways emerge, new avenues for lignin utilisation are also being created (McCann and Carpita, 2015). Furthermore, refinement of biomass downstream processing has enhanced lignin recovery, and this coupled with genetic engineering may enable new uses for lignin; such as low-cost carbon fibres, engineered plastics and thermoplastic elastomers, polymeric foams, fungible fuels, and commodity chemicals; reviewed by Ragauskas *et al.* (2014). These technical advances may eventually lead to cost-effective utilisation of lignin-derived chemicals for parallel biomaterial production, which in turn will add value to lignocellulosic biomass applications, and thus enhance the economic viability of lignocellulosic biofuels.

It is possible that in cell walls with reduced interconnectedness with lignin, certain compensatory effects may become more relevant in providing structural support. An effect

which may increase cell wall recalcitrance to deconstruction is the reduction of methyl-esterification of HG. From a biomass processing point of view, the removal of these ester-linked substituents with the aim of increasing saccharification yields can be achieved by dilute or mild alkali pretreatments; thus facilitating immensely industrial processing. In relation to structural compensatory effects, a rather analogous observation may have been made in the present study. It has been suggested that HG with a low degree of esterification may be increased in situations where supplemental structural support is required, such as in response to cellulose depletion (Wolf *et al.*, 2009). Indeed, both the glycome profiling, and the *in situ* immunolabelling approaches revealed that, when compared to stems, leaf biomass not only contains lower amounts of glucans, but also higher levels of HG in general, and particularly of de-methyl-esterified HG. Thus, HG might play more vital roles in maintaining cell wall structure in leaves than it does in stems. Furthermore, it has been demonstrated that increased levels of de-methyl-esterified HG has a negative effect on cell wall saccharification (Lionetti *et al.*, 2010). With the application of the alkaline pretreatment, although no extensive disruption of the main cell wall polysaccharides was detected, minor components, such as HG, are known to be removed by 0.1M KOH (DeMartini *et al.*, 2013). As a consequence, with 0.1M KOH, the removal of HG from the biomass would have a bigger impact on decreasing cell wall recalcitrance in leaves than in stems. Once again, these observations refer to the importance of understanding how cell wall components interact with each other and respond to downstream processing approaches to optimise lignocellulosic biomass deconstruction.

Other levels of compositional variability with the potential to affect miscanthus biomass deconstruction may lie in the fact that distinct compositional variation trends are seen along development in stem and in leaf, and also in different genotypes. Data from this thesis suggests that overall variation in structural cell wall components between mature and immature plants: in stems, is primarily associated to non-matrix cell wall components (cellulose and lignin), and

to a lesser extent to pectin; whereas in leaves, overall biomass composition varies less than in stems, but significant differences are seen in the more labile and less abundant glycan epitopes (amenable to be extracted with ammonium oxalate and sodium carbonate during the sequential extraction). Additionally, Glc contents were typically higher in stem tissues than in leaf tissues, but the enzymatic release of Glc was higher in pretreated mature leaf samples, confirming that the usability of the monosaccharides contained in miscanthus lignocellulosic biomass is also distinct between different tissues. Ultimately, no single genotype showed a general tendency for a typically high or low sugar yield in all conditions studied. However, for individual tissues it was seen that some genotypes displayed generally above or below average values; which provides further evidence for the hypotheses that there may be a genotype-specific element in cell wall assembly (perhaps associated to the structural requirements demanded by their phenotypes), and that there is an independent control of cell wall composition in different tissues (Murray *et al.*, 2008).

Several factors may affect the recalcitrance to deconstruction of the cell wall polymers, namely: the level of intertwining of the polysaccharides and of their embedding within lignin; the location of the polysaccharides within the cell wall; and the age, function or type of tissue being used, which may, for example, present differing degrees of cell wall thickening. As a result, in energy crop improvement efforts, whether by traditional plant breeding approaches or by genetic engineering, cell wall components which affect recalcitrance should be considered. Merely increasing biomass yields should not be the single strategy, as high biomass producers may not always be the most cost-effective varieties, and also high carbohydrate content is not always synonymous of high saccharification efficiency. Thus, attempts to generate plant varieties which are less recalcitrant, even if at the cost of biomass yield reductions, could be a worthy route to explore in plant breeding. Ultimately, it is likely that

less recalcitrant biomass could allow substantial savings in transport and in downstream biomass processing.

By the time of submission of this thesis, the results derived from the studies herein included have already generated novel publications, which may influence new research approaches and data interpretation. In an initial study (da Costa *et al.*, 2014) cell wall biomass was analysed for 25 miscanthus genotypes, considering different developmental stages and stem vs. leaf compositional variability, by FTIR spectroscopy and lignin determination. In addition, the *C. phytofermentans* bioassay was used to assess cell wall digestibility and conversion to ethanol. Results from this study led to the hypothesis that divergent carbohydrate compositions and modifications in stem and leaf tissues are major determinants for observed differences in cell wall quality. Subsequently, parts of the experimental methods used in this study were compiled into a full, detailed protocol focusing on cell wall biomass preparation and FTIR spectroscopy to study cell wall composition (da Costa *et al.*, 2015). The resulting publication is now part of an easy-to-use depository of life science protocols; made open access to enhance research by promoting the free-exchange of experimental procedures. From these publications, new research directions are emerging with more focus on the composition of polysaccharide fractions of the cell wall, and on the exploration of polysaccharide cross-linking between themselves and with non-carbohydrate portions of the cell wall. Glycome profiling and *in situ* immunolabelling were two key approaches used at the second stage of the studies. Both may be generally described as employing glycan-directed monoclonal antibodies to assess the distribution of cell wall polysaccharide epitopes in different cell wall biomass fractions, or in whole tissue cross sections, respectively. Outcomes of these and other studies presented in previous chapters have generated sufficient data for perhaps two new peer-reviewed publications. For the first manuscript it is intended to represent the most comprehensive report published to date on the glycan profile of *Miscanthus* spp. cell walls. The aim of this paper is

to function as a follow up of the previous publications, and should focus on the clarification of glycan compositional variability between miscanthus tissues collected at varying developmental stages. At a subsequent stage, the preparation of a second manuscript is planned, which will focus more on genotypic differences and on how cell wall composition may impact miscanthus biomass deconstruction approaches. Moreover, observations made regarding the distinct glycan epitope immunolabelling patterns observed in leaf-specific tissues (such as bulliform cells and stomatal complexes) may lead to new views of the functions of specific cell wall polysaccharides on specific cell types.

Due to time and funding constraints inherent to the project, there were several experimental approaches which were not performed, but could enrich the conclusions presented in this thesis. Here follows a brief presentation of these new research directions. With regard to lignin composition of the cell wall, it has been reported that changes in lignin composition are accompanied by changes in lignin structure, which may influence the deconstruction of cell wall biomass. As an example, with higher S/G ratios in poplar biomass, sugar release is generally higher than in tissues with lower ratios (Studer *et al.*, 2011). In miscanthus, genotypic differences in these ratios are also known to occur (Villaverde *et al.*, 2009); however limited information is available for leaf and stem individually and for different developmental stages. Given that in the present study FTIR data suggested that there are significant lignin compositional modifications between miscanthus biomass from different harvests and tissues, it would be interesting to assess these differences directly. An analytical approach which may be employed is thioacidolysis, which would allow determination of relative lignin monomer proportions in the cell wall, and subsequent deduction of their impact on recalcitrance. Furthermore, additional information could be generated concerning the impact of alkaline and perhaps other pretreatment technologies on lignin structure. Yet another approach to determine not only lignin abundance but also lignin distribution could rely on the

utilisation of lignin staining dyes (such as phloroglucinol), or lignin-directed molecular probes. Additionally, the distribution of HCAs may be determined via their autofluorescence. Such strategies could allow the determination of overlapping distribution patterns of lignin and other cell wall components, perhaps contributing to our understanding of the assembly of lignin-carbohydrate complexes.

Also related to the cross-linking of wall polymers, the identity, abundance and distribution of ether-bound ferulates, and of di- and oligoferulates, were not determined in the present study. The determination of these cell wall parameters could lead to pertinent observations relevant to understand the full picture of the effect of polymer cross-linking on cell wall deconstruction.

Data presented in previous chapters revealed that Glc abundance in the cell wall is not always significantly or even positively correlated with saccharification efficiency. These observations led to the hypothesis that glucan structural features, such as cellulose crystallinity may have a substantial effect on cell wall deconstruction. Furthermore, several authors have suggested that AX ornamentation and the degree of cellulose crystallinity may be associated (Xu *et al.*, 2012; Li *et al.*, 2013a). Consequently, it would be very pertinent to include the determination of cellulose crystallinity indices in a future research proposal.

Despite being a small component of grass lignocellulosic biomass, pectic components may have substantial influence on the deconstruction of the cell wall. In the present study it was hypothesised that the positive effect of a mild alkaline pretreatment on the enhancement of saccharification yields could be partially associated with the disruption or even removal of HG from the wall biomass. However, this probable effect of the pretreatment has not been directly assessed. Possible strategies to gather this information could employ glycome profiling, or perhaps epitope detection chromatography (Cornuault *et al.*, 2014), to analyse the cell wall extracts produced during pretreatment. Alternatively, acid solutions (TFA or H_2SO_4)

may be added to the supernatants derived from the pretreatment, in order to hydrolyse any glycans which may occur in solution, and thus allow the detection and quantification of resulting monosaccharides by HPAEC.

Any of these new research directions have individual value; however, greater outcomes may be generated if all were to be integrated in a tour de force of characterisation of the cell wall. Such an initiative would not only complement, but also expand the conclusions already reached as part of the present thesis; as new approaches (such as selective enzymatic hydrolysis) may be integrated in the project, as a means to determine the effects on recalcitrance of disturbing specific cell wall features. Additionally, by employing well characterised enzymes in a defined succession, the results could be interpreted as partly mimicking the reactions that occur when plant biomass is attacked by microbes. Modifications at the cell wall level could be assessed by approaches such as *in situ* immunolabelling, and resulting information could allow the development of new and more efficient lignocellulosic biomass processing approaches. Furthermore, the benefits of such an endeavour would not remain solely in the realm of industrial applications of lignocellulosic biomass. Given that the study of how the cell wall is disassembled will provide valuable information about how it is assembled, generated information will contribute to a deeper fundamental knowledge of plant cell walls.

7. REFERENCES

7. REFERENCES

ABIDI, N., CABRALES, L. & HAIGLER, C. H. 2014. Changes in the cell wall and cellulose content of developing cotton fibers investigated by FTIR spectroscopy. *Carbohydrate Polymers,* 100**,** 9 – 16.

ADAPA, P. K., KARUNAKARAN, C., TABIL, L. G. & SCHOENAU, G. J. 2009. Potential applications of infrared and Raman spectromicroscopy for agricultural biomass. *Agricultural Engineering International: CIGR Journal,* Vol. XI.

AGGER, J., VIKSO-NIELSEN, A. & MEYER, A. S. 2010. Enzymatic xylose release from pretreated corn bran arabinoxylan: differential effects of deacetylation and deferuloylation on insoluble and soluble substrate fractions. *J Agric Food Chem,* 58**,** 6141 – 6148.

AHLGREN, P. & GORING, D. 1971. Removal of wood components during chlorite delignification of black spruce. *Canadian journal of chemistry,* 49**,** 1272 – 1275.

AIST, J. R. 1976. Papillae and related wound plugs of plant cells. *Annual Review of Phytopathology,* 14**,** 145 – 163.

AKIN, D. E., BORNEMAN, W. S., RIGSBY, L. L. & MARTIN, S. A. 1993. *p*-Coumaroyl and feruloyl arabinoxylans from plant cell walls as substrates for ruminal bacteria. *Applied and Environmental Microbiology,* 59**,** 644 – 647.

ALBERSHEIM, P. 2011. *Plant cell walls: from chemistry to biology,* New York, Garland Science.

ALLISON, G. G., MORRIS, C., CLIFTON-BROWN, J., LISTER, S. J. & DONNISON, I. S. 2011. Genotypic variation in cell wall composition in a diverse set of 244 accessions of *Miscanthus*. *Biomass & Bioenergy,* 35**,** 4740 – 4747.

ALLISON, G. G., THAIN, S. C., MORRIS, P., MORRIS, C., HAWKINS, S., HAUCK, B., BARRACLOUGH, T., YATES, N., SHIELD, I., BRIDGWATER, A. V. & DONNISON, I. S. 2009. Quantification of hydroxycinnamic acids and lignin in perennial forage and energy grasses by Fourier-transform infrared spectroscopy and partial least squares regression. *Bioresource Technology,* 100**,** 1252 – 1261.

ALONSO-SIMÓN, A., ENCINA, A. E., GARCÍA-ANGULO, P., ÁLVAREZ, J. M. & ACEBES, J. L. 2004. FTIR spectroscopy monitoring of cell wall modifications during the habituation of bean (*Phaseolus vulgaris* L.) callus cultures to dichlobenil. *Plant Science,* 167**,** 1273 – 1281.

ANDERSON, K., WHEAT, R., CONANT, N. & CLINGENPEEL, W. 1974. Composition of the cell wall and other fractions of the autolyzed yeast form of *Histoplasma capsulatum*. *Mycopathologia et mycologia applicata,* 54**,** 439 – 451.

ANTHON, G. E. & BARRETT, D. M. 2006. Characterization of the temperature activation of pectin methylesterase in green beans and tomatoes. *Journal of Agricultural and Food Chemistry,* 54**,** 204 – 211.

ATMODJO, M. A., SAKURAGI, Y., ZHU, X., BURRELL, A. J., MOHANTY, S. S., ATWOOD, J. A., 3RD, ORLANDO, R., SCHELLER, H. V. & MOHNEN, D. 2011. Galacturonosyltransferase (GAUT)1 and GAUT7 are the core of a plant cell wall pectin biosynthetic homogalacturonan:galacturonosyltransferase complex. *Proc Natl Acad Sci U S A,* 108**,** 20225 – 20230.

AVCI, U., PATTATHIL, S. & HAHN, M. G. 2012. Immunological approaches to plant cell wall and biomass characterization: immunolocalization of glycan epitopes. *In:*

HIMMEL, M. E. (ed.) *Biomass Conversion: Methods and Protocols* New York, New York, USA: Humana Press.
BALCH, W. E., FOX, G. E., MAGRUM, L. J., WOESE, C. R. & WOLFE, R. S. 1979. Methanogens: reevaluation of a unique biological group. *Microbiol Rev,* 43**,** 260 – 296.
BARNETT, J. R. & BONHAM, V. A. 2004. Cellulose microfibril angle in the cell wall of wood fibres. *Biol Rev Camb Philos Soc,* 79**,** 461 – 472.
BASUMALLICK, L. & ROHRER, J. S. 2014. Thermo Scientific application note 1089: determination of carbohydrates in acid hydrolysates of wood. [Accessed http://www.dionex.com/en-us/webdocs/115227-AN1089-IC-Carbohydrates-Wood-Acid-Hydrolysates-AN70941-E.pdf; accessed April, 25, 2014].
BATEMAN, D. F. 1976. Plant cell wall hydrolysis by pathogens. *In:* FRIEND, J. & THRELFALL, D. R. (eds.) *Biochemical aspects of plant-parasite relationship.* London, UK: Academic Press.
BÉDOUET, L., DENYS, E., COURTOIS, B. & COURTOIS, J. 2006. Changes in esterified pectins during development in the flax stems and leaves. *Carbohydrate polymers,* 65**,** 165 – 173.
BELLISSIMI, E., van DIJKEN, J. P., PRONK, J. T. & van MARIS, A. J. A. 2009. Effects of acetic acid on the kinetics of xylose fermentation by an engineered, xylose-isomerase-based *Saccharomyces cerevisiae* strain. *FEMS Yeast Research,* 9**,** 358 – 364.
BERLIN, A., BALAKSHIN, M., GILKES, N., KADLA, J., MAXIMENKO, V., KUBO, S. & SADDLER, J. 2006. Inhibition of cellulase, xylanase and β-glucosidase activities by softwood lignin preparations. *Journal of Biotechnology,* 125**,** 198 – 209.
BIELY, P. 2012. Microbial carbohydrate esterases deacetylating plant polysaccharides. *Biotechnology Advances,* 30**,** 1575 – 1588.
BISWAL, A. K., HAO, Z., PATTATHIL, S., YANG, X., WINKELER, K., COLLINS, C., MOHANTY, S. S., RICHARDSON, E. A., GELINEO-ALBERSHEIM, I., HUNT, K., RYNO, D., SYKES, R. W., TURNER, G. B., ZIEBELL, A., GJERSING, E., LUKOWITZ, W., DAVIS, M. F., DECKER, S. R., HAHN, M. G. & MOHNEN, D. 2015. Downregulation of GAUT12 in *Populus deltoides* by RNA silencing results in reduced recalcitrance, increased growth and reduced xylan and pectin in a woody biofuel feedstock. *Biotechnol Biofuels,* 8**,** 41.
BOERJAN, W., RALPH, J. & BAUCHER, M. 2003. Lignin biosynthesis. *Annu Rev Plant Biol,* 54**,** 519 – 546.
BONAWITZ, N. D. & CHAPPLE, C. 2010. the genetics of lignin biosynthesis: connecting genotype to phenotype. *Annual Review of Genetics,* 44**,** 337 – 363.
BOOTTEN, T. J., HARRIS, P. J., MELTON, L. D. & NEWMAN, R. H. 2004. Solid-state 13C-NMR spectroscopy shows that the xyloglucans in the primary cell walls of mung bean (*Vigna radiata* L.) occur in different domains: a new model for xyloglucan-cellulose interactions in the cell wall. *J Exp Bot,* 55**,** 571 – 583.
BOSCH, M., CHEUNG, A. Y. & HEPLER, P. K. 2005. Pectin methylesterase, a regulator of pollen tube growth. *Plant Physiology,* 138**,** 1334 – 1346.
BOUTON, S., LEBOEUF, E., MOUILLE, G., LEYDECKER, M. T., TALBOTEC, J., GRANIER, F., LAHAYE, M., HOFTE, H. & TRUONG, H. N. 2002. QUASIMODO1 encodes a putative membrane-bound glycosyltransferase required for normal pectin synthesis and cell adhesion in *Arabidopsis*. *Plant Cell,* 14**,** 2577 – 2590.
BRENNAN, M. & HARRIS, P. J. 2011. Distribution of fucosylated xyloglucans among the walls of different cell types in monocotyledons determined by immunofluorescence microscopy. *Mol Plant,* 4**,** 144-156.
BROWN, J. A. & FRY, S. C. 1993. Novel *O*-D-galacturonoyl esters in the pectic polysaccharides of suspension-cultured plant cells. *Plant Physiology,* 103**,** 993 – 999.

BRUNOW, G. 2001. Methods to reveal the structure of lignin. *In:* HOFRICHTER, M. & STEINBÜCHEL, A. (eds.) *Lignin, Humic Substances and Coal.* Weinheim, Germany: Wiley-VCH Verlag GmbH & Co. KGaA.

BUANAFINA, M. M. D. O. 2009. Feruloylation in grasses: current and future perspectives. *Molecular Plant,* 2**,** 861 – 872.

BUANAFINA, M. M. D. O., LANGDON, T., HAUCK, B., DALTON, S. & MORRIS, P. 2006. Manipulating the phenolic acid content and digestibility of italian ryegrass (*Lolium multiflorum*) by vacuolar-targeted expression of a fungal ferulic acid esterase. *In:* McMILLAN, J., ADNEY, W., MIELENZ, J. & KLASSON, K. T. (eds.) *Twenty-Seventh Symposium on Biotechnology for Fuels and Chemicals.* Humana Press.

BUCKERIDGE, M. S. & de SOUZA, A. P. 2014. Breaking the "Glycomic Code" of cell wall polysaccharides may improve second-generation bioenergy production from biomass. *BioEnergy Research,* 7**,** 1065 – 1073.

BUCKERIDGE, M. S., RAYON, C., URBANOWICZ, B., TINÉ, M. A. S. & CARPITA, N. C. 2004. Mixed linkage (1→3),(1→4)-β-D-glucans of grasses. *Cereal Chemistry Journal,* 81**,** 115 – 127.

BURGERT, I. 2006. Exploring the micromechanical design of plant cell walls. *American Journal of Botany,* 93**,** 1391 – 1401.

BURTON, R. A., GIBEAUT, D. M., BACIC, A., FINDLAY, K., ROBERTS, K., HAMILTON, A., BAULCOMBE, D. C. & FINCHER, G. B. 2000. Virus-Induced Silencing of a Plant Cellulose Synthase Gene. *The Plant Cell,* 12**,** 691 – 705.

BUSSE-WICHER, M., GOMES, T. C. F., TRYFONA, T., NIKOLOVSKI, N., STOTT, K., GRANTHAM, N. J., BOLAM, D. N., SKAF, M. S. & DUPREE, P. 2014. The pattern of xylan acetylation suggests xylan may interact with cellulose microfibrils as a twofold helical screw in the secondary plant cell wall of *Arabidopsis thaliana*. *The Plant Journal,* 79**,** 492 – 506.

BUTLER, J. E., NI, L., NESSLER, R., JOSHI, K. S., SUTER, M., ROSENBERG, B., CHANG, J., BROWN, W. R. & CANTARERO, L. A. 1992. The physical and functional behavior of capture antibodies adsorbed on polystyrene. *Journal of Immunological Methods,* 150**,** 77 – 90.

CAFFALL, K. H. & MOHNEN, D. 2009. The structure, function, and biosynthesis of plant cell wall pectic polysaccharides. *Carbohydrate Research,* 344**,** 1879 – 1900.

CAO, Y., LI, J., YU, L., CHAI, G., HE, G., HU, R., QI, G., KONG, Y., FU, C. & ZHOU, G. 2014. Cell wall polysaccharide distribution in *Miscanthus lutarioriparius* stem using immuno-detection. *Plant Cell Reports***,** 1 – 11.

CARPITA, N. C. 1996. Structure and biogenesis of the cell walls of grasses. *Annual Review of Plant Physiology and Plant Molecular Biology,* 47**,** 445 – 476.

CARPITA, N. C., DEFERNEZ, M., FINDLAY, K., WELLS, B., SHOUE, D. A., CATCHPOLE, G., WILSON, R. H. & McCANN, M. C. 2001. Cell wall architecture of the elongating maize coleoptile. *Plant Physiology,* 127**,** 551 – 565.

CARPITA, N. C. & GIBEAUT, D. M. 1993. Structural models of primary cell walls in flowering plants: consistency of molecular structure with the physical properties of the walls during growth. *The Plant Journal,* 3**,** 1 – 30.

CARPITA, N. C. & McCANN, M. C. 2015. Characterizing visible and invisible cell wall mutant phenotypes. *Journal of Experimental Botany,* 66**,** 4145 – 4163.

CARROLL, A. & SOMERVILLE, C. 2009. Cellulosic biofuels. *Annual Review of Plant Biology,* 60**,** 165 – 182.

CCRC. 2007. *Plant Cell Walls. Complex Carbohydrate Research Center* [Online]. University of Georgia. Available: http://www.ccrc.uga.edu/~mao/cellwall/main.htm [Accessed 14 February 2015.

CHABBERT, B., TOLLIER, M., MONTIES, B., BARRIERE, Y. & ARGILLIER, O. 1994. Biological variability in lignification of maize: Expression of the brown midrib bm3 mutation in three maize cultivars. *J Sci Food Agric,* 64**,** 349 – 355.

CHANG, V. S. & HOLTZAPPLE, M. T. 2000. Fundamental factors affecting biomass enzymatic reactivity. *Appl Biochem Biotechnol,* 84 – 86**,** 5 – 37.

CHANG, X. F., CHANDRA, R., BERLETH, T. & BEATSON, R. P. 2008. Rapid, microscale, acetyl bromide-based method for high-throughput determination of lignin content in *Arabidopsis thaliana*. *Journal of Agricultural and Food Chemistry,* 56**,** 6825 – 6834.

CHEN, L., AUH, C., CHEN, F., CHENG, X., ALJOE, H., DIXON, R. & WANG, Z. 2002. Lignin Deposition and Associated Changes in Anatomy, Enzyme Activity, Gene Expression, and Ruminal Degradability in Stems of Tall Fescue at Different Developmental Stages. *J Agric Food Chem,* 50**,** 5558 – 5565.

CHEN, X.-Y. & KIM, J.-Y. 2009. Callose synthesis in higher plants. *Plant Signaling & Behavior,* 4**,** 489 – 492.

CHEN, X., SHEKIRO, J., FRANDEN, M., WANG, W., ZHANG, M., KUHN, E., JOHNSON, D. & TUCKER, M. 2012. The impacts of deacetylation prior to dilute acid pretreatment on the bioethanol process. *Biotechnology for Biofuels,* 5**,** 8.

CHEN, X., SHEKIRO, J., PSCHORN, T., SABOURIN, M., TAO, L., ELANDER, R., PARK, S., JENNINGS, E., NELSON, R., TRASS, O., FLANEGAN, K., WANG, W., HIMMEL, M., JOHNSON, D. & TUCKER, M. 2014. A highly efficient dilute alkali deacetylation and mechanical (disc) refining process for the conversion of renewable biomass to lower cost sugars. *Biotechnology for Biofuels,* 7**,** 98.

CHEN, Y., STEVENS, M., ZHU, Y., HOLMES, J. & XU, H. 2013. Understanding of alkaline pretreatment parameters for corn stover enzymatic saccharification. *Biotechnology for Biofuels,* 6**,** 8.

CHOWDHURY, J., HENDERSON, M., SCHWEIZER, P., BURTON, R. A., FINCHER, G. B. & LITTLE, A. 2014. Differential accumulation of callose, arabinoxylan and cellulose in nonpenetrated versus penetrated papillae on leaves of barley infected with *Blumeria graminis* f. sp. *hordei*. *New Phytologist,* 204**,** 650 – 660.

CHRISTENSEN, U., ALONSO-SIMON, A., SCHELLER, H. V., WILLATS, W. G. & HARHOLT, J. 2010. Characterization of the primary cell walls of seedlings of *Brachypodium distachyon* – a potential model plant for temperate grasses. *Phytochemistry,* 71**,** 62 – 69.

CHUNDAWAT, S. P., VENKATESH, B. & DALE, B. E. 2007. Effect of particle size based separation of milled corn stover on AFEX pretreatment and enzymatic digestibility. *Biotechnol Bioeng,* 96**,** 219 – 231.

CHUNDAWAT, S. P. S., BECKHAM, G. T., HIMMEL, M. E. & DALE, B. E. 2011. Deconstruction of lignocellulosic biomass to fuels and chemicals. *In:* PRAUSNITZ, J. M. (ed.) *Annual Review of Chemical and Biomolecular Engineering, Vol 2.*

CLAUSEN, M. H., WILLATS, W. G. T. & KNOX, J. P. 2003. Synthetic methyl hexagalacturonate hapten inhibitors of anti-homogalacturonan monoclonal antibodies LM7, JIM5 and JIM7. *Carbohydrate Research,* 338**,** 1797 – 1800.

CLIFTON-BROWN, J., LEWANDOWSKI, I., ANDERSSON, B., BASCH, G., CHRISTIAN, D., KJELDSEN, J., JORGENSEN, U., MORTENSEN, J., RICHE, A. & SCHWARZ, K. 2001. Performance of 15 *Miscanthus* genotypes at five sites in Europe. *Agron J,* 93**,** 1013 – 1019.

CLIFTON-BROWN, J., ROBSON, P., DAVEY, C., FARRAR, K., HAYES, C., HUANG, L., JENSEN, E., JONES, L., HINTON-JONES, M., MADDISON, A., MEYER, H., NORRIS, J., PURDY, S., RODGERS, C., SCHWARZ, K.-U., SALVATORE, C., SLAVOV, G., VALENTINE, J., WEBSTER, R., YOUELL, S. & DONNISON, I.

2013. Breeding miscanthus for bioenergy. *Bioenergy Feedstocks*. John Wiley & Sons, Inc.

COHEN, J. 1973. Eta-squared and partial eta-squared in fixed factor ANOVA designs. *Educational and Psychological Measurement,* 33**,** 107 – 112.

COIMBRA, M. A., BARROS, A., RUTLEDGE, D. N. & DELGADILLO, I. 1999. FTIR spectroscopy as a tool for the analysis of olive pulp cell-wall polysaccharide extracts. *Carbohydrate Research,* 317**,** 145 – 154.

COLBERT, J. T. & EVERT, R. F. 1982. Leaf vasculature in sugarcane (*Saccharum officinarum* L.). *Planta,* 156**,** 136 – 151.

COLLINS, H. M., BURTON, R. A., TOPPING, D. L., LIAO, M.-L., BACIC, A. & FINCHER, G. B. 2010. Variability in fine structures of noncellulosic cell wall polysaccharides from cereal grains: Potential importance in human health and nutrition. *Cereal Chemistry Journal,* 87**,** 272 – 282.

CORNUAULT, V., BUFFETTO, F., RYDAHL, M. G., MARCUS, S. E., TORODE, T. A., XUE, J., CREPEAU, M. J., FARIA-BLANC, N., WILLATS, W. G., DUPREE, P., RALET, M. C. & KNOX, J. P. 2015. Monoclonal antibodies indicate low-abundance links between heteroxylan and other glycans of plant cell walls. *Planta,* 242, 1321 – 1334.

CORNUAULT, V., MANFIELD, I. W., RALET, M.-C. & KNOX, J. P. 2014. Epitope detection chromatography: a method to dissect the structural heterogeneity and inter-connections of plant cell-wall matrix glycans. *The Plant Journal,* 78**,** 715 – 722.

CORRADINI, C., CAVAZZA, A. & BIGNARDI, C. 2012. High-performance anion-exchange chromatography coupled with pulsed electrochemical detection as a powerful tool to evaluate carbohydrates of food interest: principles and applications. *International Journal of Carbohydrate Chemistry,* 2012**,** 1 – 13.

CORREIA, M. A., MAZUMDER, K., BRAS, J. L., FIRBANK, S. J., ZHU, Y., LEWIS, R. J., YORK, W. S., FONTES, C. M. & GILBERT, H. J. 2011. Structure and function of an arabinoxylan-specific xylanase. *J Biol Chem,* 286**,** 22510 – 22520.

da COSTA, R. M. F., ALLISON, G. & BOSCH, M. 2015. Cell wall biomass preparation and Fourier transform mid-infrared (FTIR) spectroscopy to study cell wall composition. *Bio-protocol,* 5**,** e1494. http://www.bio-protocol.org/e1494.

da COSTA, R. M. F., LEE, S. J., ALLISON, G. G., HAZEN, S. P., WINTERS, A. & BOSCH, M. 2014. Genotype, development and tissue-derived variation of cell-wall properties in the lignocellulosic energy crop *Miscanthus*. *Annals of Botany,* 114**,** 1265 – 1277.

DARVILL, A. G., McNEIL, M. & ALBERSHEIM, P. 1978. Structure of plant cell walls: VIII. A new pectic polysaccharide. *Plant Physiology,* 62**,** 418 – 422.

DARVILL, J. E., McNEIL, M., DARVILL, A. G. & ALBERSHEIM, P. 1980. Structure of plant cell walls: XI. glucuronoarabinoxylan, a second hemicellulose in the primary cell walls of suspension-cultured sycamore cells. *Plant Physiol,* 66**,** 1135 – 1139.

de SOUZA, A., LEITE, D., PATTATHIL, S., HAHN, M. & BUCKERIDGE, M. 2013. composition and structure of sugarcane cell wall polysaccharides: implications for second-generation bioethanol Production. *BioEnergy Research,* 6**,** 564 – 579.

de SOUZA, A. P., KAMEI, C. L., TORRES, A. F., PATTATHIL, S., HAHN, M. G., TRINDADE, L. M. & BUCKERIDGE, M. S. 2015. How cell wall complexity influences saccharification efficiency in Miscanthus sinensis. *J Exp Bot,* 66**,** 4351 – 4365.

de VETTEN, N. C. & HUBER, D. J. 1990. Cell wall changes during the expansion and senescence of carnation (*Dianthus caryophyllus*) petals. *Physiologia Plantarum,* 78**,** 447 – 454.

DECKER, S. R., BRUNECKY, R., TUCKER, M. P., HIMMEL, M. E. & SELIG, M. J. 2009. High-throughput screening techniques for biomass conversion. *BioEnergy Research,* 2**,** 179 – 192.

DEFRA 2007. Planting and growing *Miscanthus* best practice guidelines department for environment, Food & Rural Affairs.

DEL RÍO, J. C., MARQUES, G., RENCORET, J., MARTÍNEZ FERRER, Á. T. & GUTIÉRREZ SUÁREZ, A. 2007. Occurrence of naturally acetylated lignin units. *Journal of Agricultural and Food Chemistry,* 55**,** 5461 – 5468.

DEMARTINI, J. D., PATTATHIL, S., AVCI, U., SZEKALSKI, K., MAZUMDER, K., HAHN, M. G. & WYMAN, C. E. 2011. Application of monoclonal antibodies to investigate plant cell wall deconstruction for biofuels production. *Energy & Environmental Science,* 4**,** 4332 – 4339.

DEMARTINI, J. D., PATTATHIL, S., MILLER, J. S., LI, H., HAHN, M. G. & WYMAN, C. E. 2013. Investigating plant cell wall components that affect biomass recalcitrance in poplar and switchgrass. *Energy & Environmental Science,* 6**,** 898 – 909.

DERKACHEVA, O. & SUKHOV, D. 2008. Investigation of lignins by FTIR spectroscopy. *Macromolecular Symposia,* 265**,** 61 – 68.

DING, S.-Y., LIU, Y.-S., ZENG, Y., HIMMEL, M. E., BAKER, J. O. & BAYER, E. A. 2012. How does plant cell wall nanoscale architecture correlate with enzymatic digestibility? *Science,* 338**,** 1055 – 1060.

DIONEX 2000. Technical Note 20 - Analysis of carbohydrates by high performance anion exchange chromatography with pulsed amperometric detection (HPAE-PAD). *IC and HPLC Technical Notes.*

DIONEX 2013. CarboPac SA10 – 4µm column product manual. Thermo Fisher Scientific.

DOMON, J.-M., BALDWIN, L., ACKET, S., CAUDEVILLE, E., ARNOULT, S., ZUB, H., GILLET, F., LEJEUNE-HÉNAUT, I., BRANCOURT-HULMEL, M., PELLOUX, J. & RAYON, C. 2013. Cell wall compositional modifications of *Miscanthus* ecotypes in response to cold acclimation. *Phytochemistry,* 85**,** 51 – 61.

DONALDSON, L. A. & KNOX, J. P. 2012. Localization of cell wall polysaccharides in normal and compression wood of radiata pine: Relationships with lignification and microfibril orientation. *Plant Physiology,* 158**,** 642 – 653.

DU, L., YU, P., ROSSNAGEL, B. G., CHRISTENSEN, D. A. & McKINNON, J. J. 2009. Physicochemical characteristics, hydroxycinnamic acids (ferulic acid, *p*-coumaric acid) and their ratio, and *in situ* biodegradability: Comparison of genotypic differences among six barley varieties. *Journal of Agricultural and Food Chemistry,* 57**,** 4777 – 4783.

DUBOIS, M., GILLES, K. A., HAMILTON, J. K., REBERS, P. T. & SMITH, F. 1956. Colorimetric method for determination of sugars and related substances. *Analytical chemistry,* 28**,** 350 – 356.

DWIYANTI, M. S., STEWART, J. R. & YAMADA, T. 2013. Germplasm resources of *Miscanthus* and their application in breeding. *Bioenergy Feedstocks.* John Wiley & Sons, Inc.

EDELMANN, H. G. & FRY, S. C. 1992. Factors that affect the extraction of xyloglucan from the primary cell walls of suspension-cultured rose cells. *Carbohydrate Research,* 228**,** 423 – 431.

ENCINA, A. & FRY, S. C. 2005. Oxidative coupling of a feruloyl-arabinoxylan trisaccharide (FAXX) in the walls of living maize cells requires endogenous hydrogen peroxide and is controlled by a low-M_r apoplastic inhibitor. *Planta,* 223**,** 77 – 89.

ENGVALL, E. & PERLMANN, P. 1971. Enzyme-linked immunosorbent assay (ELISA) quantitative assay of immunoglobulin G. *Immunochemistry,* 8**,** 871 – 874.

ESAU, K. 1977. *Anatomy of Seed Plants,* London, UK, Wiley.
EVERT, R. F. 2006. *Esau's Plant Anatomy: Meristems, Cells, and Tissues of the Plant Body: Their Structure, Function, and Development,* Hoboken, New Jersey, USA, John Wiley & Sons.
FAULDS, C. B. & WILLIAMSON, G. 1999. The role of hydroxycinnamates in the plant cell wall. *Journal of the Science of Food and Agriculture,* 79**,** 393 – 395.
FELTUS, F. A. & VANDENBRINK, J. P. 2012. Bioenergy grass feedstock: current options and prospects for trait improvement using emerging genetic, genomic, and systems biology toolkits. *Biotechnology for Biofuels,* 5**,** 80.
FENGEL, D. & WEGENER, G. 1979. Hydrolysis of polysaccharides with trifluoroacetic acid and its application to rapid wood and pulp analysis. *Hydrolysis of Cellulose: Mechanisms of Enzymatic and Acid Catalysis.* Washington, DC, USA: American Chemical Society.
FENGEL, D. & WEGENER, G. 1984. *Wood: chemistry, ultrastructure, reactions,* W. de Gruyter.
FERGUSON, M. W., WYCOFF, K. L. & AYERS, A. R. 1988. Use of cluster analysis with monoclonal antibodies for taxonomic differentiation of phytopathogenic fungi and for screening and clustering antibodies. *Current Microbiology,* 17**,** 127 – 132.
FLENLEY, J. R. 2011. Why is pollen yellow? And why are there so many species in the tropical rain forest? *Journal of Biogeography,* 38**,** 809 – 816.
FOSTER, C. E., MARTIN, T. M. & PAULY, M. 2010. Comprehensive Compositional Analysis of Plant Cell Walls (Lignocellulosic biomass) Part I: Lignin. *J Vis Exp,* 37**,** e1745.
FRY, S. C. 1988. *The growing plant cell wall: Chemical and metabolic analysis,* Essex, longman scientific and technical.
FRY, S. C. 2010. Cell wall polysaccharide composition and covalent crosslinking. *In:* ULVSKOV, P. (ed.) *Annual Plant Reviews, Plant Polysaccharides: Biosynthesis and Bioengineering.* Oxford. UK: Wiley-Blackwell.
FUKUSHIMA, R. S. & DEHORITY, B. A. 2000. Feasibility of using lignin isolated from forages by solubilization in acetyl bromide as a standard for lignin analyses. *J Anim Sci,* 78**,** 3135 – 3143.
FUKUSHIMA, R. S. & HATFIELD, R. D. 2004. Comparison of the acetyl bromide spectrophotometric method with other analytical lignin methods for determining lignin concentration in forage samples. *Journal of Agricultural and Food Chemistry,* 52**,** 3713 – 3720.
GIBEAUT, D. M., PAULY, M., BACIC, A. & FINCHER, G. B. 2005. Changes in cell wall polysaccharides in developing barley (*Hordeum vulgare*) coleoptiles. *Planta,* 221**,** 729 – 38.
GILLE, S. & PAULY, M. 2012. *O*-acetylation of Plant Cell Wall Polysaccharides. *Frontiers in Plant Science,* 3**,** 12.
GLOVER, B. J. 2010. Epidermis: Outer Cell Layer of the Plant. *Encyclopedia of Life Sciences.* Chichester, UK: John Wiley & Sons, Ltd.
GOMEZ, L. D., BRISTOW, J. K., STATHAM, E. R. & McQUEEN-MASON, S. J. 2008. Analysis of saccharification in *Brachypodium distachyon* stems under mild conditions of hydrolysis. *Biotechnology for biofuels,* 1**,** 15.
GOMEZ, L. D., WHITEHEAD, C., BARAKATE, A., HALPIN, C. & McQUEEN-MASON, S. 2010. Automated saccharification assay for determination of digestibility in plant materials. *Biotechnology for Biofuels,* 3**,** 23.

GOMEZ, L. D., WHITEHEAD, C., ROBERTS, P. & McQUEEN-MASON, S. J. 2011. High-throughput saccharification assay for lignocellulosic materials. *Journal of visualized experiments: JoVE*.

GORZSÁS, A., STENLUND, H., PERSSON, P., TRYGG, J. & SUNDBERG, B. 2011. Cell-specific chemotyping and multivariate imaging by combined FT-IR microspectroscopy and orthogonal projections to latent structures (OPLS) analysis reveals the chemical landscape of secondary xylem. *The Plant Journal,* 66**,** 903 – 914.

GRABBER, J. H., RALPH, J., LAPIERRE, C. & BARRIÈRE, Y. 2004. Genetic and molecular basis of grass cell-wall degradability. I. Lignin–cell wall matrix interactions. *Comptes Rendus Biologies,* 327**,** 455 – 465.

GRANDIS, A., de SOUZA, A. P., TAVARES, E. Q. P. & BUCKERIDGE, M. S. 2014. Using natural plant cell wall degradation mechanisms to improve second generation bioethanol. *In:* McCANN, M. C., BUCKERIDGE, M. S. & CARPITA, N. C. (eds.) *Plants and BioEnergy.* Springer New York.

GREEN, D. & PERRY, R. 1997. *Perry's Chemical Engineers' Handbook, Eighth Edition,* New York, New York, USA, McGraw-Hill.

GROHMANN, K., MITCHELL, D. J., HIMMEL, M. E., DALE, B. E. & SCHROEDER, H. A. 1989. The role of ester groups in resistance of plant cell wall polysaccharides to enzymatic hydrolysis. *Applied Biochemistry and Biotechnology,* 20/21**,** 45 – 61.

GUZMÁN, P., FERNÁNDEZ, V., GARCÍA, M. L., KHAYET, M., FERNÁNDEZ, A. & GIL, L. 2014. Localization of polysaccharides in isolated and intact cuticles of eucalypt, poplar and pear leaves by enzyme-gold labelling. *Plant Physiology and Biochemistry,* 76**,** 1 – 6.

GWON, J. G., LEE, S. Y., DOH, G. H. & KIM, J. H. 2010. Characterization of chemically modified wood fibers using FTIR spectroscopy for biocomposites. *Journal of Applied Polymer Science,* 116**,** 3212 – 3219.

HAHN, M. G., LERNER, D. R., FITTER, M. S., NORMAN, P. M. & LAMB, C. J. 1987. Characterization of monoclonal antibodies to protoplast membranes of *Nicotiana tabacum* identified by an enzyme-linked immunosorbent assay. *Planta,* 171**,** 453 – 465.

HALL, M., BANSAL, P., LEE, J. H., REALFF, M. J. & BOMMARIUS, A. S. 2010. Cellulose crystallinity – a key predictor of the enzymatic hydrolysis rate. *FEBS Journal,* 277**,** 1571 – 1582.

HARRIS, P. J. & STONE, B. A. 2008. Chemistry and molecular organization of plant cell walls. *In:* HIMMEL, M. E. (ed.) *Biomass recalcitrance: deconstructing the plant cell wall for bioenergy.* London, UK: Blackwell Publishing Ltd.

HARTLEY, R. D. 1972. *p*-Coumaric and ferulic acid components of cell walls of ryegrass and their relationships with lignin and digestibility. *Journal of the Science of Food and Agriculture,* 23**,** 1347 – 1354.

HATFIELD, R. D., GRABBER, J., RALPH, J. & BREI, K. 1999a. Using the acetyl bromide assay to determine lignin concentrations in herbaceous plants: Some cautionary notes. *Journal of Agricultural and Food Chemistry,* 47**,** 628 – 632.

HATFIELD, R. D., MARITA, J. M., FROST, K., GRABBER, J., RALPH, J., LU, F. & KIM, H. 2009. Grass lignin acylation: *p*-coumaroyl transferase activity and cell wall characteristics of C3 and C4 grasses. *Planta,* 229**,** 1253 – 1267.

HATFIELD, R. D., RALPH, J. & GRABBER, J. H. 1999b. Cell wall cross-linking by ferulates and diferulates in grasses. *Journal of the Science of Food and Agriculture,* 79**,** 403 – 407.

HATFIELD, R. D., WILSON, J. R. & MERTENS, D. R. 1999c. Composition of cell walls isolated from cell types of grain sorghum stems. *Journal of the Science of Food and Agriculture,* 79**,** 891 – 899.

HAYASHI, T. 1989. Xyloglucans in the primary-cell wall. *Annual Review of Plant Physiology and Plant Molecular Biology,* 40**,** 139 – 168.
HEATON, E. A., CLIFTON-BROWN, J., VOIGT, T. B., JONES, M. B. & LONG, S. P. 2004. *Miscanthus* for renewable energy generation: european union experience and projections for Illinois. *Mitigation and Adaptation Strategies for Global Change,* 9**,** 433 – 451.
HEATON, E. A., DOHLEMAN, F. G. & LONG, S. P. 2008. Meeting US biofuel goals with less land: the potential of *Miscanthus*. *Global Change Biology,* 14**,** 2000 – 2014.
HENDRIKS, A. T. W. M. & ZEEMAN, G. 2009. Pretreatments to enhance the digestibility of lignocellulosic biomass. *Bioresource Technology,* 100**,** 10 – 18.
HIMMEL, M. E., DING, S.-Y., JOHNSON, D. K., ADNEY, W. S., NIMLOS, M. R., BRADY, J. W. & FOUST, T. D. 2007. Biomass Recalcitrance: Engineering Plants and Enzymes for Biofuels Production. *Science,* 315**,** 804 – 807.
HIMMEL, M. E. & PICATAGGIO, S. K. 2008. Our challenge is to acquire deeper understanding of biomass recalcitrance and conversion. *In:* HIMMEL, M. E. (ed.) *Biomass recalcitrance: deconstructing the plant cell wall for bioenergy.* London, UK: Blackwell Publishing Ltd.
HODGSON, E. M., FAHMI, R., YATES, N., BARRACLOUGH, T., SHIELD, I., ALLISON, G., BRIDGWATER, A. V. & DONNISON, I. S. 2010. *Miscanthus* as a feedstock for fast-pyrolysis: Does agronomic treatment affect quality? *Bioresource Technology,* 101**,** 6185 – 6191.
HODGSON, E. M., NOWAKOWSKI, D. J., SHIELD, I., RICHE, A., BRIDGWATER, A. V., CLIFTON-BROWN, J. C. & DONNISON, I. S. 2011. Variation in *Miscanthus* chemical composition and implications for conversion by pyrolysis and thermo-chemical bio-refining for fuels and chemicals. *Bioresource Technology,* 102**,** 3411 – 3418.
HUANG, R., SU, R., QI, W. & HE, Z. 2011. Bioconversion of lignocellulose into bioethanol: Process intensification and mechanism research. *BioEnergy Research,* 4**,** 225 – 245.
HUNGATE, R. E. 1969. A roll tube method for cultivation of strict anaerobes. *In:* NORRIS, J. R. & RIBBONS, D. W. (eds.) *Methods in Microbiology.* New York: Academic Press.
IIYAMA, K., LAM, T. B. T. & STONE, B. A. 1990. Phenolic acid bridges between polysaccharides and lignin in wheat internodes. *Phytochemistry,* 29**,** 733 – 737.
IIYAMA, K., LAM, T. B. T. & STONE, B. A. 1994. Covalent cross-links in the cell wall. *Plant Physiology,* 104**,** 315 – 320.
IKEGAWA, T., MAYAMA, S., NAKAYASHIKI, H. & KATO, H. 1996. Accumulation of diferulic acid during the hypersensitive response of oat leaves to *Puccinia coronata* f. sp. *avenae* and its role in the resistance of oat tissues to cell wall degrading enzymes. *Physiological and Molecular Plant Pathology,* 48**,** 245 – 256.
IPCC 2007. Summary for Policymakers. *In:* SOLOMON, S., D., Q., MANNING, M., CHEN, Z., MARQUIS, M., AVERYT, K. B., TIGNOR, M. & MILLER, H. L. (eds.) *Climate Change 2007: The Physical Science Basis. Contribution of Working Group I to the Fourth Assessment Report of the Intergovernmental Panel on Climate Change.* Cambridge, United Kingdom and New York, NY, USA: Cambridge University Press.
ISHII, T. 1997a. *O*-acetylated oligosaccharides from pectins of potato tuber cell walls. *Plant Physiology,* 113**,** 1265 – 1272.
ISHII, T. 1997b. Structure and functions of feruloylated polysaccharides. *Plant Science,* 127**,** 111 – 127.
ISHII, T., MATSUNAGA, T., PELLERIN, P., O'NEILL, M. A., DARVILL, A. & ALBERSHEIM, P. 1999. The plant cell wall polysaccharide rhamnogalacturonan II self-assembles into a covalently cross-linked dimer. *J Biol Chem,* 274**,** 13098 – 13104.

ISTEK, A. & GONTEKI, E. 2009. Utilization of sodium borohydride ($NaBH_4$) in kraft pulping process. *Journal of Environmental Biology,* 30**,** 951 – 953.
ITO, S., SUZUKI, Y., MIYAMOTO, K., UEDA, J. & YAMAGUCHI, I. 2005. AtFLA11, a fasciclin-like arabinogalactan-protein, specifically localized in sclerenchyma cells. *Biosci Biotechnol Biochem,* 69**,** 1963 – 1969.
JACKSON, M. G. 1977. Review article: The alkali treatment of straws. *Animal Feed Science and Technology,* 2**,** 105 – 130.
JACOBS, A. K., LIPKA, V., BURTON, R. A., PANSTRUGA, R., STRIZHOV, N., SCHULZE-LEFERT, P. & FINCHER, G. B. 2003. An *Arabidopsis* callose synthase, GSL5, is required for wound and papillary callose formation. *The Plant Cell,* 15**,** 2503 – 2513.
JAHN, C. E., McKAY, J. K., MAULEON, R., STEPHENS, J., McNALLY, K. L., BUSH, D. R., LEUNG, H. & LEACH, J. E. 2011. Genetic variation in biomass traits among 20 diverse rice varieties. *Plant Physiology,* 155**,** 157 – 168.
JARVIS, M. C. 1998. Intercellular separation forces generated by intracellular pressure. *Plant, Cell & Environment,* 21**,** 1307 – 1310.
JENSEN, E., FARRAR, K., THOMAS-JONES, S., HASTINGS, A., DONNISON, I. & CLIFTON-BROWN, J. 2011. Characterization of flowering time diversity in Miscanthus species. *GCB Bioenergy,* 3**,** 387 – 400.
JENSEN, K. J. & JANES, K. A. 2012. Modeling the latent dimensions of multivariate signaling datasets. *Physical biology,* 9**,** 045004.
JI, Z., ZHANG, X., LING, Z., ZHOU, X., RAMASWAMY, S. & XU, F. 2015. Visualization of *Miscanthus* × *giganteus* cell wall deconstruction subjected to dilute acid pretreatment for enhanced enzymatic digestibility. *Biotechnol Biofuels,* 8**,** 103.
JIANG, W., PENG, H., LI, H. & XU, J. 2014. Effect of acetylation/deacetylation on enzymatic hydrolysis of corn stalk. *Biomass and Bioenergy,* 71**,** 294 – 298.
JONES, L., MILNE, J. L., ASHFORD, D. & McQUEEN-MASON, S. J. 2003. Cell wall arabinan is essential for guard cell function. *Proceedings of the National Academy of Sciences,* 100**,** 11783 – 11788.
JÖNSSON, L., ALRIKSSON, B. & NILVEBRANT, N.-O. 2013. Bioconversion of lignocellulose: inhibitors and detoxification. *Biotechnology for Biofuels,* 6**,** 16.
JOSEPHY, P. D., ELING, T. & MASON, R. P. 1982. The horseradish peroxidase-catalyzed oxidation of 3,5,3',5'-tetramethylbenzidine. Free radical and charge-transfer complex intermediates. *Journal of Biological Chemistry,* 257**,** 3669 – 3675.
JUNG, H.-J. G. 2003. Maize stem tissues: ferulate deposition in developing internode cell walls. *Phytochemistry,* 63**,** 543 – 549.
JUNG, H.-J. G. 2012. Forage digestibility: the intersection of cell wall lignification and plant tissue anatomy. *Department of Agronomy and Plant Genetics. Department of Animal Sciences, University of Minnesota, USA.*
JUNG, H.-J. G., RALPH, J. & HATFIELD, R. D. 1991. Degradability of phenolic acid-hemicellulose esters: A model system. *Journal of the Science of Food and Agriculture,* 56**,** 469 – 478.
JUNG, H. & ENGELS, F. 2002. Alfalfa stem tissues. *Crop science,* 42**,** 524 – 534.
JUNG, H. G. & DEETZ, D. A. 1993. Cell Wall Lignification and Degradability. *In:* JUNG, H. G., BUXTON, D. R., HATFIELD, R. D. & RALPH, J. (eds.) *Forage Cell Wall Structure and Digestibility.* American Society of Agronomy, Crop Science Society of America, Soil Science Society of America.
KABEL, M. A., BOS, G., ZEEVALKING, J., VORAGEN, A. G. J. & SCHOLS, H. A. 2007. Effect of pretreatment severity on xylan solubility and enzymatic breakdown of the remaining cellulose from wheat straw. *Bioresource Technology,* 98**,** 2034 – 2042.

KAČURÁKOVÁ, M., CAPEK, P., SASINKOVÁ, V., WELLNER, N. & EBRINGEROVÁ, A. 2000. FT-IR study of plant cell wall model compounds: pectic polysaccharides and hemicelluloses. *Carbohydrate Polymers,* 43**,** 195 – 203.

KATAOKA, Y. & KONDO, T. 1998. FT-IR microscopic analysis of changing cellulose crystalline structure during wood cell wall formation. *Macromolecules,* 31**,** 760 – 764.

KEEGSTRA, K. 2010. Plant cell walls. *Plant Physiology,* 154**,** 483 – 486.

KERSTIENS, G. 2010. Plant cuticle. *Encyclopedia of Life Sciences.* Chichester, UK: John Wiley & Sons, Ltd.

KEWELOH, H., WEYRAUCH, G. & REHM, H.-J. 1990. Phenol-induced membrane changes in free and immobilized *Escherichia coli*. *Applied Microbiology and Biotechnology,* 33**,** 66 – 71.

KIEMLE, S. N., ZHANG, X., ESKER, A. R., TORIZ, G., GATENHOLM, P. & COSGROVE, D. J. 2014. Role of (1,3)(1,4)-β-glucan in cell walls: interaction with cellulose. *Biomacromolecules,* 15**,** 1727 – 1736.

KIM, T. & LEE, Y. Y. 2005. Pretreatment of corn stover by soaking in aqueous ammonia. *Applied Biochemistry and Biotechnology,* 124**,** 1119-1131.

KNOX, J. P. 1997. The use of antibodies to study the architecture and developmental regulation of plant cell walls. *Int Rev Cytol,* 171**,** 79 – 120.

KNOX, J. P., LINSTEAD, P. J., COOPER, J. P. C. & ROBERTS, K. 1991. Developmentally regulated epitopes of cell surface arabinogalactan proteins and their relation to root tissue pattern formation. *The Plant Journal,* 1**,** 317 – 326.

KNOX, J. P., LINSTEAD, P. J., KING, J., COOPER, C. & ROBERTS, K. 1990. Pectin esterification is spatially regulated both within cell walls and between developing tissues of root apices. *Planta,* 181**,** 512 – 521.

KNOX, J. P., PEART, J. & NEILL, S. J. 1995. Identification of novel cell surface epitopes using a leaf epidermal-strip assay system. *Planta,* 196**,** 266 – 270.

KOMALAVILAS, P. & MORT, A. J. 1989. The acetylation at *O*-3 of galacturonic acid in the rhamnose-rich portion of pectins. *Carbohydrate Research,* 187**,** 261 – 272.

KONDO, T., MIZUNO, K. & KATO, T. 1990. Cell wall-bound *p*-coumaric and ferulic acids in italian ryegrass *Canadian Journal of Plant Science,* 70**,** 495 – 499.

KONG, F., ENGLER, C. & SOLTES, E. 1992. Effects of cell-wall acetate, xylan backbone, and lignin on enzymatic hydrolysis of aspen wood. *Applied Biochemistry and Biotechnology,* 34 – 35**,** 23 – 35.

KONG, Y., ZHOU, G., YIN, Y., XU, Y., PATTATHIL, S. & HAHN, M. G. 2011. Molecular analysis of a family of *Arabidopsis* genes related to galacturonosyltransferases. *Plant Physiology,* 155**,** 1791 – 1805.

KOUWIJZER, M., SCHOLS, H. & PÉREZ, S. 1996. Acetylation of rhamnogalacturonan I and homogalacturonan: Theoretical calculations. *In:* VISSER, J. & VORAGEN, A. G. J. (eds.) *Progress in Biotechnology.* Elsevier.

KRAKOWSKY, M. D., LEE, M. & COORS, J. G. 2006. Quantitative trait loci for cell wall components in recombinant inbred lines of maize (*Zea mays* L.) II: leaf sheath tissue. *Theoretical and Applied Genetics,* 112**,** 717 – 726.

KRISTENSEN, J. B., THYGESEN, L. G., FELBY, C., JØRGENSEN, H. & ELDER, T. 2008. Cell-wall structural changes in wheat straw pretreated for bioethanol production. *Biotechnol Biofuels,* 1**,** 5.

KULKARNI, A. R., PATTATHIL, S., HAHN, M. G., YORK, W. S. & O'NEILL, M. A. 2012. Comparison of arabinoxylan structure in bioenergy and model grasses. *Industrial Biotechnology,* 8**,** 222 – 229.

KUMAR, R. & WYMAN, C. 2009. Effect of xylanase supplementation of cellulase on digestion of corn stover solids prepared by leading pretreatment technologies. *Bioresour Technol,* 100**,** 4203 – 4213.

LABAVITCH, J. M. & RAY, P. M. 1978. Structure of hemicellulosic polysaccharides of *Avena sativa* coleoptile cell walls. *Phytochemistry,* 17**,** 933 – 937.

LABBÉ, N., RIALS, T. G., KELLEY, S. S., CHENG, Z.-M., KIM, J.-Y. & LI, Y. 2005. FT-IR imaging and pyrolysis-molecular beam mass spectrometry: new tools to investigate wood tissues. *Wood Science and Technology,* 39**,** 61 – 76.

LAM, T. B. T., IIYAMA, K. & STONE, B. A. 1990. Distribution of free and combined phenolic acids in wheat internodes. *Phytochemistry,* 29**,** 429 – 433.

LAM, T. B. T., KADOYA, K. & IIYAMA, K. 2001. Bonding of hydroxycinnamic acids to lignin: ferulic and *p*-coumaric acids are predominantly linked at the benzyl position of lignin, not the β-position, in grass cell walls. *Phytochemistry,* 57**,** 987 – 992.

LAMPORT, D. T. A., VARNAI, P. & SEAL, C. E. 2014. Back to the future with the AGP–Ca^{2+} flux capacitor. *Annals of Botany,* 114**,** 1069 – 1085.

LAN, T. Q., LOU, H. & ZHU, J. Y. 2013. Enzymatic Saccharification of lignocelluloses should be conducted at elevated pH 5.2–6.2. *BioEnergy Research,* 6**,** 476 – 485.

LE NGOC HUYEN, T., RÉMOND, C., DHEILLY, R. M. & CHABBERT, B. 2010. Effect of harvesting date on the composition and saccharification of *Miscanthus* × *giganteus*. *Bioresource Technology,* 101**,** 8224 – 8231.

LEE, C., TENG, Q., ZHONG, R. & YE, Z.-H. 2014. Alterations of the degree of xylan acetylation in *Arabidopsis* xylan mutants. *Plant Signaling & Behavior,* 9**,** e27797.

LEE, K. J. D., CORNUAULT, V., MANFIELD, I. W., RALET, M.-C. & PAUL KNOX, J. 2013. Multi-scale spatial heterogeneity of pectic rhamnogalacturonan I (RG–I) structural features in tobacco seed endosperm cell walls. *The Plant Journal,* 75**,** 1018 – 1027.

LEE, S. J., WARNICK, T. A., LESCHINE, S. B. & HAZEN, S. P. 2012a. A high-throughput biological conversion assay for determining lignocellulosic quality. *In:* NORMANLY, J. (ed.) *High-Throughput Phenotyping in Plants.* Humana Press.

LEE, S. J., WARNICK, T. A., PATTATHIL, S., ALVELO-MAUROSA, J. G., SERAPIGLIA, M. J., McCORMICK, H., BROWN, V., YOUNG, N. F., SCHNELL, D. J., SMART, L. B., HAHN, M. G., PEDERSEN, J. F., LESCHINE, S. B. & HAZEN, S. P. 2012b. Biological conversion assay using *Clostridium phytofermentans* to estimate plant feedstock quality. *Biotechnology for Biofuels,* 5**,** 5.

LEROUX, O. 2012. Collenchyma: a versatile mechanical tissue with dynamic cell walls. *Annals of Botany,* 110**,** 1083 – 1098.

LEVINE, T. R. & HULLETT, C. R. 2002. Eta squared, partial eta squared, and misreporting of effect size in communication research. *Human Communication Research,* 28**,** 612 – 625.

LI, F., REN, S., ZHANG, W., XU, Z., XIE, G., CHEN, Y., TU, Y., LI, Q., ZHOU, S., LI, Y., TU, F., LIU, L., WANG, Y., JIANG, J., QIN, J., LI, S., LI, Q., JING, H. C., ZHOU, F., GUTTERSON, N. & PENG, L. 2013a. Arabinose substitution degree in xylan positively affects lignocellulose enzymatic digestibility after various $NaOH/H_2SO_4$ pretreatments in *Miscanthus*. *Bioresour Technol,* 130**,** 629 – 637.

LI, H.-Q., LI, C.-L., SANG, T. & XU, J. 2013b. Pretreatment on *Miscanthus lutarioriparious* by liquid hot water for efficient ethanol production. *Biotechnology for Biofuels,* 6**,** 76.

LI, M., PATTATHIL, S., HAHN, M. G. & HODGE, D. B. 2014a. Identification of features associated with plant cell wall recalcitrance to pretreatment by alkaline hydrogen peroxide in diverse bioenergy feedstocks using glycome profiling. *RSC Advances,* 4**,** 17282 – 17292.

LI, Z., ZHAO, C., ZHA, Y., WAN, C., SI, S., LIU, F., ZHANG, R., LI, F., YU, B., YI, Z., XU, N., PENG, L. & LI, Q. 2014b. The minor wall-networks between monolignols and interlinked-phenolics predominantly affect biomass enzymatic digestibility in *Miscanthus*. *PLoS ONE,* 9**,** e105115.

LIBERMAN, M., MUTAFTSCHIEV, S., JAUNEAU, A., VIAN, B., CATESSON, A. M. & GOLDBERG, R. 1999. Mung bean hypocotyl homogalacturonan: Localization, organization and origin. *Annals of Botany,* 84**,** 225 – 233.

LINERS, F., GASPAR, T. & CUTSEM, P. 1994. Acetyl- and methyl-esterification of pectins of friable and compact sugar-beet calli: consequences for intercellular adhesion. *Planta,* 192**,** 545 – 556.

LINERS, F., LETESSON, J.-J., DIDEMBOURG, C. & van CUTSEM, P. 1989. Monoclonal antibodies against pectin: Recognition of a conformation induced by calcium. *Plant Physiology,* 91**,** 1419 – 1424.

LIONETTI, V., FRANCOCCI, F., FERRARI, S., VOLPI, C., BELLINCAMPI, D., GALLETTI, R., D'OVIDIO, R., de LORENZO, G. & CERVONE, F. 2010. Engineering the cell wall by reducing de-methyl-esterified homogalacturonan improves saccharification of plant tissues for bioconversion. *Proceedings of the National Academy of Sciences,* 107**,** 616 – 621.

LIU, C., XIAO, L., JIANG, J., WANG, W., GU, F., SONG, D., YI, Z., JIN, Y. & LI, L. 2013. Biomass properties from different *Miscanthus* species. *Food and Energy Security,* 2**,** 12 – 19.

LIU, T., WILLIAMS, D., PATTATHIL, S., LI, M., HAHN, M. & HODGE, D. 2014. Coupling alkaline pre-extraction with alkaline-oxidative post-treatment of corn stover to enhance enzymatic hydrolysis and fermentability. *Biotechnology for Biofuels,* 7**,** 48.

LÓPEZ-CASADO, G., MATAS, A. J., DOMÍNGUEZ, E., CUARTERO, J. & HEREDIA, A. 2007. Biomechanics of isolated tomato (*Solanum lycopersicum* L.) fruit cuticles: the role of the cutin matrix and polysaccharides. *Journal of Experimental Botany,* 58**,** 3875 – 3883.

LOUGH, W. J. & WAINER, I. W. 1996. *High Performance Liquid Chromatography: Fundamental Principles and Practice,* Glasgow, UK, Blackie Academic Professional, an imprint of Chapman Hall.

LOVE, G. D., SNAPE, C. E. & JARVIS, M. C. 1998. Comparison of leaf and stem cell-wall components in barley straw by solid-state ^{13}C NMR. *Phytochemistry,* 49**,** 1191 – 1194.

LOZOVAYA, V. V., GORSHKOVA, T. A., YABLOKOVA, E. V., RUMYANTSEVA, N. I., VALIEVA, A., ULANOV, A. & WIDHOLM, J. M. 1999. Cold alkali can extract phenolic acids that are ether linked to cell wall components in dicotyledonous plants (buckwheat, soybean and flax). *Phytochemistry,* 50**,** 395 – 400.

LU, F. & RALPH, J. 1997. Derivatization followed by reductive cleavage (DFRC method), a new method for lignin analysis: Protocol for analysis of DFRC monomers. *J Agric Food Chem,* 45**,** 2590 – 2592.

LYGIN, A. V., UPTON, J., DOHLEMAN, F. G., JUVIK, J., ZABOTINA, O. A., WIDHOLM, J. M. & LOZOVAYA, V. V. 2011. Composition of cell wall phenolics and polysaccharides of the potential bioenergy crop – *Miscanthus*. *Global Change Biology Bioenergy,* 3**,** 333 – 345.

MacADAM, J. W., NELSON, C. J. & SHARP, R. E. 1992. Peroxidase activity in the leaf elongation zone of tall fescue: I. spatial distribution of ionically bound peroxidase activity in genotypes differing in length of the elongation zone. *Plant Physiology,* 99**,** 872 – 878.

MANABE, Y., NAFISI, M., VERHERTBRUGGEN, Y., ORFILA, C., GILLE, S., RAUTENGARTEN, C., CHERK, C., MARCUS, S. E., SOMERVILLE, S., PAULY,

M., KNOX, J. P., SAKURAGI, Y. & SCHELLER, H. V. 2011. Loss-of-function mutation of REDUCED WALL ACETYLATION2 in *Arabidopsis* leads to reduced cell wall acetylation and increased resistance to *Botrytis cinerea*. *Plant Physiology,* 155**,** 1068 – 1078.

MANABE, Y., VERHERTBRUGGEN, Y., GILLE, S., HARHOLT, J., CHONG, S.-L., PAWAR, P. M.-A., MELLEROWICZ, E. J., TENKANEN, M., CHENG, K., PAULY, M. & SCHELLER, H. V. 2013. Reduced wall acetylation proteins play vital and distinct roles in cell wall *O*-acetylation in *Arabidopsis*. *Plant Physiology,* 163**,** 1107 – 1117.

MANFIELD, I. W., ORFILA, C., McCARTNEY, L., HARHOLT, J., BERNAL, A. J., SCHELLER, H. V., GILMARTIN, P. M., MIKKELSEN, J. D., PAUL KNOX, J. & WILLATS, W. G. 2004. Novel cell wall architecture of isoxaben-habituated *Arabidopsis* suspension-cultured cells: global transcript profiling and cellular analysis. *Plant J,* 40**,** 260 – 275.

MANN, D. G. J., LABBÉ, N., SYKES, R., GRACOM, K., KLINE, L., SWAMIDOSS, I., BURRIS, J., DAVIS, M. & STEWART JR., C. N. 2009. Rapid assessment of lignin content and structure in switchgrass (*Panicum virgatum* L.) grown under different environmental conditions. *BioEnergy Research,* 2**,** 246 – 256.

MARCUS, S., VERHERTBRUGGEN, Y., HERVE, C., ORDAZ-ORTIZ, J., FARKAS, V., PEDERSEN, H., WILLATS, W. & KNOX, J. P. 2008. Pectic homogalacturonan masks abundant sets of xyloglucan epitopes in plant cell walls. *BMC Plant Biology,* 8**,** 60.

MARCUS, S. E., BLAKE, A. W., BENIANS, T. A. S., LEE, K. J. D., POYSER, C., DONALDSON, L., LEROUX, O., ROGOWSKI, A., PETERSEN, H. L., BORASTON, A., GILBERT, H. J., WILLATS, W. G. T. & PAUL KNOX, J. 2010. Restricted access of proteins to mannan polysaccharides in intact plant cell walls. *The Plant Journal,* 64**,** 191 – 203.

MARRY, M., McCANN, M. C., KOLPAK, F., WHITE, A. R., STACEY, N. J. & ROBERTS, K. 2000. Extraction of pectic polysaccharides from sugar-beet cell walls. *Journal of the Science of Food and Agriculture,* 80**,** 17 – 28.

MASUKO, T., MINAMI, A., IWASAKI, N., MAJIMA, T., NISHIMURA, S.-I. & LEE, Y. C. 2005. Carbohydrate analysis by a phenol-sulfuric acid method in microplate format. *Analytical biochemistry,* 339**,** 69 – 72.

MATOS, D. A., WHITNEY, I. P., HARRINGTON, M. J. & HAZEN, S. P. 2013. Cell walls and the developmental anatomy of the *Brachypodium distachyon* stem internode. *PLoS ONE,* 8**,** e80640.

McCANN, M. C., BUSH, M., MILIONI, D., SADO, P., STACEY, N. J., CATCHPOLE, G., DEFERNEZ, M., CARPITA, N. C., HOFTE, H., ULVSKOV, P., WILSON, R. H. & ROBERTS, K. 2001. Approaches to understanding the functional architecture of the plant cell wall. *Phytochemistry,* 57**,** 811 – 821.

McCANN, M. C. & CARPITA, N. C. 2008. Designing the deconstruction of plant cell walls. *Current Opinion in Plant Biology,* 11**,** 314 – 320.

McCANN, M. C. & CARPITA, N. C. 2015. Biomass recalcitrance: a multi-scale, multi-factor and conversion-specific property. *Journal of Experimental Botany*.

McCANN, M. C., DEFERNEZ, M., URBANOWICZ, B. R., TEWARI, J. C., LANGEWISCH, T., OLEK, A., WELLS, B., WILSON, R. H. & CARPITA, N. C. 2007. Neural network analyses of infrared spectra for classifying cell wall architectures. *Plant Physiology,* 143**,** 1314 – 1326.

McCANN, M. C. & KNOX, J. P. 2010. Plant cell wall biology: polysaccharides in architectural and developmental contexts. *In:* ULVSKOV, P. (ed.) *Annual Plant Reviews: Plant Polysaccharides, Biosynthesis and Bioengineering.* Oxford. UK: Wiley-Blackwell.

McCARTNEY, D. H., BLOCK, H. C., DUBESKI, P. L. & OHAMA, A. J. 2006. Review: The composition and availability of straw and chaff from small grain cereals for beef cattle in western Canada. *Canadian Journal of Animal Science,* 86**,** 443-455.

McNEIL, M., DARVILL, A. G., FRY, S. C. & ALBERSHEIM, P. 1984. Structure and function of the primary cell walls of plants. *Annual review of biochemistry,* 53**,** 625 – 663.

MÉCHIN, V., ARGILLIER, O., MENANTEAU, V., BARRIÈRE, Y., MILA, I., POLLET, B. & LAPIERRE, C. 2000. Relationship of cell wall composition to in vitro cell wall digestibility of maize inbred line stems. *Journal of the Science of Food and Agriculture,* 80**,** 574 – 580.

MEIKLE, P. J., BONIG, I., HOOGENRAAD, N. J., CLARKE, A. E. & STONE, B. A. 1991. The location of (1→3)-β-glucans in the walls of pollen tubes of *Nicotiana alata* using a (1→3)-β-glucan-specific monoclonal antibody. *Planta,* 185**,** 1 – 8.

MEIKLE, P. J., HOOGENRAAD, N. J., BONIG, I., CLARKE, A. E. & STONE, B. A. 1994. A (1→3,1→4)-β-glucan-specific monoclonal antibody and its use in the quantitation and immunocytochemical location of (1→3,1→4)-β-glucans. *The Plant Journal,* 5**,** 1 – 9.

MELTON, L. D., McNEIL, M., DARVILL, A. G., ALBERSHEIM, P. & DELL, A. 1986. Structural characterization of oligosaccharides isolated from the pectic polysaccharide rhamnogalacturonan II. *Carbohydrate Research,* 146**,** 279 – 305.

MELTON, L. D. & SMITH, B. G. 2001. Determination of neutral sugars by gas chromatography of their alditol acetates. *Current Protocols in Food Analytical Chemistry.* John Wiley & Sons, Inc.

MIRA, N. P., TEIXEIRA, M. C. & SÁ-CORREIA, I. 2010. Adaptive response and tolerance to weak acids in *Saccharomyces cerevisiae*: a genome-wide view. *Omics,* 14**,** 525 – 540.

MITCHELL, D. J., GROHMANN, K., HIMMEL, M. E., DALE, B. E. & SCHROEDER, H. A. 1990. Effect of the degree of acetylation on the enzymatic digestion of acetylated xylans. *Journal of Wood Chemistry and Technology,* 10**,** 111 – 121.

MOHNEN, D. 1999. Biosynthesis of pectins and galactomannans. *In:* BARTON, D., NAKANISHI, K. & METH-COHN, O. (eds.) *Comprehensive Natural Products Chemistry.* Amsterdam, Netherlands: Elsevier Science Publishers.

MOHNEN, D. 2008. Pectin structure and biosynthesis. *Current Opinion in Plant Biology,* 11**,** 266 – 277.

MOLINARI, H. B. C., PELLNY, T. K., FREEMAN, J., SHEWRY, P. R. & MITCHELL, R. A. C. 2013. Grass cell wall feruloylation: distribution of bound ferulate and candidate gene expression in *Brachypodium distachyon*. *Frontiers in Plant Science,* 4.

MONTI, A., di VIRGILIO, N. & VENTURI, G. 2008. Mineral composition and ash content of six major energy crops. *Biomass and Bioenergy,* 32**,** 216 – 223.

MONTIES, B. 1989. Lignins. *In:* DEY, P. M. & HARBORNE, J. B. (eds.) *Methods in Plant Biochemistry.* New York: Academic Press.

MOORE, P. J., DARVILL, A. G., ALBERSHEIM, P. & STAEHELIN, L. A. 1986. Immunogold localization of xyloglucan and rhamnogalacturonan I in the cell walls of suspension-cultured sycamore cells. *Plant Physiol,* 82**,** 787 – 794.

MORALES-DELAROSA, S., CAMPOS-MARTIN, J. & FIERRO, J. G. 2014. Optimization of the process of chemical hydrolysis of cellulose to glucose. *Cellulose,* 21**,** 2397 – 2407.

MORGAN, N. Y. & SMITH, P. D. 2011. HPLC Detectors. *In:* CONRRADINI, D. (ed.) *Handbook of HPLC.* 2 ed. Boca Raton, Florida, USA: CRC Press.

MOSIER, N., WYMAN, C., DALE, B., ELANDER, R., LEE, Y. Y., HOLTZAPPLE, M. & LADISCH, M. 2005. Features of promising technologies for pretreatment of lignocellulosic biomass. *Bioresource Technology,* 96**,** 673 – 686.

MOUILLE, G., RALET, M. C., CAVELIER, C., ELAND, C., EFFROY, D., HEMATY, K., McCARTNEY, L., TRUONG, H. N., GAUDON, V., THIBAULT, J. F., MARCHANT, A. & HOFTE, H. 2007. Homogalacturonan synthesis in *Arabidopsis thaliana* requires a Golgi-localized protein with a putative methyltransferase domain. *Plant J,* 50**,** 605 – 614.

MOUILLE, G., ROBIN, S., LECOMTE, M., PAGANT, S. & HOFTE, H. 2003. Classification and identification of *Arabidopsis* cell wall mutants using Fourier-Transform InfraRed (FT-IR) microspectroscopy. *Plant Journal,* 35**,** 393 – 404.

MOWAT, D. N., FULKERSON, R. S., TOSSELL, W. E. & WINCH, J. E. 1965. The *in vitro* digestibility and protein content of leaf and stem portions of forages. *Canadian Journal of Plant Science,* 45**,** 321 – 331.

MURRAY, S. C., ROONEY, W. L., MITCHELL, S. E., SHARMA, A., KLEIN, P. E., MULLET, J. E. & KRESOVICH, S. 2008. Genetic improvement of sorghum as a biofuel feedstock: II. QTL for stem and leaf structural carbohydrates. *Crop Science,* 48**,** 2180 – 2193.

NEDUKHA, O. M. 2015. Callose: Localization, functions, and synthesis in plant cells. *Cytology and Genetics,* 49**,** 49 – 57.

NIELSEN, S. S. 2010. Phenol-sulfuric acid method for total carbohydrates. *In:* NIELSEN, S. S. (ed.) *Food Analysis Laboratory Manual.* Springer US.

NISHIYAMA, Y., LANGAN, P. & CHANZY, H. 2002. Crystal structure and hydrogen-bonding system in cellulose Iβ from synchrotron X-ray and neutron fiber diffraction. *Journal of the American Chemical Society,* 124**,** 9074 – 9082.

O'BRIEN, T. P., FEDER, N. & McCULLY, M. E. 1964. Polychromatic staining of plant cell walls by toluidine blue O. *Protoplasma,* 59**,** 368 – 373.

O'NEIL, M. & YORK, W. S. 2003. The composition and structure of plant primary cell walls. *In:* ROSE, J. K. C. (ed.) *The Plant Cell Wall.* Boca Raton, Florida, USA: CRC Press.

O'NEILL, M., ALBERSHEIM, P. & DARVILL, A. 1990. The pectic polysaccharides of primary cell walls. *In:* DEY, P. M. (ed.) *Methods in Plant Biochemistry.* Academic Press.

O'NEILL, M. A., EBERHARD, S., ALBERSHEIM, P. & DARVILL, A. G. 2001. Requirement of borate cross-linking of cell wall rhamnogalacturonan II for *Arabidopsis* growth. *Science,* 294**,** 846 – 849.

O'NEILL, M. A., ISHII, T., ALBERSHEIM, P. & DARVILL, A. G. 2004. Rhamnogalacturonan II: structure and function of a borate cross-linked cell wall pectic polysaccharide. *Annu Rev Plant Biol,* 55**,** 109 – 139.

OH, S. Y., YOO, D. I., SHIN, Y. & SEO, G. 2005. FTIR analysis of cellulose treated with sodium hydroxide and carbon dioxide. *Carbohydrate Research,* 340**,** 417 – 428.

OLSON, C. L. 1976. On choosing a test statistic in multivariate analysis of variance. *Psychological Bulletin,* 83**,** 579.

ONG, L., CHUAH, C. & CHEW, A. 2010. Comparison of sodium hydroxide and potassium hydroxide followed by heat treatment on rice straw for cellulase production under solid state fermentation. *Journal of Applied Sciences,* 10**,** 2608 – 2612.

PARIPATI, P. & DADI, A. P. 2014. *Pretreatment and fractionation of lignocellulosic biomass*. USA patent application.

PARK, Y. B., LEE, C. M., KOO, B.-W., PARK, S., COSGROVE, D. J. & KIM, S. H. 2013. Monitoring meso-scale ordering of cellulose in intact plant cell walls using sum frequency generation spectroscopy. *Plant physiology,* 163**,** 907 – 913.

PATTATHIL, S., AVCI, U., BALDWIN, D., SWENNES, A. G., McGILL, J. A., POPPER, Z., BOOTTEN, T., ALBERT, A., DAVIS, R. H., CHENNAREDDY, C., DONG, R., O'SHEA, B., ROSSI, R., LEOFF, C., FRESHOUR, G., NARRA, R., O'NEIL, M., YORK, W. S. & HAHN, M. G. 2010. A comprehensive toolkit of plant cell wall glycan-directed monoclonal antibodies. *Plant Physiology,* 153**,** 514 – 525.

PATTATHIL, S., AVCI, U., MILLER, J. & HAHN, M. G. 2012. Immunological approaches to plant cell wall and biomass characterization: glycome profiling. *In:* HIMMEL, M. E. (ed.) *Biomass Conversion: Methods and Protocols* New York, New York, USA: Humana Press.

PATTATHIL, S., HAHN, M. G., DALE, B. E. & CHUNDAWAT, S. P. S. 2015. Insights into plant cell wall structure, architecture, and integrity using glycome profiling of native and AFEXTM-pre-treated biomass. *Journal of Experimental Botany,* 66**,** 4279 – 4294.

PAULIE, S., PERLMANN, H. & PERLMANN, P. 2005. Enzyme-linked Immunosorbent Assay. *eLS.* John Wiley & Sons, Ltd.

PAULY, M., ALBERSHEIM, P., DARVILL, A. & YORK, W. S. 1999. Molecular domains of the cellulose/xyloglucan network in the cell walls of higher plants. *Plant J,* 20**,** 629 – 639.

PAULY, M. & KEEGSTRA, K. 2008. Cell-wall carbohydrates and their modification as a resource for biofuels. *Plant J,* 54**,** 559 – 568.

PAULY, M. & KEEGSTRA, K. 2010. Plant cell wall polymers as precursors for biofuels. *Current Opinion in Plant Biology,* 13**,** 304 – 311.

PAULY, M. & SCHELLER, H. V. 2000. *O*-Acetylation of plant cell wall polysaccharides: identification and partial characterization of a rhamnogalacturonan *O*-acetyl-transferase from potato suspension-cultured cells. *Planta,* 210**,** 659 – 667.

PAWAR, P. M.-A., KOUTANIEMI, S., TENKANEN, M. & MELLEROWICZ, E. J. 2013. Acetylation of woody lignocellulose: significance and regulation. *Frontiers in plant science,* 4**,** 118.

PELL, G., TAYLOR, E. J., GLOSTER, T. M., TURKENBURG, J. P., FONTES, C. M. G. A., FERREIRA, L. M. A., NAGY, T., CLARK, S. J., DAVIES, G. J. & GILBERT, H. J. 2004. The mechanisms by which family 10 glycoside hydrolases bind decorated substrates. *Journal of Biological Chemistry,* 279**,** 9597 – 9605.

PERSSON, P., ANDERSSON, J., GORTON, L., LARSSON, S., NILVEBRANT, N.-O. & JÖNSSON, L. J. 2002. Effect of different forms of alkali treatment on specific fermentation inhibitors and on the fermentability of lignocellulose hydrolysates for production of fuel ethanol. *Journal of Agricultural and Food Chemistry,* 50**,** 5318 – 5325.

PERSSON, S., CAFFALL, K. H., FRESHOUR, G., HILLEY, M. T., BAUER, S., POINDEXTER, P., HAHN, M. G., MOHNEN, D. & SOMERVILLE, C. 2007. The arabidopsis irregular xylem8 mutant is deficient in glucuronoxylan and homogalacturonan, which are essential for secondary cell wall integrity. *The Plant Cell Online,* 19**,** 237 – 255.

PETTI, C., HARMAN-WARE, A., TATENO, M., KUSHWAHA, R., SHEARER, A., DOWNIE, A., CROCKER, M. & DEBOLT, S. 2013. Sorghum mutant RG displays antithetic leaf shoot lignin accumulation resulting in improved stem saccharification properties. *Biotechnology for Biofuels,* 6**,** 146.

PETTOLINO, F. A., WALSH, C., FINCHER, G. B. & BACIC, A. 2012. Determining the polysaccharide composition of plant cell walls. *Nat Protoc,* 7**,** 1590 – 607.

PHENOMENEX. 2015. *Rezex HPLC Information: ROA-Organic Acid H+ (8%) Phase Information* [Online]. Available:

https://www.phenomenex.com/Products/HPLCDetail/rezex [Accessed 30 January 2015].
PHILIPPE, S., SAULNIER, L. & GUILLON, F. 2006. Arabinoxylan and (1→3),(1→4)-β-glucan deposition in cell walls during wheat endosperm development. *Planta,* 224**,** 449 – 461.
PIQUEMAL, J., LAPIERRE, C., MYTON, K., O'CONNELL, A., SCHUCH, W., GRIMA-PETTENATI, J. & BOUDET, A.-M. 1998. Down-regulation of cinnamoyl-CoA reductase induces significant changes of lignin profiles in transgenic tobacco plants. *The Plant Journal,* 13**,** 71 – 83.
PUHLMANN, J., BUCHELI, E., SWAIN, M. J., DUNNING, N., ALBERSHEIM, P., DARVILL, A. G. & HAHN, M. G. 1994. Generation of monoclonal antibodies against plant cell-wall polysaccharides (I. Characterization of a monoclonal antibody to a terminal α-(1→2)-Linked Fucosyl-Containing Epitope. *Plant Physiology,* 104**,** 699 – 710.
PURDY, S. J., MADDISON, A. L., JONES, L. E., WEBSTER, R. J., ANDRALOJC, J., DONNISON, I. & CLIFTON-BROWN, J. 2013. Characterization of chilling-shock responses in four genotypes of Miscanthus reveals the superior tolerance of *M.* × *giganteus* compared with *M. sinensis* and *M. sacchariflorus*. *Annals of Botany,* 111**,** 999 – 1013.
QING, Q., YANG, B. & WYMAN, C. E. 2010. Xylooligomers are strong inhibitors of cellulose hydrolysis by enzymes. *Bioresour Technol,* 101**,** 9624 – 9630.
RAGAUSKAS, A. J., BECKHAM, G. T., BIDDY, M. J., CHANDRA, R., CHEN, F., DAVIS, M. F., DAVISON, B. H., DIXON, R. A., GILNA, P., KELLER, M., LANGAN, P., NASKAR, A. K., SADDLER, J. N., TSCHAPLINSKI, T. J., TUSKAN, G. A. & WYMAN, C. E. 2014. Lignin valorization: Improving lignin processing in the biorefinery. *Science,* 344.
RALET, M. C., CREPEAU, M. J., LEFEBVRE, J., MOUILLE, G., HOFTE, H. & THIBAULT, J. F. 2008. Reduced number of homogalacturonan domains in pectins of an *Arabidopsis* mutant enhances the flexibility of the polymer. *Biomacromolecules,* 9**,** 1454 – 1460.
RALPH, J. 2010. Hydroxycinnamates in lignification. *Phytochemistry Reviews,* 9**,** 65 – 83.
RALPH, J., GRABBER, J. H. & HATFIELD, R. D. 1995. Lignin-ferulate cross-links in grasses – Active incorporation of ferulate polysaccharide esters into ryegrass lignins. *Carbohydrate Research,* 275**,** 167 – 178.
RALPH, J., HATFIELD, R. D., QUIDEAU, S., HELM, R. F., GRABBER, J. H. & JUNG, H.-J. G. 1994a. Pathway of *p*-coumaric acid incorporation into maize lignin as revealed by NMR. *Journal of the American Chemical Society,* 116**,** 9448 – 9456.
RALPH, J., QUIDEAU, S., GRABBER, J. H. & HATFIELD, R. D. 1994b. Identification and synthesis of new ferulic acid dehydrodimers present in grass cell-walls. *Journal of the Chemical Society-Perkin Transactions 1***,** 3485 – 3498.
RANCOUR, D., MARITA, J. & HATFIELD, R. D. 2012. Cell wall composition throughout development for the model grass *Brachypodium distanchyon*. *Frontiers in Plant Science,* 3**,** 266.
RAYMUNDO-PIÑERO, E., AZAÏS, P., CACCIAGUERRA, T., CAZORLA-AMORÓS, D., LINARES-SOLANO, A. & BÉGUIN, F. 2005. KOH and NaOH activation mechanisms of multiwalled carbon nanotubes with different structural organisation. *Carbon,* 43**,** 786 – 795.
RIDLEY, B. L., O'NEILL, M. A. & MOHNEN, D. 2001. Pectins: structure, biosynthesis, and oligogalacturonide-related signaling. *Phytochemistry,* 57**,** 929 – 967.

RINALDI, R. & SCHÜTH, F. 2009. Acid hydrolysis of cellulose as the entry point into biorefinery schemes. *ChemSusChem,* 2**,** 1096 – 1107.

ROBERTS, K., PHILLIPS, J., SHAW, P., GRIEF, C. & SMITH, E. 1985. An immunological approach to the plant cell wall. *In:* BRETT, C. T. & HILLMAN, J. R. (eds.) *Biochemistry of plant cell walls.* Cambridge, UK: Cambridge University Press.

ROBSON, P., JENSEN, E., HAWKINS, S., WHITE, S. R., KENOBI, K., CLIFTON-BROWN, J., DONNISON, I. & FARRAR, K. 2013. Accelerating the domestication of a bioenergy crop: identifying and modelling morphological targets for sustainable yield increase in *Miscanthus*. *Journal of Experimental Botany,* 64**,** 4143 – 4155.

ROBSON, P., MOS, M., CLIFTON-BROWN, J. & DONNISON, I. 2012. Phenotypic variation in senescence in *Miscanthus*: Towards optimising biomass quality and quantity. *BioEnergy Research,* 5**,** 95 – 105.

ROELFSEMA, M. R. G. & HEDRICH, R. 2009. Stomata. *eLS.* John Wiley & Sons, Ltd.

ROSGAARD, L., PEDERSEN, S., LANGSTON, J., AKERHIELM, D., CHERRY, J. R. & MEYER, A. S. 2007. Evaluation of minimal *Trichoderma reesei* cellulase mixtures on differently pretreated barley straw substrates. *Biotechnology Progress,* 23**,** 1270 – 1276.

RUSSELL, S. H. & EVERT, R. F. 1985. Leaf vasculature in *Zea mays* L. *Planta,* 164**,** 448 – 458.

SAEMAN, J. F., MOORE, W. E. & MILLETT, M. A. 1963. Sugar units present. Hydrolysis and quantitative paper chromatography. *In:* WHISTLER, R. L. (ed.) *Cellulose.* New York, New York: Academic Press.

SAGAN, C. 1980. *Cosmos,* London, UK, Macdonald & Co. Ltd.

SAHA, B. C., ITEN, L. B., COTTA, M. A. & WU, Y. V. 2005. Dilute acid pretreatment, enzymatic saccharification, and fermentation of rice hulls to ethanol. *Biotechnology Progress,* 21**,** 816 – 822.

SAMUELS, A. L., GIDDINGS, T. H., JR. & STAEHELIN, L. A. 1995. Cytokinesis in tobacco BY-2 and root tip cells: a new model of cell plate formation in higher plants. *J Cell Biol,* 130**,** 1345 – 1357.

SASSNER, P., MARTENSSON, C. G., GALBE, M. & ZACCHI, G. 2008. Steam pretreatment of H_2SO_4-impregnated *Salix* for the production of bioethanol. *Bioresour Technol,* 99**,** 137 – 145.

SAULNIER, L., CRÉPEAU, M.-J., LAHAYE, M., THIBAULT, J.-F., GARCIA-CONESA, M. T., KROON, P. A. & WILLIAMSON, G. 1999. Isolation and structural determination of two 5,5′-diferuloyl oligosaccharides indicate that maize heteroxylans are covalently cross-linked by oxidatively coupled ferulates. *Carbohydrate Research,* 320**,** 82 – 92.

SCHELLER, H. V. & ULVSKOV, P. 2010. Hemicelluloses. *In:* MERCHANT, S., BRIGGS, W. R. & ORT, D. (eds.) *Annual Review of Plant Biology, Vol 61.*

SCHOLS, H. A. & VORAGEN, A. G. J. 1994. Occurrence of pectic hairy regions in various plant cell wall materials and their degradability by rhamnogalacturonase. *Carbohydrate Research,* 256**,** 83 – 95.

SCHULZ, H. & BARANSKA, M. 2007. Identification and quantification of valuable plant substances by IR and Raman spectroscopy. *Vibrational Spectroscopy,* 43**,** 13 – 25.

SCOTT, R. P. W. 1998. Liquid Chromatography Detectors. *In:* KATZ, E., EKSTEEN, R., SCHOENMAKERS, P. & MILLER, N. (eds.) *Handbook of HPLC.* New York, New York, USA: Marcel Dekker, Inc.

SEIFERT, G. J. & ROBERTS, K. 2007. The Biology of Arabinogalactan Proteins. *Annual Review of Plant Biology,* 58**,** 137 – 161.

SELIG, M., TUCKER, M., LAW, C., DOEPPKE, C., HIMMEL, M. & DECKER, S. 2011. High throughput determination of glucan and xylan fractions in lignocelluloses. *Biotechnol Lett,* 33**,** 961 – 967.

SELIG, M. J., ADNEY, W. S., HIMMEL, M. E. & DECKER, S. R. 2009. The impact of cell wall acetylation on corn stover hydrolysis by cellulolytic and xylanolytic enzymes. *Cellulose,* 16**,** 711 – 722.

SÉNÉ, C., McCANN, M. C., WILSON, R. H. & GRINTER, R. 1994. Fourier-Transform Raman and Fourier-Transform Infrared Spectroscopy (An Investigation of Five Higher Plant Cell Walls and Their Components). *Plant Physiology,* 106**,** 1623 – 1631.

SHANE, M. W., STIGTER, K., FEDOSEJEVS, E. T. & PLAXTON, W. C. 2014. Senescence-inducible cell wall and intracellular purple acid phosphatases: implications for phosphorus remobilization in *Hakea prostrata* (Proteaceae) and *Arabidopsis thaliana* (Brassicaceae). *Journal of Experimental Botany,* 65**,** 6097 – 6106.

SHARMA, R., PALLED, V., SHARMA-SHIVAPPA, R. & OSBORNE, J. 2013. Potential of potassium hydroxide pretreatment of switchgrass for fermentable sugar production. *Applied Biochemistry and Biotechnology,* 169**,** 761 – 772.

SHEN, H., FU, C. X., XIAO, X. R., RAY, T., TANG, Y. H., WANG, Z. Y. & CHEN, F. 2009. Developmental control of lignification in stems of lowland switchgrass variety alamo and the effects on saccharification efficiency. *BioEnergy Research,* 2**,** 233 – 245.

SHEN, H., POOVAIAH, C., ZIEBELL, A., TSCHAPLINSKI, T., PATTATHIL, S., GJERSING, E., ENGLE, N., KATAHIRA, R., PU, Y., SYKES, R., CHEN, F., RAGAUSKAS, A., MIELENZ, J., HAHN, M., DAVIS, M., STEWART, C. N. & DIXON, R. 2013. Enhanced characteristics of genetically modified switchgrass (*Panicum virgatum* L.) for high biofuel production. *Biotechnology for Biofuels,* 6**,** 71.

SHOWALTER, A. M. 2001. Arabinogalactan-proteins: structure, expression and function. *Cell Mol Life Sci,* 58**,** 1399 – 417.

SI, S., CHEN, Y., FAN, C., HU, H., LI, Y., HUANG, J., LIAO, H., HAO, B., LI, Q., PENG, L. & TU, Y. 2015. Lignin extraction distinctively enhances biomass enzymatic saccharification in hemicelluloses-rich *Miscanthus* species under various alkali and acid pretreatments. *Bioresource Technology,* doi: http://dx.doi.org/10.1016/j.biortech.2015.02.031.

SLAVOV, G., ROBSON, P., JENSEN, E., HODGSON, E., FARRAR, K., ALLISON, G., HAWKINS, S., THOMAS-JONES, S., MA, X. F., HUANG, L., SWALLER, T., FLAVELL, R., CLIFTON-BROWN, J. & DONNISON, I. 2013. Contrasting geographic patterns of genetic variation for molecular markers vs. phenotypic traits in the energy grass *Miscanthus sinensis*. *Global Change Biology Bioenergy,* 5**,** 562 – 571.

SLUITER, A., HAMES, B., RUIZ, R., SCARLATA, C., SLUITER, J., TEMPLETON, D. & CROCKER, D. 2012. Determination of structural carbohydrates and lignin in biomass. *NREL Laboratory analytical procedure*.

SMITH, B. C. 2011. *Fundamentals of Fourier Transform Infrared Spectroscopy, Second Edition,* Boca Raton, Florida, USA, CRC Press.

SMITH, R. & SLATER, F. M. 2011. Mobilization of minerals and moisture loss during senescence of the energy crops *Miscanthus* × *giganteus*, *Arundo donax* and *Phalaris arundinacea* in Wales, UK. *GCB Bioenergy,* 3**,** 148 – 157.

SØRENSEN, A., TELLER, P., HILSTROM, T. & AHRING, B. 2008. Hydrolysis of *Miscanthus* for bioethanol production using dilute acid presoaking combined with wet explosion pre-treatment and enzymatic treatment. *Bioresour Technol,* 99**,** 6602 – 6607.

SØRENSEN, I. & WILLATS, W. G. T. 2011. Screening and Characterization of Plant Cell Walls Using Carbohydrate Microarrays. *In:* POPPER, Z. (ed.) *The plant cell wall. Methods and protocols.* New York: Humana Press.

SPIRIDON, I. & POPA, V. I. 1998. Hemicelluloses: Structure and Properties. *In:* DUMITRIU, S. (ed.) *Polysaccharides: Structural Diversity and Functional Versatility.* New York, NY (USA): CRC Press.

SRIDHARAN, G. & SHANKAR, A. A. 2012. Toluidine blue: A review of its chemistry and clinical utility. *Journal of Oral and Maxillofacial Pathology : JOMFP,* 16**,** 251 – 255.

STAEHELIN, L. A. & HEPLER, P. K. 1996. Cytokinesis in higher plants. *Cell,* 84**,** 821 – 824.

STONE, B. A. 2006. Callose and Related Glucans. *Encyclopedia of Life Sciences.* Chichester, UK: John Wiley & Sons, Ltd.

STUDER, M. H., DEMARTINI, J. D., DAVIS, M. F., SYKES, R. W., DAVISON, B., KELLER, M., TUSKAN, G. A. & WYMAN, C. E. 2011. Lignin content in natural *Populus* variants affects sugar release. *Proceedings of the National Academy of Sciences,* 108**,** 6300 – 6305.

SUN, R., XIAO, B. & LAWTHER, J. M. 1998. Fractional and structural characterization of ball-milled and enzyme lignins from wheat straw. *Journal of Applied Polymer Science,* 68**,** 1633 – 1641.

SUZUKI, K., KITAMURA, S., KATO, Y. & ITOH, T. 2000. Highly substituted glucuronoarabinoxylans (hsGAXs) and low-branched xylans show a distinct localization pattern in the tissues of *Zea mays* L. *Plant Cell Physiol,* 41**,** 948 – 959.

SVETEK, J., YADAV, M. P. & NOTHNAGEL, E. A. 1999. Presence of a glycosylphosphatidylinositol lipid anchor on rose arabinogalactan proteins. *Journal of Biological Chemistry,* 274**,** 14724 – 14733.

SWADESH, J. K. 2000. Chapter 5: Ion Exchange Chromatography. *HPLC: Practical and Industrial Applications.* 2 ed. Boca Raton, Florida, USA: CRC Press.

TAKAHASHI, N. & KOSHIJIMA, T. 1988. Ester linkages between lignin and glucuronoxylan in a lignin-carbohydrate complex from beech (*Fagus crenata*) wood. *Wood Science and Technology,* 22**,** 231 – 241.

TAN, L., EBERHARD, S., PATTATHIL, S., WARDER, C., GLUSHKA, J., YUAN, C., HAO, Z., ZHU, X., AVCI, U., MILLER, J. S., BALDWIN, D., PHAM, C., ORLANDO, R., DARVILL, A., HAHN, M. G., KIELISZEWSKI, M. J. & MOHNEN, D. 2013. An arabidopsis cell wall proteoglycan consists of pectin and arabinoxylan covalently linked to an arabinogalactan protein. *The Plant Cell,* 25**,** 270 – 287.

TAN, L., PU, Y., PATTATHIL, S., AVCI, U., QIAN, J., ARTER, A., CHEN, L., HAHN, M. G., RAGAUSKAS, A. J. & KIELISZEWSKI, M. J. 2014. Changes in cell wall properties coincide with overexpression of extensin fusion proteins in suspension cultured tobacco cells. *PLoS ONE,* 9**,** e115906.

TANAKA, K. & HADDAD, P. R. 2000. Ion exclusion chromatography: liquid chromatography. *Encyclopedia of Separation Science.* London, UK: Academic Press.

TELEMAN, A., LUNDQVIST, J., TJERNELD, F., STALBRAND, H. & DAHLMAN, O. 2000. Characterization of acetylated 4-*O*-methylglucuronoxylan isolated from aspen employing ^{1}H and ^{13}C NMR spectroscopy. *Carbohydr Res,* 329**,** 807 – 815.

THOMAS, J. R., DARVILL, A. G. & ALBERSHEIM, P. 1989a. Isolation and structural characterization of the pectic polysaccharide rhamnogalacturonan II from walls of suspension-cultured rice cells. *Carbohydrate Research,* 185**,** 261 – 277.

THOMAS, J. R., DARVILL, A. G. & ALBERSHEIM, P. 1989b. Rhamnogalacturonan I, a pectic polysaccharide that is a component of monocot cell-walls. *Carbohydrate Research,* 185**,** 279 – 305.

TOBIMATSU, Y., ELUMALAI, S., GRABBER, J. H., DAVIDSON, C. L., PAN, X. & RALPH, J. 2012. Hydroxycinnamate conjugates as potential monolignol replacements: *in vitro* lignification and cell wall studies with rosmarinic acid. *ChemSusChem,* 5**,** 676 – 686.

TOLONEN, A. C., HAAS, W., CHILAKA, A. C., AACH, J., GYGI, S. P. & CHURCH, G. M. 2011. Proteome-wide systems analysis of a cellulosic biofuel-producing microbe. *Molecular Systems Biology,* 7.

van BEL, A. J. E. 2003. The phloem, a miracle of ingenuity. *Plant, Cell & Environment,* 26**,** 125 – 149.

van der WEIJDE, T., ALVIM KAMEI, C. L., TORRES, A. F., VERMERRIS, W., DOLSTRA, O., VISSER, R. G. F. & TRINDADE, L. M. 2013. The potential of C_4 grasses for cellulosic biofuel production. *Frontiers in Plant Science,* 4**,** 107.

van ZYL, W. H., LYND, L. R., DEN HAAN, R. & McBRIDE, J. E. 2007. Consolidated bioprocessing for bioethanol production using *Saccharomyces cerevisiae*. *Adv Biochem Eng Biotechnol,* 108**,** 205 – 235.

VANHOLME, R., DEMEDTS, B., MORREEL, K., RALPH, J. & BOERJAN, W. 2010. Lignin biosynthesis and structure. *Plant Physiology,* 153**,** 895 – 905.

VÁRNAI, A., COSTA, T., FAULDS, C., MILAGRES, A., SIIKA-AHO, M. & FERRAZ, A. 2014. Effects of enzymatic removal of plant cell wall acylation (acetylation, *p*-coumaroylation, and feruloylation) on accessibility of cellulose and xylan in natural (non-pretreated) sugar cane fractions. *Biotechnology for Biofuels,* 7**,** 153.

VEGA-SÁNCHEZ, M. E., LOQUÉ, D., LAO, J., CATENA, M., VERHERTBRUGGEN, Y., HERTER, T., YANG, F., HARHOLT, J., EBERT, B., BAIDOO, E. E. K., KEASLING, J. D., SCHELLER, H. V., HEAZLEWOOD, J. L. & RONALD, P. C. 2015. Engineering temporal accumulation of a low recalcitrance polysaccharide leads to increased C6 sugar content in plant cell walls. *Plant Biotechnology Journal,* 13**,** 903 – 914.

VEGA-SANCHEZ, M. E., VERHERTBRUGGEN, Y., CHRISTENSEN, U., CHEN, X., SHARMA, V., VARANASI, P., JOBLING, S. A., TALBOT, M., WHITE, R. G., JOO, M., SINGH, S., AUER, M., SCHELLER, H. V. & RONALD, P. C. 2012. Loss of Cellulose synthase-like F6 function affects mixed-linkage glucan deposition, cell wall mechanical properties, and defense responses in vegetative tissues of rice. *Plant Physiol,* 159**,** 56 – 69.

VEGA-SÁNCHEZ, M. E., VERHERTBRUGGEN, Y., SCHELLER, H. V. & RONALD, P. C. 2013. Abundance of mixed linkage glucan in mature tissues and secondary cell walls of grasses. *Plant Signaling & Behavior,* 8**,** e23143.

VERHERTBRUGGEN, Y., MARCUS, S. E., HAEGER, A., ORDAZ-ORTIZ, J. J. & KNOX, J. P. 2009. An extended set of monoclonal antibodies to pectic homogalacturonan. *Carbohydr Res,* 344**,** 1858 – 1862.

VILLAVERDE, J. J., LI, J., EK, M., LIGERO, P. & de VEGA, A. 2009. Native lignin structure of *Miscanthus* × *giganteus* and its changes during acetic and formic acid fractionation. *Journal of Agricultural and Food Chemistry,* 57**,** 6262 – 6270.

VOGEL, J. 2008. Unique aspects of the grass cell wall. *Current Opinion in Plant Biology,* 11**,** 301–307.

WADA, S. & RAY, P. M. 1978. Matrix polysaccharides of oat coleoptile cell walls. *Phytochemistry,* 17**,** 923 – 931.

WAKSMUNDZKA-HAJNOS, M. & SHERMA, J. 2010. *High Performance Liquid Chromatography in Phytochemical Analysis,* Boca Raton. Florida, USA, CRC Press.

WALDRON, K. W., PARR, A. J., NG, A. & RALPH, J. 1996. Cell wall esterified phenolic dimers: identification and quantification by reverse phase high performance liquid chromatography and diode array detection. *Phytochemical Analysis,* 7**,** 305 – 312.

WARNE, R. T. 2014. A primer on multivariate analysis of variance (MANOVA) for behavioral scientists. *Practical Assessment, Research & Evaluation,* 19**,** 2.

WARNICK, T. A., METHE, B. A. & LESCHINE, S. B. 2002. *Clostridium phytofermentans* sp. nov., a cellulolytic mesophile from forest soil. *Int J Syst Evol Microbiol,* 52**,** 1155 – 1160.

WEN, J. L., XIAO, L. P., SUN, Y. C., SUN, S. N., XU, F., SUN, R. C. & ZHANG, X. L. 2011. Comparative study of alkali-soluble hemicelluloses isolated from bamboo (*Bambusa rigida*). *Carbohydr Res,* 346**,** 111 – 120.

WENDE, G. & FRY, S. C. 1997a. 2-*O*-β-D-xylopyranosyl-(5-*O*-feruloyl)-L-arabinose, a widespread component of grass cell walls. *Phytochemistry,* 44**,** 1019 – 1030.

WENDE, G. & FRY, S. C. 1997b. *O*-feruloylated, *O*-acetylated oligosaccharides as side-chains of grass xylans. *Phytochemistry,* 44**,** 1011 – 1018.

WHITCOMBE, A. J., O'NEILL, M. A., STEFFAN, W., ALBERSHEIM, P. & DARVILL, A. G. 1995. Structural characterization of the pectic polysaccharide, rhamnogalacturonan-II. *Carbohydr Res,* 271**,** 15 – 29.

WI, S. G., SINGH, A. P., LEE, K. H. & KIM, Y. S. 2005. The pattern of distribution of pectin, peroxidase and lignin in the middle lamella of secondary xylem fibres in alfalfa (*Medicago sativa*). *Ann Bot,* 95**,** 863 – 868.

WILKERSON, C. G., MANSFIELD, S. D., LU, F., WITHERS, S., PARK, J.-Y., KARLEN, S. D., GONZALES-VIGIL, E., PADMAKSHAN, D., UNDA, F., RENCORET, J. & RALPH, J. 2014. Monolignol ferulate transferase introduces chemically labile linkages into the lignin backbone. *Science,* 344**,** 90 – 93.

WILLATS, W. G. T., LIMBERG, G., BUCHHOLT, H. C., van ALEBEEK, G.-J., BENEN, J., CHRISTENSEN, T. M. I. E., VISSER, J., VORAGEN, A., MIKKELSEN, J. D. & KNOX, J. P. 2000a. Analysis of pectic epitopes recognised by hybridoma and phage display monoclonal antibodies using defined oligosaccharides, polysaccharides, and enzymatic degradation. *Carbohydrate Research,* 327**,** 309 – 320.

WILLATS, W. G. T., ORFILA, C., LIMBERG, G., BUCHHOLT, H. C., van ALEBEEK, G.-J. W. M., VORAGEN, A. G. J., MARCUS, S. E., CHRISTENSEN, T. M. I. E., MIKKELSEN, J. D., MURRAY, B. S. & KNOX, J. P. 2001a. Modulation of the degree and pattern of methyl-esterification of pectic homogalacturonan in plant cell walls: Implications for pectin methyl esterase action, matrix properties, and cell adhesion. *Journal of Biological Chemistry,* 276**,** 19404 – 19413.

WILLATS, W. G. T., STEELE-KING, C. G., McCARTNEY, L., ORFILA, C., MARCUS, S. E. & KNOX, J. P. 2000b. Making and using antibody probes to study plant cell walls. *Plant Physiology and Biochemistry,* 38**,** 27 – 36.

WILLATS, W. T., McCARTNEY, L., MACKIE, W. & KNOX, J. P. 2001b. Pectin: cell biology and prospects for functional analysis. *Plant Molecular Biology,* 47**,** 9 – 27.

WILLIAMSON, G., KROON, P. A. & FAULDS, C. B. 1998. Hairy plant polysaccharides: a close shave with microbial esterases. *Microbiology,* 144 (Pt 8)**,** 2011 – 2023.

WILSON, R. H., SMITH, A. C., KACURAKOVA, M., SAUNDERS, P. K., WELLNER, N. & WALDRON, K. W. 2000. The mechanical properties and molecular dynamics of plant cell wall polysaccharides studied by Fourier-transform infrared spectroscopy. *Plant Physiology,* 124**,** 397 – 406.

WILSON, S. M., HO, Y. Y., LAMPUGNANI, E. R., van de MEENE, A. M. L., BAIN, M. P., BACIC, A. & DOBLIN, M. S. 2015. Determining the subcellular location of synthesis and assembly of the cell wall polysaccharide (1,3; 1,4)-β-D-glucan in grasses. *The Plant Cell,* 27**,** 754 – 771.

WOLF, S., MOUILLE, G. & PELLOUX, J. 2009. homogalacturonan methyl-esterification and plant development. *Molecular Plant,* 2**,** 851 – 860.

WYMAN, C. E., DALE, B. E., BALAN, V., ELANDER, R. T., HOLTZAPPLE, M. T., RAMIREZ, R. S., LADISCH, M. R., MOSIER, N. S., LEE, Y. Y., GUPTA, R.,

THOMAS, S. R., HAMES, B. R., WARNER, R. & KUMAR, R. 2013. Comparative performance of leading pretreatment technologies for biological conversion of corn stover, poplar wood, and switchgrass to sugars. *Aqueous Pretreatment of Plant Biomass for Biological and Chemical Conversion to Fuels and Chemicals.* John Wiley & Sons, Ltd.

XIE, B. & HONG, Z. 2011. Unplugging the callose plug from sieve pores. *Plant Signaling & Behavior,* 6**,** 491 – 493.

XIE, B., WANG, X., ZHU, M., ZHANG, Z. & HONG, Z. 2011. CalS7 encodes a callose synthase responsible for callose deposition in the phloem. *Plant J,* 65**,** 1 – 14.

XIMENES, E., KIM, Y., MOSIER, N., DIEN, B. & LADISCH, M. 2011. Deactivation of cellulases by phenols. *Enzyme Microb Tech,* 48**,** 54 – 60.

XIONG, G., CHENG, K. & PAULY, M. 2013. Xylan *O*-acetylation impacts xylem development and enzymatic recalcitrance as indicated by the *Arabidopsis* mutant tbl29. *Molecular Plant,* 6**,** 1373 – 1375.

XU, F. 2010. Structure, ultrastructure, and chemical composition. *In:* SUN, R.-C. (ed.) *Cereal Straw as a Resource for Sustainable Biomaterials and Biofuels.* Amsterdam, Netherlands: Elsevier.

XU, N., ZHANG, W., REN, S., LIU, F., ZHAO, C., LIAO, H., XU, Z., HUANG, J., LI, Q., TU, Y., YU, B., WANG, Y., JIANG, J., QIN, J. & PENG, L. 2012. Hemicelluloses negatively affect lignocellulose crystallinity for high biomass digestibility under NaOH and H_2SO4 pretreatments in *Miscanthus*. *Biotechnology for Biofuels,* 5**,** 58.

XUE, J., BOSCH, M. & KNOX, J. P. 2013. Heterogeneity and glycan masking of cell wall microstructures in the stems of *Miscanthus* × *giganteus*, and its parents *M. sinensis* and *M. sacchariflorus*. *PLoS ONE,* 8**,** e82114.

YAN, J., CHEN, W., LUO, F. A. N., MA, H., MENG, A., LI, X., ZHU, M., LI, S., ZHOU, H., ZHU, W., HAN, B. I. N., GE, S., LI, J. & SANG, T. A. O. 2012. Variability and adaptability of *Miscanthus* species evaluated for energy crop domestication. *GCB Bioenergy,* 4**,** 49 – 60.

YORK, W. S. & O'NEILL, M. A. 2008. Biochemical control of xylan biosynthesis – which end is up? *Current Opinion in Plant Biology,* 11**,** 258 – 265.

YOSHIDA, M., LIU, Y., UCHIDA, S., KAWARADA, K., UKAGAMI, Y., ICHINOSE, H., KANEKO, S. & FUKUDA, K. 2008. Effects of cellulose crystallinity, hemicellulose, and lignin on the enzymatic hydrolysis of *Miscanthus* sinensis to monosaccharides. *Biosci Biotechnol Biochem,* 72**,** 805 – 810.

YOUL, J. J., BACIC, A. & OXLEY, D. 1998. Arabinogalactan-proteins from *Nicotiana alata* and *Pyrus communis* contain glycosylphosphatidylinositol membrane anchors. *Proceedings of the National Academy of Sciences,* 95**,** 7921 – 7926.

ZABOTINA, O. A., van de VEN, W. T. G., FRESHOUR, G., DRAKAKAKI, G., CAVALIER, D., MOUILLE, G., HAHN, M. G., KEEGSTRA, K. & RAIKHEL, N. V. 2008. Arabidopsis XXT5 gene encodes a putative α-1,6-xylosyltransferase that is involved in xyloglucan biosynthesis. *The Plant Journal,* 56**,** 101 – 115.

ZHANG, G. F. & STAEHELIN, L. A. 1992. Functional compartmentation of the Golgi apparatus of plant cells : immunocytochemical analysis of high-pressure frozen- and freeze-substituted sycamore maple suspension culture cells. *Plant Physiol,* 99**,** 1070 – 83.

ZHANG, T., WYMAN, C., JAKOB, K. & YANG, B. 2012. Rapid selection and identification of *Miscanthus* genotypes with enhanced glucan and xylan yields from hydrothermal pretreatment followed by enzymatic hydrolysis. *Biotechnology for Biofuels,* 5**,** 56.

ZHANG, Y. & LEE, Y. C. 2002. High-performance anion-exchange chromatography of carbohydrates on pellicular resin columns. *In:* EL-RASSI, Z. (ed.) *Carbohydrate*

Analysis by Modern Chromatography and Electrophoresis. Amsterdam, The Netherlands: Elsevier Science.

ZHENG, Y., PAN, Z., ZHANG, R., WANG, D. & JENKINS, B. 2008. Non-ionic surfactants and non-catalytic protein treatment on enzymatic hydrolysis of pretreated creeping wild ryegrass. *Appl Biochem Biotechnol,* 146**,** 231 – 248.

ZHOU, G., TAYLOR, G. & POLLE, A. 2011. FTIR-ATR-based prediction and modelling of lignin and energy contents reveals independent intra-specific variation of these traits in bioenergy poplars. *Plant methods,* 7**,** 1 – 10.

ZYKWINSKA, A. W., RALET, M. C., GARNIER, C. D. & THIBAULT, J. F. 2005. Evidence for *in vitro* binding of pectin side chains to cellulose. *Plant Physiol,* 139**,** 397 – 407.

8. APPENDICES

8. APPENDICES

8.1. APPENDIX A: LIGNIN PRECURSORS AND POLYMER UNITS

Lignin precursor monomers derive primarily from the three monolignols (*p*-coumaryl, coniferyl and synapyl alcohols), which once integrated in the lignin polymer are generally denoted as *p*-hydroxyphenyl (H lignin), guaiacyl (G lignin), and syringyl (S-lignin) units. *O*-Me designates methoxyl substitutions. (adapted from Boerjan *et al.* (2003).

Monolignols (lignin precursors)

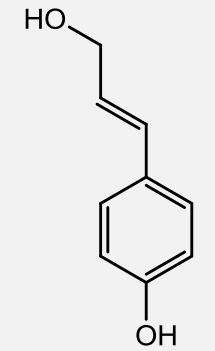

p-coumaryl alcohol

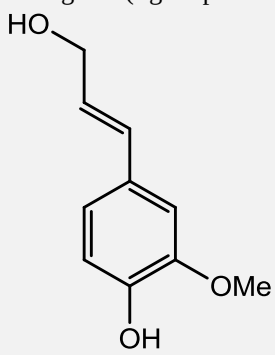

coniferyl alcohol

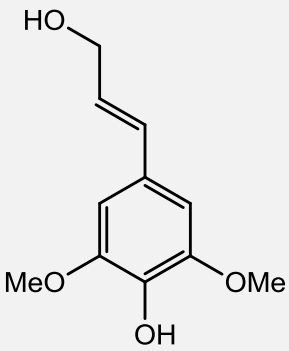

synapyl alcohol

Lignin polymer units

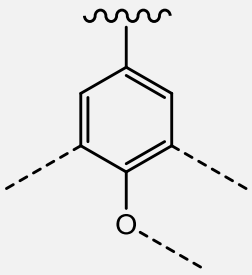

General *p*-hydroxyphenyl unit

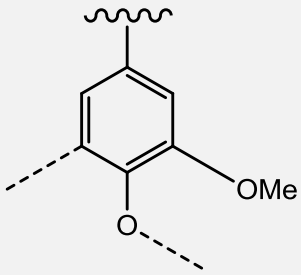

General guaiacyl unit

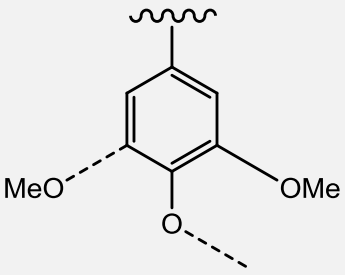

General syringyl unit

8.2. APPENDIX B: CELL WALL MONOSACCHARIDES

Thirteen different monosaccharides, including three hexoses, two deoxyhexoses, three pentoses, two uronic acids, two ketoses, and an acid pentose, account for the monomer subunits of cellulose, matrix polysaccharides (hemicelluloses and pectins), as well for the glyco- units of the primary cell wall structural glycoproteins (Albersheim, 2011).

Hexoses

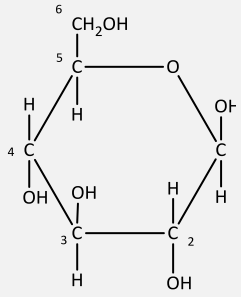

D-Glucose
(Glc)

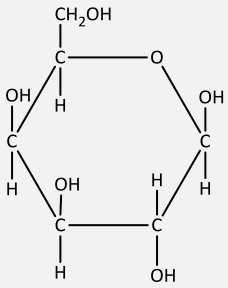

D-Galactose
(Gal)

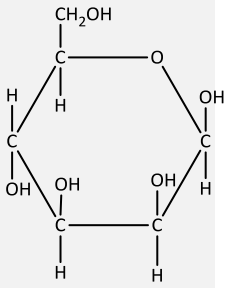

D-Mannose
(Man)

Deoxyhexoses (lack an OH group at C6)

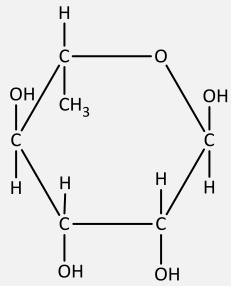

L-Rhamnose
(Rha)

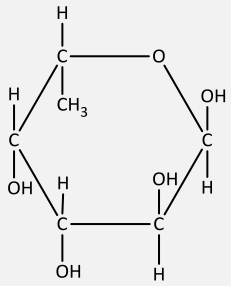

L-Fucose
(Fuc)

Pentoses

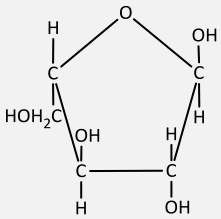

L-Arabinose
(Ara)

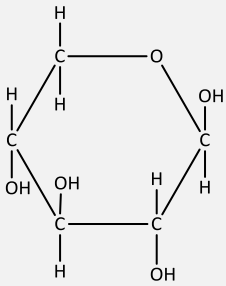

D-Xylose
(Xyl)

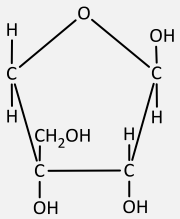

D-Apiose
(Api)

Acidic Sugars (contain COOH groups)

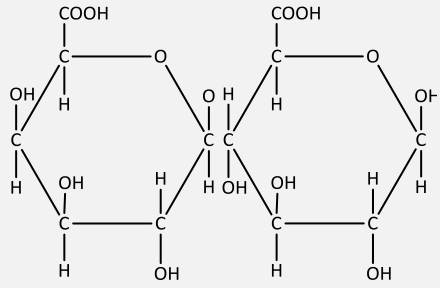

D-Galacturonic acid
(GalA)

D-Glucuronic acid
(GlcA)

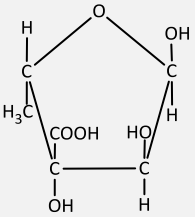

L-Aceric acid
(AceA)

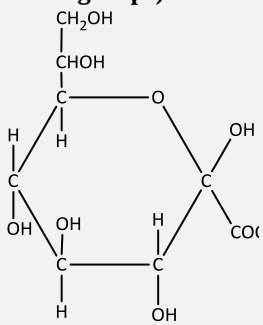

3-deoxy-D-Manno-octulosonic
(KDO)

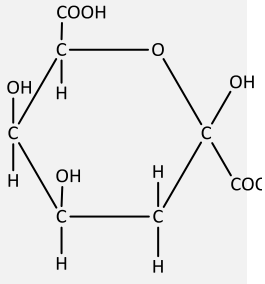

3-deoxy-D-Lyxo-2-heptulosaric a
(DHA)

8.3. APPENDIX C: LIST OF ALL USED MONOCLONAL ANTIBODIES

Listing of plant cell wall glycan-directed monoclonal antibodies (mAbs) used in the glycome profiling screening. The groupings of antibodies are based on a hierarchical clustering of ELISA data generated from a screen of all mAbs against a panel of plant polysaccharide preparations (Pattathil *et al.*, 2010), which grouped the mAbs according to the predominant polysaccharides recognised. Most listed items contain a web link to the WallMabDB plant cell wall monoclonal antibody database (http://www.wallmabdb.net), which provides detailed descriptions of each mAb, including immunogen, antibody isotype, epitope structure (to the current known extent), supplier information, and related literature citations.

Glycan Group Recognised	mAb Name
Non-Fucosylated Xyloglucan-1	CCRC-M95 CCRC-M101
Non-Fucosylated Xyloglucan-2	CCRC-M104 CCRC-M89 CCRC-M93 CCRC-M87 CCRC-M88
Non-Fucosylated Xyloglucan-3	CCRC-M100 CCRC-M103
Non-Fucosylated Xyloglucan-4	CCRC-M58 CCRC-M86 CCRC-M55 CCRC-M52 CCRC-M99
Non-Fucosylated Xyloglucan-5	CCRC-M54 CCRC-M48 CCRC-M49 CCRC-M96 CCRC-M50 CCRC-M51 CCRC-M53
Non-Fucosylated Xyloglucan-6	CCRC-M57
Fucosylated Xyloglucan	CCRC-M102 CCRC-M39 CCRC-M106 CCRC-M84 CCRC-M1
Xylan-1/XG	CCRC-M111 CCRC-M108 CCRC-M109
Xylan-2	CCRC-M119 CCRC-M115 CCRC-M110 CCRC-M105
Xylan-3	CCRC-M117 CCRC-M113 CCRC-M120 CCRC-M118 CCRC-M116 CCRC-M114
Xylan-4	CCRC-M154 CCRC-M150

Glycan Group Recognised	mAbNames
Xylan-5	CCRC-M144 CCRC-M146 CCRC-M145 CCRC-M155
Xylan-6	CCRC-M153 CCRC-M151 CCRC-M148 CCRC-M140 CCRC-M139 CCRC-M138
Xylan-7	CCRC-M160 CCRC-M137 CCRC-M152 CCRC-M149
Galactomannan-1	CCRC-M75 CCRC-M70 CCRC-M74
Galactomannan-2	CCRC-M166 CCRC-M168 CCRC-M174 CCRC-M175
Glucomannan	CCRC-M169 CCRC-M170
β-Glucan	LAMP BG1
HG Backbone-1	CCRC-M131 CCRC-M38 JIM5
HG Backbone-2	JIM136 JIM7
RG-I Backbone	CCRC-M69 CCRC-M35 CCRC-M36 CCRC-M14 CCRC-M129 CCRC-M72
Linseed Mucilage RG-I	JIM3 CCRC-M40 CCRC-M161 CCRC-M164
Physcomitrella Pectin	CCRC-M98 CCRC-M94
RG-Ia	CCRC-M5 CCRC-M2
RG-Ib	JIM137 JIM101 CCRC-M61 CCRC-M30
RG-Ic	CCRC-M23 CCRC-M17 CCRC-M19 CCRC-M18 CCRC-M56 CCRC-M16

Glycan Group	mAbNames
RG-I/Arabinogalactan	CCRC-M60 CCRC-M41 CCRC-M80 CCRC-M79 CCRC-M44 CCRC-M33 CCRC-M32 CCRC-M13 CCRC-M42 CCRC-M24 CCRC-M12 CCRC-M7 CCRC-M77 CCRC-M25 CCRC-M9 CCRC-M128 CCRC-M126 CCRC-M134 CCRC-M125 CCRC-M123 CCRC-M122 CCRC-M121 CCRC-M112 CCRC-M21 JIM131 CCRC-M22 JIM132 JIM1 CCRC-M15 CCRC-M8 JIM16
Arabinogalactan-1	JIM93 JIM94 JIM11 MAC204 JIM20
Arabinogalactan-2	JIM14 JIM19 JIM12 CCRC-M133 CCRC-M107
Arabinogalactan-3	JIM4 CCRC-M31 JIM17 CCRC-M26 JIM15 JIM8 CCRC-M85 CCRC-M81 MAC266 PN16.4B4
Arabinogalactan-4	MAC207 JIM133 JIM13 CCRC-M92 CCRC-M91 CCRC-M78
Unidentified	MAC265 CCRC-M97

8.4. APPENDIX D: ELISA PROCEDURE

The enzyme-linked immunosorbent assay (ELISA) employed consists of an indirect method of detection. Indirect ELISA is a two-step ELISA which involves two binding process, one with a primary antibody and another with a labelled secondary antibody. The primary antibody is incubated with the antigens, followed by the incubation with the secondary antibody. The ELISA procedure is here described:

1. Coating of the ELISA plates: All cell wall extracts are diluted to a predetermined concentration and a volume of each sample is dispensed into each well of an ELISA plate. Subsequently, the samples in the wells are left to evaporate to dryness overnight in a ventilated incubator set at 37°C. The number of wells coated with the epitopes should equalise the number of mAbs to be tested, plus controls. The image below represents the typical layout of the 384-well plates used (diagonal duplication of 16 mAbs for 11 samples plus negative controls).

	Sample 1		Sample 2		Sample 3		Sample 4		Sample 5		H2O control		Sample 6		Sample 7		Sample 8		Sample 9		Sample 10		Sample 11	
	1	2	3	4	5	6	7	8	9	10	11	12	13	14	15	16	17	18	19	20	21	22	23	24
A	mAb1	mAb2	mAb1	mAb2	mAb1	mAb2	mAb1	mAb2	mAb1	mAb2	mAb1	mAb2	mAb1	mAb2	mAb1	mAb2	mAb1	mAb2	mAb1	mAb2	mAb1	mAb2	mAb1	mAb2
B	mAb2	mAb1	mAb2	mAb1	mAb2	mAb1	mAb2	mAb1	mAb2	mAb1	mAb2	mAb1	mAb2	mAb1	mAb2	mAb1	mAb2	mAb1	mAb2	mAb1	mAb2	mAb1	mAb2	mAb1
C	mAb3	mAb4	mAb3	mAb4	mAb3	mAb4	mAb3	mAb4	mAb3	mAb4	mAb3	mAb4	mAb3	mAb4	mAb3	mAb4	mAb3	mAb4	mAb3	mAb4	mAb3	mAb4	mAb3	mAb4
D	mAb4	mAb3	mAb4	mAb3	mAb4	mAb3	mAb4	mAb3	mAb4	mAb3	mAb4	mAb3	mAb4	mAb3	mAb4	mAb3	mAb4	mAb3	mAb4	mAb3	mAb4	mAb3	mAb4	mAb3
E	mAb5	mAb6	mAb5	mAb6	mAb5	mAb6	mAb5	mAb6	mAb5	mAb6	mAb5	mAb6	mAb5	mAb6	mAb5	mAb6	mAb5	mAb6	mAb5	mAb6	mAb5	mAb6	mAb5	mAb6
F	mAb6	mAb5	mAb6	mAb5	mAb6	mAb5	mAb6	mAb5	mAb6	mAb5	mAb6	mAb5	mAb6	mAb5	mAb6	mAb5	mAb6	mAb5	mAb6	mAb5	mAb6	mAb5	mAb6	mAb5
G	mAb7	mAb8	mAb7	mAb8	mAb7	mAb8	mAb7	mAb8	mAb7	mAb8	mAb7	mAb8	mAb7	mAb8	mAb7	mAb8	mAb7	mAb8	mAb7	mAb8	mAb7	mAb8	mAb7	mAb8
H	mAb8	mAb7	mAb8	mAb7	mAb8	mAb7	mAb8	mAb7	mAb8	mAb7	mAb8	mAb7	mAb8	mAb7	mAb8	mAb7	mAb8	mAb7	mAb8	mAb7	mAb8	mAb7	mAb8	mAb7
I	mAb9	mAb10	mAb9	mAb10	mAb9	mAb10	mAb9	mAb10	mAb9	mAb10	mAb9	mAb10	mAb9	mAb10	mAb9	mAb10	mAb9	mAb10	mAb9	mAb10	mAb9	mAb10	mAb9	mAb10
J	mAb10	mAb9	mAb10	mAb9	mAb10	mAb9	mAb10	mAb9	mAb10	mAb9	mAb10	mAb9	mAb10	mAb9	mAb10	mAb9	mAb10	mAb9	mAb10	mAb9	mAb10	mAb9	mAb10	mAb9
K	mAb11	mAb12	mAb11	mAb12	mAb11	mAb12	mAb11	mAb12	mAb11	mAb12	mAb11	mAb12	mAb11	mAb12	mAb11	mAb12	mAb11	mAb12	mAb11	mAb12	mAb11	mAb12	mAb11	mAb12
L	mAb12	mAb11	mAb12	mAb11	mAb12	mAb11	mAb12	mAb11	mAb12	mAb11	mAb12	mAb11	mAb12	mAb11	mAb12	mAb11	mAb12	mAb11	mAb12	mAb11	mAb12	mAb11	mAb12	mAb11
M	mAb13	mAb14	mAb13	mAb14	mAb13	mAb14	mAb13	mAb14	mAb13	mAb14	mAb13	mAb14	mAb13	mAb14	mAb13	mAb14	mAb13	mAb14	mAb13	mAb14	mAb13	mAb14	mAb13	mAb14
N	mAb14	mAb13	mAb14	mAb13	mAb14	mAb13	mAb14	mAb13	mAb14	mAb13	mAb14	mAb13	mAb14	mAb13	mAb14	mAb13	mAb14	mAb13	mAb14	mAb13	mAb14	mAb13	mAb14	mAb13
O	mAb15	mAb16	mAb15	mAb16	mAb15	mAb16	mAb15	mAb16	mAb15	mAb16	mAb15	mAb16	mAb15	mAb16	mAb15	mAb16	mAb15	mAb16	mAb15	mAb16	mAb15	mAb16	mAb15	mAb16
P	mAb16	mAb15	mAb16	mAb15	mAb16	mAb15	mAb16	mAb15	mAb16	mAb15	mAb16	mAb15	mAb16	mAb15	mAb16	mAb15	mAb16	mAb15	mAb16	mAb15	mAb16	mAb15	mAb16	mAb15

2. Blocking: Non-specific sites in the coated ELISA plates are blocked by addition of a blocking buffer followed by 1h incubation at room temperature.

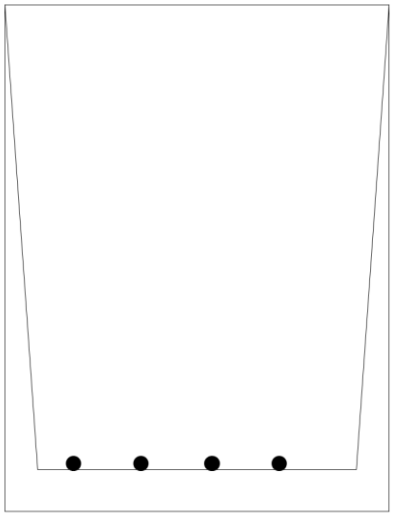

3. Primary antibodies: Blocking buffer is aspirated from each well and a volume of the primary mAb is dispensed into each well, followed by 1h incubation at room temperature.

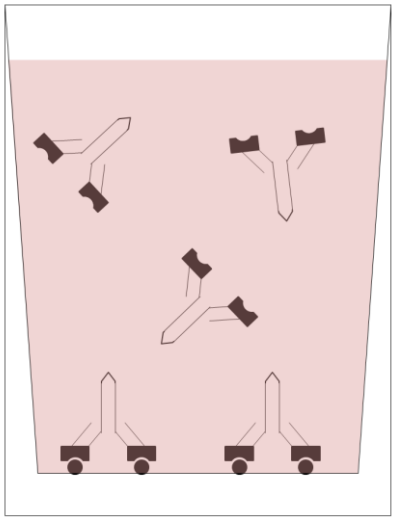

4. Washing of primary mAbs: The primary antibodies are aspirated from each well and a wash buffer is added, left for 5 seconds, and then aspirated. This step is performed three times.

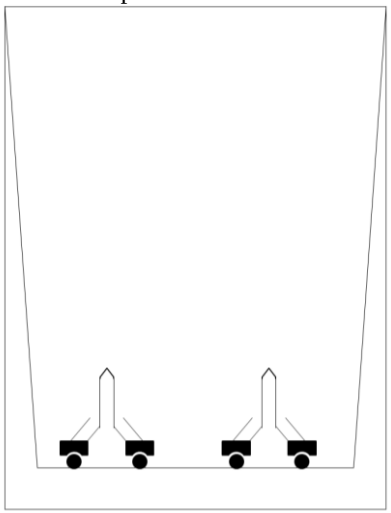

5. Secondary antibodies: After washing, a volume of horseradish peroxidase-conjugated goat secondary mAb is added to each well. Anti-mouse or anti-rat secondary mAbs are dispensed into the respective mouse (for example, CCRC series) and rat (for example, JIM series) primary mAb-bound wells and incubated at room temperature for 1 hour.

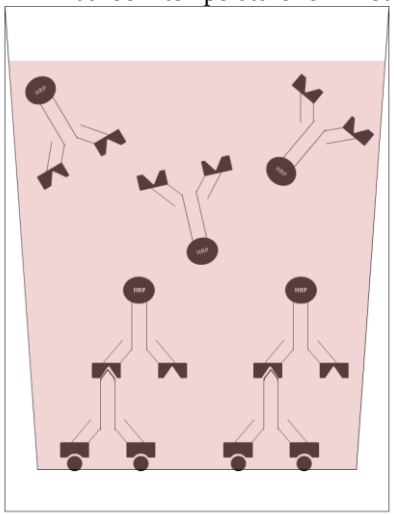

6. Washing of secondary mAbs: The secondary antibodies are aspirated from each well and a wash buffer is added, left for 5 seconds, and then completely aspirated. This step is performed five times.

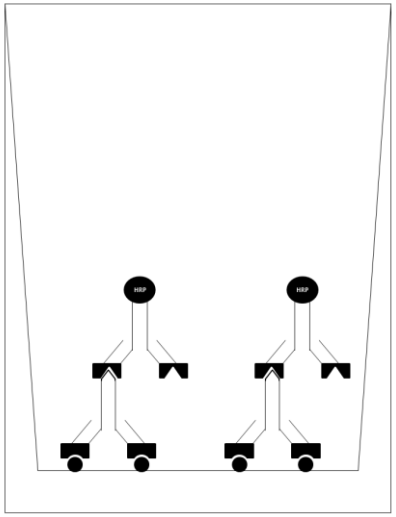

7. Substrate addition and termination: A volume of tetramethylbenzidine (TMB) substrate is dispensed into each well, incubated for precisely 20 minutes, and then the reaction is stopped with sulphuric acid (forming a yellow detectable product).

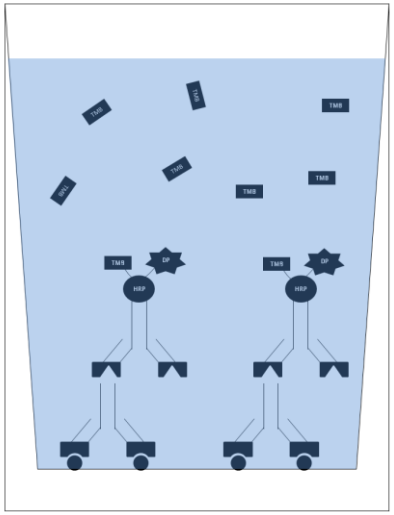

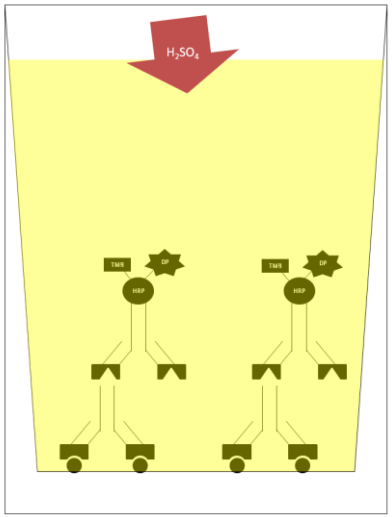

8. Quantitation: Immediately after termination, the net optical density is measured for the colour formation in the wells of ELISA plates, using a plate reader at 450nm and subtracting a background reading at 655nm.

8.5. APPENDIX E: GENERATION AND CHARACTERISATION OF MONOCLONAL ANTIBODIES

All mAbs used in this study were obtained as hybridoma cell culture supernatants. Hahn *et al.* (1987) describe a procedure for mAb generation, which despite having been used for the CCRC series of mAbs, it is generally similar to the methods used for the remaining mAb series[*]. An outline of the methods used for mAb production is presented below[†].

For the generation of cell wall glycan-directed mAbs, the first step is the isolation and purification of cell wall polysaccharides from various plant species or from the growth media of suspension-cultured cells. Subsequently, oligosaccharide fragments are generated by selective enzymatic fragmentation of the isolated polysaccharides; thus forming the immunogens which will later allow the targeting of specific structural features of a cell wall structural carbohydrate.

Oligosaccharides and polysaccharides have a hemiacetal function at their reducing end (1 in the reaction below), which occurs in equilibrium with an open chain aldehyde (2). Primary amines can then react reversibly with free carbonyls to form a Schiff base (3), which is converted to a stable secondary amine (4) by reduction.

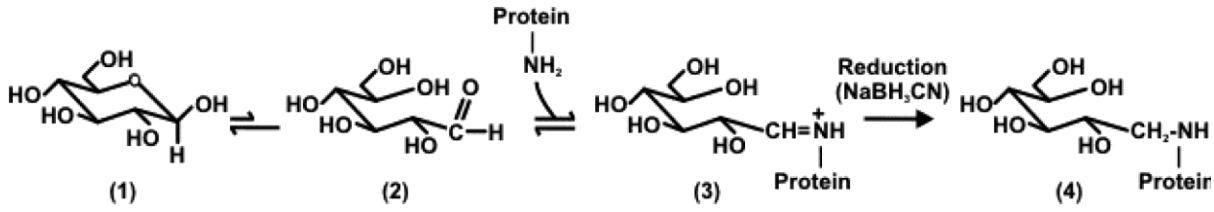

[*] Note that despite most mAbs having been produced from mouse tissues, MAC265, MAC266, and the LM and JIM series were prepared using rat tissues.
[†] Adapted from http://www.ccrc.uga.edu/~mao/wallmab/Respoly/respoly.htm.

This reaction performed under mild conditions has little impact on the attached saccharides, and therefore it is used to couple the isolated glycans to proteins and thus produce neoglycoconjugates to be used as immunogens.

To generate hybridoma cell lines, mice (or rats) can subsequently be immunised with the neoglycoconjugates and their sera monitored for the presence of mAbs which recognise the neoglycoconjugates. When mAb concentrations are sufficiently high, the murine splenic lymphocytes are isolated and fused with tumour cells (e.g., myeloma cells) to form hybridomas. Hybridoma cells are grown at a density of one cell per well, individual mAb-producing cells are selected, and the growth procedure is repeated until mAb-producing hybridoma lines are obtained, each derived from a single cell.

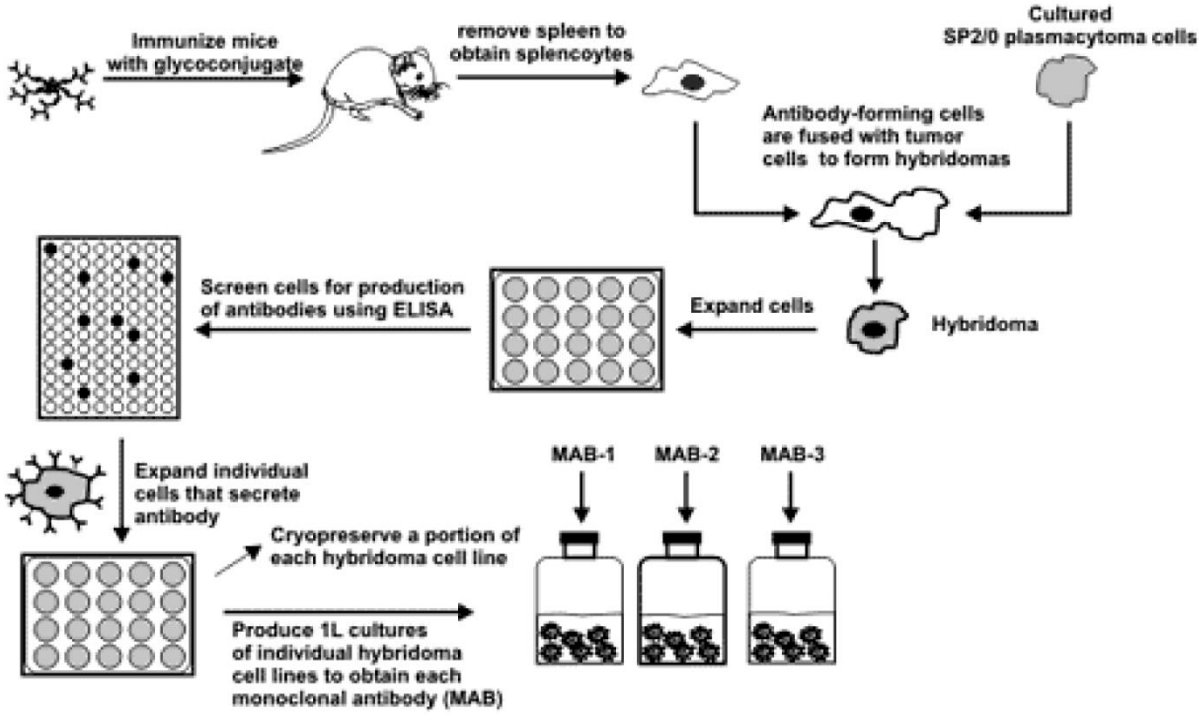

Determining the binding specificities is essential to enhance the value of mAbs as diagnostic tools, and ELISA may be used for this end; as it allows grouping of the various mAbs according to their specificities against structurally defined plant cell wall polysaccharide antigens. For the mAbs used in this study (Appendix C), an extensive study on their

characterisation, which also summarises previous work, can be found in Pattathil *et al.* (2010). These authors screened a large collection of mAbs against diverse plant polysaccharide preparations, whose detailed chemical compositions had either been previously known or was determined during the study. In this paper it was reported that despite some mAbs being polymer-specific, most would bind to specific epitopes occurring in more than one polysaccharide. Subsequent hierarchical clustering analysis, performed according to Ferguson *et al.* (1988), revealed that based on commonalities in glycan recognition, the mAbs could be grouped into several well-resolved major clades, and several subclasses consisting of the major cell wall matrix polysaccharides.

8.6. APPENDIX F: TOTAL SUGAR ESTIMATION OF THE CELL WALL MATERIAL AND COMPOSITIONAL ANALYSIS OF THE POST-SEQUENTIAL EXTRACTION RESIDUE

A further analytical study was performed on the CWM and on the residues remaining after the sequential extraction discussed in chapter 5. Initially, in order to provide a term of comparison, the phenol-sulphuric acid assay (Section 5.1.2) was performed on samples which had been previously acid-hydrolysed according to the methods described in section 4.1.2. Total carbohydrate estimated as glucose equivalents by the phenol-sulphuric acid assay (Table F1) revealed that generally stem tissues contained higher amounts of carbohydrate than leaves, at all developmental stages and for both the CWM and for the residue. In the cell wall isolated from stem samples, the total carbohydrate declined throughout development, which is consistent with the data presented in Table 4.1. By contrast, according to this method, there seems to be an increase in the total carbohydrate in leaf CWM samples as they mature and enter senescence. However, given that the absorptivity is not identical for all cell wall carbohydrates (Nielsen, 2010), this variation in leaf carbohydrate is more likely to reflect a change in the proportion of the different cell wall monosaccharides than an increase in absolute sugar amounts. By comparing these results with the sum of individual sugars determined by HPAEC-PAD (Table 4.1) it is clear that the phenol-sulphuric acid assay leads to an underestimation of the carbohydrates present in the cell wall.

With the purpose of determining which cell wall polymers were more resistant to the sequential extraction (Section 5.1), the residue samples were acid-hydrolysed and analysed by HPAEC-PAD (Section 4.1.2). Results of this assay (Table F2) revealed that the most abundantly released monosaccharide from the residue was glucose, which on average represented more than 80% of the residue samples. Secondly, xylose was detected, but it represented an average of less than 2% of the residues, with stem samples typically containing higher amounts of this monosaccharide. In addition, genotypes sac01 and sin08 had above

average percentages of Glc and Xyl at most developmental stages or tissues being analysed. Fuc, Ara and Gal were detected at trace or even negligible amounts, indicating that the polymers where these monosaccharides occur in the cell wall had been extensively removed during the sequential extraction. As a result, these observations reveal that only cellulose and residual portions of xylans remain in the samples after the sequential extraction; thus corroborating the efficiency of the sequential extraction in removing the matrix polysaccharides from miscanthus cell wall. Given that the residues here analysed are the product of an increasingly harsh cell wall fractionation procedure, the facts that higher amounts of Xyl are detected in stem samples than in leaves, and that differences are observed between genotypes, may suggest that in stems and in certain genotypes there is a higher proportion of strongly bound Xyl-containing hemicelluloses (presumably xylan and XG; see section 5.1.4), which cannot be removed by the sequential extraction.

To test if the sodium chlorite treatment (Section 5.1.2) had achieved a complete delignification of the cell wall samples, the acetyl bromide method (Section 2.4.2) was performed on the residues (Table F3). Acetyl bromide lignin represented less than 1% of the remaining leaf residue content; whereas in stems, the average lignin content that remained in the samples after the sequential extraction was higher, as it reached a maximum of 1.24% in senesced samples. However, the sodium chlorite treatment effectively removed an average of nearly 98% of the lignin from the cell walls (compare Tables 2.4 and F3).

Based on the reduced arabinose and lignin contents, analysing these residues for HCAs was considered unnecessary. Other constituents presumably include remnants of the chemicals used during the sequential extraction (ammonium oxalate, sodium carbonate, potassium hydroxide, sodium borohydride, sodium chlorite; section 5.1.2), in addition, humidity of the samples is also likely to be higher, particularly as a result of the hygroscopic effect of potassium hydroxide.

Table F1. Total carbohydrate content of miscanthus CWM estimated by the phenol-sulphuric acid assay. Values represent the mg of carbohydrate per g of cell wall material dry weight (between parenthesis is the same value expressed as percentage of the CWM).

			CWM
Active Growth	**Leaf**	gig01	560.29 (56%)
		hyb03	531.77 (53%)
		sac01	587.94 (59%)
		sin08	540.76 (54%)
		sin09	529.56 (53%)
		sin11	555.43 (56%)
		sin13	510.99 (51%)
		sin15	559.00 (56%)
		Mean	**546.97 (55%)**
	Stem	gig01	655.50 (66%)
		hyb03	603.61 (60%)
		sac01	652.57 (65%)
		sin08	617.37 (62%)
		sin09	587.00 (59%)
		sin11	606.83 (61%)
		sin13	610.92 (61%)
		sin15	608.84 (61%)
		Mean	**617.83 (62%)**
Peak Biomass	**Leaf**	gig01	551.46 (55%)
		hyb03	540.14 (54%)
		sac01	520.21 (52%)
		sin08	510.13 (51%)
		sin09	597.65 (60%)
		sin11	552.76 (55%)
		sin13	574.27 (57%)
		sin15	575.40 (58%)
		Mean	**552.75 (55%)**
	Stem	gig01	593.10 (59%)
		hyb03	593.89 (59%)
		sac01	636.34 (64%)
		sin08	614.49 (61%)
		sin09	575.27 (58%)
		sin11	599.13 (60%)
		sin13	628.11 (63%)
		sin15	638.34 (64%)
		Mean	**609.83 (61%)**
Senescence	**Leaf**	gig01	587.91 (59%)
		hyb03	577.82 (58%)
		sac01	587.23 (59%)
		sin08	602.08 (60%)
		sin09	598.33 (60%)
		sin11	599.86 (60%)
		sin13	540.51 (54%)
		sin15	616.24 (62%)
		Mean	**588.75 (59%)**
	Stem	gig01	578.30 (58%)
		hyb03	587.21 (59%)
		sac01	661.27 (66%)
		sin08	601.38 (60%)
		sin09	569.88 (57%)
		sin11	579.35 (58%)
		sin13	586.77 (59%)
		sin15	599.23 (60%)
		Mean	**595.42 (60%)**

Table F2. Monosaccharide contents of the residue left after the sequential extraction (Chapter 5) determined by HPAEC-PAD. Values are expressed as percentage of the residue sample at three developmental stages for each genotype and are the mean ± standard deviation.

			Fucose	Arabinose	Galactose	Glucose	Xylose
Active Growth	**Leaf**	gig01	<0.001	<0.001	<0.001	64.71 ± 0.36	0.81 ± 0.13
		hyb03	<0.001	<0.001	<0.001	85.39 ± 2.25	0.84 ± 0.31
		sac01	<0.001	<0.001	<0.001	95.19 ± 0.91	2.81 ± 0.14
		sin08	<0.001	<0.001	<0.001	84.05 ± 0.23	0.72 ± 0.25
		sin09	<0.001	<0.001	<0.001	81.47 ± 1.29	0.67 ± 0.13
		sin11	<0.001	<0.001	<0.001	96.78 ± 0.57	2.11 ± 0.38
		sin13	<0.001	<0.001	<0.001	82.99 ± 0.09	0.88 ± 0.24
		sin15	<0.001	<0.001	<0.001	84.70 ± 0.21	0.84 ± 0.17
		Mean	**<0.001**	**<0.001**	**<0.001**	**84.41 ± 9.78**	**1.21 ± 0.80**
	Stem	gig01	<0.001	<0.001	<0.001	70.01 ± 0.09	1.43 ± 0.06
		hyb03	<0.001	<0.001	<0.001	92.69 ± 0.01	1.28 ± 0.33
		sac01	<0.001	<0.001	<0.001	96.16 ± 0.01	3.40 ± 0.07
		sin08	<0.001	<0.001	<0.001	79.35 ± 0.75	1.56 ± 0.06
		sin09	<0.001	<0.001	<0.001	91.92 ± 0.74	1.85 ± 0.12
		sin11	<0.001	<0.001	<0.001	96.20 ± 0.61	3.31 ± 0.01
		sin13	<0.001	<0.001	<0.001	71.45 ± 0.48	1.05 ± 0.02
		sin15	<0.001	<0.001	<0.001	70.72 ± 0.30	1.34 ± 0.06
		Mean	**<0.001**	**<0.001**	**<0.001**	**83.56 ± 11.86**	**1.90 ± 0.93**
Peak Biomass	**Leaf**	gig01	<0.001	<0.001	<0.001	93.97 ± 3.97	2.16 ± 0.20
		hyb03	<0.001	<0.001	<0.001	78.78 ± 1.33	0.97 ± 0.31
		sac01	<0.001	<0.001	<0.001	92.17 ± 0.63	2.08 ± 0.05
		sin08	<0.001	<0.001	<0.001	86.07 ± 0.19	0.84 ± 0.19
		sin09	<0.001	<0.001	<0.001	74.92 ± 1.44	0.44 ± 0.11
		sin11	<0.001	<0.001	<0.001	96.09 ± 0.89	1.63 ± 0.19
		sin13	<0.001	<0.001	<0.001	83.98 ± 0.28	0.86 ± 0.15
		sin15	<0.001	<0.001	<0.001	77.62 ± 0.50	0.89 ± 0.14
		Mean	**<0.001**	**<0.001**	**<0.001**	**85.45 ± 8.02**	**1.23 ± 0.64**
	Stem	gig01	<0.001	<0.001	<0.001	95.00 ± 0.75	2.03 ± 0.05
		hyb03	<0.001	<0.001	<0.001	88.02 ± 1.94	1.36 ± 0.47
		sac01	<0.001	<0.001	<0.001	85.29 ± 0.50	2.53 ± 0.08
		sin08	<0.001	<0.001	<0.001	87.59 ± 4.53	1.88 ± 0.14
		sin09	<0.001	<0.001	<0.001	74.03 ± 0.37	0.89 ± 0.21
		sin11	<0.001	<0.001	<0.001	90.00 ± 1.28	2.66 ± 0.05
		sin13	<0.001	<0.001	<0.001	84.81 ± 0.50	1.76 ± 0.15
		sin15	<0.001	<0.001	<0.001	90.74 ± 1.58	1.58 ± 0.00
		Mean	**<0.001**	**<0.001**	**<0.001**	**86.93 ± 6.14**	**1.84 ± 0.58**
Senescence	**Leaf**	gig01	<0.001	<0.001	<0.001	87.13 ± 0.07	2.17 ± 0.14
		hyb03	<0.001	<0.001	<0.001	91.97 ± 2.11	1.77 ± 0.37
		sac01	<0.001	<0.001	<0.001	83.47 ± 0.79	1.20 ± 0.14
		sin08	<0.001	<0.001	<0.001	81.07 ± 1.01	1.57 ± 0.27
		sin09	<0.001	<0.001	<0.001	74.24 ± 0.64	0.95 ± 0.06
		sin11	<0.001	<0.001	<0.001	62.17 ± 0.08	1.60 ± 0.07
		sin13	<0.001	<0.001	<0.001	83.10 ± 1.05	0.82 ± 0.30
		sin15	<0.001	<0.001	<0.001	87.40 ± 0.84	1.25 ± 0.25
		Mean	**<0.001**	**<0.001**	**<0.001**	**81.32 ± 9.33**	**1.42 ± 0.45**
	Stem	gig01	<0.001	<0.001	<0.001	80.44 ± 0.70	1.84 ± 0.06
		hyb03	<0.001	<0.001	<0.001	87.70 ± 0.55	1.41 ± 0.06
		sac01	<0.001	<0.001	<0.001	88.70 ± 0.08	2.50 ± 0.04
		sin08	<0.001	<0.001	<0.001	87.58 ± 0.32	1.97 ± 0.01
		sin09	<0.001	<0.001	<0.001	83.93 ± 0.85	1.31 ± 0.08
		sin11	<0.001	<0.001	<0.001	96.67 ± 0.60	3.08 ± 0.03
		sin13	<0.001	<0.001	<0.001	96.97 ± 3.82	2.32 ± 0.03
		sin15	<0.001	<0.001	<0.001	84.34 ± 0.77	1.57 ± 0.26
		Mean	**<0.001**	**<0.001**	**<0.001**	**88.29 ± 5.89**	**2.00 ± 0.60**

Table F3. Acetyl bromide lignin (ABSL) percentage of the residue left after the sequential extraction (Chapter 5). Values are mean ± standard deviation.

			ABSL (% Residue)
Active Growth	**Leaf**	gig01	0.53 ± 0.05
		hyb03	0.63 ± 0.00
		sac01	0.69 ± 0.00
		sin08	0.79 ± 0.05
		sin09	0.59 ± 0.05
		sin11	0.94 ± 0.15
		sin13	0.78 ± 0.03
		sin15	0.87 ± 0.07
		Mean	**0.73 ± 0.14**
	Stem	gig01	0.75 ± 0.08
		hyb03	0.64 ± 0.03
		sac01	0.89 ± 0.03
		sin08	1.01 ± 0.07
		sin09	1.11 ± 0.02
		sin11	1.49 ± 0.14
		sin13	0.81 ± 0.00
		sin15	1.44 ± 0.10
		Mean	**1.02 ± 0.31**
Peak Biomass	**Leaf**	gig01	0.80 ± 0.11
		hyb03	0.53 ± 0.03
		sac01	0.64 ± 0.02
		sin08	0.91 ± 0.03
		sin09	0.60 ± 0.02
		sin11	1.00 ± 0.04
		sin13	1.21 ± 0.12
		sin15	1.18 ± 0.03
		Mean	**0.86 ± 0.26**
	Stem	gig01	1.26 ± 0.04
		hyb03	0.93 ± 0.03
		sac01	0.79 ± 0.01
		sin08	1.65 ± 0.03
		sin09	0.83 ± 0.01
		sin11	1.33 ± 0.02
		sin13	1.16 ± 0.03
		sin15	1.39 ± 0.01
		Mean	**1.17 ± 0.30**
Senescence	**Leaf**	gig01	0.99 ± 0.05
		hyb03	0.77 ± 0.02
		sac01	0.67 ± 0.03
		sin08	1.17 ± 0.01
		sin09	0.73 ± 0.02
		sin11	0.87 ± 0.00
		sin13	1.13 ± 0.10
		sin15	1.21 ± 0.10
		Mean	**0.94 ± 0.21**
	Stem	gig01	1.00 ± 0.01
		hyb03	1.02 ± 0.15
		sac01	0.93 ± 0.12
		sin08	1.29 ± 0.17
		sin09	0.99 ± 0.01
		sin11	1.61 ± 0.04
		sin13	1.64 ± 0.01
		sin15	1.46 ± 0.05
		Mean	**1.24 ± 0.30**

8.7. APPENDIX G: MANOVA RESULTS FOR THE GLYCOME PROFILING DATA

Table G1. StatSoft Statistica software output. Results for two test statistics are reported: Wilk's lambda and Pillai's trace. Both are test statistics for the same null hypothesis, although their formulas differ (Olson, 1976; Warne, 2014). MANOVA performed including only the mAbs which bound to miscanthus cell wall glycan epitopes during glycome profiling. Not included mAb subclasses: Xylan-2 (CCRC-M119, CCRC-M115, CCRC-M110, CCRC-M105); Galactomannan-1 (CCRC-M75, CCRC-M70, CCRC-M74); Galactomannan-2 (CCRC-M168, CCRC-M174, CCRC-M175); Glucomannan (CCRC-M169, CCRC-M170); Physcomitrella Pectin (CCRC-M98, CCRC-M94); RG-Ia (CCRC-M5, CCRC-M2).

Effect	Test	Value	*F*-ratio	Effect degrees of freedom	Error degrees of freedom	*P*-value
Intercept	Wilk's	0.0000	38844.53	70	1.00	0.0040
	Pillai's	1.0000	38113.34	70	1.00	0.0041
Extract	Wilk's	0.0000	720.54	350	10.62	<0.0001
	Pillai's	4.9992	430.33	350	25.00	<0.0001
Genotype	Wilk's	0.0000	18.54	490	20.81	<0.0001
	Pillai's	6.9226	8.95	490	49.00	<0.0001
Development	Wilk's	0.0000	30.30	140	2.00	0.0325
	Pillai's	1.9987	43.22	140	4.00	0.0011
Tissue	Wilk's	0.0000	884.15	70	1.00	0.0267
	Pillai's	1.0000	884.13	70	1.00	0.0267
Extract × Genotype	Wilk's	0.0000	5.17	2450	404.52	<0.0001
	Pillai's	28.3015	2.11	2450	1225.00	<0.0001
Extract × Development	Wilk's	0.0000	7.95	700	42.22	<0.0001
	Pillai's	9.5442	2.99	700	100.00	<0.0001
Genotype × Development	Wilk's	0.0000	3.76	980	81.00	<0.0001
	Pillai's	12.4533	1.61	980	196.00	<0.0001
Extract × Tissue	Wilk's	0.0000	45.92	350	10.62	<0.0001
	Pillai's	4.9765	15.15	350	25.00	<0.0001
Genotype × Tissue	Wilk's	0.0000	7.72	490	20.81	<0.0001
	Pillai's	6.7874	3.19	490	49.00	<0.0001
Development × Tissue	Wilk's	0.0000	10.16	140	2.00	0.0937
	Pillai's	1.9958	13.66	140	4.00	0.0098
Extract × Genotype × Development	Wilk's	0.0000	2.20	4900	991.95	<0.0001
	Pillai's	37.9452	1.18	4900	4900.00	<0.0001
Extract × Genotype × Tissue	Wilk's	0.0000	2.44	2450	404.52	<0.0001
	Pillai's	24.7774	1.21	2450	1225.00	<0.0001
Extract × Development × Tissue	Wilk's	0.0000	4.41	700	42.22	<0.0001
	Pillai's	9.1103	1.46	700	100.00	0.0092
Genotype × Development × Tissue	Wilk's	0.0000	1.84	980	81.00	0.0004
	Pillai's	11.8474	1.10	980	196.00	0.2024

8.8. APPENDIX H: SUPPLEMENTARY DATA FOR GLYCOME PROFILING PCA

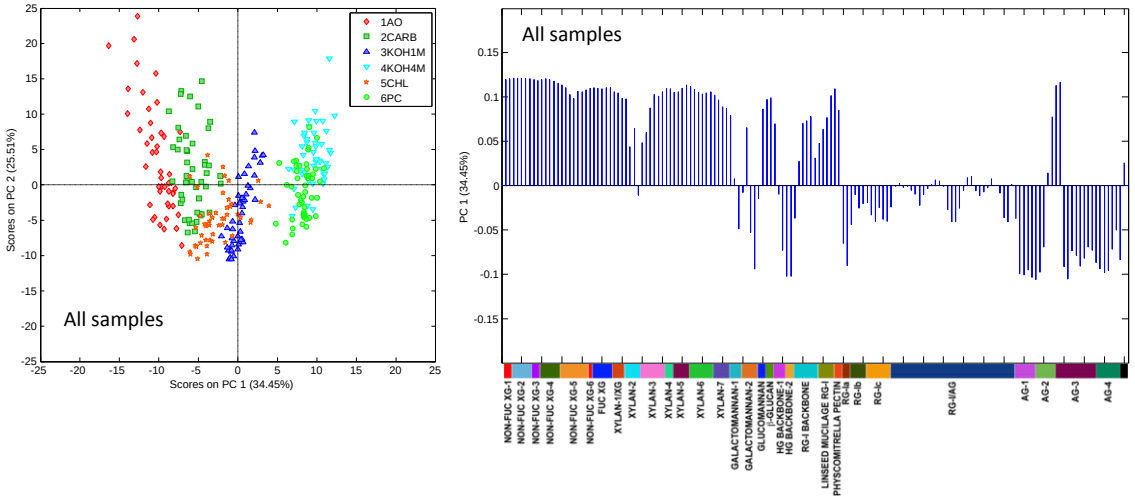

Fig. 8.8.A. Principal components analysis of glycome profiling data. Plot of principal component one (PC1) and principal component two (PC2) scores and corresponding loadings plots of the PC along which clusters emerged. Data is presented for all samples from the six fractions obtained during the sequential extraction (Section 5.1). Abbreviations: L, leaf samples; S, stem samples.

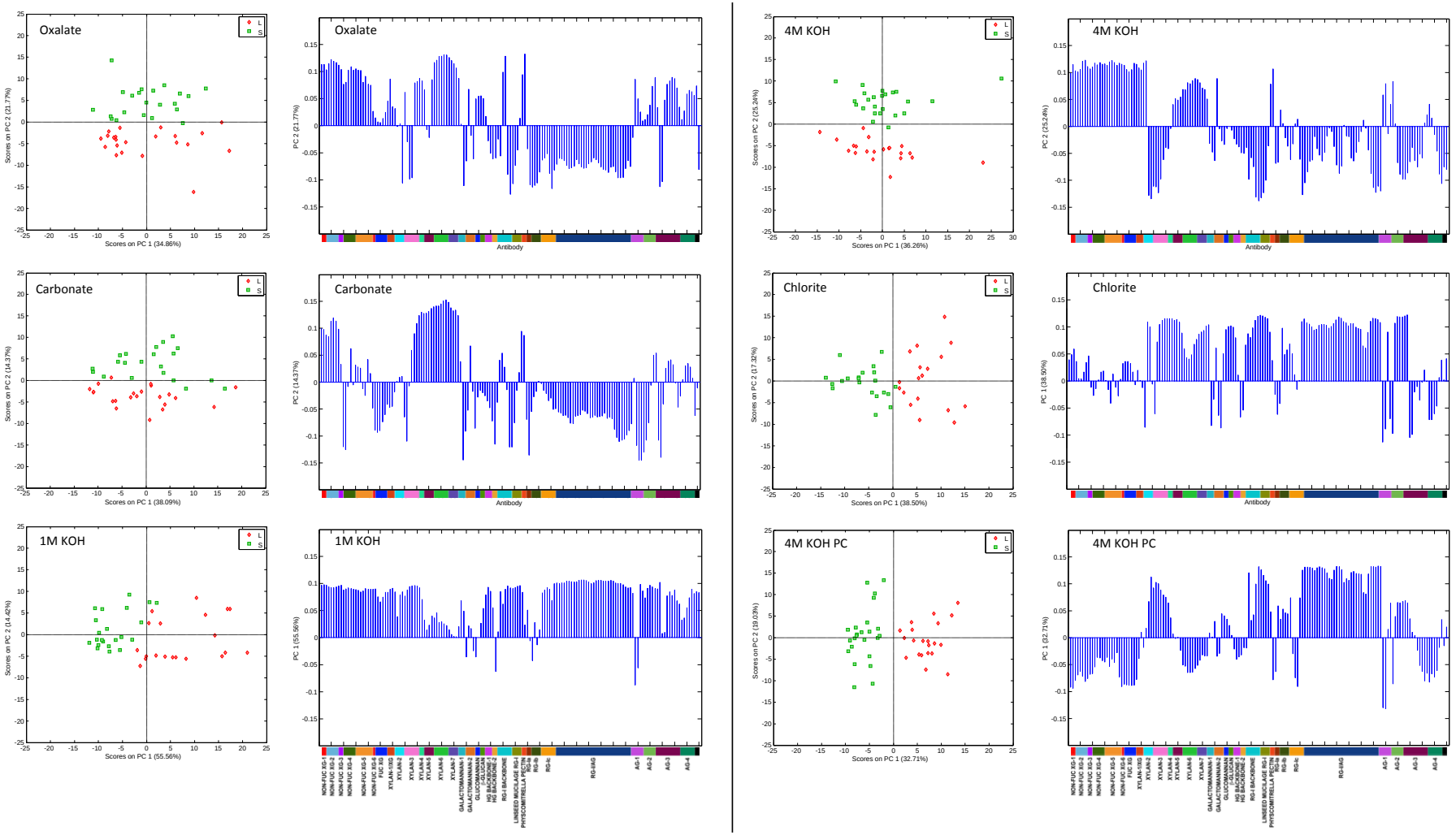

Fig. 8.8.B. Principal components analysis of glycome profiling data. Plot of principal component one (PC1) and principal component two (PC2) scores and corresponding loadings plots of the PC along which clusters emerged. Data is presented for each individual extraction step performed during the sequential extraction (Section 5.1). Abbreviations: L, leaf samples; S, stem samples.

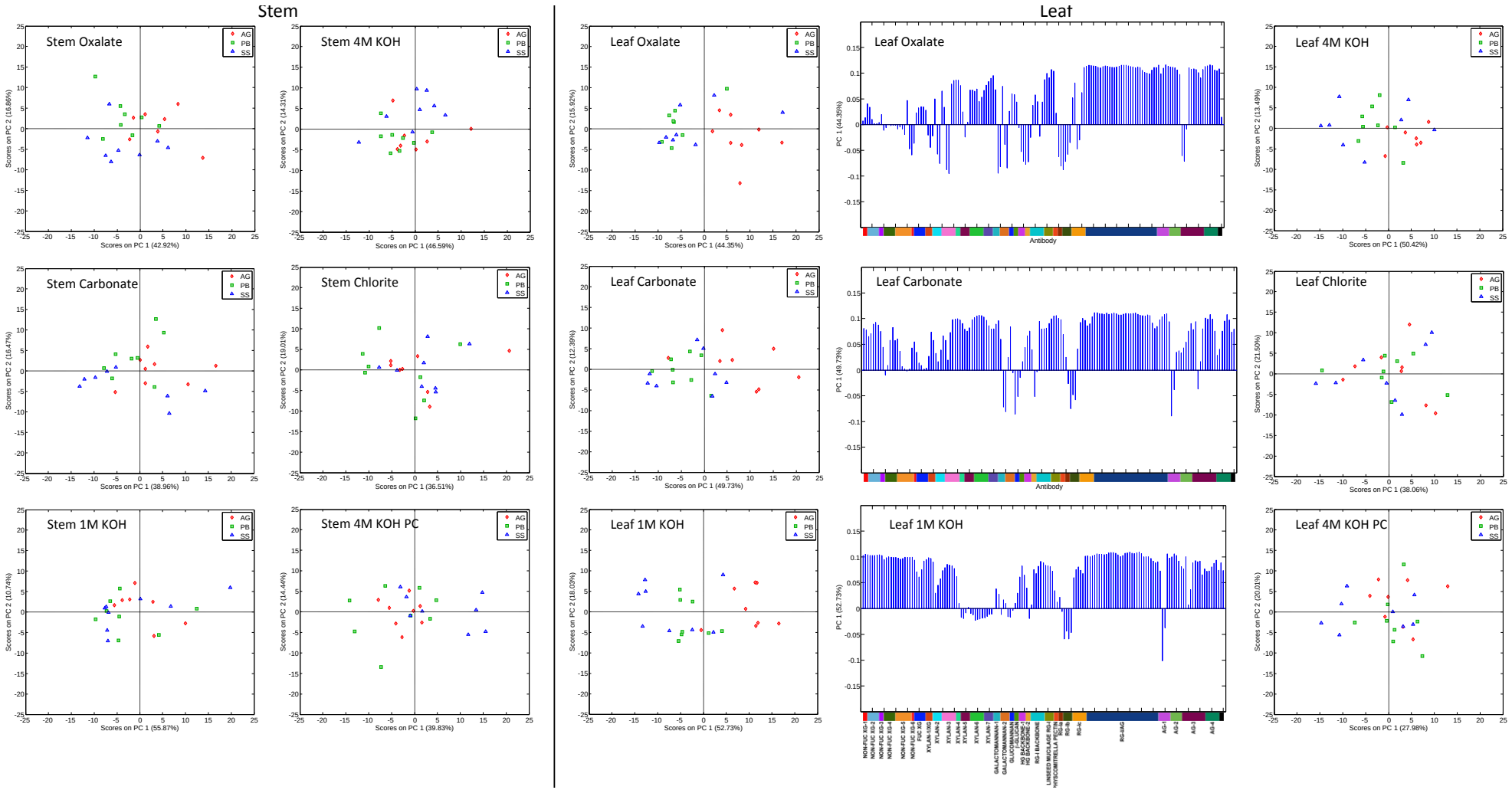

Fig. 8.8.C. Principal components analysis of glycome profiling data. Plot of principal component one (PC1) and principal component two (PC2) scores for each individual extraction step performed during the sequential extraction (Section 5.1) presented independently for each tissue: stem samples on the left panel and leaf on the right. Corresponding loadings plots are presented for the PC analyses where clusters emerged. Abbreviations: AG, active growth; PB, peak biomass; SS, senesced stage.

8.9. APPENDIX I: SUPPLEMENTARY DATA ON MAB BINDINGS

Detail of the mean binding intensities of each mAb used in glycome profiling (Section 5.1). Data is provided for the six cell wall fractions produced during the sequential extraction, for both tissues and for the three developmental stages: actively growing (red line), peak biomass (green line) and senescence (blue line).

Non-Fuc XG – Oxalate

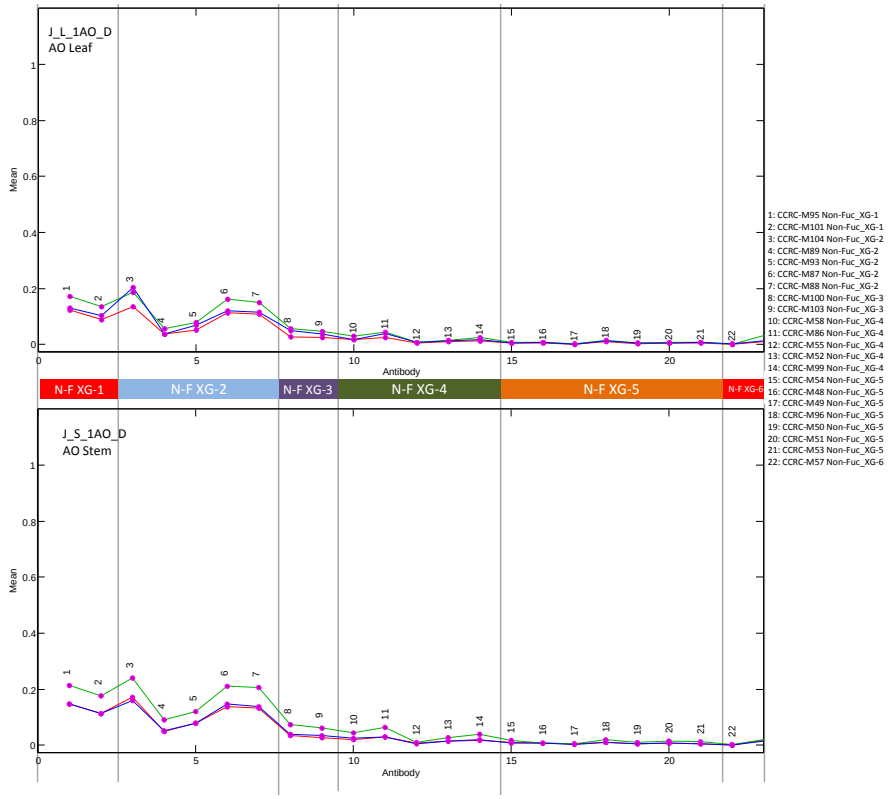

Non-Fuc XG – Carbonate

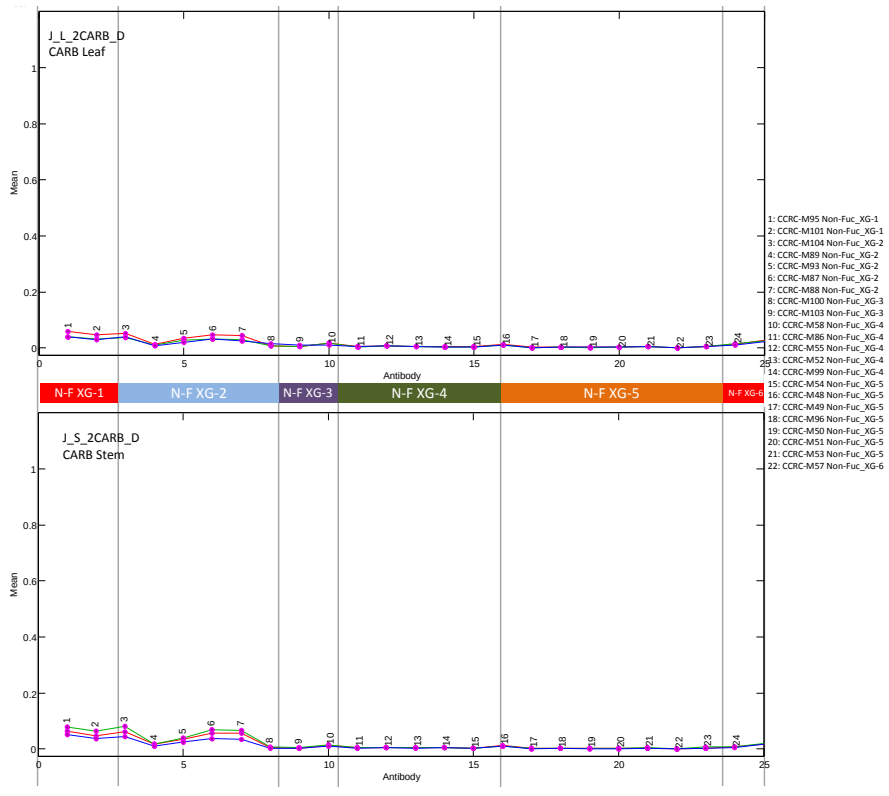

Non-Fuc XG – 1M KOH

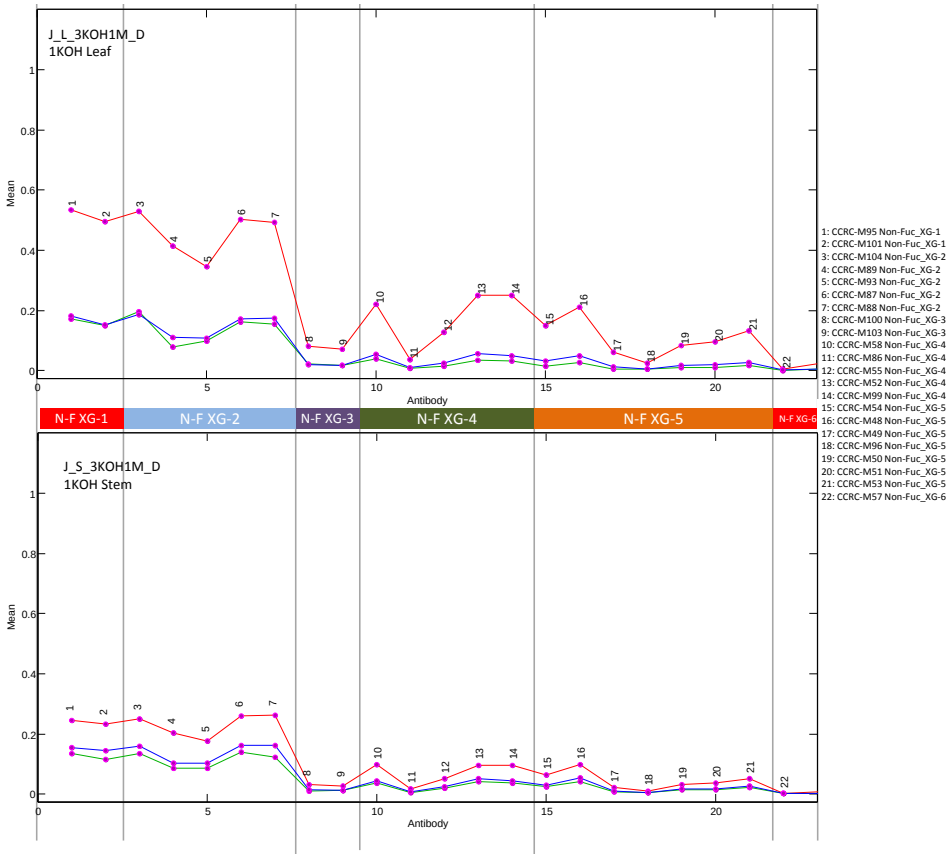

Non-Fuc XG – 4M KOH

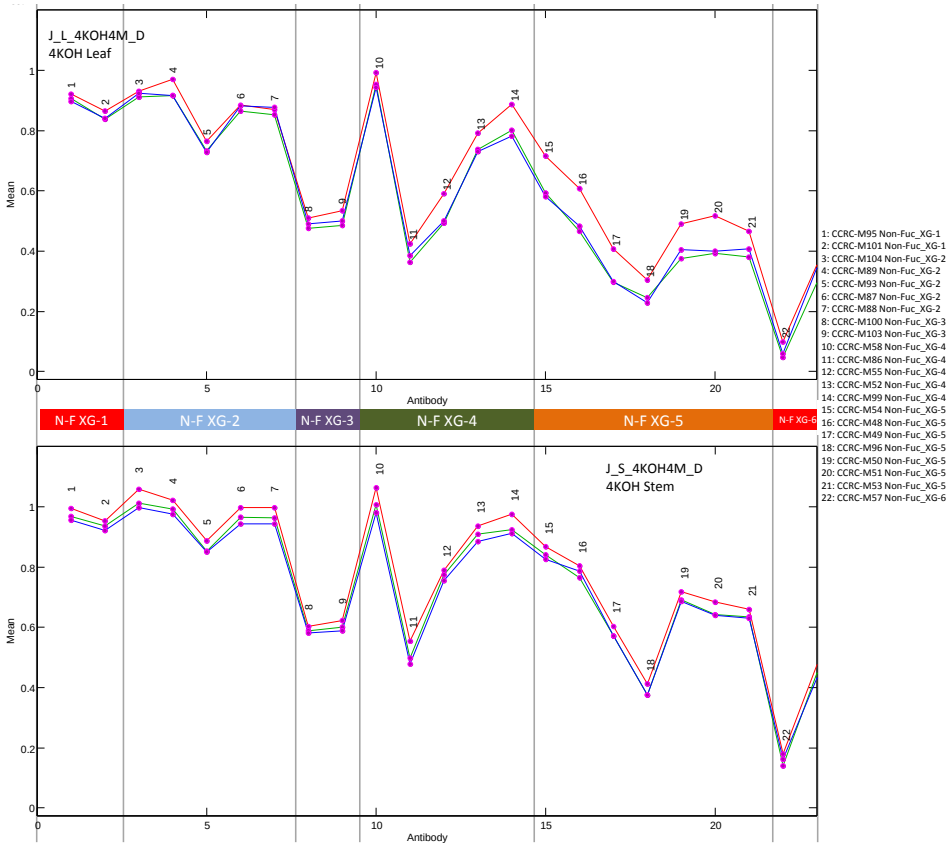

Non-Fuc XG – Chlorite

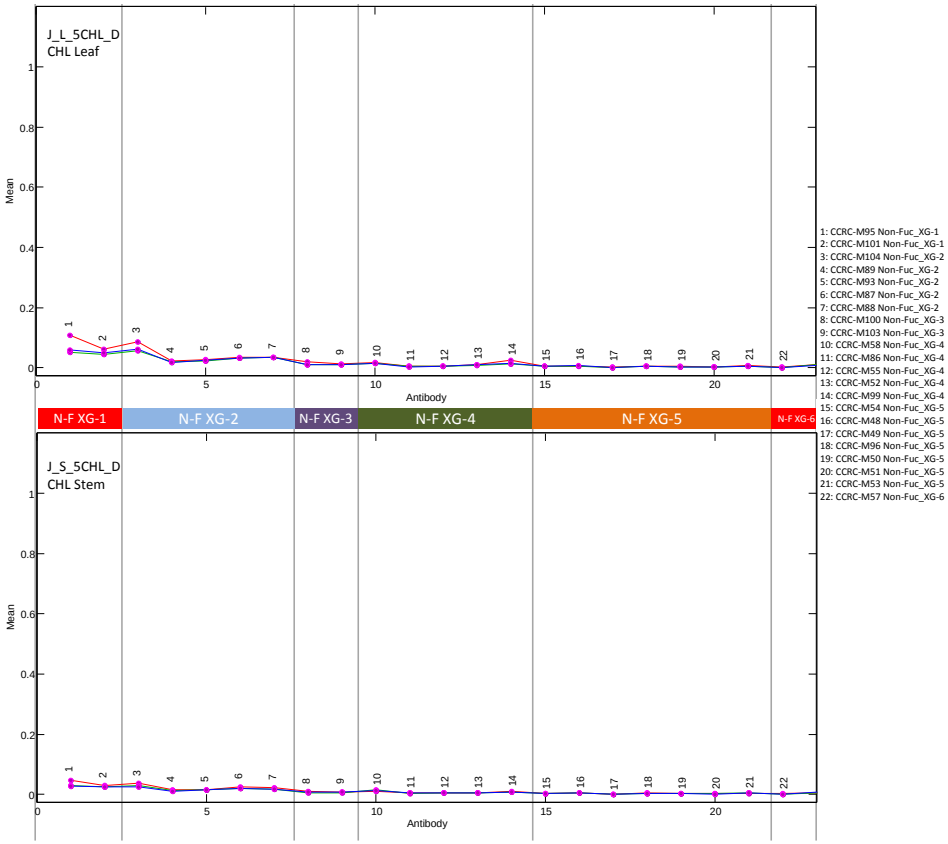

Non-Fuc XG – 4M KOH PC

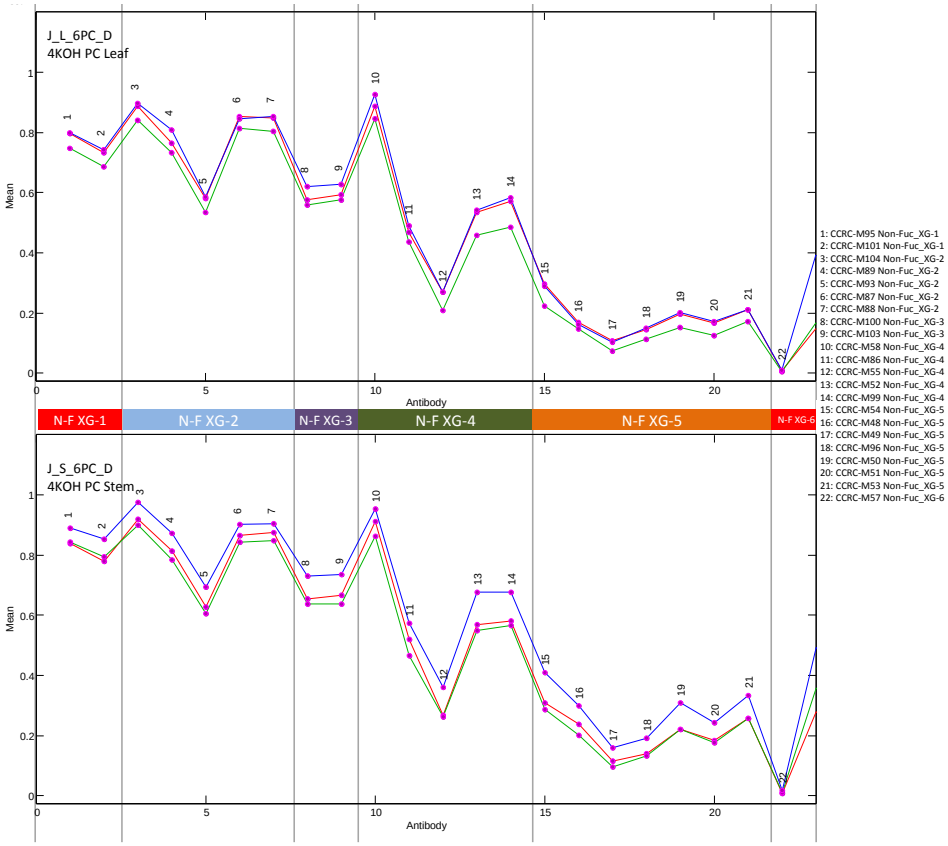

Fuc XG – Oxalate

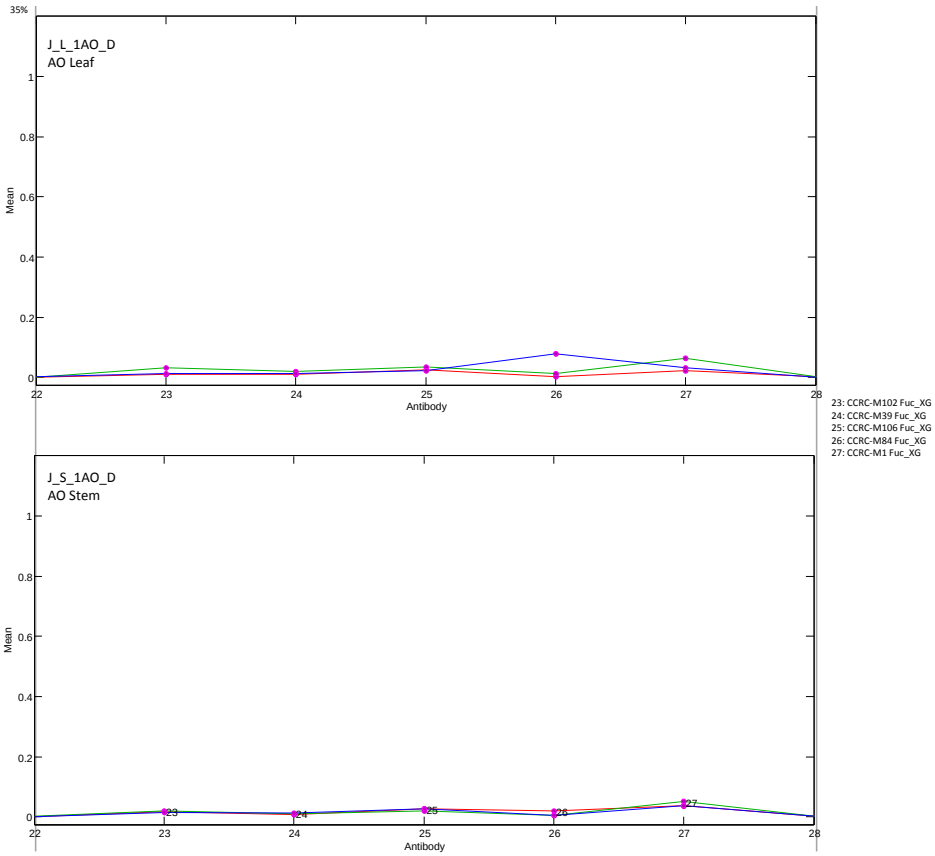

Fuc XG – Carbonate

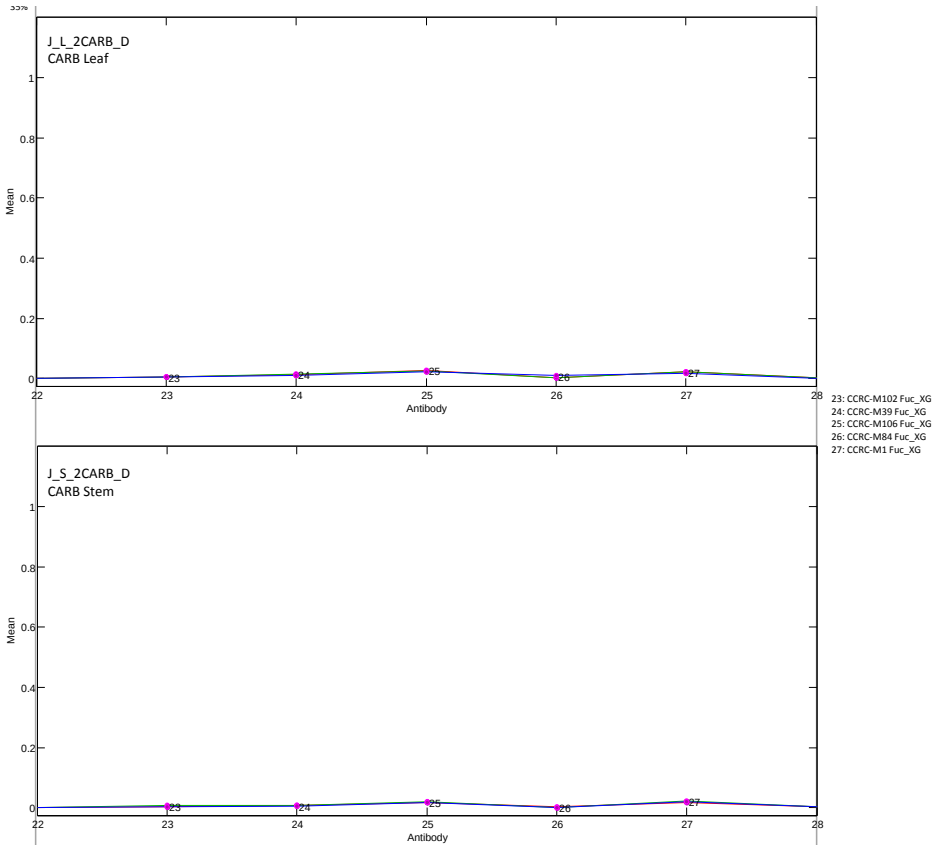

Fuc XG – 1M KOH

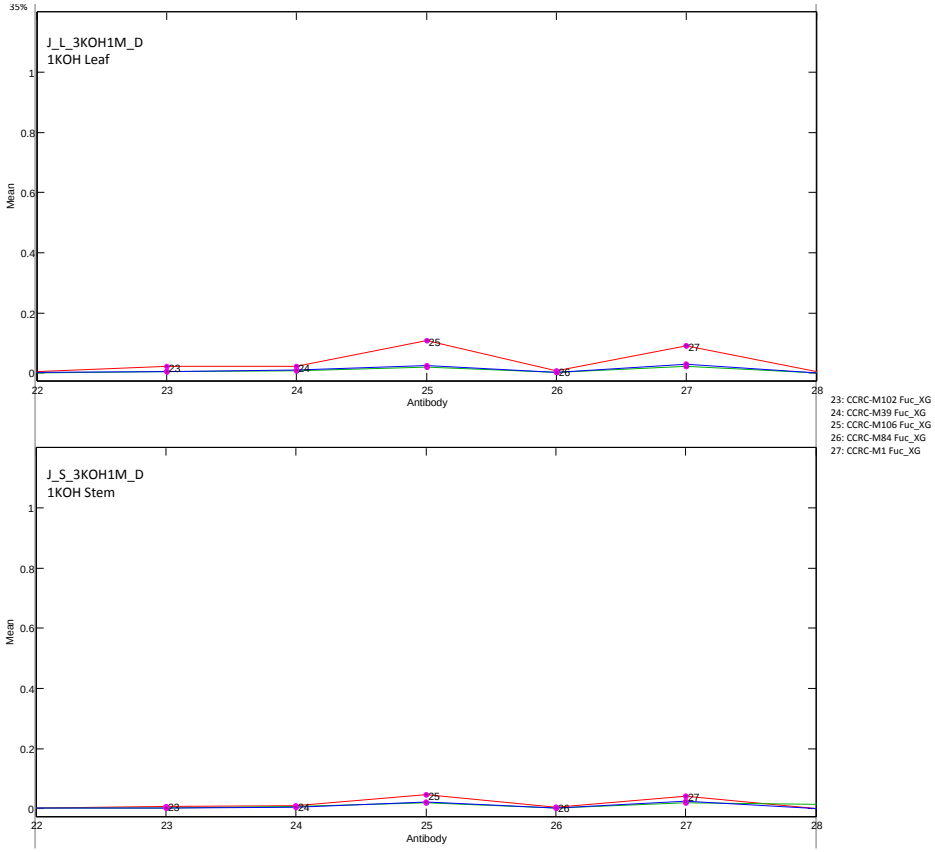

Fuc XG – 4M KOH

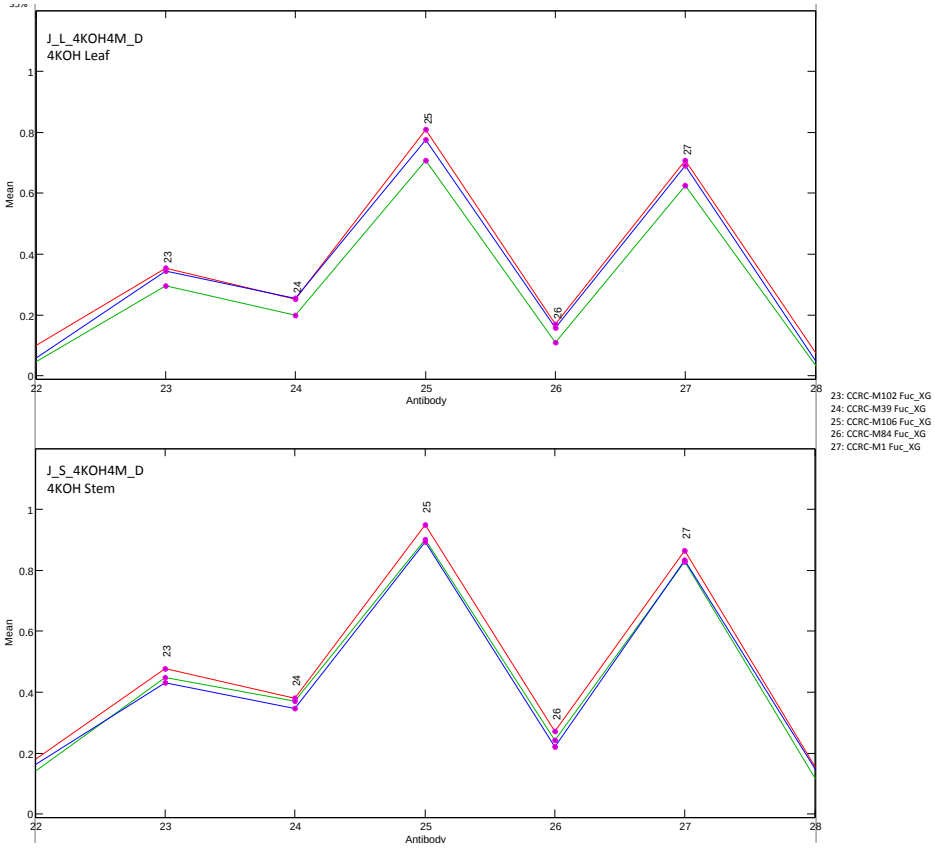

Fuc XG – Chlorite

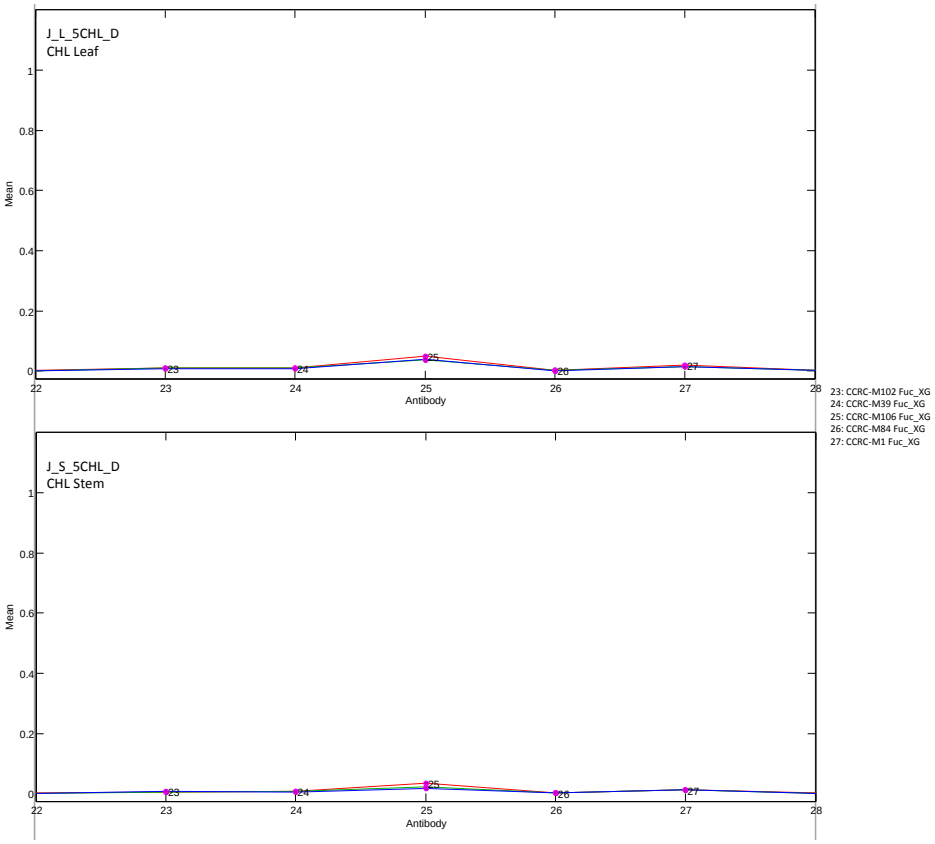

Fuc XG – 4M KOH PC

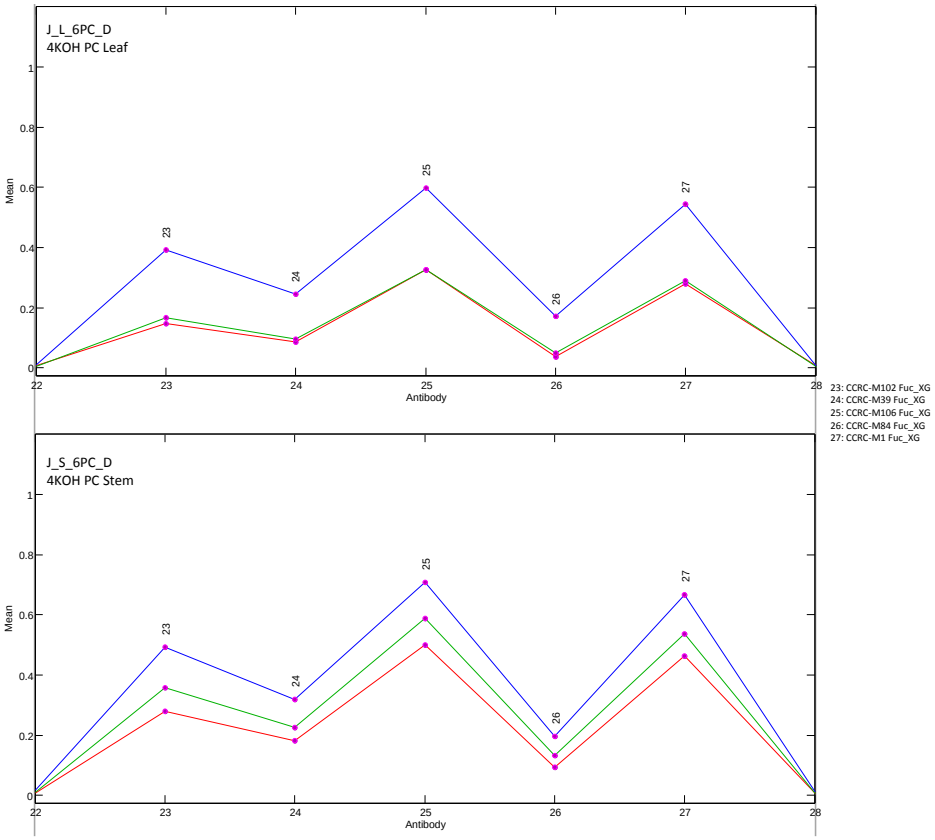

Xylan – Oxalate

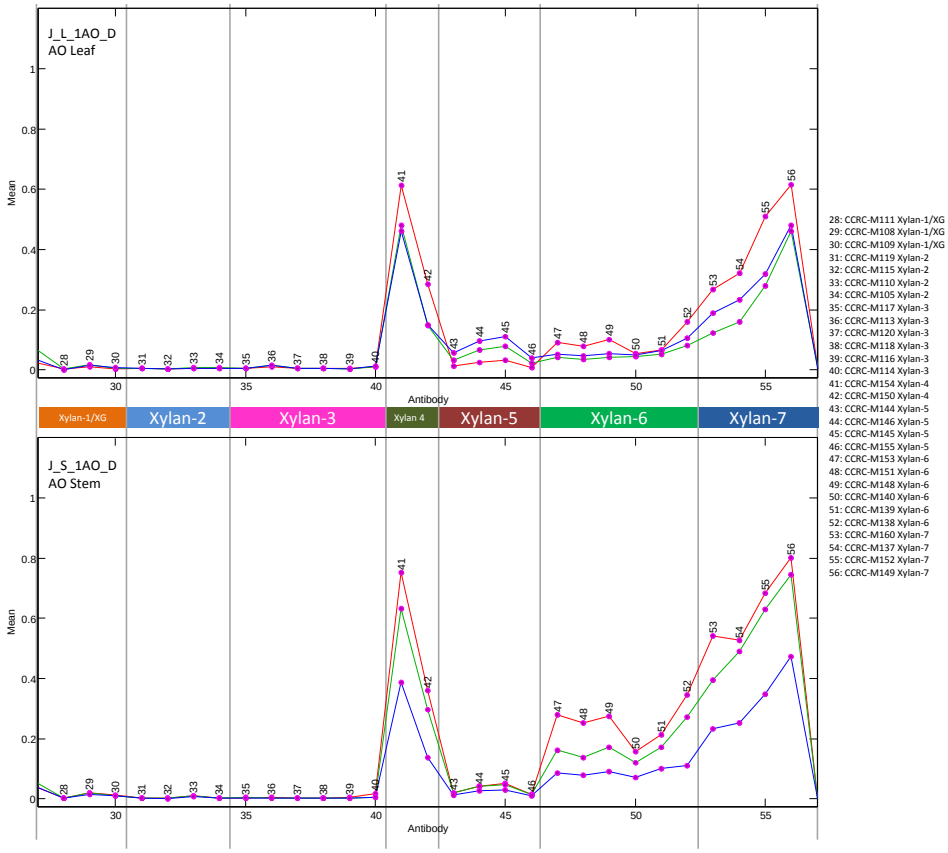

Xylan – Carbonate

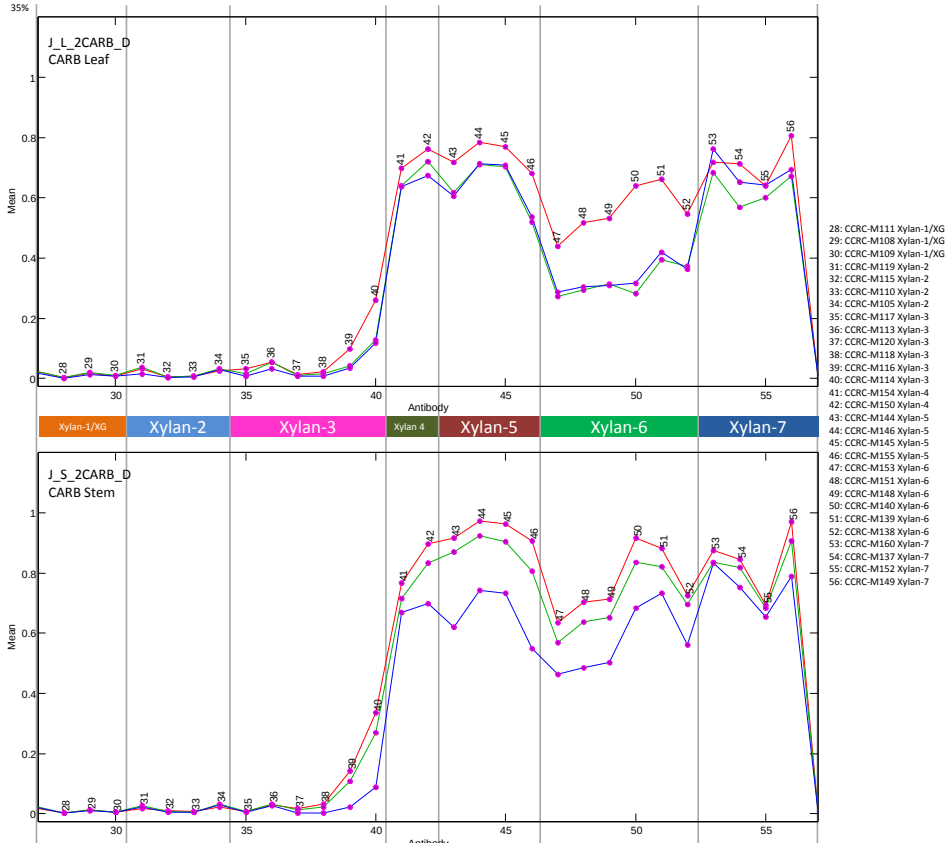

Xylan – 1M KOH

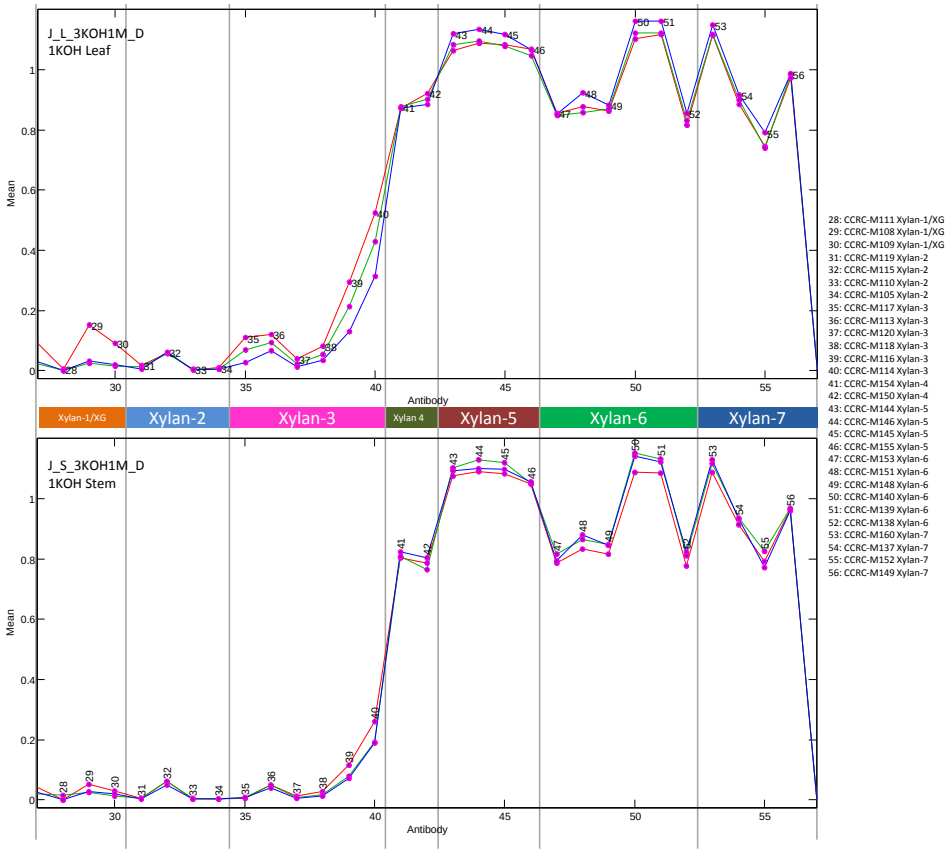

Xylan – 4M KOH

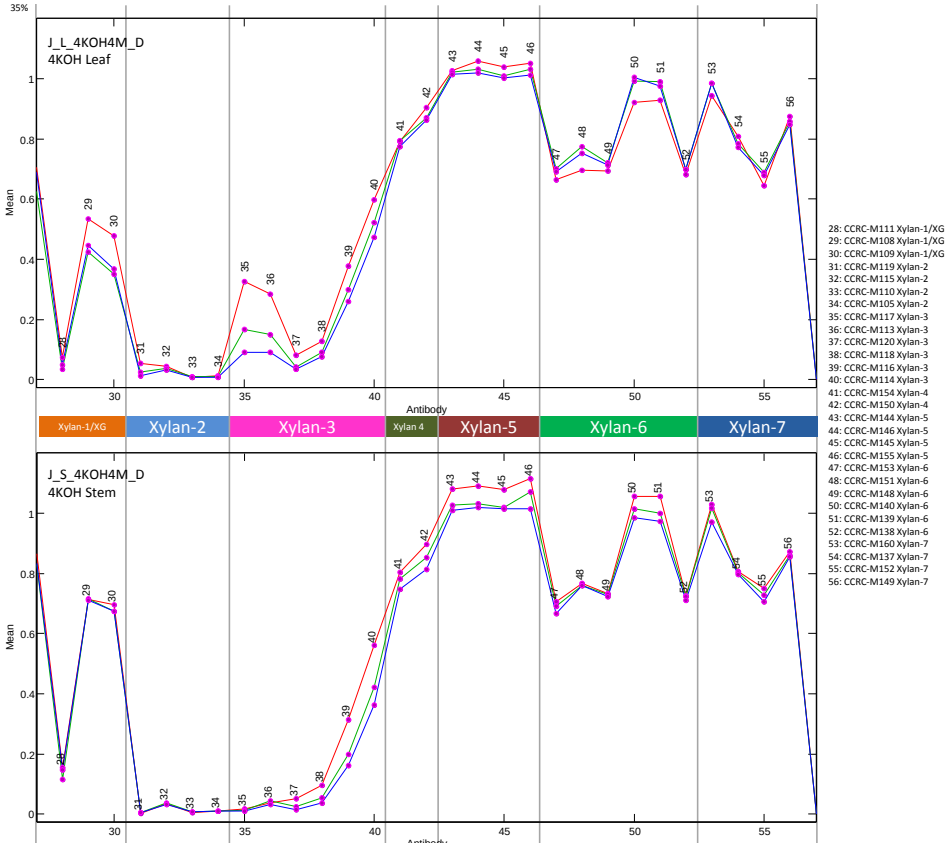

Xylan – Chlorite

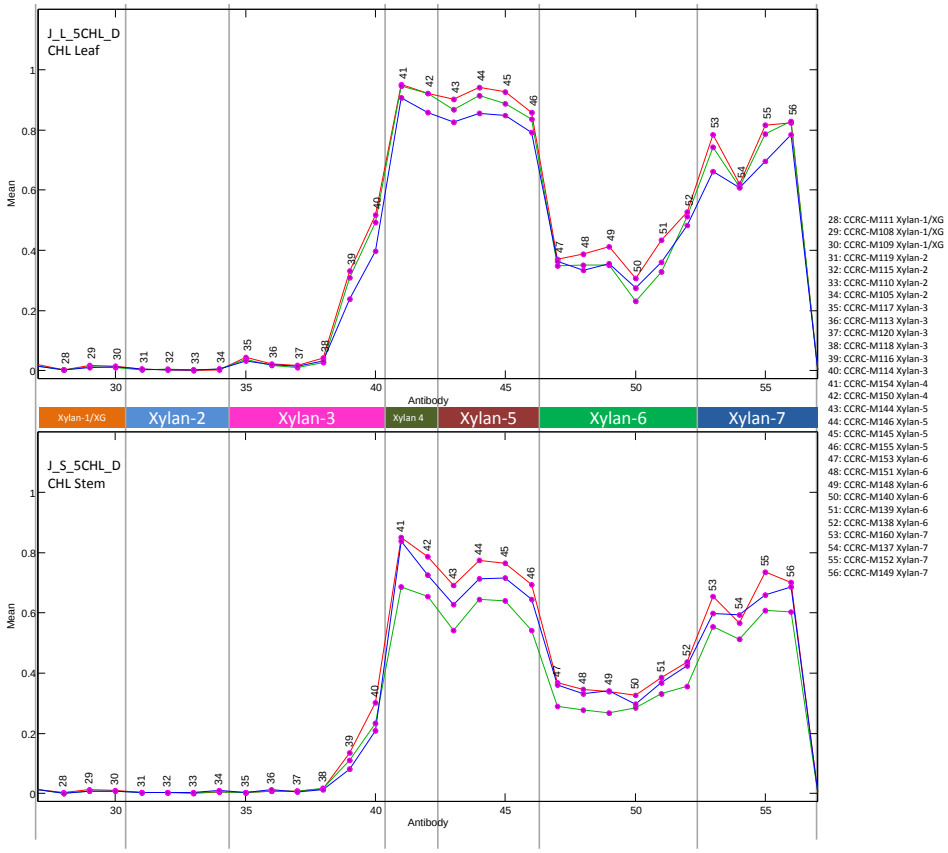

Xylan – 4M KOH PC

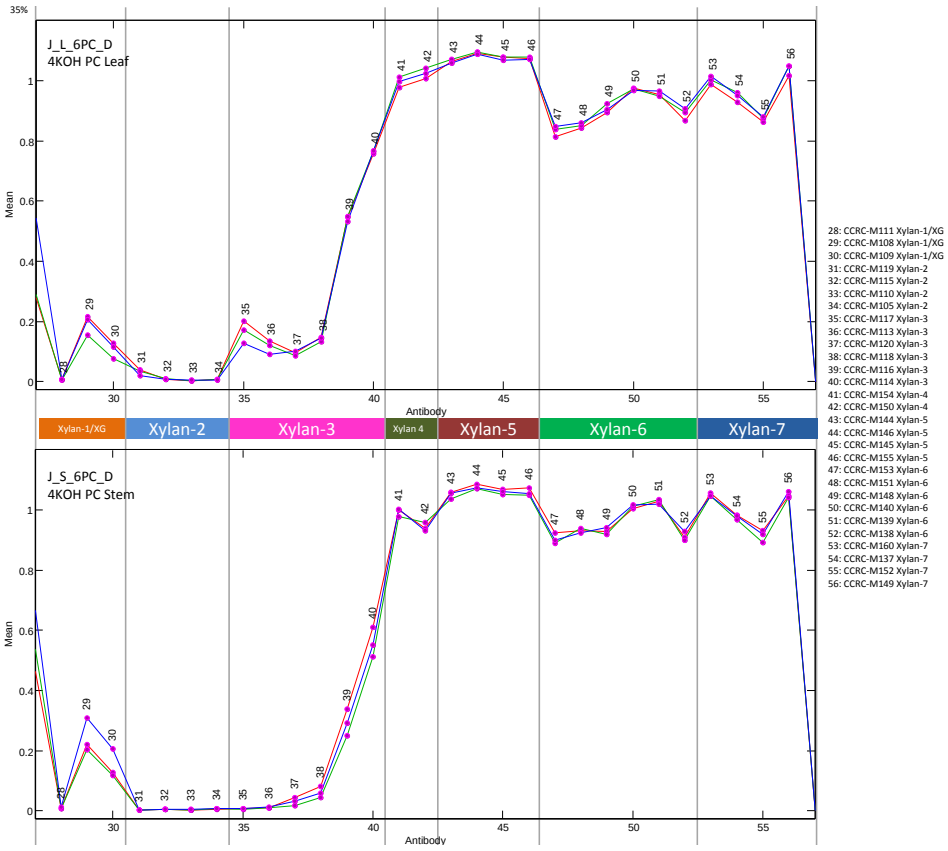

β-glucan – Oxalate

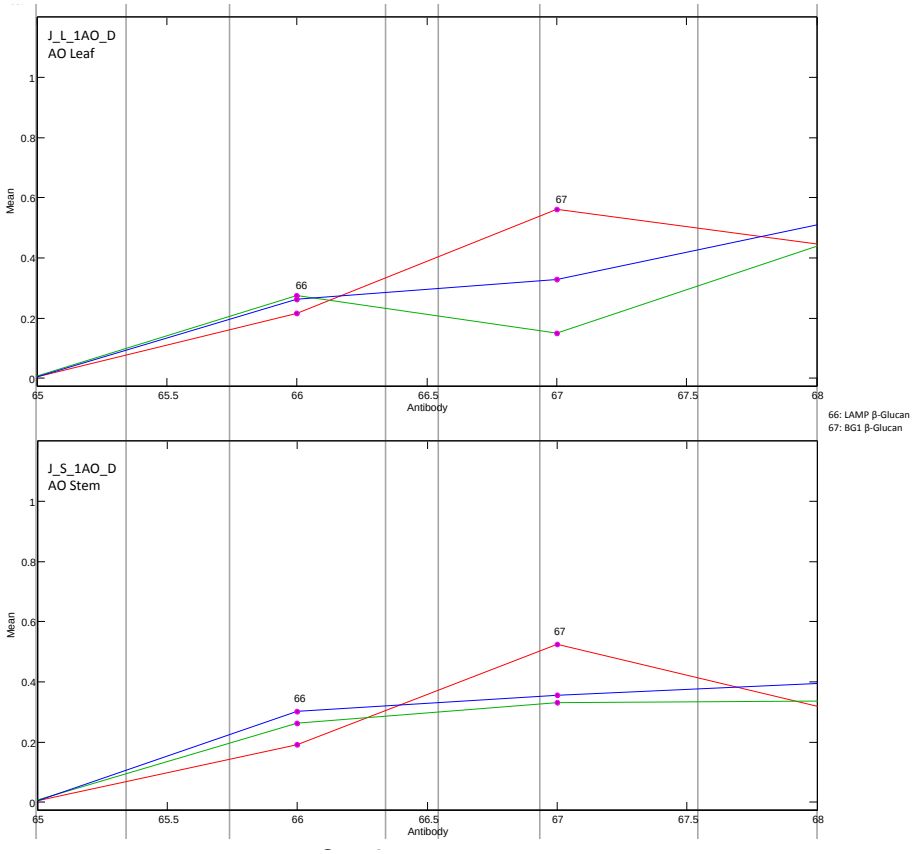

β-glucan – Carbonate

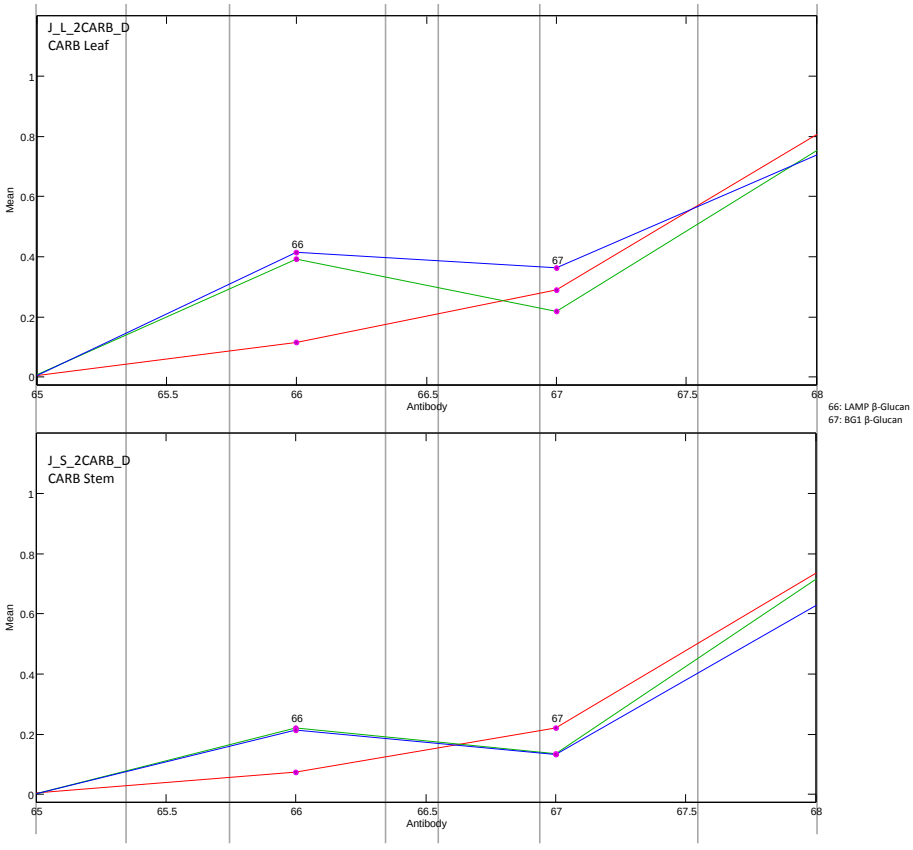

β-glucan – 1M KOH

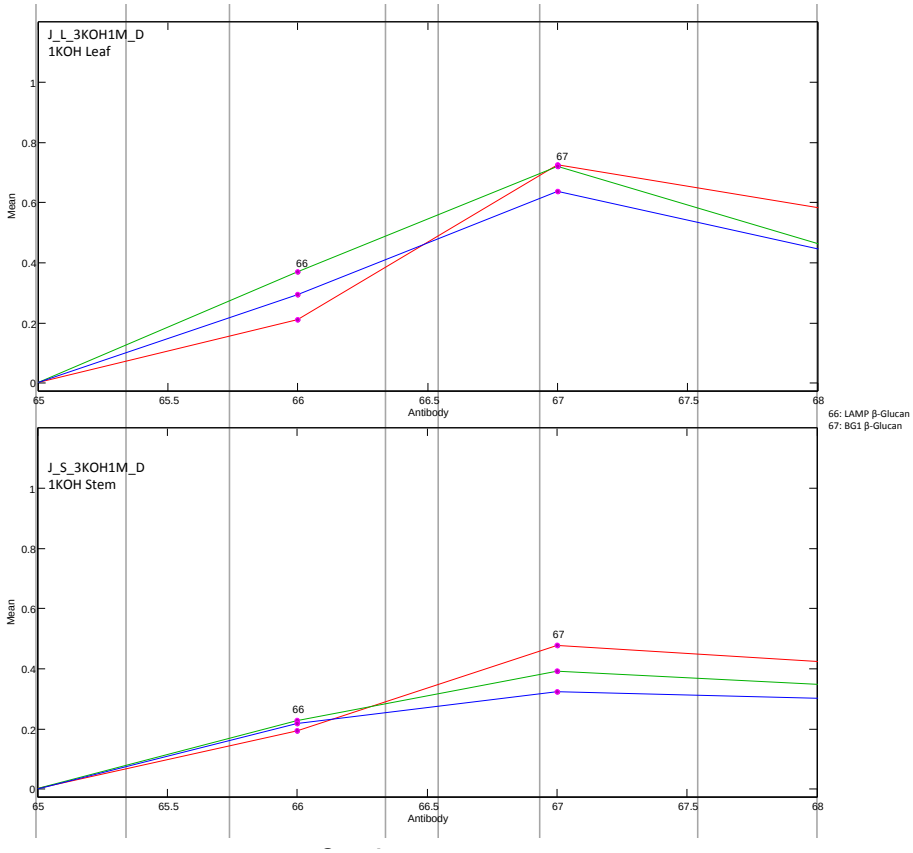

β-glucan – 4M KOH

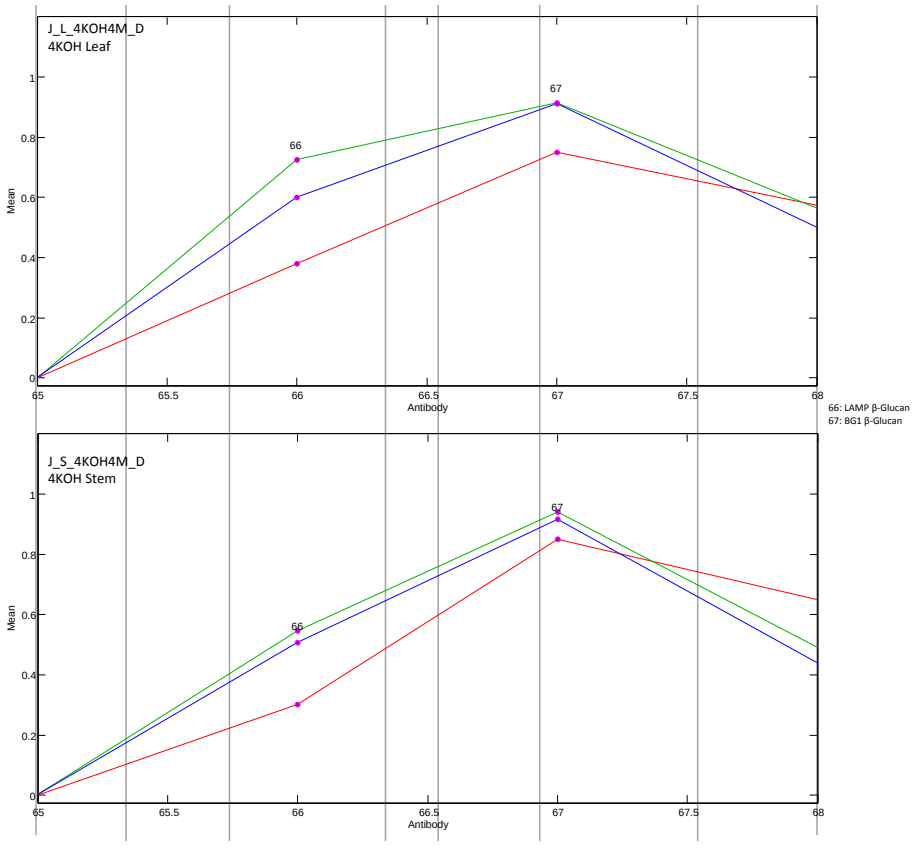

β-glucan – Chlorite

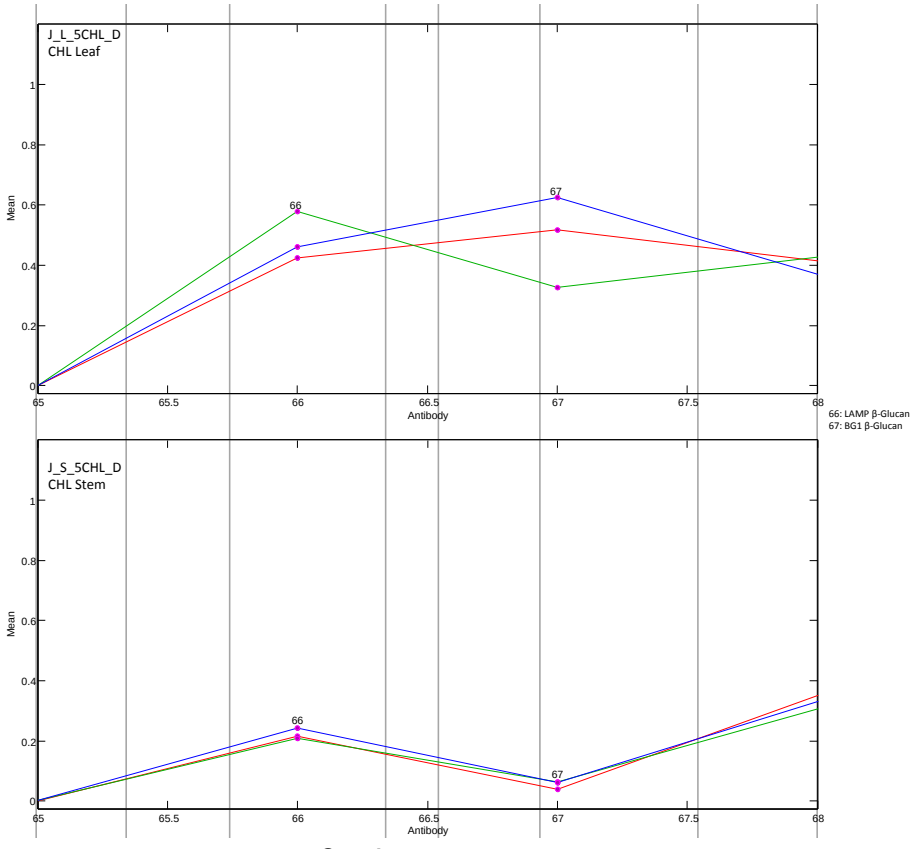

β-glucan – 4M KOH PC

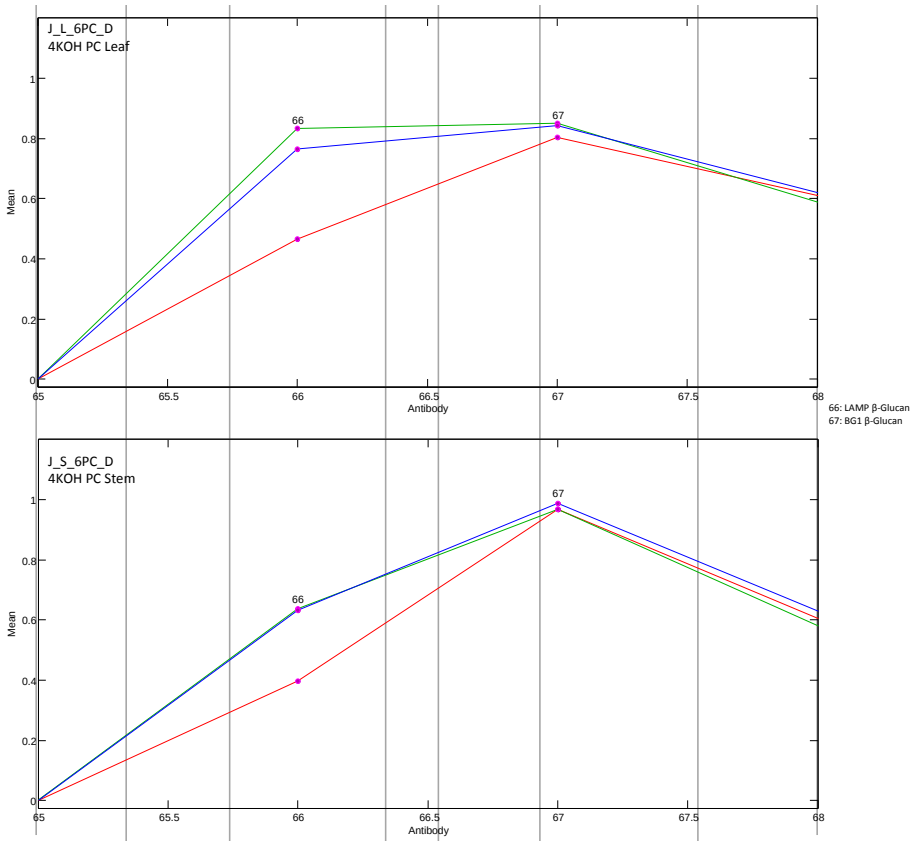

Pectins – Oxalate

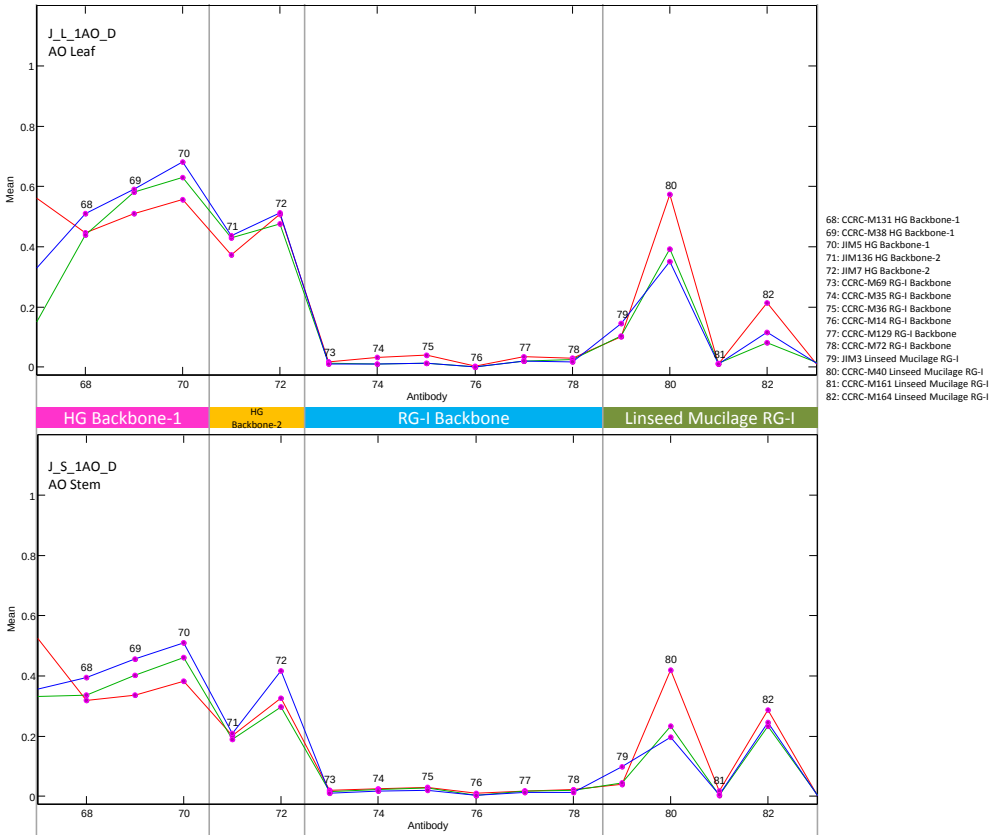

Pectins – Carbonate

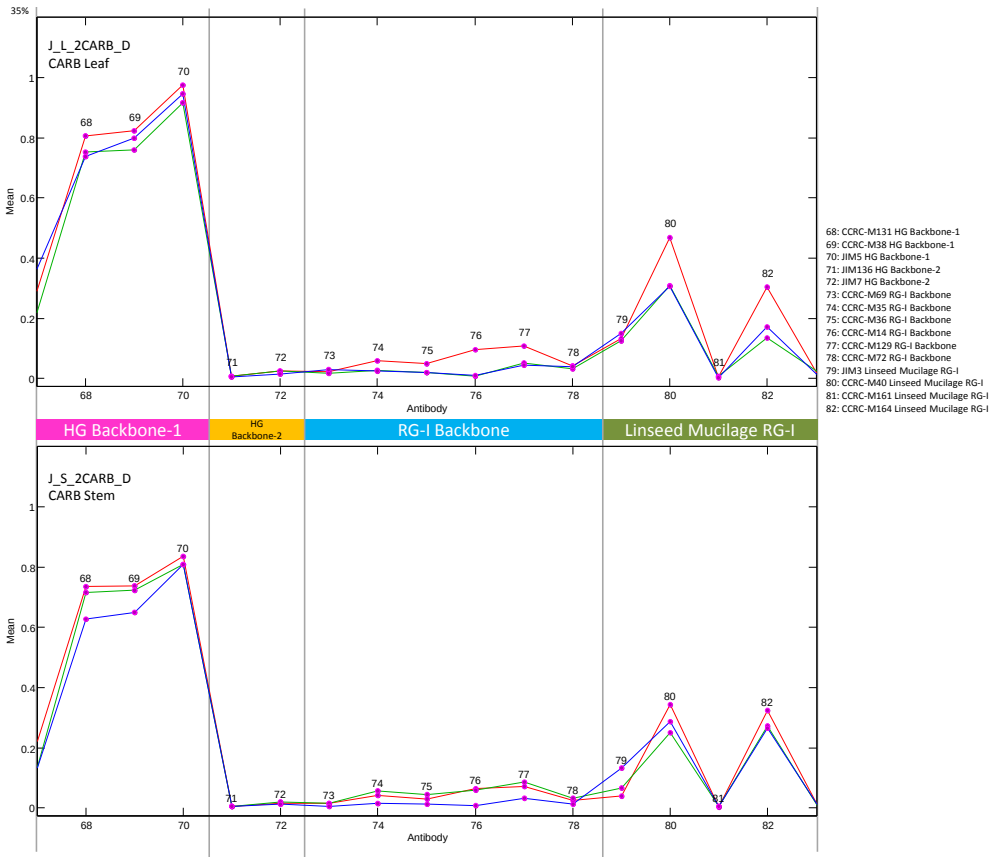

Pectins – 1M KOH

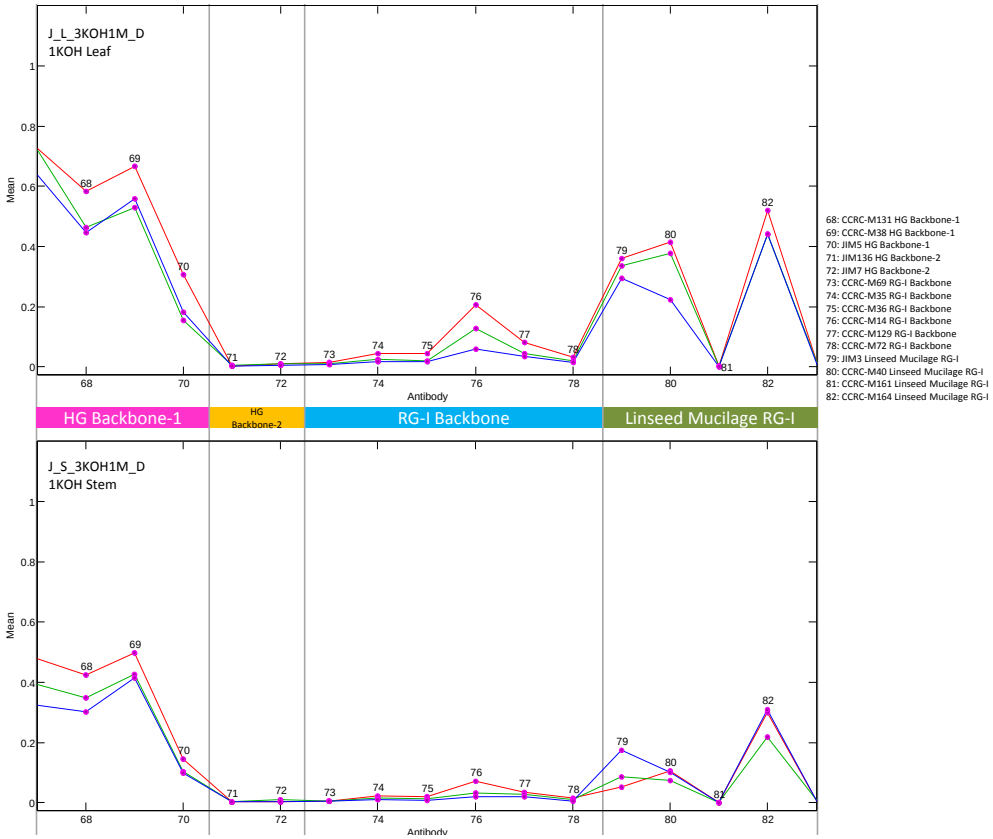

Pectins – 4M KOH

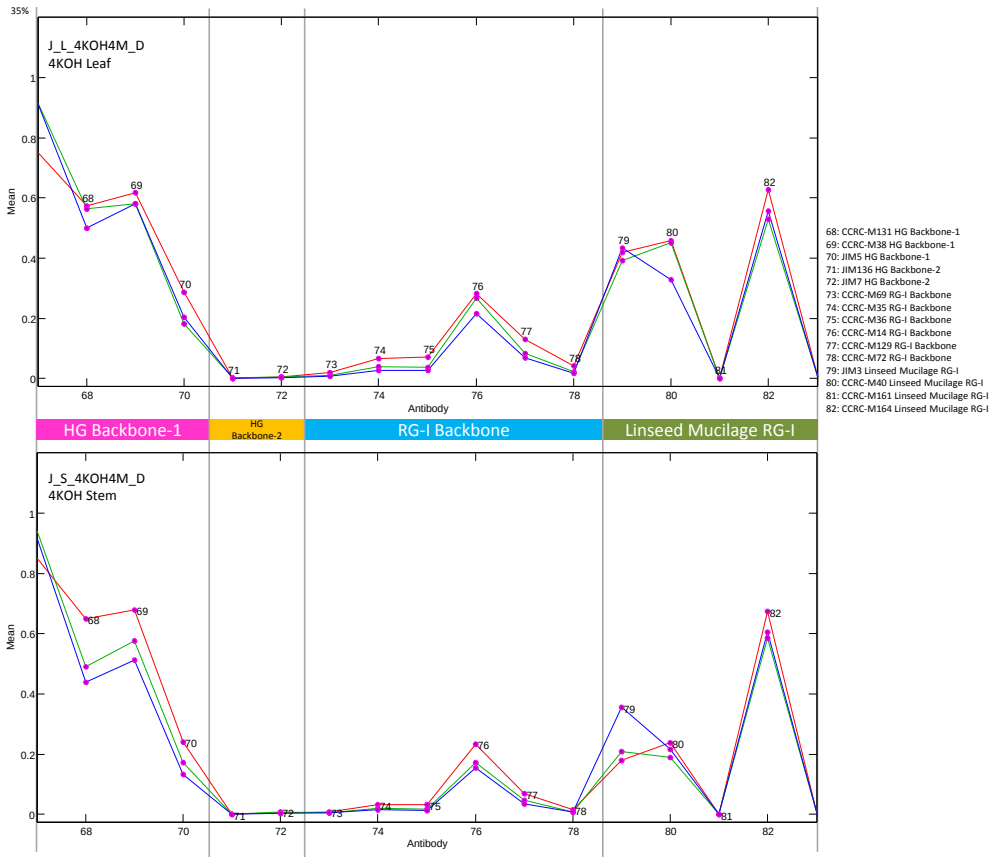

Pectins – Chlorite

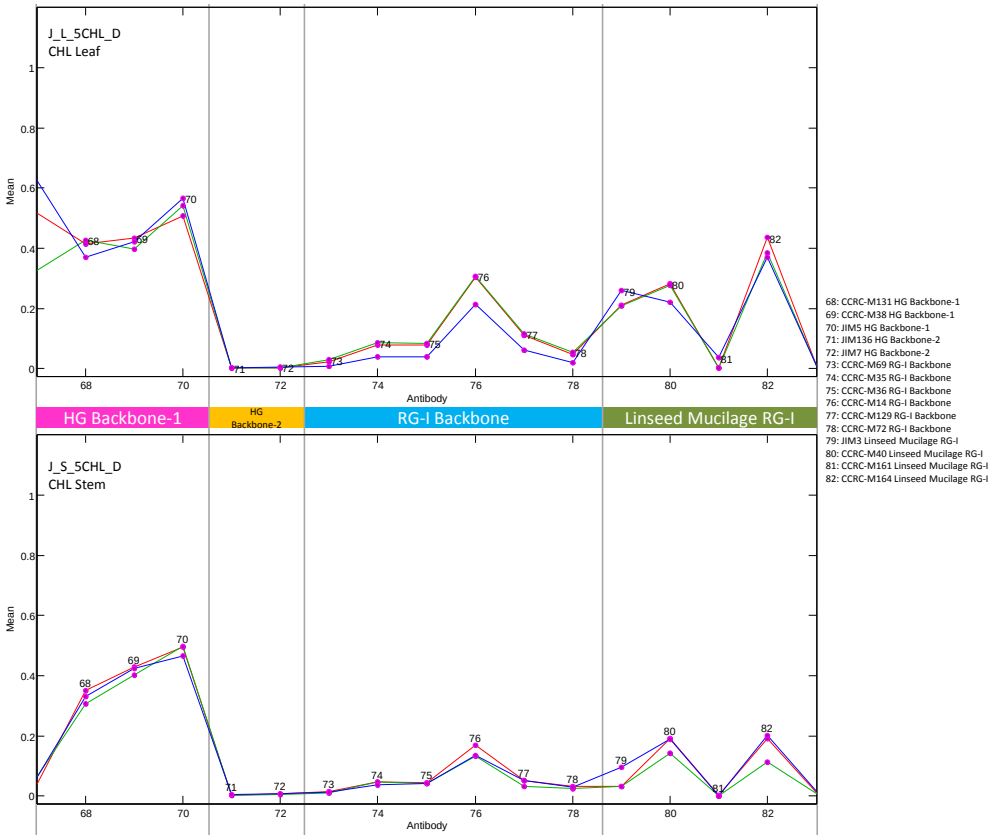

Pectins – 4M KOH PC

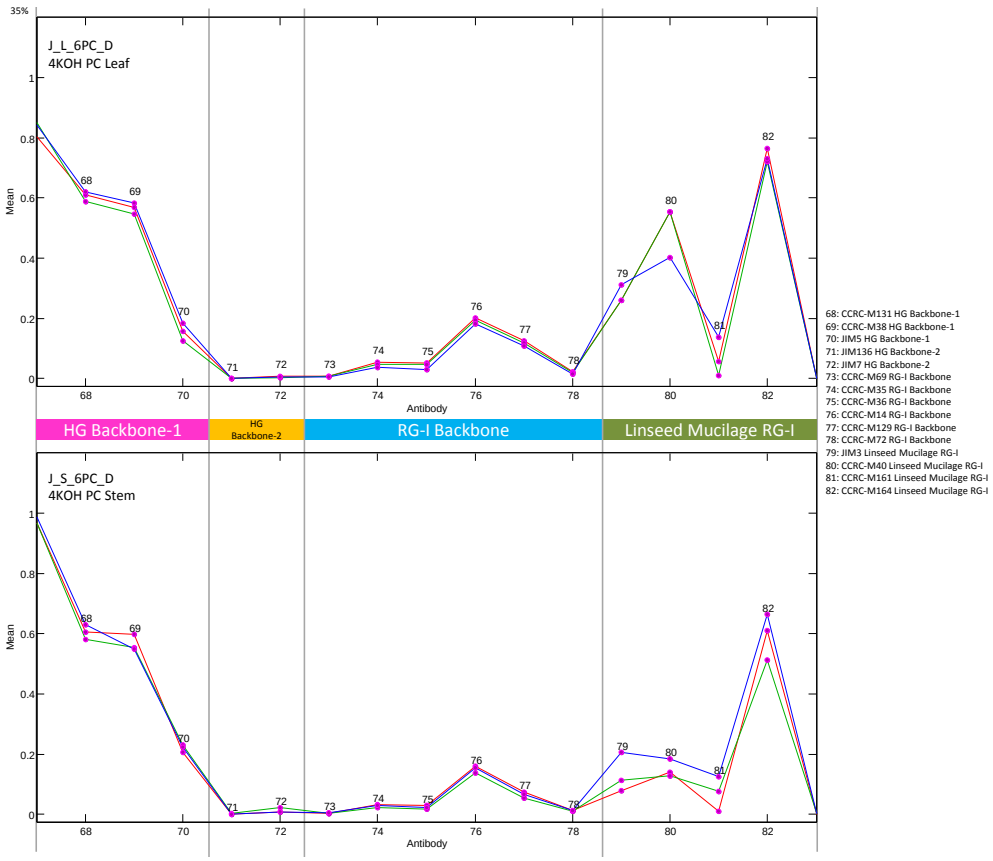

RG-I – Oxalate

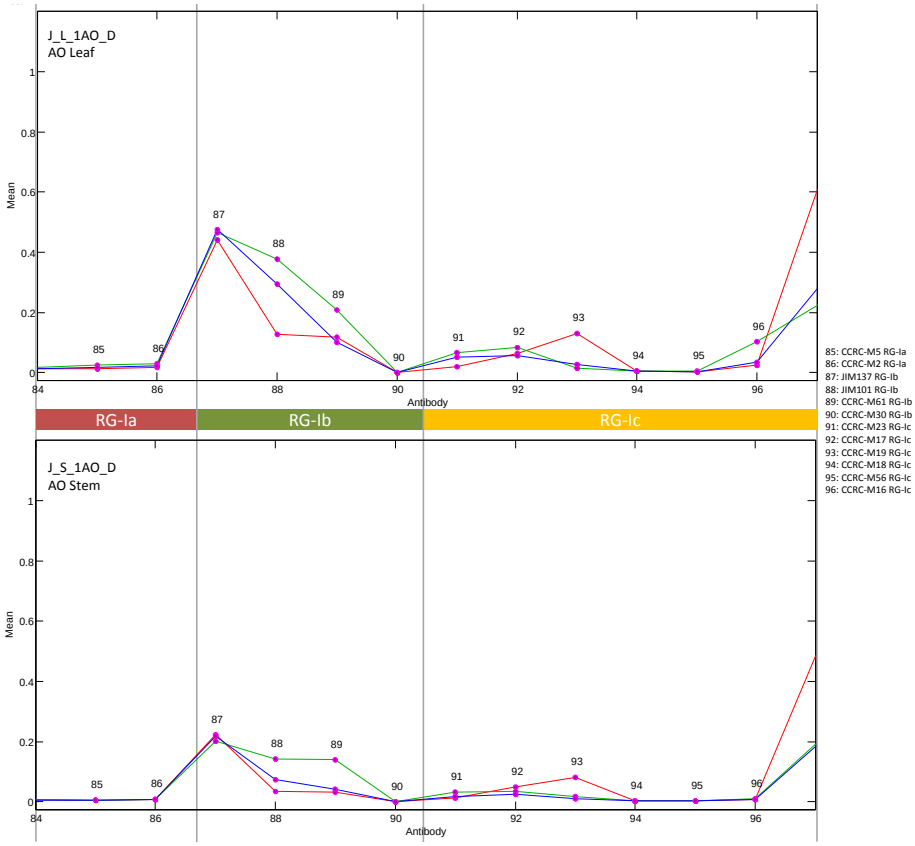

RG-I – Carbonate

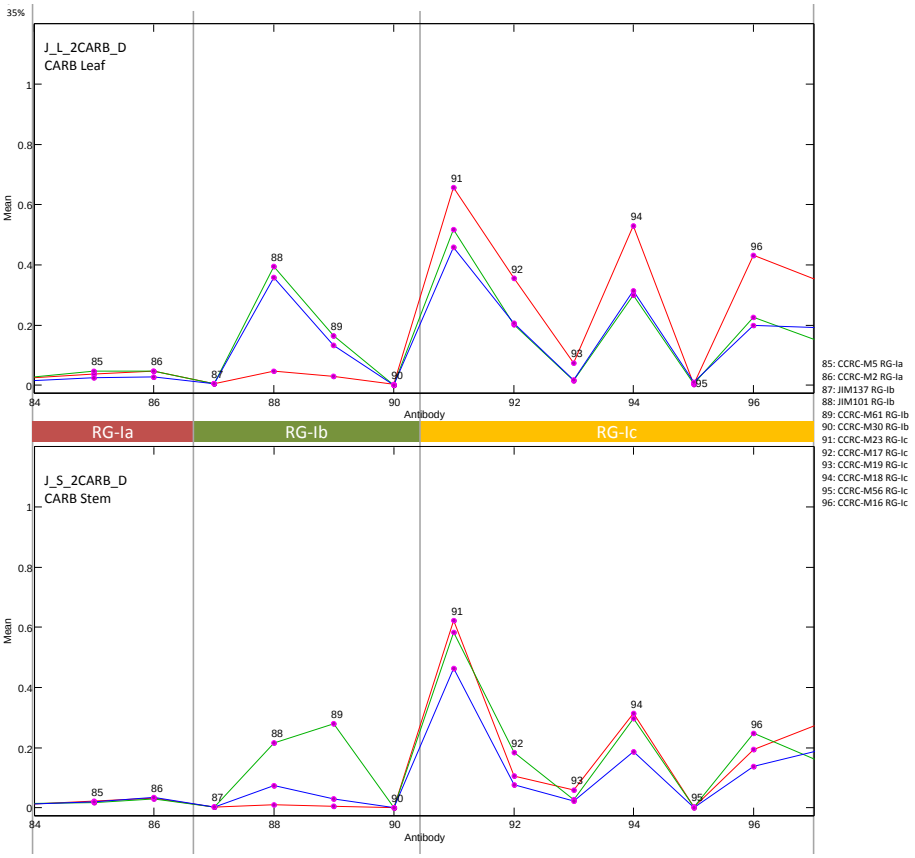

RG-I – 1M KOH

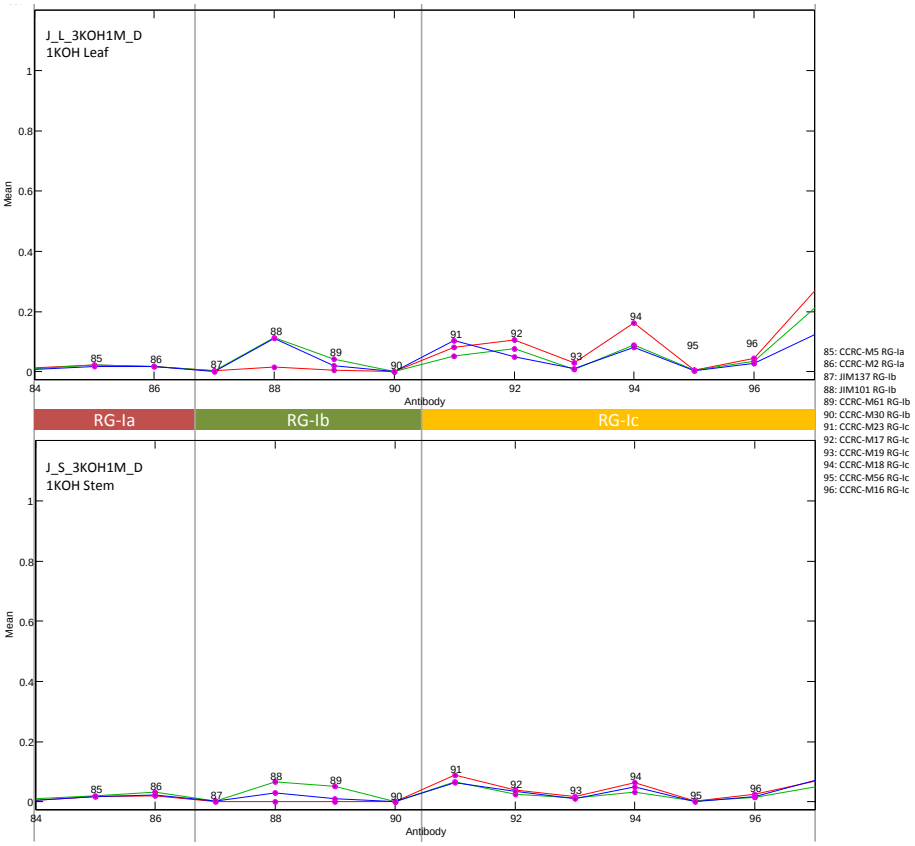

RG-I – 4M KOH

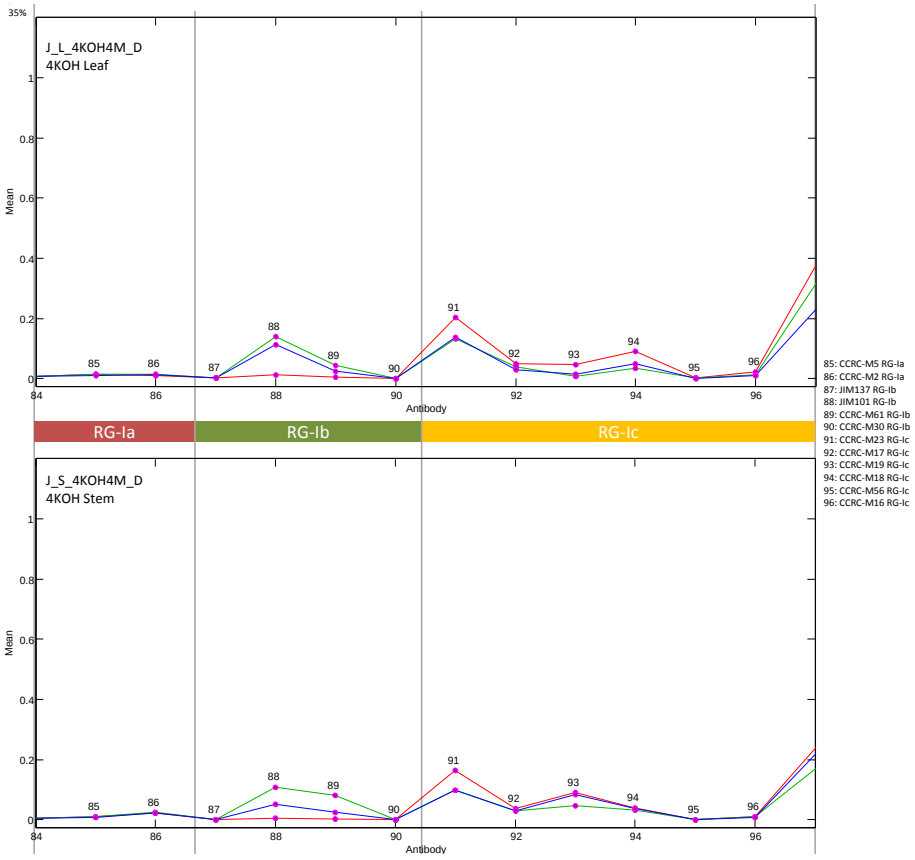

RG-I – 1M Chlorite

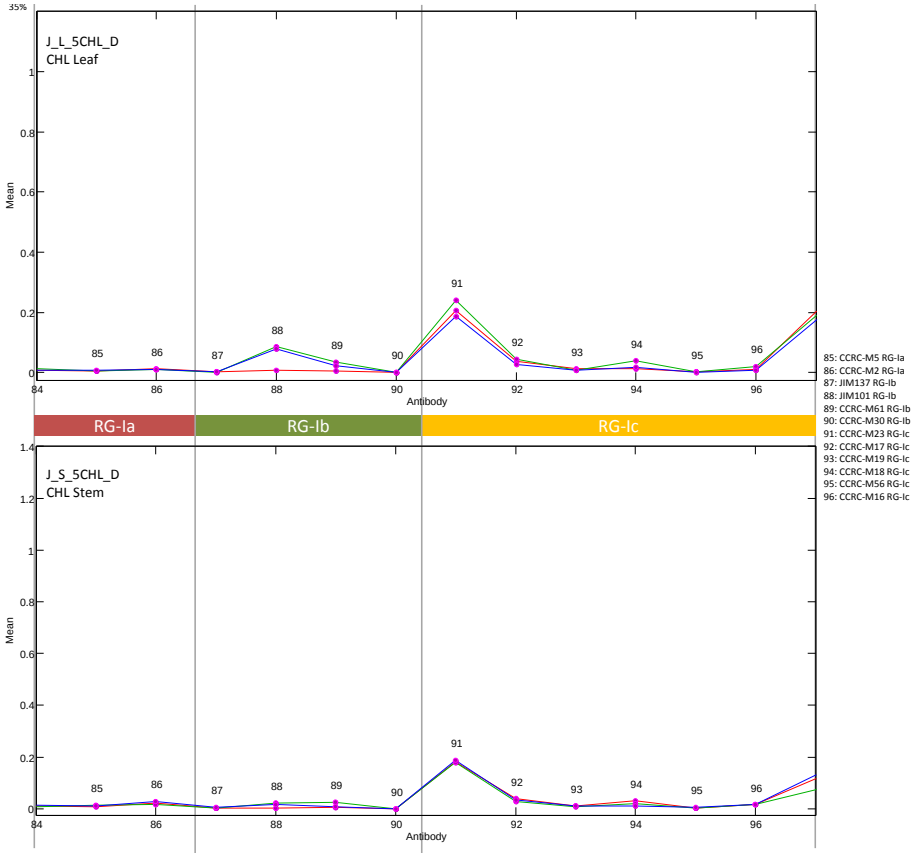

RG-I – 4M KOH PC

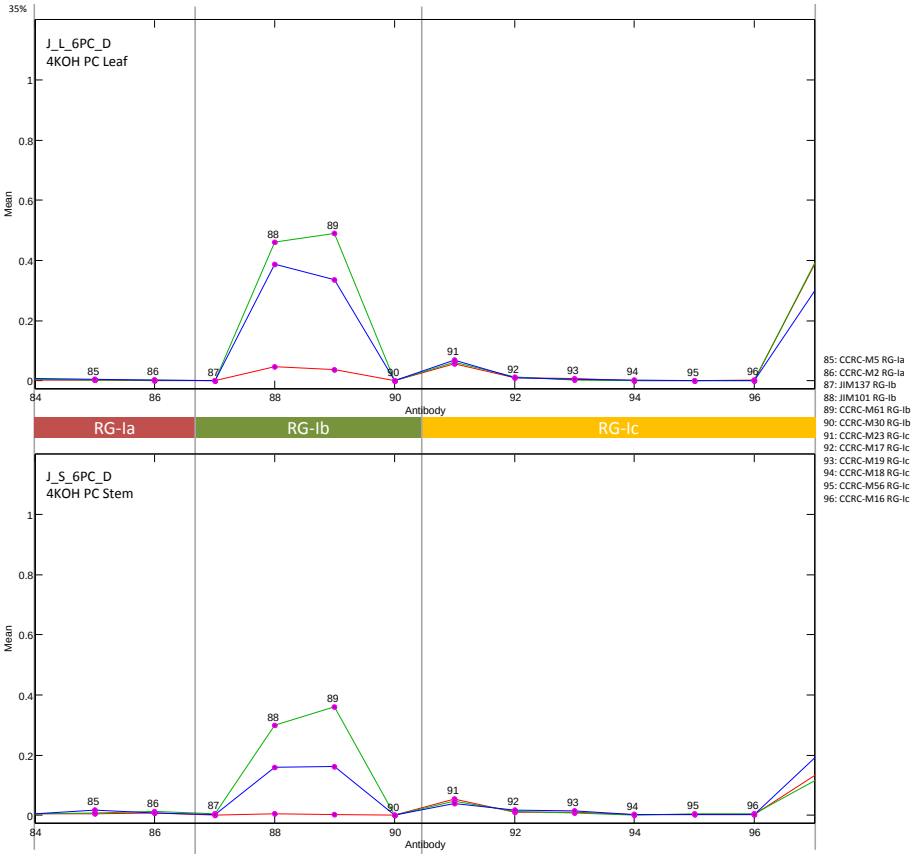

RG-I/AG – Oxalate

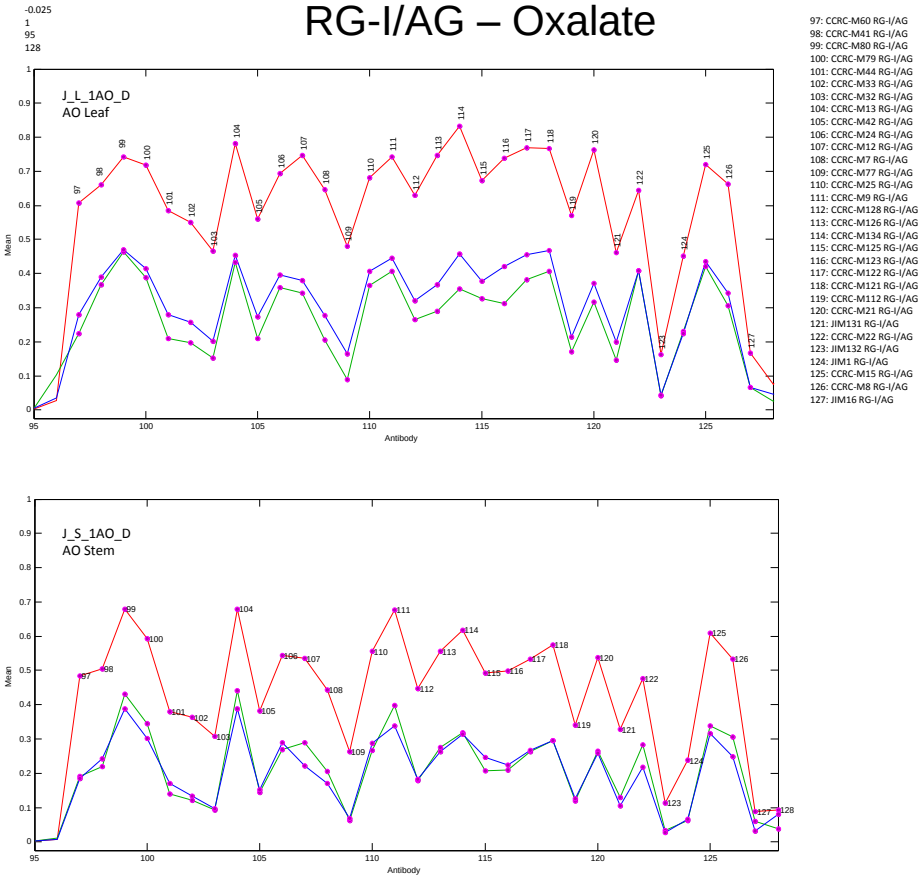

RG-I/AG – Carbonate

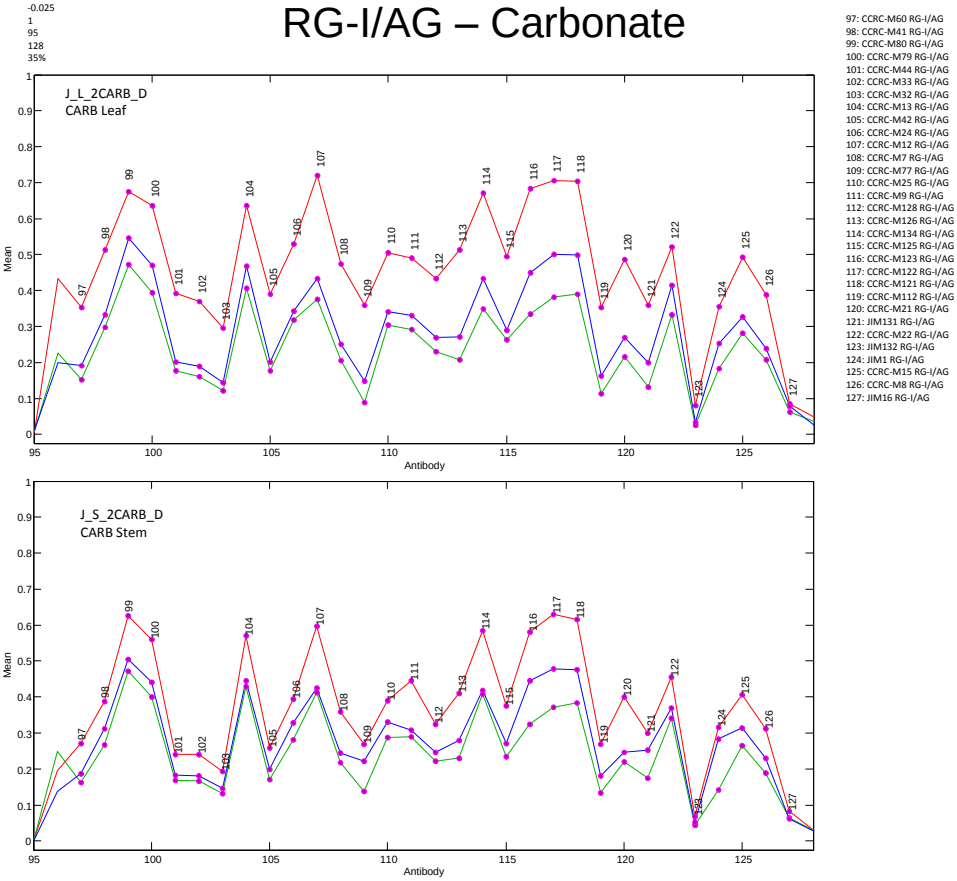

RG-I/AG – 1M KOH

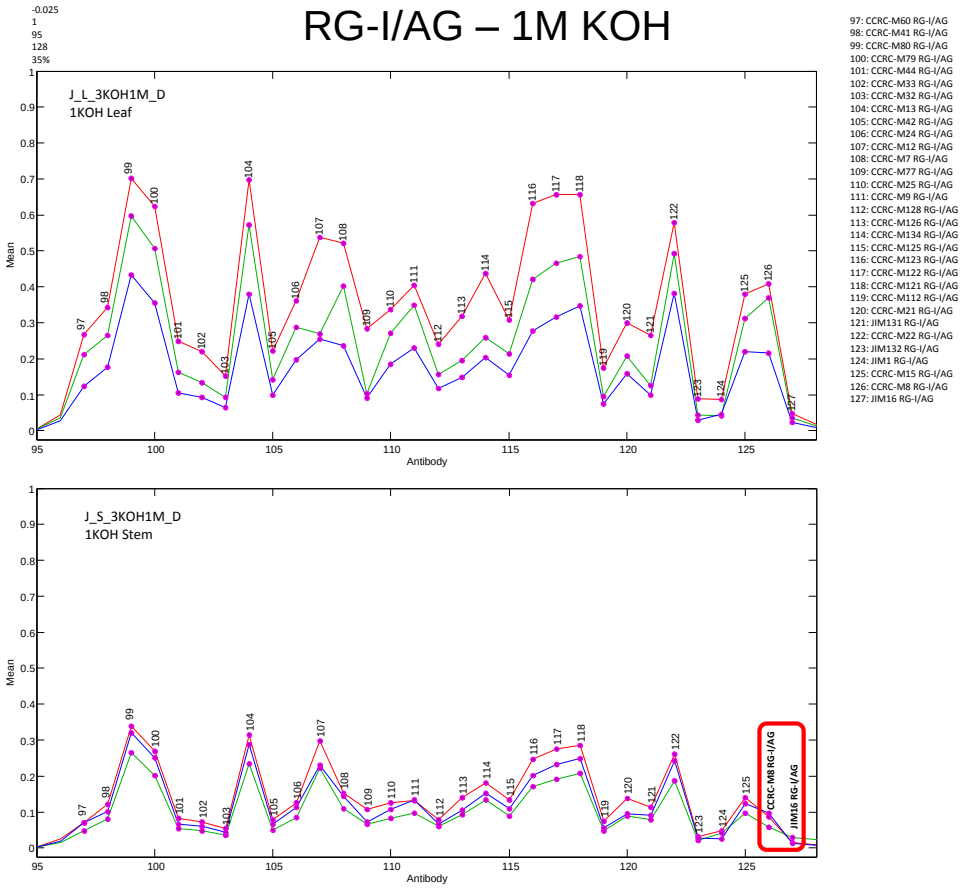

97: CCRC-M60 RG-I/AG
98: CCRC-M41 RG-I/AG
99: CCRC-M80 RG-I/AG
100: CCRC-M79 RG-I/AG
101: CCRC-M44 RG-I/AG
102: CCRC-M33 RG-I/AG
103: CCRC-M32 RG-I/AG
104: CCRC-M13 RG-I/AG
105: CCRC-M42 RG-I/AG
106: CCRC-M24 RG-I/AG
107: CCRC-M12 RG-I/AG
108: CCRC-M7 RG-I/AG
109: CCRC-M77 RG-I/AG
110: CCRC-M25 RG-I/AG
111: CCRC-M9 RG-I/AG
112: CCRC-M128 RG-I/AG
113: CCRC-M126 RG-I/AG
114: CCRC-M134 RG-I/AG
115: CCRC-M125 RG-I/AG
116: CCRC-M123 RG-I/AG
117: CCRC-M122 RG-I/AG
118: CCRC-M121 RG-I/AG
119: CCRC-M112 RG-I/AG
120: CCRC-M21 RG-I/AG
121: JIM131 RG-I/AG
122: CCRC-M22 RG-I/AG
123: JIM132 RG-I/AG
124: JIM1 RG-I/AG
125: CCRC-M15 RG-I/AG
126: CCRC-M8 RG-I/AG
127: JIM16 RG-I/AG

RG-I/AG – 4M KOH

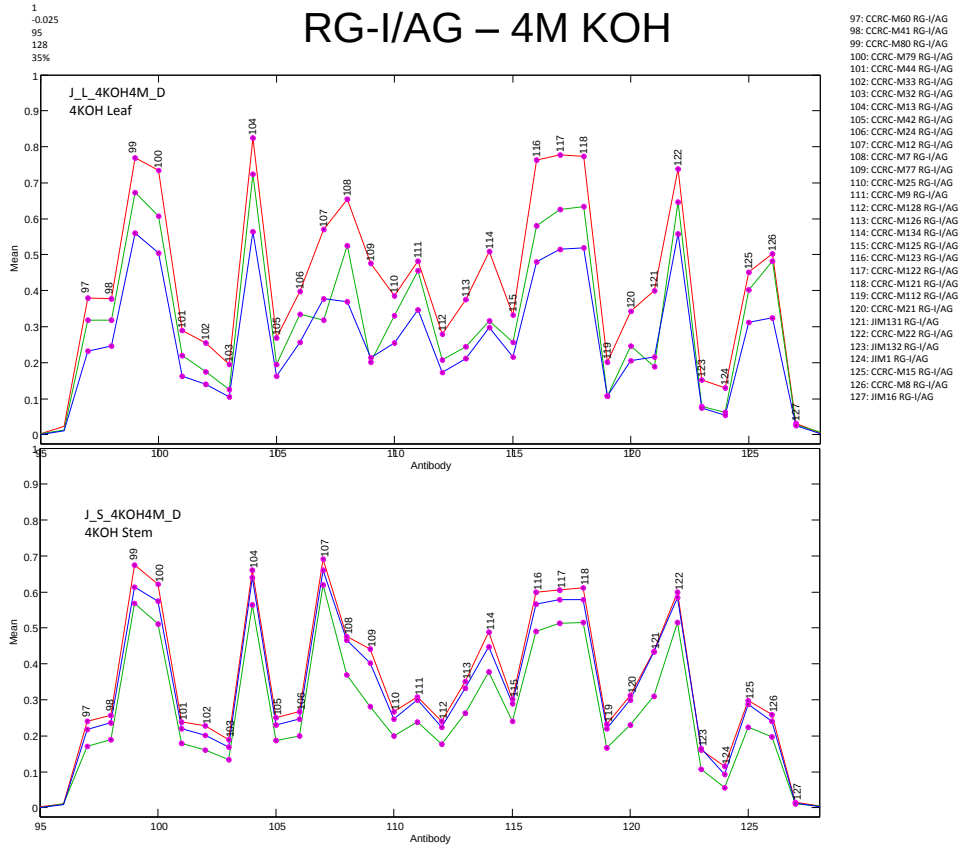

97: CCRC-M60 RG-I/AG
98: CCRC-M41 RG-I/AG
99: CCRC-M80 RG-I/AG
100: CCRC-M79 RG-I/AG
101: CCRC-M44 RG-I/AG
102: CCRC-M33 RG-I/AG
103: CCRC-M32 RG-I/AG
104: CCRC-M13 RG-I/AG
105: CCRC-M42 RG-I/AG
106: CCRC-M24 RG-I/AG
107: CCRC-M12 RG-I/AG
108: CCRC-M7 RG-I/AG
109: CCRC-M77 RG-I/AG
110: CCRC-M25 RG-I/AG
111: CCRC-M9 RG-I/AG
112: CCRC-M128 RG-I/AG
113: CCRC-M126 RG-I/AG
114: CCRC-M134 RG-I/AG
115: CCRC-M125 RG-I/AG
116: CCRC-M123 RG-I/AG
117: CCRC-M122 RG-I/AG
118: CCRC-M121 RG-I/AG
119: CCRC-M112 RG-I/AG
120: CCRC-M21 RG-I/AG
121: JIM131 RG-I/AG
122: CCRC-M22 RG-I/AG
123: JIM132 RG-I/AG
124: JIM1 RG-I/AG
125: CCRC-M15 RG-I/AG
126: CCRC-M8 RG-I/AG
127: JIM16 RG-I/AG

RG-I/AG – Chlorite

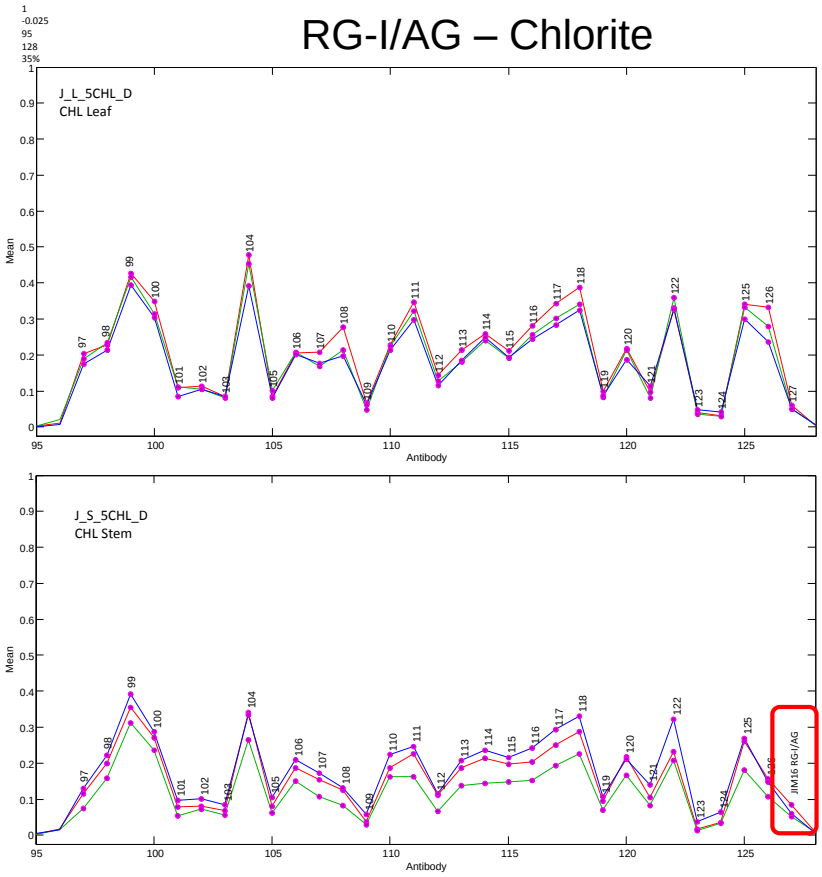

97: CCRC-M60 RG-I/AG
98: CCRC-M41 RG-I/AG
99: CCRC-M80 RG-I/AG
100: CCRC-M79 RG-I/AG
101: CCRC-M44 RG-I/AG
102: CCRC-M33 RG-I/AG
103: CCRC-M32 RG-I/AG
104: CCRC-M13 RG-I/AG
105: CCRC-M42 RG-I/AG
106: CCRC-M24 RG-I/AG
107: CCRC-M12 RG-I/AG
108: CCRC-M7 RG-I/AG
109: CCRC-M77 RG-I/AG
110: CCRC-M25 RG-I/AG
111: CCRC-M9 RG-I/AG
112: CCRC-M128 RG-I/AG
113: CCRC-M126 RG-I/AG
114: CCRC-M134 RG-I/AG
115: CCRC-M125 RG-I/AG
116: CCRC-M123 RG-I/AG
117: CCRC-M122 RG-I/AG
118: CCRC-M121 RG-I/AG
119: CCRC-M112 RG-I/AG
120: CCRC-M21 RG-I/AG
121: JIM131 RG-I/AG
122: CCRC-M22 RG-I/AG
123: JIM132 RG-I/AG
124: JIM1 RG-I/AG
125: CCRC-M15 RG-I/AG
126: CCRC-M8 RG-I/AG
127: JIM16 RG-I/AG

RG-I/AG – 4M KOH PC

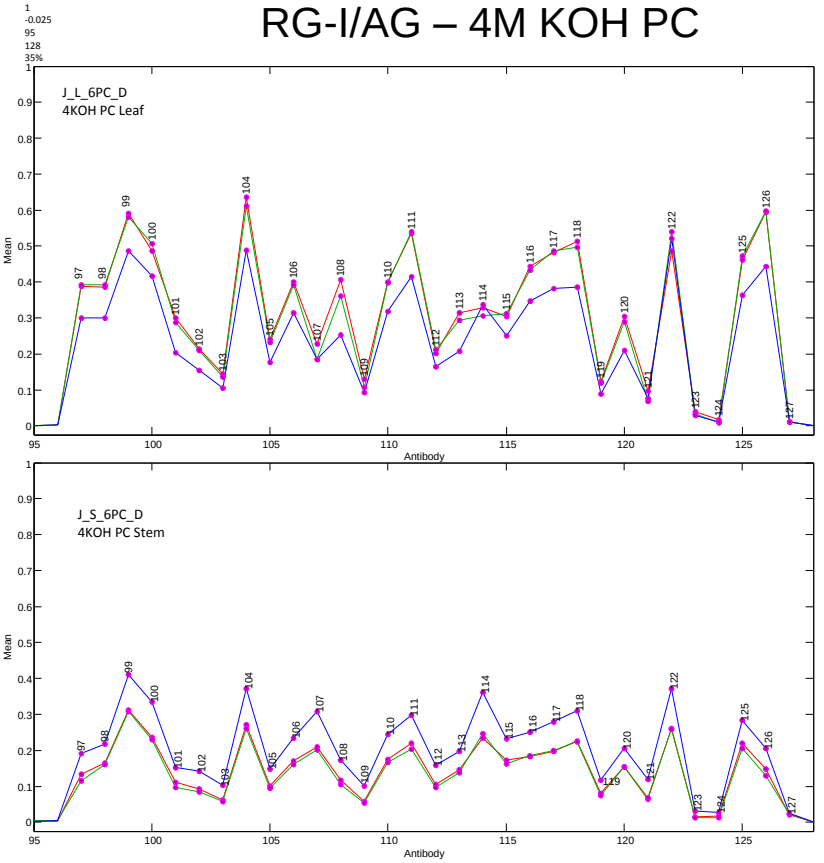

97: CCRC-M60 RG-I/AG
98: CCRC-M41 RG-I/AG
99: CCRC-M80 RG-I/AG
100: CCRC-M79 RG-I/AG
101: CCRC-M44 RG-I/AG
102: CCRC-M33 RG-I/AG
103: CCRC-M32 RG-I/AG
104: CCRC-M13 RG-I/AG
105: CCRC-M42 RG-I/AG
106: CCRC-M24 RG-I/AG
107: CCRC-M12 RG-I/AG
108: CCRC-M7 RG-I/AG
109: CCRC-M77 RG-I/AG
110: CCRC-M25 RG-I/AG
111: CCRC-M9 RG-I/AG
112: CCRC-M128 RG-I/AG
113: CCRC-M126 RG-I/AG
114: CCRC-M134 RG-I/AG
115: CCRC-M125 RG-I/AG
116: CCRC-M123 RG-I/AG
117: CCRC-M122 RG-I/AG
118: CCRC-M121 RG-I/AG
119: CCRC-M112 RG-I/AG
120: CCRC-M21 RG-I/AG
121: JIM131 RG-I/AG
122: CCRC-M22 RG-I/AG
123: JIM132 RG-I/AG
124: JIM1 RG-I/AG
125: CCRC-M15 RG-I/AG
126: CCRC-M8 RG-I/AG
127: JIM16 RG-I/AG

Arabinogalactans – Oxalate

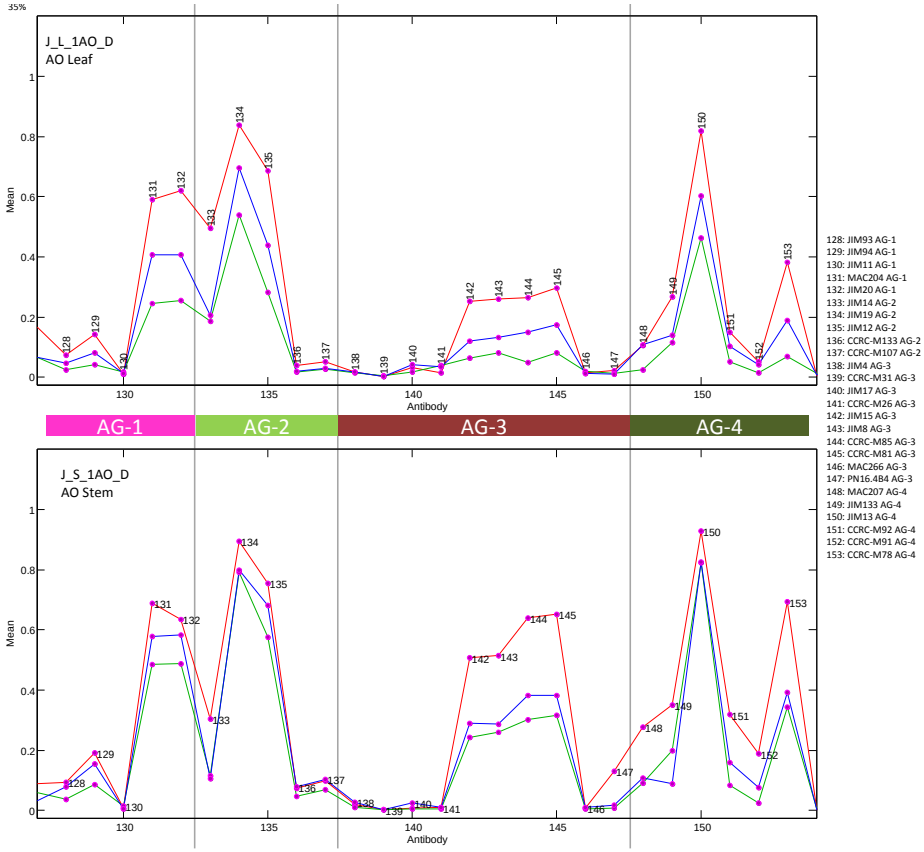

Arabinogalactans – Carbonate

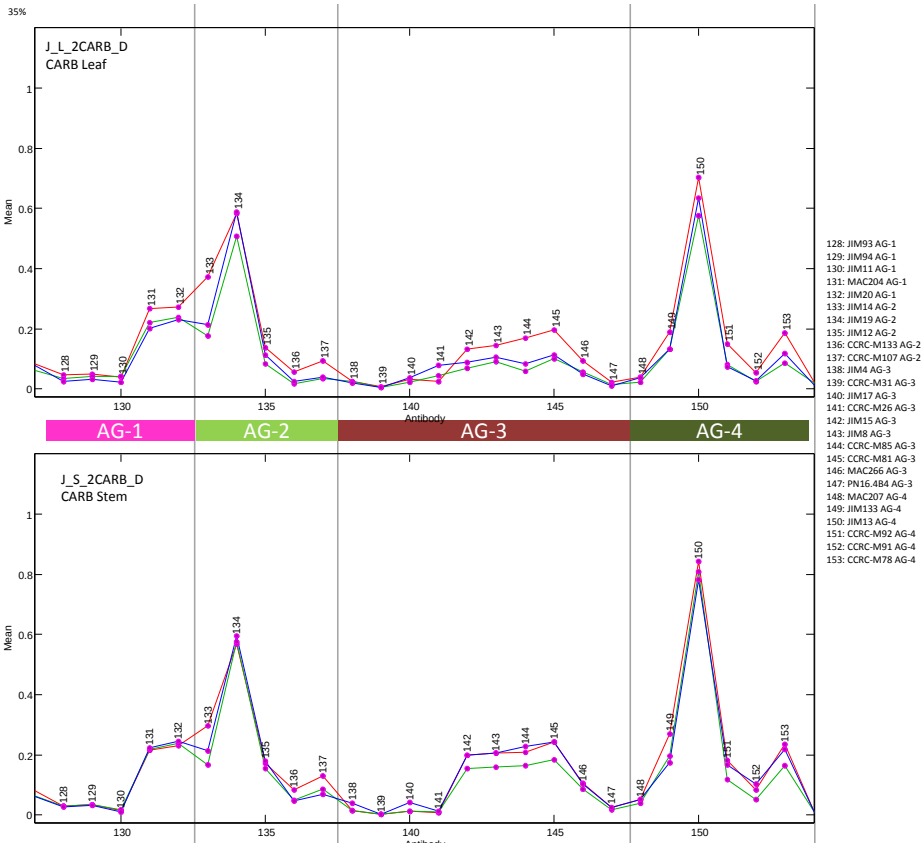

Arabinogalactans – 1M KOH

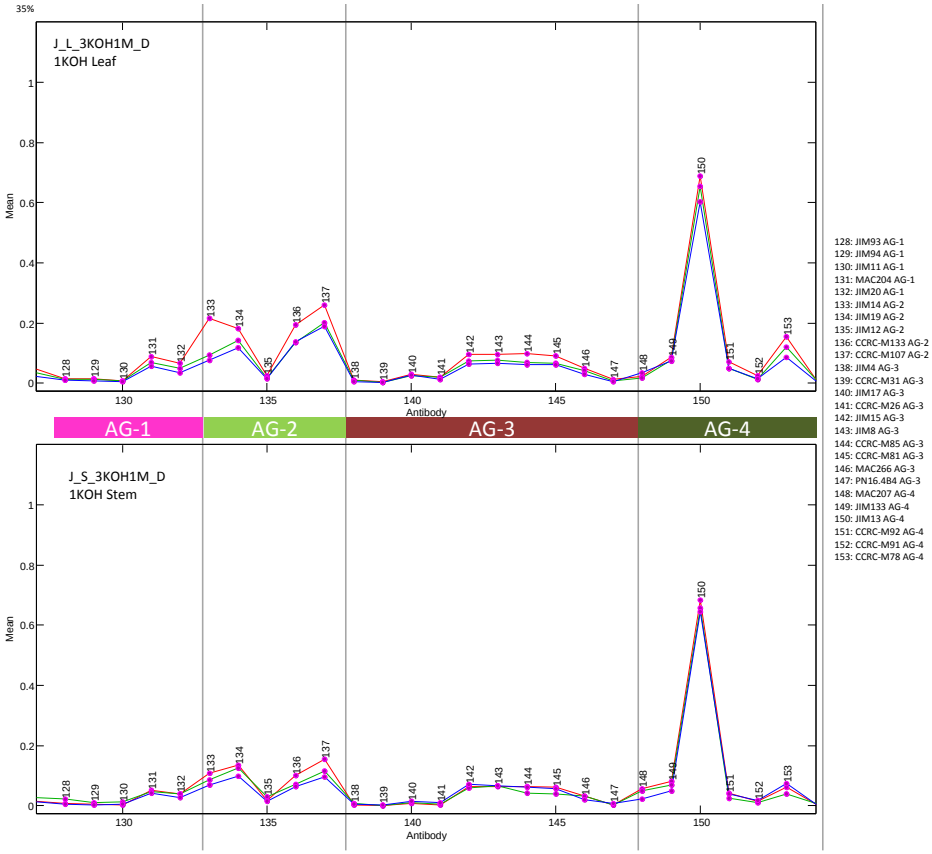

Arabinogalactans – 4M KOH

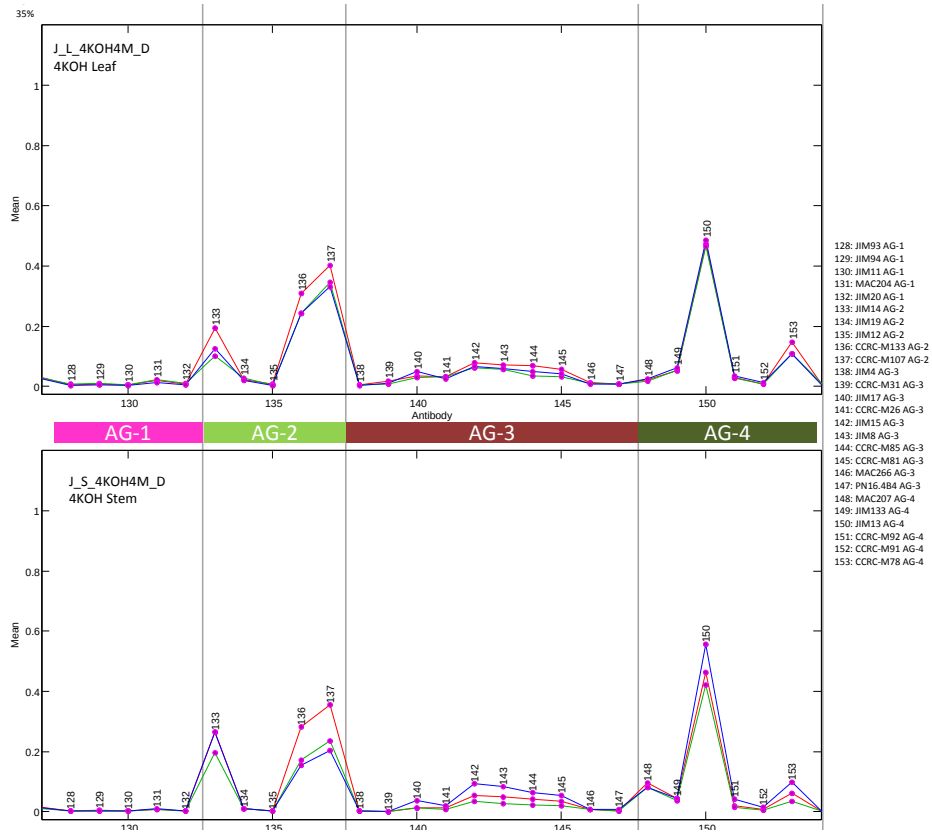

Arabinogalactans – Chlorite

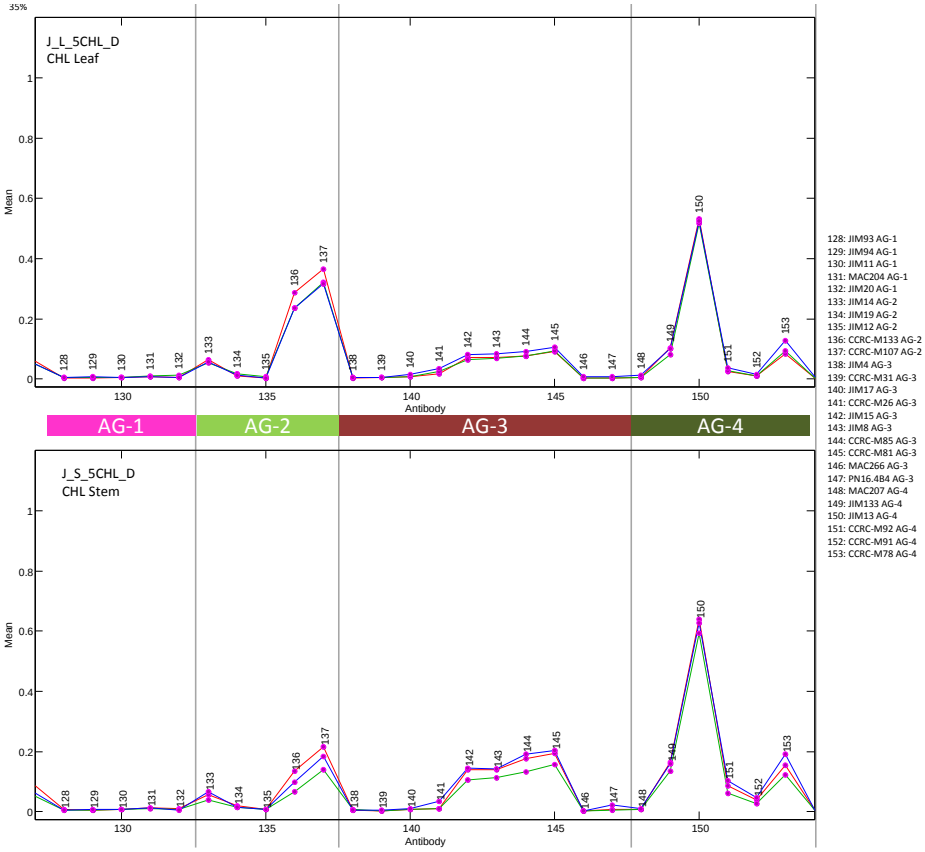

Arabinogalactans – 4M KOH PC

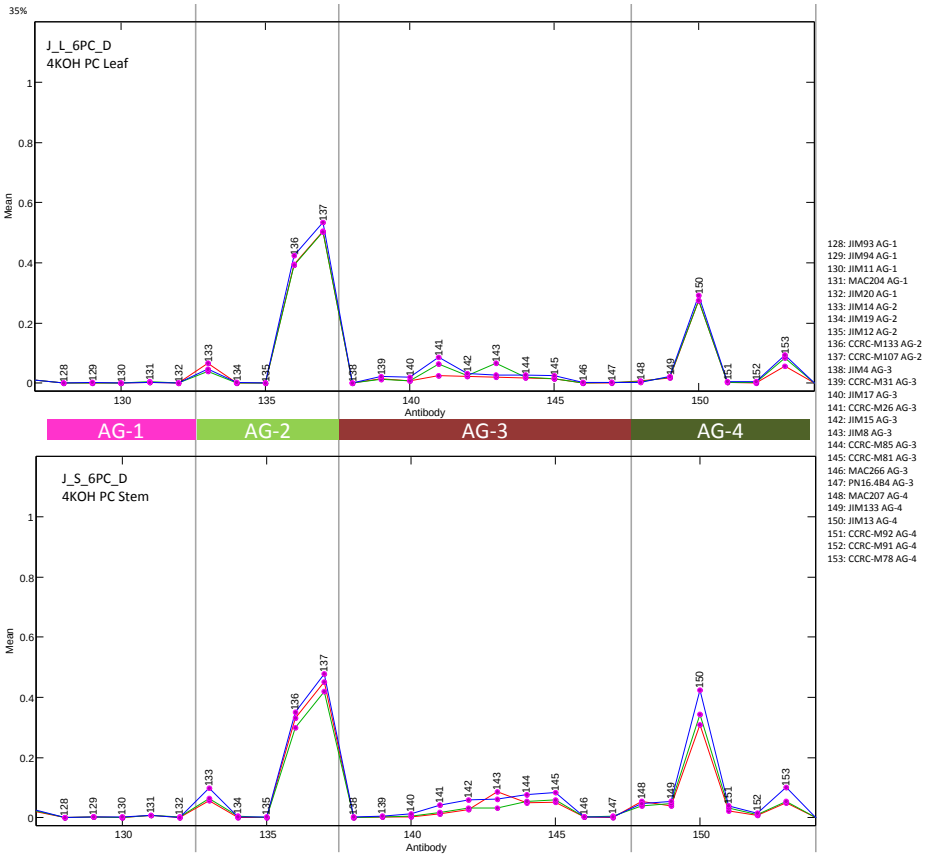

8.10. APPENDIX J: SUPPLEMENTAL IMMUNOLABELLING MICROGRAPHS

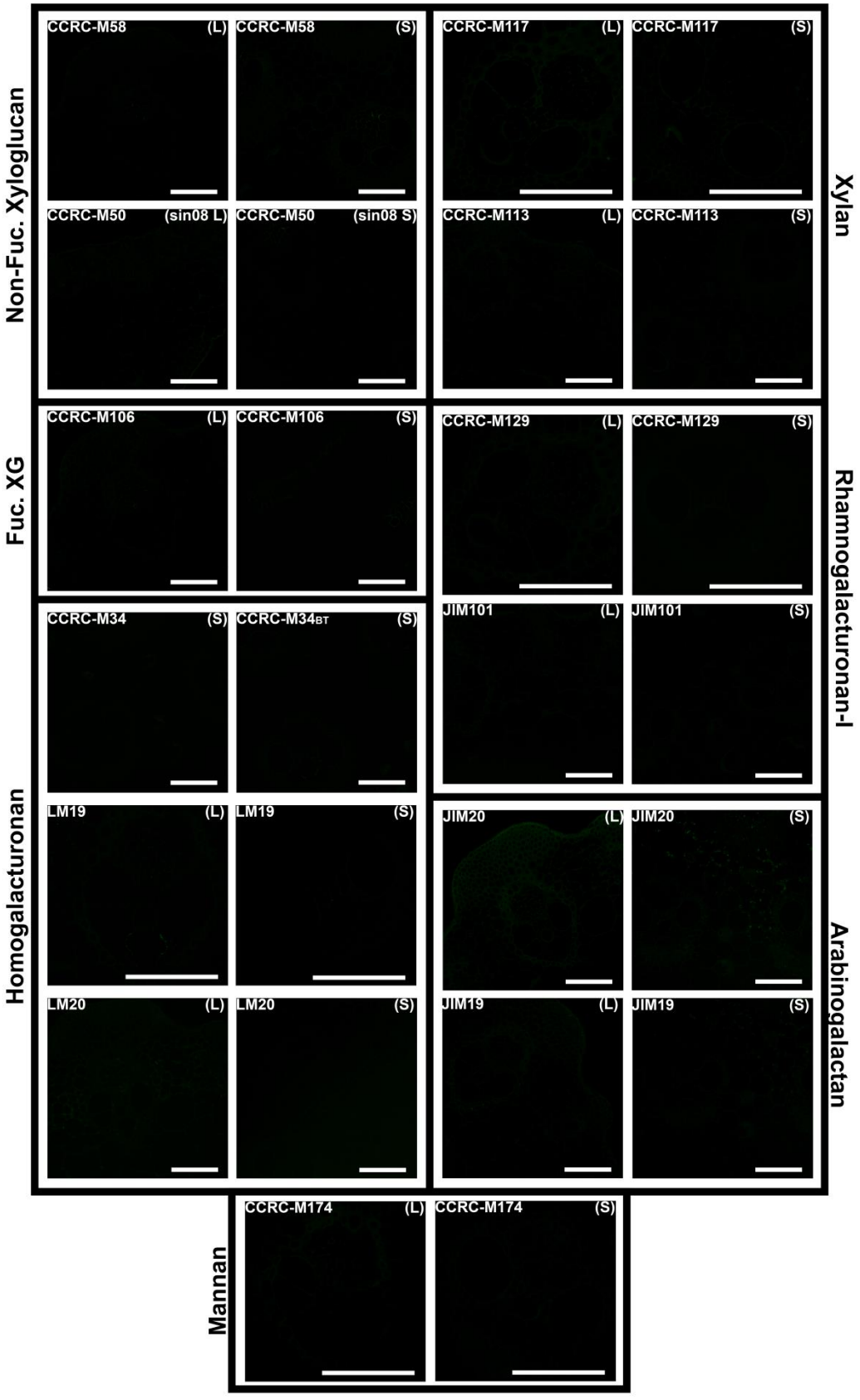

Fig. 8.10A. Letters between parenthesis indicate the corresponding tissue (L: leaf; S: stem). All micrographs are taken from gig01, except for CCRC-M50, which consists of sin08 sections. (bar=100µm)

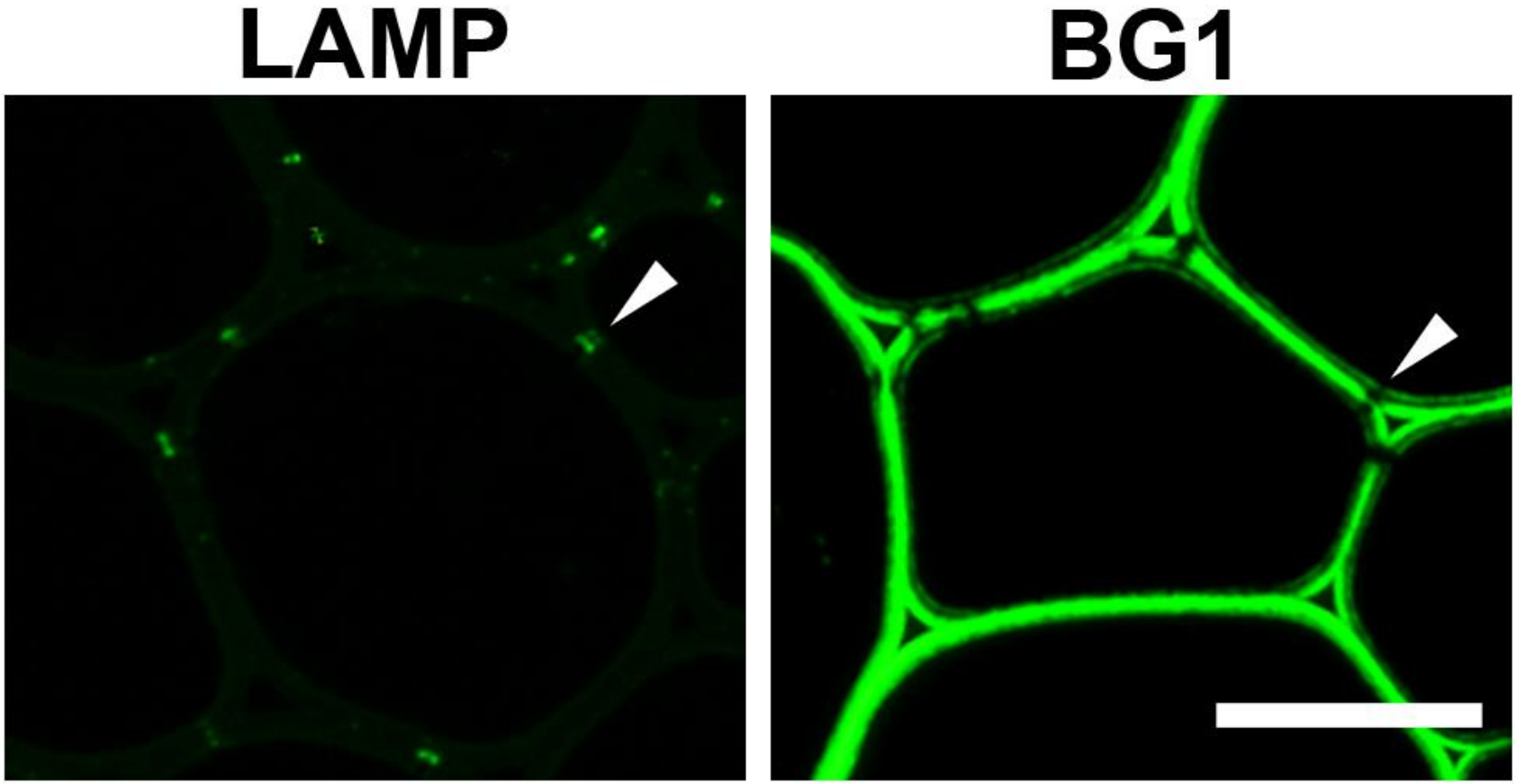

Fig. 8.10B. Detail of the immunofluorescent labelling of transverse sections from miscanthus genotype sin11 with β-glucan binding mAbs. Arrowheads indicate plasmodesmatal regions. For LAMP, the cross-section belongs to a stem sample, for BG1, the cross-section belongs to a leaf sample. Scale bar: 25µm.